

Notice 1

Under the Copyright Act 1968, this thesis must be used only under the normal conditions of scholarly fair dealing. In particular no results or conclusions should be extracted from it, nor should it be copied or closely paraphrased in whole or in part without the written consent of the author. Proper written acknowledgement should be made for any assistance obtained from this thesis.

Notice 2

I certify that I have made all reasonable efforts to secure copyright permissions for third-party content included in this thesis and have not knowingly added copyright content to my work without the owner's permission.

Targeting Phosphodiesterase Inhibition for Novel Antimalarial Therapies

Brittany L. Howard

B. Med. Chem. (Honours)

A thesis submitted in fulfillment of the requirements for the degree of
Doctor of Philosophy.

Department of Medicinal Chemistry
Faculty of Pharmacy and Pharmaceutical Sciences
Monash University
381 Royal Parade, Parkville, Victoria, Australia, 3052

January, 2013



Table of contents

Statement of originality.....	v
Acknowledgements.....	vi
Abbreviations and acronyms.....	viii
Figures, schemes and tables.....	xii
Publications and presentations.....	xxvi
Abstract.....	xxix
 Chapter 1: Malaria and the phosphodiesterase enzymes	1
1.1 Malaria.....	1
1.2 The <i>Plasmodium falciparum</i> parasite life-cycle.....	4
1.3 Currently employed antimalarial drugs.....	6
1.3.1 Chloroquine, amino alcohols and 4-aminoquinolines.....	6
1.3.2 Artemisinin and other endoperoxides.....	8
1.3.3 Other antimalarial drugs.....	9
1.4 <i>Plasmodium falciparum</i> resistance.....	14
1.5 The current antimalarial drug pipeline.....	16
1.5.1 Optimisation of a known antimalarial chemotype.....	19
The endoperoxide chemotype.....	19
The 4-aminoquinoline chemotype.....	20
The 8-aminoquinoline chemotype.....	21
The amino-alcohol chemotype.....	22
Chimeric chemotypes.....	23
Novel antimalarial chemotypes.....	23
1.5.2 Target-based screening – the genomic approach.....	24
1.5.3 Whole cell phenotypic screening.....	25
1.5.4 Combination therapies using existing antimalarials.....	27
1.5.5 Repurposing of drug chemotypes.....	28
1.6 Cyclic nucleotide phosphodiesterase enzymes.....	30
1.7 Architecture of the human phosphodiesterase enzymes.....	32
1.8 Human phosphodiesterase enzyme inhibitors.....	36
1.9 <i>Plasmodium falciparum</i> phosphodiesterase enzymes.....	40
1.10 Summary and aims of this thesis.....	44

Chapter 2: Homology modelling of <i>Plasmodium falciparum</i> phosphodiesterases and molecular docking	47
2.1 Introduction	47
2.2 Homology modelling of the <i>Plasmodium falciparum</i> phosphodiesterases	49
2.2.1 Protein sequence comparison	49
2.2.2 Homology modelling	51
2.2.3 Active site analysis	54
2.3 Docking into the developed <i>Plasmodium falciparum</i> phosphodiesterase enzymes homology models	59
2.3.1 Docking of human phosphodiesterase inhibitors	59
2.3.2 Docking of human phosphodiesterase 9 and 1 inhibitors	64
2.4 Gaining selectivity for the <i>Plasmodium falciparum</i> phosphodiesterases	66
2.5 Using the molecular docking results to shape the synthetic strategy	68
Chapter 3: Human phosphodiesterase 9 and 1 inhibitors as antiplasmodial compounds	70
3.1 Introduction	70
3.2 Synthesis of 5-(3-chlorobenzyl)-3-isopropyl-1 <i>H</i> -pyrazolo[4,3- <i>d</i>]pyrimidin-7(6 <i>H</i>)-one	74
3.3 Synthesis of a focussed pyrazolopyrimidinone library	81
3.4 Synthesis of 5-benzyl-3-isopropyl-1-methyl-1 <i>H</i> -pyrazolo[4,3- <i>d</i>]pyrimidin-7(6 <i>H</i>)-one	83
3.5 Biological assessment of the synthesised pyrazolopyrimidinones	83
3.5.1 <i>Plasmodium falciparum</i> growth inhibition	84
3.5.2 Human phosphodiesterase inhibition	88
3.6 Docking studies of the synthesised pyrazolopyrimidinone compounds	90
3.7 Chapter conclusions and future directions	95
Chapter 4: Synthetic studies of novel flavonoid mimetics	97
4.1 Introduction	97
4.1.1 Flavonoids as human phosphodiesterase inhibitors and antiplasmodial compounds	98
Flavonoids as human phosphodiesterase inhibitors	99
Flavonoids as antiplasmodial compounds	101
4.1.2 Prominent recurring structural features among human phosphodiesterase inhibitors	103
4.1.3 Poorly represented flavonoid-like compound classes	103
4.2 Synthetic studies of the 2-phenylbenzoxazepinone compound class	105
4.2.1 Synthetic access to the 2-phenylbenzoxazepinone compounds	105
4.2.2 Synthesis of 2-phenyl-3,4-dihydrobenzo[<i>f</i>][1,4]oxazepin-5(2 <i>H</i>)-one	107
4.2.3 Synthesis of 7,8-dimethoxy-2-phenyl-3,4-dihydrobenzo[<i>f</i>][1,4]-oxazepin-5(2 <i>H</i>)-one	110
4.2.4 Biological assessment of 2-phenyl-3,4-dihydrobenzo[<i>f</i>][1,4]-oxazepin-5(2 <i>H</i>)-one	113
4.2.5 Section discussion	113

4.3	Synthetic studies of the 2-phenylbenzoxepinone compound class	115
4.3.1	Synthetic access to the 2-phenylbenzoxepinone compounds	115
4.3.2	Attempted synthesis of 2-phenyl-3,4-dihydrobenzo[<i>b</i>]-oxepin-5(2 <i>H</i>)-one	117
4.3.3	Section discussion	124
4.4	Synthetic studies of the 8-phenylbenzosuberone compound class	124
4.4.1	Synthetic access to the 8-phenylbenzosuberone compounds	124
4.4.2	Attempted synthesis of 8-phenyl-6,7,8,9-tetrahydro-5 <i>H</i> -benzo[7]annulen-5-one	127
4.4.3	Synthesis of 2,3-dimethoxy-8-phenyl-6,7,8,9-tetrahydro-5 <i>H</i> -benzo[7]annulen-5-one	129
4.4.4	Section discussion	136
4.5	Chapter conclusions and future directions	136
 Chapter 5: Chromanone analogues of LY294002 as phosphodiesterase inhibitors		
		138
5.1	Introduction	138
5.2	Synthesis of 6-methyl-8-phenyl-2-(tetrahydro-2 <i>H</i> -pyran-4-yl)chroman-4-one	142
5.2.1	Pathway one	142
5.2.2	Pathway two	145
5.3	Synthesis of a focussed 2-tetrahydropyranchromanone library	146
5.4	Biological assessment of the synthesised 2-tetrahydropyranchromanones	152
5.4.1	<i>Plasmodium falciparum</i> growth inhibition	152
5.4.2	Human phosphodiesterase inhibition	155
5.5	Chapter discussion	158
5.6	Chapter conclusions and future directions	161
 Chapter 6: Conclusions and future directions		
		163
 Chapter 7: Experimental		
		169
7.1	Computational chemistry general experimental	169
7.1.1	Sequence alignment and template selection	169
7.1.2	Model building and minimisation	170
7.1.3	Docking	170
7.2	Synthetic chemistry general experimental	171
7.2.1	Chapter 3 experimental	174
7.2.2	Chapter 4 experimental	195
7.2.3	Chapter 5 experimental	215
7.3	Biological assay general experimental	240
7.3.1	<i>Plasmodium falciparum</i> growth inhibition assay	240
7.3.2	Human phosphodiesterase inhibition assay	241
	BPS Bioscience assays	241
	Scottish Biomedical assays	242

Chapter 8: References	243
Appendices	290
Appendix 1: Chapter 2 publication	291
Appendix 2: Sequence alignment of the catalytic domain of human and protozoan phosphodiesterases	302
Appendix 3: Calculated physicochemical properties of synthesised compounds	308
Appendix 4: Summary of biological activities of synthesised compounds	316
Appendix 5: IC ₅₀ curves of synthesised compounds	320

Statement of originality

To the best of the author's knowledge and belief, this thesis contains no material which has been accepted for the award of any other degree or diploma in any University or other institution, and contains no material previously published or written by another person except where due reference is made.

Brittany L. Howard

January, 2013

Acknowledgements

I will begin by acknowledging my supervisors, Dr. David Manallack and Dr. Philip Thompson, who have overseen every aspect of this research. You have both extended your support beyond the role of a supervisor, and I am immensely thankful for the opportunities you have both provided me with. David – your dedication to your students is what sets you apart, and for which I have been incredibly fortunate. Phil – the single most important skill you have instilled in me is to always see the bigger picture, both in work and in life. I will carry this with me in my journeys.

I wish to acknowledge Dr. Paul Gilson. Teaching a chemist to do biology is no easy feat, and your commitment to this work is greatly appreciated.

Thank you to past and present members of the research group; Simon Mountford, Ian Jennings, Joyce Zheng, Kade Roberts, Michelle Camerino, Jo-Anne Pinson, Jacob Nankervis, Tim Blackmore, Will Nguyen, Susan Northfield, Diana Neale, Michelle Miller, Syazwani Amran, and Oscr Lui (and honorary Thompson group members, Chris Opie and Natalie Vinh). Suze and Dee – I don't think I could have survived Friday afternoons without our hour of Maru! You are all talented scientists and lovely people to have met.

My appreciation extends to the staff and students within the medicinal chemistry department. In particular I wish to acknowledge Brad Doak, for your advice and friendship. You are gifted.

Of course, I want to thank my Mum and Dad. Without your unwavering support, this simply would not have been possible. You have tolerated years of study and my associated bad moods. Thank you. Beyond my parents, I wish to acknowledge the support of Brayden, Bridie, Nana (the greatest Nana in the world) and Pa.

Trent – thank you for so much, not the least of which for your patience and understanding. You have been my center of gravity throughout all of this. I think I will choose to express my gratitude by finally buying you a kitten as you’ve always wanted!

Abbreviations and acronyms

# acc	number of hydrogen bond acceptors
# don	number of hydrogen bond donors
μL	microliter
μM	micromolar
¹³ C NMR	Carbon NMR
1D	one-dimensional
¹ H NMR	Proton NMR
2D	two-dimensional
3D7	chloroquine-sensitive <i>Plasmodium falciparum</i> strain
7G8	chloroquine-resistant <i>Plasmodium falciparum</i> strain
Å	Angstrom
ADP	adenosine diphosphate
AIBN	azobisisobutyronitrile
aq.	aqueous
Ar	aryl
ATP	adenosine triphosphate
BACE	Beta-secretase
°C	degrees Celsius
cAMP	cyclic adenosine monophosphate
cGMP	cyclic guanosine monophosphate
cLogD _{7.4}	calculated logarithm of the distribution coefficient (at physiological pH)
cLogP	calculated logarithm of the partition coefficient
conc.	concentrated

DCE	dichloroethane
DIPEA	diisopropylethylamine (Hünig's base)
DMF	dimethylformamide
DMSO	dimethylsulfoxide
e.g.	for example
EC ₅₀	half maximal effective concentration
ESI	electrospray ionisation
exp.	experimental
g	gram
GSK	GlaxoSmithKline
h	hour(s)
<i>h</i>	human
H-bond	hydrogen bond
HCTU	1 <i>H</i> -benzotriazolium-1-[bis(dimethylamino)methylene] -5chlorohexafluorophosphate-(1-),3-oxide
HeLa	Henrietta Lacks 'immortal' cells
HIV	Human Immunodeficiency Virus
HRMS	high resolution mass spectrometry
Hz	hertz
I.R.	infrared
IBMX	3-isobutyl-1-methylxanthine
IC ₅₀	half maximal inhibitory concentration
<i>J</i>	coupling constant
K	Kelvin
L	litres
LCMS	liquid chromatography mass spectrometry
LDH	lactate dehydrogenase
lit.	literature
<i>Lmj</i>	<i>Leishmania major</i>
logD	the logarithm of the distribution coefficient
logP	the logarithm of the partition coefficient
M	molar
M.p.	melting point
mg	milligrams

MHz	megahertz
min	minute(s)
mL	millilitres
mm	millimetres
mM	millimolar
mmol	millimole(s)
MW	microwave
NF54	chloroquine-sensitive <i>Plasmodium falciparum</i> strain
nm	nanometres
nM	nanomolar
NMR	nuclear magnetic resonance
PARP	poly(ADP-ribose) polymerase
PDB	Protein Data Bank
PDE	Phosphodiesterase (enzyme)
<i>Pf</i>	<i>Plasmodium falciparum</i>
pH	power of hydrogen
PI3K	phosphoinositide 3-kinase
pK_a	negative logarithm of the acid dissociation constant
PKA	Protein kinase A
PPA	polyphosphoric acid
ppm	parts per million
PSA	polar surface area
PyBroP	bromo- <i>tris</i> -pyrrolidino-phosphonium hexafluorophosphate
R _f	retention factor
RMSD	root mean squared deviation
RP-HPLC	reverse phase high performance liquid chromatography
rt	room temperature
s	second(s)
SAR	structure-activity relationship
SP	standard precision
t	time
$t_{1/2}$	half-life
t.l.c.	thin-layer chromatography
TBAB	tetra- <i>n</i> -butylammonium bromide

<i>Tbr</i>	<i>Trypanosoma brucei</i>
TFA	trifluoroacetic acid
THF	tetrahydrofuran
t_R	retention time
TsOH	<i>para</i> -toluenesulfonic acid
vdW	van der Waals
w2mef	chloroquine-resistant <i>Plasmodium falciparum</i> strain
XP	extra precision
δ	chemical shift (ppm)

Amino acids are referred to as their standard one or three letter codes, unless otherwise stated.

Figures, schemes and tables

Chapter 1

Figure 1.1. The *P. falciparum* life-cycle, as described by Pasvol.

Table 1.2. Structures of the antimalarial drugs, compound class and mechanism of action.

Table 1.3. The common antimalarial therapies and the mechanisms by which parasite resistance arises.

Table 1.4. The MMV Global Malaria Portfolio as of the third quarter, 2012.

Figure 1.5. Structures of several compounds from the endoperoxide chemical class that are being optimised for antimalarial activity.

Figure 1.6. Structures of several compounds from the 4-aminoquinoline chemical class that are being optimised for antimalarial activity.

Figure 1.7. Structures of several compounds from the 8-aminoquinoline chemical class that are being optimised for antimalarial activity.

Figure 1.8. Structures of several compounds from the amino-alcohol chemical class that are being optimised for antimalarial activity.

Figure 1.9. Structures of several chimeric compounds that are currently being optimised for antimalarial activity.

Figure 1.10. Structures of several compounds from novel chemical classes that are being optimised for antimalarial activity.

Table 1.11. A summary of *P. falciparum* 3D7 high-throughput screening.

Figure 1.12. Structures of aforementioned antimalarial drugs employed in combination therapies.

Figure 1.13. A tadalafil analogue, **67**, synthesised by Deprez *et al.* and its activity and selectivity over human PDE5.

Table 1.14. The human PDE isoforms, their substrate preference, classical inhibitors and potential clinical application.

Figure 1.15. The general structures of the different PDE families, adapted from Conti *et al.*

Figure 1.16. The secondary structure of the catalytic domain of PDE4B2B, with the helices divided into sub-regions as described by Xu *et al.* The N-terminal sub-region (residues 152 to 274) is coloured in blue, the middle sub-region (residues 275-347) in red, and the C-terminal sub-region (residues 348 to 489) in purple.

Figure 1.17. The binding site of PDE4B2B showing the position of the metal ions zinc (grey sphere) and magnesium (purple sphere). The purine-scanning glutamine (Gln443) as well as the phenylalanine (Phe446) and isoleucine (Ile410) residues of the hydrophobic clamp are shown as sticks. Numbering is taken from the 1XMY crystal structure.

Figure 1.18. Structures of human PDE inhibitors.

Figure 1.19. Structures of several human PDE inhibitors, with the common structural features highlighted (the purine-like moiety is highlighted in purple, and the catechol ether moiety is highlighted in blue).

Table 1.20. The structural characteristics of the *Pf*PDEs.

Table 1.21. Schematic representation of the *P. falciparum* life-cycle and the expression of the *Pf*PDE isoforms throughout.

Table 1.22. The inhibitory activities of various *h*PDE inhibitors and chloroquine on *Pf*PDE α .

Chapter 2

Table 2.1. The percentage homologies of the human and parasitic PDE enzymes.

Figure 2.2. Superimposition of each of the developed *Pf*PDE homology models with the *h*PDE9 crystal structure template (shown in grey) (clockwise from top left, *Pf*PDE α - δ).

Figure 2.3. Ramachandran analysis of each of the *Pf*PDE homology models (clockwise from top left, *Pf*PDE α - δ).

Figure 2.4. The active site of the homology model of *Pf*PDE α with cGMP bound. Highlighted is the purine-scanning glutamine (Gln884), as well as the hydrophobic clamp residues (Phe887 and Ile850). Metal ions and water molecules are represented as spheres, and hydrogen bonds are shown as dashed lines. Numbering is taken from the *Pf*PDE α sequence.

Table 2.5. The alignment of the key PDE binding residues across the *h*PDEs, *Pf*PDEs and *Lmj*PDE.

Figure 2.6. Dendrogram analysis of the catalytic domains of the *h*PDEs, *Pf*PDEs, and *Lmj*PDE.

Figure 2.7. Dendrogram analysis of the 25 residues (from Table 2.5) associated with enzyme activity of the *h*PDEs, *Pf*PDEs and *Lmj*PDE.

Figure 2.8. The docked pose of (a) zaprinast and (b) sildenafil in the *Pf*PDE α homology model. Highlighted is the purine-scanning glutamine (Gln884), as well as the hydrophobic clamp residues (Phe887 and Ile850). Metal ions and water molecules are

represented as spheres, and hydrogen bonds are shown as dashed lines. Numbering is taken from the *PfPDE α* sequence.

Figure 2.9. The docked pose of E4021 in the *PfPDE α* homology model. Highlighted is the purine-scanning glutamine (Gln884), as well as the hydrophobic clamp residues (Phe887 and Ile850). Metal ions and water molecules are represented as spheres, and hydrogen bonds are shown as dashed lines. Numbering is taken from the *PfPDE α* sequence.

Figure 2.10. Docking of PDE inhibitors into the *PfPDE α* homology model. Highlighted is the purine-scanning glutamine (Gln884), as well as the phenylalanine residue (Phe887) of the hydrophobic clamp. Metal ions and water molecules are represented as spheres, and hydrogen bonds are shown as dashed lines. (a) dipyridamole, (b) EHNA, (c) IBMX, (d) rolipram, (e) milrinone, (f) vinpocetine, (g) pentoxifylline, (h) theophylline, (i) papaverine.

Figure 2.11. The structure of the tadalafil analogue, **76**, published by Beghyn *et al.*

Figure 2.12. Structures of *hPDE1* and *hPDE9* inhibitors developed by DeNinno *et al.*

Figure 2.13. The docked pose of (a) **77** and (b) **78** in the *PfPDE α* homology model. Highlighted is the purine-scanning glutamine (Gln884), as well as the hydrophobic clamp residues (Phe887 and Ile850). Metal ions and water molecules are represented as spheres, and hydrogen bonds are shown as dashed lines.

Chapter 3

Figure 3.1. Structure of the *hPDE9* and *hPDE1* inhibitor, **77**, identified by DeNinno *et al.* that was investigated in molecular modelling work (Chapter 2).

Figure 3.2. Structures of *hPDE* inhibitors that are representative of the guanine isostere family.

Figure 3.3. A summary of the guanine isosteres reported as *h*PD_E inhibitor scaffolds.

Scheme 3.4. General synthesis of guanine isosteres (**84**) from a key heterocyclic core (**82**).

Scheme 3.5. General reaction scheme of the condensation of a key pyrazole precursor (**85**) with various carboxylic acids (**86**) to give substituted pyrazolopyrimidinone compounds (**87**).

Figure 3.6. The envisaged derivatisations to **77** in the synthesis of pyrazolopyrimidinone analogues; modification to the benzyl substituent in blue, modification to the core bicyclic system in green, modification to the 9-isopropyl group in purple, modification to the endocyclic *N*¹ in pink.

Scheme 3.7. Synthesis of the key pyrazole precursor (**85**) adapted from the procedure of DeNinno *et al.*¹⁹⁹ and the subsequent synthesis of the target compound (**77**). (a) Na_(s), CH₃CH₂OH, N₂, rt, 1 h, then 60 °C, 1 h, 98%; (b) NH₂NH₂·H₂O, CH₃CH₂OH, N₂, rt, 18 h, then NH₂NH₂·H₂O, 60 °C, 3 h, 64%; (c) 1 M aq. NaOH, 1,4-dioxane, 50 °C, 1 h, 74%; (d) conc. H₂SO₄, 70% aq. HNO₃, 60 °C, 1 h, 30%; (e) conc. H₂SO₄, CH₃OH, 55 °C, 16 h, 66%; (f) Mg₃N₂, CH₃OH, 0 °C to 80 °C, 24 h, 88%; (g) Pd/C, H₂, CH₃CH₂OH, rt, 20 h, 68%; (h) PyBroP, DCE, MW, 120 °C, 20 min, then *t*BuOK, *i*PrOH, MW, 130 °C, 40 min, 63%.

Scheme 3.8. Conversion of the carboxylic acid (**93**) to the corresponding amide (**95**) via the ethyl ester intermediate (**96**), adapted from Robins *et al.* (a) conc. H₂SO₄, CH₃CH₂OH, toluene, 78 °C, 24 h, 92%; (b) conc. NH₄OH, 100 °C, 2 h, unisolated.

Scheme 3.9. Conversion of the carboxylic acid (**93**) to the corresponding amide (**95**) via the methyl ester intermediate (**94**), adapted from Bridgwood *et al.* (a) conc. H₂SO₄, CH₃OH, 55 °C, 16 h; 66%; (b) Mg₃N₂, CH₃OH, 0 °C to 80 °C, 24 h, 88%.

Scheme 3.10. Synthesis of **77** (via **97**) using amide coupling conditions. (a) HCTU, DIPA, DMF, rt, 20 min, then **85** in DMF, rt, 24 h, 12%. (b) PyBroP, DCE, MW, 120 °C, 20 min; (c) *t*BuOK, *i*PrOH, MW, 130 °C, 40 min, 63%.

Table 3.11. The structures of synthesised pyrazolopyrimidinone analogues (**77**, **98-116**).

Scheme 3.12. Synthesis of 5-benzyl-3-isopropyl-1-methyl-1*H*-pyrazolo[4,3-*d*]pyrimidin-7(6*H*)-one (**117**) from **99**. (a) (CH₃O)₂SO₂, CH₃C(O)CH₃, 60 °C, 16 h, 63%.

Table 3.13. Determined IC₅₀ value ranges of the synthesised pyrazolopyrimidinones for *P. falciparum* (3D7) growth inhibition.

Figure 3.14. IC₅₀ curves of compounds **99** and **105** against *P. falciparum* growth. Each value represents the mean of duplicate determinations where each replicate was within 4% of the mean value.

Figure 3.15. Percentage inhibition of human PDE activity of compounds **99** and **105** at 1 μM concentration. Each value represents the mean of duplicate determinations where each replicate was within 7% of the mean value.

Table 3.16. Human PDE9 IC₅₀ values of zaprinast and selected pyrazolopyrimidinone analogues.

Figure 3.17. Docked poses of *para*-substituted pyrazolopyrimidinone compounds (**104**, **106**, **109-111**, **113**, **114**) into the *Pf*PDEα model. (a) *Pf*PDEα model is shown as helices; (b) *Pf*PDEα model is shown as a rendered surface. Hydrogen bonds are shown as dashed lines. Purine-scanning glutamine (Gln884) and hydrophobic clamp residues (Phe887 and Ile850) are shown as purple sticks. Numbering is taken from the *Pf*PDEα sequence. Water molecules and ions are shown as spheres.

Figure 3.18. (a) Docked poses of compounds **99** (pink) and **100** (blue); (b) **98** (green); (c) **102** (pink) and **103** (blue); (d) **101** (green) into the *Pf*PDEα model. Hydrogen bonds

are shown as dashed lines. Purine-scanning glutamine (Gln884) and hydrophobic clamp residues (Phe887 and Ile850) are shown as purple sticks. Numbering is taken from the *PfPDE α* sequence. Water molecules and ions are shown as spheres.

Figure 3.19. Docked poses of compounds with *ortho*-, *meta*- and *para*-substituents into the *PfPDE α* model. (a) chlorobenzyl analogues **105** (green), **77** (blue), **104** (red); (b) methylbenzyl analogues **108** (green), **107** (blue), **106** (red). Highlighted as sticks are the purine-scanning glutamine (Gln884) and the hydrophobic clamp residues (Phe887 and Ile850). Numbering is taken from the *PfPDE α* sequence.

Figure 3.20. Docking of compounds **77** (blue), **105** (purple) and **99** (green) into the *hPDE9* crystal structure (3DYN). Highlighted as sticks are the purine-scanning glutamine (Gln453) as well as the hydrophobic clamp residues (Phe456 and Leu420) and an adjacent phenylalanine residue (Phe441). Numbering is taken from the 3DYN crystal structure.

Chapter 4

Figure 4.1. Subclasses of different flavonoids, and the structures of several commonly found flavonoids.

Table 4.2. Flavonoid inhibition of cAMP and cGMP phosphodiesterases.

Table 4.3. IC₅₀ values (μ M) of flavonoids on human phosphodiesterase isozymes.

Figure 4.4. Structures of the antiplasmodial flavonoids, **118** and **119**, as reported by Tasdemir *et al.*

Figure 4.5. Scaffolds of 6,7-fused ring system compound classes; 2-phenylbenzoxazepinone (**121**), 2-phenylbenzoxepinone (**122**), 8-phenylbenzosuberone (**123**) and a representative from the benzodiazepine class, diazepam (**124**).

Figure 4.6. Sites of interest for 1,(2)-dimethoxylation on the 2-phenylbenzoxazepinone, 2-phenylbenzoxepinone and 8-phenylbenzosuberone compound classes.

Scheme 4.7. Schmidt reaction of 2-phenylchroman-4-one (**125**) described by Misiti and Rimatori to give several isolable and characterised products. (a) NaN_3 , $\text{CH}_3\text{CO}_2\text{H}$, conc. H_2SO_4 , 40-50 °C, 45 min, **121** (83%), **126** (3%), **127** (5%).

Scheme 4.8. The envisaged Beckmann rearrangement of the oxime intermediate (**128**) to the corresponding 2-phenylbenzoxazepinone (**121**) from 2-phenylchroman-4-one (**125**) starting material.

Scheme 4.9. The Schmidt reaction of 2-phenylchroman-4-one (**125**) to give 2-phenylbenzoxazepinone (**121**) and a tetrazole by-product (**127**). (a) NaN_3 , conc. H_2SO_4 , toluene, rt, 16 h, **121** (64%), **127** (8%), **125** (12%).

Table 4.10. Comparison of literature (lit.) and experimental (exp.) values in the characterisation of the Schmidt reaction products and by-products.

Scheme 4.11. Synthesis of the oxime intermediates of 3,4-dihydronaphthalen-1(2*H*)-one (**129**) and chroman-4-one (**130**) and subsequent Beckmann rearrangement. (a) $\text{NH}_2\text{OH}\cdot\text{HCl}$, $\text{CH}_3\text{CO}_2\text{Na}$, $\text{CH}_3\text{CH}_2\text{OH}$, 78 °C, 2 h; (b) TsOH , ZnBr_2 , CH_3CN , 5 h.

Scheme 4.12. Synthesis of 2-phenylbenzoxazepinone (**121**) *via* the Beckmann rearrangement of (*E*)-2-phenylchroman-4-one oxime (**135**). (a) $\text{NH}_2\text{OH}\cdot\text{HCl}$, $\text{CH}_3\text{CO}_2\text{Na}$, $\text{CH}_3\text{CH}_2\text{OH}$, 78 °C, 2 h, 92%; (b) PPA, 120 °C, 2 h, then H_2O , 75 °C, 2 h, 79%.

Scheme 4.13. Synthesis of substituted flavanones (**136**) *via* chalcone intermediates (**137**) through reaction of a 2'-hydroxyacetophenone with a benzaldehyde.

Scheme 4.14. Two-step synthesis of 6-methoxy-2-phenylchroman-4-one (**138**) *via* the corresponding chalcone intermediate (**139**). (a) $\text{Ba}(\text{OH})_2\cdot 8\text{H}_2\text{O}$, $\text{CH}_3\text{CH}_2\text{OH}$, 40 °C, 16 h, 97%; (b) $\text{CH}_3\text{CO}_2\text{Na}$, $\text{CH}_3\text{CH}_2\text{OH}$, 78 °C, 16 h, 90%.

Table 4.15. Investigation of temperature and time effects in the synthesis of (*E*)-1-(2-hydroxy-5-methoxyphenyl)-3-phenylprop-2-en-1-one (**139**) using the procedure of Chimenti *et al.*

Figure 4.16. Synthesised flavanone compounds (**138**, **140-142**) with various methoxy substituents.

Scheme 4.17. The previously established Schmidt reaction and Beckmann rearrangement conditions failed to produce any of the methoxy-substituted 2-phenylbenzoxazepinones (**143** and **144**).

Figure 4.18. 2-Phenylbenzoxazepinone (**121**) docked into the *PfPDEα* homology model. (a) the *R* enantiomer and (b) the *S* enantiomer. Highlighted as sticks are the purine-scanning glutamine (Gln884), as well as the hydrophobic clamp residues (Phe887 and Ile850). Numbering is taken from the *PfPDEα* sequence. Metal ions and water molecules are represented as spheres, and hydrogen bonds are shown with dashed lines.

Scheme 4.19. Attempted synthesis of 2-phenylbenzoxepinone (**122**) through dehydrative ring formation of the butyric acid (**149**) as reported by Tatsuoka *et al.* (a) PPA, rt, 6 h.

Scheme 4.20. Literature synthesis of 2-phenylbenzoxepinone (**122**) *via* the cyclopropane intermediate (**151**). (a) (CH₃)₃S(O)I, NaH, DMSO, rt, then **150** in DMSO over 3 min, then rt, 2 h, 51%; (b) (*n*Bu)₃SnH, AIBN, toluene, 90-100 °C, 1 h, 85%.

Scheme 4.21. Literature syntheses of the key 4-phenoxy-4-phenylbutanoic acid precursor (**145**) and subsequent reaction to give 5-phenyl-4,5-dihydrobenzo[*b*]oxepin-2(3*H*)-one (**152**). (a) NaOCH₃, CH₃OH, 65 °C, 1 h, then γ -phenyl- γ -butyrolactone, 150 °C, 85%; (b) 75% PPA, rt, 5 h, 30%. (c) 75% PPA, rt, 5 h, 30%.³⁰⁵

Scheme 4.22. Synthesis of 7,8-dimethoxy-5-phenyl-4,5-dihydrobenzo[*b*]oxepin-2(3*H*)-one (**153**). (a) PPA, rt, 7 h, 82%.

Scheme 4.23. Synthesis of 7-methoxy-2-phenyl-3,4-dihydrobenzo[*b*]oxepin-5(2*H*)-one (**154**). (a) PPA, rt, 7 h, 46%.

Scheme 4.24. Proposed reaction mechanism for the synthesis of 5-phenyl-4,5-dihydrobenzo[*b*]oxepin-2(3*H*)-one (**152**) from either 4-phenoxy-4-phenylbutanoic acid (**145**) (shown in blue) or from the reaction of γ -phenyl- γ -butyrolactone with phenol (shown in purple).

Figure 4.25. Corey-Chaykovsky reaction using dimethylsulfoxonium methylide (**157**) or dimethylsulfonium methylide (**158**).

Scheme 4.26. Trial reaction to test for dimethylsulfoxonium methylide (**157**) preparation using 2-cyclohexenone (**159**). (a) $(\text{CH}_3)_3\text{S}(\text{O})\text{I}$, NaH, DMSO, rt, 40 min, then **159** in DMSO over 3 min, then 50 °C, 2 h, 88%.

Scheme 4.27. Reaction of 2-phenyl-4*H*-chromen-4-one (**150**) to give the desired cyclopropane product (**151**) and by-product **161**. (a) $(\text{CH}_3)_3\text{S}(\text{O})\text{I}$, NaH, DMSO, rt, 40 min, then **150** in DMSO over 3 min, then 50 °C, 2 h, **151** (12%), **161** (68%).

Scheme 4.28. Literature report of the nitro-activated cyclopropane (**162**) reacting with water to form 2-hydroxy-4-nitro-3,4-dihydrobenzo[*b*]oxepin-5(2*H*)-one (**163**).

Scheme 4.29. Attempted Pereyre's reductive cleavage of the cyclopropane (**151**) to give 2-phenylbenzoxepinone (**122**). (a) $(n\text{Bu})_3\text{SnH}$, AIBN, toluene, 90-100 °C, 1 h.

Scheme 4.30. Friedel-Crafts intramolecular acylation reaction of diphenylvaleric acid (**165**) in the synthesis of 9-phenylbenzosuberone (**164**). (a) AlCl_3 , CS_2 , 46 °C, 12 h, 59%.

Scheme 4.31. Friedel-Crafts intramolecular acylation reaction of 5-phenylpentanoic acid (**167**) in the synthesis of benzosuberone (**166**). (a) PPA, rt, 6 h, 92%.

Scheme 4.32. It can be envisaged that both 8-phenylbenzosuberone (**123**) and 4-benzyl-3,4-dihydronaphthalen-1(2*H*)-one (**169**) can be synthesised through an intramolecular Friedel-Crafts acylation reaction of 4,5-bis-(4'-methoxyphenyl)pentanoic acid (**168**).

Scheme 4.33. Synthesis of 2,3-dimethoxy-8-phenylbenzosuberone (**171**) as described by Thompson. (a) PPA, 100 °C, 4 h, 48% (**171/172** (7:3)).

Scheme 4.34. Synthesis of 4-benzyl-3,4-dihydronaphthalen-1(2*H*)-one (**169**). (a) *t*BuOK, ethyl acrylate, *t*BuOH, rt, 2 h, 98%; (b) 1,4-dioxane/1 M aq. NaOH (1:1), 100 °C, 2 h, 95%; (c) (CH₃CH₂)₃SiH, CF₃CO₂H, N₂, rt, 16 h, 85%; (d) PPA, 80 °C, 4 h, 67%.

Scheme 4.35. Synthesis of 2,3-dimethoxy-8-phenylbenzosuberone (**171**) and 4-(3,4-dimethoxybenzyl)-3,4-dihydronaphthalen-1(2*H*)-one (**172**). (a) (COCl)₂, CH₂Cl₂, 60 °C, 1 h, then 1,2-dimethoxybenzene, AlCl₃, rt to 60 °C, 4 h, 85%; (b) *t*BuOK, ethyl acrylate, *t*BuOH, rt, 2 h, 93%; (c) 1,4-dioxane/1 M aq. NaOH (1:1), 100 °C, 2 h, 96%; (d) (CH₃CH₂)₃SiH, CF₃CO₂H, N₂, rt, 1 h; (e) (CH₃CH₂)₃SiH, rt, 15 h, 92%; (f) PPA, 80 °C, 4 h, 92% (**175/176** (4:1)).

Figure 4.36. Chiral chromatography profile at 254 nm of the reaction mixture of the benzosuberone (**171**) and the tetralone (**172**) compounds using the Cellulose 1 column.

Figure 4.37. Chiral chromatography profile at 254 nm of the reaction mixture of the benzosuberone (**171**) and the tetralone (**172**) compounds using the Cellulose 2 column.

Figure 4.38. Chiral chromatography profile at 254 nm of the reaction mixture of the benzosuberone (**171**) and the tetralone (**172**) compounds using the Amylose 2 column.

Figure 4.39. Collected fractions from the chiral HPLC separation of the benzosuberone (**171**) and the tetralone (**172**) compounds using the Amylose 2 stationary phase and eluting with 20% ethanol in petroleum spirits. Fractions were collected in order A, B, C, D.

Figure 4.40. Chiral chromatography profile at 254 nm (Amylose 2, 20% ethanol in petroleum spirits) of purified 2,3-dimethoxy-8-phenylbenzosuberone (**171**).

Figure 4.41. The assigned aromatic region of the ¹H NMR spectrum of 2,3-dimethoxy-8-phenylbenzosuberone (**171**). Chemical shift (δ) in ppm is shown along the x-axis.

Chapter 5

Figure 5.1. The structure of the synthetic chromone, LY294002 (**182**).

Table 5.2. LY294002 (**182**) inhibition of human PDE isoforms.

Figure 5.3. JN8-6 (**183**) inhibition of human PDE isoforms.

Figure 5.4. 8-Phenyl-substituted analogue (**184**) and the chromanone core scaffold (**185**).

Scheme 5.5. Envisaged synthetic pathways to 8-phenyl-2-(tetrahydro-2*H*-pyran-4-yl)chroman-4-one (**188**) (pathway one in purple, pathway two in red).

Scheme 5.6. Synthesis of 6-methyl-8-phenyl-2-(tetrahydro-2*H*-pyran-4-yl)chroman-4-one (**188**). (a) Br₂, CH₃CO₂H, CH₃CO₂Na, 0 °C to rt, 24 h, then Br₂, CH₃CO₂H, 0 °C to rt, 24 h, 96%; (b) Na₂B₄O₇·10H₂O, CH₃CH₂OH, 78 °C, 48 h, 87%; (c) C₆H₅B(OH)₂, Cs₂CO₃, Pd(CH₃CO₂)₂, PCy₃, (*n*Bu)₄NBr, 1,4-dioxane/H₂O (6:1), MW, 150 °C, 30 min, 94%.

Scheme 5.7. Alternate synthesis of 6-methyl-8-phenyl-2-(tetrahydro-2*H*-pyran-4-yl)chroman-4-one (**188**). (a) C₆H₅B(OH)₂, K₂CO₃, Pd(OH)₂, DMF/H₂O (9:1), MW, 130 °C, 2.5 h, 92%; (b) tetrahydro-2*H*-pyran-4-carbaldehyde, Na₂B₄O₇·10H₂O, CH₃CH₂OH/H₂O (1:1.6), 78 °C, 72 h, 41%.

Scheme 5.8. Synthesis of 2-tetrahydropyranchromanone analogues through a Suzuki-Miyaura coupling of **187** with boronic acids. (a) Cs₂CO₃, Pd(OCOCH₃)₂, PCy₃, (*n*Bu)₄NBr, 1,4-dioxane/H₂O (6:1), MW, 150 °C, 30 min.

Table 5.9. The structures of the synthesised 2-tetrahydropyranchromanones (**188**, **190-206**).

Scheme 5.10. Oxidation of 2-phenylchroman-4-one (**125**) to 2-phenyl-4*H*-chromen-4-one (**207**) (a) I₂, pyridine, 90 °C, 3 h, 57%.

Scheme 5.11. Oxidation of 8-(3,4-dimethoxyphenyl)-6-methyl-2-(tetrahydro-2*H*-pyran-4-yl)chroman-4-one (**190**) to 8-(3,4-dimethoxyphenyl)-6-methyl-2-(tetrahydro-2*H*-pyran-4-yl)-4*H*-chromen-4-one (**208**). (a) I₂, pyridine, 90 °C, 16 h, 22%.

Scheme 5.12. Synthesis of methyl-2-(tetrahydro-2*H*-pyran-4-yl)chroman-4-one (**209**). (a) piperidine, CH₃CH₂OH, 78 °C, 48 h, 38%.

Figure 5.13. 6-methoxy-8-phenyl-2-(tetrahydro-2*H*-pyran-4-yl)chroman-4-one (**210**).

Scheme 5.14. Attempted synthesis of 6-methoxy-8-phenyl-2-(tetrahydro-2*H*-pyran-4-yl)chroman-4-one (**210**). (a) Br₂, CH₃CO₂H, CH₃CO₂Na, 0 °C to rt, 24 h, then Br₂, CH₃CO₂H, 0 °C to rt, 24 h, 88%; (b) tetrahydro-2*H*-pyran-4-carbaldehyde, Na₂B₄O₇·10H₂O, CH₃CH₂OH, 78 °C, 48 h, 7%; (c) C₆H₅B(OH)₂, Cs₂CO₃, Pd(CH₃CO₂)₂, PCy₃, (*n*Bu)₄NBr, 1,4-dioxane/H₂O (6:1), MW, 150 °C, 30 min, unisolated.

Table 5.15. Determined IC₅₀ ranges of the synthesised 2-tetrahydropyranchromanones and related compounds for *P. falciparum* (3D7) growth inhibition.

Table 5.16. Determined inhibitory activities of chromanone compounds.

Figure 5.17. The docking pose of the (a) *R* (pink) and (b) *S* (blue) enantiomers of **190** in the *Pf*PDEα homology model. Hydrogen bonds are shown as dashed lines. Purine-scanning glutamine (Gln884) and hydrophobic clamp residues (Phe887 and Ile850) are shown as purple sticks. Numbering is taken from the *Pf*PDEα sequence. Water molecules and ions are shown as spheres.

Figure 5.18. The docking pose of **208** (green) in the *Pf*PDEα homology model. Hydrogen bonds are shown as dashed lines. Purine-scanning glutamine (Gln884) and hydrophobic clamp residues (Phe887 and Ile850) are shown as purple sticks. Numbering is taken from the *Pf*PDEα sequence. Water molecules and ions are shown as spheres.

Appendices

Table A3. Calculated physicochemical properties of synthesised compounds.

Table A4. Summary of the biological activities of synthesised compounds.

Publications and presentations

Publications

Howard, B. L.; Thompson, P. E.; Manallack, D. T. Active site similarity between human and *Plasmodium falciparum* phosphodiesterases: Considerations for antimalarial drug design. *Journal of Computer-Aided Molecular Design* **2011**, 25, 753-762.

Oral presentations

Howard, B. L.; Thompson, P. E.; Manallack, D. T. Homology modelling of malarial phosphodiesterase enzymes. *AMMA M⁴, Melbourne Meeting of Molecular Modellers, Melbourne. 2009.*

Howard, B. L.; Thompson, P. E.; Manallack, D. T. *Plasmodium falciparum* phosphodiesterases for the investigation of malaria. *Cancer Therapeutics (CTx) Symposium, Melbourne. 2010.*

Howard, B. L.; Thompson, P. E.; Manallack, D. T. Malaria. *3MT Monash University, Melbourne. 2010.*

Howard, B. L.; Thompson, P. E.; Manallack, D. T. Inhibitors of *Plasmodium falciparum* phosphodiesterases as novel antimalarial therapies. *Gordon Research Conference on Cyclic Nucleotide Phosphodiesterases, Italy. 2012.*

Howard, B. L.; Thompson, P. E.; Manallack, D. T. Inhibitors of *Plasmodium falciparum* phosphodiesterases as novel antimalarial therapies. *Cancer Therapeutics (CTx) Symposium, Melbourne. 2012.*

Howard, B. L.; Thompson, P. E.; Manallack, D. T. Synthesis of novel chromone scaffolds as a new class of PDE inhibitors. *RACI Synthesis Symposium, Melbourne. 2012.*

Poster presentations

Howard, B. L.; Thompson, P. E.; Manallack, D. T. Phosphodiesterase inhibitors and malaria. *MIPS 4th Annual Postgraduate Research Symposium, Melbourne. 2009.*

Howard, B. L.; Thompson, P. E.; Manallack, D. T. Phosphodiesterase inhibitors and malaria. *M⁴, Melbourne Meeting of Molecular Modellers, Melbourne. 2009.*

Howard, B. L.; Thompson, P. E.; Manallack, D. T. Inhibitors of *Plasmodium falciparum* phosphodiesterases for the investigation of malaria. *Gordon Research Conference on Cyclic Nucleotide Phosphodiesterases, USA. 2010.*

Howard, B. L.; Thompson, P. E.; Manallack, D. T. Inhibitors of *Plasmodium falciparum* phosphodiesterases for the investigation of malaria. *2010 National Medicinal Chemistry Symposium, USA. 2010.*

Howard, B. L.; Thompson, P. E.; Manallack, D. T. Inhibitors of *Plasmodium falciparum* phosphodiesterases for the investigation of malaria. *RACI 13th National Convention (RACI 2010) in conjunction with 12th IUPAC International Congress of Pesticide Chemistry, Melbourne. 2010.*

Howard, B. L.; Thompson, P. E.; Manallack, D. T. Inhibitors of *Plasmodium falciparum* phosphodiesterases for the investigation of malaria. *RACI 34th Annual Synthesis Symposium, Melbourne. 2010.*

Howard, B. L.; Thompson, P. E.; Manallack, D. T. Inhibitors of *Plasmodium falciparum* phosphodiesterases for the investigation of malaria. *Cancer Therapeutics (CTx) Symposium, Melbourne. 2011.*

Howard, B. L.; Thompson, P. E.; Manallack, D. T. Inhibitors of *Plasmodium falciparum* phosphodiesterases for the investigation of malaria. *RACI Biomolecular Division Conference: Biomolecular at the Beach, Melbourne. 2011.*

Howard, B. L.; Thompson, P. E.; Manallack, D. T. Inhibitors of *Plasmodium falciparum* phosphodiesterases for the investigation of malaria. *IUPAC International Conference on Organic Synthesis (ICOS-19), Melbourne. 2012.*

Abstract

Malaria is an infectious disease that is responsible for approximately one million deaths across the world each year. The emergence and rapid spread of resistance to the established antimalarial drugs demands the development of a new generation of medicines to treat the many millions of people who are likely to be infected by chloroquine- and even artemisinin-resistant *Plasmodium* parasites.

The primary theme explored within this thesis has been application of the “inverted silver bullet” approach to antimalarial drug discovery. This strategy involves investigating targets that are well conserved between the parasite and human host, and for which good inhibitors of the human homologue are known. The cyclic nucleotide phosphodiesterase (PDE) enzymes fit this profile. The human PDEs (*hPDE*1-11) and *Plasmodium falciparum* PDEs (*PfPDE* α - δ) are predicted to be structurally homologous. They also meet the second criterion in that inhibitors of the human forms are established as drugs, such as sildenafil (Viagra[®]). There is also evidence that inhibiting the *PfPDE*s will dramatically alter the cell biology of the protozoa, perhaps most significantly its asexual reproduction.

Two variations of this strategy have been examined in this thesis. In Chapters 2 and 3, a direct inhibitor repurposing strategy has been followed. Homology models of the *Pf*PDEs were developed based upon *h*PDE9 from which an analogy was identified between the binding sites of the four *Pf*PDEs and *h*PDE1. This led to a series of 1*H*-pyrazolo[4,3-*d*]pyrimidin-7(6*H*)-one derivatives, known *h*PDE1 and *h*PDE9 inhibitors, being selected for re-examination as inhibitors of *Plasmodium falciparum* parasite growth. The synthesis of target compounds was achieved in a divergent, nine-step synthesis. Gratifyingly, 6 of 22 compounds were identified as submicromolar IC₅₀ inhibitors of parasite growth, with 5-benzyl-3-isopropyl-1*H*-pyrazolo[4,3-*d*]pyrimidin-7(6*H*)-one (IC₅₀ = 0.08-0.72 μM), and 5-(2-chlorobenzyl)-3-isopropyl-1*H*-pyrazolo[4,3-*d*]pyrimidin-7(6*H*)-one (IC₅₀ = 0.06-0.97 μM) emerging as superior compounds. The latter also demonstrated decreased activity against *h*PDE isoforms (*h*PDE9 IC₅₀ = 1.8 μM) compared to the former. This demonstrates the potential to gain selectivity for *P. falciparum* growth inhibition over *h*PDE inhibition. However, it remains unknown if the observed antiparasmodial activity is occurring through *Pf*PDE inhibition, and so future work should focus on the validation of this mechanism or the identification of an alternative.

In Chapters 4 and 5, an approach geared to generating novel chemotypes was examined. The reported antiparasmodial and *h*PDE inhibitory activity of flavonoid structures provided a starting point to scarcely reported classes of bicyclic compounds. The synthesis of three series of 6,7-fused ring system-based scaffolds was explored, and while progress was made toward each, the synthetic challenges prevented full assessment of their potential. Instead, a fourth series, the 2-tetrahydropyranchromanones, was synthesised and found to contain effective inhibitors

of both *Plasmodium falciparum* growth and *hPDE* activity. In particular, 8-(3,4-dimethoxyphenyl)-6-methyl-2-(tetrahydro-2*H*-pyran-4-yl)chroman-4-one demonstrated antiplasmodial activity ($IC_{50} = 2.6-10\ \mu M$) as well as showing inhibitory activity against *hPDE4* and *hPDE1*. As above, the mechanism(s) underpinning the antiplasmodial activity remain to be established.

All in all, this thesis strongly supports the concept of the “inverted silver bullet” approach to drug discovery and presents at least two series of compounds that represent good starting points for the ongoing development of novel antimalarial therapies. If formal attribution of a PDE inhibition mechanism is elucidated, the work will provide a powerful endorsement of the use of protein structure-based design in identifying compounds likely to be effective and expediting the drug discovery process, particularly in comparison to the mass screening strategies undertaken elsewhere. The work also highlights that many chemicals in “druggable” chemical space have still not been synthesised, so the search for structural novelty could lead to the ready identification of many new bioactive molecules.

Chapter 1

Malaria and the phosphodiesterase enzymes

1.1 Malaria

Malaria is an infectious disease caused by protozoan parasites of the genus *Plasmodium*.¹ The disease was first attributed to a parasitic infection when, in 1880, Charles Laveran noted living, crescent-shaped bodies in blood samples of malaria patients. In 1897, it was definitively determined that the mode of transmission of malaria between humans was *via* mosquitoes.² It is now known that five *Plasmodium* strains are capable of causing malaria in humans (*P. falciparum*, *P. vivax*, *P. malariae*, *P. ovale* and *P. knowlesi*) and all are transmitted through the bite of infected female *Anopheles* mosquitoes.³⁻⁵ Infection with the *Plasmodium falciparum* parasite accounts for the majority of human malaria infections and is responsible for the most severe disease and mortality.⁶

The earliest malaria infections have been traced back to Mediterranean regions and from here it was thought to have spread throughout Europe. European soldiers are believed

responsible for exporting the disease to India and Africa in the 17th and 18th centuries. Following this, the importation of African slaves into the 'New World' meant that, by the early 1800s, malaria was worldwide in its geographic distribution.² Malaria became a major scourge of world health and played its part in the success and failure of armies as well as the progression of industrialisation. A global eradication program was initiated by the World Health Organisation (WHO) in the 1950s that was centred around the development of the dichloro-diphenyl-trichloroethane (DDT) insecticide.⁷ Initially, this campaign was successful in countries such as Sri Lanka, India, and the former Soviet Union. However, this was not sustained due to the cost of the program and the emergence of DDT-resistant *Plasmodium* strains.⁸ Further to this, controversy arose surrounding the health risks of DDT use which included breast and pancreatic cancer, as well as reproductive irregularities.^{9,10}

There were an estimated 216 million cases of malaria in 2010, of which 86% of those infected were children under five years of age.¹¹ While the global incidence of malaria has decreased over the 2000-2010 period, the proportion of African malaria cases has shown an increase from 74% to 81%. This is believed to be directly related to poor diagnosis and treatment within poverty-stricken areas, as well as the emergence and rapid spread of drug resistance.¹¹ Despite this, prevention strategies have resulted in a decrease in child mortality rates of more than 25% since 2000. This can be attributed to the distribution of 145 million insecticide-treated nets in 2010 and an increase in the number of rapid diagnostic tests delivered to affected regions.¹¹

Currently, 3.3 billion people inhabit areas that put them at risk of contracting malaria, with tourists returning from malaria endemic areas expanding the area at risk.¹² The most significant endemic regions include the sub-Saharan Africa countries of Nigeria, the Democratic Republic of Congo, Burkina Faso, Mozambique, Cote d'Ivoire and Mali. In total, 106 malaria endemic countries were identified by the WHO in 2010.¹¹

The 2011 WHO World Malaria Report attributed more than 90% of reported malaria cases to infection with the *P. falciparum* parasite, which is the only species capable of causing severe malaria in humans.¹¹ Infection with *P. malariae*, *P. ovale*, and *P. vivax* is rarely fatal and although human infection with *P. knowlesi* can result in severe malaria, its infection incidence is more prevalent in macaques than humans.^{3,13}

In 99% of *P. falciparum* infections the presenting clinical symptoms are similar to that observed in cases of common influenza infection, which frequently include fever, headaches and diaphoresis. Other common symptoms include dizziness, nausea, malaise, myalgia, abdominal pain and a dry cough. In these instances, the infection is treated with standard antimalarial drugs or is eventually overcome by host immune responses.¹⁴ However, 1% of *P. falciparum* infections develop into severe malaria. Severe malaria is recognised as a disorder that affects several organs simultaneously. The major complications associated with severe malaria include cerebral oedema, pulmonary oedema, severe anaemia, acute renal failure and internal bleeding. Additional complications include metabolic acidosis and hypoglycaemia. These complications develop rapidly and death can result within hours of the symptoms first presenting.¹² In 2010, severe malaria resulted in an estimated 655,000 deaths.¹⁴

1.2 The *Plasmodium falciparum* parasite life-cycle

In developing an antimalarial, it is essential to understand the *Plasmodium falciparum* life-cycle. The life-cycle of the *P. falciparum* parasite consists of two distinct stages; a sexual reproductive stage in the mosquito and an asexual reproductive stage in the human host (Figure 1.1).¹⁵⁻¹⁷ The duration of one *P. falciparum* cycle is approximately 48 hours.¹²

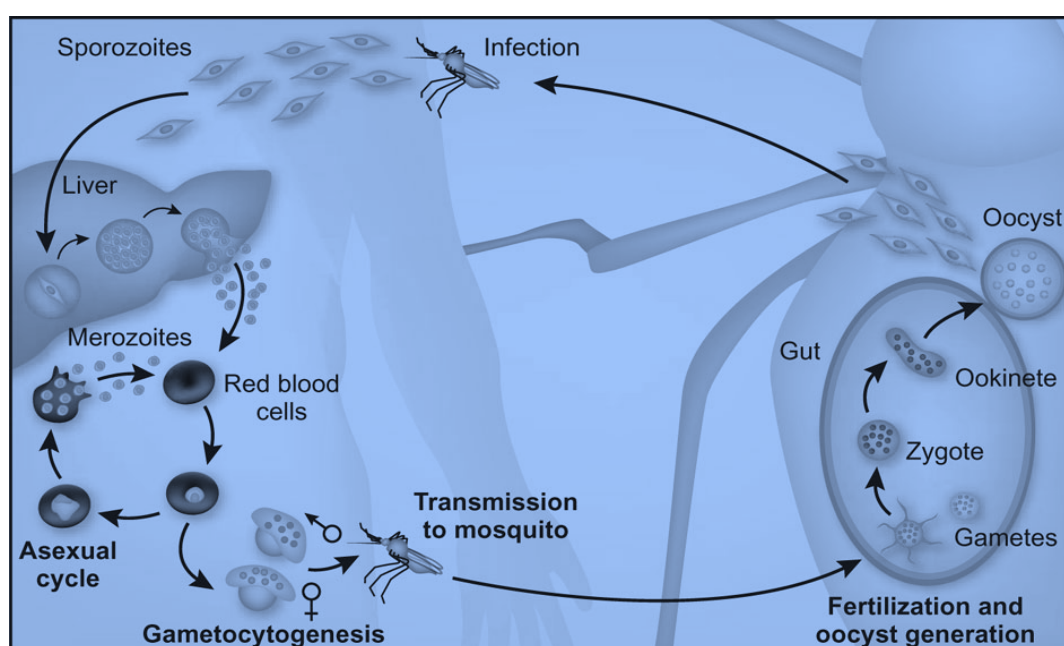


Figure 1.1. The *P. falciparum* life-cycle, as described by Pasvol.¹⁸

Initially, the female *Anopheles* mosquito transfers the sporozoites from her salivary glands to the human host upon feeding. Within an hour of being deposited into the skin, the sporozoites enter the bloodstream and invade hepatocytes. It is here that they undergo mitotic division to develop into liver schizonts, each containing about 10,000 merozoites. After five days, the schizonts release the merozoites into the circulatory system where they next invade the erythrocytes. Within the next 48 hours, the merozoites develop firstly into ring, then trophozoite and finally schizont stages. Many rounds of asexual reproduction occur within the erythrocytes, dramatically increasing

the number of parasites. In non-immune humans, the infection is amplified about 20-fold with each cycle.¹² Although the mechanism is poorly understood, it has been observed that some parasites are converted from asexual to sexual stages. The young, sexual stages mature into male or female gametocytes over the next fifteen days. When the mosquito next feeds on the human host, the mature gametocytes are transferred through the blood meal to the *Anopheles* mosquito. They are then fertilised within the mosquito midgut to form a motile ookinete, which translocates from inside the mosquito gut to the outside of the gut wall in the haemocyte. Here, it forms an oocyst and produces thousands of haploid sporozoites that then migrate to the salivary glands where they are ready to be transferred to the next human host.¹⁵

The key differences between the five strains of *Plasmodium* parasites lie within their life-cycle. Unlike in cases of *P. falciparum* infection, some of the liver parasites become dormant in *P. vivax* and *P. ovale* infections.^{19,20} The reactivation of these dormant forms can vary from a period of three weeks to several years. Unless these hypnozoites are eliminated from the host, the malaria symptoms will continue to relapse periodically.²⁰

A second difference lies in the time for which it takes the parasite to replicate in the host. This varies between 24 hours in *P. knowlesi*, 48 hours in *P. falciparum* and *P. vivax*, and 72 hours for *P. malariae*.²¹ The different variation in replication times means that infection with *P. knowlesi* can become life-threatening if not treated expeditiously and that different diagnostic tools are required for early detection.³

The third difference lies in the timing at which the gametocytes appear in the bloodstream.²² For example, in *P. vivax* the gametocytes appear concurrently or even before the asexual parasites, while in *P. falciparum* the gametocytes do not appear until several days after the initial parasitaemia and fever. Therefore, the additional challenge of treating *P. vivax* infection is that the treatment must be able to kill existing gametocytes rather than simply preventing their differentiation.²²

1.3 Currently employed antimalarial drugs

A variety of therapeutic agents have been employed over the years to target malaria, and a brief summary follows with reference to the chemical structures illustrated in Table 1.2. The current front-line therapies for *P. falciparum* malaria are the artemisinins, and in areas where resistance is yet to develop, chloroquine.

1.3.1 Chloroquine, amino alcohols and 4-aminoquinolines

Quinine (**1**), an amino alcohol, was the first compound to be used as an antimalarial therapy, with its use dating back to at least the 17th century. It is a natural product isolated from the bark of the *Cinchona calisaya* tree, and was first tested in malaria patients in 1891 by Ehrlich.²³ It is currently employed in treating severe cases of malaria and also as a second line treatment for cases of resistant malaria.⁵

The structurally related compound, pamaquine (**2**), was discovered by Farbenindustrie during the 1920s.²⁴ Pamaquine had an advantage over quinine in that it could act against both gametocytes and liver stage parasites.^{25,26} The year 1930 saw the development of

quinacrine (**3**), which is based on an acridine scaffold rather than a quinoline scaffold.²⁵ While this compound has a range of side effects, it proved highly successful in combating malaria during World War II.^{27,28} In the 1950s, the better tolerated primaquine (**4**) was introduced and it remains the only treatment against *P. vivax* liver infections.²⁹ In 1999, bulaquine (**5**) (the butyrolactone enamine prodrug of primaquine) was approved in India for *P. vivax* malaria.³⁰

Chloroquine (**6**) is a 4-aminoquinoline and was the mainstay of malaria prophylaxis and treatment for the second half of the 20th century,³¹ as well as being the drug of choice in the WHO Global Eradication Program.²⁴ Chloroquine is well-tolerated but has a narrow therapeutic ratio – the therapeutic dose is 10 mg/kg, a dose of 20 mg/kg causes serious toxic effects, and a dose of 30 mg/kg is potentially lethal.³² Despite its overwhelming importance, the mechanism of action of chloroquine and its analogues is still a matter of debate.³³⁻³⁵ There is however, common agreement that both quinine and chloroquine cause parasite death by disrupting the parasite's ability to form haemozoin during the erythrocytic asexual cycle of the parasite.³⁶⁻⁴⁰ This results in cell lysis and parasite cell autodigestion.⁴¹

Further research afforded many more 4-aminoquinolines and related amino-alcohols, including amodiaquine (**7**), mefloquine (**8**), halofantrine (**9**), lumefantrine (**10**) and pyronaridine (**11**).⁴² Interestingly, pyronaridine, an azacrine-type Mannich base, is structurally related to chloroquine but has proven active against chloroquine resistant *P. falciparum* strains. The 4-aminoquinolines and amino-alcohols all suffer from safety issues which include cardiovascular effects, central nervous system effects, reactive

metabolite formation, and generally a low clinical therapeutic ratio.⁴³ Overcoming these limitations is the challenge for the next generation of antimalarials.⁴⁴

1.3.2 Artemisinin and other endoperoxides

Artemisinin (**12**), a sesquiterpene lactone peroxide, was discovered by Chinese scientists in 1972 after it was isolated from the leaves of the sweet wormwood, *Artemisia annua*, as part of the Chinese Government's 'Program 523'.⁴⁵⁻⁴⁸ The program was developed to search for new antimalarial compounds in the face of chloroquine resistance.²⁵ From a medicinal chemistry perspective, artemisinin is an unlikely drug candidate due to its structure containing highly reactive acetal, lactone, ketal and endoperoxide functional groups that render the compound as metabolically unstable. As a consequence, bioavailability is limited and efficacy is reduced. Artemisinin has a very short half-life, and is converted to the active metabolite, dihydroartemisinin (DHA) (**13**) following first-pass metabolism.³⁰

The next generations of artemisinin drugs were designed to overcome these shortcomings. These synthetic derivatives include artemether (**14**), arteether (**15**) and artesunate (**16**). All have been shown as being more active than both artemisinin and DHA and the entire family of compounds are active against all existing drug-resistant strains of *P. falciparum*.⁴⁹

Artemisinin and its derivatives are highly potent and rapid-acting. The artemisinins are unique in that they act on all stages of the parasite intra-erythrocytic life-cycle and are therefore capable of rapidly killing all of the blood stages of the parasite. They reduce

parasite numbers by approximately 10,000 per erythrocytic cycle, the highest ratio among all licensed antimalarial drugs.⁵⁰ In addition, the artemisinins also kill gametocyte parasite stages and this results in reduced transmission from humans to mosquitoes.^{43,49} Although the exact molecular targets of the artemisinins are not well defined, it is believed that they alkylate multiple targets such as haeme, parasite neutral lipid bodies and proteins.⁵¹

1.3.3 Other antimalarial drugs

From the hydroxyquinone chemical family, lapachol (**17**) was initially reported in the 19th century and is currently used to treat malaria in South America.⁵² The close synthetic derivative, lapinone (**18**), is active against *P. vivax* malaria. However, due to poor bioavailability it requires intravenous administration over four days.⁵³ Overcoming the poor bioavailability of lapinone lead to atovaquone (**19**), one of the active ingredients in Malarone[®] (atovaquone/proguanil), which is used as a prophylactic drug for travelers.⁵⁴

Antibacterial antifolates were shown to have antimalarial activity in the early 20th century and since then, several parasite-specific medicines have been developed.²⁹ The diaminopyrimidine warhead of pyrimethamine (**20**) mimics the natural co-factors dihydrofolate and tetrahydrofolate and subsequently inhibits *Plasmodium* dihydrofolate reductase (DHFR).²⁹ The diaminodihydrotriazine, proguanil (**21**), is often used in synergy with atovaquone and works by affecting the mitochondrial membrane potential of the parasite.⁵⁵ Cycloguanil (**22**) mimics the natural enzyme substrates in a similar way to pyrimethamine, and is an active metabolite of proguanil that is generated

through CYP2C19-mediated metabolism.⁵⁶ Chlorproguanil (**23**) behaves in a similar manner, cyclising *in vivo* to a chloro-cycloguanil metabolite.

Tetracycline (**24**) and the semi-synthetic derivative, doxycycline (**25**), both consist of a four-ring system with considerable complexity and substitution. Tetracycline, a secondary metabolite from *Streptomyces actinobacteria*, is effective in causing parasite death by blocking the expression of apicoplast genes which results in nonfunctional apicoplasts in the daughter parasites. This is referred to as the ‘delayed death phenotype’ because parasite death does not occur until the next replication cycle. As a consequence of this, the tetracyclines can be used clinically or in prophylaxis.⁵⁷ Clindamycin (**26**) is derived from the lincosamide family. It acts through a translational mechanism, inhibiting the early stages of parasite protein synthesis through binding to the 50S ribosome.

Sulfadoxine (**27**), a bisaryl sulfonamide, and dapsone (**28**), a symmetrical bisaryl sulfone, act against the parasite by mimicking *para*-aminobenzoic acid (PABA). They disrupt the folate pathway upstream of dihydrofolate reductase-thymidylate synthase (DHFR-TS) by inhibiting *Plasmodium* dihydropteroate synthetase (DHPS).²⁹

Table 1.2. Structures of the antimalarial drugs, compound class and mechanism of action.

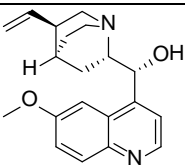
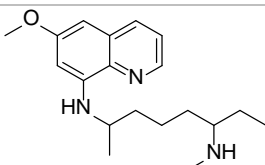
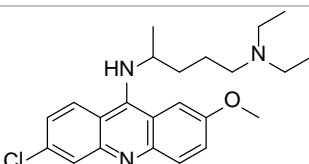
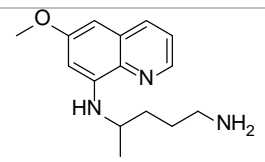
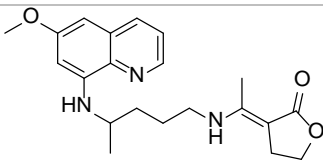
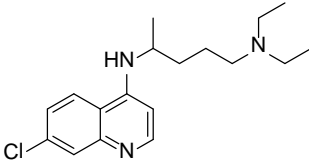
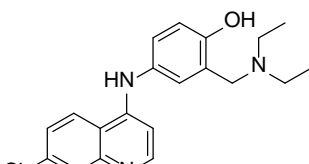
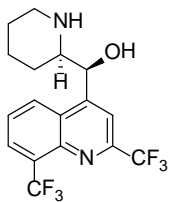
Name	Structure and compound class	Mechanism of action	Reference
Quinine (1)	 Amino alcohol	Binds to haematin to prevent polymerisation.	36
Pamaquine (2)	 8-Aminoquinoline	Effective against the hypnozoites of <i>P. vivax</i> malaria. No longer used clinically.	59
Quinacrine (3)	 4-Aminoacridine	Mechanism of action is not fully understood.	59, 63
Primaquine (4)	 8-Aminoquinoline	Effective against the intrahepatic hypnozoite form of <i>P. vivax</i> .	60
Bulaquine (5)	 8-Aminoquinoline	Enamine prodrug of primaquine for <i>P. vivax</i> malaria.	61
Chloroquine (6)	 4-Aminoquinoline	Inhibits haeme polymerisation and therefore disrupts parasite haemoglobin metabolism.	36, 37, 60
Amodiaquine (7)	 4-Aminoquinoline	Similar mechanism of action to chloroquine.	36, 38, 64
Mefloquine (8)	 Amino alcohol	Similar mechanism of action to quinine.	65

Table 1.2 continued. Structures of the antimalarial drugs, compound class and mechanism of action.

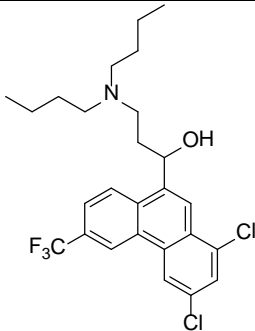
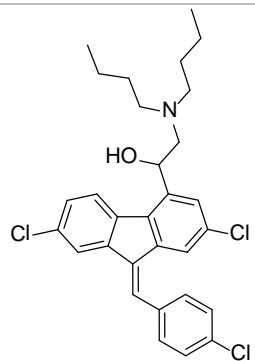
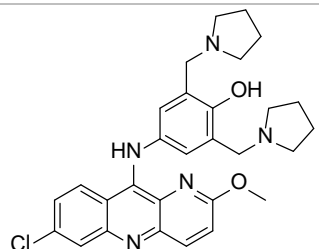
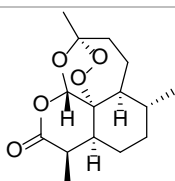
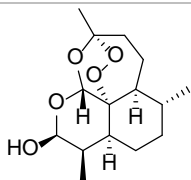
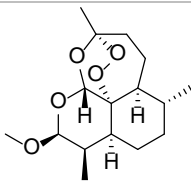
Name	Structure and compound class	Mechanism of action	Reference
Halofantrine (9)	 <p>Amino alcohol</p>	Similar mechanism of action to quinine.	66
Lumefantrine (10)	 <p>Amino alcohol</p>	Similar mechanism of action to quinine.	65
Pyronaridine (11)	 <p>Azacrine</p>	Inhibits parasite uptake of hypoxanthine.	25, 42
Artemisinin (12)	 <p>Endoperoxide</p>	Peroxide is believed to homolytically cleave in the presence of Fe ²⁺ to form carbon-centered radicals.	54, 67, 68
Dihydroartemisinin (DHA) (13)	 <p>Endoperoxide</p>	Mechanism of action similar to artemisinin.	67, 69
Artemether (14)	 <p>Endoperoxide</p>	Mechanism of action similar to artemisinin.	67, 70

Table 1.2 continued. Structures of the antimalarial drugs, compound class and mechanism of action.

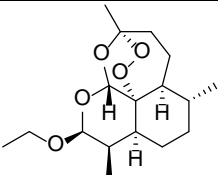
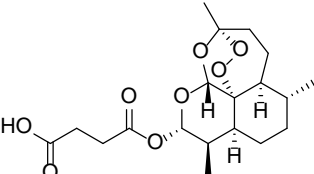
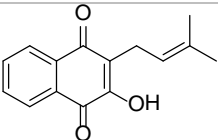
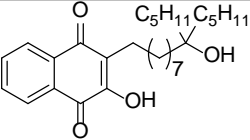
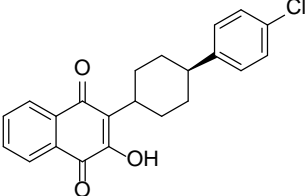
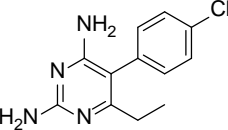
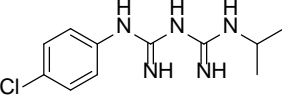
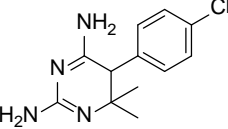
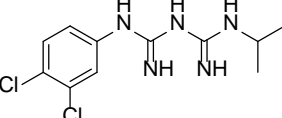
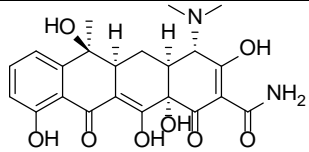
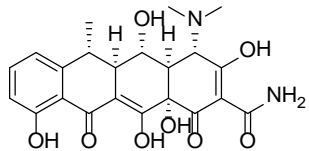
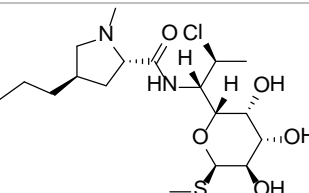
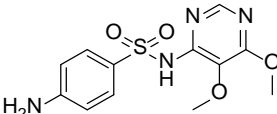
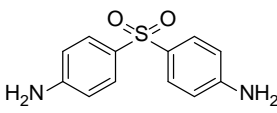
Name	Structure and compound class	Mechanism of action	Reference
Arteether (15)	 Endoperoxide	Mechanism of action similar to artemisinin.	67, 68, 71
Artesunate (16)	 Endoperoxide	Mechanism of action similar to artemisinin.	72
Lapachol (17)	 Hydroxyquinone	Inhibits the cell respiratory mechanism and host electron transport system.	54
Lapinone (18)	 Hydroxyquinone	Mechanism of action similar to lapachol.	53, 54
Atovaquone (19)	 Hydroxyquinone	Mechanism of action similar to lapachol.	53, 54, 65
Pyrimethamine (20)	 Diaminopyrimidine	Inhibits DHFR.	73
Proguanil (21)	 Diamino-dihydrotriazine	Metabolised <i>in vivo</i> to give cycloguanil, which is a DHFR inhibitor.	55, 69, 74
Cycloguanil (22)	 Diamino-dihydrotriazine	Mechanism of action similar to pyrimethamine.	73
Chlorproguanil (23)	 Diamino-dihydrotriazine	Mechanism of action similar to proguanil.	71

Table 1.2 continued. Structures of the antimalarial drugs, compound class and mechanism of action.

Name	Structure and compound class	Mechanism of action	Reference
Tetracycline (24)	 <p>Tetracycline</p>	Blocks the expression of apicoplast genes.	57, 75
Doxycycline (25)	 <p>Doxycycline</p>	Mechanism of action similar to doxycycline.	57, 76
Clindamycin (26)	 <p>Lincosamide</p>	Mechanism of action similar to doxycycline.	57, 76
Sulfadoxine (27)	 <p>Anilinesulfonamide</p>	Inhibits DHPS by competing with PABA.	77, 78
Dapsone (28)	 <p>Anilinesulfone</p>	Mechanism of action similar to sulfadoxine.	78

1.4 *Plasmodium falciparum* resistance

In 1955, the ‘Global Malaria Eradication Programme’ was launched by the WHO and saw chloroquine chemotherapy implemented to complement vector control measures. The program resulted in 27 countries being declared malaria-free.⁶ However, the extensive deployment of antimalarial drugs in the last fifty years, particularly chloroquine, has put a tremendous amount of selection pressure on human malaria parasites to evolve mechanisms of resistance.⁷⁹ This emergence of resistance has been

the main contributor to the global resurgence of malaria over the past thirty years.⁸⁰

Genetically, resistance to antimalarial drugs is thought to be rare and spontaneous and also independent of the drug being employed for treatment. However, a longer antimalarial half-life ($t_{1/2}$) allows for longer sub-therapeutic exposure of the parasite to the drug, increasing the opportunity for resistance to occur. The exact genetic event is either a change or mutation in the copy number of genes encoding or relating to the drug's parasite target or influx/efflux pumps that affect intraparasitic concentrations of the drug. For the parasite to develop resistance it may require only a single genetic event, or instead multiple unlinked events may be necessary.

Currently, chloroquine resistance is observed in more than 80% of wild *P. falciparum* isolates in all malaria-endemic areas.⁸¹ Even more alarming has been the much more rapid development of resistance to sulfadoxine-pyrimethamine, which is now also widespread. It took only six years of use for mefloquine resistance to develop, though this is currently confined to its main areas of use (Thailand, Cambodia and Vietnam).⁸² In fact, significant resistance has developed to all antimalarial drug classes, with one exception – the artemisinins. As such, current antimalarial treatments consist of an artemisinin component.

The true extent of the effect of resistance on morbidity and mortality are often underestimated.^{83,84} As a consequence, it is essential to predict the emergence and spread of resistance to both currently effective and newly introduced antimalarial

compounds in order to increase their lifespan of effectiveness. A summary of the parasite resistance mechanisms to common antimalarial drugs is shown in Table 1.3.

Table 1.3. The common antimalarial therapies and the mechanisms by which parasite resistance arises.

Antimalarial	Resistance mechanism
Chloroquine (6) ($t_{1/2}$ = 8 weeks)	Mutations in the transporter genes <i>pfert</i> and <i>pfmdr1</i> . ^{85,86} This limits the accumulation of chloroquine in the parasite's digestive food vacuole. ^{84,87-90}
Quinine (1) ($t_{1/2}$ = 8-10 hours)	Mutations in the transporter genes (<i>pfert</i> , <i>pfmdr1</i>). This limits the accumulation of quinine in the parasite's digestive food vacuole. ⁹¹⁻⁹⁴
Mefloquine (8) ($t_{1/2}$ = 14-18 days) ⁹⁵	Amplification of the <i>pfmdr1</i> gene, which limits accumulation of mefloquine in the parasite's digestive food vacuole. ⁹⁶
Lumefantrine (10) ($t_{1/2}$ = 3-5 days)	Mutations and polymorphisms in <i>pfmdr1</i> . ⁹⁷⁻⁹⁹
Atovaquone (19) ($t_{1/2}$ = 2-3 days) ¹⁰⁰	Single nucleotide polymorphisms in the cytochrome <i>b</i> gene. ¹⁰¹
Sulfadoxine- Pyrimethamine ($t_{1/2}$ = 4-5 days)	Point mutations in the genes encoding the target enzymes, <i>PfDHPS</i> (dihydropteroate synthetase) and <i>PfDHFR</i> (dihydrofolate reductase). ⁸⁶
Artemisinin (12) ($t_{1/2}$ = 0.5-1.4 hours) ¹⁰²	Mutations in <i>pfatp6</i> and polymorphisms in <i>ubp1</i> . ^{103,104}

pfert – *Plasmodium falciparum* chloroquine resistance transporter, *pfmdr1* – *Plasmodium falciparum* multidrug resistance protein-1, *pfatp6* – the sarco/endoplasmic reticulum Ca^{2+} ATPase orthologue of *Plasmodium falciparum*, *ubp1* – upstream binding protein-1.

1.5 The current antimalarial drug pipeline

The prospect of developing new antimalarial drugs received a massive boost when the Bill and Melinda Gates Foundation confirmed their commitment to the discovery of new medicines, with the ultimate goal of malaria eradication.¹⁰⁵ This objective was supported by the WHO and its Roll Back Malaria (RBM) partnership. The eradication agenda presented Target Product Profiles (TPPs) to the malaria research community. The agenda recognised the necessity for a steady pipeline of novel antimalarials with new mechanisms of action in order to counteract potential drug resistance. The TPPs dictated that new medicines must be active against the asexual blood stages of

P. falciparum as well as having the ability to block the transmission of the parasite to other human hosts *via* the mosquito vector.³⁰ In addition, the new medicines must be able to target dormant liver-stage parasites in the case of *P. vivax* infections. Broader challenges for the new drugs include reducing the total therapeutic dose, decreasing the risks of adverse cardiovascular, haematological, gastrointestinal and central nervous system effects, and reducing the cost of formulation.³⁰

As part of the Gates Foundation's commitment to discovering new antimalarials, the Medicines for Malaria Venture (MMV) was launched in 1999. This scientific portfolio (Table 1.4, classified by therapeutic type) is the most robust and diverse portfolio of antimalarial drug projects in history and has the ultimate goal of building a strong pipeline of molecules leading to a new generation of medicines that will form a critical part of the arsenal required to eradicate malaria. As of 2012, the MMV science portfolio comprised numerous projects at various research and development stages. The projects are both academic and industrial programs.¹⁰⁷

In general, there are five main approaches pursued in discovering new antimalarials; (1) optimising a known antimalarial chemotype, (2) performing target-based screening, (3) undertaking whole cell phenotypic screening, (4) establishing new formulations of existing antimalarials, and (5) repurposing drug chemotypes, each of which are discussed below.

Table 1.4. The MMV Global Malaria Portfolio as of the third quarter, 2012.

<i>Global Malaria Portfolio, 3Q 2012</i>						
Translational			Development			
Preclinical	Phase I	Phase IIa	Phase IIb/III	Registration	Phase IV	
RKA182 Liverpool	AQ13 Immtech	Ferroquine Sanofi	Pyramax Paediatric Shin Poong/ University of Iowa	Mefloquine Artesunate Farmaguinhos/DNDi/	Coartem®-D Novartis	novel classes/mechanisms
NPC-1161-B University of Mississippi	CDRI 97-78 Ipca	OZ439 Monash/UNMC/STI	Eurartesim® Paediatric Sigma-Tau	Atresunate I.R. WHO/TDR	Eurartesim® Sigma-Tau	
BCX4945 Biocryst/Albert Einstein College of Medicine	GNF156 Novartis	NITD609 Novartis	Arterolane/PQP Ranbaxy		Pyramax® Shin Poong/ University of Iowa	endoperoxides
DSM265 UTSW/UW/Monash	N-tert-butyl isoquine Liverpool School of Tropical Hygiene/GSK	Fosmidomycin piperazine Jomaa Pharma GmbH	Azithromycin chloroquine Pfizer		Artesunate for injection Guilim	
P218 DHFR Biotec/Monash/ LSHTM		Artemisone UHKST	Co-trimoxazole Bactrim Institute of Tropical Medicine		ASAQ Winthrop Sanofi/DNDi	4-aminoquinolines
21A092 Drexel/Med/UW		Methylene blue AQ University of heidelberg	Tafenoquine GSK		SP-AQ Guilim	8-aminoquinolines
ELQ-300 USF/VAMC		SAR97276 Sanofi	Argemone Mexicana Mali/Geneva			natural products
			Nauclea pobeguinii DRC/Antwerp			combinations

1.5.1 Optimisation of a known antimalarial chemotype

Working in the same chemical space as registered antimalarial medicines provides an increase in confidence that the compounds will work due to the success of their chemical predecessors. This approach has been validated in the case of the aminoquinolines and artemisinin compounds. It is however, essential that the next generation of compounds address the deficiencies of their progenitors. With the ongoing problem of resistance, a main objective is to synthesise molecules active against *Plasmodium* strains that are resistant to the first generation drugs. Several known antimalarial chemotypes are being pursued as ‘next generation’ compounds, and are discussed below.

The endoperoxide chemotype

The endoperoxide functionality of the artemisinins (the active moiety) has attracted several medicinal chemistry programs. Several research groups have attempted to reduce the complexity of the chemotype whilst maintaining biological activity.^{29,30} This resulted in the synthesis of artemisone (**29**),^{67,109} arterolane (formerly OZ277) (**30**),¹¹⁰ and OZ439 (**31**).¹¹¹⁻¹¹³ Several further synthetic peroxides (**32-36**), including CDRI-97-78 (**37**), are being investigated for antimalarial activity (Figure 1.5).¹¹⁴⁻¹¹⁸

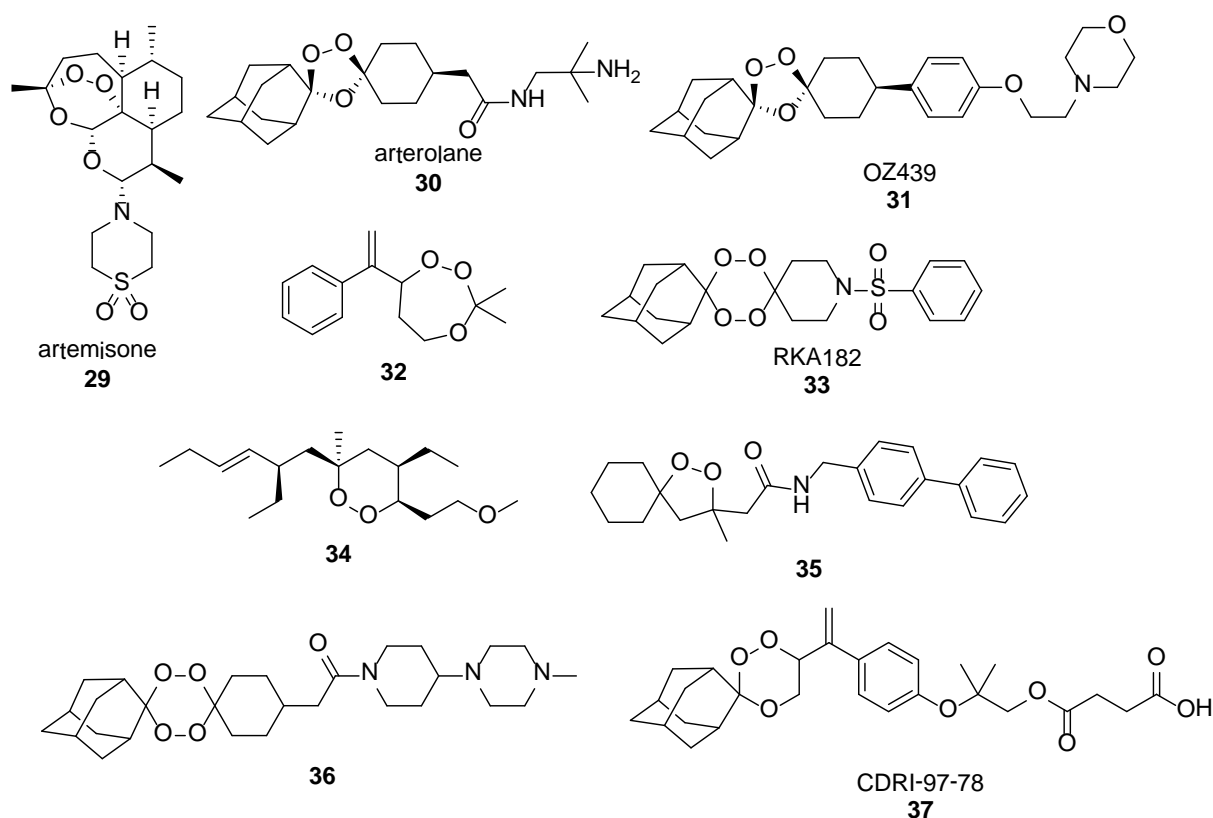


Figure 1.5. Structures of several compounds from the endoperoxide chemical class that are being optimised for antimalarial activity.

The 4-aminoquinoline chemotype

Given the earlier success of the 4-aminoquinoline chemotype with drugs such as chloroquine (**6**), it should be of no surprise to learn that there are several 4-aminoquinolines in the antimalarial pipeline. These include ferroquine (**38**),¹¹⁹⁻¹²¹ isoquine (**39**),¹²² and AQ-13 (**40**) (Figure 1.6).^{44,123} It is essential that these next generation compounds show activity in relevant clinical isolates resistant to chloroquine and amodiaquine, as well as improved cardiovascular and CNS effects. A main strategy is to introduce diversity into the side-chain, of which there are currently several lead compounds (**41-46**).¹²⁴⁻¹³⁴

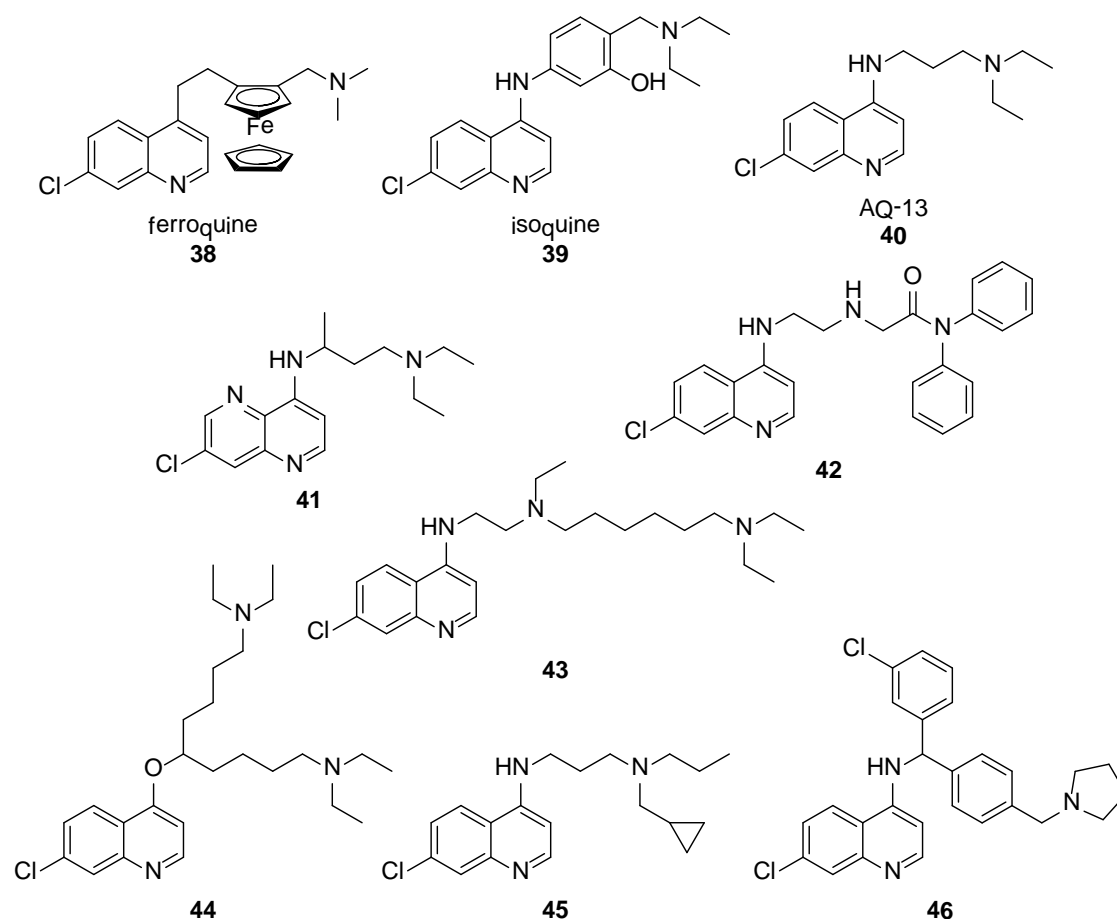


Figure 1.6. Structures of several compounds from the 4-aminoquinoline chemical class that are being optimised for antimalarial activity.

The 8-aminoquinoline chemotype

The 8-aminoquinoline chemotype is the focus of several medicinal chemistry campaigns. The only approved antimalarial with the ability to eliminate liver stage parasites (hypnozoites) is primaquine (**4**). However, there are significant drawbacks associated with the use of primaquine including the long duration of treatment and the risk of haemolytic anaemia in some patients.³⁰ Tafenoquine (**47**) and (-)-NPC-1161-B (**48**) have emerged as potential primaquine replacements, and have been shown to have anti-relapse efficacy as well as significantly longer half-lives (Figure 1.7).^{135,43,136} Other modifications to the chemotype include the synthesis of the prodrug **49**, as well as **50** and **51**.

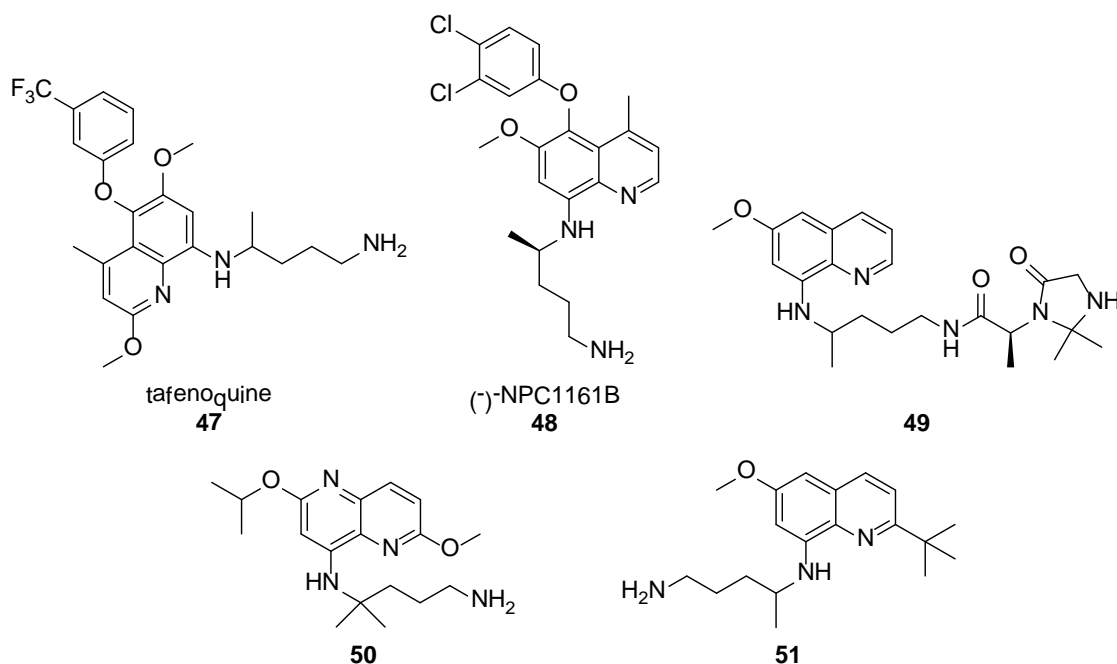


Figure 1.7. Structures of several compounds from the 8-aminoquinoline chemical class that are being optimised for antimalarial activity.

The amino-alcohol chemotype

The liabilities of the amino alcohols include low absorption (lumefantrine), nausea and vomiting (mefloquine), cardiovascular issues (halofantrine) and negative psychological side effects (mefloquine).³⁰ To overcome these shortcomings, medicinal chemistry projects have focussed on modifying the core scaffolds of these compounds, of which WR308396 (**52**), **53** and **54** are the most promising (Figure 1.8).^{137,138}

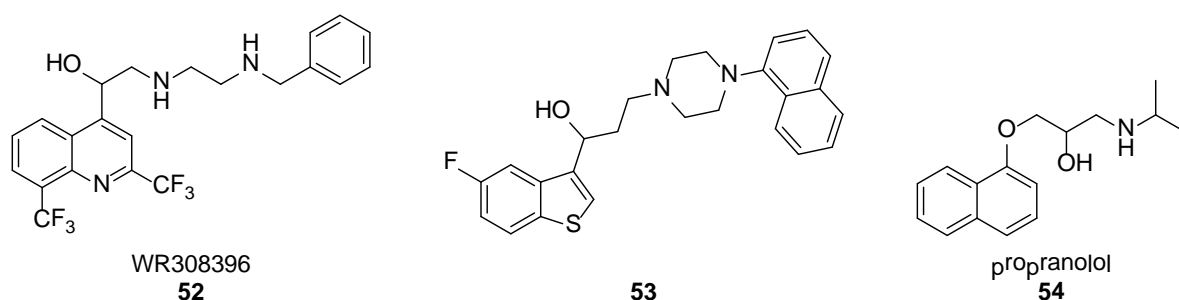


Figure 1.8. Structures of several compounds from the amino-alcohol chemical class that are being optimised for antimalarial activity.

Chimeric chemotypes

Chimeric molecules containing both the 4-aminoquinoline moiety of chloroquine and the trioxane moiety of artemisinin have been synthesised based on the assumption that both moieties act on haeme.^{24,139,140} The most active reported compounds of this class are trioxaquine (**55**), as well as the biologically cleavable (**56**) and the non-cleavable (**57**) chimeras of mefloquine and an artemisinin (Figure 1.9).¹⁴¹

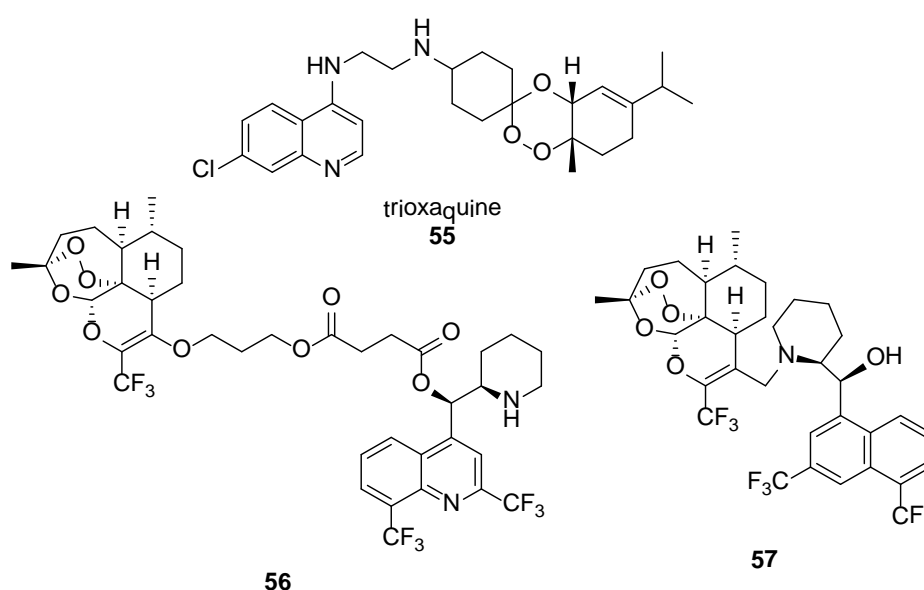
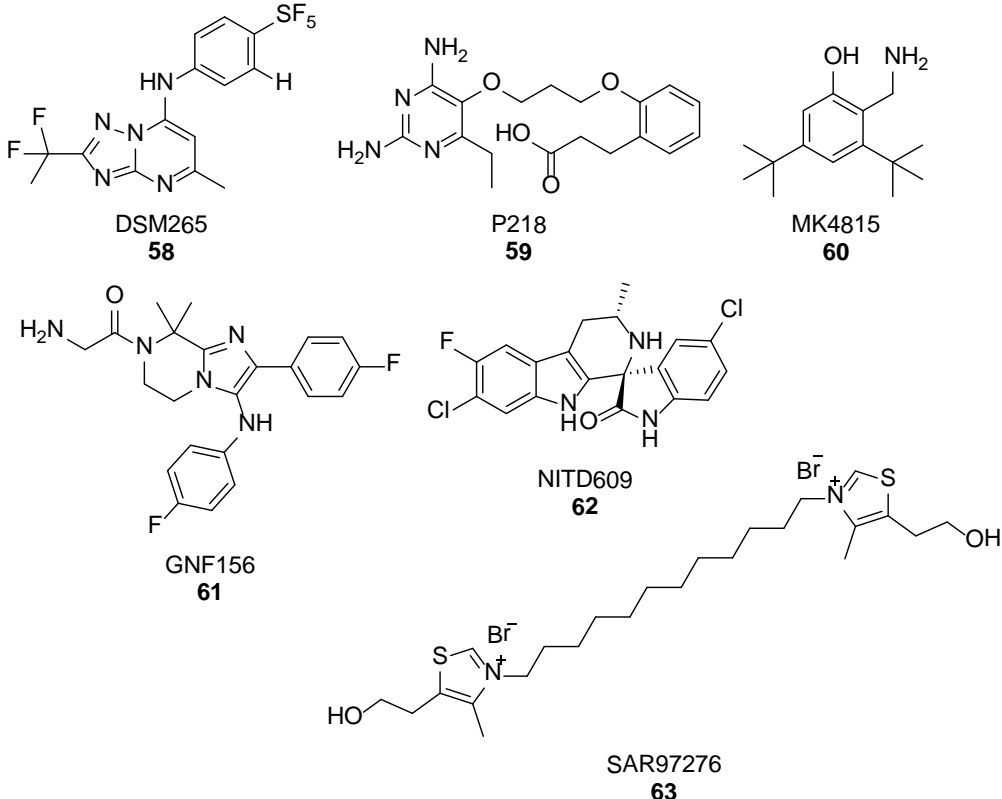


Figure 1.9. The structures of several chimeric compounds that are currently being optimised for antimalarial activity.

Novel antimalarial chemotypes

Several novel chemotypes acting at various targets with various mechanisms of action are being investigated as antimalarials (Figure 1.10). Amongst many, these include the triazolopyrimidines (DSM265, **58**),¹⁴² pyrimidine-2,4-diamines (P218, **59**),⁴³ aminocresols (MK4815, **60**),^{43,29} imidazolopiperazines (GNF156, **61**),^{43,143,144} spiroindolones (NITD609, **62**),¹⁴⁵ and albitazoliums (SAR97276, **63**).³⁰ These



From this, biochemical screening of an isolated protein target has been adopted extensively within the pharmaceutical industry and has proven a valuable approach in a large number of drug discovery projects.¹⁴⁹ Examples of this approach within the malaria field include the targeting of enzymes such as *P. falciparum* dihydroorotate dehydrogenase (DHODH) and the *Pf* falcipains. The global malaria portfolio consists of numerous projects focussed on discrete protein targets.¹⁰⁷ Despite significant effort, target-based screening has not fulfilled its promise and target validation has proved challenging – progressing from *in vitro* enzyme inhibitors to killing parasites is not simple.^{43,150}

1.5.3 Whole cell phenotypic screening

As the erythrocytic stages of *P. falciparum* parasites can now be maintained in culture, the cost and speed of testing compounds against the whole parasite in human erythrocytes has improved by almost two orders of magnitude. Mass screening in 1,536-well formats has become a viable and extremely attractive option.³⁰ Furthermore, to be active, a compound has to cross several biological membranes; erythrocytic cell membrane, parasite plasma membrane, parasitophorous vacuolar membrane and potentially other parasitic sub-cellular membranes.¹⁵¹ Whole cell phenotypic screening eliminates compounds incapable of doing so.

A disadvantage of this approach is that whole cell screening against the parasite gives very little, if any, information about the mechanism of action. To identify the potential target, affinity methodologies involving immobilised ligands, whole parasite extracts and mass spectrometric methods may be needed.¹⁵² On the other hand, a potential

advantage of this approach is that such compounds identified from phenotypic screens do not necessarily have a unique protein target and should therefore, theoretically be less susceptible to resistance formation.

In May 2010, the results from screening approximately 4.5 million compounds were published in studies supported by GlaxoSmithKline (GSK), St. Jude Children's Research Hospital and Novartis (Table 1.11).¹⁵³⁻¹⁵⁵ There were 20,000 compounds identified with antimalarial activity (IC₅₀ values of 1 μ M or less in *P. falciparum*-infected 3D7 erythrocytes). This movement represented a dramatic change in the availability of chemotypes as starting points for antimalarial drug discovery projects.

Table 1.11. A summary of *P. falciparum* 3D7 high-throughput screening.

Organisation	Library Size	3D7 screening concentration	Number of confirmed hits	Hit rate (%)
GSK	1,986,056	2 μ M	13,533	0.68
Novartis	1,700,000	1.25 μ M	5,973	0.34
Broad Institute	79,294	30 μ M/6 μ M	134	0.17
St. Jude	309,474	7 μ M	1,134	0.37

Investigation of the potential mechanisms of action of these compounds based on the human or microbiological target data was also carried out. In the GSK screen it was hypothesised that approximately 70% of the compounds were acting through G protein-coupled receptors (GPCRs) or kinase targets.^{30,154} In the St. Jude's screen, three previously validated drug targets (*Pf* DHODH, haemozoin formation and *Pf* falcipains) as well as 15 new inhibitors of novel malaria proteins (including *Pf* choline kinase, dUTPase, GSK3 and thioredoxin) were identified.^{30,155}

1.5.4 Combination therapies using existing antimalarials

Another popular approach to treating malaria is to develop new combinations of existing antimalarial therapies. The complex macrocyclic antibiotic, azithromycin, is currently undergoing Phase III clinical trials in combination with chloroquine. It is slow-acting and is known to disrupt parasite protein synthesis in a manner similar to the lincosamides.^{57,76} In addition, azithromycin appears to work clinically as a chloroquine-resistance reversal agent.³⁰ Specifically, the fixed-dose combination has been developed for the prevention of infection during pregnancy.⁴³

Fosmidomycin (**64**), naturally produced by *Streptomyces lavendulae*, was originally investigated as an antibacterial agent but was later shown to be effective in killing malaria blood schizonts (Figure 1.12).¹⁵⁹ It is a phosphonic acid *N*-hydroxyformamide derivative that acts as a potent inhibitor of 1-deoxy-D-xylulose-5-phosphate (DOXP) reductoisomerase. Inhibition of this pathway prevents isoprenoid synthesis in the parasite, leading to its death. Fosmidomycin in combination with piperazine is currently undergoing Phase II clinical trials.²⁹

The trimethoprim-sulfamethoxazole (**65** and **66**) combination, Co-trimoxazole Bactrim[®], was originally used for antibacterial infections but is now being explored clinically as an alternative to sulfadoxine-pyrimethamine as well as a preventative antimalarial in pregnancy. Sulfamethoxazole acts as a DHPS inhibitor and trimethoprim exerts its effects through DHFR inhibition (Figure 1.12).²⁹

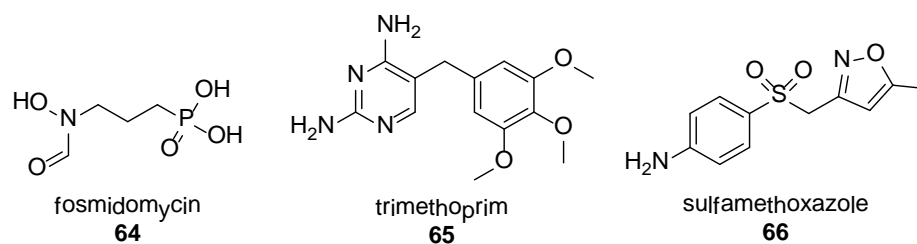


Figure 1.12. Structures of aforementioned antimalarial drugs employed in combination therapies.

Several fixed-dose artemisinin combination therapies are soon to be launched including Pyramax[®] (and Pyramax Paediatric[®]), Eurartesim[®] (and Eurartesim Paediatric[®]) and mefloquine-artesunate. The artemether-lumefantrine combination, Coartem-D[®], has also shown good antimalarial efficacy.¹⁶⁰ Amodiaquine combinations are also heading toward the market with artesunate-amodiaquine (ASAQ Winthrop) and sulfadoxine-pyrimethamine-amodiaquine (SP-AQ) formulations in the pipeline.^{29,43}

1.5.5 Repurposing of drug chemotypes

Repurposing drugs with known human therapeutic activity as antimalarials has also proven successful in treating malaria. The tetracyclines, a group of broad-spectrum antibiotics most commonly prescribed in the treatment of severe acne, have been repurposed as antimalarials and are now prescribed for both treatment and prophylaxis (discussed in section 1.3.3).⁵⁷ An advantage of employing antibacterials as antimalarials is that they have a well understood safety profile (including during pregnancy), which is of particular importance in antimalarial therapies as it enables them to be prescribed during the first trimester. However, a disadvantage of repurposing this chemotype is that the rate at which antibacterial resistance will develop is increased.¹⁶¹

This drug repurposing approach has its obvious merits and has attracted more attention in recent times. It is possible to prioritise novel targets based on the likelihood of finding a small molecule inhibitor through ‘orthologue’ searching.¹⁶² This has been referred to by Seebeck as the ‘inverted silver bullet’ approach and involves searching for drug targets that are well conserved between the parasite and the human host and for which good inhibitors of the human homologue exist as drugs.¹⁶³ This is in direct opposition to Ehrlich’s ‘magic bullet,’ which describes targeting pathways that are essential for the parasite, though non-essential or entirely absent in the human host. For Seebeck and co-workers, this inverted silver bullet approach led to the identification of *P. falciparum* phosphodiesterase (*Pf*PDE) enzymes as potential targets.

The first iteration of this approach was the examination of a range of human PDE inhibitors as inhibitors of a *Pf*PDE and of parasite growth.¹⁶ This strategy has also been further pursued in recent literature. Deprez and co-workers identified a series of human PDE5 inhibitors based upon tadalafil that also show activity against the whole *P. falciparum* parasite.^{164,165} A series of synthesised tadalafil analogues inhibited parasite growth and one example, compound **67**, retained antiparasmodial activity while almost all human PDE5 activity was abolished (Figure 1.13).¹⁶⁵ While the further progression of that work has been limited by poor understanding of the *Pf*PDE biology,¹⁶⁶ the principle of taking a human PDE inhibitor and developing an antimalarial drug was clearly exemplified.

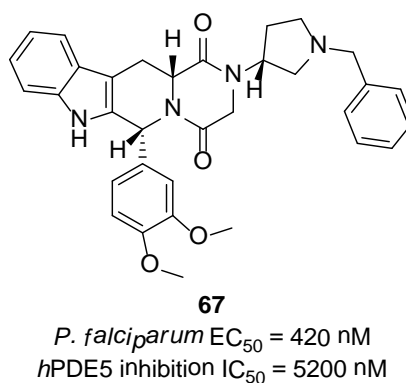


Figure 1.13. A tadalafil analogue, **67**, synthesised by Deprez *et al.* and its activity and selectivity over human PDE5.^{164,165}

Drug repurposing using the wealth of human enzyme inhibitors in order to generate drugs for neglected diseases has become a popular research topic. Pollastri and co-workers have investigated the repurposing of human PDE4 inhibitors as *Trypanosoma brucei* PDE (*TbrPDE*) inhibitors with some success.¹⁶⁷⁻¹⁶⁹ The MMV also have projects targeting the *P. falciparum* kinome based upon previously described human kinase inhibitors.³⁰ This proposition forms the basis for this thesis and a more detailed discussion of phosphodiesterase (PDE) enzyme structure, function and inhibition (both in humans and *P. falciparum*) follows.

1.6 Cyclic nucleotide phosphodiesterase enzymes

As described above, the phosphodiesterase enzymes (PDEs) appear to be a promising target for new antimalarial drugs. The PDEs are a superfamily of metal ion-dependent enzymes which hydrolyse the cellular second messengers cyclic adenosine monophosphate (cAMP) and cyclic guanosine monophosphate (cGMP), thereby attenuating the myriad of cell signalling functions that are carried out by these cyclic nucleotides. Perhaps most notably, numerous G protein-coupled receptors (GPCRs) act

by stimulation of adenylate cyclase and so PDEs may be considered key regulators of GPCR function.¹⁷⁰⁻¹⁷⁶

The PDEs have been the subject of numerous reviews (with respect to classification, function, and physiological and pathological importance),¹⁷⁶⁻¹⁷⁹ and as such only a brief summary is provided here. Originally, the PDEs were classified according to their substrate specificity and their modes of regulation. As the primary amino acid sequences and nucleotide sequences became available, it was possible to classify the PDEs based on sequence homologies.¹⁷⁷ It is now known that there are 21 genes encoding for eleven families of human phosphodiesterases (*hPDE1-11*) and more than 100 isoforms through alternative mRNA splicing.^{170,177,179,180} The different PDE families are specific for either cAMP or cGMP, or are dual-specific with both cAMP and cGMP hydrolysing capabilities (Table 1.14).

The biological roles of PDE isoforms are varied and, in many cases interconnected, as many tissues express multiple isoforms. Some of those are highlighted in Table 1.14. PDEs 1, 2, 3 and 4 are expressed in multiple tissues while the other PDEs are more localised. Despite this, PDEs 5-11 are critical factors in key cyclic nucleotide pathways and are usually found in high abundance within localised tissues.

Table 1.14. The human PDE isoforms, their substrate preference, classical inhibitors and potential clinical application.^{181,182}

PDE family	PDE subtypes	Specificity	Classical inhibitors	Clinical application
1	A, B, C	cAMP/cGMP	Nimodipine Vinpocetine	Dementia, memory loss
2	A	cAMP/cGMP	EHNA	Sepsis, acute respiratory distress syndrome
3	A, B	cAMP/cGMP	Cilostamide Milrinone	Congestive heart failure, thrombosis
4	A, B, C, D	cAMP	Rolipram Roflumilast	Asthma, COPD, bipolar depression
5	A	cGMP	Zaprinast E4021 Sildenafil Vardenafil Tadalafil	Chronic renal failure, pulmonary hypertension, erectile dysfunction,
6	A, B, C	cGMP	Dipyridamole Zaprinast E4021 Sildenafil	Adversely affects vision, so no known clinical application
7	A, B	cAMP	Dipyridamole Thiadiazole	Immunological diseases
8	A, B	cAMP	Dipyridamole	Immunological diseases
9	A	cGMP	Zaprinast	Diabetes, dementia
10	A	cAMP/cGMP	Dipyridamole Papaverine	Schizophrenia
11	A	cAMP/cGMP	Tadalafil Zaprinast Dipyridamole	Improvement of human testicular functions

1.7 Architecture of the human phosphodiesterase enzymes

The first crystal structure of a human PDE isoforms was published in 2000.¹⁸³ The structure of *hPDE4B2B* provided an insight to the mechanism of PDE catalysis. Since this time, many structures of PDE catalytic domains have been solved as either the apo-enzyme or with bound substrate. Analyses of the crystal structures have shown several structural features that are shared among the PDE families that are believed to play a pivotal role in the binding of the substrate.¹⁸⁴

The human PDEs share three structural features; (1) an N-terminal splicing region, (2) a regulatory domain, and (3) a C-terminal catalytic domain. Beyond the catalytic domain is a C-terminal extension, though its function remains unknown.^{171,184} The N-terminal splicing region shows no sequence homology across or within human PDE families.¹⁷¹ Instead, it is believed to serve specific regulatory functions such as autoinhibition of the catalytic domains and control of the subcellular localisation.¹⁷⁰ The regulatory domains of the human PDEs consist of several structural motifs (Figure 1.15). Their function is believed to involve communicating with other cellular components and the regulation of catalytic activity, however, the mechanisms behind these functions are not fully understood.¹⁷¹ In PDE1 this is a calmodulin-binding site, a phosphatidic acid binding site in PDE4, a PAS domain in PDE8, autoinhibitory sequences in PDE1 and PDE4, a membrane association domain in PDE2-4, and allosteric cGMP binding sites in PDE2, PDE5, PDE6, PDE10 and PDE11.^{171,181}

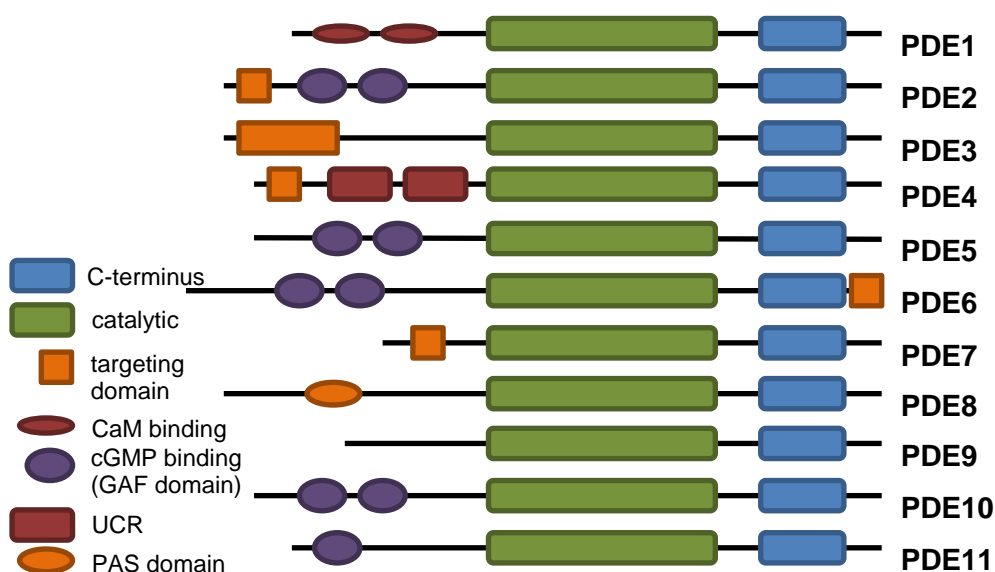


Figure 1.15. The general structures of the different PDE families, adapted from Conti *et al.*¹⁷⁹

In all human PDEs, a conserved C-terminal catalytic domain is located at the core of the enzyme and consists of approximately 270 residues.^{176,181} There are 16 invariant amino acids across all human PDE catalytic domains, 11 of which are present in the substrate binding region.¹⁸⁴ The catalytic domains comprise 16 α -helices which are further divided into three sub-regions; helices 1-7, 8-11, and 12-16 (Figure 1.16).¹⁸³ The substrate binding region lies at the interface of these three sub-regions and takes the form of a deep hydrophobic pocket that can further be divided into four subtypes; a metal-binding site, core pocket, hydrophobic pocket and lid region.^{173,174,184} The active site is approximately 15 Å in depth with an opening of approximately 10 Å \times 20 Å.

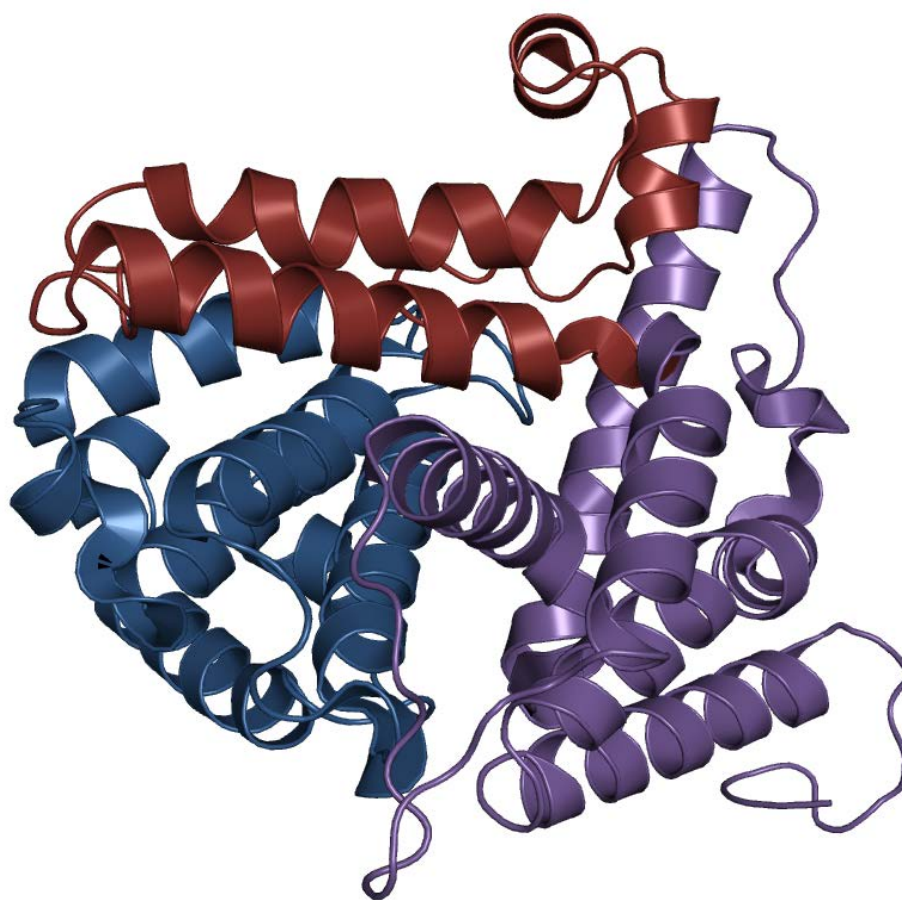


Figure 1.16. The secondary structure of the catalytic domain of PDE4B2B, with the helices divided into sub-regions as described by Xu *et al.*¹⁸³ The N-terminal sub-region (residues 152 to 274) is coloured in blue, the middle sub-region (residues 275-347) in red, and the C-terminal sub-region (residues 348 to 489) in purple.

The metal-binding site consists of a zinc ion (Zn^{2+}) and a second metal ion that is most probably a magnesium ion (Mg^{2+}). Both ions adopt near-perfect octahedral coordination geometry.^{184,185} The zinc ion is coordinated by two invariant histidine residues, two invariant aspartate residues and two water molecules. One of each of the aspartate residues and water molecules bridges to the magnesium ion, which is coordinated by a further four water molecules. The presence of two metal ions implies a binuclear catalytic mechanism for the cleavage of the cyclic phosphate group of the endogenous ligands (Figure 1.17).¹⁸⁴

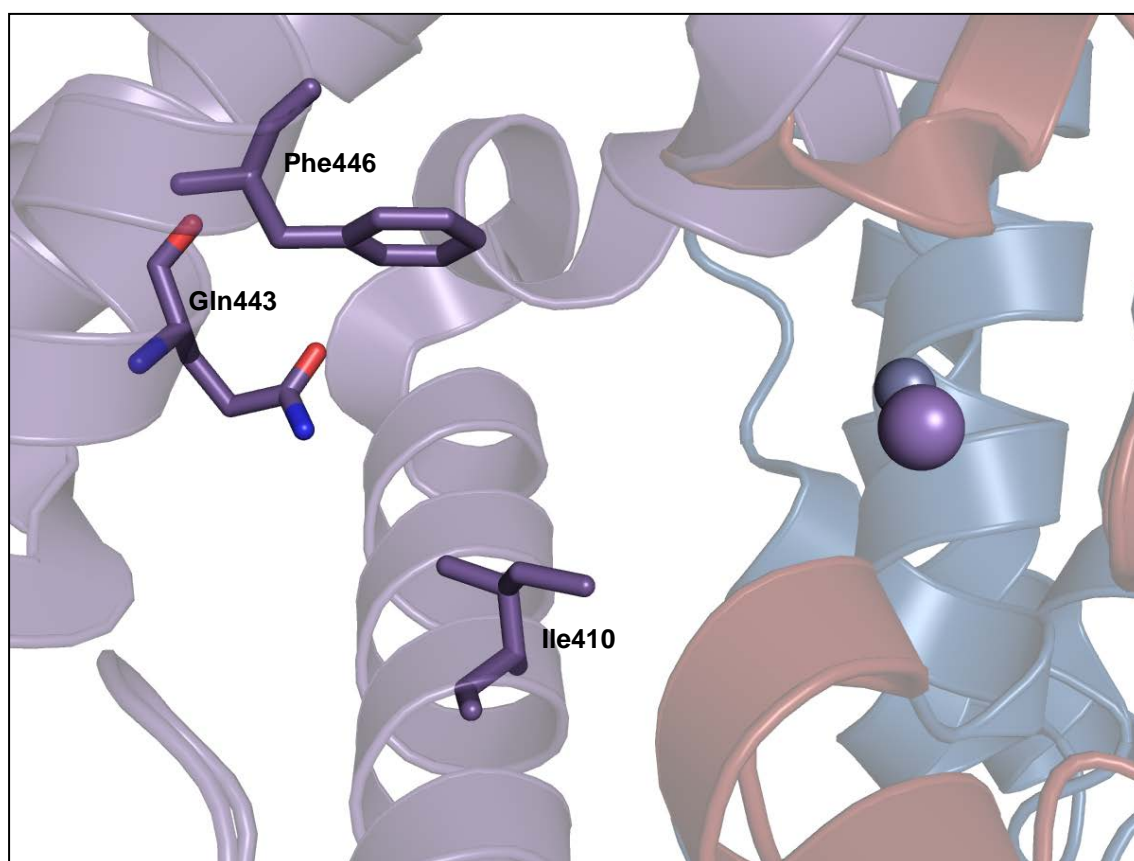


Figure 1.17. The binding site of PDE4B2B showing the position of the metal ions, zinc (grey sphere) and magnesium (purple sphere). The purine-scanning glutamine (Gln443) as well as the phenylalanine (Phe446) and isoleucine (Ile410) residues of the hydrophobic clamp are shown as sticks. Numbering is taken from the 1XMY crystal structure.¹⁸⁵

The substrate binding region also contains an invariant glutamine residue referred to as the ‘purine-scanning glutamine’ (Figure 1.17). The orientation of this invariant residue has been shown to directly dictate enzyme specificity for cAMP or cGMP.¹⁷³ The residue forms essential hydrogen bonds to the purine ring of the substrate and so substrate specificity is determined by the adjacent residues and the manner in which they serve to orient the purine-scanning glutamine. A conserved phenylalanine residue resides at the top of the binding site and, together with a small hydrophilic residue at the base of the binding site, forms the ‘hydrophobic clamp’ (Figure 1.17). This phenylalanine residue forms π -stacking arrangements with cAMP and cGMP, which are believed to be critical for substrate binding.

1.8 Human phosphodiesterase enzyme inhibitors

Since the late 1970s, PDE inhibitors have been sought as potential therapeutics and some have reached clinical application. In recent years, there has been an increased focus on identifying isoform selective inhibitors and there are many extensive reviews of PDE inhibitors.^{177,182,186-188} Here, reference is made to a selection of inhibitors relevant to this thesis and their structures are illustrated in Figure 1.18.

A range of diseases have been treated with non-selective PDE inhibitors, including papaverine (**68**) and theophylline (**69**), which are the mainstay of non-selective *h*PDE inhibitors. Papaverine was first recognised as a mediator of vasorelaxation and was found to exert its effect through inhibition of human PDE5.¹⁸² This discovery spurred further investigation into human PDE5 and its therapeutic potential.

Zaprinast (**70**) was the first PDE5 inhibitor to be characterised, and remains one of the very few cGMP-specific PDE inhibitors. In fact, zaprinast was used widely to explore the role and function of the PDE5 isozyme.¹⁸⁹ It was initially developed as an antiallergy compound (through mast cell stabilisation), though demonstrated vasodilation *in vitro*.^{182,190,191} It is the archetype for PDE5 inhibitors and is capable of inhibiting *h*PDE5 with an IC₅₀ value of 0.81 µM.¹⁹² It has also been used extensively as a human PDE9 inhibitor (IC₅₀ = 29-46 µM),¹⁹² primarily due to a lack of other potent and/or selective PDE9 inhibitors.

The most famous of all human PDE inhibitors is sildenafil (**71**), which is now marketed as Viagra[®] for the treatment of erectile dysfunction, albeit through a somewhat serendipitous discovery. Following the observation that zaprinast was shown to induce an increase in cGMP associated with a vasorelaxing effect,¹⁹⁰ the structurally-related compound, sildenafil, was initially developed as an antihypertensive or coronary vasodilator. During clinical trials, it was unexpectedly discovered that sildenafil sustained male erections.¹⁸⁶ Currently, three *h*PDE5 inhibitors exist on the market; sildenafil (Viagra[®]), tadalafil (Cialis[®]) (**72**), and vardenafil (Levitra[®]) (**73**), and all are prescribed for erectile dysfunction.

Rolipram (**74**) is a human PDE4 inhibitor that was developed in the early 1970s as a potential antidepressant.¹⁹³⁻¹⁹⁵ Although rolipram was effective as an antidepressant, clinical development was terminated due to the unwanted side effects associated with its use. The structurally-related *h*PDE4 inhibitor, roflumilast (**75**), was subsequently

developed. It is now marketed as Daxas[®] and is used in the treatment of inflammatory disorders such as asthma and chronic obstructive pulmonary disease (COPD).¹⁸²

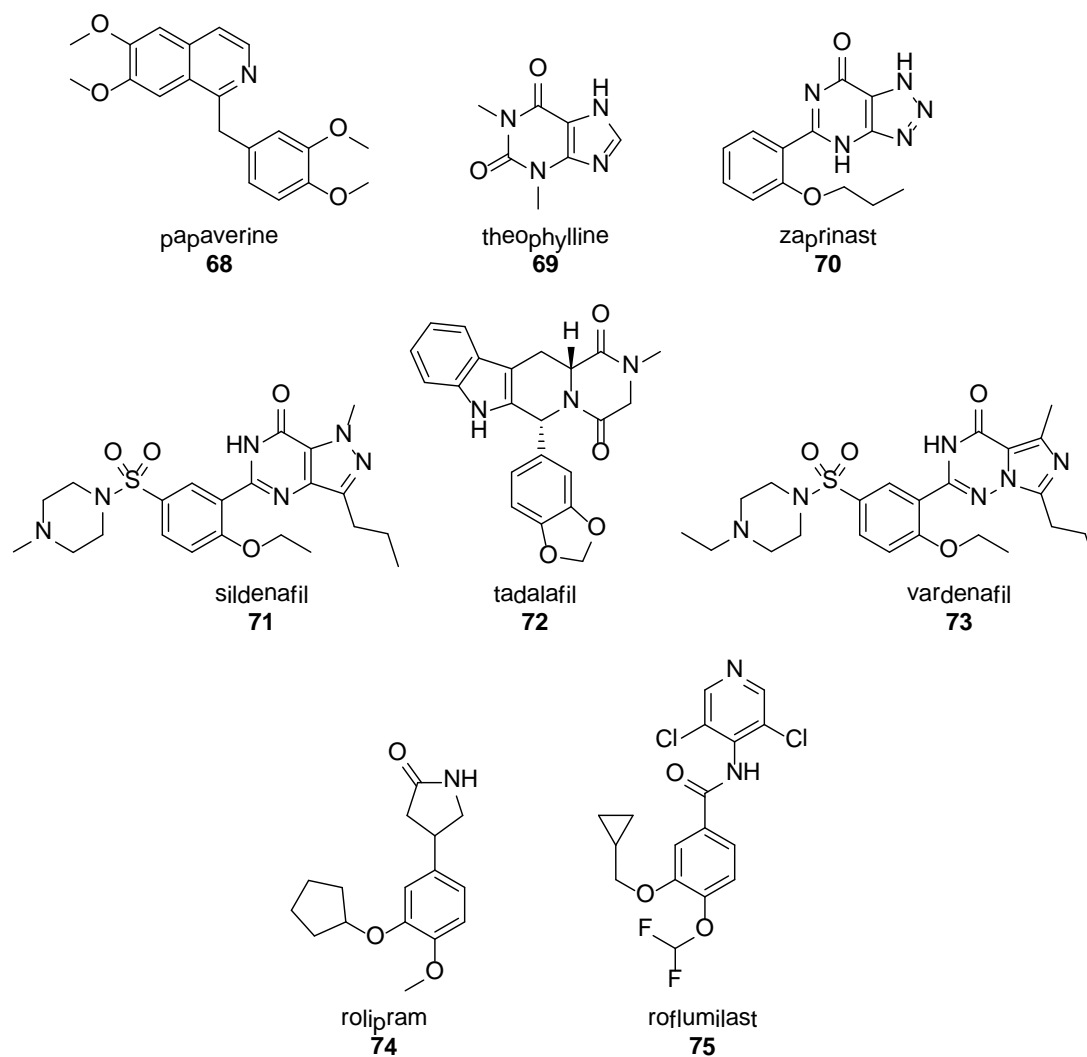


Figure 1.18. Structures of human PDE inhibitors.

As the examples above show, the identification of key inhibitor chemotypes can lead to the development of selective and potent therapeutics. Given the high structural similarity among the human PDE isoforms, it is not surprising that common structural features have been observed (Figure 1.19).

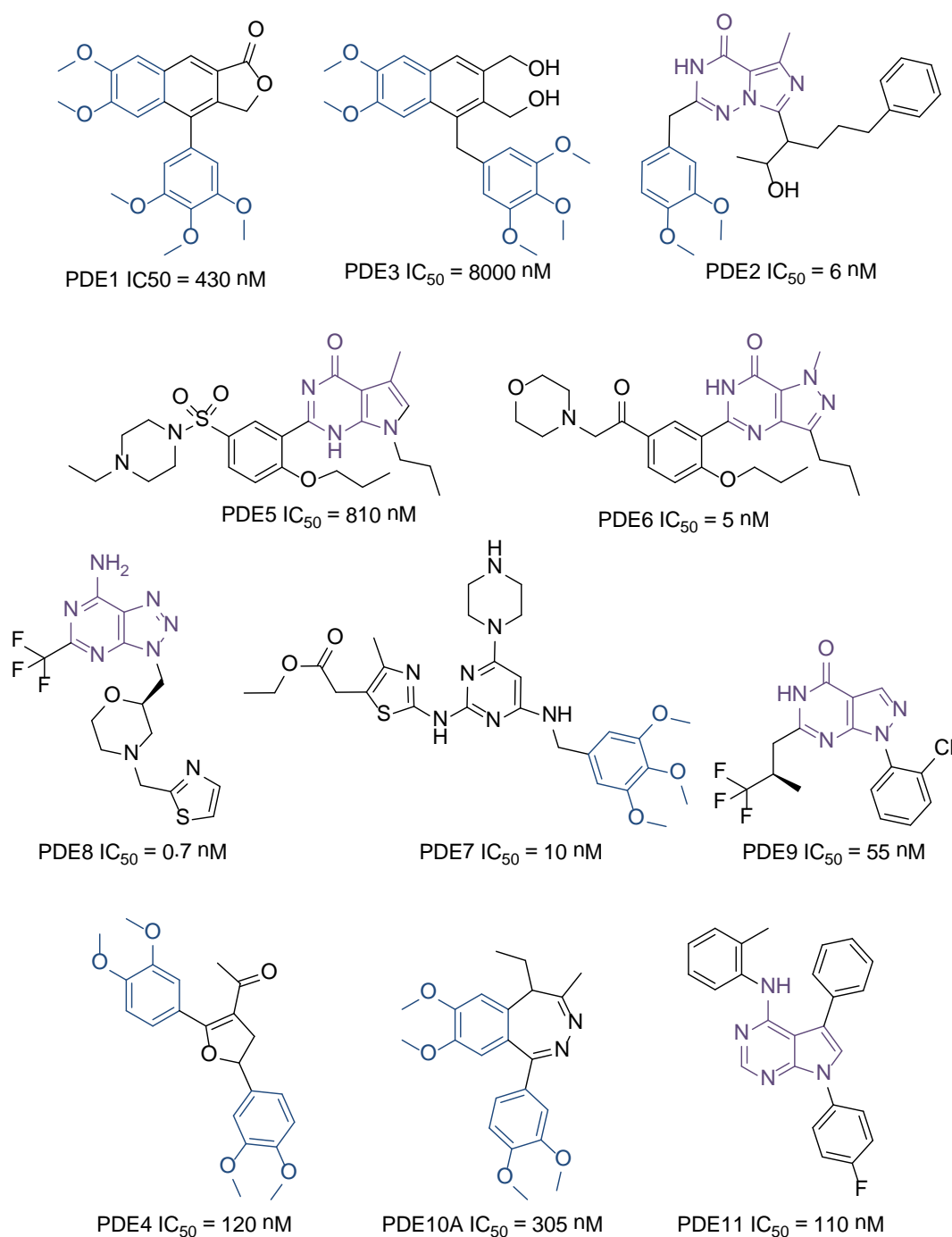


Figure 1.19. Structures of several human PDE inhibitors, with the common structural features highlighted (the purine-like moiety is highlighted in purple, and the catechol ether moiety is highlighted in blue).

Many *h*PDE inhibitors incorporate the purine moiety of the cyclic nucleotides (cAMP or cGMP) as the basic scaffold to act as substrate mimics (highlighted in purple in Figure 1.19), as in theophylline, zaprinast and sildenafil. Additional elements are then included to enhance affinity and selectivity for a particular PDE isozyme. Similarly, a

common catechol ether moiety emerges (highlighted in blue in Figure 1.19), as exemplified by the structures of papaverine and rolipram. In addition, many compounds contain an aromatic bicyclic system with an aromatic pendant, as seen in papaverine, tofisopam, and trequinsin. From these chemotypes, compounds that inhibit each of the 11 *hPDE* sub-types have been synthesised, biologically assessed, and shown to be active.

In summary, the history of the development of human PDE inhibitors has shown that there are a number of unique chemical scaffolds that have suitable architecture for inhibition of the enzyme. In pursuing an inverted silver bullet strategy for *PfPDE* inhibitors, there is an excellent selection of plausible starting points from which to choose.

1.9 *Plasmodium falciparum* phosphodiesterase enzymes

Protozoal phosphodiesterases differ from their metazoan counterparts in two main aspects; (1) in humans, all PDEs belong to the class I superfamily of PDEs and share a conserved catalytic domain, and (2) the protozoal PDEs contain less variety within the regulatory domains. The kinetoplastids are an order of unicellular eukaryotes which includes several parasites that are major human parasites. For example, human sleeping sickness is caused by *Trypanosoma brucei*; Chagas disease is caused by *Trypanosoma cruzi*; and human leishmaniasis is caused by several species of the genus *Leishmania*, and as previously discussed, malaria is caused by *Plasmodium* species. The PDEs of these parasites are being investigated as potential drug targets. All kinetoplastids appear to comprise the same set of four families of class I PDEs and no class II PDEs.¹⁸⁷

The *P. falciparum* parasite was predicted to contain four phosphodiesterase genes.¹⁶³ The amino acid sequence identities between the *Plasmodium falciparum* phosphodiesterase (*PfPDE*) catalytic domains vary from 30% to 40%, indicating that they represent four distinct PDE families.¹⁸⁷ The *PfPDEs* were first reported by Yuasa and co-workers in 2005 following the identification of the intracellular cyclic nucleotides, cAMP and cGMP.^{16,196,197} The levels of cAMP and cGMP are believed to be regulated within the parasite as they are in humans *via* production through adenylate and guanylate cyclases and inactivation through PDE hydrolysis.¹⁶

Given the implication of cyclic nucleotide signalling within *P. falciparum* and its known disruption on parasite cell biology (including hepatocyte infection, gametocytogenesis, cell cycle control, exocytosis and regulation of ookinete gliding)^{163,166,198} Wentzinger and co-workers examined the potential of the *PfPDEs* as drug targets, and their summary of the characteristics of these enzymes is provided in Table 1.20.

Table 1.20. The structural characteristics of the *PfPDEs*.

<i>PfPDE</i> α	<i>PfPDE</i> β	<i>PfPDE</i> γ	<i>PfPDE</i> δ
Located on chromosome 12	Located on chromosome 13	Located on chromosome 13	Located on chromosome 14
<i>PfPDE</i> α A – 954 amino acids <i>PfPDE</i> α B – 892 amino acids	1139 amino acids	769 amino acids	815 amino acids
<i>PfPDE</i> α A – 6 helices <i>PfPDE</i> α B – 4 helices	6 helices	6 helices	6 helices

The gene encoding for *Pf*PDE α produces two alternative splice variants, *Pf*PDE α A and *Pf*PDE α B. *Pf*PDE α B results from the removal of an additional exon from the mRNA, resulting in a loss of transmembrane helices four and five. However, this is not expected to alter the topology of the protein.¹⁶³

The prediction that the *Pf*PDEs contain four to six transmembrane helices has indicated that the *Pf*PDEs are integral membrane proteins. This has been supported experimentally when it was shown that essentially all PDE activity was associated with the membrane fraction. This is unlike the human PDEs, where only *h*PDE3 and *h*PDE4 are known to associate with membranes.¹⁶³

It has also been predicted that the catalytic domains of *Pf*PDE β and *Pf*PDE δ are exposed outwards of the parasite toward the lumen of the parasitophorous vacuole. Conversely, *Pf*PDE α A, *Pf*PDE α B and *Pf*PDE γ are intracellular facing and are exposed toward the cytoplasm of the parasite.

The recombinant expression of the *Pf*PDEs has been attempted in several systems with limited success. *Pf*PDE α was eventually expressed in *E. Coli* however, only at low levels. This recombinant enzyme was determined as being cGMP-specific.¹⁶³

*Pf*PDE α was investigated as a drug target by constructing a knock-out strain for this gene. Knocking out the gene produced no major phenotype despite *Pf*PDE α being well expressed in the erythrocytic stage of *P. falciparum* infection. Both merozoite

production and cell proliferation were unaffected. This suggests that the negative effects of deleting *PfPDEα* are counterbalanced by the up-regulation of the other *PfPDEs*, or that *PfPDEα* is simply not essential within the parasite. Along with *PfPDEα*, *PfPDEβ* is predominant in the erythrocyte stage. This indicates that *PfPDEβ* is the major and possibly essential PDE in the erythrocyte cycle of *P. falciparum*, making it a viable antimalarial drug target (Figure 1.21).¹⁶³

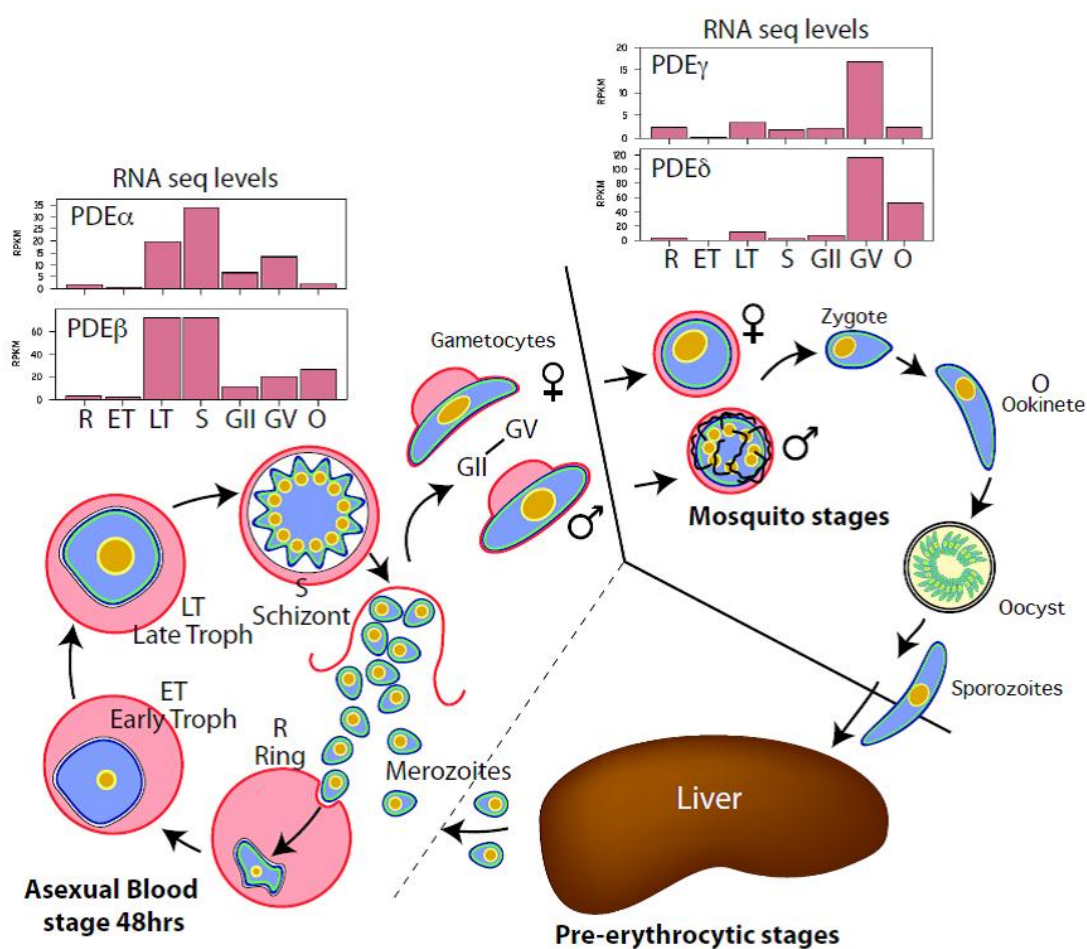


Figure 1.21. Schematic representation of the *P. falciparum* life-cycle and the expression of the *PfPDE* isoforms throughout.

The effects of several *hPDE* inhibitors on *PfPDEα* were examined by Yuasa *et al.* (Table 1.22). This showed compounds that inhibit *hPDE5* demonstrated inhibitory effects on *PfPDEα*, with zaprinast determined to be the most effective *PfPDEα* blocker

with an IC_{50} value of $3.8 \pm 0.23 \mu M$. When tested against the whole parasite, zaprinast inhibited parasite growth with an ED_{50} value of $35 \pm 4.2 \mu M$.¹⁶ Certainly this study, together with that referred to earlier relating to tadalafil analogues (Figure 1.13), demonstrate the enormous potential for *Pf*PDE inhibitors as possible antimalarial drugs.

Table 1.22. The inhibitory activities of various *h*PDE inhibitors and chloroquine on *Pf*PDE α .¹⁶

Inhibitor	IC_{50} for <i>Pf</i> PDE α (μM)
Chloroquine	>100
IBMX	>100
Papaverine	>100
Theophylline	>100
Pentoxifylline	>100
Vinpocetine	>100
EHNA	>100
Milrinone	>100
Rolipram	>100
Sildenafil	56 ± 11
E4021	46 ± 1.8
Dipyridamole	22 ± 0.58
Zaprinast	3.8 ± 0.23

Partially purified *Pf*PDE α proteins produced in *E. Coli* were used for the assay. $0.6 \mu M$ concentrations of cGMP were used. The bivalent cation used was 1 mM MnCl_2 . IC_{50} values were calculated by linear regression. Assays were performed in duplicate. Data is expressed as the mean \pm SEM of three independent determinations.

1.10 Summary and aims of this thesis

Malaria is a global health crisis which is being further potentiated by the development of resistance to the currently employed antimalarial therapies. Initiatives such as the Medicines for Malaria Venture (MMV) demonstrate the scope for drug discovery towards the development of new antimalarial compounds. While several approaches to developing new medicines have been validated, the repurposing of known drugs has several merits (as discussed in section 1.5.5).

Given the role of the phosphodiesterase enzymes within the *Plasmodium falciparum* parasite and evidence that targeting the enzymes disrupts the cell biology of the protozoa, the *Pf*PDEs present as novel therapeutic targets. Applying a drug repurposing strategy may be particularly fruitful given the abundance of known human PDE inhibitors. Adding to this, several common structural features among these inhibitors delineates distinct compound chemotypes that can be incorporated into the design of a new class of *Pf*PDE inhibitors.

The aim of this work is to apply the accumulated knowledge and experience of *h*PDE drug discovery to the objective of designing inhibitors of the *Pf*PDEs that might facilitate the development of new antimalarial drugs. In Chapter 2, the prospect of drug repurposing strategies led by computer-assisted structure-based design techniques is examined. A question that has been posed is whether the structural data relating to human PDEs can be used to generate useful models of the *Pf*PDEs that may then assist in the screening of the thousands of known inhibitors of *h*PDE isoforms. In Chapter 3, the results from Chapter 2 have been applied directly in repurposing a series of *h*PDE inhibitors described by Pfizer.¹⁹⁹ These compounds were found to inhibit *Pf*PDE growth consistent with the hypothesis, and are exciting leads to take further in unravelling the basic roles of *Pf*PDEs in the parasite life-cycle.

In Chapters 4 and 5, an alternative approach was taken. Conscious of the potential that new chemotypes might have on the PDE inhibitor field in general, novel structural classes that build on the previously identified anti-PDE and antimalarial activity of natural product flavonoids have been pursued. Four rarely studied compound classes

were assessed and while progress was made for each chemotype, it was a new class of synthetic chromanones that inhibited both *hPDE* and *Plasmodium falciparum* proliferation that provided an exciting new avenue for exploration.

Chapter 2

Homology modelling of *Plasmodium falciparum* phosphodiesterases and molecular docking

2.1 Introduction

In the absence of crystal structures of the *Plasmodium falciparum* phosphodiesterase enzymes (*PfPDEs*), the development of homology models of the enzymes was envisaged to serve as a useful tool in the development of enzyme inhibitors. The similarity between the *hPDEs* and *PfPDEs* has been recognised previously, and Wentzinger and Seebeck suggested that the sequences of the *PfPDEs* conformed to the general Class I grouping of mammalian PDEs.¹⁶³ This is further supported by the crystal structure of the protozoan *Leishmania major* phosphodiesterase enzyme (*LmjPDEB1*) which similarly adopts the general fold of the Class I PDEs, drawing the link between mammalian and protozoan PDEs.

The primary aim of molecular modelling is to employ theoretical methods and computational techniques to simulate the behaviour of molecular systems. With regard to drug discovery, being able to simulate a molecular system can provide vital clues to the type of molecules that may produce or block a biological response. Within

molecular modelling, homology modelling, also referred to as comparative modelling, is a commonly employed technique in which a three-dimensional protein structure is predicted *in silico*.²⁰⁰⁻²⁰²

In order to produce a feasible homology model of a target protein the experimentally determined crystal structure of a suitable protein is required as the template structure. The quality of the homology model depends heavily on similarities in the sequence alignment between the target sequence and that of the template protein.

One of the first steps in the process is to optimally align the target and template sequences. Following this, the target sequence is modelled to overlay it on the backbone of the template protein crystal structure. Often, several stages of refinement are required to improve the quality of the homology model.

The aim of this work was to develop homology models of each of the four *Plasmodium falciparum* phosphodiesterase enzymes (*PfPDE* α - δ) to use in molecular docking studies. To achieve this, the closest human phosphodiesterase enzyme homologue had to be identified to serve as a template structure. Models are then built and refined to provide putative enzyme structures that retain the hallmark features of the PDEs. Finally, molecular docking studies were conducted to examine the binding of cGMP and cAMP, the likely substrates of the *PfPDE*s, as well as zaprinast, which has been shown to inhibit *PfPDE* α .¹⁶ The computational methods for this work are described in detail in section 7.1. Following model validation, the aim was to identify compounds, known or novel, that potentially act as *PfPDE* inhibitors.

2.2 Homology modelling of the *Plasmodium falciparum* phosphodiesterases

2.2.1 Protein sequence comparison

Unlike other PDEs, all four *Pf*PDEs have been predicted to contain three to six transmembrane helices that suggests they are integral membrane proteins. The amino acid sequences of the four *Pf*PDEs vary from 30% to 40% identity between the putative catalytic domains, indicating that they represent four distinct PDE families (Table 2.1).¹⁶³

Table 2.1. The percentage homologies of the human and parasitic PDE enzymes.

		<i>Pf</i> PDE α	<i>Pf</i> PDE β	<i>Pf</i> PDE γ	<i>Pf</i> PDE δ	<i>Lmj</i> PDEB1
<i>Pf</i> PDE	α	100				21.9
	β	30.9	100			23.1
	γ	29.8	36.8	100		21.9
	δ	25.3	27.8	27	100	21.1
<i>h</i> PDE	1A	21.2	26.7	24.6	21.1	24
	1B	23.6	25.8	26.3	21.9	24.6
	1C	20.9	25.2	25.8	22.7	24.1
	2A	23.9	24.9	24.3	18.4	28.3
	3A	22.6	22.8	23.9	20.2	21.4
	3B	21.2	23.1	24.9	20	23.2
	4A	24.1	24.9	25.6	19.9	27.7
	4B	25.4	24.4	26.5	18.9	28
	4C	23.9	24.7	26.8	20.6	27.9
	4D	24.3	25.6	27.4	18.2	27.6
	5A	19.9	23.3	22.5	20.2	27.8
	6A	20.4	21.8	22.4	17.4	25.7
	6B	21.5	23.2	23	16.5	24.9
	6C	20.3	23.8	23	18.5	26
	7A	26.5	27.3	24.6	22.5	26.9
	7B	21.6	24.8	22.1	23.2	26
	8A	22.5	24	26.4	21.3	26.2
	8B	23.2	24	26.1	19.2	26.4
	9A	26.8	27.5	23.1	21.1	25.7
	10A	20.9	22.9	22.1	17.6	26.4
	11A	21.3	25.8	23.4	18.2	30.7

Sequence alignment using ClustalW was performed for the catalytic domains of the four *P. falciparum* PDEs, *L. major* PDEB1 and 21 human PDEs (Appendix 2).²⁰³ Manual adjustments to the alignment derived from ClustalW were needed to ensure that conserved residues and other important structural features were preserved. The five protozoan PDEs were found to have 16-27% sequence identity to the human PDE enzymes (Table 2.1) with approximately 50% of residues being indicated as similar or highly similar. It was noted that *hPDE9* had the highest homology for *PfPDE* α (26.8%) and β (27.5%), and *PDE7A* was quite similar.

There are 16 amino acids that are absolutely conserved among the 21 human PDE enzymes and of these, 13 are also fully conserved across the four *PfPDE* enzymes (the catalytic sequence alignment is provided in Appendix 2). The changes that would result from the lack of conservation of the three non-binding site residues are not expected to alter the gross structure of the proteins. An invariant asparagine in the *hPDE* enzymes (N253; the numbering used in this chapter refers to the PDB: 3DYN crystal structure)¹⁷⁰ at the beginning of helix 6 is conserved in *PfPDE* β , γ and δ but was found to be a threonine residue in *PfPDE* α . In the *hPDE*s this asparagine residue may provide structural stability to the enzyme by forming a hydrogen bond with adjacent backbone amides of isoleucine, valine and alanine residues. Within helix 9, serine replaces a conserved alanine (A312) in *PfPDE* α , β and γ . This alanine residue is positioned in a cavity on the outside of the protein where there is sufficient room to accommodate the additional hydroxyl group of the serine. Thirdly, histidine (H324) in helix 10 is replaced by a tyrosine residue in all four *PfPDE*s and appears to be coupled to a complimentary charge at an acidic residue (usually aspartic acid; *hPDE1* is the only exception, where it is a glutamic acid) between helices 7 and 8 (D295). This acidic residue in human

enzymes is replaced with a glycine residue in the *Pf*PDE enzymes and this allows room for the tyrosine residue.

2.2.2 Homology modelling

Centred upon the sequence alignment (Appendix 2), *h*PDE9 seemed a suitable starting point for creating homology models of each of the four *Pf*PDEs. The models were constructed based on the coordinates of the *h*PDE9A crystal structure (PDB code: 3DYN) (Figure 2.2).¹⁷⁰

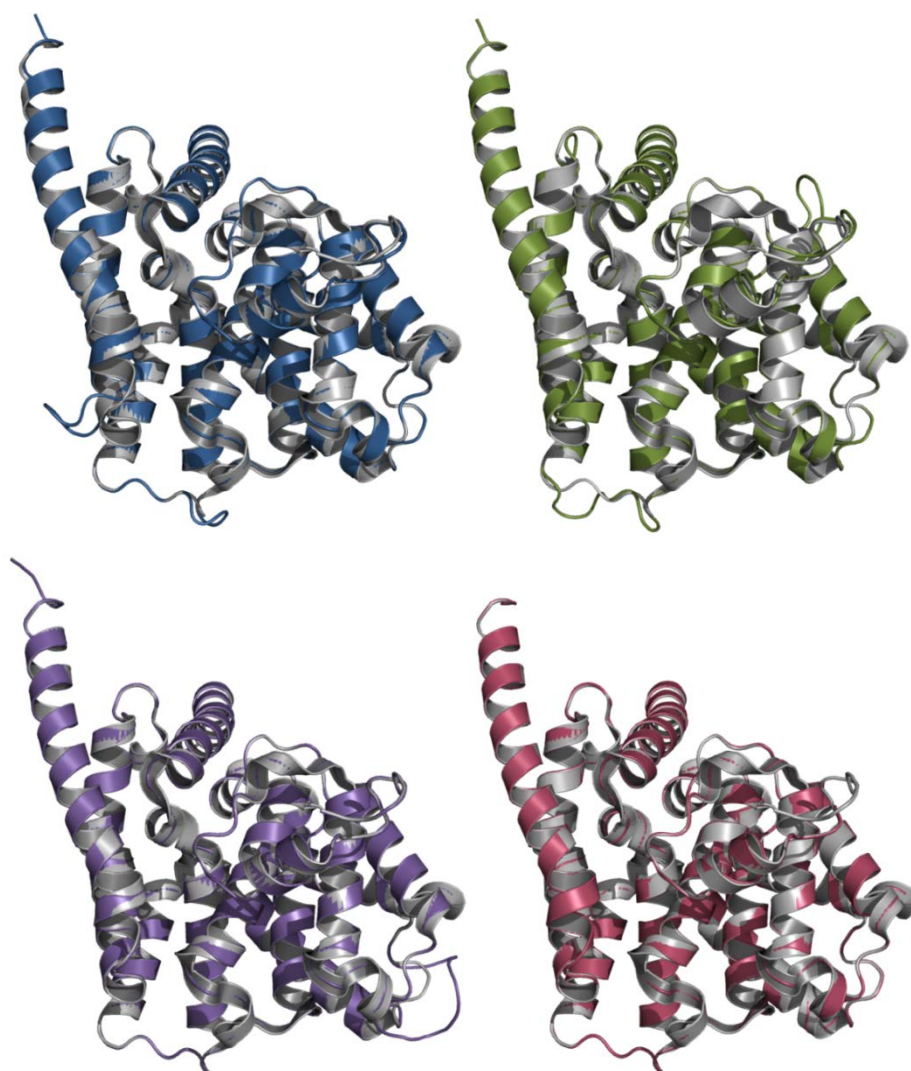


Figure 2.2. Superimposition of each of the developed *Pf*PDE homology models with the *h*PDE9 crystal structure template (shown in grey) (clockwise from top left, *Pf*PDE α - δ).

In this crystal structure, *hPDE9A* is in complex with the endogenous ligand, cGMP, at 2.1 Å resolution. When each of the homology models is superimposed onto the *hPDE9A* crystal structure template, the only noticeable deviations from that structure arose from small insertions in the loop regions (Figure 2.2). These insertions are not in close proximity to the binding site in any of the models generated, and would not be expected to significantly affect substrate or inhibitor binding. Each of the homology models was assessed using MolProbity,²⁰⁴ and Ramachandran plot analyses showed backbone phi and psi angles in the expected regions (Figure 2.3). Further refinement of the *PfPDE* homology models was not required.

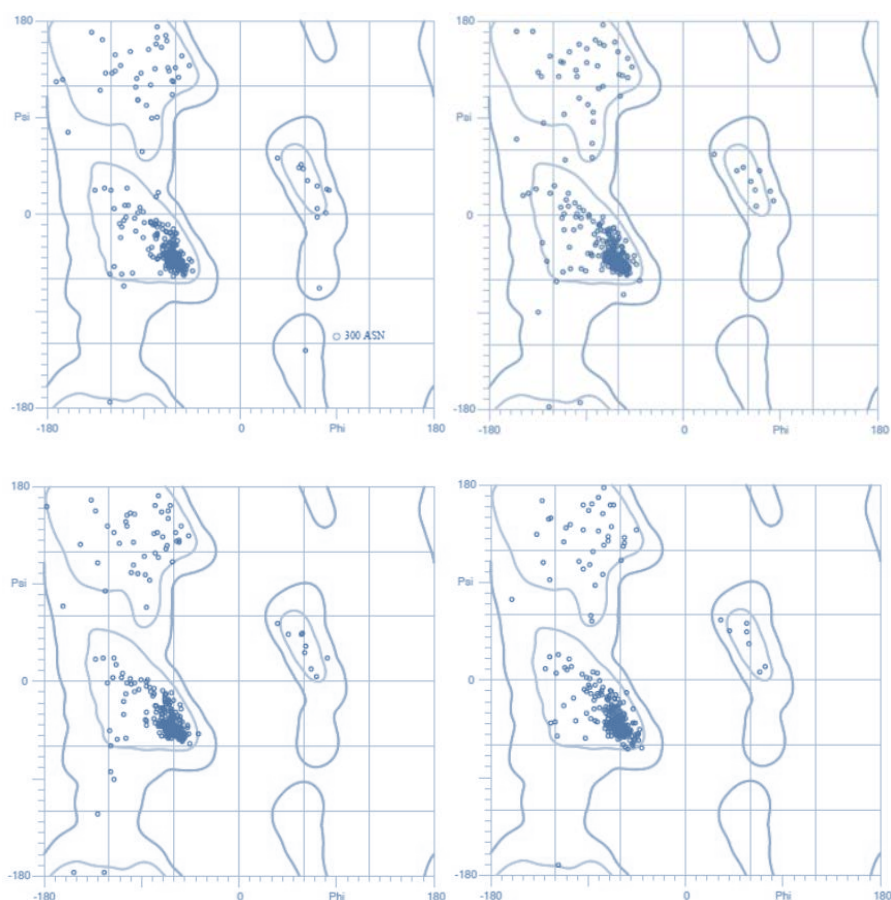


Figure 2.3. Ramachandran analysis of each of the *PfPDE* homology models (clockwise from top left, *PfPDE* α - δ).

The models were built retaining cGMP, the metal ions and the coordinated water molecules in the binding site to ensure the binding cavity would not collapse during the building or minimisation of the models. This helped maintain the integrity of the hydrogen bond network within the binding site and ensured that the hydrophobic clamp remained in position. Thus the resultant models are constructed around these features, yielding a cGMP substrate-bound conformer of the *Pf*PDEs (Figure 2.4). Removal of the endogenous ligand and subsequent full minimisation of the homology models did not result in any significant change to the positions of the metal ions nor to the shape or volume of the binding cavity. These ‘cGMP-specific’ models were considered to be suitable for further modelling work. Experimental work by Yuasa and co-workers had previously shown *Pf*PDE α to be cGMP specific.¹⁶

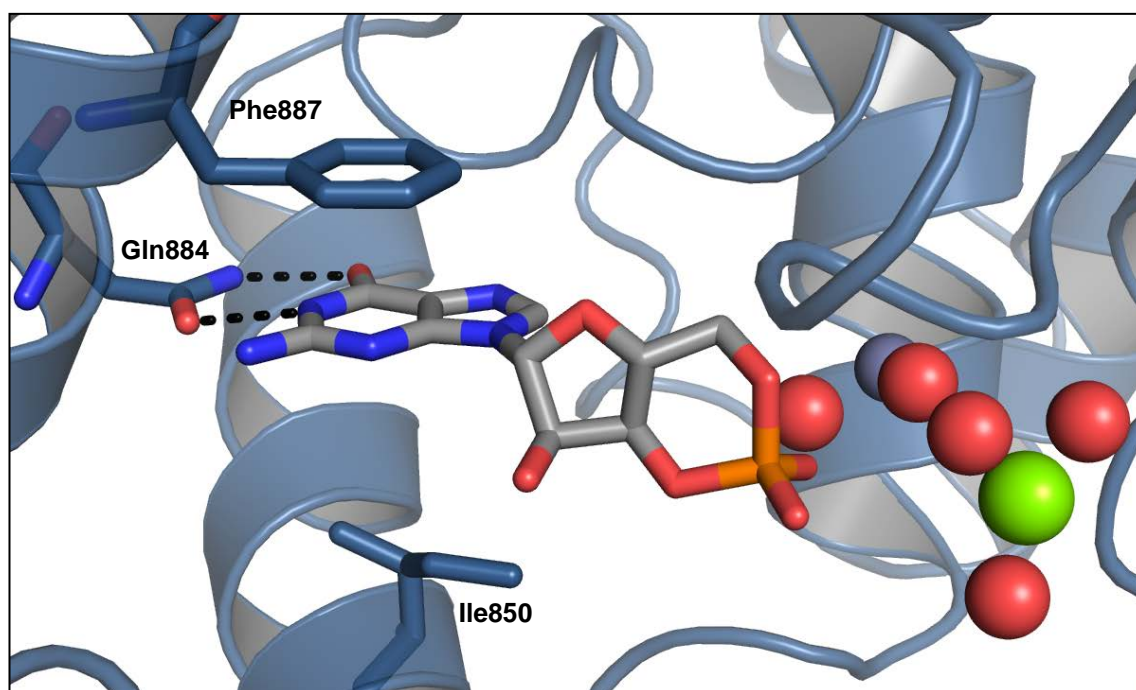


Figure 2.4. The active site of the homology model of *Pf*PDE α with cGMP bound. Highlighted is the purine-scanning glutamine (Gln884), as well as the hydrophobic clamp residues (Phe887 and Ile850). Metal ions and water molecules are represented as spheres, and hydrogen bonds are shown as dashed lines. Numbering is taken from the *Pf*PDE α sequence.

2.2.3 Active site analysis

With *Pf*PDE models established that preserved the basic fold of the PDE catalytic domain, the residues of the active site of the *Pf*PDEs were examined next. This analysis may be a means to understand or predict the cyclic nucleotide or inhibitor selectivity of each of the isozymes. Firstly, the sequence similarity at the cyclic nucleotide binding site was assessed by sequence alignment of the key PDE residues (previously determined by Manallack *et al.*¹⁸⁴) in the metal-binding (M), hydrophobic pocket (H), lid (L) and core pocket (Q) regions as defined by Sung *et al.* (Table 2.5).²⁰⁵

Human PDE binding sites are characterised primarily by a conserved glutamine ‘purine-scanning’ residue (Gln453, R6 in Table 2.5) and a ‘hydrophobic clamp’ comprised of an aromatic residue at the roof of the binding site (Phe456 in 3DYN) and a hydrophobic residue (isoleucine, valine or leucine) at the bottom of the binding site (Leu420 in 3DYN, R5 in Table 2.5).^{171,184} This forms the basis of adenine or guanine binding of the cyclic nucleotides. In the *Pf*PDE models, this construct is retained; the purine-scanning glutamine residue is conserved, the phenylalanine residue is also conserved, while at the bottom of the site the second ‘hydrophobic clamp’ residue varies between hydrophobic residues – isoleucine (α), valine (β,δ) and leucine (γ) (Table 2.5).

Table 2.5. The alignment of the key PDE binding residues across the *h*PDEs, *Pf*PDEs and *Lmj*PDE.

3DYN residue	Region	hPDE											pPDE				LmjPDE
		1 (A, B, C)	2	3	4	5	6	7 (A, C)	8	9	10	11	α	β	γ	δ	B1
292	(i)	H	H	H	H	H	H	H	H	H	H	H	H	H	H	H	H
293	(i)	D	D	D	D	D	D	D	D	D	D	D	D	D	D	D	D
296	(i)	H	H	H	H	H	H	H	H	H	H	H	H	H	H	H	H
322	(i)	E	E	E	E	E	E	E	E	E	E	E	E	E	E	E	E
325	(i)	H	H	H	H	H	H	H	H	H	H	H	H	H	H	H	H
402	(i)	D	D	D	D	D	D	D	D	D	D	D	D	D	D	D	D
251	(R3)	Y	Y	Y	Y	Y	Y	Y	Y	F	Y	Y	Y	Y	Y	Y	Y
405	(R1)	H	D	G	N	A	A	N	N	N	S	A	H	H	H	H	N
413	(R2)	H	T	H	Y	Q	Q	S	C	A	T	S	H	H	H	H	S
420	Q+H	L	I	I	I	V	V	V	I	L	I	V	I	V	L	V	V
423		E	E	E	E	E	E	E	E	E	E	E	E	E	E	E	E
453	(R6)(i)	Q	Q	Q	Q	Q	Q	Q	Q	Q	Q	Q	Q	Q	Q	Q	Q
456		F	F	F	F	F	F	F	F	F	F	W	F	F	F	F	F
490	(R7)	W	W	W	Y	W	W	W	W	Y	W	W	W	W	W	W	I
421		M, L, M	Y	V	M	A	A	T, C	S	L	Y	T	N ^a	L	V	S	T
424		F	F	F	F	F	F	F	Y	Y	F	F	F	F	F	F	F
441		L(ii)	M	F	M	L	M	L	V	F	M	I	C ^a	L	L	I	M
301		N	N	N	N	N	N	Q	N	N	N	N	N	N	N	N	N
302		N, N, S	S	A	Q	S	L	P	S	T	S	A	Y ^a	L	I	S	S
303		F	F	F	F	Y	Y	F	F	Y	Y	Y	F	F	F	Y	F
452		S	L	L	S	M	L	I	S	A	G	L	S	S	I ^c	T ^d	G
455		G	S	S	G	G	G	G	S	G	G	E	D ^a	T	T	Y ^d	G
459		F	H	H	Y	A	F	Y	Y	F	A	S	H	F	E ^c	I ^d	F
406	(R8)	P	Q	P	P	I	I	P	P	E	V	V	S ^a	G ^b	N ^c	T ^d	V
417	(iii)	T	A	T	T	A	A	S	A	V	A	A	T	C ^b	V	T	A

(i) indicates an invariant residue, (ii) while a list of amino acids has been compiled for this hydrophobic region position, this amino acid falls in a loop region. Each of the PDEs have differing lengths for this loop and thus in a 3-dimensional sense it may be difficult to make comparisons. Having said that, PDEs 3, 4, 5 and 9 overlay quite well while PDE1 is distorted at this point, (iii) no region assigned to this residue. ^a denotes this residue as unique to *Pf*PDE α at this position. ^b denotes this residue as unique to *Pf*PDE β at this position. ^c denotes this residue as unique to *Pf*PDE γ at this position. ^d denotes this residue as unique to *Pf*PDE δ at this position.

With regard to the purine-scanning glutamine (Gln453, R6 in Table 2.5), it has been shown that in *hPDEs* the terminal carboxamide group of this residue exists in either one of two conformations (through a 180° rotation) and forms complementary hydrogen bonds to either of the cyclic nucleotide substrates. This ‘glutamine switch’ mechanism has been proposed to explain PDE substrate preference for cAMP and cGMP. Both cAMP- and cGMP-specific enzymes hold the glutamine in the appropriate conformation through a network of hydrogen bonds.¹⁷³ *hPDE9A* is a cGMP-specific isozyme and the crystal structure shows that the purine-scanning glutamine (Gln453) is anchored *via* hydrogen bonding to an adjacent glutamine (Gln406) which locks it into a cGMP-specific conformation. In dual-specific PDEs, this glutamine residue is free to rotate and adopt either conformation, allowing both cAMP and cGMP to bind as substrates.¹⁷³ The ability of the *PfPDE* models to accommodate cAMP was investigated through a manual rotation of the carboxamide group of the purine-scanning glutamine residue (Gln453, R6 in Table 2.6), and energy minimisation of the structure. Notably, a steric clash with the adjacent histidine residues (R1 and R2, Table 2.6) prevented the glutamine from presenting a conformer suitable for cAMP binding in any of the four *PfPDEs*. This clash could not be relieved by energy minimisation or by any manual rotation of the histidine residues. This may support the observation that *PfPDEα* is cGMP specific. As each *PfPDE* shares histidine residues in positions R1 and R2, this suggests that they too may be cGMP-selective.¹⁸⁵ That none of the four identified isozymes can hydrolyse cAMP would be surprising given the apparent role of *PfPKA* in parasite signalling.²⁰⁶

Another region of interest is located adjacent to the purine-scanning glutamine in the active site. In *Leishmania major* and *Trypanosoma brucei* protozoa, the residue preceding this glutamine is a glycine residue. This effectively opens up a pocket near

the glutamine residue that is apparent only in the *hPDE10* isozyme and has been suggested as a selectivity pocket for drug design against these parasites.²⁰⁷ As the *PfPDE* enzymes do not share the glycine residue adjacent to the purine-scanning glutamine, it is predicted that the additional pocket found in *hPDE10* and other protozoan PDE enzymes will not exist in the *PfPDEs*.

A closer examination of the cyclic nucleotide binding site residues was made to assess other relationships that might exist within and between *PfPDE* and *hPDE* isoforms. This analysis highlighted potentially important differences between the *PfPDEs* and *hPDE9A* from which the models were built. Most strikingly, the relationship to *hPDE9A* in the binding site is lost at positions R1 and R2 (Table 2.5) and all of the *PfPDEs* have two histidine residues, a motif that is shared only with the *hPDE1* isozyme. The relationship to *hPDE1* is strongest for *PfPDE β* and *PfPDE γ* , which are also highly similar to each other in the catalytic pocket. *PfPDE α* was found to be most similar to PDE3 in this region, showing the same residues in positions R4 and R5 in the active site. *PfPDE δ* in contrast, shows similarity to *hPDEs* 5, 6 and 11 and this may be attributed to residues within the lid region as well as position R5 (Val) in the active site. On balance however, the residues closely associated with the active site (i.e. R1-R8) suggest that the *PfPDEs* appear to be mostly *hPDE1*-like (particularly R1 and R2).

While the analyses above are described based upon an empirical observation, an attempt was made to use some less biased tools such as dendrogram analyses. This analysis aligns multiple amino acid sequences and is employed to demonstrate similarity among members of a family.²⁰⁸ Dendrogram analysis of the overall catalytic domain showed that the *PfPDE* sequences group together clearly in distinct pairs (α,δ and β,γ) compared

to the human which also group into their established families (Figure 2.6). A similar grouping was demonstrated by Yuasa *et al.* who also showed that the catalytic sequences of the *Pf*PDEs are most closely related to *h*PDE9.¹⁶

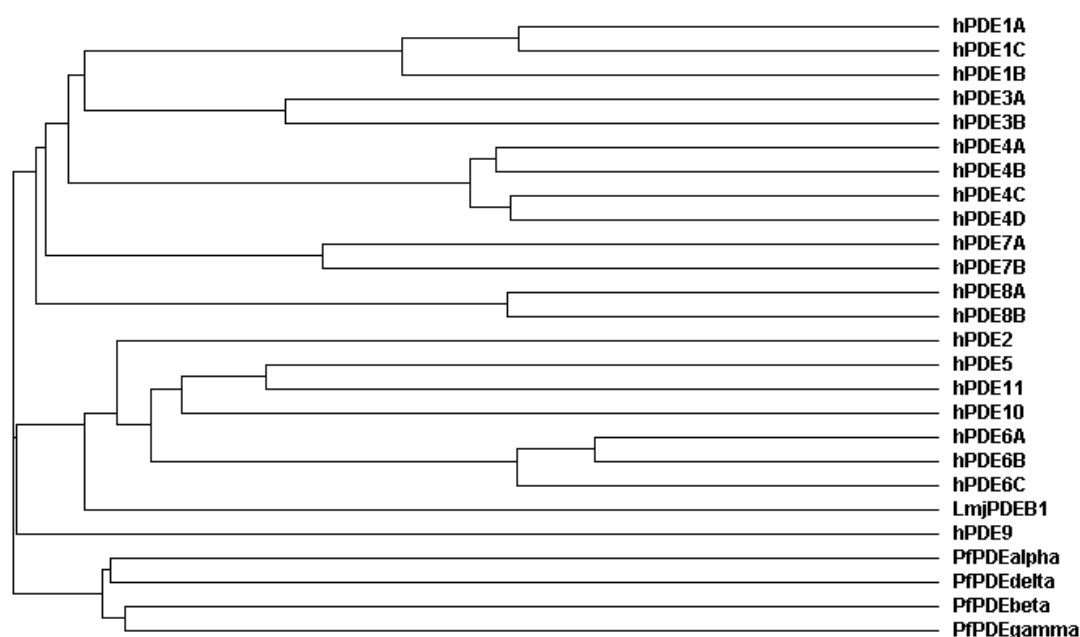


Figure 2.6. Dendrogram analysis of the catalytic domains of the *h*PDEs, *Pf*PDEs, and *Lmj*PDE.

Interestingly, the same process applied to assess the similarity of the substrate binding site residues (from Table 2.5) yields a potentially more fruitful analysis. Note from the figure below (Figure 2.7), that the *Pf*PDEs are dispersed among the branches. Consistent with our other observations, *Pf*PDE β and γ are related to the *h*PDE1 family, whereas *Pf*PDE α links to *h*PDE3, and *Pf*PDE δ to PDE5, 6 and 11.

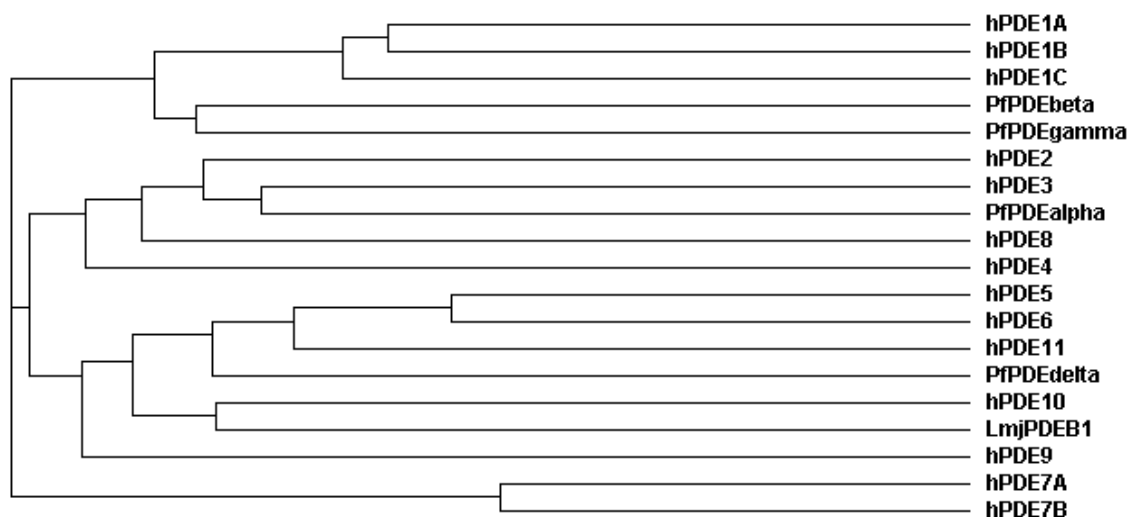


Figure 2.7. Dendrogram analysis of the 25 residues (from Table 2.5) associated with enzyme activity of the *hPDEs*, *PfPDEs* and *LmjPDE*.

In summary, the collected studies of amino acid sequence and structure suggest that the *PfPDE* isoforms can be successfully modelled based upon the structures of the *hPDEs*. At the catalytic site, the residue sequence show a stronger similarity to *hPDE1*, based in particular on the active site histidine residues. The elements identified inspire the design of *PfPDE* inhibitors centred upon *hPDE* inhibitors.

2.3 Docking into the developed *Plasmodium falciparum* phosphodiesterase enzyme homology models

2.3.1 Docking of human phosphodiesterase inhibitors

The purpose of the developed homology models is primarily to facilitate the design of new inhibitors of the *PfPDEs*, which will be crucial in delineating isozyme function and validating the clinical potential of *PfPDE* inhibition. To date, the only pharmacological data relating to *PfPDE* activity concerns a selection of PDE inhibitors screened against

PfPDEα.¹⁶³ As such, homology models could provide the opportunity to perform large scale virtual screens of chemical libraries to enrich the selection of compounds from which inhibitors could be identified, prior to the availability of *in vitro* assays.

Yuasa and co-workers reported the inhibitory activity of several *hPDE* inhibitors against *PfPDEα* (Table 1.22, Chapter 1).¹⁶ Of the compounds tested, the *hPDE1/5* inhibitor, zaprinast (*hPDE1* IC_{50} = 6 μ M, *hPDE5A* IC_{50} = 0.81 μ M, *hPDE9A* IC_{50} = 29-46 μ M)¹⁹² was the most potent inhibitor with an IC_{50} value of 3.8 μ M.¹⁶³ The *hPDE* inhibitors E4021 (*hPDE5A* IC_{50} = 6.2 nM)¹⁹² and sildenafil (*hPDE5A* IC_{50} = 1.6 nM, *hPDE9A* IC_{50} = 2.6-11 μ M)¹⁹² were also reported to exhibit moderate activity against *PfPDEα* (IC_{50} values of 46 and 56 μ M, respectively).²⁰⁹

Zaprinast was docked into the *PfPDEα* model and adopted a pose analogous to the binding of the pyrazolopyrimidinone core of sildenafil in the *hPDE5A* crystal structures, 1TBF and 1UDT (Figure 2.8).^{173,205} The expected contacts to the purine-scanning glutamine were evident, as well as aromatic stacking with the phenylalanine residue of the hydrophobic clamp. Furthermore, the pendant aryl groups superimpose although the alkoxy groups project in different directions. The docked binding mode of sildenafil in the *PfPDEα* model, while also similar to the *hPDE5A* crystal structure binding modes (1TBF and 1UDT),^{173,205} does not hydrogen bond as closely to the purine-scanning glutamine (Figure 2.8). This appears to be due to a steric clash between the histidine residue (R1, Table 2.5) and the pyrazole *N*-methyl substituent of sildenafil. In *hPDE5A*, the presence of a smaller alanine residue in this position avoids this clash. Interestingly, the bicyclic ring system of zaprinast lacks the *N*-methyl substituent and is thus able to fully enter the binding site to make the key interactions with the purine-

scanning glutamine. Sildenafil also has additional interactions with the *hPDE5A* binding site through the bulky sulfonamide group that are not reproduced in *PfPDEα*.

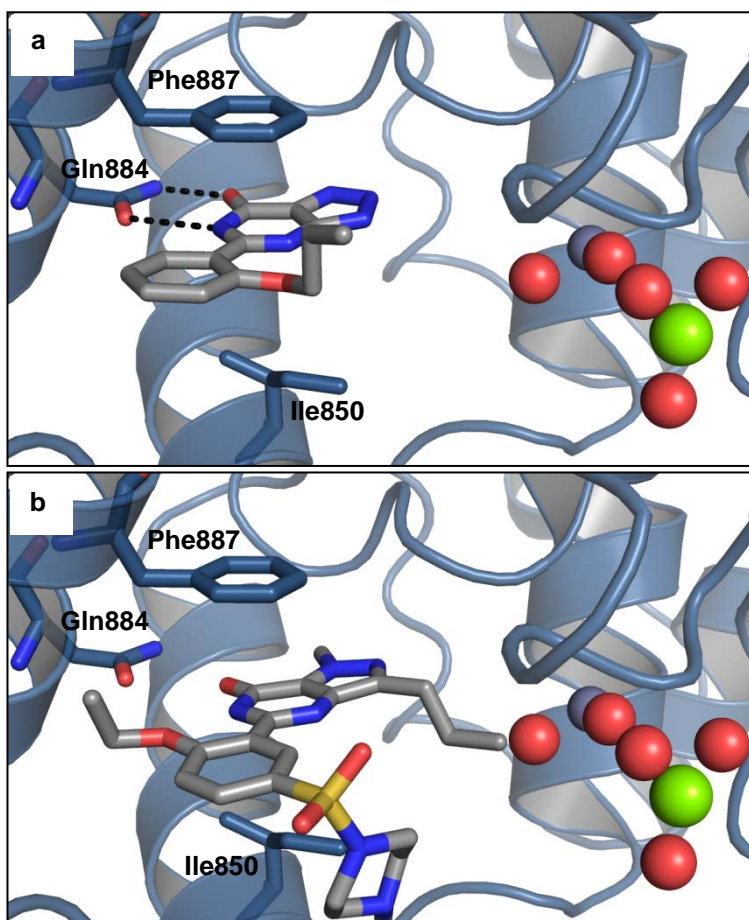


Figure 2.8. The docked pose of zaprinast (a) and sildenafil (b) in the *PfPDEα* homology model. Highlighted is the purine-scanning glutamine (Gln884), as well as the hydrophobic clamp residues (Phe887 and Ile850). Metal ions and water molecules are represented as spheres, and hydrogen bonds are shown as dashed lines.

While crystal structures are not available to show the binding mode of E4021 in any PDE enzyme, this ligand was docked into the binding site of *PfPDEα* (Figure 2.9). Docking suggests a binding mode for E4021 where the catechol ring interacts with the purine-scanning glutamine through a single hydrogen bond and the piperidine carboxylic acid terminus resides near the metal ions of the binding site. When E4021 was docked into the *hPDE5A* crystal structures 1UDT and 1TBF, the binding mode

showed that the ether oxygen in the 3-position also formed a hydrogen bond with the purine-scanning glutamine.

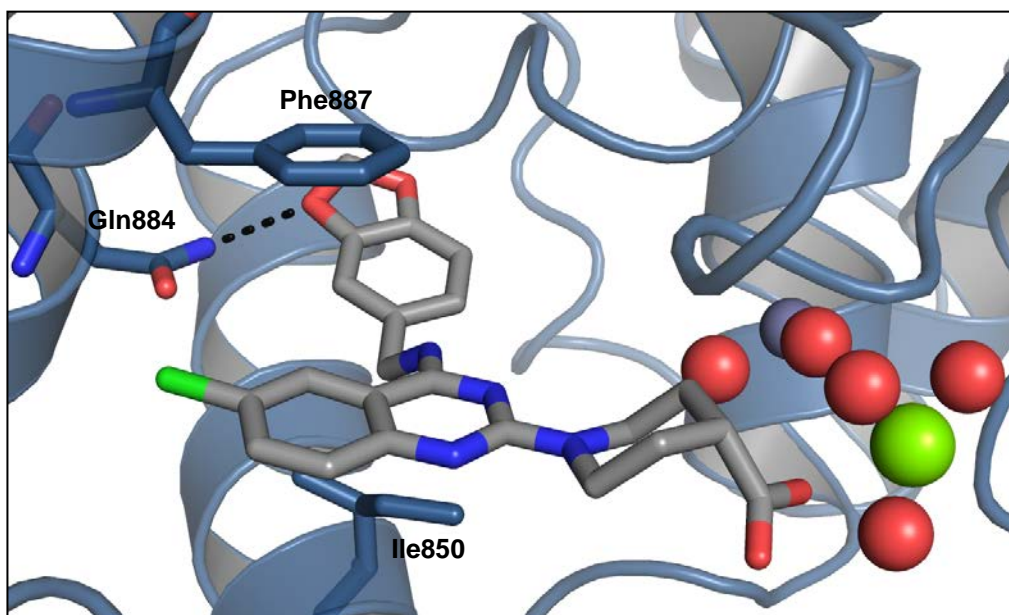


Figure 2.9. The docked pose of E4021 in the *PfPDEα* homology model. Highlighted is the purine-scanning glutamine (Gln884), as well as the hydrophobic clamp residues (Phe887 and Ile850). Metal ions and water molecules are represented as spheres, and hydrogen bonds are shown as dashed lines. Numbering is taken from the *PfPDEα* sequence.

The inhibitory effects of other *hPDE* inhibitors against *PfPDEα* were assessed by Yuasa *et al.*,¹⁶ though several showed no activity ($>100\ \mu\text{M}$) (Table 1.22). These inactive compounds were also docked into the *PfPDEα* model (Figure 2.10). While some demonstrated hydrogen bonds to the purine-scanning glutamine, the docking work does not appear able to significantly distinguish between active and inactive compounds, both through a visual inspection of the docked poses and through docking G-score analysis.

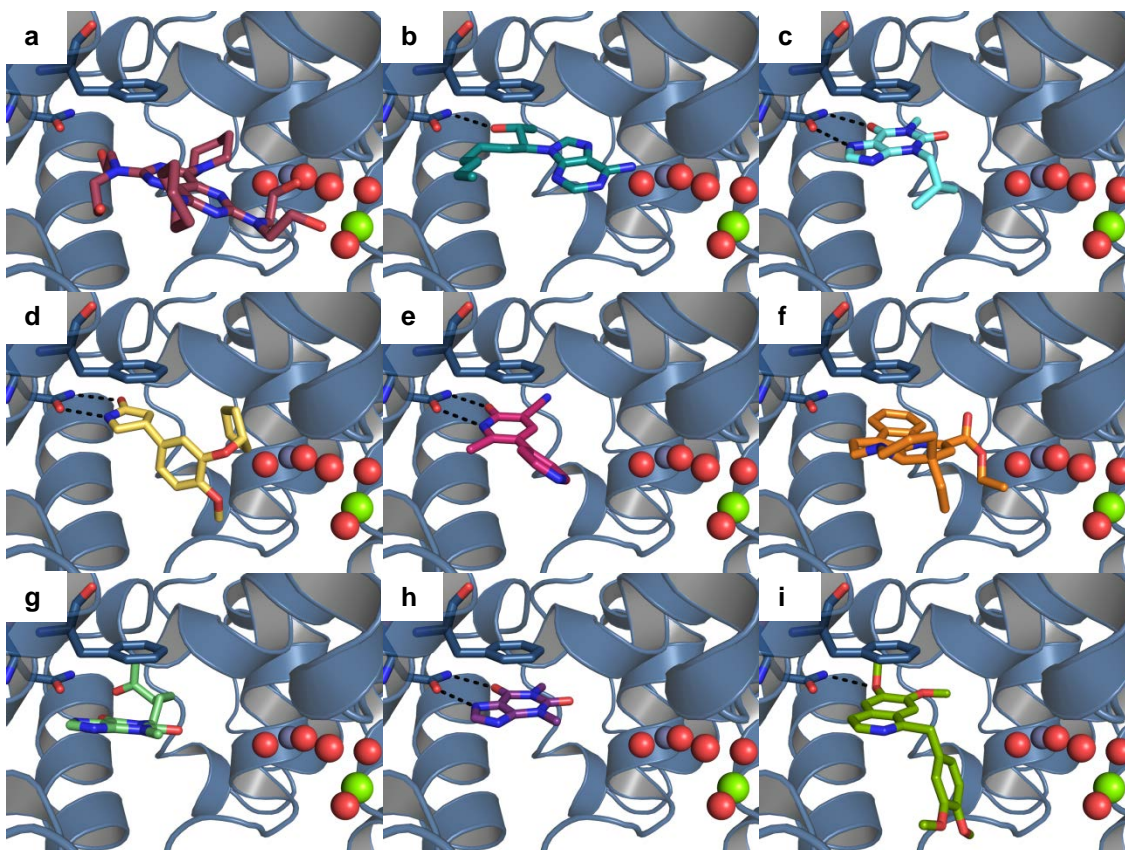


Figure 2.10. Docking of PDE inhibitors into the *PfPDEα* homology model. Highlighted is the purine-scanning glutamine (Gln884), as well as the phenylalanine residue (Phe887) of the hydrophobic clamp. Metal ions and water molecules are represented as spheres, and hydrogen bonds are shown as dashed lines. (a) dipyridamole, (b) EHNA, (c) IBMX, (d) rolipram, (e) milrinone, (f) vinpocetine, (g) pentoxifylline, (h) theophylline, (i) papaverine.

Very recently, Beghyn *et al.* implemented what they described as a ‘drug to genome to drug’ approach to inhibitor design and tested a series of *PfPDE* inhibitors based on tadalafil.^{164,165} Docking of compound **76** (Figure 2.11) from the Beghyn study was undertaken using the *PfPDEα* model.

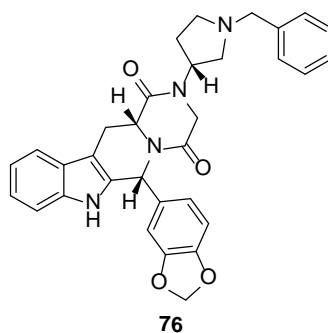


Figure 2.11. The structure of the tadalafil analogue, **76**, published by Beghyn *et al.*¹⁶⁵

Given that the binding mode of tadalafil in *hPDE5A* (PDB code 1XOZ) places the benzodioxole in a pocket adjacent to the purine-scanning glutamine, then a similar sized pocket would be required to successfully dock this compound into the *PfPDE α* model. However, as the *PfPDE* homology models do not possess a cavity of the right dimensions, the tadalafil analogue could not be successfully docked. Interestingly, the bottom of the *hPDE5A* binding pocket is lined with an alanine residue (A783, 1XOZ) while the *PfPDEs* have larger amino acids in this position (N, L, V, S for α , β , γ and δ , respectively). In addition, the *hPDE5A* binding pocket in structure 1XOZ is made larger by the movement of helix 15 in a direction away from the metal atoms. The size of the amino acids, plus large scale protein movement results in a pocket that is capable of binding the benzodioxole group. This is precluded in our models.

In summary, our docking analysis of the known and potential *PfPDE* inhibitors has shown several results. The docking mode of zaprinast appears convincing in light of the crystal structures of sildenafil in *hPDE5A* and may also explain the relative potency of the two molecules against *PfPDE α* . Given that the inhibitory effects of *hPDE* inhibitors have only been assessed against the *PfPDE α* isoform thus far,¹⁶ this molecular modelling work has heavily focussed on investigating the docking results of these inhibitors against the *PfPDE α* homology model. Ongoing studies will seek to identify potential binding modes of known *hPDE* inhibitors in the other *PfPDE* isoforms (β - δ) to elucidate the potential for gaining isoform selectivity.

2.3.2 Docking of human phosphodiesterase 9 and 1 inhibitors

As the sequence analyses comparing the human and *PfPDE* enzymes showed similarity to *hPDE9* (with respect to the overall catalytic domain) and *hPDE1* (within the active

site), a logical starting point in searching for potential *Pf*PDE inhibitors was to investigate *h*PDE1 and *h*PDE9 inhibitors. DeNinno and co-workers had recently published a series of such compounds.²⁹ In particular, the pyrazolopyrimidinone compounds **77** and **78** were shown to have good activity at *h*PDE1 and *h*PDE9, with compound **78** exhibiting good selectivity for *h*PDE9 over *h*PDE1 (Figure 2.12).

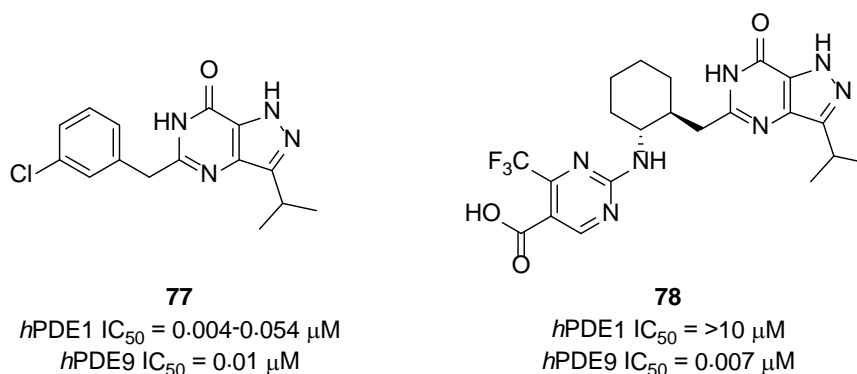


Figure 2.12. Structures of *h*PDE1 and *h*PDE9 inhibitors developed by DeNinno *et al.*¹⁹⁹

These compounds were docked into the *Pf*PDE homology models and their proposed binding modes were examined (Figure 2.13). The docking poses showed that these two compounds (**77** and **78**) each made two contacts to the ‘purine-scanning’ glutamine as well as a π -stacking interaction with the phenylalanine residue of the hydrophobic clamp, in a manner that is seen in the binding mode of all *h*PDE inhibitors. Like zaprinast, **77** showed a ‘guanine-type’ binding mode analogous to the binding of the endogenous ligand (cGMP). However, **78** was predicted to bind in a mode that is unique among *h*PDE structures co-crystallised with inhibitors.

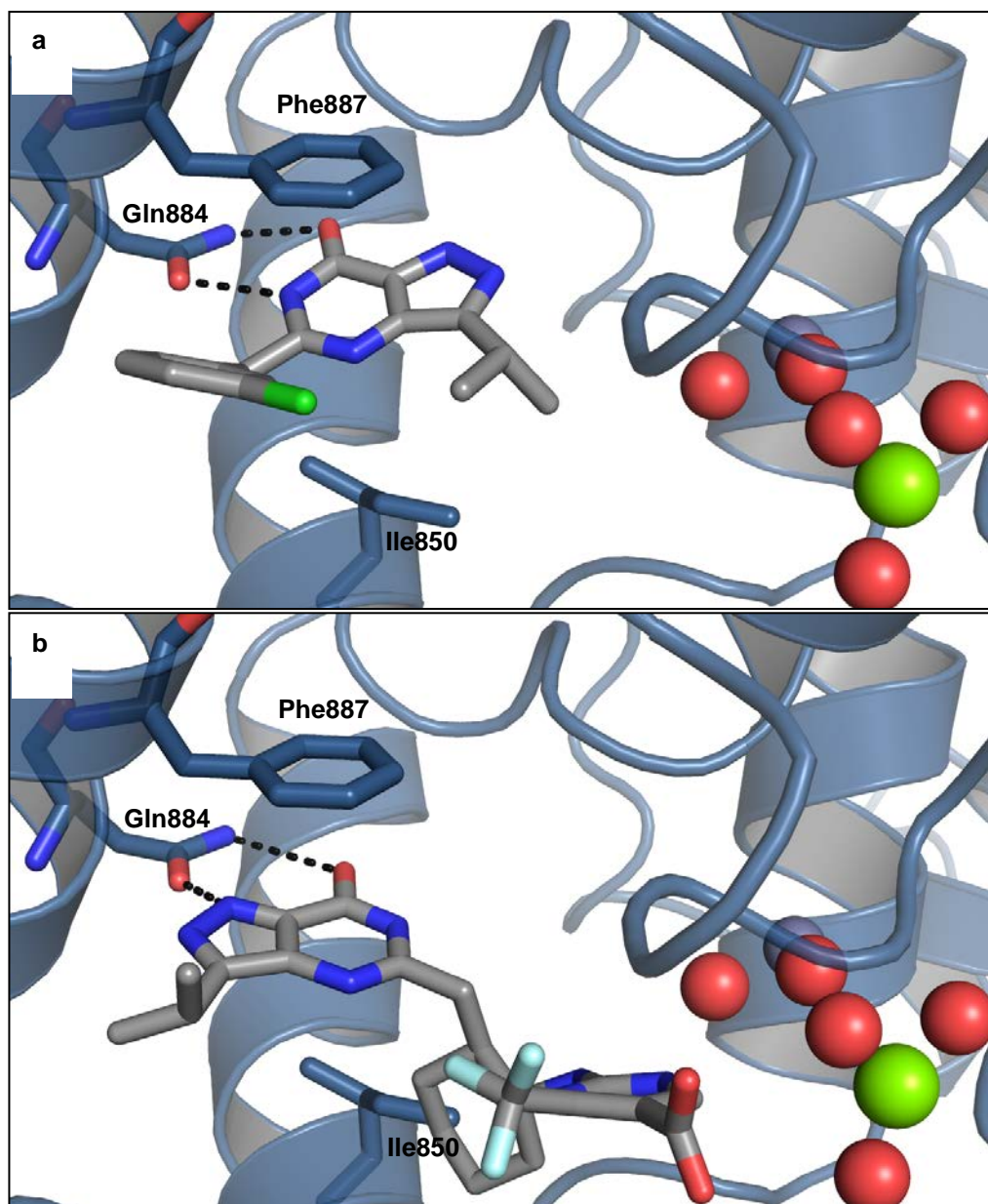


Figure 2.13. The docked pose of (a) **77** and (b) **78** in the *PfPDEα* homology model. Highlighted is the purine-scanning glutamine (Gln884), as well as the hydrophobic clamp residues (Phe887 and Ile850). Metal ions and water molecules are represented as spheres, and hydrogen bonds are shown as dashed lines.

2.4 Gaining selectivity for the *Plasmodium falciparum* phosphodiesterases

Prior studies on the *PfPDE* biochemistry of zaprinast and tadalafil analogues, as well as the docking of the *hPDE9A* and *hPDE1* selective inhibitors (section 2.3.2) showed the

potential for developing *Pf*PDE inhibitors from *h*PDE ligands. An important further element is the need to remove *h*PDE potency while retaining *Pf*PDE potency to achieve selectivity for the *Pf*PDEs. From the docking results, it would appear that there may be several chemical fragments that could be explored to develop *Pf*PDE inhibitors, such as the benzodioxole group of E4021 or the guanine-like structures of zaprinast and sildenafil. It is clear however, that to obtain *Pf*PDE selectivity, binding site residues that are unique to the enzyme of interest need to be targeted. This approach has been successful in the development of highly selective and potent *h*PDE inhibitors. It is therefore logical to target differences within the 25 binding site residues associated with the active site (Table 2.5). Of the 25 amino acids, five residues within *Pf*PDE α are unique to this isozyme. It is proposed that targeting these particular residues will introduce selectivity for *Pf*PDE α over both other *Pf*PDEs and the *h*PDEs. In a similar manner, targeting residues identified as being unique to *Pf*PDE β , γ and δ may offer a means by which selectivity toward each isozyme may be achieved.

Beghyn and co-workers designed a set of tadalafil analogues where the *N*-methyl group was replaced with benzyl-substituted pyrrolidine or piperidine rings. These substituents are thought to be oriented towards the periphery of the active site where they encounter residues unique to the *Pf*PDEs. While further assays are needed to confirm their ability to inhibit the *Pf*PDEs, these results are very positive and have encouraged design and synthesis work centred on a drug repurposing strategy.^{164,165}

Other means of gaining selectivity may be achieved through substitution from the 5-position of the guanine ring of cGMP and its related analogues to specifically target the R8 residue in the *Pf*PDEs (Table 2.5). As the R8 residue is unique to each *Pf*PDE, this

simplistic approach could provide the basis through which selectivity may be obtained. Notwithstanding that their inhibitory potency is unknown, the DeNinno compounds **77** and **78**, which have been extended from this 2-position, show promising results when docked into each of the *Pf*PDE models. The chlorobenzyl group at the 2-position of **77** appears to extend toward the unique serine residue in *Pf*PDE α . In the case of **78**, docking favours an interaction between the pyrimidinetrifluoro carboxylic acid moiety and the metal binding site within the enzyme. In addition, extending the molecule toward the unique tyrosine residue in each of the *Pf*PDEs should not be overlooked in a design strategy.

2.5 Using the molecular docking results to shape the synthetic strategy

In anticipation of the potential of the four *Pf*PDE isozymes as targets for antimalarial drug design, homology models have been constructed based on sequence data and homology to their human counterparts. Interestingly, the models show that the binding site topology of the *Pf*PDEs have a high resemblance to *h*PDE1 and the modelling work explains the cGMP selectivity observed with *Pf*PDE α . Docking of the reported *Pf*PDE α inhibitors zaprinast, E4021 and sildenafil, suggested plausible binding modes consistent with their relative potencies. The docking studies also support the pursuit of *h*PDE9 and *h*PDE1 inhibitors as starting points for the design of *Pf*PDE inhibitors.

It is envisaged that the homology modelling and docking studies undertaken may provide a useful tool for screening compound libraries, either diversity-based or developed from the large *h*PDE inhibitor pool. The generalised homology to *h*PDEs,

coupled with observable differences in the binding sites, might support the structure-based design of pan-*Pf*PDE inhibitors that select against human isoforms, or also potentially *Pf*PDE-isoform selective inhibitors.

Chapter 3

Human phosphodiesterase 9 and 1 inhibitors as antiplasmodial compounds

3.1 Introduction

In Chapter 2, a pathway for the identification of *Pf*PDE inhibitors was outlined. This work determined the enzymes as being most similar to *h*PDE9 and *h*PDE1 and as a consequence, inhibitors of these human enzymes should be investigated for their effects on *Plasmodium falciparum* growth. A series of *h*PDE9 and *h*PDE1 inhibitors, described by DeNinno and co-workers in 2009, were considered to be suitable candidates for further study.¹⁹⁹ In particular, the pyrazolopyrimidinone compound **77** (Figure 3.1) demonstrated a guanine-like binding pose when docked into the *Pf*PDE α homology model, resembling that of the endogenous ligand (cGMP). On this basis, the synthesis of a series of analogues in this class was pursued.

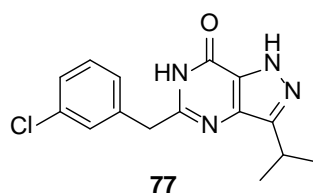


Figure 3.1. Structure of the *h*PDE9 and *h*PDE1 inhibitor, **77**, identified by DeNinno *et al.* that was investigated in molecular modelling work (Chapter 2).¹⁹⁹

As a class, the pyrazolopyrimidinones have long been associated with biological activity. Analogues were reported by Rose as far back as 1952, and in 1987 their close relationship to the purine structure saw them pursued as adenosine agonists.^{210,211} Formycin B (**79**) was investigated in the 1960s for its antibacterial activity and has since been examined in *Leishmania major* and *Trypanosoma brucei* parasite studies.²¹²⁻²¹⁴ More recently, the compound class has been utilised as *h*PDE inhibitors, and perhaps the most famous representative of the class is sildenafil (**71**), the *h*PDE5 inhibitor (Figure 3.2).

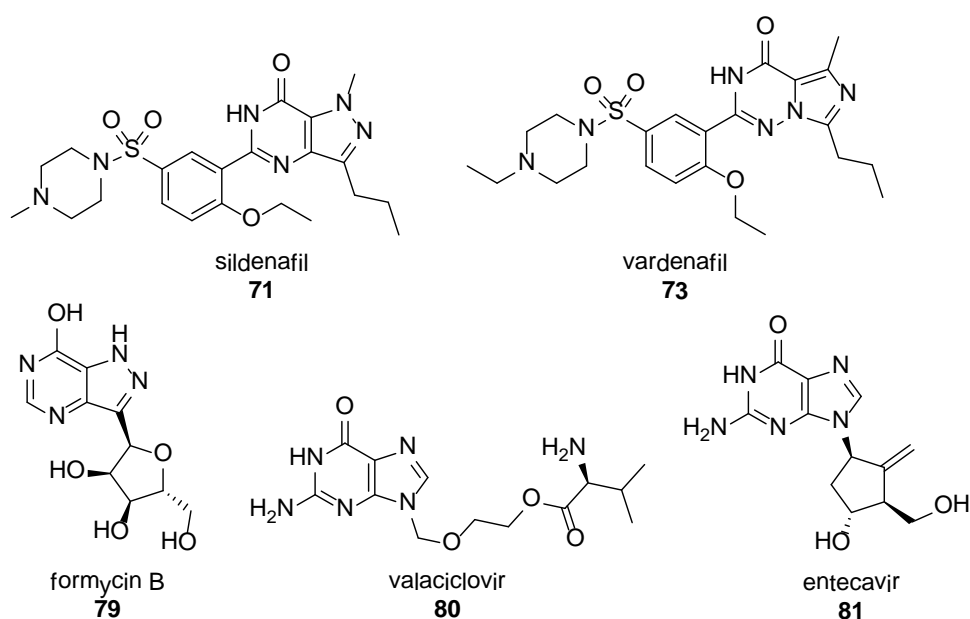


Figure 3.2. Structures of *h*PDE inhibitors that are representative of the guanine isostere family.

In many respects, the class can be included in a broader group of “guanine isosteres” that also include marketed drugs such as valaciclovir (**80**) (marketed as Valtrex[®]), entecavir (**81**) (marketed as Baraclude[®]), and vardenafil (**73**) (marketed as Levitra[®]) (Figure 3.2).^{215,216} In 2005, a review summarised other guanine isosteres that are represented in reported *h*PD_E inhibitor scaffolds (Figure 3.3).²¹⁷

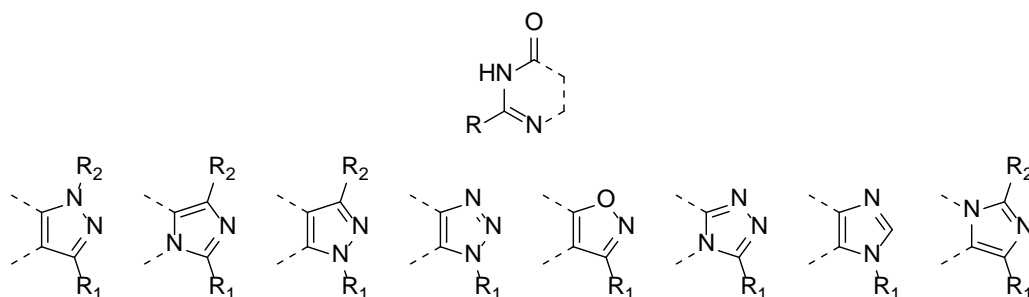
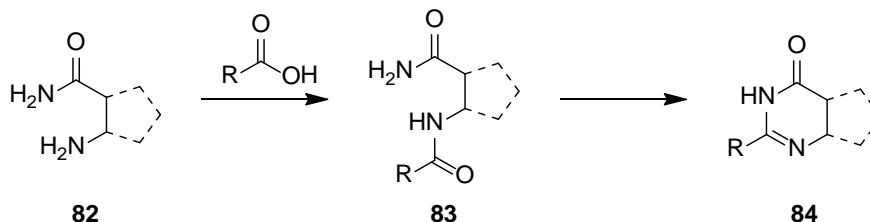


Figure 3.3. A summary of the guanine isosteres reported as *h*PD_E inhibitor scaffolds.²¹⁷

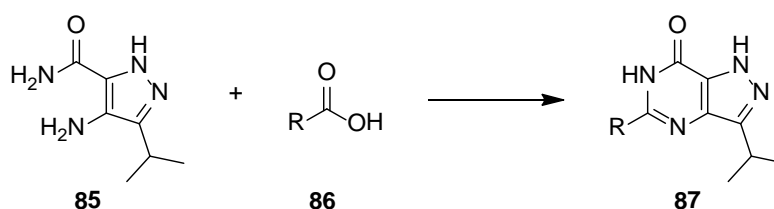
In the synthesis of most of these scaffolds, a key five-membered heterocycle with a primary amine is firstly synthesised (**82**). From here, analogues are generated through a coupling reaction of this amine with a carboxylic acid before a cyclisation of the diamide intermediate (**83**) to give the bicyclic core scaffold (**84**) (Scheme 3.4).



Scheme 3.4. General synthesis of guanine isosteres (**84**) from a key heterocyclic core (**82**).

Compound **77** and various analogues described by DeNinno *et al.* were prepared in this way (adapted from the reported synthesis of sildenafil by Terrett *et al.*²¹⁸). Condensation

reactions of a key pyrazole precursor (**85**) with a range of substituted carboxylic acids (**86**) was achieved by DeNinno *et al.* using a parallel synthesis protocol and afforded 20 substituted pyrazolopyrimidinone compounds (**87**) (Scheme 3.5).



Scheme 3.5. General reaction scheme of the condensation of a key pyrazole precursor (**85**) with various carboxylic acids (**86**) to give substituted pyrazolopyrimidinone compounds (**87**).

For the purpose of this work, the synthesis of 5-(3-chlorobenzyl)-3-isopropyl-1*H*-pyrazolo[4,3-*d*]pyrimidin-7(6*H*)-one (**77**) was the initial starting point, however, it was envisaged that analogues of **77** could be synthesised through variation of the benzyl substituent (electron-donating/withdrawing, steric effects), the position of the substituent on the aromatic ring (*ortho*-, *meta*-, *para*-substitutions), and the linker length between the core scaffold and the aromatic moiety (methylene, ethylene). In addition, it was envisaged that *N*¹-alkylation, replacement of the 9-isopropyl group with alternate moieties, and other guanine isostere analogues, may be obtained through variation of the scaffold of **77** (Figure 3.6).

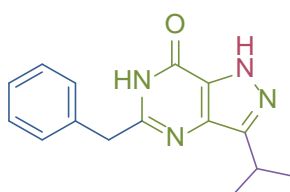


Figure 3.6. The envisaged derivatisations in the syntheses of pyrazolopyrimidinone analogues; modification to the benzyl substituent in blue, modification to the core bicyclic system in green, modification to the 9-isopropyl group in purple, modification to the endocyclic *N*¹ in pink.

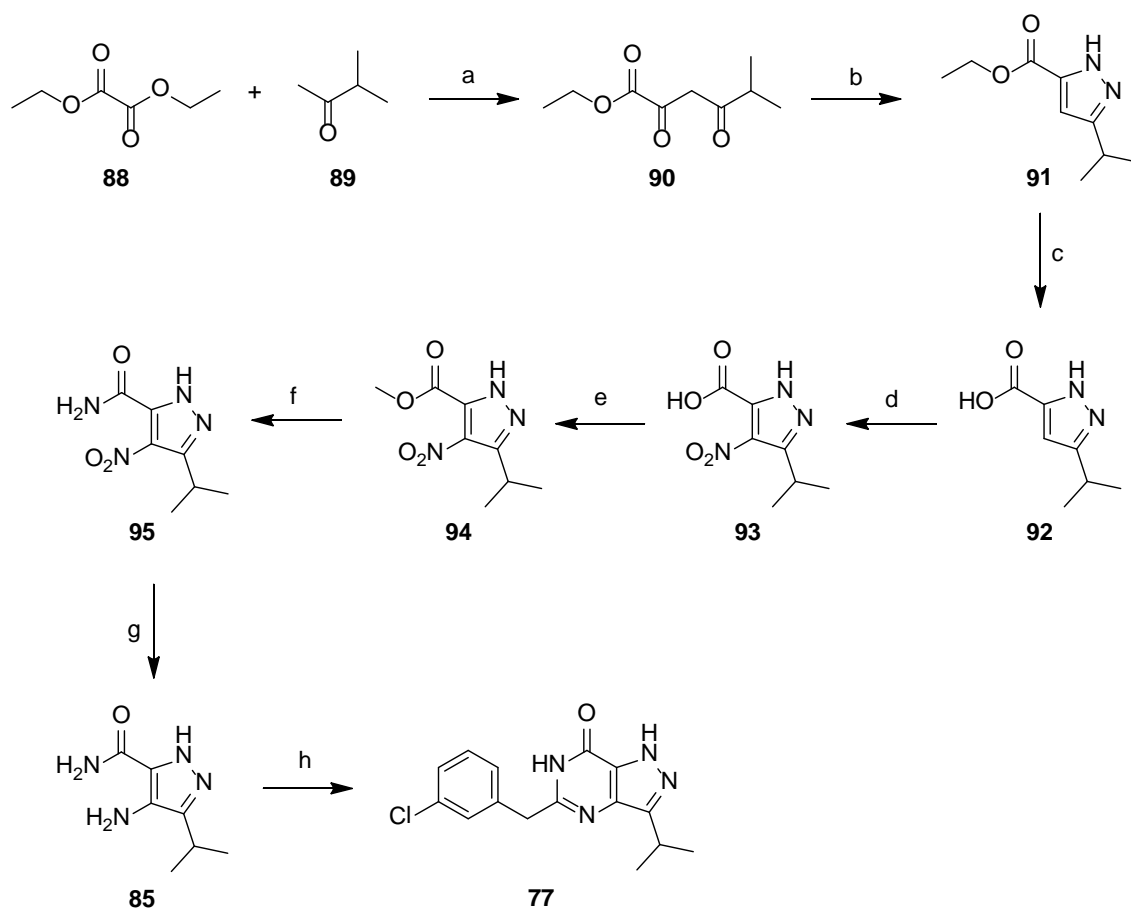
In the absence of *Pf*PDE enzymatic assays, it was thought that the compounds will be assessed for antiparasmodial activity *via* testing in whole *P. falciparum* parasite assays. It was recognised that activity in this whole cell assay may be due to non-*Pf*PDE related mechanisms however, active antiparasmodial compounds may arise from this work that would also be of interest. Such active compounds to emerge from this work may also have the capacity to identify the roles played by PDEs in *P. falciparum* parasite signalling.

3.2 Synthesis of 5-(3-chlorobenzyl)-3-isopropyl-1*H*-pyrazolo[4,3-*d*]pyrimidin-7(6*H*)-one

The synthesis of compound **77** was achieved by an adaptation of the procedure described by DeNinno *et al.* (Scheme 3.7).¹⁹⁹ While the key intermediate (**85**) is commercially available, it was considered useful to establish the synthetic route so that potential analogues, for example through changes at the 9-isopropyl group, could be considered. The nine step synthesis was successfully achieved, albeit with some revisions as detailed here. Characterisation data of the intermediates and final product were consistent with that previously described.¹⁹⁹

In the first step, diethyloxalate (**88**) underwent a Claisen-Schmidt condensation with the enolate anion of 3-methyl-2-butanone (**89**) to afford ethyl-5-methyl-2,4-dioxohexanoate (**90**) in 98% yield. Treatment of **90** with hydrazine hydrate in ethanol gave the cyclised pyrazole ethyl ester (**91**) in 64% yield. The ¹H NMR spectrum showed an aromatic proton at δ 6.17 ppm consistent with the single proton of the pyrazole ring in **91**, as well as the signals associated with the ethyl ester and isopropyl group which are well-defined

in the ^1H NMR spectrum.¹⁹⁹ The ester of **91** was hydrolysed under basic conditions to give the corresponding carboxylic acid (**92**) in 74% yield. No purification steps were necessary throughout this sequence with **92** obtained in >95% purity as determined by ^1H NMR spectroscopy and analytical RP-HPLC. Using literature procedures, the nitration of **92** was achieved in 30% yield in comparison to the literature report of 70%.¹⁹⁹ Analytical RP-HPLC showed significant conversion of **92** to **93** after 1 hour, but difficulties in isolation limited the yield.

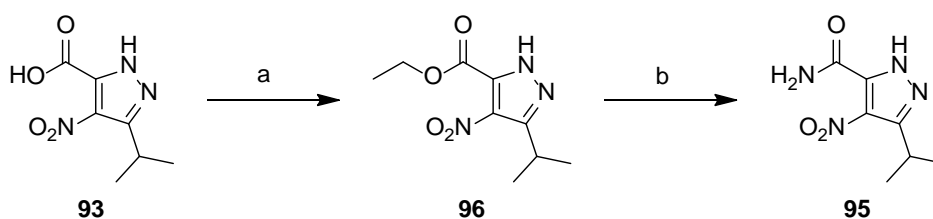


Scheme 3.7. Synthesis of the key pyrazole precursor (**85**) adapted from the procedure of DeNinno *et al.*¹⁹⁹ and the subsequent synthesis of the target compound (**77**). (a) $\text{Na}_{(\text{s})}$, $\text{CH}_3\text{CH}_2\text{OH}$, N_2 , rt, 1 h, then 60°C , 1 h, 98%; (b) $\text{NH}_2\text{NH}_2\cdot\text{H}_2\text{O}$, $\text{CH}_3\text{CH}_2\text{OH}$, N_2 , rt, 18 h, then $\text{NH}_2\text{NH}_2\cdot\text{H}_2\text{O}$, 60°C , 3 h, 64%; (c) 1 M aq. NaOH , 1,4-dioxane, 50°C , 1 h, 74%; (d) conc. H_2SO_4 , 70% aq. HNO_3 , 60°C , 1 h, 30%; (e) conc. H_2SO_4 , CH_3OH , 55°C , 16 h, 66%; (f) Mg_3N_2 , CH_3OH , 0°C to 80°C , 24 h, 88%; (g) Pd/C , H_2 , $\text{CH}_3\text{CH}_2\text{OH}$, rt, 20 h, 68%; (h) PyBroP , DCE , MW, 120°C , 20 min, then $i\text{BuOK}$, $i\text{PrOH}$, MW, 130°C , 40 min, 63%.

The conversion of the carboxylic acid (**93**) to the corresponding amide (**95**) proved surprisingly challenging, although difficulties in achieving this deceptively simple transformation had been reported by others.²¹⁹ In the procedure of DeNinno *et al.*, the acid (**93**) was firstly converted to the corresponding acid chloride intermediate through treatment with oxalyl chloride, and was then successively treated with gaseous ammonia to afford **95** in 60% yield.¹⁹⁹ The reaction work-up involved several steps, which may account for some loss of product. Attempts following this procedure failed to give useful yields and/or quantities of product, which was compounded by the laboratory being ill-equipped for the convenient and safe handling of ammonia gas.

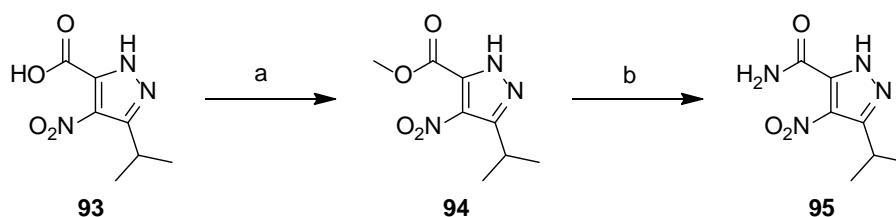
As a consequence, alternative methods for the conversion of **93** to **95** were explored. Treatment of the acid chloride with aqueous ammonia gave **95** in 22% yield. The ¹H NMR spectrum of **95** displayed a broad singlet at δ 8.21 ppm, characteristic of amide protons.¹⁹⁹ While modestly successful, substituting gaseous ammonia for aqueous ammonia results in competing formation of carboxylic acid starting material (**93**). In addition, several repeats of the experimental conditions with aqueous ammonia gave inconsistent results.

As another alternative, the reported aminolysis of the ethyl ester was examined (Scheme 3.8).²²⁰ The carboxylic acid (**93**) was converted to the ethyl ester (**96**) and then treated with ammonium hydroxide at 100 °C for 2 hours.²²⁰ After this time, LCMS analysis showed approximately 15% conversion to the desired amide (**95**) ([M-H]⁺ molecular ion at m/z 197.3) but the remainder was the carboxylic acid (**93**) ([M-H]⁺ molecular ion at m/z 198.2).



Scheme 3.8. Conversion of the carboxylic acid (**93**) to the corresponding amide (**95**) via the ethyl ester intermediate (**96**), adapted from Robins *et al.*²²⁰ (a) conc. H₂SO₄, CH₃CH₂OH, toluene, 78 °C, 24 h, 92%; (b) conc. NH₄OH, 100 °C, 2 h, unisolated.

With competing hydrolysis under aqueous conditions posing a significant problem, the use of anhydrous conditions appeared important. Ley and co-workers investigated the possibility of ammonia gas evolution upon reaction of magnesium nitride with protic solvents.^{219,221} Ironically, the group embarked on the investigation due to noted difficulties in the synthesis of the *h*PDE5 inhibitor, sildenafil. Following these procedures, the carboxylic acid (**93**) was first converted to the methyl ester (**94**) in 66% yield (Scheme 3.9).²²¹ Compound **94** was subsequently treated with magnesium nitride in methanol at 0 °C. The vial was immediately sealed and the reaction warmed to room temperature before stirring was continued at 80 °C for 24 hours. After work-up, the amide (**95**) was afforded in 88% yield and high purity. The identity of **95** was confirmed with the [M-H]⁺ molecular ion at *m/z* 197.3 and a characteristic amide signal in the ¹H NMR spectrum at δ 8.21 ppm, consistent with the reported data.¹⁹⁹



Scheme 3.9. Conversion of the carboxylic acid (**93**) to the corresponding amide (**95**) via the methyl ester intermediate (**94**), adapted from Bridgwood *et al.*²²¹ (a) conc. H₂SO₄, CH₃OH, 55 °C, 16 h; 66%; (b) Mg₃N₂, CH₃OH, 0 °C to 80 °C, 24 h, 88%.

While this procedure worked well on a small scale (100 mg), difficulties were encountered on scale-up due to the reactivity of magnesium nitride. When using larger vials, the internal pressure build-up was a concern, so multiple small-scale reactions were run in parallel to generate useful amounts of material.

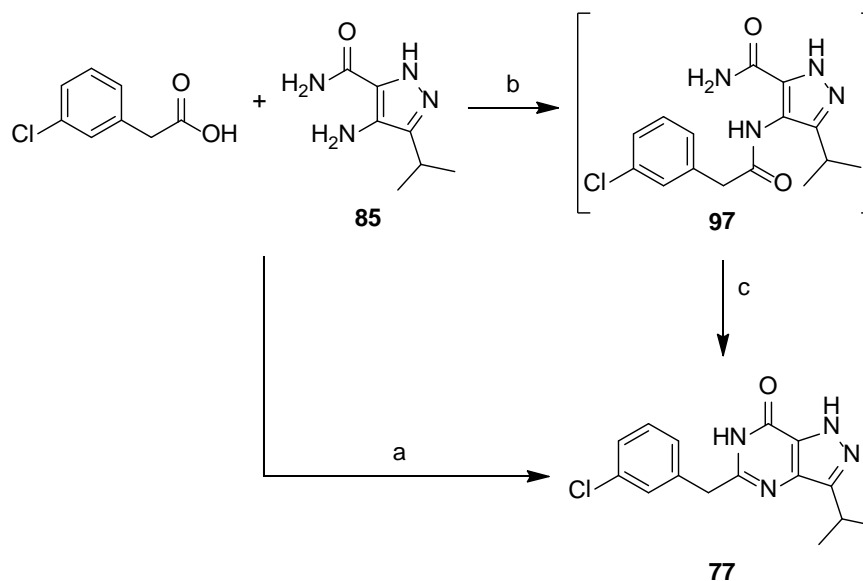
Resuming the pathway of Scheme 3.7, the nitro group of **95** was reduced to the primary amine of **85** in 68% yield. The identity of **85** was confirmed by ^1H NMR and ^{13}C NMR spectra and the $[\text{M}-\text{H}]^+$ molecular ion of m/z 167.2, all of which were consistent with reported values.^{199,222} This key intermediate, **85**, was also found to be identical to a purchased commercial sample (Fluorochem, UK).

The final steps in the synthesis of **77** were the amide coupling of **85** with *m*-chlorophenylacetic acid to afford the amide, followed by a subsequent cyclisation reaction. DeNinno *et al.* performed the amide coupling by activating phenylacetic acid using carbonyldiimidazole in pyridine for 2 hours, which then coupled to the primary amine of **85**. Base-catalysed cyclisation was achieved with potassium *t*-butoxide.¹⁹⁹

An alternative amide coupling reagent, 1*H*-benzotriazolium-1-[*bis*(dimethylamino)-methylene]-5-chloro-hexafluorophosphate-(1-),3-oxide (HCTU), was investigated principally due to its rapid reactivity but also ready availability in-house. Firstly, *m*-chlorophenylacetic acid was treated with four equivalents of HCTU and a mild base, diisopropylamine (DIPA), in dimethylformamide at room temperature for 20 minutes. Following this activation of the carboxylic acid, **85** in dimethylformamide was added to the reaction mixture. The reaction was monitored by LCMS analysis and the amide-

coupled intermediate (**97**) was detectable (Scheme 3.10). Some conversion to the fully cyclised product (**77**) was observed after 24 hours. Compound **77** was recovered in 12% yield following purification by column chromatography. Its identity was confirmed through ^1H NMR and ^{13}C NMR spectra, which corresponded well to that reported by DeNinno *et al.*¹⁹⁹ Although compound **77** was previously reported in the literature and the ^1H NMR spectroscopic data was consistent with those reports,¹⁹⁹ the acquired ^{13}C NMR spectrum showed either very weak or no signals for the quaternary carbons of the pyrazolo[4,3-*d*]pyrimidinone rings. While the seven carbons of the *m*-chlorobenzyl substituent were all evident as were the isopropyl carbons, it is possible to see only small and broad signals that are tentatively attributed to the remaining carbons. Varying the NMR solvent did not strengthen these signals. In part, this might be attributed to tautomerism of the ring systems.

Bromo-*tris*-pyrrolidino-phosphonium hexafluorophosphate (PyBroP) was examined as an alternative amide coupling reagent, as was the use of microwave heating. As such, treatment of **85** with PyBroP and triethylamine in 1,2-dichloroethane at 120 °C for 20 minutes with the use of microwave heating showed complete conversion to the amide-coupled intermediate (**97**) (Scheme 3.10). Phosphoramidate and pyrrolidine by-products were removed from the reaction mixture with a short silica plug eluting with ethyl acetate, leaving **97** in good purity as determined by analytical RP-HPLC.



Scheme 3.10. Synthesis of **77** (via **97**) using amide coupling conditions. (a) HCTU, DIPA, DMF, rt, 20 min, then **85** in DMF, rt, 24 h, 12%. (b) PyBroP, DCE, MW, 120 °C, 20 min; (c) *t*BuOK, *i*PrOH, MW, 130 °C, 40 min, 63%.

The intermediate, **97**, was then dissolved in isopropanol and reacted with potassium *t*-butoxide using microwave heating at 130 °C for 40 minutes. Complete conversion to the cyclised pyrazolopyrimidinone (**77**) had occurred as determined by LCMS analysis. After column chromatography, **77** was obtained in 63% yield over the two steps. The use of PyBroP for the coupling reaction and the isolation of the amide-coupled intermediate gave a marked improvement on the previous reaction conditions employing HCTU. Similar PyBroP coupling conditions in the syntheses of analogues of this compound class were later published by Wang *et al.* in 2012.¹⁶⁸

In summary, the nine-step synthesis of (2-(3-chlorobenzyl)-1H-pyrazolo[4,3-d]pyrimidin-7(6H)-one (**77**) had been completed, with some revisions from the synthesis of DeNinno *et al.*¹⁹⁹ In particular, the use of magnesium nitride as an ammonia source was very successful, although further optimisation of the conditions would be required to scale-up the synthetic route for bulk syntheses (e.g. high pressure-

safe reaction vessels). Herein, the amounts retrieved were suitable for the synthesis of a small library of analogues as follows.

3.3 Synthesis of a focussed pyrazolopyrimidinone library

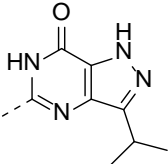
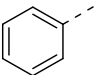
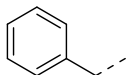
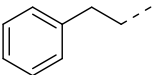
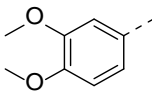
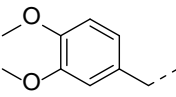
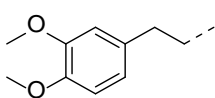
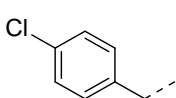
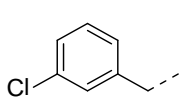
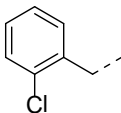
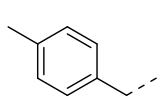
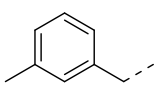
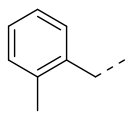
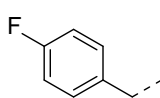
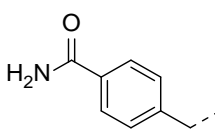
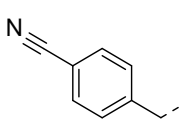
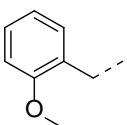
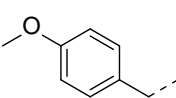
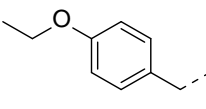
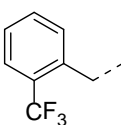
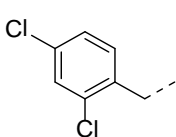
Synthesis of the pyrazolopyrimidinone compounds (**98-116**, Table 3.11) by reaction of the key intermediate (**85**) and a range of carboxylic acids was carried out in the manner described in section 3.2 and proceeded smoothly in most cases. The predicted physicochemical properties of the analogues were monitored to ensure the maintenance of drug-like properties (Appendix 3).

When *p*-cyanophenylacetic acid was coupled to **85**, both the target *p*-cyanobenzyl analogue (**111**) and a *p*-carboxamide analogue (**110**) were obtained. Under aqueous basic conditions, nitrile groups can undergo base-catalysed hydrolysis to the corresponding amide.²²³ It is possible that water in the solvent (most probably tetrahydrofuran) together with potassium *t*-butoxide resulted in nitrile hydrolysis to the corresponding carboxamide (**110**).

The isolated yields of these compounds varied from 10-77% with no apparent relationship between the nature of the product and its yield. Signals within the ¹H NMR spectra were consistent with the expected chemical shifts and splittings, although the chemical shift of the methylene protons in substituted benzyl analogues showed considerable variation. For example, the methylene signal of the *m*-chlorobenzyl analogue (**77**) resides at δ 4.56 ppm, while the methylene signal of the *p*-fluorobenzyl

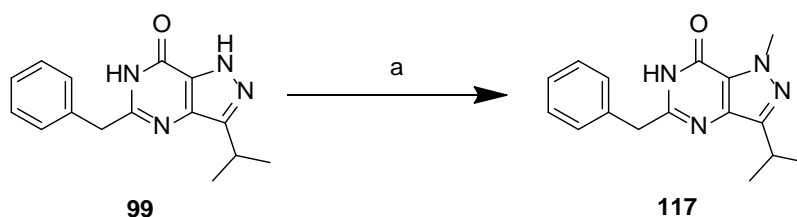
analogue (**109**) resides at δ 3.35 ppm, which highlights the different electronic effects of the various substituents. The 9-isopropyl protons appear at consistent chemical shifts within the ^1H NMR spectra. The ^{13}C NMR spectra were comparable to that observed with **77**, that is, the quaternary carbons of the pyrazolo[4,3-*d*]pyrimidinone core often did not appear as defined signals within the spectra. Each of the compounds displayed parent adducts in the positive ion mass spectrum except for **102**. In this instance, the $[\text{M}-\text{H}]^+$ molecular ion could be detected in the negative ion mass spectrum.

Table 3.11. Structures of synthesised pyrazolopyrimidinone analogues (**77**, **98-116**).

				
				
98	99	100	101	102
				
103	104	77	105	106
				
107	108	109	110	111
				
112	113	114	115	116

3.4 Synthesis of 5-benzyl-3-isopropyl-1-methyl-1*H*-pyrazolo[4,3-*d*]pyrimidin-7(6*H*)-one

The *N*¹-methyl-substituted analogue of compound **99** was prepared to investigate the influence of such a substitution on antiparasmodial activity. 5-Benzyl-3-isopropyl-1-methyl-1*H*-pyrazolo[4,3-*d*]pyrimidin-7(6*H*)-one (**99**) was methylated on the endocyclic *N*¹-position with dimethylsulfate according to the procedure described by Kankan and Rao to afford **117** in 63% yield after column chromatography (Scheme 3.12).²²⁴ The identity of **117** was confirmed through ¹H NMR and ¹³C NMR spectroscopy, and the [M+H]⁺ molecular ion at *m/z* 283.2.



Scheme 3.12. Synthesis of 5-benzyl-3-isopropyl-1-methyl-1*H*-pyrazolo[4,3-*d*]pyrimidin-7(6*H*)-one (**117**) from **99**. (a) (CH₃O)₂SO₂, CH₃C(O)CH₃, 60 °C, 16 h, 63%.

3.5 Biological assessment of the synthesised pyrazolopyrimidinones

The objective of the biological studies of the pyrazolopyrimidinone compounds was to determine if they had the ability to inhibit *P. falciparum* growth. As with many similar campaigns, achieving a threshold level of activity would be the measure of success and justify the further pursuit of this class of compounds. As described in Chapter 1, the mass screens of GSK and Novartis identified IC₅₀ values of 1 μM as their benchmark. Secondly though, it was hoped that some separation in the antiparasmodial activity from *h*PDDE activity would be observed.

3.5.1 *Plasmodium falciparum* growth inhibition

The synthesised pyrazolopyrimidinone compounds described above (**77**, **98-117**), were tested for antiplasmodial activity through a measurement of whole parasite growth inhibition. This assay is the same as that employed in the 2009 GSK malaria screen by Gamo *et al.*¹⁵⁴ The *P. falciparum* parasite strains employed in the assays were 3D7 (chloroquine-sensitive) parasites. Parasite strains were cultured using standard procedures as previously described by Trager and Jensen and were synchronised to the schizont stage for the assay.²²⁵ *P. falciparum* growth inhibition was assessed using the lactate dehydrogenase (LDH) assay described by Gamo *et al.*¹⁵⁴ In brief, the parasites were firstly cultured in red blood cells to reach a level of 0.1% parasitaemia. This was typically over a period of 48 hours. The suspensions of parasites in red blood cells were then treated with test compound or dimethylsulfoxide (DMSO) vehicle and then incubated for 72 hours. The treated parasites were put through a freeze/thaw cycle for 4 hours in order to lyse the cells. The lysates were then treated with Malstat reagent which contains the substrate, lactic acid, and 3-acetylpyridine adenine dinucleotide (APAD), a *Pf*-LDH specific cofactor.²²⁶ With the turnover of the enzyme, APAD-H is produced which reacts with the other reagent of the assay, nitro blue tetrazolium, under phenazine methosulfate catalysis to produce an insoluble formazan dye. The colour thus develops as a function of LDH activity which is a surrogate for the number of live parasites in the well, and therefore inversely proportional to the effectiveness of the antiplasmodial compound.²²⁷

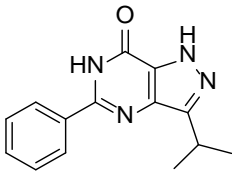
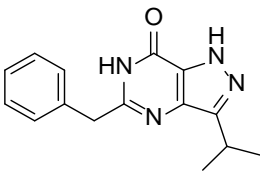
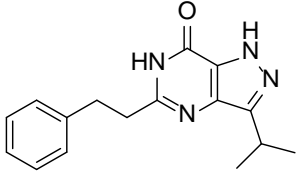
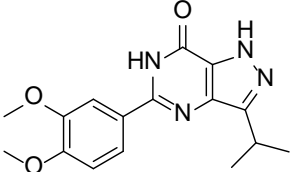
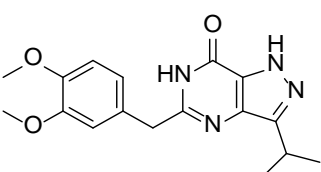
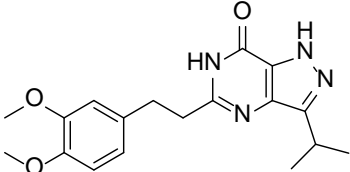
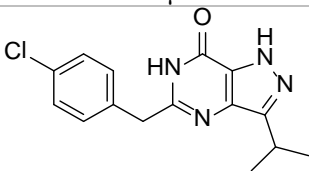
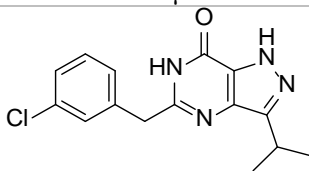
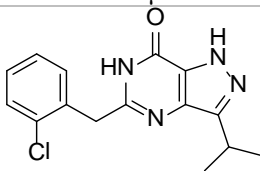
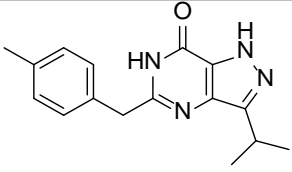
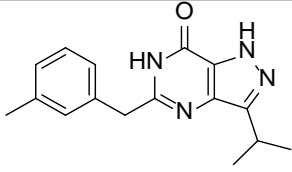
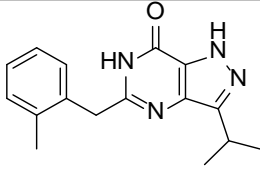
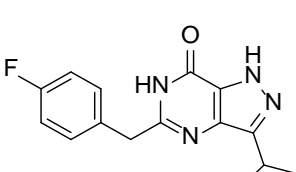
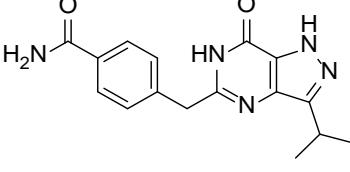
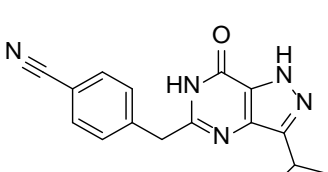
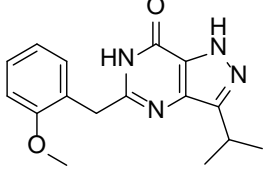
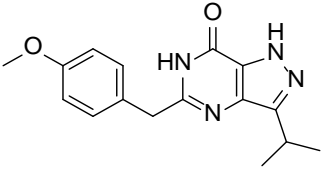
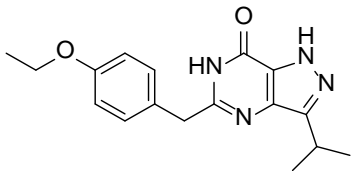
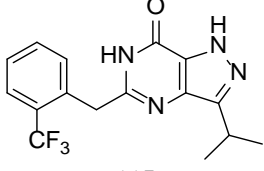
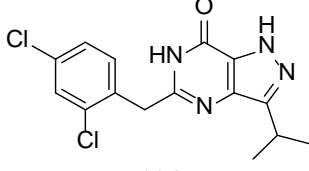
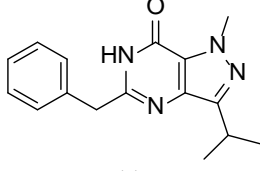
The initial procedure needed some adaptation. It was determined that 30 μ L of parasite sample and 75 μ L of Malstat reagent gave consistent absorbance readings. Each compound was initially assessed for growth inhibition at final concentrations of

100 μM , 33.3 μM , 11.1 μM , 3.7 μM , 1.23 μM and 0.41 μM . Where necessary, individual compounds were further assessed at concentrations three-fold above and three-fold below the approximate IC_{50} value in order to obtain full dose-response curves (performed in triplicate). Zaprinast was employed as a control within the assay, and its antiplasmodial activity was comparable to that observed within the literature.¹⁶

Under these conditions, the intra-assay variability was quite low indicating good precision in the assay format. However, the IC_{50} values were found to vary up to ten-fold from one assay to another. This seems likely to be a result of variations at the level of the parasite culture. These variations from one assay to another include that the parasites may be synchronised at slightly different life-cycle stages, the parasites may vary in health, and the red blood cell population may influence the state of the parasites. There may also be systematic variation in the colorimetric assay, for example, extended exposure to light may influence assay development. Although this variability is undesirable, it is consistent with data seen in the literature, where IC_{50} values for compounds tested in whole parasite assays vary from laboratory to laboratory.

The IC_{50} value ranges determined for the test compounds as *P. falciparum* growth inhibitors against the 3D7 parasite strain are shown in Table 3.13. Within the assay, zaprinast inhibited *P. falciparum* growth with an IC_{50} value of 22-124 μM . Given that 10-fold variations in IC_{50} values were observed within the assays, the antiplasmodial activity of zaprinast can be considered consistent with literature reports.¹⁶ The dose-response curves of compounds **99** and **105** are shown in Figure 3.14, while the remainder are provided in Appendix 5.

Table 3.13. Determined IC₅₀ value ranges of the synthesised pyrazolopyrimidinones for *P. falciparum* (3D7) growth inhibition.

 <p>98 3.7-10.4 μM</p>	 <p>99 0.08-0.72 μM</p>	 <p>100 1.6-2.7 μM</p>
 <p>101 >100 μM</p>	 <p>102 33-92 μM</p>	 <p>103 27-54 μM</p>
 <p>104 0.26-1.7 μM</p>	 <p>77 16- >100 μM</p>	 <p>105 0.06-0.97 μM</p>
 <p>106 3.3-6.6 μM</p>	 <p>107 2.0-4.6 μM</p>	 <p>108 0.64-1.2 μM</p>
 <p>109 0.22-1.5 μM</p>	 <p>110 2.0-3.3 μM</p>	 <p>111 8.0-9.7 μM</p>
 <p>112 >100 μM</p>	 <p>113 3.2-4.7 μM</p>	 <p>114 2.4-5.3 μM</p>
 <p>115 0.61-0.84 μM</p>	 <p>116 5.0-7.2 μM</p>	 <p>117 >100 μM</p>

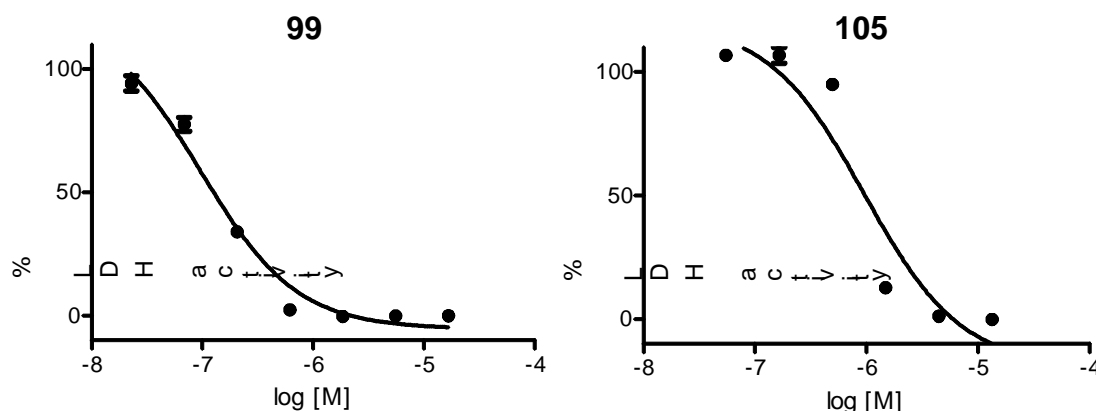


Figure 3.14. IC₅₀ curves of compounds **99** and **105** against *P. falciparum* growth. Each value represents the mean of duplicate determinations where each replicate was within 4% of the mean value.

Of the 21 compounds assessed here, six compounds (**99**, **104**, **105**, **108**, **109**, **115**) showed activity below or near an IC₅₀ value of 1 μ M, eleven compounds (**98**, **100**, **102**, **103**, **106**, **107**, **110**, **111**, **113**, **114**, **116**) showed intermediate activity, and the remaining compounds (**101**, **77**, **112**, **117**) displayed poor activity. Despite the shortcomings of the assay in terms of IC₅₀ variability, it should be noted that the general trends in compound activities were consistent. In other words, the rank order of potencies was conserved between experiments. The variability does mean however, that the data lacks the granularity to decipher some potentially useful structure-activity information. Having said this, some valuable insights could be gained and are discussed in more detail below.

Firstly, many of the *para*-benzyl-substituted compounds, such as **99**, are good inhibitors, including the *p*-chloro (**104**), *p*-methyl (**106**), *p*-fluoro (**109**), and *p*-carboxamide (**110**) compounds. The *p*-cyano (**111**) and *p*-methoxy (**113**) compounds are somewhat less active. *Ortho*-substituted analogues also perform well, such as the *o*-

chloro (**105**), *o*-methyl (**108**) and *o*-trifluoromethyl (**115**) compounds. The two *meta*-benzyl examples, including the target compound, *m*-chloro (**77**), as well as the *m*-methyl compound (**107**), are of poor and moderate potency, respectively. Other more bulky substitutions such as catechol ethers compounds (**101-103**) and the 2,4-dichloro compound (**116**) are less active. The *N*¹-methyl compound (**117**) was inactive in the assay, showing the importance of the endocyclic nitrogen in **99**.

3.5.2 Human phosphodiesterase inhibition

After examining the results of the LDH *P. falciparum* growth inhibition assay, compounds **99** and **105** were selected for assessment of human PDE inhibition. While the *m*-chloro analogue (**77**) has been shown to inhibit *hPDE9* and *hPDE1*, there have been no reports of the activity of the other synthesised compounds against these or other *hPDE* isoforms. The enzymatic assays were conducted externally under contract. The compounds were first screened at 1 μ M concentration for inhibition of *hPDE1-11*, and the results are shown in Figure 3.15. Both compounds showed a preference for *hPDE9*, as well as *hPDE5*, *hPDE6* and *hPDE1*. Compound **99** was a more potent inhibitor of the *hPDE* isoforms than **105** in this screening assay.

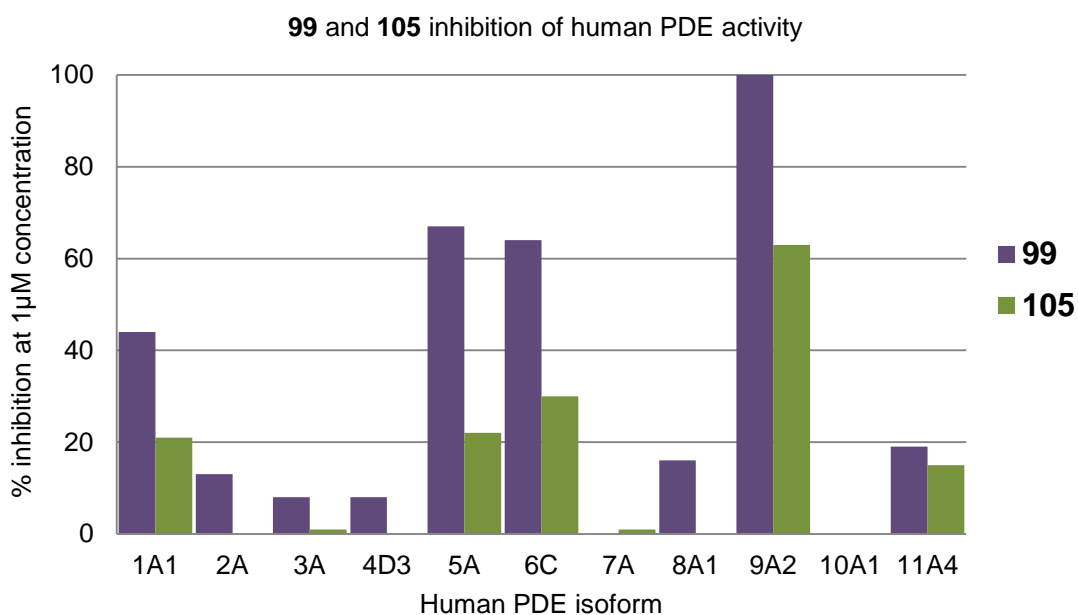


Figure 3.15. Percentage inhibition of human PDE activity of compounds **99** and **105** at 1 μ M concentration. Each value represents the mean of duplicate determinations where each replicate was within 7% of the mean value.

Following this, further assays were conducted to determine the IC_{50} values of the compounds *versus* *hPDE9*. Compound **99** was a very potent inhibitor of *hPDE9* with an IC_{50} value of 29 nM, while **105** showed an IC_{50} of 1.8 μ M. It should be noted that against *hPDE9*, **77** has a reported IC_{50} value of 10 nM and zaprinast has an IC_{50} value of 29-46 μ M (Table 3.16).¹⁹² In summary, the results show the capacity of the inhibitors to retain antiparasmodial activity while the strongest activity against the human form of the enzyme was reduced.

Table 3.16. Human PDE9 IC_{50} values of zaprinast and selected pyrazolopyrimidinone analogues.

Compound	<i>hPDE9</i> IC_{50} (μ M)	<i>Pf</i> inhibition (μ M)
Zaprinast	29-46	124
77	0.01 ¹⁹⁹	16- >100
99	0.03	0.08-0.72
105	1.80	0.06-0.97

3.6 Docking studies of the synthesised pyrazolopyrimidinone compounds

As well as uncovering active “hits,” this work has provided the basis for building structure-activity data and also the possibility of refining the developed *Pf*PDE models. While it is not certain that these compounds inhibit the *Pf*PDEs, or if so which isoform(s), the possibility still remains. With the *Pf*PDE models from Chapter 2 in hand, each of the 21 pyrazolopyrimidinone compounds was docked to examine any potential relationship between *in silico* *Pf*PDE docking scores and parasite inhibition.

The *para*-substituted benzyl analogues, which were generally more active compounds, all docked readily into the *Pf*PDE α model and favoured the guanine-like binding mode of cGMP (Figure 3.17). These docked analogues all make two hydrogen bond contacts to the purine-scanning glutamine residue, which is considered a hallmark feature of substrate and inhibitor binding.

An aromatic π -stacking interaction with the hydrophobic clamp is also observed. Viewing the surface of the *Pf*PDE α model with the pyrazolopyrimidinone compounds docked perhaps provides the best depiction of how the ligands sit within the binding cavity (Figure 3.17). In each case, the benzyl substituent points toward the external surface of the enzyme, although the substituents make no obvious direct interaction with the enzyme.

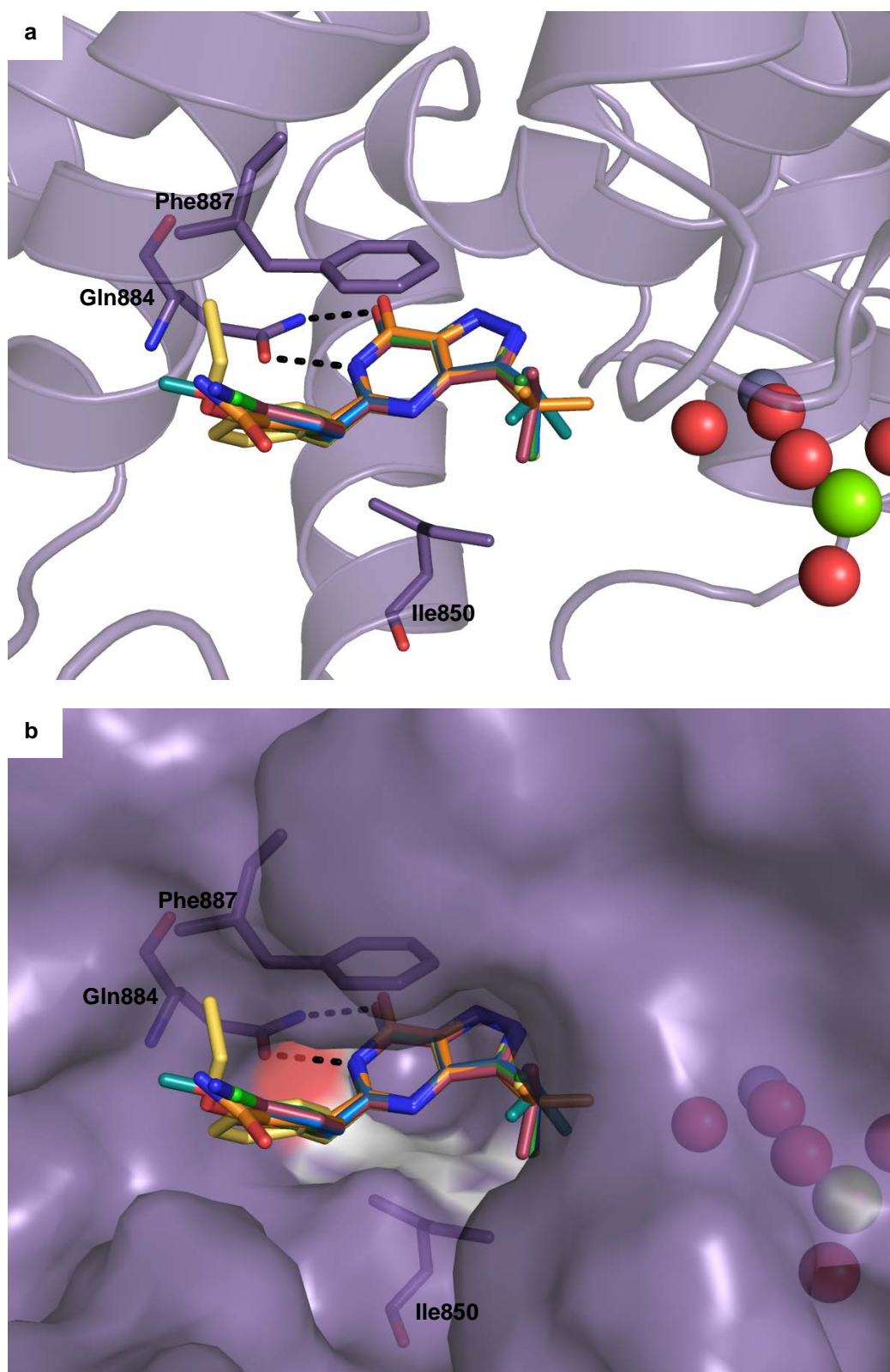


Figure 3.17. Docked poses of *para*-substituted pyrazolopyrimidinone compounds (**104**, **106**, **109-111**, **113**, **114**) into the *PfPDEα* model. (a) *PfPDEα* model is shown as helices; (b) *PfPDEα* model is shown as a rendered surface. Hydrogen bonds are shown as dashed lines. Purine-scanning glutamine (Gln884) and hydrophobic clamp residues (Phe887 and Ile850) are shown as purple sticks. Numbering is taken from the *PfPDEα* sequence. Water molecules and ions are shown as spheres.

The length of the aryl pendant group has a significant impact on activity, as in the case of the unsubstituted aryl compounds, **98**, **99** and **100**. The benzyl-substituted compound (**99**) is most active but when docked into the *Pf*PDE α model, the less active phenethyl compound (**100**) showed no great change in binding mode in comparison to the benzyl compound (**99**). The phenyl compound (**98**), which is equipotent to **100**, showed a 90° rotation in the plane of the binding site (Figure 3.18).

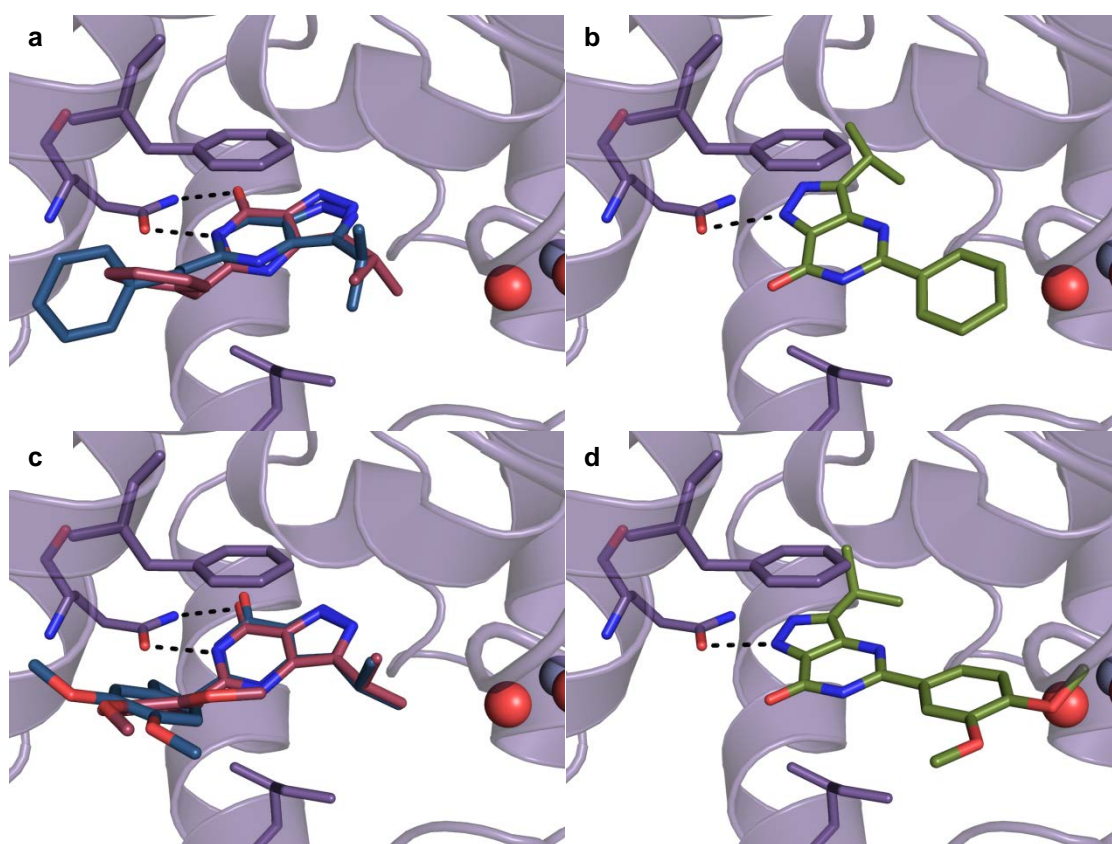


Figure 3.18. (a) Docked poses of compounds **99** (pink) and **100** (blue); (b) **98** (green); (c) **102** (pink) and **103** (blue); (d) **101** (green) into the *Pf*PDE α model. Hydrogen bonds are shown as dashed lines. Purine-scanning glutamine (Gln884) and hydrophobic clamp residues (Phe887 and Ile850) are shown as purple sticks. Numbering is taken from the *Pf*PDE α sequence. Water molecules and ions are shown as spheres.

When the catechol ether compounds, **101**, **102** and **103**, were docked into the *Pf*PDE α model, the docking results were identical to that observed in the unsubstituted cases above, although these compounds were significantly less active (Figure 3.18).

Interestingly, some solutions from the docking of **101-103** showed poses of the catechol ether where hydrogen bonding occurs between the methoxy substituents and the purine-scanning glutamine residue. A similar binding mode is observed in *h*PDE structures co-crystallised with catechol ether-containing PDE inhibitors, such as rolipram (PDB: 1XMY) and roflumilast (1XMU),¹⁸⁵ and this common structural moiety is explored in greater detail in Chapters 4 and 5.

Unfortunately, the *Pf*PDE homology models are unable to account for the differences in the observed activity of *ortho*-, *meta*- and *para*-substituents. In both of the series explored, the chloro-substituents (**104**, **77** and **105**) and methyl-substituents (**106**, **107**, **108**), the docked poses gave no insight as to why different biological activities are observed (Figure 3.19).

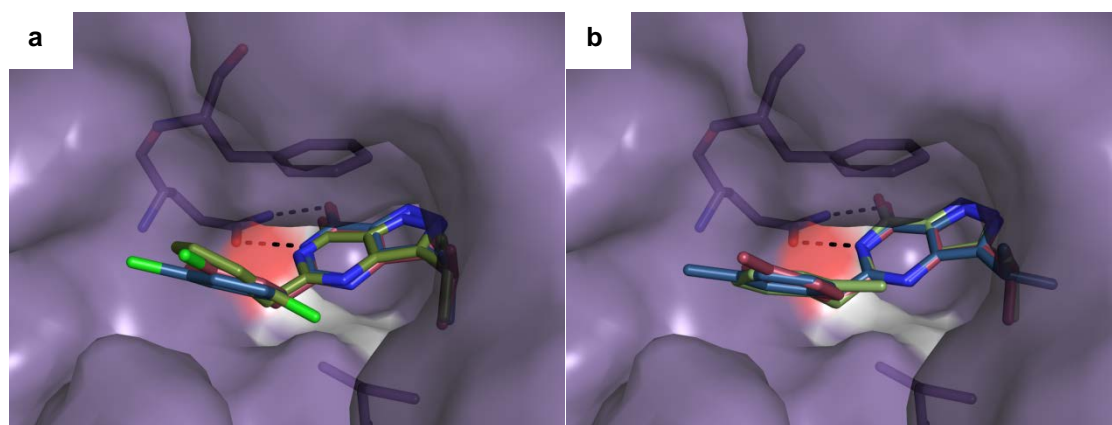


Figure 3.19. Docked poses of *ortho*-, *meta*- and *para*-substituents into the *Pf*PDE α model. (a) chlorobenzyl analogues **105** (green), **77** (blue), **104** (red); (b) methylbenzyl analogues **108** (green), **107** (blue), **106** (red). Highlighted as sticks are the purine-scanning glutamine (Gln884) and the hydrophobic clamp residues (Phe887 and Ile850). Numbering is taken from the *Pf*PDE α sequence.

Testing against the *h*PDE isoforms shows a marked reduction in *h*PDE9 inhibitory activity when comparing the benzyl (**99**) to the *o*-chlorobenzyl analogue (**105**). It was

envisaged that docking each of these compounds into the *h*PDE9 crystal structure (3DYN) may provide an explanation for the difference in determined affinities. If this was the case, then it may be possible to use this information to further reduce *h*PDE9 activity and gain selectivity for the *Pf*PDEs. However, when **99** and **105** were docked into *h*PDE9 (3DYN), a very similar binding pose was observed for each (Figure 3.20). The only noticeable difference was the angle of the benzyl substituent relative to an adjacent phenylalanine residue (Phe441), although the function of this residue within the binding site is not apparent. Potentially, this reduced aromatic interaction could be responsible for the reduction in observed *h*PDE9 affinity of **105**. It is unclear, however, how the chloro-substituent affects the binding mode when placed in the *ortho*-position (**105**) compared to the *meta*-position (**77**).

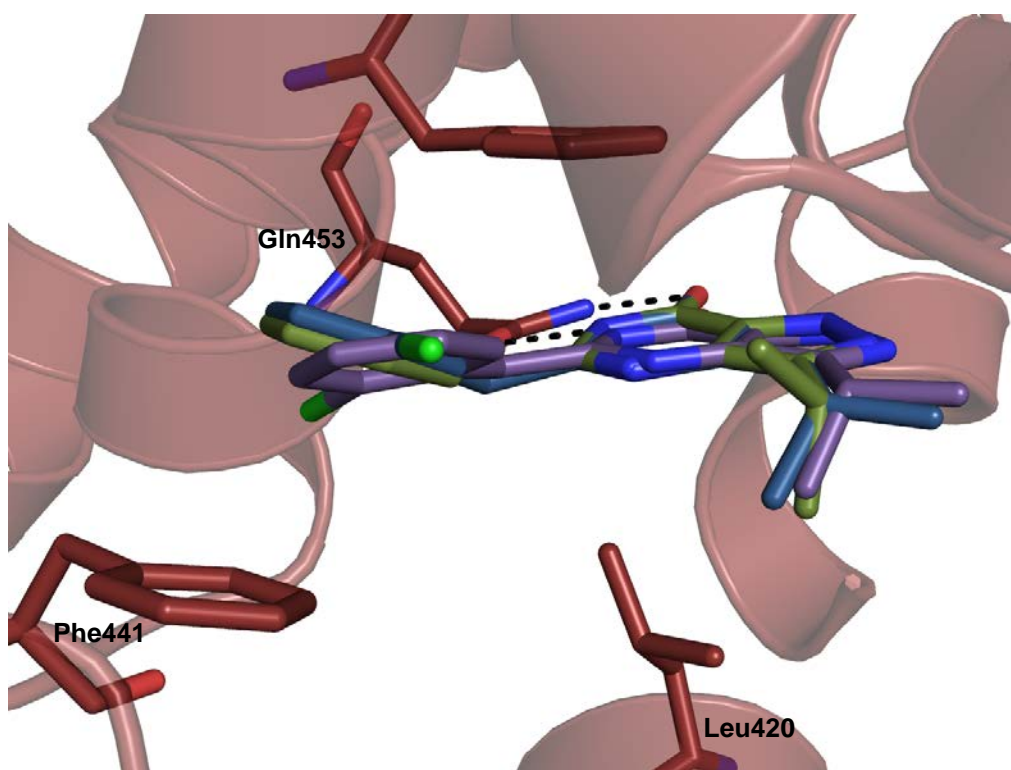


Figure 3.20. Docking of compounds **77** (blue), **105** (purple) and **99** (green) into the *h*PDE9 crystal structure (3DYN). Highlighted as sticks are the purine-scanning glutamine (Gln453) as well as the hydrophobic clamp residues (Phe456 and Leu420) and an adjacent phenylalanine residue (Phe441). Numbering is taken from the 3DYN crystal structure.

3.7 Chapter conclusions and future directions

Within this work, a series of human PDE9 and PDE1 inhibitors were synthesised and assessed for antiparasmodial activity. The compounds were generated through an optimised synthetic pathway to the key pyrazole intermediate (**85**), before final cyclisation reactions with carboxylic acids to give the corresponding pyrazolopyrimidinone compounds.

The assay conditions to measure *P. falciparum* growth were optimised for the testing of the synthesised pyrazolopyrimidinone compounds. As observed in the literature, variations were seen in determined IC₅₀ values for the individual compounds. The improvement of the reproducibility or development of an alternate assay to measure parasite growth may be required to improve the quality of the assay data. Despite this, the assay results were used to identify active and poorly active antiparasmodial compounds. Furthermore, some tentative structure-activity relationship data was generated for the pyrazolopyrimidinone compounds. This investigation resulted in a compound, **105**, that demonstrated sub-micromolar antiparasmodial activity as well as a significant decrease in all human PDE activity in comparison to the initial lead compound (**77**). The mechanism of the observed antiparasmodial activity remains to be elucidated. As such, compound **105** can be utilised in ongoing biochemistry work. For example, measurement of cGMP and cAMP levels of *P. falciparum* cell lysates when treated with the inhibitor could be undertaken. Increased cellular levels of either or both cyclic nucleotides would infer a PDE inhibitory mechanism. Furthermore, the development of a labelled pyrazolopyrimidinone, for example by biotinylation, would allow for affinity-based assays to be performed as a means to isolate and identify the target(s) of these compounds.

The developed pyrazolopyrimidinone compounds represent a “drug repurposing” strategy that has been used in rational design and compares well against mass chemical screening efforts. With careful evaluation of a target structure, considered selection of template molecule, and design of a limited synthetic compound library, 6 compounds out of 21 were obtained that would have been “hits” in the GSK or Novartis mass screening programs – a 28% hit rate. This work has resulted in a series of active compounds that will serve as a suitable starting point for further medicinal chemistry efforts, as well as a useful tool for the ongoing understanding of *P. falciparum* cyclic nucleotide biochemistry.

Chapter 4

Synthetic studies of novel flavonoid mimetics

4.1 Introduction

In Chapters 1-3, the “inverted silver bullet” paradigm was assessed by examining the capacity for *h*PDE inhibitors to inhibit *Plasmodium falciparum* parasite growth. Chapter 3, in particular, showed the fruitful application of that approach. However, it was also apparent that the synthesised compounds of this work were not chemically novel and therefore, it may be best to leave the further pursuit of these compounds to the companies who own them. Taken further though, the premise provides a motive for the pursuit of novel compound classes to add to the chemical entities that can be described as PDE inhibitors and/or antiplasmodial compounds.

This chapter describes efforts made in the pursuit of such novel compound classes. A survey of relevant literature identified a number of significant observations that underpin the hypothesis of this work:

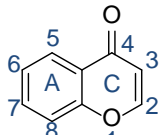
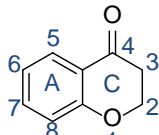
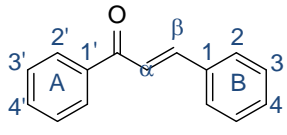
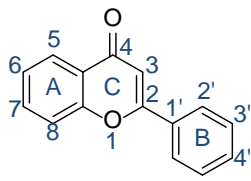
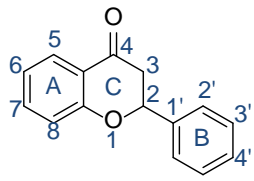
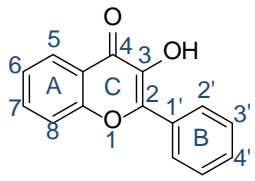
- 1) the flavonoid class of natural products are well represented as both human PDE inhibitors and antiplasmodial compounds;

- 2) there are prominent recurring structural features among human PDE inhibitors;
and
- 3) there are a number of compound classes that might be considered flavonoid-like that are yet to be explored as PDE inhibitors and additionally, are very poorly represented in the literature.

Each of these concepts is expanded upon in sections 4.1.1–4.1.3. The hypothesis is that novel synthetic flavonoid-related compounds would be able to inhibit human PDE isoforms and/or inhibit *Plasmodium falciparum* parasite growth, providing new starting points for antimalarial drug design.

4.1.1 Flavonoids as human phosphodiesterase inhibitors and antiplasmodial compounds

The flavonoids are a group of polyphenolic compounds that are widely distributed throughout the plant kingdom and to date, more than 6000 flavonoids have been identified.²²⁸ They have been shown to exhibit many biological activities, though the mechanisms behind many of these are not fully understood. Flavonoids have been demonstrated to show antioxidant effects,²²⁹ cardio-protective effects,^{230,231} anti-inflammatory activity,²³² anti-ulcer activity,²³² anti-spasmodic effects,²³³ anti-mutagenic effects,²³⁴ anti-microbial activity,²³⁵ anti-tumour²³⁵ and anti-HIV activity.^{230,236} Flavonoid compounds are separated into distinct subclasses, and the structures of several commonly found flavonoids are shown in Figure 4.1.

<div style="display: flex; justify-content: space-around; align-items: flex-end;"> <div style="text-align: center;">  <p>chromone</p> </div> <div style="text-align: center;">  <p>chromanone</p> </div> <div style="text-align: center;">  <p>chalcone</p> </div> </div>								
<div style="display: flex; justify-content: space-around; align-items: flex-end;"> <div style="text-align: center;">  <p>flavone</p> </div> <div style="text-align: center;">  <p>flavanone</p> </div> <div style="text-align: center;">  <p>flavonol</p> </div> </div>								
	3	5	6	7	2'	3'	4'	5'
Flavanones								
Hesperitin	H	OH	H	OH	H	OH	OCH ₃	H
Naringin	H	OH	H	OR	H	H	OH	H
Naringenin	H	OH	H	OH	H	H	OH	H
Flavones								
Flavone	H	H	H	H	H	H	H	H
Luteolin	H	OH	H	OH	H	OH	OH	H
Chrysin	H	OH	H	OH	H	H	H	H
Apigenin	H	OH	H	OH	H	H	OH	H
Acacetin	H	OH	H	OH	H	H	OCH ₃	H
Casticin	OCH ₃	OH	OCH ₃	OCH ₃	H	OH	OCH ₃	H
Flavonols								
Kaempferol	OH	OH	H	OH	H	H	OH	H
Quercetin	OH	OH	H	OH	H	OH	OH	H
Fisetin	OH	H	H	OH	H	OH	OH	H

OCH₃ = methoxy, R = rutinoside

Figure 4.1. Subclasses of different flavonoids, and the structures of several commonly found flavonoids.

Flavonoids as human phosphodiesterase inhibitors

In 1978, Beretz and co-workers were among the first to demonstrate the ability of the flavonoids to inhibit both cGMP and cAMP phosphodiesterases with activity comparable to the known *h*PDE inhibitors, papaverine, theophylline and 3-isobutyl-1-methylxanthine (IBMX) (summarised in Table 4.2).^{237,238} Other studies by Ferrell *et al.* and Kuppusamy and Das restated quercetin and luteolin as PDE inhibitors.^{239,240} It should be noted that this work predates the identification of many of the *h*PDE subtypes.

Table 4.2. Flavonoid inhibition of cAMP and cGMP phosphodiesterases.^{237,238}

Compound	IC ₅₀ (μM)	
	cAMP	cGMP
Quercetin	3.6	15
Apigenin	9.2	35
Kaempferol	2.7	
Luteolin	8.7	
Flavone	>100	
Naringenin	45	
Papaverine	5	11
Theophylline	300	310
IBMX	35	7

More recent work has revealed several flavonoid inhibitors of the phosphodiesterase isoforms. Orallo *et al.* demonstrated that the flavanone, naringenin, was capable of inhibiting *hPDE* 1, 4 and 5.²⁴¹ Ning *et al.* showed the flavone glycoside from horny goat weed, icariin, as having *hPDE*5 inhibitory activity and also as being more effective in maintaining cGMP levels than zaprinast.²⁴² In fact, several literature reports have described the *hPDE* inhibitory effects of a range of other flavones and chalcones.²⁴³⁻²⁴⁸ In 2004, Ko *et al.* studied the inhibitory effects of a series of flavonoid compounds on *hPDE*s 1-5.²⁴⁹ In this study, luteolin and quercetin were shown to inhibit each of the five isozymes to some extent while the flavanone, hesperetin, showed selectivity for *hPDE*4. (Table 4.3).

Table 4.3. IC₅₀ values (μM) of flavonoids on human phosphodiesterase isozymes.

Flavonoid	<i>hPDE</i> isozyme				
	1	2	3	4	5
Luteolin	21.5 ± 2.9	13.3 ± 0.8	10.1 ± 1.8	19.1 ± 2.4	19.3 ± 3.2
Quercetin	27.8 ± 5.7	17.9 ± 3.4	5.6 ± 1.0	9.9 ± 2.5	>100
Hesperetin	>100	>100	>100	28.2 ± 1.1	>100

Flavonoids as antiplasmodial compounds

The antiplasmodial activity of natural and synthetic flavonoids has been demonstrated.²⁵⁰⁻²⁵³ This activity has been observed when the compounds have been assessed both alone and through synergistic effects with known antimalarial compounds, such as artemisinin. Artemisinin is the main antiplasmodial agent of *Artemisia annua* however, numerous flavonoid compounds have also been isolated from the plant.²⁵⁴ Of the flavonoid compounds present in *Artemisia annua*, several reports have demonstrated synergistic antimalarial effects when their use is combined with artemisinin; Elford and co-workers demonstrated the synergistic antimalarial effects of casticin (a flavone) with artemisinin,⁷¹ and Liu and co-workers have demonstrated a similar effect of chrysophanol-D with artemisinin.²⁵⁵

More recently, reports have emerged of flavonoids alone exhibiting antiplasmodial activity. Lehané *et al.* identified several common dietary flavonoids which inhibit the growth of the intraerythrocytic malaria parasite.²²⁸ Of the eleven dietary flavonoids tested, eight showed antiplasmodial activity against *P. falciparum* (3D7) with IC₅₀ values between 11 µM and 66 µM. In addition to this, all showed activity against a chloroquine-resistant strain (7G8). Luteolin was the most active against both strains (IC₅₀ values of 11 µM and 12 µM for 3D7 and 7G8 strains, respectively) and was further found to prevent the progression of parasite growth beyond the trophozoite stage. Additionally, quercetin and chrysin showed 3D7 inhibition with IC₅₀ values of 15 µM and 18 µM, respectively. Most promisingly, luteolin was found to produce an additive antiplasmodial effect when used in conjunction with chloroquine and artemisinin.

The antiplasmodial activity of luteolin was further examined in a 2006 report by Tasdemir *et al.*²⁵³ Here, luteolin was shown to inhibit a chloroquine-sensitive *P. falciparum* strain (NF54) with an IC₅₀ value of 10.7 μ M. Among the other flavonoids assessed for antiplasmodial activity, the catechol ether-substituted compounds, 5,4-dihydroxy-6,7-dimethoxyflavanone (**118**) and cirsimaritin (**119**) (Figure 4.4), showed IC₅₀ values of 8.8 μ M and 16.9 μ M against parasite growth, respectively. In 2007, Lim *et al.* compared the antimalarial effects of twenty flavonoids and chalcones, many of which were similar in structure to the naturally occurring casticin.²⁵⁶ They concluded that the most active compounds were 3'-methyl-substituted flavanones.

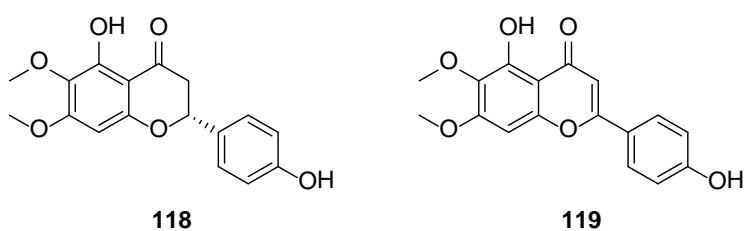


Figure 4.4. Structures of the antiplasmodial flavonoids, **118** and **119**, as reported by Tasdemir *et al.*²⁵³

There is a considerable overlap of compounds that exhibit antiplasmodial activity and those that inhibit human PDE activity. Luteolin is a notable example from those discussed above. Tasdemir and co-workers hypothesised that the flavonoids were exhibiting antiplasmodial effects through inhibition of fatty acid biosynthesis, and demonstrated inhibition of the FabG, FabZ and FabI enzymes that supported this to some extent. On the other hand, given its described ability to inhibit the phosphodiesterase enzymes, it may be possible that luteolin, and perhaps other antiplasmodial flavonoids, are acting through *P. falciparum* phosphodiesterase (*PfPDE*) inhibition. In light of these observations, it would appear worthwhile to investigate

whether flavonoid antiparasmodial compounds are acting *via* a phosphodiesterase inhibitory mechanism of action.

4.1.2 Prominent recurring structural features among human phosphodiesterase inhibitors

As described in Chapter 1, while the structures of the most well characterised PDE inhibitors are diverse and belonging to multiple chemical classes, they consistently present certain identifiable features (Figure 1.19). First among these common structural motifs is a bicyclic core with an aromatic pendant. In numerous cases also, 1,2-dimethoxy or alkoxy (catechol ether) groups are attached to this bicyclic core or the aromatic pendant. Papaverine (**68**) and tofisopam (**120**) are prominent examples of compounds bearing these features. In the crystal structure of rolipram bound to *h*PDE4D, the catechol ether hydrogen bonds to the purine-scanning glutamine residue.¹⁸⁵ This structural motif is also a feature of the flavonoid compounds, although these are typically hydroxyl-substituted (polyphenolic). The bicyclic moiety may act as an isostere to the bicyclic core of the cyclic nucleotides (e.g. adenosine or guanine), and the catechol ethers or phenols could provide the hydrogen donor or acceptor functions of the natural substrates.

4.1.3 Poorly represented flavonoid-like compound classes

In the quest for novel phosphodiesterase inhibitor chemotypes, the concept of ring expansion of flavanone-like structures to 6,7-fused ring systems, as exemplified by tofisopam (**120**) (Figure 4.5), presented an attractive prospect. The activities of flavanones, such as naringenin and hesperitin, suggest that non-planar bicyclic systems

can possess PDE inhibitory activity (Table 4.3) and that pursuing these classes might provide an opportunity to survey new chemical space.

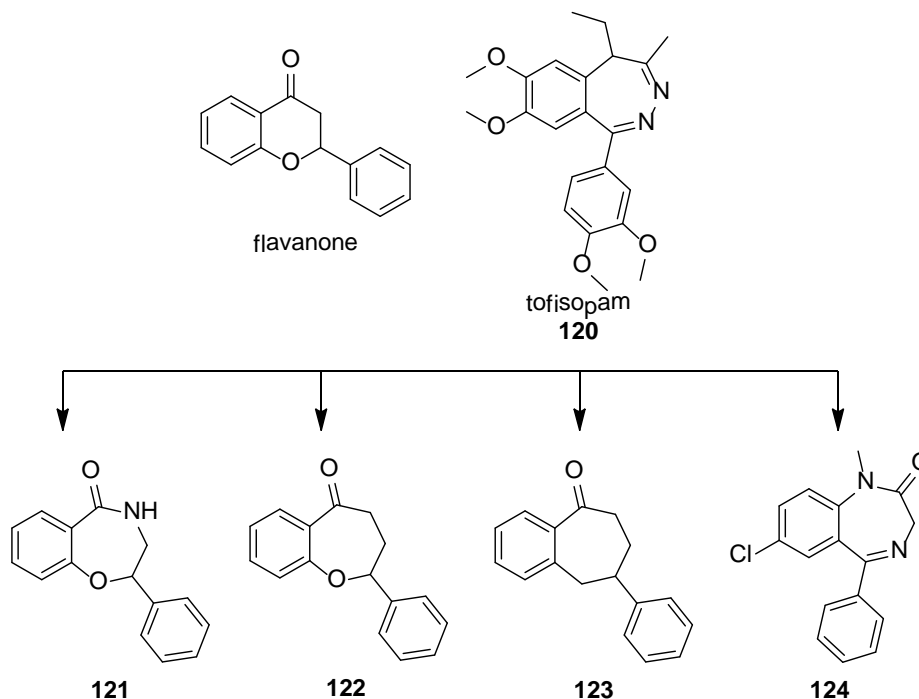


Figure 4.5. Scaffolds of 6,7-fused ring system compound classes; 2-phenylbenzoxazepinone (**121**), 2-phenylbenzoxepinone (**122**), 8-phenylbenzosuberone (**123**) and a representative from the benzodiazepine class, diazepam (**124**).

A series of compounds for synthesis was selected from the relatively simple skeletons shown in Figure 4.5 (**121-123**). Of course, the benzodiazepines (diazepam, **124**) as a compound class are well reported within the literature and have been utilised primarily as anti-depressant and anti-psychotic drugs.²⁵⁷⁻²⁵⁹ Conversely, the 2-phenylbenzoxazepinones, 2-phenylbenzoxepinones and 8-phenylbenzosuberones all remain relatively unreported within the literature and bear resemblance to a flavanone scaffold. As a consequence, these three 6,7-fused ring system compound classes (**121-123**) emerged as novel scaffolds of interest. In addition, an aim was to focus attention on those structures for which a 1,2-dimethoxy functionality (or catechol ether) was

synthetically accessible, either as part of the 6,7-fused ring system or as a pendant ring (Figure 4.6). It should be noted that the structurally related 9-phenylbenzosuberone and 5-phenylbenzazepinone compounds are well reported within the literature.²⁶⁰⁻²⁶⁶

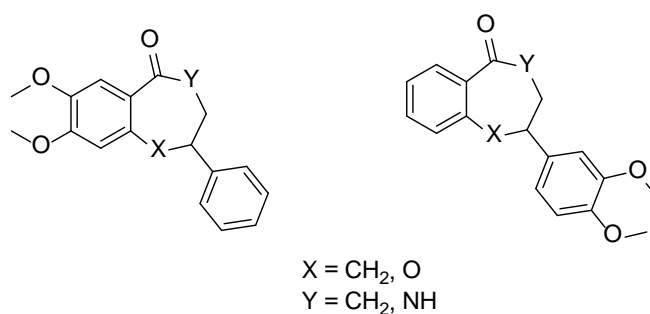


Figure 4.6. Sites of interest for 1,(2)-dimethoxylation on the 2-phenylbenzoxazepinone, 2-phenylbenzoxepinone and 8-phenylbenzosuberone compound classes.

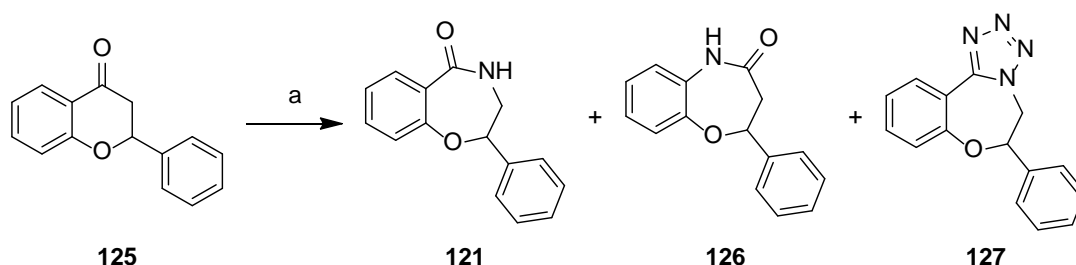
In this chapter, the syntheses of the phenyl-substituted benzoxazepinone, benzoxepinone, and benzosuberone compound classes have been investigated with the goal of identifying novel scaffolds worth pursuing in a medicinal chemistry campaign against PDE and/or *P. falciparum* targets.

4.2 Synthetic studies of the 2-phenylbenzoxazepinone compound class

4.2.1 Synthetic access to the 2-phenylbenzoxazepinone compounds

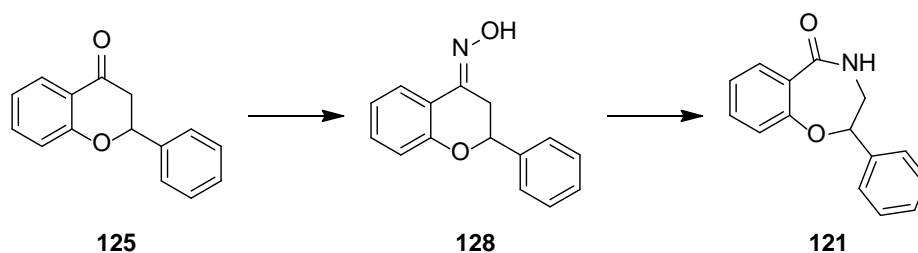
The benzoxazepinone class of compounds are recognised as benzodiazepine analogues and are also reported within the literature as poly(ADP-ribose) polymerase (PARP) inhibitors.²⁶⁷⁻²⁷⁰ The 2-phenylbenzoxazepinones are most commonly synthesised through either a Schmidt reaction or Beckmann rearrangement of the corresponding flavanone.²⁷¹⁻²⁷³

The Schmidt reaction describes the acid-mediated conversion of ketones to amides, particularly cyclic ketones to lactams, with ring expansion.^{274,275-280} The synthesis of 2-phenylbenzoxazepinone (2-phenyl-3,4-dihydrobenzo[*f*][1,4]oxazepin-5(2*H*)-one) (**121**) *via* the Schmidt reaction has been reported previously.^{281,282} Misiti and Rimatori described the reaction of 2-phenylchroman-4-one (**125**) with sodium azide under acidic conditions to afford predominantly **121** (83%) and two other products – the reverse “aryl-migration” product (**126**) and the tetrazole (**127**) (Scheme 4.7).²⁸²



Scheme 4.7. Schmidt reaction of 2-phenylchroman-4-one (**125**) described by Misiti and Rimatori to give several isolable and characterised products. (a) NaN_3 , $\text{CH}_3\text{CO}_2\text{H}$, conc. H_2SO_4 , 40-50 °C, 45 min, **121** (83%), **126** (3%), **127** (5%).²⁸²

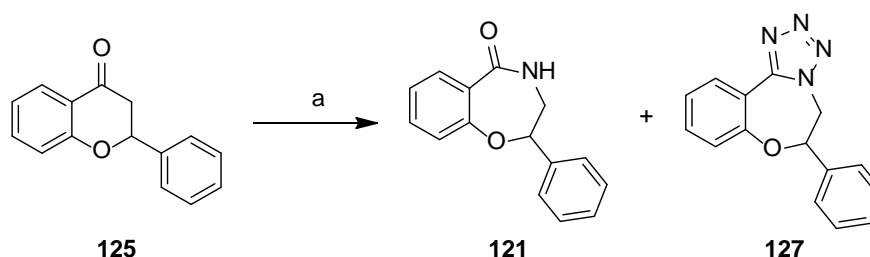
The Beckmann rearrangement is the acid-catalysed rearrangement of oximes to amides,²⁸³ and is also widely reported within the literature.²⁸⁴⁻²⁸⁸ As with the Schmidt reaction, both alkyl- and aryl-migratory products can result from the Beckmann rearrangement, though alkyl migration is more commonly observed. It should be noted that the Beckmann rearrangement of 2-phenylchroman-4-one (**125**) to 2-phenylbenzoxazepinone (**121**) has not been reported (Scheme 4.8).



Scheme 4.8. The envisaged Beckmann rearrangement of the oxime intermediate (**128**) to the corresponding 2-phenylbenzoxazepinone (**121**) from 2-phenylchroman-4-one (**125**) starting material.

4.2.2 Synthesis of 2-phenyl-3,4-dihydrobenzo[*f*][1,4]oxazepin-5(2*H*)-one

In the first instance, the synthesis of 2-phenylbenzoxazepinone (**121**) was achieved *via* the Schmidt reaction. Commercially available 2-phenylchroman-4-one (**125**) was treated with sodium azide and concentrated sulfuric acid in toluene for 16 hours.²⁸⁹ Compound **121** was isolated by column chromatography in good yield (64%), as was some tetrazole by-product (**127**) (8%) and unreacted 2-phenylchroman-4-one (**125**) (12%) (Scheme 4.9). No sign of the aryl-migratory product (**126**) was observed. Mass spectrometry was particularly useful in identifying the product components as the ¹H NMR spectrum of each (**121**, **127** and **125**) were not significantly different. In fact, the most distinguishing signal within the ¹H NMR spectrum comes from the lone methylene signal that proved critical in the characterisation of the alkyl-migratory product (δ 3.57-3.42 ppm). Comparison to the reported melting points supported the assignments (Table 4.10), and 2D NMR (HMBC and HSQC) spectroscopy was also utilised.



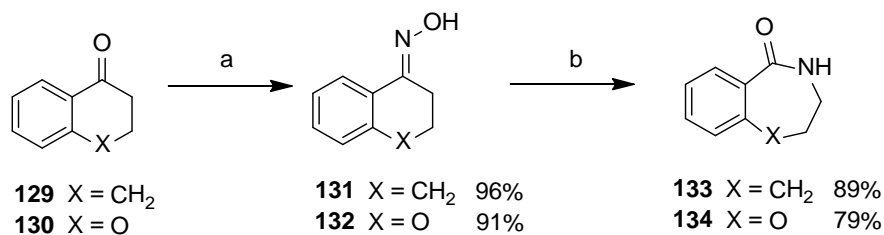
Scheme 4.9. The Schmidt reaction of 2-phenylchroman-4-one (**125**) to give 2-phenylbenzoxazepinone (**121**) and the tetrazole by-product (**127**). (a) NaN₃, conc. H₂SO₄, toluene, rt, 16 h, **121** (64%), **127** (8%), **125** (12%).

Table 4.10. Comparison of literature (lit.) and experimental (exp.) values in the characterisation of the Schmidt reaction products and by-products.

	CH ₂ (δ ppm)		CH (δ ppm)		M.p. ($^{\circ}$ C)	
	Lit.	Exp.	Lit.	Exp.	Lit.	Exp.
2-Phenylchroman-4-one (125)	3.08-2.88 ²⁹⁰	3.16-2.90	5.47 ²⁹⁰	5.52	76-78 ²⁹¹	76-77
Alkyl-migratory product (121)	3.48 ²⁸²	3.57-3.42	5.35 ²⁸²	5.33	125-126 ²⁸²	125-126
Aryl-migratory product (126)	3.05 ²⁸²	-	5.62 ²⁸²	-	141-142 ²⁸²	-
Tetrazole by-product (127)	5.30-4.65 ²⁸²	5.23-5.12	-	4.85	137-138 ²⁸²	137-138

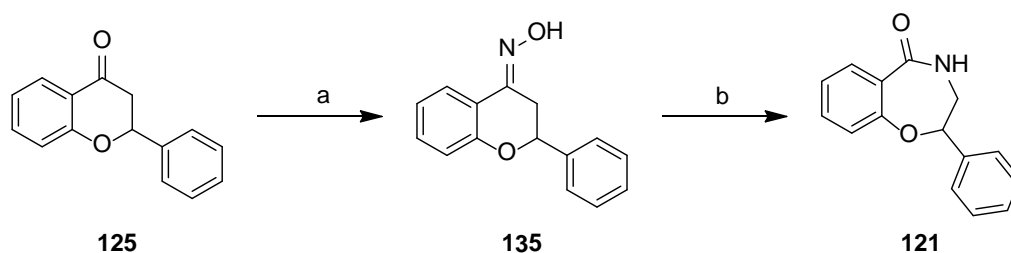
In order to increase the conversion to the alkyl-migratory product (**121**) and simultaneously reduce the formation of the tetrazole by-product (**127**), alternate Schmidt reaction conditions were explored. Both aqueous acidic conditions and the use of Lewis acid catalysis were examined.^{289,292} The most successful result came from the use of iron (III) chloride as a Lewis acid according to the procedure of Yadav *et al.*, which gave **121** in 82% yield as well as some tetrazole by-product (**127**) (12%).²⁷¹

To avoid the problem of competing tetrazole by-product formation, the Beckmann rearrangement of the corresponding oxime was attempted. Simple substrates, 3,4-dihydronaphthalen-1(2*H*)-one (**129**) and chroman-4-one (**130**), gave the corresponding Beckmann rearrangement products (**133** and **134**, respectively) in high yields using *p*-toluenesulfonylchloride and zinc (II) bromide as catalyst (Scheme 4.11).²⁹³



Scheme 4.11. Synthesis of the oxime intermediates of 3,4-dihydronaphthalen-1(2*H*)-one (**129**) and chroman-4-one (**130**) and subsequent Beckmann rearrangement. (a) NH₂OH·HCl, CH₃CO₂Na, CH₃CH₂OH, 78 °C, 2 h; (b) TsOH, ZnBr₂, CH₃CN, 5 h.

2-Phenylchroman-4-one (**125**) was also successfully converted to (*Z*)-2-phenylchroman-4-one oxime (**135**) (Scheme 4.12). As there was no addition or loss of signals in either the ¹H NMR or ¹³C NMR spectra, and chemical shifts perturbations were minimal, the presence of oxime material was confirmed by detection of its molecular ion in the mass spectrum. The oxime (**135**) underwent facile Beckmann rearrangement under a range of conditions, including catalysis by *p*-toluenesulfonylchloride and zinc (II) bromide as above,²⁹³ or *p*-toluenesulfonic acid and zinc (II) chloride.²⁹⁴ The reaction with polyphosphoric acid performed best and afforded **121** in 79% yield (Scheme 4.12).²⁸⁹



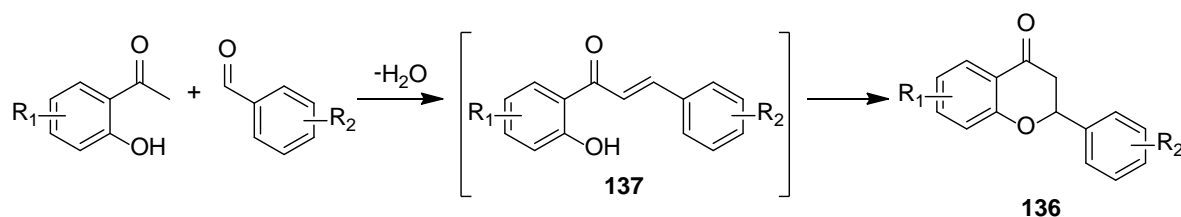
Scheme 4.12. Synthesis of 2-phenylbenzoxazepinone (**121**) via the Beckmann rearrangement of (*E*)-2-phenylchroman-4-one oxime (**135**). (a) NH₂OH·HCl, CH₃CO₂Na, CH₃CH₂OH, 78 °C, 2 h, 92%; (b) PPA, 120 °C, 2 h, then H₂O, 75 °C, 2 h, 79%.

Although the Schmidt reaction avoids the intermediate preparation of the oxime, formation of the tetrazole by-product is not desirable in the syntheses of further analogues. From these results, the Beckmann rearrangement of the corresponding oxime

using polyphosphoric acid appeared to be the most efficient strategy in the synthesis of 2-phenylbenzoxazepinone (**121**) and potentially further analogues.

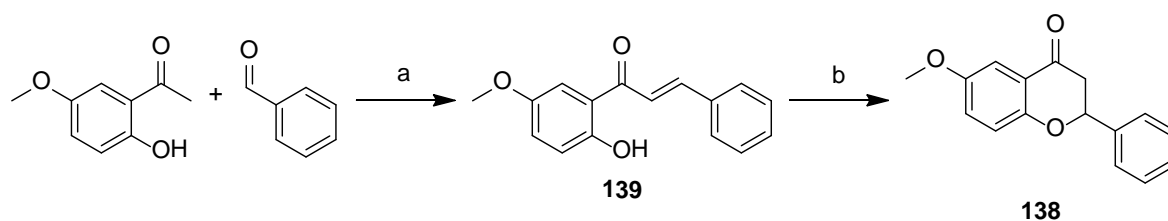
4.2.3 Synthesis of 7,8-dimethoxy-2-phenyl-3,4-dihydrobenzo[*f*][1,4]oxazepin-5(2*H*)-one

With the successful synthesis of 2-phenylbenzoxazepinone (**121**) through both the Schmidt reaction and Beckmann rearrangement, attention turned to analogues bearing desired substitutions, such as the methoxy or catechol ether examples, described in section 4.1.2. Of course, preparation of these depended on the availability of precursor flavanones. Most commonly, flavanones (**136**) are prepared by the reaction of a substituted 2'-hydroxyacetophenone with a substituted benzaldehyde (Scheme 4.13). The reaction proceeds *via* a chalcone intermediate (**137**), which can be isolated (two-step procedure) or directly cyclised in the reaction (one-step procedure).



Scheme 4.13. Synthesis of substituted flavanones (**136**) *via* chalcone intermediates (**137**) through reaction of a 2'-hydroxyacetophenone with a benzaldehyde.

Firstly, the synthesis of 6-methoxy-2-phenylchroman-4-one (**138**) was performed (Scheme 4.14). This involved the reaction of 1-(2-hydroxy-5-methoxyphenyl)ethanone with benzaldehyde, which proceeds through the intermediate chalcone (**139**). Several literature procedures and adaptations thereof were explored,^{295,296} and the conditions were shown to impact significantly on the results.



Scheme 4.14. Two-step synthesis of 6-methoxy-2-phenylchroman-4-one (**138**) via the corresponding chalcone intermediate (**139**). (a) $\text{Ba}(\text{OH})_2 \cdot 8\text{H}_2\text{O}$, $\text{CH}_3\text{CH}_2\text{OH}$, 40 °C, 16 h, 97%; (b) $\text{CH}_3\text{CO}_2\text{Na}$, $\text{CH}_3\text{CH}_2\text{OH}$, 78 °C, 16 h, 90%.

A two-step procedure described by both Sathyanarayana and later by Chimenti and co-workers proved the most reliable, and it was found that by careful selection of temperature and reaction time (40 °C for 16 hours), complete conversion to the intermediate chalcone could be obtained (at higher temperatures, degradation occurred) (Table 4.15).^{297,298} Under these conditions, purification of the chalcone was unnecessary.

Table 4.15. Investigation of temperature and time effects in the synthesis of (*E*)-1-(2-hydroxy-5-methoxyphenyl)-3-phenylprop-2-en-1-one (**139**) using the procedure of Chimenti *et al.*²⁹⁸

Reaction conditions	Conversion to 139 ^a (%)	Isolable yield (%)
Ethanol, 30 °C, 24 h	72	68
Ethanol, 40 °C, 24 h	89	84
Ethanol, 40 °C, 16 h	100	97
Ethanol, 60 °C, 16 h	51	-
Ethanol, 78 °C, 16 h	33	-

^a conversion determined by LCMS analysis.

The cyclisation of the chalcone (**139**) to afford the flavanone (**138**), as outlined by Chimenti *et al.*, was successful (Figure 4.14).²⁹⁹ Alternative base- and acid-catalysed cyclisation conditions were examined, but offered no advantage. This two-step

procedure described by Chimenti *et al.*²⁹⁸ was also employed in the synthesis of flavanones **140-142** (Figure 4.16). The yields for both the condensation reaction and subsequent cyclisation were each >90% in the preparation of each analogue.

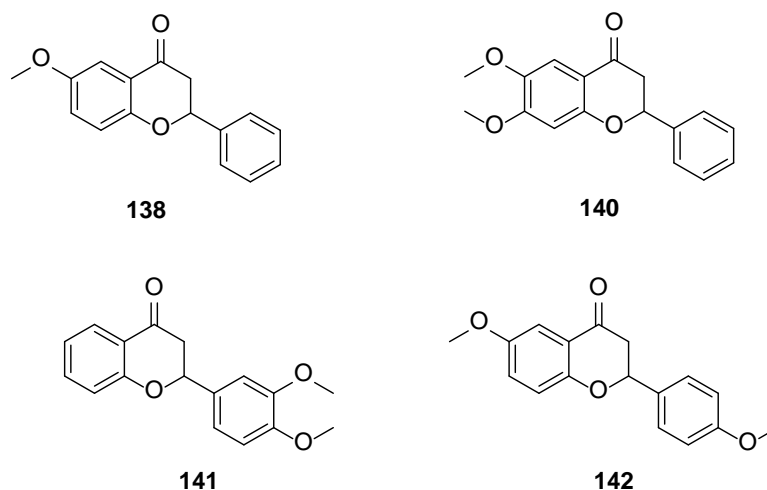
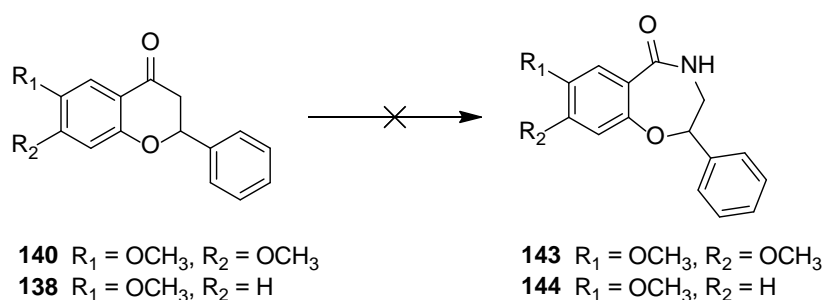


Figure 4.16. Synthesised flavanone compounds (**138**, **140-142**) with various methoxy substituents.

The synthesis of 7,8-dimethoxy-2-phenylbenzoxazepinone (7,8-dimethoxy-2-phenyl-3,4-dihydrobenzo[*f*][1,4]oxazepin-5(2*H*)-one) (**143**) was then investigated as a prioritised target due to the presence of a catechol ether functionality (Scheme 4.17). Disappointingly, neither the Schmidt reaction nor Beckmann rearrangement conditions (outlined in Schemes 4.9 and 4.12) gave any conversion to **143** from the corresponding 6,7-dimethoxy-2-phenylchroman-4-one (**140**). Similarly, these reaction conditions failed in the synthesis of the 7-methoxy analogue (**144**) (Scheme 4.17).



Scheme 4.17. The previously established Schmidt reaction and Beckmann rearrangement conditions failed to produce any of the methoxy-substituted 2-phenylbenzoxazepinones (**143** and **144**).

Whilst there are many literature procedures outlining numerous reaction conditions, it would seem apparent that the conditions explored within this work are not generally applicable. Unless the presence of the methoxy substituents were a specific case or alternate conditions can be found, the use of the Schmidt reaction and Beckmann rearrangement to generate analogues of the 2-phenylbenzoxazepinone class of 6,7-fused ring system scaffolds would appear limited.

4.2.4 Biological assessment of 2-phenyl-3,4-dihydrobenzo[f][1,4]oxazepin-5(2*H*)-one

The successfully synthesised compound, 2-phenylbenzoxazepinone (**121**), was assessed for *P. falciparum* growth inhibition and proved to be a moderately active inhibitor. Under the LDH assay conditions described in Chapter 3, **121** had an IC₅₀ value of 7.6-9.4 µM. The tetrazole by-product (**127**) was also assessed but did not inhibit parasite growth (IC₅₀ > 100 µM). **121** was also assessed for human PDE inhibition. At 1 µM concentration, **121** demonstrated 62% inhibition of *h*PDE1, yet poor inhibition at *h*PDE9 and *h*PDE4 (Appendix 4).

4.2.5 Section discussion

While the synthetic program relating to this class was cut short, the antiplasmodial activity as well as *h*PDE1 inhibition of 2-phenylbenzoxazepinone (**121**) may represent a starting point for further investigation. When both enantiomers were docked into the *Pf*PDEα homology model (Figure 4.18), the amide of **121** made two hydrogen bond contacts to the purine-scanning glutamine residue. This binding mode is observed in all

human PDE crystal structures with bound ligands and is believed essential in PDE inhibition.

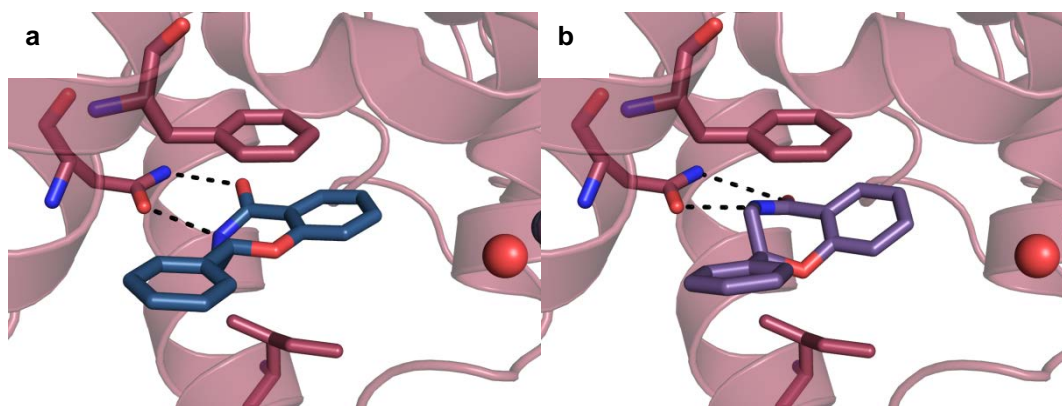


Figure 4.18. 2-Phenylbenzoxazepinone (**121**) docked into the *PfPDEα* homology model. (a) the *R* enantiomer and (b) the *S* enantiomer. Highlighted as sticks are the purine-scanning glutamine (Gln884), as well as the hydrophobic clamp residues (Phe887 and Ile850). Numbering is taken from the *PfPDEα* sequence. Metal ions and water molecules are represented as spheres, and hydrogen bonds are shown with dashed lines.

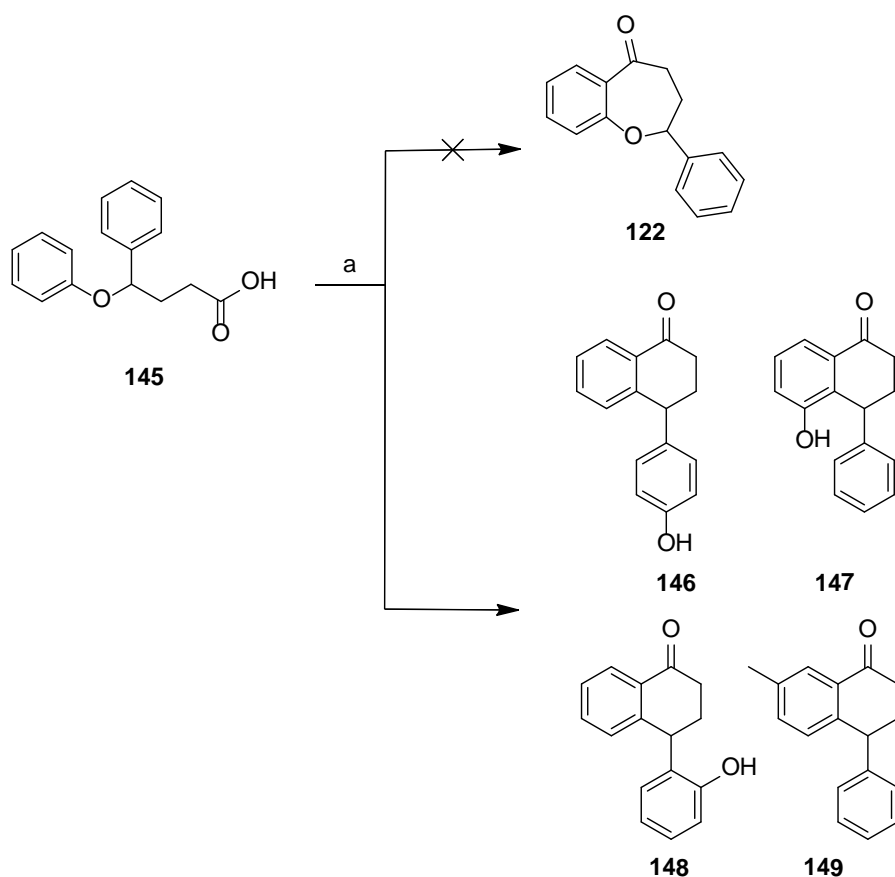
While such evidence supports the hypothesis of antiplasmodial activity occurring through a PDE inhibition mechanism, challenges encountered in the syntheses of the derivatised 6,7-fused ring system scaffold will need to be overcome if the compound class is to be pursued as antiplasmodial compounds. Given that neither the activity nor predicted binding mode is dependent upon the presence of catechol ether groups, the exploration of other substituent types might provide access to more potent human PDE inhibitors or antiplasmodial compounds.

4.3 Synthetic studies of the 2-phenylbenzoxepinone compound class

4.3.1 Synthetic access to the 2-phenylbenzoxepinone compounds

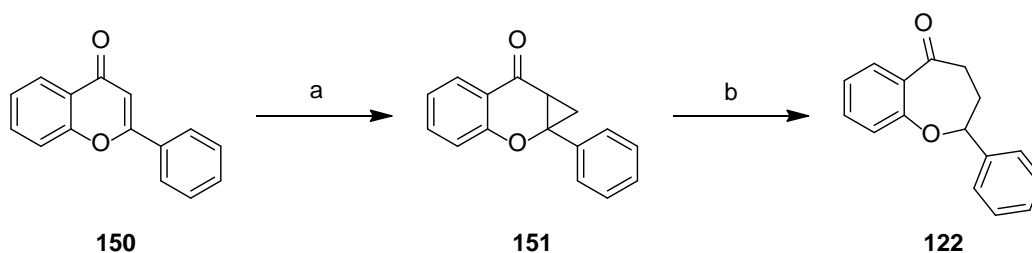
In the ongoing pursuit of novel chemotypes to act as antiplasmodial and/or PDE inhibitors, attention turned to the 2-phenylbenzoxepinone compound class. The only literature report of a 2-phenylbenzoxepinone comes from Tatsuoka *et al.* in 1990.³⁰⁰ The 2-phenylbenzoxepinone (2-phenyl-3,4-dihydrobenzo[*b*]oxepin-5(2*H*)-one) compound (**122**) and a series of analogues were synthesised in an effort to offer useful frameworks “For the purpose of synthesising pharmacologically active compounds.” However, no pharmacological activity was reported.

It would be expected that this class might be accessed through cycliacylation of a phenoxybutanoyl precursor. Indeed, well-known unsubstituted compounds have been prepared in this way.³⁰¹⁻³⁰³ However, when Tatsuoka *et al.* attempted the synthesis of **122** through dehydrative ring formation of the corresponding butyric acid (**145**), a complex mixture of α -tetralone derivatives **146-149** was obtained, as identified through spectroscopic analyses (Scheme 4.19).³⁰⁰



Scheme 4.19. Attempted synthesis of 2-phenylbenzoxepinone (**122**) through dehydrative ring formation of the butyric acid (**145**) as reported by Tatsuoka *et al.* (a) PPA, rt, 6 h.³⁰⁰

Ultimately, Tatsuoka and co-workers achieved the synthesis of **122** by ring expansion of 2-phenyl-4*H*-chromen-4-one (**150**) – cyclopropanation of **150** was followed by reductive cleavage of the cyclopropyl ketone (**151**) (Scheme 4.20).³⁰⁴ Moreover, the synthesis could be extended to aryl substituent substrates. It was found that in general, electron donating substituents on the fused benzene ring (i.e. methoxy) gave the 2-phenylbenzoxepinone product in a much higher yield than in the presence of electron withdrawing groups (i.e. trifluoromethyl, ester).

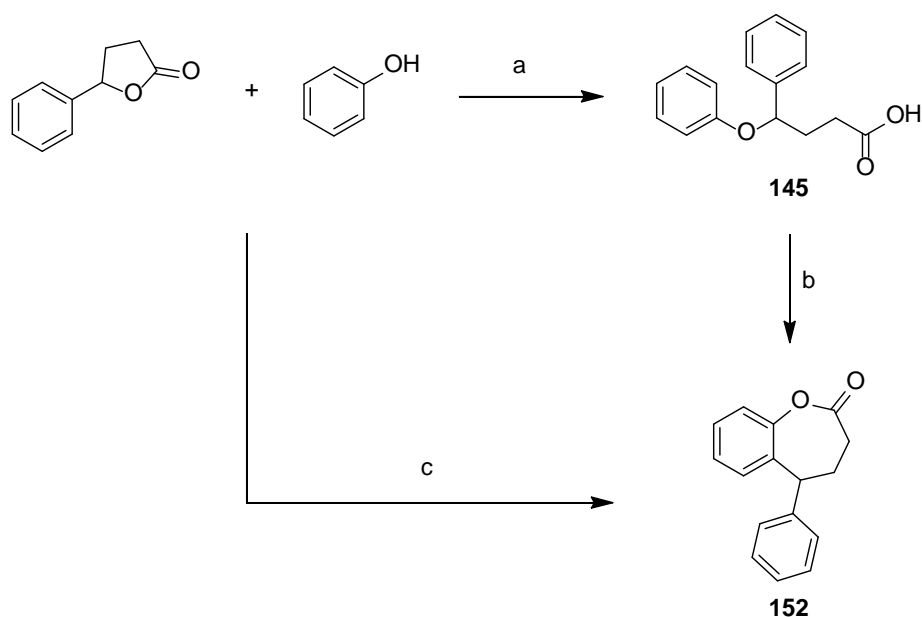


Scheme 4.20. Literature synthesis of 2-phenylbenzoxepinone (**122**) via the cyclopropane intermediate (**151**). (a) $(\text{CH}_3)_3\text{S}(\text{O})\text{I}$, NaH, DMSO, rt, then **150** in DMSO over 3 min, then rt, 2 h, 51%; (b) $(n\text{Bu})_3\text{SnH}$, AIBN, toluene, 90-100 °C, 1 h, 85%.

4.3.2 Attempted synthesis of 2-phenyl-3,4-dihydrobenzo[*b*]-oxepin-5(2*H*)-one

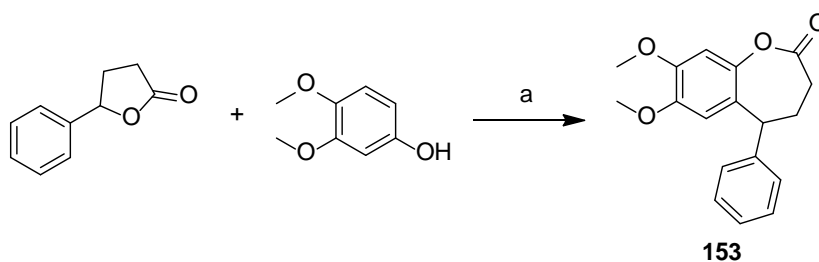
Despite Tatsuoka *et al.* previously being unsuccessful with a Friedel-Crafts cycliacylation, it was believed that a viable synthesis might be successful with appropriate conditions.³⁰⁰ As discussed below (section 4.5), it was the success with analogous substituted 8-phenylbenzosuberone compounds that provided hope for success.

Interestingly, Tatsuoka *et al.* had reported the reaction of γ -phenyl- γ -butyrolactone with phenol to yield the key 4-phenoxy-4-phenylbutanoic acid precursor (**145**) within a 1985 patent.³⁰⁵ Perhaps ominously, they also reported the conversion of **145** under Friedel-Crafts acylation conditions to the lactone (**152**), a structural isomer of 2-phenylbenzoxepinone (**122**) (Scheme 4.21). In fact, complete conversion of γ -phenyl- γ -butyrolactone and phenol to **152** under acidic conditions was also reported. This contradicted the earlier result described above (from the same group) where a Friedel-Crafts reaction of **145** instead afforded a complex mixture of α -tetralones **146-149**.



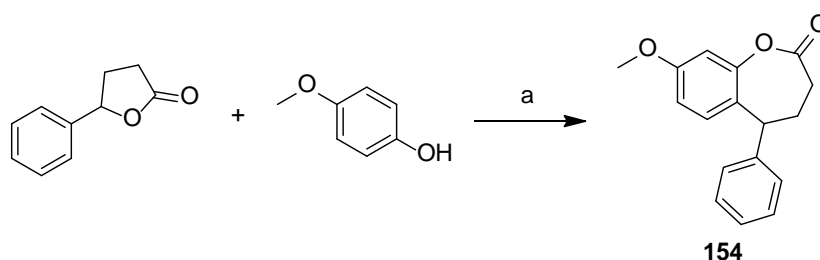
Scheme 4.21. Literature syntheses of the key 4-phenoxy-4-phenylbutanoic acid precursor (**145**) and subsequent reaction to give 5-phenyl-4,5-dihydrobenzo[*b*]oxepin-2(3*H*)-one (**152**). (a) NaOCH₃, CH₃OH, 65 °C, 1 h, then γ -phenyl- γ -butyrolactone, 150 °C, 85%; (b) 75% PPA, rt, 5 h, 30%. (c) 75% PPA, rt, 5 h, 30%.³⁰⁵

To examine this reaction further, γ -phenyl- γ -butyrolactone was reacted with 3,4-dimethoxyphenol in polyphosphoric acid at room temperature for 7 hours (Scheme 4.22).³⁰⁵ The product obtained was 7,8-dimethoxy-5-phenyl-4,5-dihydrobenzo[*b*]oxepin-2(3*H*)-one (**153**). No α -tetralone products were observed nor was there any sign of the target 2-phenylbenzoxepinone (**122**). The identity of **153** was confirmed by both 1D and 2D NMR experiments as well as the [M+H]⁺ molecular ion at *m/z* 239.3.



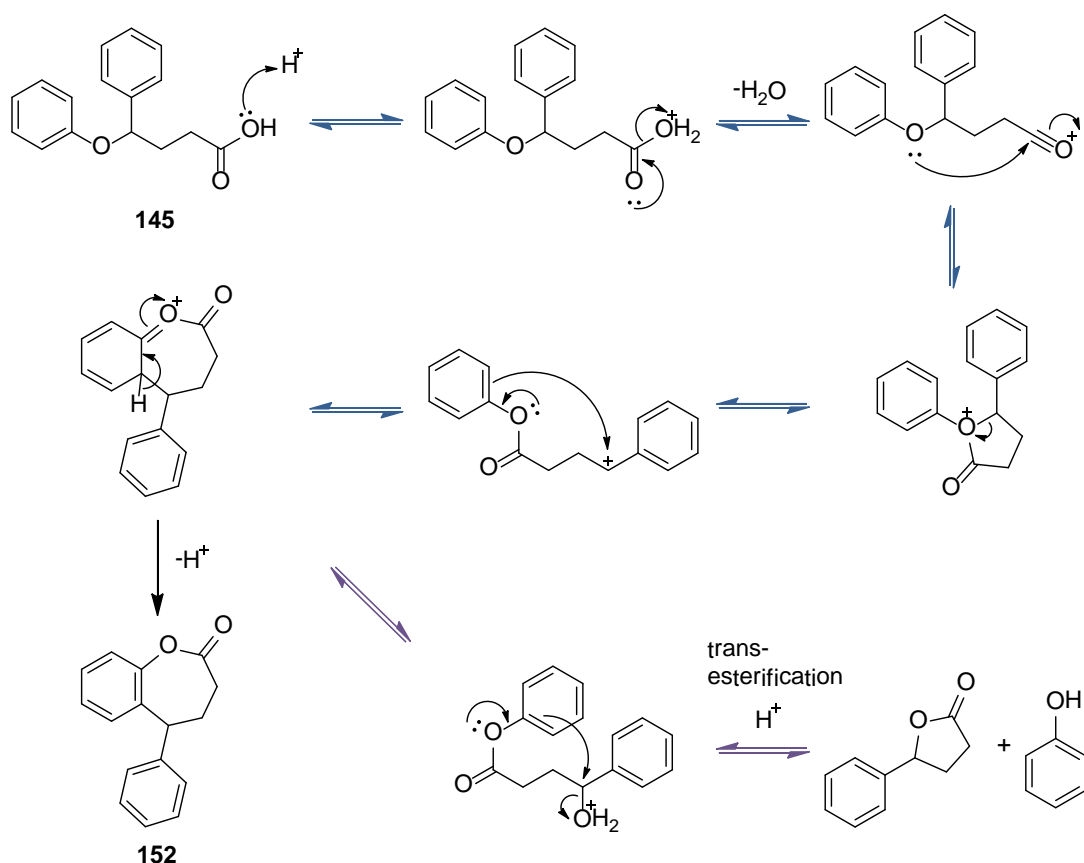
Scheme 4.22. Synthesis of 7,8-dimethoxy-5-phenyl-4,5-dihydrobenzo[*b*]oxepin-2(3*H*)-one (**153**). (a) PPA, rt, 7 h, 82%.

A similar result was observed when γ -phenyl- γ -butyrolactone was reacted with 4-methoxyphenol under the aforementioned acidic conditions (Scheme 4.23). 7-Methoxy-2-phenyl-3,4-dihydrobenzo[*b*]oxepin-5(2*H*)-one (**154**) was isolated in 46% with no evidence of either 7-methoxy-2-phenyl-3,4-dihydrobenzo[*b*]oxepin-5(2*H*)-one or α -tetralone by-products. Again, both 1D and 2D NMR experiments were required to characterise the product.



Scheme 4.23. Synthesis of 7-methoxy-2-phenyl-3,4-dihydrobenzo[*b*]oxepin-5(2*H*)-one (**154**). (a) PPA, rt, 7 h, 46%.

The mechanism of the rearrangement of the key butyrolactone intermediate (**145**) under acidic conditions is not immediately obvious. However, a proposed mechanism is described in Scheme 4.24. This mechanism attempts to rationalise the formation of **152**, whether it be directly through a rearrangement and dehydration of the butyrolactone intermediate (**145**) (shown in blue arrows) (as reported by Tatsuoka *et al.*³⁰⁵) or through a one-pot reaction of γ -phenyl- γ -butyrolactone and phenol under acidic conditions (shown in purple arrows). This proposed mechanism is by no means definitive and further investigation would be required to confirm such a reaction mechanism.



Scheme 4.24. Proposed reaction mechanism for the synthesis of 5-phenyl-4,5-dihydrobenzo[*b*]oxepin-2(3*H*)-one (**152**) from either 4-phenoxy-4-phenylbutanoic acid (**145**) (shown in blue) or from the reaction of γ -phenyl- γ -butyrolactone with phenol (shown in purple).

The alternative method centred upon ring expansion from 2-phenyl-4*H*-chromen-4-one (**150**) was also attempted (Scheme 4.20).³⁰⁰ Firstly, cyclopropanation of **150** was attempted using the Corey-Chaykovsky reaction.³⁰⁶ This reaction involves the reaction of a sulfur ylide with an electrophile such as a carbonyl, olefin, imine or thiocarbonyl (**155**) to give the corresponding epoxide, cyclopropane, aziridine or thionane (**156**). The sulfur ylide can be either dimethylsulfoxonium methylide (Corey's reagent) (**157**) or dimethylsulfonium methylide (**158**) (Figure 4.25). The synthesis of dimethylsulfoxonium methylide (**157**) was first reported in 1962 and has since been used extensively within the literature.³⁰⁷⁻³¹²

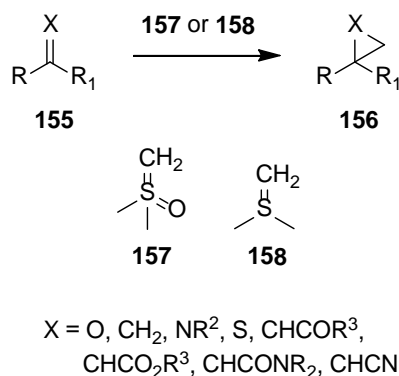
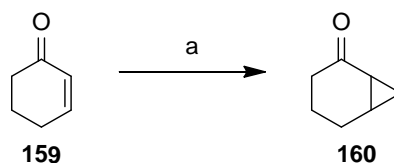


Figure 4.25. Corey-Chaykovsky reaction using dimethylsulfoxonium methylide (**157**) or dimethylsulfonium methylide (**158**).

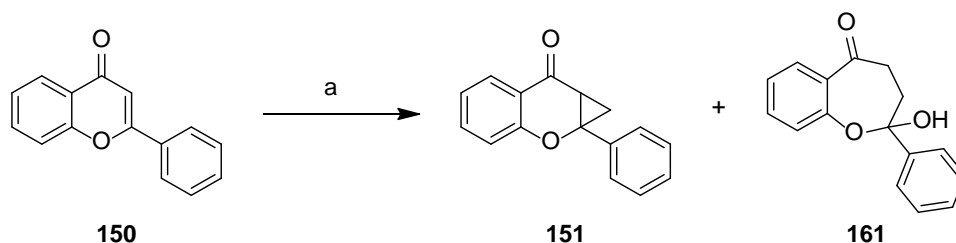
Dimethylsulfoxonium methylide (**157**) was prepared by reacting trimethylsulfoxonium iodide with sodium hydride in anhydrous dimethylsulfoxide according to literature procedures.^{306, 307, 313, 314} To test for ylide formation, the reaction was firstly trialled on a test substrate, 2-cyclohexenone (**159**) (Scheme 4.26). The ylide was allowed to form over a 40 minute period, before 2-cyclohexenone was added in a drop-wise manner according to the literature procedure.³¹⁵ The cyclopropane product (**160**) was obtained in 88% yield, which confirmed the procedure of the dimethylsulfoxonium methylide (**157**) formation.



Scheme 4.26. Trial reaction to test for dimethylsulfoxonium methylide (**157**) preparation using 2-cyclohexenone (**159**). (a) $(\text{CH}_3)_3\text{S}(\text{O})\text{I}$, NaH, DMSO, rt, 40 min, then **159** in DMSO over 3 min, then 50 °C, 2 h, 88%.

Employing the same reaction conditions as above, 2-phenyl-4*H*-chromen-4-one (**150**) was reacted with dimethylsulfoxonium methylide (**157**) at 50 °C for 2 hours (Scheme 4.27). In this instance, a mixture of products was observed by both LCMS

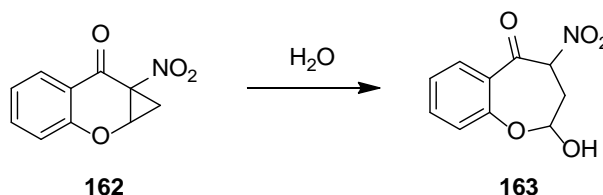
analysis and analytical RP-HPLC analysis. Following separation by column chromatography, ^1H NMR and ^{13}C NMR spectroscopy confirmed the presence of some desired cyclopropane product (**151**) (12%). The ^1H NMR spectrum of **151** displayed a doublet of doublets at δ 2.54 and 2.06 ppm that correspond to the diastereotopic protons of the cyclopropane group, as well as a triplet at δ 1.74 ppm that corresponds to the α -keto proton coupled to the diastereotopic protons. LCMS analysis showed the corresponding $[\text{M}+\text{H}]^+$ molecular ion at m/z 237.2 and RP-HPLC analysis indicated pure material. However, the major product (68%) was identified as the ring-opened 2-hydroxy-2-phenyl-3,4-dihydrobenzo[*b*]oxepin-5(2*H*)-one (**161**) (Scheme 4.27). The ^1H NMR spectrum of **161** is significantly different to **155** in the aliphatic region. A multiplet is observed at δ 3.49 ppm which integrates to the four alkyl protons of the newly formed 7-membered ring. LCMS analysis showed the $[\text{M}+\text{H}]^+$ molecular ion at m/z 256.2, consistent with the ring-expanded hemiketal product (**161**).



Scheme 4.27. Reaction of 2-phenyl-4*H*-chromen-4-one (**150**) to give the desired cyclopropane product (**151**) and by-product **161**. (a) $(\text{CH}_3)_3\text{S}(\text{O})\text{I}$, NaH, DMSO, rt, 40 min, then **150** in DMSO over 3 min, then 50 °C, 2 h, **151** (12%), **161** (68%).

A similar by-product has been noted within the literature, whereby a nitro-activated cyclopropane (**162**) was observed to react smoothly with water and open to 2-hydroxy-4-nitro-3,4-dihydrobenzo[*b*]oxepin-5(2*H*)-one (**163**) (Scheme 4.28).³¹⁶ In this case, it can be envisaged that the cyclopropane ring opens to give an oxonium ion and an enolate, which is stabilised by the α -nitro substituent. From here, the addition of water

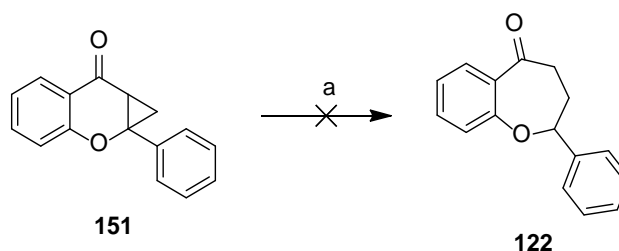
results in **163**. Similarly, it is proposed that following cyclopropane ring opening of compound **151**, the pendant phenyl ring serves to stabilise the oxonium ion, and the subsequent addition of water gives the hemiketal, **161**.



Scheme 4.28. Literature report of the nitro-activated cyclopropane (**162**) reacting with water to form 2-hydroxy-4-nitro-3,4-dihydrobenzo[*b*]oxepin-5(2*H*)-one (**163**).³¹⁶

Interestingly, this observed side-reaction could be prevented by cooling the reaction mixture to 0 °C prior to quenching of the reaction. Under these conditions, the desired cyclopropane product (**151**) was obtained in 81% yield. No ring-expanded material (**161**) was observed, just a small amount of the 2-phenyl-4*H*-chromen-4-one starting material (**150**).

The reductive cleavage (Pereyre's reaction) was performed on the cyclopropane product (**151**) using the conditions of Tatsuoka *et al.*³⁰⁰ A solution of **151** in toluene was heated with one equivalent of tri-*n*-butyltin hydride in the presence of azobisisobutyronitrile for 1.5 hours (Scheme 4.29). While the product obtained was a mixture, analysis by ¹H NMR spectroscopy and LCMS suggested that the desired product (**122**) was present but significant starting material (**151**) remained. However, longer reaction times resulted in the formation of degradation products. Unfortunately, **122** could not be retrieved in pure form either by column chromatography, RP-HPLC or crystallisation.



Scheme 4.29. Attempted Pereyre's reductive cleavage of the cyclopropane (**151**) to give 2-phenylbenzoxepinone (**122**). (a) $(n\text{Bu})_3\text{SnH}$, AIBN, toluene, 90-100 °C, 1.5 h.

4.3.3 Section discussion

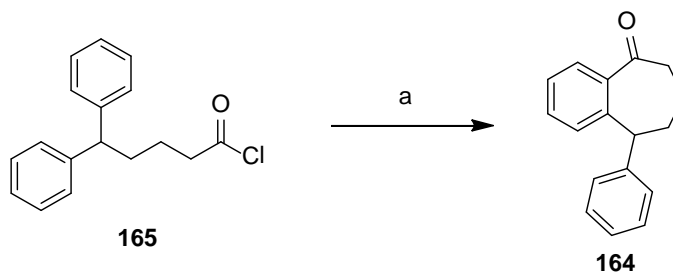
While this was an encouraging outcome, there remained significant further optimisation of the synthetic route to access the 2-phenylbenzoxepinone compounds. At this stage, as progress was being made on other targets, work toward the synthesis of the 2-phenylbenzoxepinones compound class was suspended. In order to reach the target compounds, optimisation of both the synthetic and purification procedures would be required. This would include the exploration of chemical substituents which may improve product conversion, as well as the development of purification strategies to isolate the desired products.

4.4 Synthetic studies of the 8-phenylbenzosuberone compound class

4.4.1 Synthetic access to the 8-phenylbenzosuberone compound class

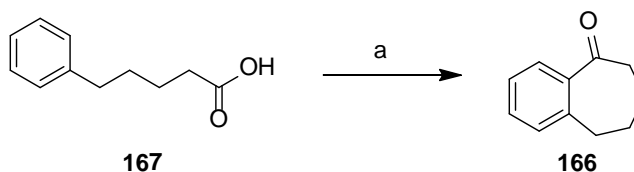
The third 6,7-bicyclic ring system examined was the 8-phenylbenzosuberone (8-phenyl-6,7,8,9-tetrahydro-5*H*-benzo[7]annulen-5-one) structure (**123**). The parent compound is unreported within the literature, which is somewhat surprising given that aryl substitution at each of the other positions of the cycloheptane ring has been described.^{260-266,317-319} The synthesis of 9-phenylbenzosuberone (9-phenyl-6,7,8,9-tetrahydro-5*H*-benzo[7]annulen-5-one) (**164**) was first reported in 1958 by Klemm and

Bower.²⁶¹ Similar to unsubstituted benzosuberone,³²⁰⁻³²⁵ **164** was synthesised *via* a Friedel-Crafts intramolecular acylation reaction of the corresponding diphenylvaleric acid (**165**) (Scheme 4.30). This process for the preparation of 9-phenylbenzosuberone was patented by Kofron in 1968.²⁶²



Scheme 4.30. Friedel-Crafts intramolecular acylation reaction of diphenylvaleric acid (**165**) in the synthesis of 9-phenylbenzosuberone (**164**). (a) AlCl_3 , CS_2 , 46°C , 12 h, 59%.²⁶¹

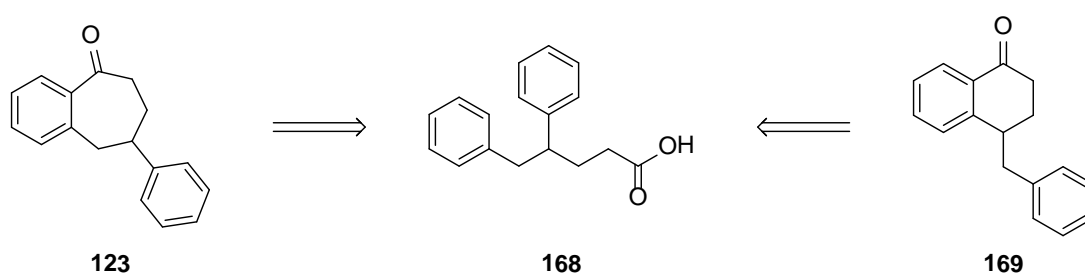
The synthesis of benzosuberone (**166**) is well reported within the literature.³²⁶⁻³²⁹ Most commonly, as seen above, it has been synthesised through a Friedel-Crafts intramolecular acylation reaction of the 5-phenylpentanoic acid (**167**) (Scheme 4.31).^{320-325,330}



Scheme 4.31. Friedel-Crafts intramolecular acylation reaction of 5-phenylpentanoic acid (**167**) in the synthesis of benzosuberone (**166**). (a) PPA, rt, 6 h, 92%.³³⁰

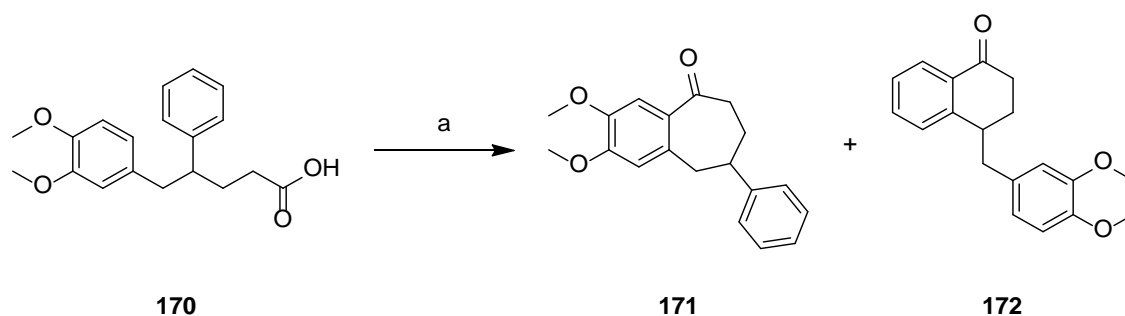
In considering the synthesis of 8-phenylbenzosuberone (**123**), the desired precursor to the Friedel-Crafts intramolecular acylation reaction is 4,5-bis-(4'-methoxyphenyl)pentanoic acid (**168**), but it is also apparent that this substrate cyclises onto the 4-phenyl substituent giving 4-benzyl-3,4-dihydronaphthalen-1(2*H*)-one (**169**)

(Scheme 4.32). Along these lines, Hatam and Whiting had cyclised the 4,5-bis-(4'-methoxyphenyl)pentanoic acid (**168**) using Friedel-Crafts acylation conditions and noted no evidence of the benzosuberone-based product. To be successful in the synthesis of 8-phenylbenzosuberone, a process to circumvent this side reaction would be necessary.



Scheme 4.32. It can be envisaged that both 8-phenylbenzosuberone (**123**) and 4-benzyl-3,4-dihydronaphthalen-1(2*H*)-one (**169**) can be synthesised through an intramolecular Friedel-Crafts acylation reaction of 4,5-bis-(4'-methoxyphenyl)pentanoic acid (**168**).

A preliminary study of this reaction was performed by Thompson who confirmed that the intramolecular Friedel-Crafts acylation reaction of 4,5-bis-(4'-methoxyphenyl)pentanoic acid (**168**) gave exclusively the 6-membered tetralone product, **169**, when cyclised *via* Friedel-Crafts acylation (using either aluminium trichloride reaction conditions or polyphosphoric acid reaction conditions).³³¹ The use of activating or deactivating aryl substituents was consequently investigated. As such, the Friedel-Crafts acylation reaction of 5-(3,4-dimethoxyphenyl)-4-phenylpentanoic acid (**170**) appeared to give a 7:3 mixture of the 2,3-dimethoxy-8-phenylbenzosuberone (**171**) and the 6-membered tetralone (**172**) (Scheme 4.33). However, the compounds were unable to be isolated in pure form.

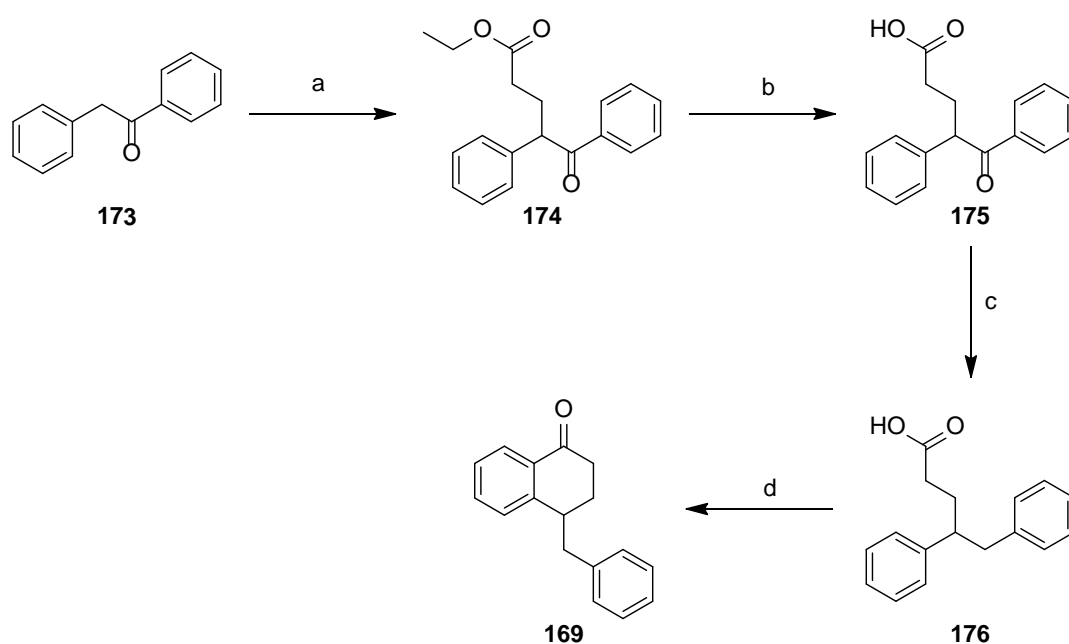


Scheme 4.33. Synthesis of 2,3-dimethoxy-8-phenylbenzosuberone (**171**) as described by Thompson. (a) PPA, 100 °C, 4 h, 48% (**171/172** (7:3)).³³¹

While incomplete, these data emphasised the possibility of accessing these hitherto undescribed 8-phenylbenzosuberone derivatives for which there was also the prospect of further derivatisation. This work examines the potential of accessing these compounds in pure form by modified synthesis or isolation procedures.

4.4.2 Attempted synthesis of 8-phenyl-6,7,8,9-tetrahydro-5*H*-benzo[7]annulen-5-one

The synthesis of 8-phenylbenzosuberone (**123**), or be it 4-benzyl-3,4-dihydronaphthalen-1(2*H*)-one (**169**), was examined to establish the synthetic procedures for preparing the key precursors, the 4,5-diarylpentanoic acids (**168** and **170**), as shown in Scheme 4.34. First, deoxybenzoin (**173**) underwent Michael addition with ethyl acrylate to give the corresponding ethyl ester (**174**) in 98% yield. The melting point (55–56 °C) was comparable to the literature value (45–57 °C).³³² The ethyl ester (**174**) was hydrolysed under basic conditions to afford the acid (**175**) in 95% yield.



Scheme 4.34. Synthesis of 4-benzyl-3,4-dihydronaphthalen-1(2H)-one (**169**). (a) *t*BuOK, ethyl acrylate, *t*BuOH, rt, 2 h, 98%; (b) 1,4-dioxane/1 M aq. NaOH (1:1), 100 °C, 2 h, 95%; (c) (CH₃CH₂)₃SiH, CF₃CO₂H, N₂, rt, 16 h, 85%; (d) PPA, 80 °C, 4 h, 67%.

Reduction of the keto function of **175** was attempted using Wolff-Kishner conditions as described by Reddy and Rao,³³³ but was unsuccessful, perhaps due to challenges in achieving the high temperatures needed for hydrazone decomposition. Reduction of the ketone using the Kursanov-Parnes conditions,³³⁴ triethylsilane in trifluoroacetic acid, was successful and gave the corresponding methylene compound (**176**) which was isolated in 85% yield. The ¹H NMR spectrum displayed a signal at δ 3.05 – 2.95 ppm corresponding to the benzylic protons and the [M-H]⁺ molecular ion was observed at *m/z* 253.2, both of which compared well with literature values.³³⁵ The final step was the Friedel-Crafts intramolecular acylation of the acid (**176**) which was performed in neat polyphosphoric acid at 80 °C for 4 hours. The 6-membered tetralone (**169**) was obtained exclusively, as previously observed by Thompson, with no trace of 8-phenylbenzosuberone (**123**) as determined by ¹H NMR spectroscopy and chiral HPLC.³³¹ Compound **169** was isolated in 67% yield and good purity (>95%). ¹H NMR spectroscopy shows the benzylic methylene protons as a multiplet at δ 3.02 – 2.87 ppm.

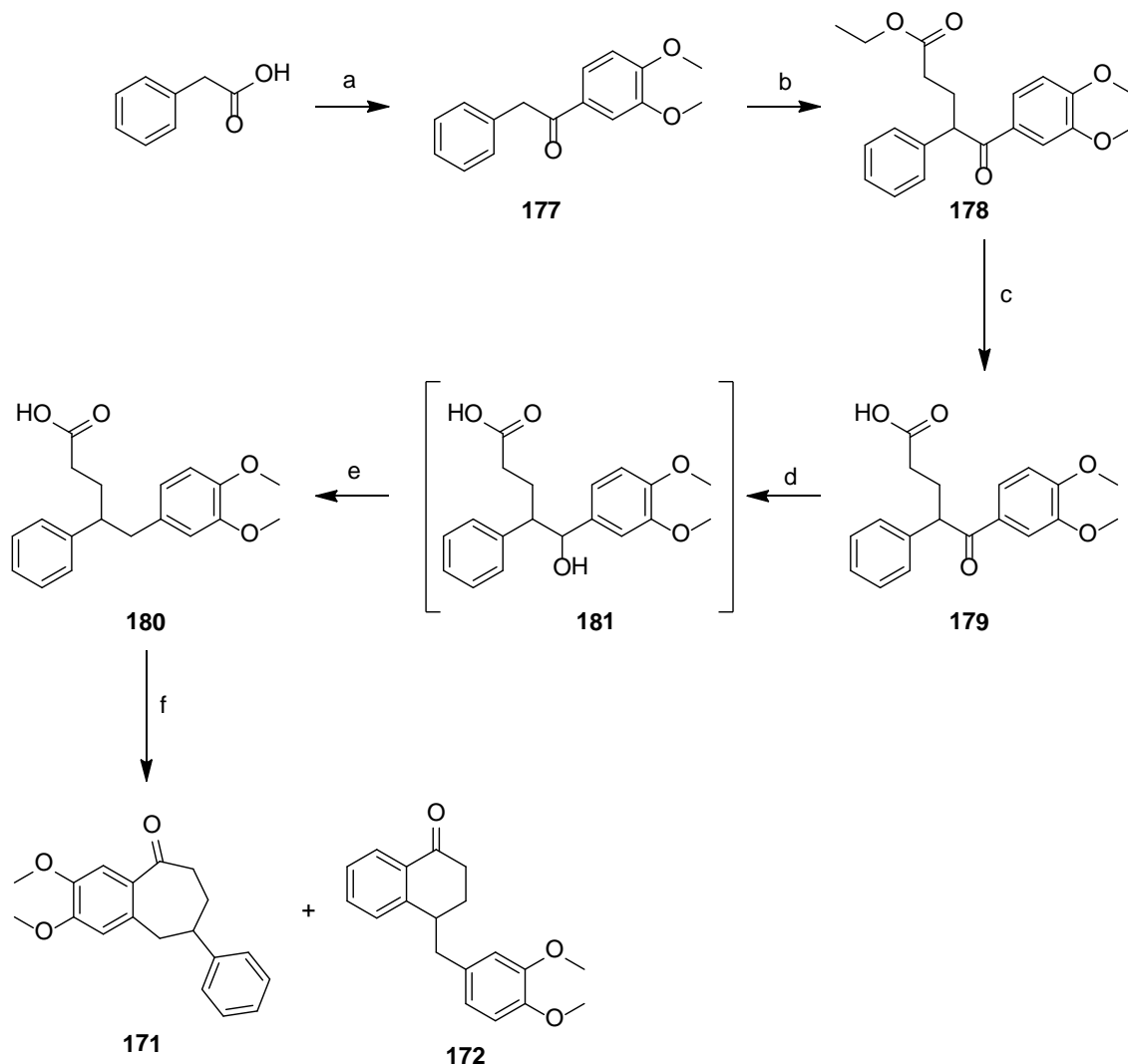
This spectral data correlated well with literature reports.³³⁵⁻³³⁷ While not affording the target compound, a robust synthetic route had been established that should be suited to the synthesis of analogue compounds, including poly-methoxylated 8-phenylbenzosuberone compounds.

4.4.3 Synthesis of 2,3-dimethoxy-8-phenyl-6,7,8,9-tetrahydro-5H-benzo[7]annulen-5-one

For the attempted synthesis of 2,3-dimethoxy-8-phenylbenzosuberone (2,3-dimethoxy-8-phenyl-6,7,8,9-tetrahydro-5H-benzo[7]annulen-5-one) (**171**), the synthesis of the key carboxylic acid derivative, 5-(3,4-dimethoxyphenyl)-4-phenylpentanoic acid (**170**), was achieved in a manner similar to that described above (Scheme 4.35). Firstly, the starting deoxybenzoin (**177**) was prepared by a Friedel-Crafts intermolecular acylation reaction of veratrole with phenylacetyl chloride (prepared from phenyl acetic acid and oxalyl chloride in dichloromethane) in the presence of aluminium trichloride. This afforded 1-(3,4-dimethoxyphenyl)-2-phenylethanone (**177**) in 85% yield. This one-pot procedure gave a better yield than that using thionyl chloride in the preparation of the acid chloride. The ¹H NMR spectrum of **177** showed the characteristic splitting pattern of the 1,2,4-trisubstituted benzene ring and the melting point corresponded to literature values.^{338,339}

Alkylation of 1-(3,4-dimethoxyphenyl)-2-phenylethanone (**177**) with ethyl acrylate by Michael addition gave the ester compound (**178**) in 93% yield and good purity (>90%) as shown by analytical RP-HPLC. Compound **178** is not reported in the literature, so its identity was confirmed by the molecular ion at *m/z* 357.2, and analysis of the ¹H NMR

and ^{13}C NMR spectra. The ethyl ester was hydrolysed under basic conditions to afford the corresponding acid (**179**) in 96% yield.



Scheme 4.35. Synthesis of 2,3-dimethoxy-8-phenylbenzosuberone (**171**) and 4-(3,4-dimethoxybenzyl)-3,4-dihydronaphthalen-1(2H)-one (**172**). (a) $(\text{COCl})_2$, CH_2Cl_2 , 60°C , 1 h, then dimethoxybenzene, AlCl_3 , rt to 60°C , 4 h, 85%; (b) $t\text{BuOK}$, ethyl acrylate, $t\text{BuOH}$, rt, 2 h, 93%; (c) 1,4-dioxane/1M aq. NaOH (1:1), 100°C , 2 h, 96%; (d) $(\text{CH}_3\text{CH}_2)_3\text{SiH}$, $\text{CF}_3\text{CO}_2\text{H}$, N_2 , rt, 1 h; (e) $(\text{CH}_3\text{CH}_2)_3\text{SiH}$, rt, 15 h, 92%; (f) PPA, 80°C , 4 h, 92% (**175/176** (4:1)).

The reduction of the ketone was attempted using Kursanov-Parnes conditions (described in section 4.4.2), though it was found to be more resistant than the earlier case. After stirring at room temperature for 7 days, only 50% conversion to the fully reduced methylene compound (**180**) was observed, with the remainder being that of the

partially reduced alcohol intermediate (**181**) (the $[M-H]^+$ molecular ion was observed at m/z 329.3). The reaction was successfully driven to completion by addition of a further two equivalents of triethylsilane and stirring for a further 4 days. Compound **180** is unreported within the literature, however key NMR data correlated to that observed with the unsubstituted equivalent (**176**).

Upon closer examination, it was found that the Kursanov-Parnes reaction proceeded almost instantaneously to the alcohol intermediate (**181**) and that the subsequent reduction to the methylene (**180**) was the rate-limiting step. Thus in a modified procedure, 1 hour after commencement of the reaction two further equivalents of triethylsilane were added and 100% conversion to the methylene product was observed by analytical RP-HPLC within 16 hours. It should be noted that Wolff-Kishner conditions again failed to yield the reduced ketone compound (**180**), with several degradation products evident from analytical RP-HPLC.

Compound **180** was subjected to a Friedel-Crafts intramolecular acylation reaction in polyphosphoric acid (as described earlier). As anticipated, a mixture of the 7-membered benzosuberone (**171**) and 6-membered benzyltetralone (**172**) was obtained in approximately a 4:1 ratio as determined by 1H NMR spectroscopy. The two compounds could not be separated by the standard techniques available. They co-eluted by both t.l.c. and analytical RP-HPLC trace. In addition, attempts to selectively crystallise one component were unsuccessful.

As these products are chiral and both present as racemic mixtures, an attempt was made to resolve them by chiral chromatography. They were analysed first by elution through

three different stationary phases; Phenomonex Lux Cellulose 1 (Figure 4.36), Cellulose 2 (Figure 4.37) and Amylose 2 (Figure 4.38) columns. The eluents were isocratic mixtures of 10-20% ethanol in petroleum spirits. The mixture of **171** and **172** could be partially resolved by analytical chiral chromatography using an Amylose 2 column (Figure 4.38) with a single benzosuberone (**171**) enantiomer and single tetralone (**172**) enantiomer able to be isolated (Figure 4.39).

The single late-running component obtained (Figure 4.40) was identified by ^1H NMR spectroscopy as an enantiomer of 2,3-dimethoxy-8-phenylbenzosuberone (**171**). A semi-preparative elution was used to isolate 8 mg of **171**.

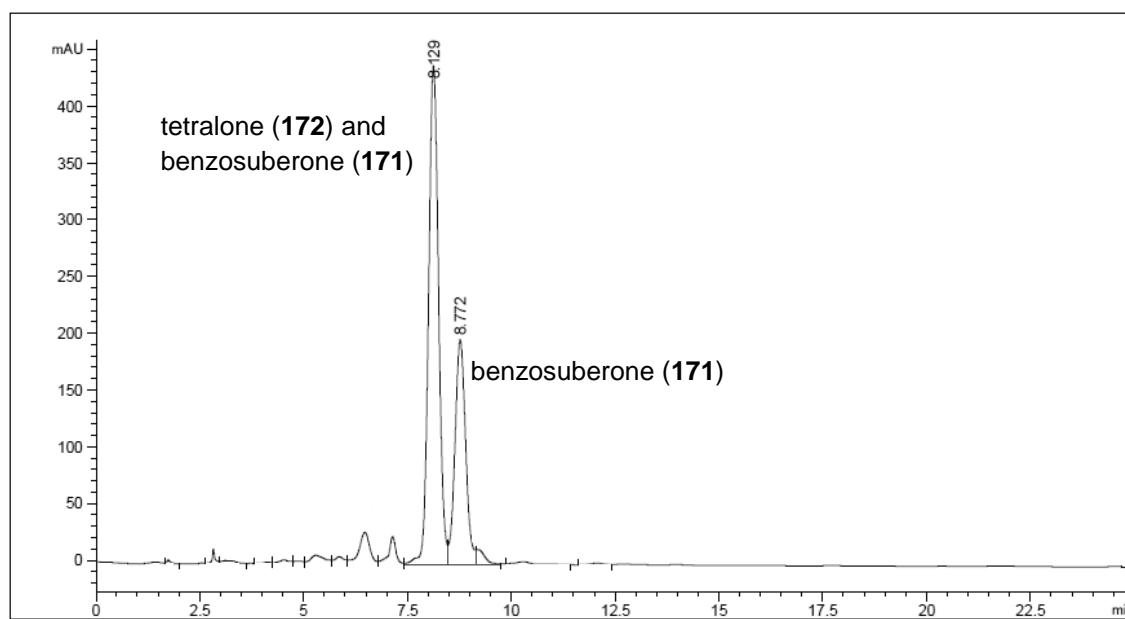


Figure 4.36. Chiral chromatography profile at 254 nm of the reaction mixture of the benzosuberone (**171**) and the tetralone (**172**) compounds using the Cellulose 1 column.

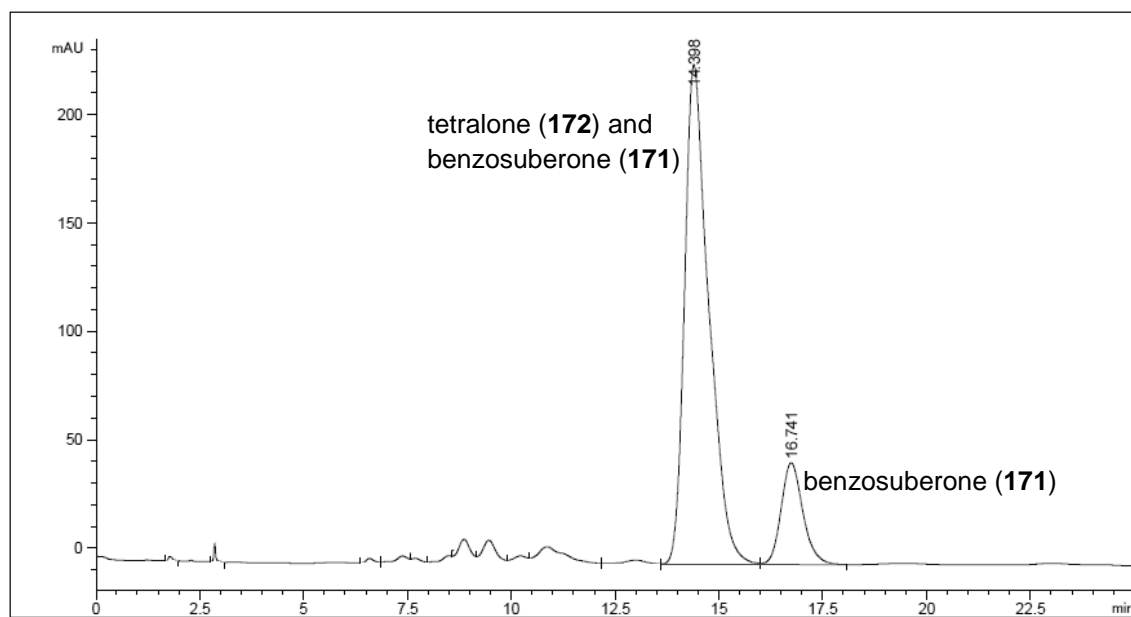


Figure 4.37. Chiral chromatography profile at 254 nm of the reaction mixture of the benzosuberone (171) and the tetralone (172) compounds using the Cellulose 2 column.

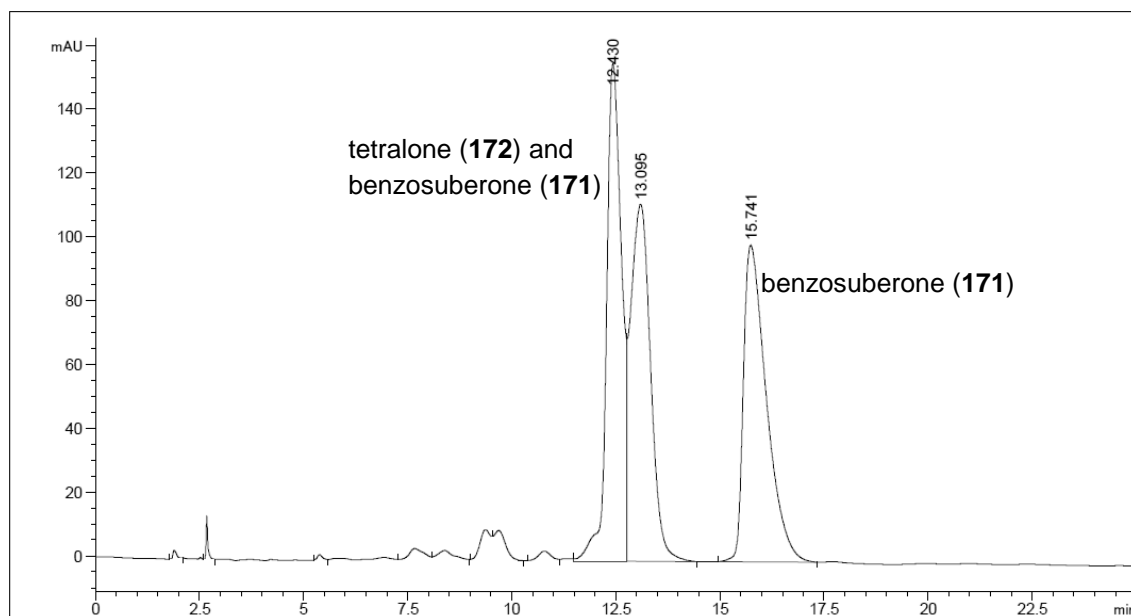


Figure 4.38. Chiral chromatography profile at 254 nm of the reaction mixture of the benzosuberone (171) and the tetralone (172) compounds using the Amylose 2 column.

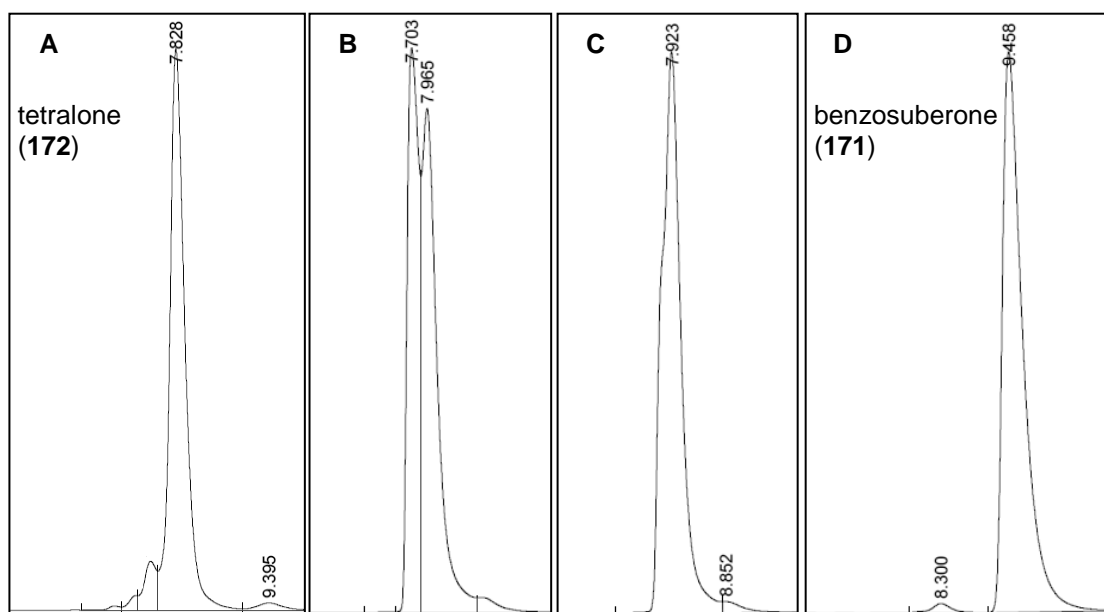


Figure 4.39. Collected fractions from the chiral HPLC separation of the benzosuberone (**171**) and the tetralone (**172**) using the Amylose 2 stationary phase and eluting with 20% ethanol in petroleum spirits. Fractions were collected in order A, B, C, D.

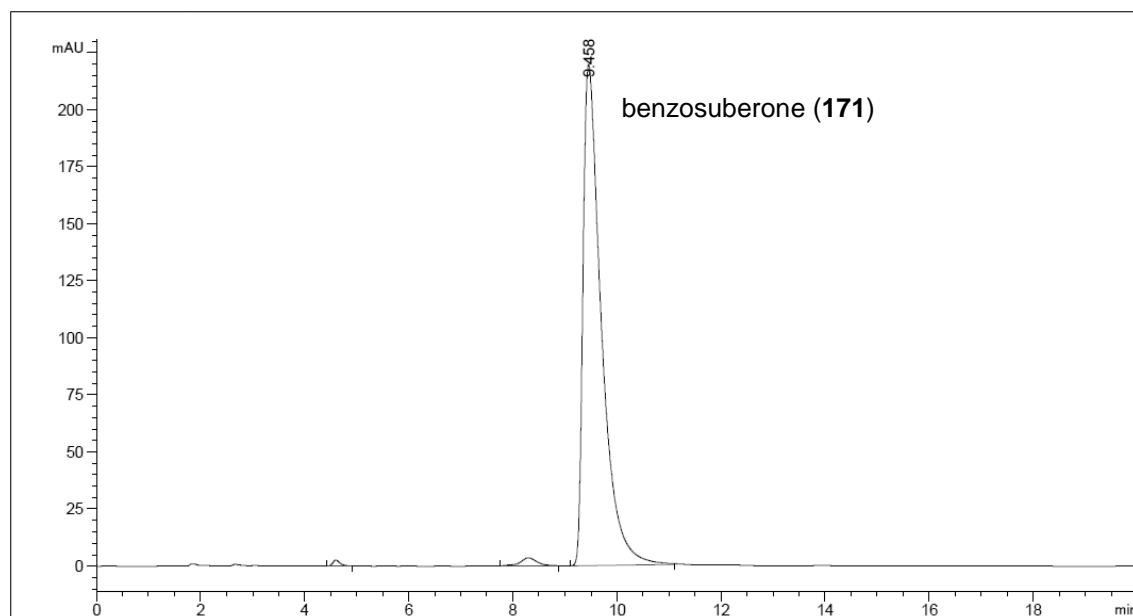


Figure 4.40. Chiral chromatography profile at 254 nm (Amylose 2, 20% ethanol in petroleum spirits) of purified 2,3-dimethoxy-8-phenylbenzosuberone (**171**).

The isolated 2,3-dimethoxy-8-phenylbenzosuberone (**171**) was characterised by ^1H NMR spectroscopy, ^{13}C NMR spectroscopy, 2D NMR spectroscopy, analytical RP-HPLC and HRMS. The splitting of the aromatic signals within the ^1H NMR spectrum was particularly important in identifying **171** from the tetralone material (**172**). As shown in Figure 4.41, the aromatic region of the ^1H NMR spectrum showed two distinct singlets (δ 7.44 and 6.54 ppm), each of which integrate to one proton, that are characteristic of the 2,3-dimethoxy-2-phenylbenzosuberone compound (**171**). The additional five protons can be accounted for in the triplet, triplet and doublet signals, all consistent with a phenyl substituent. Conversely, **172** only displays only one singlet peak in the aromatic region of the ^1H NMR spectrum (δ 6.82 ppm).

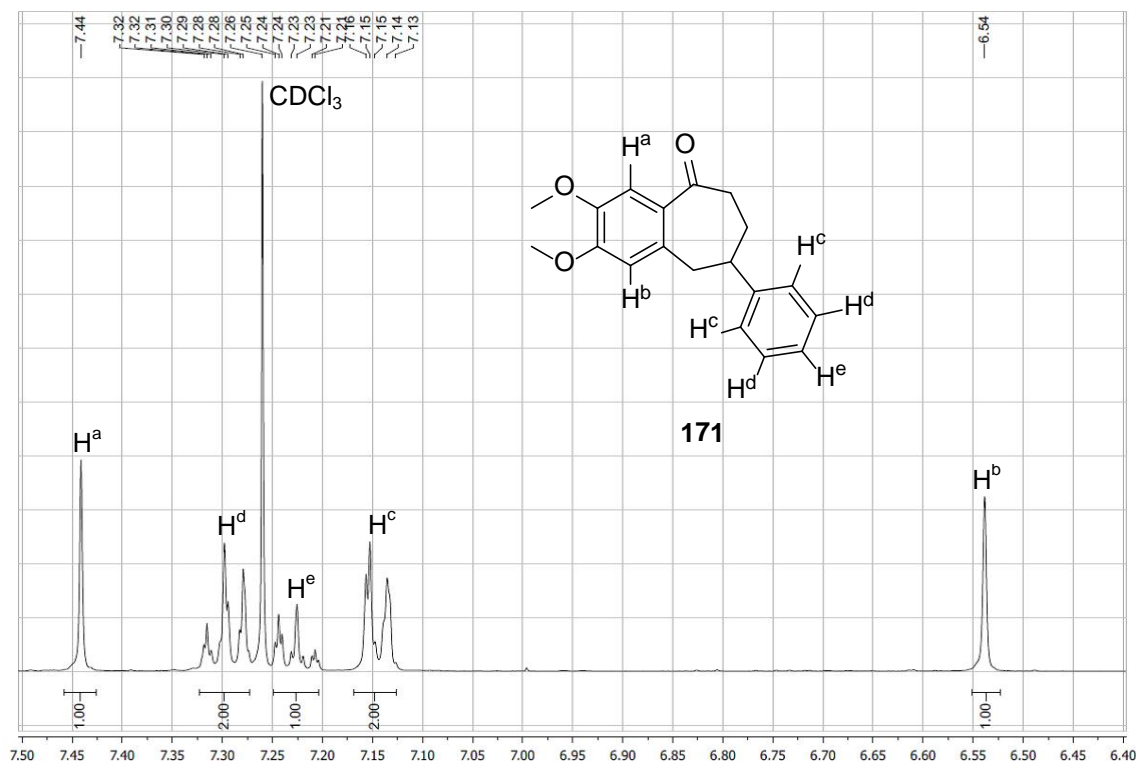


Figure 4.41. The assigned aromatic region of the ^1H NMR spectrum of 2,3-dimethoxy-8-phenylbenzosuberone (**171**). Chemical shift (δ) in ppm is shown along the x-axis.

4.4.4 Section discussion

A method for the synthesis and isolation of 2,3-dimethoxy-8-phenylbenzosuberone (**171**) has been identified within this work, and the subsequent isolation of the 6,7-fused ring system compound was achieved. This represents the first synthesis of the basic 8-phenylbenzosuberone class and provides the basis for further studies. In particular, the capacity to influence the regioselectivity of the ring formation step will be of interest in the design of substituted analogues. Also, chiral separation, useful in a synthetic sense here, highlights the potential for chiral-directed syntheses of this under-explored molecular class in the future.

4.5 Chapter conclusions and future directions

In this chapter, the syntheses of three series of relatively rare compound classes were explored. In some respects, the outcomes were disappointing with no class emerging as an obvious scaffold for further development. In other respects, some significant progress was made toward novel compound series.

The Schmidt reaction and Beckmann rearrangement were examined for the synthesis of the 2-phenylbenzoxazepinone compounds. Whilst the reaction conditions were successful with the most basic flavanone substrate, the scope of these reactions proved limited and not suitable for the generation of the methoxy functionalised analogues. However, 2-phenylbenzoxazepinone (**121**) demonstrated both antiplasmodial and *h*PDE1 activity, and therefore may serve as a suitable starting point for further investigation of the *Pf*PDEs.

The synthesis of the 2-phenylbenzoxepinone compound class was also attempted. In some respects this work was led astray by conflicting literature reports. On the other hand, it remains surprising that the various precursor carboxylic acids are so resistant to the expected Friedel-Crafts intramolecular acylation reaction. The ring expansion method appears likely to be successful, after some initial difficulties, and is worthy of further study.

The first example of the synthesis of the previously unreported 8-phenylbenzosuberone class was described. Pivotal to the success in this synthesis was the application of chiral chromatography to overcome difficulties in separation of the structural isomers. This result was important in itself, but also flags a pathway to achieve the separation of other mixtures, especially mixtures containing racemic compounds that might be poorly resolved by achiral purification methods. The likelihood of both enantiomers co-eluting with other components of a mixture would seem less likely in a chiral environment. Of course, there remains a limitation in the capacity to pursue this compound class because of the inability to obtain large amounts of pure material.

While in the context of new antimalarial compounds little was achieved, save for the activity of 2-phenylbenzoxazepinone (**121**), the work described in this chapter charts significant progress towards compound classes of potential medicinal value. Ultimately, it was the success detailed in the following chapter (Chapter 5) that took priority over these compounds being further pursued as novel PDE inhibitor scaffolds.

Chapter 5

Chromanone analogues of LY294002 as phosphodiesterase inhibitors

5.1 Introduction

In Chapter 4, three series of novel 6,7-fused ring system compounds were investigated as potential novel phosphodiesterase inhibitor scaffolds. While some progress was made in each series, these scaffolds were not pursued in further medicinal chemistry campaigns. This was, in part, due to the success of an alternate scaffold that was developed from the synthetic chromone compound, LY294002 (**182**) (Figure 5.1). The development of this scaffold as a novel antiplasmodial chemotype is described in this chapter.

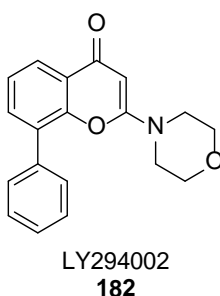


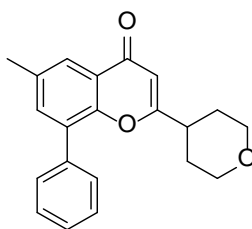
Figure 5.1. The structure of the synthetic chromone, LY294002 (**182**).

LY294002 (**182**) is a phosphoinositide 3-kinase (PI3K) inhibitor that has been widely used in the characterisation of the actions of PI3K. It has an IC_{50} value of approximately 1 μ M against the class I PI3K isoforms. Among a range of off-target activities, LY294002 has also been shown to inhibit human PDEs. In literature reports by Abbott and Thompson, LY294002 and a series of structurally related 2-morpholinochromones were shown to inhibit *hPDE2* and *hPDE3* with IC_{50} values of 40 μ M and 100 μ M, respectively.^{340,341} In the same year, Nakamura *et al.* showed that LY294002 inhibited PDE activity of the soluble fraction of adipocytes in a comparable manner to the archetypal *hPDE4* inhibitor, rolipram.³⁴² This suggested that *hPDE4* is a target of LY294002. More recently, the PDE4 activity in murine cardiac myocytes was shown to be blocked by LY294002, although an alternate PI3K-dependent mechanism of inhibition was proposed.³⁴³ In 2006, Gharbi *et al.* utilised a proteomic approach to identify numerous binding partners of an LY294002 derivative, which had been immobilised through the pendant phenyl ring, among which PDE4A in WEHI-231 cells and PDE1A and PDE10A from HeLa cells were identified.³⁴⁴ In unpublished work, LY294002 has since been assessed for activity at each human PDE isoform (Table 5.2). This work shows that LY294002 inhibits multiple PDE isoforms, particularly *hPDE10A1* and *hPDE11A*. The observed inhibition suggests that the LY294002 chromone template might serve as a useful starting point for the design and synthesis of PDE isoform-selective inhibitors.

Table 5.2. LY294002 (**182**) inhibition of human PDE isoforms.

<i>hPDE</i> isoform	1A	2A	3A	4A	4B	4C	4D	5A	6C	7A	8A	9A	10A	11A
% inhibition (10 μ M)	11	23	NI	41	45	25	41	50	25	NI	NI	NI	85	65
% inhibition (1 μ M)	NI	12	NI	NI	-	-	-	NI	NI	NI	NI	NI	11	23
IC_{50} (μ M)	-	40	100	-	-	-	-	-	-	-	-	-	1.3	4.1

Further work conducted within the laboratory investigated the replacement of the morpholine group with a tetrahydropyran group, as exemplified by compound JN8-6 (**183**) (Figure 5.3).³⁴⁵ This replacement resulted in compounds that demonstrated more potent PDE inhibition than LY294002 at certain *h*PDE isoforms, as well as significantly reduced PI3K inhibition ($IC_{50} > 8\mu M$). In particular, stronger inhibition at *h*PDE1 and *h*PDE4 was apparent (it should be noted that the single point assays were conducted at 1 μM in this case). The structure-activity relationship of the 2-tetrahydropyranochromone series continues to be pursued.



JN8-6
183

<i>h</i> PDE isoform	1A	2A	3A	4A	4B	4C	4D	5A	6C	7A	8A	9A	10A	11A
% inhibition (1 μM)	26	NI	NI	29	42	17	20	NI	12	13	NI	NI	12	23

Figure 5.3. JN8-6 (**183**) inhibition of human PDE isoforms.

The objective of the work described in this chapter was to examine an additional change to the scaffold – a formal reduction of the chromone ring to the equivalent chromanone. This has obvious parallels to the structures studied in Chapter 4, where the synthetic targets were saturated 6,7-fused ring systems that were based upon the activities of natural product flavanones.

Such a chromanone (**184**), of which the structure is shown in Figure 5.4, has not previously been reported. The parent structure (**185**) and some simple analogues are reported in just two patents; one pertaining to their use as beta secretase inhibitors, and

another as intermediates in the preparation of beta secretase inhibitors.^{346,347} This chemotype was thus available for investigation as a novel class of antiparasmodial compounds or as novel PDE inhibitors. Therefore, the aim of this chapter was to prepare and evaluate the biological activity of these compounds.

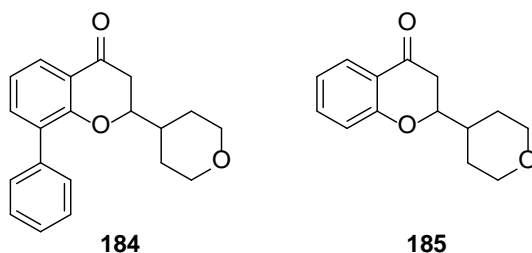
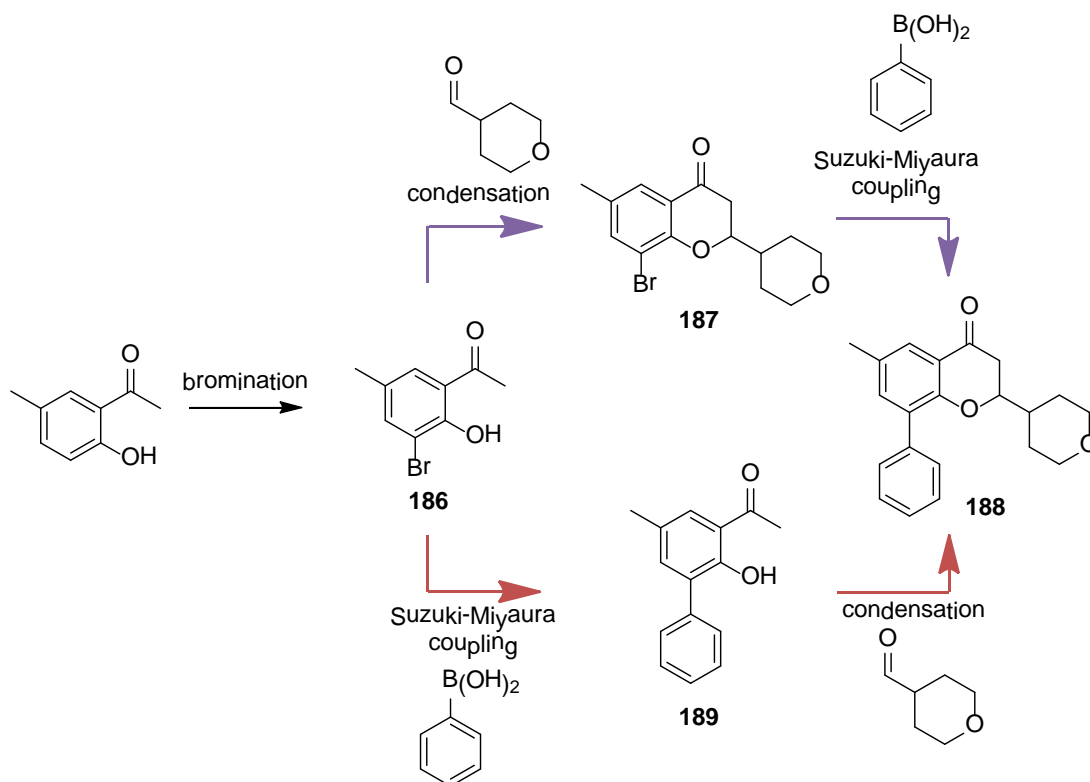


Figure 5.4. 8-Phenyl-substituted analogue (**184**) and the chromanone core scaffold (**185**).

It was envisaged that 6-methyl-8-phenyl-2-(tetrahydro-2H-pyran-4-yl)chroman-4-one (**184**) and analogues could be synthesised through either of two synthetic pathways that included pivotal sequential chromanone ring formation and pendant aryl substitution (Scheme 5.5, pathway one in purple, pathway two in red). The pathways differ only in the order of these transformations and both have been investigated. It was decided to include a 6-methyl substituent as this acts as a synthetic expedient in directing bromo substitution *ortho* to the phenol, and was apparently not detrimental to activity observed with compound JN8-6 (**183**) above.³⁴⁸

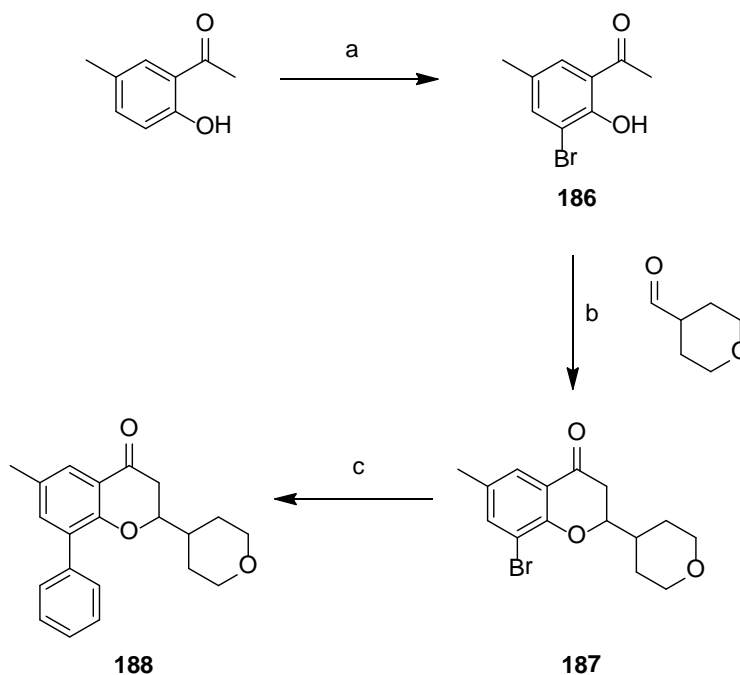


Scheme 5.5. Envisaged synthetic pathways to 8-phenyl-2-(tetrahydro-2*H*-pyran-4-yl)chroman-4-one (**188**) (pathway one in purple, pathway two in red).

5.2 Synthesis of 6-methyl-8-phenyl-2-(tetrahydro-2*H*-pyran-4-yl)chroman-4-one

5.2.1 Pathway one

To begin, 1-(2-hydroxy-5-methylphenyl)ethanone was brominated to give 1-(3-bromo-2-hydroxy-5-methylphenyl)ethanone (**186**) in high yield (96%) using the procedure of Abbott,³⁴⁸ where bromine in glacial acetic acid was added to a stirring solution of the acetophenone and sodium acetate in glacial acetic acid at 0 °C (Scheme 5.6). It was noted that initially the reaction stalled at approximately 50% conversion, but addition of a further equivalent of bromine drove the reaction to completion. The ¹H NMR spectrum was consistent with that reported.³⁴⁸ An alternative bromination procedure described by Abbott utilising chloroform as solvent gave a poorer yield.³⁴⁸



Scheme 5.6. Synthesis of 6-methyl-8-phenyl-2-(tetrahydro-2*H*-pyran-4-yl)chroman-4-one (**188**). (a) Br₂, CH₃CO₂H, CH₃CO₂Na, 0 °C to rt, 24 h, then Br₂, CH₃CO₂H, 0 °C to rt, 24 h, 96%; (b) Na₂B₄O₇·10H₂O, CH₃CH₂OH, 78 °C, 48 h, 87%; (c) C₆H₅B(OH)₂, Cs₂CO₃, Pd(CH₃CO₂)₂, PCy₃, (*n*Bu)₄NBr, 1,4-dioxane/H₂O (6:1), MW, 150 °C, 30 min, 94%.

Compound **186** then underwent a condensation reaction with tetrahydro-2*H*-pyran-4-carbaldehyde to form the key chromanone intermediate, **187** (Scheme 5.6). Under the conditions of sodium tetraborate as a base in ethanol at reflux for 48 hours, 90% conversion to **187** was observed. Recrystallisation with ethanol/ethyl acetate (5:1) gave an 87% yield of the pure material (**187**). Its identity was confirmed through ¹H NMR and ¹³C NMR spectroscopy and observation of the [M+H]⁺ molecular ion at *m/z* 325.2. The ¹H NMR spectrum of **187** is complicated due to overlapping signals and the rotation of the tetrahydropyran ring on the NMR time scale, with the symmetrical methylene carbons of the tetrahydropyran group each appearing as two signals in the ¹³C NMR spectrum when performed at standard operating temperature (298 K). Proton and carbon NMR assignments were elucidated using 2D NMR spectroscopy experiments.

In the reaction of **186** with 2-tetrahydropyrancarbaldehyde, a number of variations to the conditions were examined; for example further equivalents of the carbaldehyde were added at 24 hours and 48 hours, and the reaction time was extended to 5 days. These variations failed to produce as successful conversion to **187** but rather, degradation materials were observed by analytical RP-HPLC. Barium hydroxide was trialled in the place of sodium tetraborate in this reaction but afforded only 10% conversion to the cyclised product (**187**) and the formation of several unidentifiable by-products. A microwave irradiation procedure reporting the synthesis of 2-alkyl-substituted chromanone derivatives was also examined.³⁴⁹ In this case, a slight excess of diisopropylamine as a base was employed with microwave heating in ethanol at 170 °C for 1 hour. LCMS analysis gave no evidence of either the starting materials or the desired chromanone (**187**), but a range of other side-products were observed.

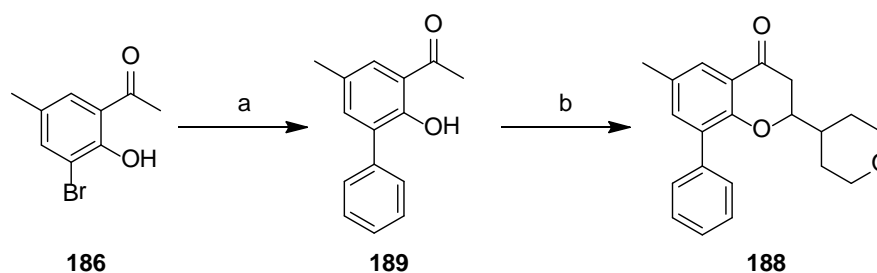
The Suzuki-Miyaura coupling of **187** to form the target compound (**188**) was achieved using a modified procedure of Bedford *et al.*^{350,351} Microwave heating, in this case, was very successful (Scheme 5.6). LCMS analysis showed near complete conversion to the desired product ($[M+H]^+$ molecular ion at m/z 323.2). Column chromatography was used to purify **188**, removing palladium residues and trace impurities. The purified 6-methyl-8-phenyl-2-(tetrahydro-2*H*-pyran-4-yl)chroman-4-one (**188**) was isolated in 94% yield.

The aliphatic proton signals of **188** are split in a similar manner to that observed with the key intermediate, **187**. The ^1H NMR spectrum showed the tetrahydropyran protons as two multiplets at δ 3.86 – 3.83 and 3.31 – 3.20 ppm. When ^{13}C NMR spectroscopy is performed at 298 K, the symmetrical CH_2 carbons of the tetrahydropyran group each

appear as two signals within the ^{13}C NMR spectrum at δ 66.61 and 66.62 ppm, and δ 27.9 and 27.8 ppm. However, ^{13}C NMR experiments performed at 323 K showed the coalescence of the two signals (δ 67.1 and 28.4 ppm), as would be expected of rotameric carbons at higher temperatures. As in the case of **187**, proton and carbon NMR assignments were elucidated using 2D NMR experiments.

5.2.2 Pathway two

The alternative synthetic pathway of initially performing the Suzuki-Miyaura coupling followed by the condensation reaction with tetrahydro-2*H*-pyran-4-carbaldehyde was also pursued (Scheme 5.5, pathway two shown in red). The synthesised 1-(3-bromo-2-hydroxy-5-methylphenyl)ethanone (**186**) was reacted with phenylboronic acid under optimised Suzuki-Miyaura coupling conditions to give the corresponding 1-(2-hydroxy-5-methyl-[1,1'-biphenyl]-3-yl)ethanone (**189**) in high yield (92%) (Scheme 5.7).



Scheme 5.7. Alternate synthesis of 6-methyl-8-phenyl-2-(tetrahydro-2*H*-pyran-4-yl)chroman-4-one (**188**). (a) $\text{C}_6\text{H}_5\text{B}(\text{OH})_2$, K_2CO_3 , $\text{Pd}(\text{OH})_2$, DMF/ H_2O (9:1), MW, 130 °C, 2.5 h, 92%; (b) tetrahydro-2*H*-pyran-4-carbaldehyde, $\text{Na}_2\text{B}_4\text{O}_7 \cdot 10\text{H}_2\text{O}$, $\text{CH}_3\text{CH}_2\text{OH}/\text{H}_2\text{O}$ (1:1.6), 78 °C, 72 h, 41%.

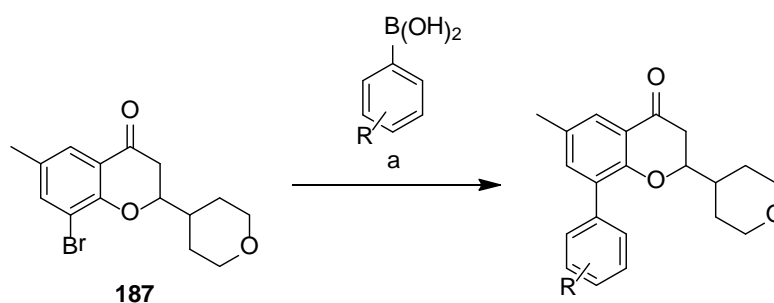
The subsequent condensation reaction to give 6-methyl-8-phenyl-2-(tetrahydro-2*H*-pyran-4-yl)chroman-4-one (**188**) proceeded in moderate yield (Scheme 5.7), with approximately 50% conversion to the desired product (**188**) (determined by analytical

RP-HPLC). 6-Methyl-8-phenyl-2-(tetrahydro-2*H*-pyran-4-yl)chroman-4-one (**188**) was isolated by column chromatography in 41% yield and gave identical analytical data to the compound obtained *via* pathway one.

A comparison of the results from pathway one and pathway two show that the former was more efficient in the synthesis of 6-methyl-8-phenyl-2-(tetrahydro-2*H*-pyran-4-yl)chroman-4-one (**188**); pathway one yielded **188** in 79%, pathway two yielded **188** in 36% (over three synthetic steps). It also gave the advantage of diversifying at the 8-position in the final step of the synthesis. Therefore, pathway one was employed in generating 2-tetrahydropyranchromanone analogues.

5.3 Synthesis of a focussed 2-tetrahydropyranchromanone library

Following the successful synthesis of the target compound, 6-methyl-8-phenyl-2-(tetrahydro-2*H*-pyran-4-yl)chroman-4-one (**188**), using the conditions established in pathway one, 2-tetrahydropyranchromanone analogues could be accessed through a Suzuki-Miyaura coupling of 8-bromo-6-methyl-2-(tetrahydro-2*H*-pyran-4-yl)chroman-4-one (**187**) with various aryl boronic acids (Scheme 5.8). A series of analogues were prepared (Figure 5.9, **188**, **190-206**) where the boronic acids employed were chosen on the basis of their aryl substituent and in-house availability. As in the case of the pyrazolopyrimidinone compounds (Chapter 3), the predicted physicochemical properties of the 2-tetrahydropyranchromanones were monitored to maintain drug-like properties (Appendix 3).



Scheme 5.8. Synthesis of 2-tetrahydropyranchromanone analogues through a Suzuki-Miyaura coupling of **187** with boronic acids. (a) Cs_2CO_3 , $\text{Pd}(\text{OCOCH}_3)_2$, PCy_3 , $(n\text{Bu})_4\text{NBr}$, 1,4-dioxane/ H_2O (6:1), MW, 150°C , 30 min.

Table 5.9. The structures of the synthesised 2-tetrahydropyranchromanones (**188**, **190-206**).

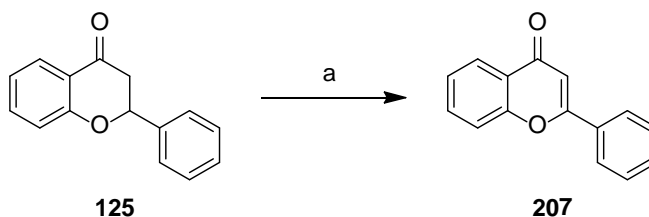
188	190	191	192	193	194
195	196	197	198	199	200
201	202	203	204	205	206

Each of the synthesised analogues was characterised by ^1H NMR spectroscopy, ^{13}C NMR spectroscopy, HRMS and analytical RP-HPLC. The molecular ion of each

compound was observed in the positive ion mass spectrum. The yields of the analogues varied (49-94%), however no relationship between the product structure and the isolable yield could be seen. The paired signals of rotameric carbons were observed within the ^{13}C NMR spectra of each synthesised analogue and were consistent with those observed for the parent compound, 6-methyl-8-phenyl-2-(tetrahydro-2*H*-pyran-4-yl)chroman-4-one (**188**).

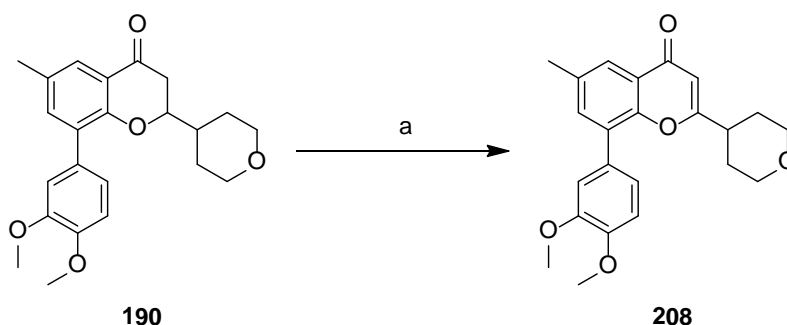
In addition to the series described above, a number of other syntheses were conducted to provide reference compounds. First, there was interest in examining the oxidation of the chromanone ring to give the corresponding chromone compounds. As described earlier, JN8-6 (**183**) shows inhibition at *h*PDE isoforms, and this route might provide an alternate pathway to accessing these compounds that would result in an extra compound for biological assessment from the single synthetic pathway.

The oxidation of flavanones to flavones has been reported using elemental iodine in pyridine.³⁵² As a test case, this reaction was successfully replicated on 2-phenylchroman-4-one itself (**125**), giving the oxidised 2-phenyl-4*H*-chromen-4-one (**207**) in 57% yield (Scheme 5.10). The ^1H NMR spectrum displays a signal at δ 6.70 ppm correlating to the newly formed α -keto methine proton.³⁵³



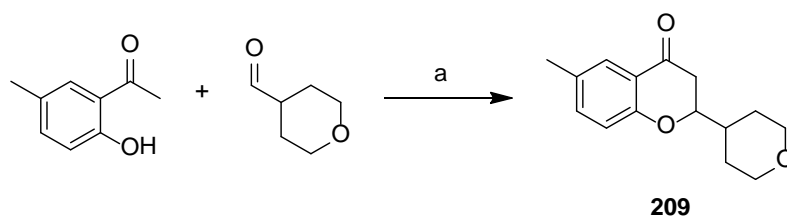
Scheme 5.10. Oxidation of 2-phenylchroman-4-one (**125**) to 2-phenyl-4*H*-chromen-4-one (**207**) (a) I_2 , pyridine, 90 °C, 3 h, 57%.

Employing these conditions, 8-(3,4-dimethoxyphenyl)-6-methyl-2-(tetrahydro-2*H*-pyran-4-yl)chroman-4-one (**190**) was oxidised with iodine in pyridine at 90 °C to give the chromone, 8-(3,4-dimethoxyphenyl)-6-methyl-2-(tetrahydro-2*H*-pyran-4-yl)-4*H*-chromen-4-one (**208**) in 22% yield following column chromatography (Scheme 5.11). A distinctive α -keto methine proton signal at δ 6.20 ppm was present in the ^1H NMR spectrum and the $[\text{M}+\text{H}]^+$ molecular ion was observed at m/z 381.2. The low yield was attributed to compound loss during the reaction work-up, particularly during several stages of washing with saturated aqueous sodium thiosulfate to remove iodine. Overall, this was a pleasing result as it may provide access to useful compounds in future work.



Scheme 5.11. Oxidation of 8-(3,4-dimethoxyphenyl)-6-methyl-2-(tetrahydro-2*H*-pyran-4-yl)chroman-4-one (**190**) to 8-(3,4-dimethoxyphenyl)-6-methyl-2-(tetrahydro-2*H*-pyran-4-yl)-4*H*-chromen-4-one (**208**). (a) I_2 , pyridine, 90 °C, 16 h, 22%.

The unsubstituted chromanone, 6-methyl-2-(tetrahydro-2*H*-pyran-4-yl)chroman-4-one (**209**) was synthesised to assess the structure-activity requirement of the 8-aryl moiety (Scheme 5.12). Condensation of 1-(2-hydroxy-5-methylphenyl)ethanone with tetrahydro-2*H*-pyran-4-carbaldehyde using piperidine as the base catalyst gave **209** in 38% yield.



Scheme 5.12. Synthesis of methyl-2-(tetrahydro-2*H*-pyran-4-yl)chroman-4-one (**209**). (a) piperidine, CH₃CH₂OH, 78 °C, 48 h, 38%.

Surprisingly, the previously established condensation conditions using sodium tetraborate as a base catalyst were unsuccessful in the synthesis of **209**. In this instance, LCMS analysis could not detect the molecular ion, but instead showed that the reacted material had formed several unidentifiable products. It is unclear why this is the case with this particular substrate.

Another simple structural variation that was envisaged was the replacement of the 6-methyl substituent with a methoxy substituent (**210**), providing a potential hydrogen bond acceptor that might promote binding to *h*PDE enzymes (Figure 5.13).³⁴⁸

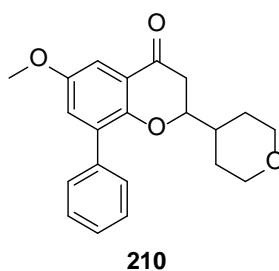
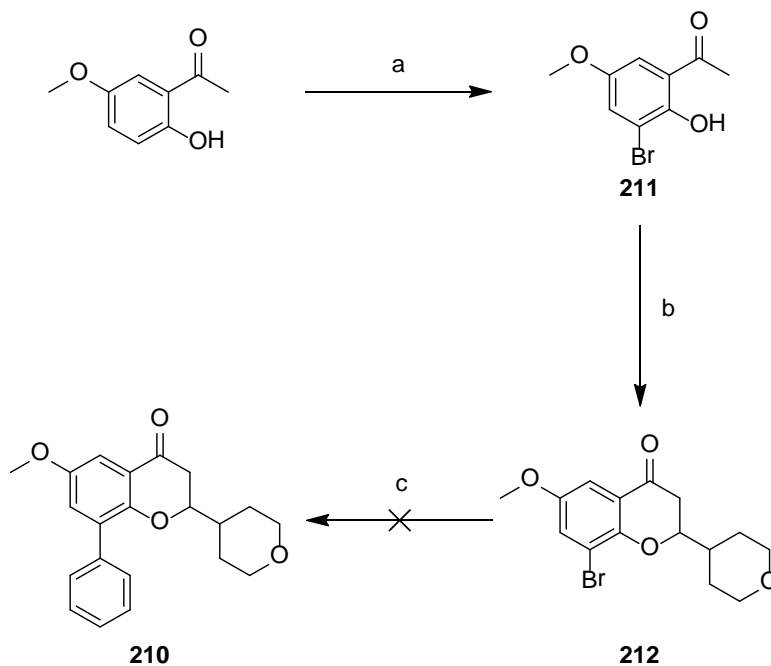


Figure 5.13. 6-methoxy-8-phenyl-2-(tetrahydro-2*H*-pyran-4-yl)chroman-4-one (**210**).

The synthesis of compound **210** was approached in a fashion analogous to the 6-methyl case (Scheme 5.14). Initially, 1-(2-hydroxy-5-methoxyphenyl)ethanone was brominated in 88% yield following recrystallisation from ethanol. 1-(3-Bromo-2-hydroxy-5-

methoxyphenyl)ethanone (**211**) was then reacted with tetrahydro-2*H*-pyran-4-carbaldehyde using the sodium tetraborate conditions previously established, though with a much poorer result. LCMS analysis of the crude reaction mixture showed only 22% conversion to the cyclised chromanone, 8-bromo-6-methoxy-2-(tetrahydro-2*H*-pyran-4-yl)chroman-4-one (**212**), and this material was isolated in just 7% yield. Finally, a Suzuki-Miyaura coupling of **212** with phenylboronic acid was attempted. While LCMS analysis of the crude reaction mixture showed a $[M+H]^+$ molecular ion at m/z 339.2 that corresponded to the 6-methoxy-8-phenyl-2-(tetrahydro-2*H*-pyran-4-yl)chroman-4-one product (**210**), this material was unable to be isolated by either column chromatography or recrystallisation. While disappointing, this result suggests that the effects associated with the presence of the methoxy substituent would need to be addressed in future work. Certainly, pathway two (Scheme 5.5) of the original synthesis is worth exploring to see if it offers any advantage.



Scheme 5.14. Attempted synthesis of 6-methoxy-8-phenyl-2-(tetrahydro-2*H*-pyran-4-yl)chroman-4-one (**210**). (a) Br₂, CH₃CO₂H, CH₃CO₂Na, 0 °C to rt, 24 h, then Br₂, CH₃CO₂H, 0 °C to rt, 24 h, 88%; (b) tetrahydro-2*H*-pyran-4-carbaldehyde, Na₂B₄O₇·10H₂O, CH₃CH₂OH, 78 °C, 48 h, 7%; (c) C₆H₅B(OH)₂, Cs₂CO₃, Pd(CH₃CO₂)₂, PCy₃, (*n*Bu)₄NBr, 1,4-dioxane/H₂O (6:1), MW, 150 °C, 30 min.

In summary, the synthetic work described within this chapter afforded eighteen chromanone-based analogues of LY294002 for evaluation in both antiplasmodial and human PDE assays. It was thought that the compounds synthesised would allow for preliminary structure-activity relationship data to be generated. Importantly, a synthetic route has been established by which further 8-aryl analogues could be potentially synthesised, and this offers the potential for expansion in the syntheses of further 2-tetrahydropyranchromanones.

5.4 Biological assessment of the synthesised

2-tetrahydropyranchromanones

5.4.1 *Plasmodium falciparum* growth inhibition

The synthesised 2-tetrahydropyranchromanones (**188**, **190-206**), as well as the oxidised chromone compound (**208**), were assessed for *Plasmodium falciparum* growth inhibition. A number of other compounds, including synthetic intermediates and flavanone analogues described in Chapter 4, were also screened for antiplasmodial activity. The compounds were assayed as per the method of Gamo *et al.*,¹⁵⁴ which was described in detail in Chapter 3, and the results are shown in Table 5.15. The dose-response curves of each of the assessed chromanones can be viewed in Appendix 5. As seen in the assessment of the antiplasmodial activity of the pyrazolopyrimidinone analogues (Chapter 3), the IC₅₀ values were found to vary as much as ten-fold between assays. However, the results again demonstrated the ability of the assay to consistently distinguish between active and inactive antiplasmodial compounds.

Table 5.15. Determined IC₅₀ ranges of the synthesised 2-tetrahydropyranchromanones and related compounds for *P. falciparum* (3D7) growth inhibition.

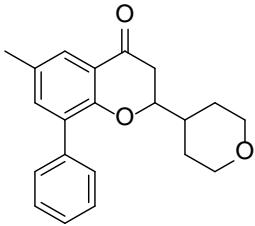
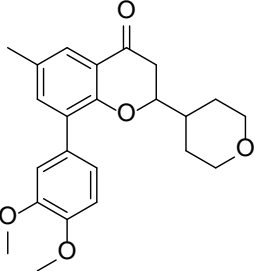
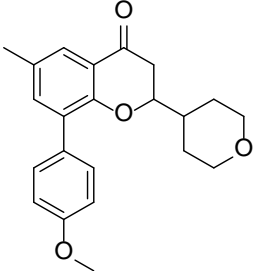
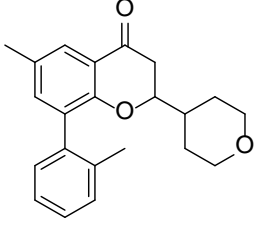
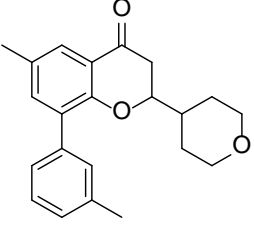
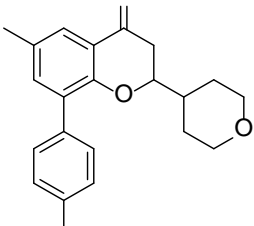
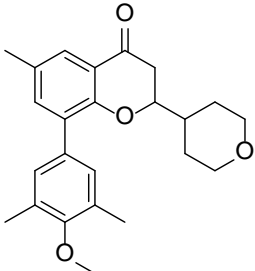
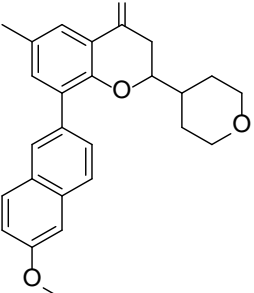
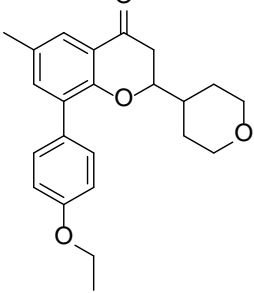
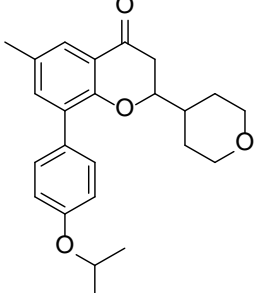
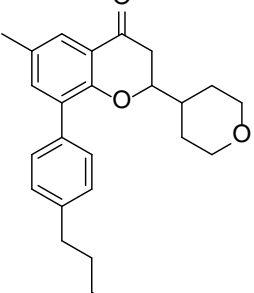
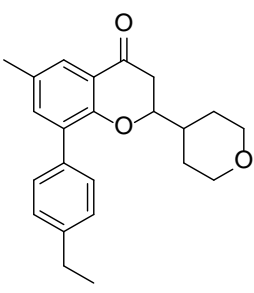
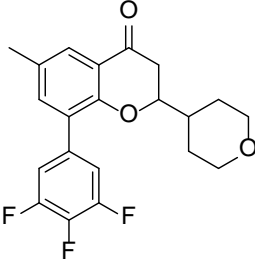
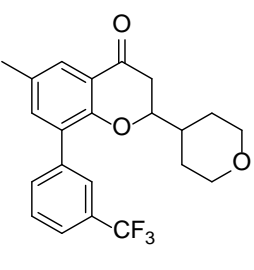
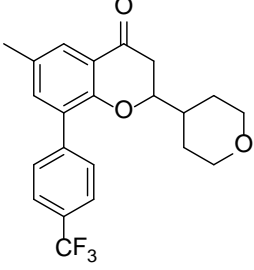
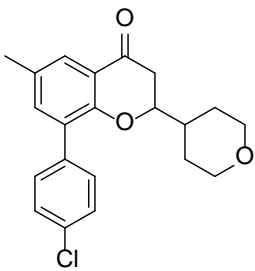
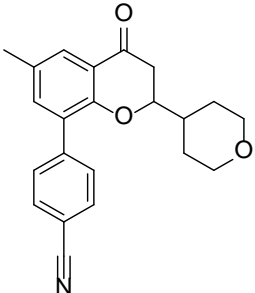
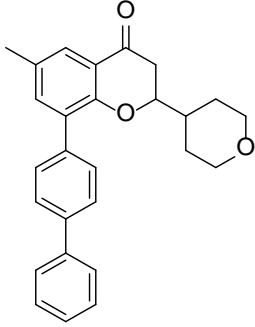
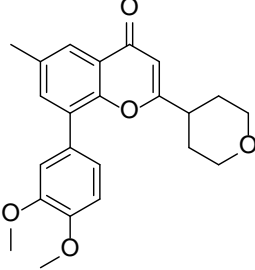
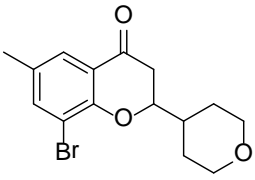
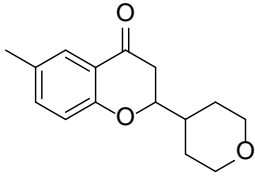
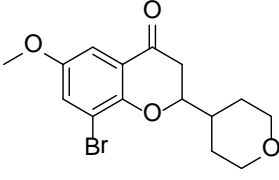
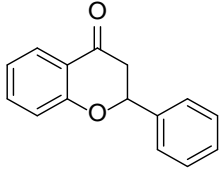
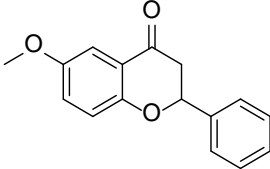
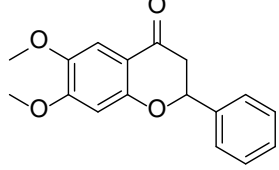
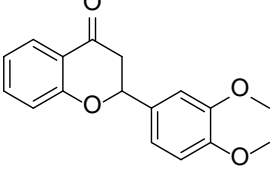
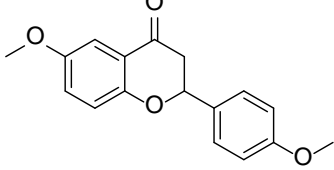
		
188 >100 μ M	190 2.6-4.1 μ M	191 5.7-9.0 μ M
		
192 >100 μ M	193 9.9-48 μ M	194 5.6-7.0 μ M
		
195 >100 μ M	196 >100 μ M	197 4.2-11 μ M
		
198 3.0-5.4 μ M	199 1.1-1.3 μ M	200 6.6-12 μ M
		
201 7.9-52 μ M	202 >100 μ M	203 1.7-3.1 μ M

Table 5.15 continued. Determined IC₅₀ ranges of the synthesised 2-tetrahydropyranchromanones and related compounds for *P. falciparum* (3D7) growth inhibition.

		
204 85->100 μ M	205 3.8-4.2 μ M	206 2.3-3.7 μ M
		
208 4.7-9.7 μ M	187 >100 μ M	209 >100 μ M
		
212 >100 μ M	125 61->100 μ M	138 >100 μ M
		
140 >100 μ M	141 42->100 μ M	142 >100 μ M

Of the 27 compounds assessed, nine compounds (**190**, **191**, **194**, **198**, **199**, **203**, **205**, **206**, **208**) showed low micromolar antiplasmodial activity, seven compounds (**193**, **197**, **200**, **201**, **204**, **125**, **141**) showed intermediate activity, and eleven compounds (**188**, **192**, **195**, **196**, **202**, **187**, **212**, **209**, **138**, **140**, **142**) showed no inhibition (>100 μ M). Of the compounds that showed low micromolar activity, the *p*-butylphenyl compound (**199**) was the most potent antiplasmodial compound with an IC₅₀ value of 1.3 μ M. In

fact, many of the *para*-phenyl-substituted analogues demonstrated low micromolar IC₅₀ values, including the *p*-methoxy (**191**), *p*-methyl (**194**), *p*-isopropoxy (**198**), *p*-trifluoromethyl (**203**), *p*-cyano (**205**) and *p*-phenyl (**206**) compounds. The *p*-ethoxy (**197**), *p*-ethyl (**200**) and *p*-chloro (**204**) compounds are somewhat less active. The *o*- (**192**), *m*- (**193**), and *p*-methyl-substituted (**194**) compounds show an order of potency of **194** > **193** > **192**. This structure-activity relationship is supported, in part, by the antiplasmodial activities of the *m*-trifluoromethyl (**202**) and *p*-trifluoromethyl (**203**) compounds. The catechol ether chromanone compound (**190**) was of particular interest as the moiety has been observed among many PDE inhibitors, as discussed in Chapter 4. The antiplasmodial activity of **190** could be directly compared to the oxidised chromone counterpart (**208**). Promisingly, the chromanone scaffold demonstrated comparable activity. Given the variation between assays, it is difficult to conclusively determine which is the more active scaffold. From the assessment of the unsubstituted 2-tetrahydropyranchromanones (**187**, **209** and **212**) it is evident that 8-aryl substitutions are essential in gaining antiplasmodial activity. Of the flavanone compounds (synthesised in Chapter 4), only the analogue with the catechol ether moiety on ring B (**141**) showed antiplasmodial activity (IC₅₀ = 42 µM).

5.4.2 Human phosphodiesterase inhibition

Most of the synthesised chromanone analogues were also assessed for inhibition of *h*PDE9 and *h*PDE1. As previously discussed, both LY294002 (**182**) and the chromone analogue, JN8-6 (**183**), showed inhibition of *h*PDE4. It was therefore felt that additional assessment of the compounds at *h*PDE4 was essential (Table 5.16). As in Chapter 3, the human PDE enzymatic assays were conducted externally under contract. The

compounds were initially assessed at 1 μM concentration, and IC_{50} values were determined for selected compounds.

Table 5.16. Determined inhibitory activities of chromanone compounds.

Compound	<i>Pf</i> parasite growth IC_{50} (μM)	<i>Human PDE % inhibition at 1 μM (IC_{50} in μM)</i>										
		1A	2A	3CAT	4CAT	5CAT	6AB	7A	8A	9A	10A	11A
182		11	(40) 23	(100) 0	41 ^b	50	25 ^c	0	0	0	(1.3) 85	(4.1) 65
188	>100	39	-	-	31	-	-	-	-	0	-	-
190	2.6- 10.2	94	13	14	(1.6) 90	45	0	33	54	2	53	51
191	9.0	73	-	-	48	-	-	-	-	0	-	-
192		3	-	-	32	-	-	-	-	10	-	-
193	48.2	6	-	-	37	-	-	-	-	76	-	-
194	5.6	84	7	8	48	30	0	0	27	0	6	24
195	>100	-	-	-	-	-	-	-	-	-	-	-
196	>100	0	-	-	4	-	-	-	-	1	-	-
197	10.7	82	-	-	31	-	-	-	-	3	-	-
198	5.4	68	-	-	22	-	-	-	-	3	-	-
199	1.3	77	-	-	22	-	-	-	-	0	-	-
200	11.6	25	-	-	44	-	-	-	-	3	-	-
201	52.0	-	-	-	-	-	-	-	-	-	-	-
202	>100	-	-	-	-	-	-	-	-	-	-	-

Table 5.16 continued. Determined inhibitory activities of chromanone compounds.

Compound	<i>Pf</i> parasite growth IC_{50} (μM)	<i>Human PDE % inhibition at 1 μM (IC_{50} in μM)</i>										
		1A	2A	3CAT	4CAT	5CAT	6AB	7A	8A	9A	10A	11A
203	3.1	74	-	-	10	-	-	-	-	6	-	-
204	85.1	6	-	-	35	-	-	-	-	1	-	-
205		72	0	3	33	34	0	4	34	1	9	32
206	3.7	0	-	-	1	-	-	-	-	0	-	-
208	9.7	99	29	29	(0.2) 94	60	0	44	83	4	82	75
187	>100	4	-	-	11	-	-	-	-	3	-	-
209	>100	68	-	-	6	-	-	-	-	0	-	-
212	>100	-	-	-	-	-	-	-	-	-	-	-

Each value represents the mean of duplicate determinations where each replicate was within 6% of the mean value. Values shown in brackets are determined IC_{50} values, in μM . Compounds **99** and **105** were assayed externally by BPS Bioscience, San Diego (see section 7.3.2 for experimental methods). The remainder of the compounds were assayed externally by Scottish Biomedical, Glasgow (see section 7.3.2 for experimental methods).

Pleasingly, many of these novel chromanone-based compounds were found to inhibit one or more of the *hPDE* isoforms. In general, inhibition of *hPDE1* and *hPDE4* predominated over *hPDE9* at 1 μM concentrations. The most active compounds were the catechol ether compounds, **190** and **208**, and both were selective for *hPDE4* inhibition over *hPDE1*. They showed almost complete inhibition of *hPDE4* activity at 1 μM concentration, and the IC_{50} values for these compounds were determined as 1.6 μM and 0.2 μM , respectively.

Four compounds (**191**, **208**, **190** and **205**) were subsequently assessed for inhibitory activity at each of the *hPDE* isoforms (*hPDE1-11*) to assess their selectivity (Table 5.16). This assessment showed some interesting results. Across all of the *hPDE* isoforms, the oxidised chromone analogue (**208**) showed greatest inhibition. Both catechol ether compounds, **190** and **208**, showed inhibition of *hPDE8* at 1 μ M (54% and 83%, respectively). They also demonstrated *hPDE10* and *hPDE11* activity, which is not surprising given that similar inhibition was observed with LY294002 (**182**).

These results highlight important structure-activity relationship data allowing the direct comparison of the chromanone (**190**) and oxidised chromone (**208**) compounds showing that the chromone compounds were more active at *hPDE4*. This is further supported by the comparison of the *hPDE4* activities of JN8-6 (**183**) and **188**, where the oxidised chromone was again more active.

5.5 Chapter discussion

With the enzyme and cell-based data in hand, it was of interest to see if any insight could be gained in regard to the possible basis for inhibition of the *PfPDEs*. Using the homology models of the *PfPDE* isozymes developed in Chapter 2, each of the 8-phenyl-2-tetrahydropyranchromanones was docked into the *PfPDE α* model to make predictions regarding likely *PfPDE* inhibition. The binding modes of both enantiomers were assessed.

The docking results failed to show binding modes of the analogues that could be described as characteristic of the class. This was not surprising as LY294002 had been

shown to exhibit a range of binding poses when docked into *h*PDE crystal structures, where interactions of the purine-scanning glutamine could be made with either the carbonyl or morpholinyl group of LY294002.

The catechol ether compounds (**190** and **208**) did prove the most potent however, and so these results were examined more closely. When either of the *R* or *S* enantiomers of the catechol ether chromanone (**190**) was docked into the *Pf*PDE α model, the only observable interaction with the enzyme came *via* a hydrogen bond between the catechol ether moiety and the purine-scanning glutamine residue (Figure 5.17). As previously discussed, hydrogen bonding between the catechol ether of *h*PDE inhibitors (such as rolipram and roflumilast) and the purine-scanning glutamine is commonly observed in *h*PDE crystal structures.¹⁸⁵

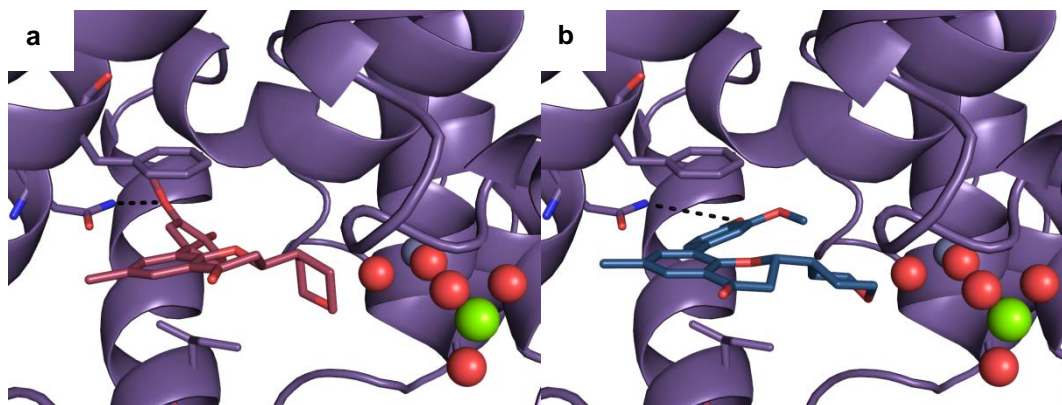


Figure 5.17. The docking pose of the (a) *R* (pink) and (b) *S* (blue) enantiomers of **190** in the *Pf*PDE α homology model. Hydrogen bonds are shown as dashed lines. Purine-scanning glutamine (Gln884) and hydrophobic clamp residues (Phe887 and Ile850) are shown as purple sticks. Numbering is taken from the *Pf*PDE α sequence. Water molecules and ions are shown as spheres.

When the oxidised catechol ether chromone (**208**) was docked into the *Pf*PDE α model, it again demonstrated a hydrogen bond between the catechol ether moiety and the

purine-scanning glutamine (Figure 5.18). Despite the chromone having a planar bicyclic core, this did not appear to attenuate the π -stacking interaction with the conserved phenylalanine residue of the hydrophobic clamp in comparison to the less planar chromanone (**190**).

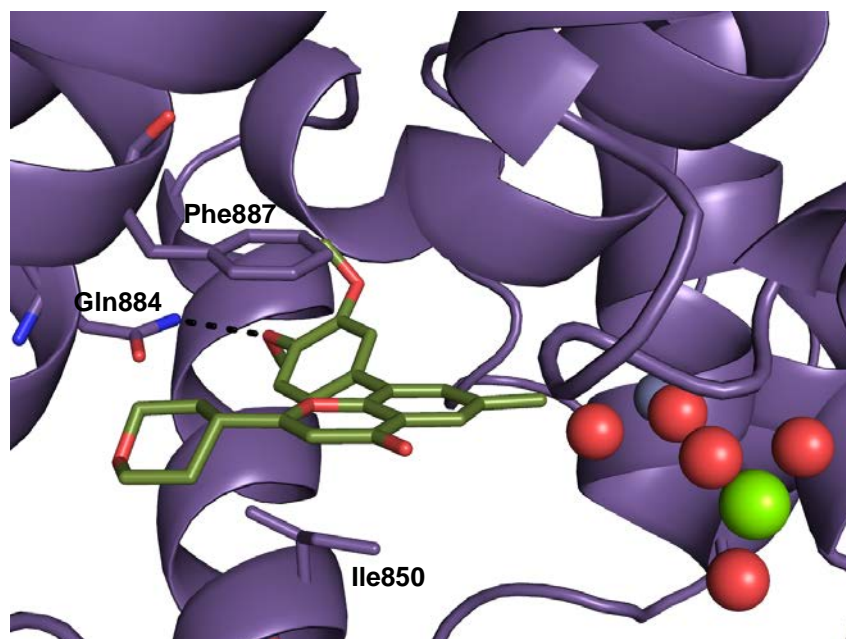


Figure 5.18. The docking pose of **208** (green) in the *PfPDEα* homology model. Hydrogen bonds are shown as dashed lines. Purine-scanning glutamine (Gln884) and hydrophobic clamp residues (Phe887 and Ile850) are shown as purple sticks. Numbering is taken from the *PfPDEα* sequence. Water molecules and ions are shown as spheres.

In summary, docking of the synthesised 8-phenyl-2-tetrahydropyranchromanone compounds into the *PfPDEα* model is not able to rationalise the variations observed in their activities. This could be due to a number of reasons; antiparasmodial activity is not occurring through a *PfPDE* mechanism, the compounds are only low micromolar inhibitors and therefore do not interact strongly with the *PfPDE* enzymes, or it could be an artefact of the *PfPDE* models and the docking process. Most likely, it is consistent with the general difficulty in docking studies using moderately potent inhibitors.

5.6 Chapter conclusions and future directions

In this chapter, a new class of compounds, the 8-(aryl)-2-(tetrahydro-2*H*-pyran-4-yl)chroman-4-ones, have been prepared and identified as novel inhibitors of both *P. falciparum* growth and the *h*PDE enzymes. As with the pyrazolopyrimidinone analogues described in Chapter 3, it remains unknown whether these compounds are inhibiting the *Pf*PDEs.

The hypothesis for the work undertaken in Chapters 4 and 5 was that novel flavonoid-like structures may provide a new PDE inhibitor scaffold, which has been largely satisfied in this work. The library of LY294002 analogues was prepared in an efficient three-step synthesis. The compounds were tested for antiparasmodial activity, and the assays were able to identify a number of active compounds. The analogues synthesised in this study represent a small starting series, and this library is amenable to expansion in the future. In addition, the results have provided some tentative, yet valuable structure-activity relationship data and lead compounds for further investigation.

Synthesised analogues of interest were also assessed for *h*PDE inhibition. Initially, this was undertaken at *h*PDE9, *h*PDE1 and *h*PDE4, given both the hypothesis discussed in Chapter 3, and the ability of LY294002 (**188**) to inhibit *h*PDE4. A number of compounds were identified that were moderate inhibitors of *h*PDE1 and *h*PDE4, and this work represents the first instance of this compound class showing such activity. These are very useful results in themselves as *h*PDE1, in particular, is both an emerging therapeutic target and is under-represented with respect to pharmacological inhibitors. It is notable that these active compounds are racemic mixtures. The single enantiomers would be worth assessing for *h*PDE activity as they may provide critical structure-

activity relationship data. It is plausible that these compounds might be co-crystallised with *h*PDE4, as has been achieved with other inhibitors in the research group.³⁴⁵

In choosing what “hits” from this program are to be taken forward, the physicochemical properties of the compounds should also be considered (Appendix 3). It is worth noting that these compounds are relatively hydrophobic and more polar substituents might be desirable. In particular, the *p*-butyl-substituted **199** is not an optimal lead compound with high *c*LogP (5.80) and *c*LogD_{7.4} (5.80) values that fall outside of Lipinski’s Rule of 5.^{354,355}

Chapter 6

Conclusions and future directions

The need for new antimalarial therapies is now more apparent than ever before, and the development of new drugs has become a major undertaking of global significance. The world's largest philanthropic organisation, the Bill and Melinda Gates Foundation, as well as the largest pharmaceutical companies, such as GlaxoSmithKline, Pfizer and Novartis, have made commitments of an enormous magnitude to maintaining a steady pipeline of novel antimalarial therapies.³⁵⁶ Indeed, the ultimate goal set forth by the Medicines for Malaria Venture (MMV) is the complete eradication of malaria.^{105,357,358}

The work in this thesis does not attempt to compete with these efforts, although it does seek to explore new strategies in antimalarial drug design. Given the immense challenges involved in the development of antimalarial therapies,³⁵⁹⁻³⁶³ not the least of which includes the emergence and rapid spread of resistance, new strategies that are more efficient or novel in approach may be beneficial, as could be the identification of new molecules with the potential to be further developed as new antimalarials.^{364,365}

In some ways, this thesis contests the role of mass chemical screening in identifying novel antiplasmodial compounds as opposed to a more rational drug discovery approach. The 2010 GSK malaria screen saw approximately 2,000,000 compounds assessed for antimalarial activity, which was measured through parasite growth inhibition. A “hit” was identified as any compound capable of inhibiting parasite growth at, or below, 1 μ M concentration. A significant drawback is that these phenotypic screens provide no explanation as to the mechanism through which the observed parasite growth inhibition is occurring. From this screen 13,533 hits resulted, a hit rate of just 0.68%, and this was considered an excellent result. In this thesis, where “rational” implies that there was basis for hypothesising that carefully designed compounds might inhibit parasite growth, around 40 compounds were prepared to yield 9 hit compounds. In comparison to mass chemical screening, this approach gave a much improved hit rate of 22%. Furthermore, this rational approach involves a postulated mechanism of action. This work serves as an advocate for rational drug discovery.

The success of the work in this thesis has surpassed expectations but equally, the described results foreshadow much future study to potentially progress the science toward the therapeutic endpoint – a new antimalarial therapy. This thesis has described two rationalised approaches, both centred on the “inverted silver bullet” paradigm, but with two distinct starting points.

Chapters 2 and 3 examined the repurposing of human phosphodiesterase inhibitors as *Plasmodium falciparum* inhibitors,³⁶⁶ a proposition that is as yet, unable to be directly tested. In this section, the power of comparative structural biology came to the fore, with the development of homology models of the *Plasmodium falciparum*

phosphodiesterases (*Pf*PDEs) revealing the possibility that *h*PDE1 and *h*PDE9 inhibitors might be an excellent starting point for developing *Pf*PDE inhibitors, in contrast to *h*PDE5 which had been proposed by others.^{165,168,169}

To an extent, this approach has succeeded. With the synthesis of a focussed library of substituted *h*PDE1 and *h*PDE9 inhibitors, the 2-substituted 3-isopropyl-1*H*-pyrazolo[4,3-*d*]pyrimidin-7(6*H*)-ones, compounds that are capable of inhibiting *Plasmodium falciparum* growth with submicromolar IC₅₀ values were identified. Direct evidence of *Pf*PDE inhibition has not been obtained but importantly, the activity was independent of *h*PDE inhibition. Regardless of the mechanism behind the observed antiparasmodial activity, the inhibition of human targets should obviously be minimised in clinical candidates.

Future work should attempt to validate the mechanism, or mechanisms, behind the observed antiparasmodial activity. Cell-based assays examining cyclic nucleotide levels should be undertaken as these compounds themselves may be used as a tool for investigating the role of cyclic nucleotide signalling within the parasite life-cycle. Preparation of recombinant *Pf*PDE enzymes for direct assays is also important for progress. The synthesis of a tagged 2-substituted 3-isopropyl-1*H*-pyrazolo[4,3-*d*]pyrimidin-7(6*H*)-one (e.g. biotin) could be used to perform pull-down assays to aid in the identification of the target, or targets, of these compounds. Of course, other *h*PDE1 and *h*PDE9 inhibitors of various chemical classes could, and will, be screened for activity against the parasite and this may yet provide more leads.

Other classes of PDE inhibitor chemotypes were the focus of Chapters 4 and 5. In this work, the objective was to develop completely new PDE inhibitors. The starting rationale in this case was the antiplasmodial activity and phosphodiesterase inhibition displayed by the flavonoid class of natural products, as was the potential to develop novel phosphodiesterase inhibitor scaffolds through relatively subtle structural modifications. It was envisaged that ring expanded flavonoid-like structures, particularly if combined with a catechol moiety, could present as novel antiplasmodial compounds and/or novel PDE inhibitors. Three series of structurally related 6,7-fused ring system scaffolds were pursued synthetically with the goal of identifying novel scaffolds worth pursuing in a medicinal chemistry campaign. While significant progress was made with each series, these compound classes suffered from synthetic liabilities that halted their progress within the scope of this thesis. Additionally, successes in Chapter 5 saw the 2-tetrahydropyranchromanone compounds emerge as a priority.

Work to follow from that described in Chapter 4 should focus on optimising synthetic routes to these compounds. Synthetic access to the 2-phenylbenzoxazepinone series could be pursued to generate analogues, especially given the first glimpse of antiplasmodial activity. Methods other than the Schmidt reaction or Beckmann rearrangement may be needed in certain cases, as the utility of these reactions was limited where methoxy substituents were present. From the studies conducted on the 2-phenylbenzoxepinone compound class, the reported two-step procedure of cyclopropanation and subsequent reductive cleavage of the cyclopropyl ketone shows promise, though further work is required to optimise this reaction and isolate target compounds. Finally, the first synthesis and purification of an 8-phenylbenzosuberone was achieved, overcoming a competing side-reaction that gives 4-benzyl-tetralones.

Chiral HPLC techniques proved crucial in isolating one of the 8-phenylbenzosuberone enantiomers from the α -tetralone structural isomer. Ongoing work surrounding this area should seek to explore the effects of different substituents in the final Friedel-Crafts intramolecular cyclisation reaction, and whether there is the potential to favour the formation of the 8-phenylbenzosuberone product over the α -tetralone by-product. For these compounds to be pursued in a medicinal chemistry campaign, the purification would require further optimisation for scale-up. In each case, optimisation of the synthesis would lead to novel compounds that are deceptively simple in structure, which might be active in malaria or other biological contexts.

Finally, in Chapter 5, the idea of taking an off-target effect of one compound and repurposing it as a lead compound for that new target was examined. Based on the scaffold of LY294002, a human PI3K inhibitor with demonstrated *h*PDE inhibition, chromanone analogues were pursued as antimalarial and/or human phosphodiesterase inhibitors. The synthesis of a series of novel 2-tetrahydropyranchromanone compounds was optimised and the compounds were assessed for antiplasmodial activity and human PDE inhibition. In particular, the analogue incorporating a catechol ether moiety, which had previously been identified as a common PDE inhibitor structural motif, showed low micromolar inhibition of *Plasmodium falciparum* growth. In addition, several of the compounds also emerged as inhibitors of *h*PDE isoforms, also a novel outcome of this work. As with the antiplasmodial compounds described in Chapter 3, a mechanism of antiplasmodial activity of the 2-tetrahydropyranchromanones remains to be elucidated. Pan-*h*PDE screening may also identify isoform-selective structure-activity relationship data.

While the efforts in Chapters 2 and 3 provide a satisfying exposition of the idea of drug repurposing, and the work has generated potent inhibitors that can be pursued in the future, it is the work in the later chapters that has unearthed some important insights for drug discovery. Given the simplicity of the structures, it might be expected that the compounds described would be well known but in fact, compounds of these classes were scarcely or completely unreported. That they are not known suggests that there is still sufficient room to explore within “druggable” chemical space.³⁶⁷⁻³⁷⁰ However, these compounds do suffer from two obvious drawbacks – they are not trivial to make and they are chiral. Drug discovery tends to shy away from these features and probably at the cost of identifying valuable new compounds.^{371,372} The work in this thesis suggests that the additional effort to overcome these facets may well be repaid in new therapies for some of the world’s most challenging diseases.

Chapter 7

Experimental

7.1 Computational chemistry general experimental

7.1.1 Sequence alignment and template selection

Protein sequences of both human and malarial PDEs were retrieved from the UniProtKB database. ClustalW²⁰³ was employed to compare the catalytic sequences to determine percentage homologies and to suggest likely catalytic sequence alignments. Further manual adjustments to the sequence alignments were undertaken to coincide with previous work in the laboratory.¹⁸⁴ Typically, this involved moving gaps out of helical regions and into loop sections. This optimised alignment utilised the 16 amino acids known to be conserved among the human enzymes as a guide to give the appropriate overlay of these invariant residues. These adjustments align residues that play a key structural role in the protein. From these analyses, potential template proteins were identified and additional criteria were examined to select the most appropriate crystal structure for homology modelling purposes, including the ligand co-crystallised with the structure as well as the crystal structure resolution.

7.1.2 Model building and minimisation

Each homology model was generated using Prime (Maestro, Schrödinger, Portland, USA) employing the optimised sequence alignment. The model building process used the PDE9 structure, 3DYN,¹⁷⁰ and retained the endogenous cGMP ligand and metal ions together with their coordinated water molecules. Minimisation of the model was undertaken using Macromodel (Maestro). Initially, amino acid side chains were minimised with the ligand, metals, water molecules and protein backbone held rigid. Steric clashes were addressed by the rotation of strained residues. Typically this was a result of the substitution of a larger amino acid for a smaller one and manual inspection was required to look for alternative conformations to reduce steric strain. This involved examining other PDE crystal structures with similar amino acids in these positions to provide clues to likely low energy conformations. Following this, the model was further minimised while maintaining the previous constraints. A final minimisation was conducted without constraints and the models were assessed using MolProbity²⁰⁴ which included a Ramachandran analysis.

7.1.3 Docking

Docking was performed using Glide (Maestro) employing the extra precision (XP) mode. Both cyclic nucleotides (cAMP and cGMP) were docked into each model. In both cases, two conformations of the terminal carboxamide of the invariant glutamine in the active site were explored. Additionally, each cyclic nucleotide was minimised in the protein using both conformations of the carboxamide of the invariant glutamine. This was undertaken to gain insight into the conformation of this residue and was applied to the docking of PDE inhibitors.

7.2 Synthetic chemistry general experimental

All materials were reagent grade and purchased commercially from Sigma-Aldrich, Alfa-Aesar, Merck, Boron Molecular, GL Biochem, Matrix Scientific, Indofine Chemicals, Fluorochem, and Apollo Scientific. All solvents were reagent grade and used as required. It should be noted that tetrahydro-2*H*-pyran-4-carbaldehyde was susceptible to degradation and required refrigeration and the reagent needed to be resealed under nitrogen to avoid degradation.

Thin layer chromatography (t.l.c.) was performed using Merck Silica Gel 60 F254 pre-coated plates (0.25 mm) and visualised by ultraviolet light as well as staining with iodine or potassium permanganate solution. Flash column chromatography used Merck Silica Gel 60, 230-400 mesh ASTM, following the method described by Still *et al.*³⁷⁴ Products were either pre-adsorbed onto silica (230-400 mesh ASTM) prior to column chromatography or dissolved in the appropriate solvent.

¹H NMR spectra were routinely recorded at 300.13 MHz using a Bruker Avance DPX-300 spectrometer or at 400.13 MHz using a Bruker Ultrashield-Avance III NMR spectrometer or at 600.13 MHz using a Varian Unity Spectrometer, all at 298 K unless otherwise stated. Data acquisition and processing was managed using XWINNMR (Bruker) software package v3.5 or Topspin v3.2 and plotting was managed using XWINPLOT or MestReNova v6.0.2. Chemical shifts (δ) for all ¹H NMR spectra were reported in parts per million (ppm) referenced to an internal standard of residual proteo-solvent: δ 2.50 ppm for *d*₆-dimethylsulfoxide (DMSO), δ 3.31 ppm *d*₄-methanol (CD₃OD), and δ 7.26 ppm for *d*-chloroform (CDCl₃).³⁷⁵ The ¹H NMR spectra were reported as follows: chemical shift (δ), multiplicity, coupling constant (*J*) in Hertz (Hz) (quoted to one decimal place), peak integration and assignment. In reporting the spectral

data, the following abbreviations have been used: s = singlet, d = doublet, t = triplet, q = quartet, sext = sextet, hept = heptet, m = multiplet, br = broad.

^{13}C NMR spectra were routinely recorded at 75.5 MHz using a Bruker Avance DPX-300 spectrometer or at 100.62 MHz using a Bruker Ultrashield-Avance III NMR spectrometer or at 150 MHz using a Varian Unity Spectrometer, all at 298 K unless otherwise stated. Data acquisition and processing were managed using XWINNMR (Bruker) software package v3.5 and plotting was managed using XWINPLOT or MestReNova v6.0.2. Chemical shifts (δ) for all ^{13}C NMR were reported in parts per million (ppm) referenced to an internal standard of residual proteo-solvent: δ 39.52 ppm for d_6 -dimethylsulfoxide (DMSO), δ 49.00 ppm for d_4 -methanol (CD_3OD), δ 77.16 ppm for d -chloroform (CDCl_3).³⁷⁵ The ^{13}C NMR spectra were reported as follows: chemical shift (δ). ^{13}C NMR signals were assigned as: (C=O) = carbonyl carbon, (C) = quaternary carbon, (CH) = methine carbon, (CH_2) = methylene carbon and (CH_3) = methyl carbon, * = rotameric carbon.

LCMS analysis was performed on a Agilent 1200 series separation module with an Agilent 6120 Quadrupole LC/MS system with a Luna 5 μm C8(2) 100 \AA 50 mm \times 4.6 mm \times 5 μm column. Buffer A: 5% Acetonitrile, 94.9% Water, 0.1% formic acid, Buffer B: 95% Acetonitrile, 19.9% Water, 0.1% formic acid. Compounds were analysed using a gradient of 0-100% buffer B in buffer A over 4 min. followed by isocratic 100% buffer B for a further 3 min. followed by gradient to 100% buffer A for 2 min. followed by isocratic 100% buffer A for 1 min. at a flow rate of 0.5 mL/min. System control and analysis was facilitated with Agilent Chemstation software.

High Resolution Mass Spectrometry analyses was performed on a Waters Micromass LCT Premier XE time-of-flight mass spectrometer fitted with an electrospray (ESI) ion source controlled by MassLynx v4.5 software. Low Resolution Mass Spectrometry analyses were performed using a Micromass Platform II single quadrupole mass spectrometer equipped with an atmospheric pressure (ESI/APCI) ion source. Sample management was facilitated by an Agilent 1100 series HPLC system and the instrument was controlled using MassLynx v3.5 software. Masses are quoted as the monoisotopic mass.

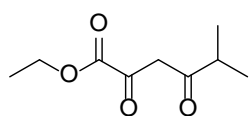
Analytical Reverse-Phase High Performance Liquid Chromatography (RP-HPLC) was conducted on a Waters Millenium 2690 system fitted with a Phenomenex[®] Luna C8, 100 Å, 5 µm (50 × 4.60 mm I.D.) column. A binary solvent system was used (solvent A: 0.1% TFA, 99.9% H₂O; solvent B: 0.1% TFA, 19.9% H₂O, 80% acetonitrile), with UV detection at 254 nm. The method used gradient elution beginning with 100% solvent A going to 20% solvent A, 80% solvent B, over 20 min at a flow rate of 1 mL/min.

Analytical and semi-preparative chiral chromatography were conducted on an Agilent Infinity 1260 system fitted with either of (a) Lux 5µ Amylose-2 250 × 10.00 mm, (b) Lux 5µ Amylose-2 150 × 4.60 mm, (c) Lux 5µ Cellulose-1 150 × 4.60 mm, (d) Lux 5µ Cellulose-2 150 × 4.60 mm column, or an (e) Lux 5µ Amylose-2 150 × 10.00 mm column in the case of semi-preparative chiral chromatography. A binary solvent system was used (solvent A: ethanol; solvent B: petroleum spirits), with UV detection at 254 nm. The method used isocratic elution of 10% solvent A and 90% solvent B, or 20% solvent A and 80% solvent B, with a flow rate of 1 mL/min.

Microwave reactions were conducted in a Biotage Initiator TM, in 2.0-5.0 mL vials according to manufacturer's instructions. Melting points (M.p.) were determined using a Mettler Toledo MP50 melting point apparatus.

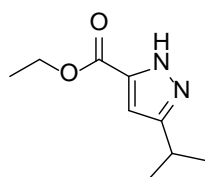
7.2.1 Chapter 3 experimental

Ethyl 5-methyl-2,4-dioxohexanoate (**90**)



Sodium (433 mg, 1.88 mmol) was dissolved in stirring ethanol (50 mL) at room temperature under an atmosphere of nitrogen. A solution of diethyloxalate (2.64 g, 17.0 mmol) in 3-methyl-2-butanone (2.05 g, 14.0 mmol) was added dropwise at room temperature over 10 min. The mixture was stirred at room temperature for 1 h then heated to 60 °C and stirred for 1 h. The reaction mixture was cooled to room temperature, poured into ice-cold 2 M aqueous hydrochloric acid (20 mL), and extracted with diethyl ether (20 mL) and ethyl acetate (20 mL). The combined organic extracts were dried (anhydrous sodium sulfate), filtered and concentrated *in vacuo* to afford **90** as a pale yellow oil (2.55 g, 13.7 mmol, 98%). ¹H NMR (300 MHz, CDCl₃) δ 6.27 (s, 2H, C(O)CH₂), 4.21 (q, *J* = 7.0 Hz, 2H, OCH₂), 2.58 - 2.49 (m, 1H, CH), 1.23 (t, *J* = 7.0 Hz, 3H, CH₂CH₃), 1.02 (d, *J* = 4.5 Hz, 6H, CHCH₃, CHCH₃). ESI-MS: *m/z* 187.2 [M+H]⁺. RP-HPLC: *t_R* 9.73 min.

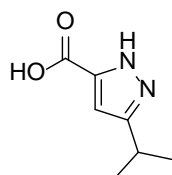
Ethyl 3-isopropyl-1*H*-pyrazole-5-carboxylate (**91**)



Hydrazine hydrate (487 mg, 9.73 mmol) was added to a solution of ethyl 5-methyl-2,4-dioxohexanoate (**90**) (2.55 g, 13.7 mmol) in ethanol (50 mL) at room temperature under an atmosphere of nitrogen. The reaction mixture was stirred for 18 h. Additional hydrazine hydrate

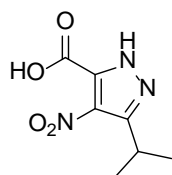
(206 mg, 4.12 mmol) was added and the mixture was stirred at 60 °C for 3 h. The mixture was concentrated *in vacuo*. The residue was dissolved in dichloromethane (80 mL) and washed with water (3 × 20 mL). The organic layer was dried (anhydrous sodium sulfate), filtered and concentrated *in vacuo* to afford **91** as a yellow oil (1.59 g, 8.73 mmol, 64%). ¹H NMR (300 MHz, CDCl₃) δ 7.24 (s, 1H, ArH), 4.32 (q, *J* = 4.8 Hz, 2H, OCH₂), 3.04 - 2.95 (m, 1H, CH), 1.26 (t, *J* = 4.8 Hz, 3H, CH₂CH₃), 1.13 (d, *J* = 4.5 Hz, 6H, CHCH₃, CHCH₃). ESI-MS: *m/z* 183.2 [M+H]⁺. RP-HPLC: *t_R* 9.26 min.

3-Isopropyl-1*H*-pyrazole-5-carboxylic acid (**92**)



Ethyl 3-isopropyl-1*H*-pyrazole-5-carboxylate (**91**) (1.48 g, 8.21 mmol) was dissolved in 1,4-dioxane (40 mL) and 1 M aqueous sodium hydroxide (35 mL) was added. The mixture was stirred at 50 °C under an atmosphere of nitrogen for 1 h and concentrated *in vacuo*. The residue was dissolved in water (50 mL) and extracted with ethyl acetate (3 × 20 mL). The organic phase was lyophilised to afford **92** as a yellow oil (931 mg, 6.04 mmol, 74%). ¹H NMR (300 MHz, CDCl₃) δ 6.46 (s, 1H, ArH), 3.09 - 2.98 (m, 1H, CH), 1.09 (d, *J* = 3.0 Hz, 6H, CH₃, CH₃). ESI-MS: *m/z* 153.2 [M-H]⁺. RP-HPLC: *t_R* 6.88 min.

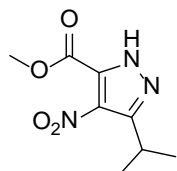
3-Isopropyl-4-nitro-1*H*-pyrazole-5-carboxylic acid (**93**)



3-Isopropyl-1*H*-pyrazole-5-carboxylic acid (**92**) (931 mg, 6.03 mmol) was added portion-wise to concentrated sulfuric acid (15 mL) at room temperature while stirring. The reaction mixture was heated to 60 °C and aqueous nitric acid (70%, 2.0 mL, 33.6 mmol) was added in a drop-wise manner. The reaction mixture was stirred at 60 °C for 1 h, cooled to room temperature, poured onto ice, and stirred for 15 min, warming to room temperature. The resulting precipitate was filtered to afford **93** as a white solid (360 mg, 1.81 mmol, 30%). ¹H NMR (300 MHz,

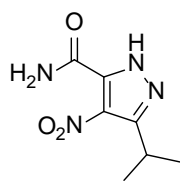
CDCl_3) δ 3.74 - 3.64 (m, 1H, CH), 1.36 (d, $J = 4.5$ Hz, 6H, CH_3 , CH_3). ESI-MS: m/z 198.2 $[\text{M}-\text{H}]^+$. RP-HPLC: t_R 6.89 min.

Methyl 3-isopropyl-4-nitro-1H-pyrazole-5-carboxylate (**94**)



To a 0 °C solution of methanol (20 mL) was added 5 drops of concentrated sulfuric acid. 3-Isopropyl-4-nitro-1H-pyrazole-5-carboxylic acid (**93**) (1.0 g, 5.02 mmol) was added, and the solution was heated at 65 °C for 16 h. The mixture was concentrated *in vacuo*, dissolved in water (30 mL) and extracted with dichloromethane (3×10 mL). The combined organic extracts were washed with saturated aqueous sodium hydrogen carbonate (10 mL), dried (anhydrous sodium sulfate), filtered and concentrated *in vacuo* to afford **94** as a yellow oil (708 mg, 3.32 mmol, 66%). ^1H NMR (400 MHz, CDCl_3) δ 3.90 (s, 3H, OCH_3), 3.62 - 3.50 (m, 1H, CH), 1.30 (d, $J = 4.5$ Hz, 6H, CH_3 , CH_3). ESI-MS: m/z 212.1 $[\text{M}-\text{H}]^+$. RP-HPLC: t_R 8.42 min.

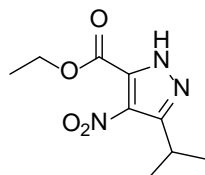
3-Isopropyl-4-nitro-1H-pyrazole-5-carboxamide (**95**)



To a microwave vial containing a stirred solution of methyl 3-isopropyl-4-nitro-1H-pyrazole-5-carboxylate (**94**) (100 mg, 0.47 mmol) in methanol (5.0 mL) was added magnesium nitride (237 mg, 2.35 mmol) at 0 °C. The vial was immediately sealed and allowed to warm to room temperature with stirring. After 1 h, the reaction mixture was heated to 80 °C for 24 h. The reaction mixture was cooled to room temperature, diluted with water (15 mL) and neutralised (pH ~ 7.0) with 1 M aqueous hydrochloric acid. The aqueous layer was extracted with chloroform (3×10 mL). The combined organic extracts were washed with saturated aqueous sodium chloride (10 mL), dried (anhydrous sodium sulfate), filtered and concentrated *in vacuo* to afford **95** as a clear oil (82 mg, 0.41 mmol, 88%). ^1H NMR

(300 MHz, CDCl₃) δ 8.21 (br s, 2H, NH₂), 3.59 - 3.52 (m, 1H, CH), 1.35 (d, J = 3.0 Hz, 6H, CH₃, CH₃). ESI-MS: m/z 197.3 [M-H⁺]⁻. RP-HPLC: t_R 5.97 min.

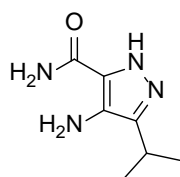
Ethyl 3-isopropyl-4-nitro-1H-pyrazole-5-carboxylate (96)



3-Isopropyl-4-nitro-1H-pyrazole-5-carboxylic acid (**93**) (735 mg, 0.40 mmol) was added to a stirring solution of ethanol (3 mL) and concentrated sulfuric acid (3 mL) in toluene (30 mL) and stirred at

78 °C for 24 h. The reaction mixture was concentrated *in vacuo*. The residue was dissolved in water (40 mL), extracted with diethyl ether (2 × 15 mL), and washed with saturated aqueous sodium carbonate (15 mL) and water (15 mL). The organic layer was dried (anhydrous sodium sulfate), filtered and concentrated *in vacuo* to afford **96** as a white solid (772 mg, 3.40 mmol, 92%). ¹H NMR (400 MHz, CDCl₃) δ 4.46 (q, J = 7.1 Hz, 2H, CH₂), 3.72 - 3.56 (m, 1H, CH), 1.42 - 1.38 (m, 9H, CH₂CH₃, CH₃, CH₃). ESI-MS: m/z 228.2 [M+H⁺]⁺. RP-HPLC: t_R 9.24 min.

4-Amino-3-isopropyl-1H-pyrazole-5-carboxamide (85)

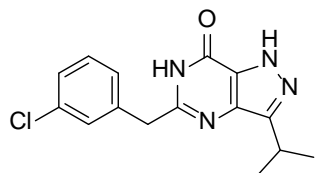


3-Isopropyl-4-nitro-1H-pyrazole-5-carboxamide (**95**) (82 mg, 0.41 mmol) was stirred in ethanol (8.0 mL) at room temperature.

Palladium on carbon catalyst (spatula tip) in ethanol (2.0 mL) was added, and the solution was flushed with nitrogen gas and placed under hydrogen gas (1 atm). The solution was stirred at room temperature for 20 h. The mixture was filtered through celite and the filtrate was concentrated *in vacuo* to afford **85** as a pale pink oil (47 mg, 0.28 mmol, 68%). ¹H NMR (300 MHz, CDCl₃) δ 2.58 - 2.55 (m, 1H, CH), 1.33 (d, J = 7.5 Hz, 6H, CH₃ and CH₃). ¹H NMR (300 MHz, DMSO) δ 12.08 (br s, 1H, NH), 7.07 (br s, 2H, NH₂), 6.51 (br s, 2H, CONH₂), 2.92 - 2.88 (m, 1H, CH), 1.20 (d, J = 7.5 Hz, 6H, CH₃, CH₃). ¹³C NMR (101 MHz, DMSO) δ 166.5 (C=O), 133.5 (C), 132.4

(C), 128.0 (C), 23.5 (CH), 21.3 (CH₃). ESI-HRMS: m/z calculated for C₇H₁₂N₄O [M+H]⁺ 169.1084, found 169.1080. RP-HPLC: t_R 2.42 min.

5-(3-Chlorobenzyl)-3-isopropyl-1H-pyrazolo[4,3-d]pyrimidin-7(6H)-one (**77**)



Method I:

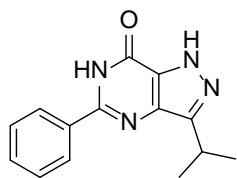
3-Chlorophenylacetic acid (203 mg, 1.19 mmol), 2-(6-chloro-1-*H*-benzotriazole-1-yl)-1,1,3,3-tetramethylammonium hexafluorophosphate (492 mg, 1.19 mmol) and diisopropylamine (297 mg, 2.94 mmol) were combined in dimethylformamide (4 mL) and stirred at room temperature for 20 min. 4-Amino-3-isopropyl-1*H*-pyrazole-5-carboxamide (**85**) (50 mg, 0.30 mmol) in dimethylformamide (2 mL) was added and stirring continued at room temperature for 48 h. The reaction mixture was diluted with aqueous acetonitrile (50%, 10 mL) and lyophilised to yield a yellow oil. Purification by column chromatography eluting with ethyl acetate afforded **77** as a white solid (11 mg, 0.04 mmol, 12%).

Method II:

4-Amino-3-isopropyl-1*H*-pyrazole-5-carboxamide (**85**) (40 mg, 0.24 mmol), 3-chlorophenylacetic acid (41 mg, 0.24 mmol), bromo-tris-pyrrolidinophosphoniumhexafluorophosphate (122 mg, 0.26 mmol) and triethylamine (49 mg, 0.48 mmol) were combined in 1,2-dichloroethane (5 mL) and heated using microwave irradiation at 120 °C for 20 min. The reaction mixture was concentrated *in vacuo* to give a yellow oil. This material was passed through a short silica plug eluting with ethyl acetate. The filtrate was concentrated *in vacuo* to give a yellow solid. This solid was combined with 1 M potassium *t*-butoxide in tetrahydrofuran (53 mg, 0.48 mmol) in isopropanol (5 mL) and heated using microwave irradiation at 130 °C for 40 min. The reaction mixture was concentrated *in vacuo*. The residue was purified by column chromatography eluting with 10% methanol in ethyl acetate to afford **77** as a white solid (45 mg, 0.15 mmol,

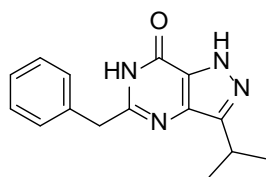
63%). ^1H NMR (400 MHz, CD_3OD) δ 7.43 (s, 1H, ArH), 7.32 (dd, $J = 4.7, 1.7$ Hz, 2H, ArH), 7.27 (dt, $J = 9.2, 4.7$ Hz, 1H, ArH), 4.56 (s, 2H, CH_2), 3.01 - 2.92 (m, 1H, CH), 1.21 (d, $J = 7.0$ Hz, 6H, CH_3 , CH_3). ^{13}C NMR (101 MHz, DMSO) δ 151.8 (C=O), 139.4 (C), 132.9 (C), 130.2 (CH), 128.7 (CH), 127.5 (CH), 126.7 (CH), 40.2 (CH_2), 25.7 (CH), 21.8 (CH_3). Note: not all ^{13}C signals visible in spectrum. ESI-HRMS: m/z calculated for $\text{C}_{15}\text{H}_{15}\text{ClN}_4\text{O}$ $[\text{M}+\text{H}^+]^+$ 303.1007, found 303.1009. RP-HPLC: t_R 8.30 min.

3-Isopropyl-5-phenyl-1H-pyrazolo[4,3-d]pyrimidin-7(6H)-one (98)

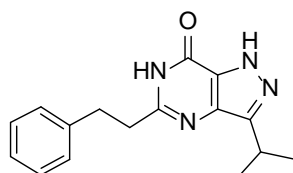


4-Amino-3-isopropyl-1H-pyrazole-5-carboxamide (**85**) (50 mg, 0.30 mmol), benzoic acid (45 mg, 0.30 mmol), bromo-tris-pyrrolidinophosphoniumhexafluorophosphate (152 mg, 0.33 mmol)

and triethylamine (60 mg, 0.59 mmol) were combined in 1,2-dichloroethane (5 mL) and heated using microwave irradiation at 120 °C for 20 min. The reaction mixture was concentrated *in vacuo* to give a yellow oil. This material was passed through a short silica plug eluting with ethyl acetate. The filtrate was concentrated *in vacuo* to give a yellow solid. This solid was combined with 1 M potassium *t*-butoxide in tetrahydrofuran (67 mg, 0.60 mmol) in isopropanol (5 mL) and heated using microwave irradiation at 130 °C for 40 min. The reaction mixture was concentrated *in vacuo*. The residue was purified by column chromatography eluting with 10% methanol in ethyl acetate to afford **98** as a white solid (40 mg, 0.16 mmol, 53%). ^1H NMR (400 MHz, DMSO) δ 8.11 - 8.06 (m, 2H, ArH), 7.54 - 7.49 (m, 3H, ArH), 3.33 (m, 1H, CH), 1.40 (d, $J = 7.5$ Hz, 6H, CH_3 , CH_3). ^{13}C NMR (101 MHz, DMSO) δ 149.5 (C=O), 130.5 (CH), 129.3 (CH), 128.5 (CH), 28.0 (CH), 21.8 (CH_3). Note: not all ^{13}C signals visible in spectrum. ESI-HRMS: m/z calculated for $\text{C}_{14}\text{H}_{14}\text{N}_4\text{O}$ $[\text{M}+\text{H}^+]^+$ 255.1240, found 255.1252. RP-HPLC: t_R 8.52 min.

5-Benzyl-3-isopropyl-1H-pyrazolo[4,3-d]pyrimidin-7(6H)-one (99)

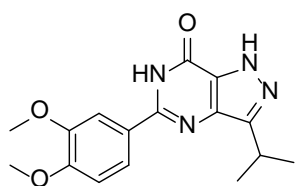
4-Amino-3-isopropyl-1H-pyrazole-5-carboxamide (**85**) (40 mg, 0.24 mmol), phenylacetic acid (32 mg, 0.24 mmol), bromo-tris-pyrrolidinophosphonium-hexafluorophosphate (122 mg, 0.26 mmol) and triethylamine (49 mg, 0.48 mmol) were combined in 1,2-dichloroethane (5 mL) and heated using microwave irradiation at 120 °C for 20 min. The reaction mixture was concentrated *in vacuo* to give a yellow oil. This material was passed through a short silica plug eluting with ethyl acetate. The filtrate was concentrated *in vacuo* to give a yellow solid. This solid was combined with 1 M potassium *t*-butoxide in tetrahydrofuran (53 mg, 0.48 mmol) in isopropanol (5 mL) and heated using microwave irradiation at 130 °C for 40 min. The reaction mixture was concentrated *in vacuo*. The residue was purified by column chromatography eluting with 10% methanol in ethyl acetate to afford **99** as a white solid (28 mg, 0.10 mmol, 42%). ¹H NMR (400 MHz, CD₃OD) 7.36 - 7.17 (m, 5H, ArH), 3.99 (s, 2H, CH₂), 3.47 - 3.37 (m, 1H, CH), 1.41 (d, *J* = 7.0 Hz, 6H, CH₃, CH₃). ¹³C NMR (101 MHz, DMSO) δ 154.0 (C=O), 137.1 (C), 128.7 (CH), 128.4 (CH), 126.6 (CH), 40.3 (CH₂), 26.1 (CH), 21.8 (CH₃). Note: not all ¹³C signals visible in spectrum. ESI-HRMS: *m/z* calculated for C₁₅H₁₆N₄O [M+H]⁺ 269.1397, found 269.1410. RP-HPLC: *t*_R 8.54 min.

3-Isopropyl-5-phenethyl-1H-pyrazolo[4,3-d]pyrimidin-7(6H)-one (100)

4-Amino-3-isopropyl-1H-pyrazole-5-carboxamide (**85**) (50 mg, 0.30 mmol), 3-phenylpropanoic acid (45 mg, 0.30 mmol), bromo-tris-pyrrolidinophosphonium-hexafluorophosphate (152 mg, 0.33 mmol) and triethylamine (60 mg, 0.59 mmol) were combined in 1,2-dichloroethane (5 mL) and heated using microwave irradiation at 120 °C for 20 min. The reaction mixture was concentrated *in vacuo* to give a yellow oil. This

material was passed through a short silica plug eluting with ethyl acetate. The filtrate was concentrated *in vacuo* to give a yellow solid. This solid was combined with 1 M potassium *t*-butoxide in tetrahydrofuran (67 mg, 0.60 mmol) in isopropanol (5 mL) and heated using microwave irradiation at 130 °C for 40 min. The reaction mixture was concentrated *in vacuo*. The residue was purified by column chromatography eluting with 10% methanol in ethyl acetate to afford **100** as a white solid (54 mg, 0.10 mmol, 42%). ¹H NMR (400 MHz, DMSO) δ 7.28 - 7.21 (m, 4H, ArH), 7.16 (ddd, *J* = 8.6, 5.4, 2.2 Hz, 1H, ArH), 3.41 - 3.33 (m, 1H, CH), 3.08 (dd, *J* = 9.0, 6.4 Hz, 2H, NCCH₂), 2.95 (dd, *J* = 9.0, 6.4 Hz, 2H, NCCH₂CH₂), 1.40 (d, *J* = 7.0 Hz, 6H, CH₃, CH₃). ¹³C NMR (101 MHz, DMSO) δ 156.8 (C=O), 139.4 (C), 128.4 (CH), 127.9 (CH), 126.8 (CH), 36.0 (CH₂), 28.9 (CH₂), 25.9 (CH), 21.9 (CH₃). Note: not all ¹³C signals visible in spectrum. ESI-HRMS: *m/z* calculated for C₁₆H₁₈N₄O [M+H]⁺ 283.1553, found 283.1550. RP-HPLC: *t*_R 8.57 min.

5-(3,4-Dimethoxyphenyl)-3-isopropyl-1*H*-pyrazolo[4,3-*d*]pyrimidin-7(6*H*)-one
(**101**)

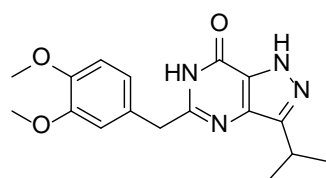


4-Amino-3-isopropyl-1*H*-pyrazole-5-carboxamide (**85**) (40 mg, 0.24 mmol), 3,4-dimethoxybenzoic acid (43 mg, 0.24 mmol), bromo-tris-pyrrolidinophosphonium-hexafluorophosphate

(122 mg, 0.26 mmol) and triethylamine (66 μL, 0.48 mmol) were combined in 1,2-dichloroethane (5 mL) and heated using microwave irradiation at 120 °C for 20 min. The reaction mixture was concentrated *in vacuo* to give a yellow oil. This material was passed through a short silica plug eluting with ethyl acetate. The filtrate was concentrated *in vacuo* to give a yellow solid. This solid was combined with 1 M potassium *t*-butoxide in tetrahydrofuran (53 mg, 0.48 mmol) in isopropanol (5 mL) and heated using microwave irradiation at 130 °C for 40 min. The reaction mixture was

concentrated *in vacuo*. The residue was purified by column chromatography eluting with 10% methanol in ethyl acetate to afford **101** as a white solid (20 mg, 0.06 mmol, 25%). ^1H NMR (400 MHz, CD_3OD) δ 7.67 - 7.58 (m, 2H, ArH), 7.08 (s, 1H, ArH), 3.94 (s, 3H, OCH₃), 3.91 (s, 3H, OCH₃), 3.58 - 3.38 (m, 1H, CH), 1.47 (d, J = 7.5 Hz, 6H, CH₃, CH₃). ^{13}C NMR (101 MHz, DMSO) δ 150.6 (C=O), 112.5 (CH), 112.2 (CH), 56.6 (CH₃), 56.5 (CH₃), 30.7 (CH), 22.4 (CH₃). Note: not all ^{13}C signals visible in spectrum. ESI-HRMS: m/z calculated for $\text{C}_{16}\text{H}_{18}\text{N}_4\text{O}_3$ $[\text{M}+\text{H}]^+$ 315.1452, found 315.1449. RP-HPLC: t_{R} 8.65 min.

5-(3,4-Dimethoxybenzyl)-3-isopropyl-1H-pyrazolo[4,3-*d*]pyrimidin-7(6H)-one (**102**)



4-Amino-3-isopropyl-1H-pyrazole-5-carboxamide (**85**)

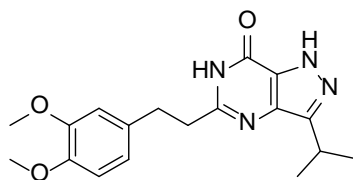
(50 mg, 0.30 mmol), 2-(3,4-dimethoxyphenyl)acetic acid

(58 mg, 0.30 mmol), bromo-tris-pyrrolidinophosphonium-

hexafluorophosphate (152 mg, 0.33 mmol) and triethylamine (82 μL , 0.59 mmol) were combined in 1,2-dichloroethane (5 mL) and heated using microwave irradiation at 120 °C for 20 min. The reaction mixture was concentrated *in vacuo* to give a yellow oil. This material was passed through a short silica plug eluting with ethyl acetate. The filtrate was concentrated *in vacuo* to give a yellow solid. This solid was combined with 1 M potassium *t*-butoxide in tetrahydrofuran (67 mg, 0.60 mmol) in isopropanol (5 mL) and heated using microwave irradiation at 130 °C for 40 min. The reaction mixture was concentrated *in vacuo*. The residue was purified by column chromatography eluting with 10% methanol in ethyl acetate to afford **102** as a white solid (75 mg, 0.23 mmol, 77%). ^1H NMR (400 MHz, CD_3OD) δ 6.99 (s, 1H, ArH), 6.86 - 6.63 (m, 2H, ArH), 3.94 (s, 2H, CH₂), 3.79 (s, 3H, OCH₃), 3.78 (s, 3H, OCH₃), 3.33 - 3.28 (m, 1H, CH), 1.41 (d, J = 7.0 Hz, 6H, CH₃, CH₃). ^{13}C NMR (101 MHz, CD_3OD) δ 150.5 (C=O), 149.7 (C), 130.4 (C), 122.1 (CH), 113.7 (CH), 113.2 (CH), 56.5 (CH₃), 56.4 (CH₃), 41.4 (CH₂),

22.3 (CH), 20.8 (CH₃). Note: not all ¹³C signals visible in spectrum. ESI-HRMS: *m/z* calculated for C₁₇H₂₀N₄O₃ [M+H]⁺ 327.1463, found 327.1478. RP-HPLC: *t*_R 7.73 min.

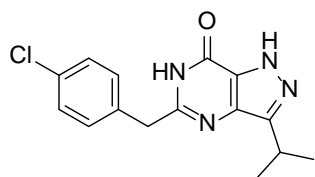
5-(3,4-Dimethoxyphenethyl)-3-isopropyl-1*H*-pyrazolo[4,3-*d*]pyrimidin-7(6*H*)-one
(103)



4-Amino-3-isopropyl-1*H*-pyrazole-5-carboxamide (85)

(50 mg, 0.30 mmol), 3-(3,4-dimethoxyphenyl)-propanoic acid (62 mg, 0.30 mmol), bromo-tris-pyrrolidino-

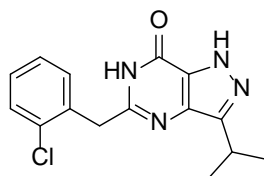
phosphoniumhexafluorophosphate (152 mg, 0.33 mmol) and triethylamine (60 mg, 0.59 mmol) were combined in 1,2-dichloroethane (5 mL) and heated using microwave irradiation at 120 °C for 20 min. The reaction mixture was concentrated *in vacuo* to give a yellow oil. This material was passed through a short silica plug eluting with ethyl acetate. The filtrate was concentrated *in vacuo* to give a yellow solid. This solid was combined with 1 M potassium *t*-butoxide in tetrahydrofuran (67 mg, 0.60 mmol) in isopropanol (5 mL) and heated using microwave irradiation at 130 °C for 40 min. The reaction mixture was concentrated *in vacuo*. The residue was purified by column chromatography eluting with 10% methanol in ethyl acetate to afford **103** as a white solid (28 mg, 0.08 mmol, 27%). ¹H NMR (400 MHz, DMSO) δ 6.86 - 6.83 (m, 2H, ArH), 6.76 - 6.74 (m, 1H, ArH), 3.69 (s, 3H, OCH₃), 3.33 (s, 3H, OCH₃), 3.28 - 3.22 (m, 1H, CH), 2.94 - 2.92 (m, 2H, NCCH₂), 2.87 - 2.85 (m, 2H, NCCH₂CH₂), 1.33 (d, *J* = 7.4 Hz, 6H, CH₃, CH₃). ¹³C NMR (101 MHz, DMSO) δ 148.5 (C=O), 120.1 (CH), 112.4 (CH), 111.9 (CH), 55.5 (CH₃), 55.3 (CH₃), 36.1 (CH₃), 32.6 (CH₂), 26.1 (CH), 21.8 (CH₃). Note: not all ¹³C signals visible in spectrum. ESI-HRMS: *m/z* calculated for C₁₈H₂₂N₄O₃ [M+H]⁺ 343.1765, found 343.1767. RP-HPLC: *t*_R 8.09 min.

5-(4-Chlorobenzyl)-3-isopropyl-1H-pyrazolo[4,3-d]pyrimidin-7(6H)-one (104)4-Amino-3-isopropyl-1H-pyrazole-5-carboxamide (**85**)

(50 mg, 0.30 mmol), 2-(4-chlorophenyl)acetic acid (51 mg,

0.30 mmol), bromo-tris-pyrrolidinophosphoniumhexafluoro-

phosphate (152 mg, 0.33 mmol) and triethylamine (60 mg, 0.59 mmol) were combined in 1,2-dichloroethane (5 mL) and heated using microwave irradiation at 120 °C for 20 min. The reaction mixture was concentrated *in vacuo* to give a yellow oil. This material was passed through a short silica plug eluting with ethyl acetate. The filtrate was concentrated *in vacuo* to give a yellow solid. This solid was combined with 1 M potassium *t*-butoxide in tetrahydrofuran (67 mg, 0.60 mmol) in isopropanol (5 mL) and heated using microwave irradiation at 130 °C for 40 min. The reaction mixture was concentrated *in vacuo*. The residue was purified by column chromatography eluting with 10% methanol in ethyl acetate to afford **104** as a white solid (14 mg, 0.05 mmol, 17%). ¹H NMR (400 MHz, CD₃OD) δ 7.31 - 7.29 (m, 2H, ArH), 7.25 - 7.23 (m, 2H, ArH), 3.68 (s, 2H, CH₂), 3.55 - 3.41 (m, 1H, CH), 1.40 (d, *J* = 7.5 Hz, 6H, CH₃, CH₃). ¹³C NMR (101 MHz, CD₃OD) δ 169.1 (C), 162.0 (C=O), 133.4 (C), 130.5 (CH), 128.7 (CH), 41.6 (CH₂), 28.3 (CH), 22.2 (CH₃). Note: not all ¹³C signals visible in spectrum. ESI-HRMS: *m/z* calculated for C₁₅H₁₅ClN₄O [M+H]⁺ 303.1007, found 303.1012. RP-HPLC: *t_R* 9.16 min.

5-(2-Chlorobenzyl)-3-isopropyl-1H-pyrazolo[4,3-d]pyrimidin-7(6H)-one (105)4-Amino-3-isopropyl-1H-pyrazole-5-carboxamide (**85**) (50 mg,

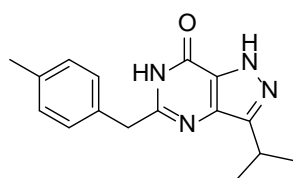
0.30 mmol), 2-(2-chlorophenyl)acetic acid (51 mg, 0.30 mmol),

bromo-tris-pyrrolidinophosphonium-hexafluorophosphate

(152 mg, 0.33 mmol) and triethylamine (60 mg, 0.59 mmol) were combined in 1,2-dichloroethane (5 mL) and heated using microwave irradiation at 120 °C for 20 min.

The reaction mixture was concentrated *in vacuo* to give a yellow oil. This material was passed through a short silica plug eluting with ethyl. The filtrate was concentrated *in vacuo* to give a yellow solid. This solid was combined with 1 M potassium *t*-butoxide in tetrahydrofuran (67 mg, 0.60 mmol) in isopropanol (5 mL) and heated using microwave irradiation at 130 °C for 40 min. The reaction mixture was concentrated *in vacuo*. The residue was purified by column chromatography eluting with 10% methanol in ethyl acetate to afford **105** as a white solid (14 mg, 0.05 mmol, 17%). ¹H NMR (400 MHz, CD₃OD) δ 7.31 - 7.29 (m, 2H, ArH), 7.25 - 7.23 (m, 2H, ArH), 3.68 (s, 2H, CH₂), 3.55 - 3.41 (m, 1H, CH), 1.40 (d, *J* = 7.5 Hz, 6H, CH₃, CH₃). ¹³C NMR (101 MHz, DMSO) δ 150.9 (C=O), 134.8 (C), 133.5 (C), 131.1 (CH), 130.4 (CH), 129.1 (CH), 128.5 (CH), 37.8 (CH₂), 26.1 (CH), 21.6 (CH₃). Note: not all ¹³C signals visible in spectrum. ESI-HRMS: *m/z* calculated for C₁₅H₁₅ClN₄O [M+H]⁺ 303.1007, found 303.1011. RP-HPLC: *t*_R 9.02 min.

3-Isopropyl-5-(4-methylbenzyl)-1*H*-pyrazolo[4,3-*d*]pyrimidin-7(6*H*)-one (**106**)

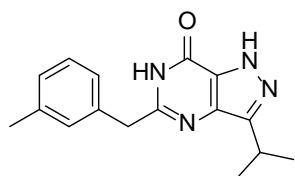


4-Amino-3-isopropyl-1*H*-pyrazole-5-carboxamide (**85**) (50 mg, 0.30 mmol), 2-(*p*-tolyl)acetic acid (45 mg, 0.30 mmol), bromo-tris-pyrrolidinophosphonium-hexafluorophosphate (152 mg,

0.33 mmol) and triethylamine (60 mg, 0.59 mmol) were combined in 1,2-dichloroethane (5 mL) and heated using microwave irradiation at 120 °C for 20 min. The reaction mixture was concentrated *in vacuo* to give a yellow oil. This material was passed through a short silica plug eluting with ethyl acetate. The filtrate was concentrated *in vacuo* to give a yellow solid. This solid was combined with 1 M potassium *t*-butoxide in tetrahydrofuran (67 mg, 0.60 mmol) in isopropanol (5 mL) and heated using microwave irradiation at 130 °C for 40 min. The reaction mixture was concentrated *in vacuo*. The residue was purified by column chromatography eluting with 10% methanol in ethyl

acetate to afford **106** as a white solid (60 mg, 0.21 mmol, 70%). ^1H NMR (400 MHz, DMSO) δ 7.23 (d, J = 8.2 Hz, 2H, ArH), 7.10 (d, J = 8.2 Hz, 2H, ArH), 3.85 (s, 2H, CH₂), 3.30 - 3.25 (m, 1H, CH), 2.24 (s, 3H, ArCH₃), 1.32 (d, J = 7.5 Hz, 6H, CH₃, CH₃). ^{13}C NMR (101 MHz, DMSO) δ 155.8 (C=O), 153.4 (C), 135.6 (C), 135.3 (C), 134.4 (C), 132.6 (C), 128.9 (CH), 128.8 (CH), 128.6 (C), 45.9 (CH₂), 24.0 (CH), 21.9 (CH₃), 20.6 (CH₃). ESI-HRMS: m/z calculated for C₁₆H₁₈N₄O [M+H]⁺ 283.1553, found 283.1557. RP-HPLC: t_R 8.22 min.

3-isopropyl-5-(3-methylbenzyl)-1H-pyrazolo[4,3-d]pyrimidin-7(6H)-one (**107**)

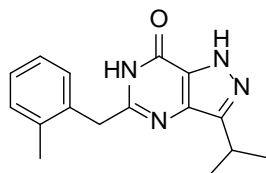


4-Amino-3-isopropyl-1H-pyrazole-5-carboxamide (**85**) (50 mg, 0.30 mmol), 2-(*m*-tolyl)acetic acid (45 mg, 0.30 mmol), bromo-tris-pyrrolidinophosphoniumhexafluoro-phosphate

(152 mg, 0.33 mmol) and triethylamine (60 mg, 0.59 mmol) were combined in 1,2-dichloroethane (5 mL) and heated using microwave irradiation at 120 °C for 20 min. The reaction mixture was concentrated *in vacuo* to give a yellow oil. This material was passed through a short silica plug eluting with ethyl acetate. The filtrate was concentrated *in vacuo* to give a yellow solid. This solid was combined 1 M potassium *t*-butoxide in tetrahydrofuran (67 mg, 0.60 mmol) in isopropanol (5 mL) and heated using microwave irradiation at 130 °C for 40 min. The reaction mixture was concentrated *in vacuo*. The residue was purified by column chromatography eluting with 10% methanol in ethyl acetate to afford **107** as a white solid (54 mg, 0.19 mmol, 63%). ^1H NMR (400 MHz, CD₃OD) δ 7.18 - 7.15 (m, 2H, ArH), 7.13 - 7.03 (m, 2H, ArH), 3.63 (s, 2H, CH₂), 3.51 - 3.41 (m, 1H, CH), 2.31 (s, 3H, ArCH₃), 1.41 (d, J = 7.5 Hz, 6H, CH₃, CH₃). ^{13}C NMR (101 MHz, CD₃OD) δ 159.9 (C=O), 131.5 (C), 130.4 (CH), 130.3 (C), 129.6 (CH), 128.8 (CH), 126.7 (CH), 43.8 (CH₂), 27.8 (CH), 22.3 (CH₃), 20.6 (CH₃).

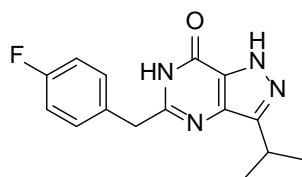
Note: not all ^{13}C signals visible in spectrum. ESI-HRMS: m/z calculated for $\text{C}_{16}\text{H}_{18}\text{N}_4\text{O}$ $[\text{M}+\text{H}]^+$ 283.1553, found 283.1555. RP-HPLC: t_R 8.22 min.

3-Isopropyl-5-(2-methylbenzyl)-1*H*-pyrazolo[4,3-*d*]pyrimidin-7(6*H*)-one (**108**)



4-Amino-3-isopropyl-1*H*-pyrazole-5-carboxamide (**85**) (50 mg, 0.30 mmol), 2-(*o*-tolyl)acetic acid (45 mg, 0.30 mmol), bromo-tris-pyrrolidinophosphonium-hexafluorophosphate (152 mg,

0.33 mmol) and triethylamine (60 mg, 0.59 mmol) were combined in 1,2-dichloroethane (5 mL) and heated using microwave irradiation at 120 °C for 20 min. The reaction mixture was concentrated *in vacuo* to give a yellow oil. This material was passed through a short silica plug eluting with ethyl acetate. The filtrate was concentrated *in vacuo* to give a yellow solid. This solid was combined with 1 M potassium *t*-butoxide in tetrahydrofuran (67 mg, 0.60 mmol) in isopropanol (5 mL) and heated using microwave irradiation at 130 °C for 40 min. The reaction mixture was concentrated *in vacuo*. The residue was purified by column chromatography eluting with 10% methanol in ethyl acetate to afford **108** as a white solid (61 mg, 0.22 mmol, 73%). ^1H NMR (400 MHz, DMSO) δ 7.21 - 7.14 (m, 2H, ArH), 7.14 - 7.09 (m, 2H, ArH), 4.82 (s, 2H, CH₂), 3.24 - 3.18 (m, 1H, CH), 2.36 (s, 3H, ArCH₃), 1.29 (d, J = 7.5 Hz, 6H, CH₃, CH₃). ^{13}C NMR (101 MHz, DMSO) δ 155.3 (C=O), 152.3 (C), 136.7 (C), 135.8 (C), 130.0 (C), 129.8 (C), 128.9 (CH), 126.7 (CH), 126.5 (C), 125.9 (CH), 125.6 (CH), 38.0 (CH₂), 25.9 (CH), 21.8 (CH₃), 19.4 (CH₃). ESI-HRMS: m/z calculated for $\text{C}_{16}\text{H}_{18}\text{N}_4\text{O}$ $[\text{M}+\text{H}]^+$ 283.1553, found 283.1558. RP-HPLC: t_R 8.94 min.

5-(4-Fluorobenzyl)-3-isopropyl-1H-pyrazolo[4,3-d]pyrimidin-7(6H)-one (109)

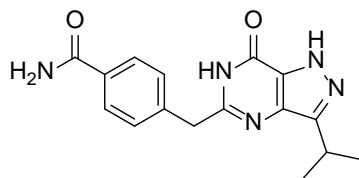
4-Amino-3-isopropyl-1H-pyrazole-5-carboxamide (85)

(50 mg, 0.30 mmol), 2-(*o*-tolyl)acetic acid (46 mg,

0.30 mmol), bromo-tris-pyrrolidinophosphoniumhexafluoro-

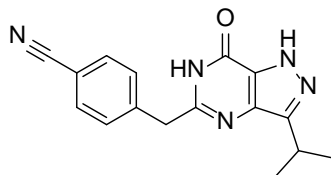
phosphate (152 mg, 0.33 mmol) and triethylamine (60 mg, 0.59 mmol) were combined in 1,2-dichloroethane (5 mL) and heated using microwave irradiation at 120 °C for 20 min. The reaction mixture was concentrated *in vacuo* to give a yellow oil. This material was passed through a short silica plug eluting with ethyl acetate. The filtrate was concentrated *in vacuo* to give a yellow solid. This solid was combined with 1 M potassium *t*-butoxide in tetrahydrofuran (67 mg, 0.60 mmol) in isopropanol (5 mL) and heated using microwave irradiation at 130 °C for 40 min. The reaction mixture was concentrated *in vacuo*. The residue was purified by column chromatography eluting with 10% methanol in ethyl acetate to afford **109** as a white solid (8 mg, 0.03 mmol, 10%). ¹H NMR (400 MHz, CD₃OD) δ 7.37 - 7.32 (m, 2H, ArH), 7.07 - 7.00 (m, 2H, ArH), 3.45 - 3.35 (m, 1H, CH), 3.35 (s, 2H, CH₂), 1.40 (d, *J* = 7.5 Hz, 6H, CH₃, CH₃). ¹³C NMR (101 MHz, CD₃OD) δ 169.0 (C), 164.6 (C=O), 131.6 (CH), 131.5 (C), 116.3 (CH), 40.9 (CH₂), 28.4 (CH), 22.3 (CH₃). Note: not all ¹³C signals visible in spectrum. ESI-HRMS: *m/z* calculated for C₁₅H₁₅FN₄O [M+H]⁺ 287.1303, found 287.1312. RP-HPLC: *t_R* 8.55 min.

4-((3-Isopropyl-7-oxo-6,7-dihydro-1H-pyrazolo[4,3-d]pyrimidin-5-yl)methyl)-benzamide (110) and 4-((3-Isopropyl-7-oxo-6,7-dihydro-1H-pyrazolo[4,3-d]pyrimidin-5-yl)methyl)benzo-nitrile (111)



4-Amino-3-isopropyl-1H-pyrazole-5-carboxamide (**85**)

(50 mg, 0.30 mmol), 2-(4-cyanophenyl)acetic acid (48 mg, 0.30 mmol), bromo-tris-pyrrolidinophosphonium-



hexafluorophosphate (152 mg, 0.33 mmol) and triethylamine (60 mg, 0.59 mmol) were combined in 1,2-dichloroethane (5 mL) and heated using microwave

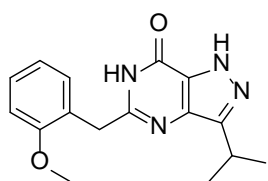
irradiation at 120 °C for 20 min. The reaction mixture was concentrated *in vacuo* to give a yellow oil. This material was passed through a short silica plug eluting with ethyl acetate. The filtrate was concentrated *in vacuo* to give a yellow solid. This solid was combined with 1 M potassium *t*-butoxide in tetrahydrofuran (67 mg, 0.60 mmol) in isopropanol (5 mL) and heated using microwave irradiation at 130 °C for 40 min. The reaction mixture was concentrated *in vacuo* to afford a mixture of **111** and **110** (1:1) as a yellow oil. Purification by column chromatography eluting with 10% methanol in ethyl acetate afforded **110** as a white solid (44 mg, 0.14 mmol, 47%) and **111** as a white solid (35 mg, 0.12 mmol, 40%).

110 - ^1H NMR (400 MHz, DMSO) δ 7.85 - 7.82 (m, 2H, ArH), 7.37 - 7.33 (m, 2H, ArH), 3.98 (s, 2H, CH₂), 3.23 - 3.21 (m, 1H, CH), 1.32 (d, J = 7.5 Hz, 6H, CH₃, CH₃). ^{13}C NMR (101 MHz, DMSO) δ 167.7 (C=O), 152.0 (C=O), 140.3 (C), 135.6 (C), 128.5 (CH), 127.6 (CH), 30.7 (CH₂), 26.2 (CH), 21.8 (CH₃). Note: not all ^{13}C signals visible in spectrum. ESI-HRMS: m/z calculated for C₁₆H₁₇N₅O₂ [M+H]⁺ 312.1455, found 312.1465. RP-HPLC: t_R 6.65 min.

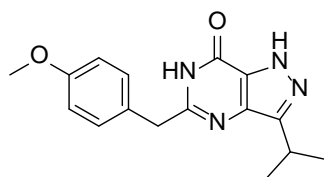
111 - ^1H NMR (400 MHz, DMSO) δ 7.79 (d, J = 8.3 Hz, 2H, ArH), 7.53 (d, J = 8.3 Hz, 2H, ArH), 4.03 (s, 2H, CH₂), 3.28 - 3.15 (m, 1H, CH), 1.30 (d, J = 7.5 Hz, 6H, CH₃,

CH_3). ^{13}C NMR (101 MHz, DMSO) δ 157.3 (C=O), 142.8 (C), 132.3 (CH), 129.9 (CH), 118.8 (C), 109.6 (C), 40.2 (CH_2), 23.6 (CH), 21.8 (CH_3). Note: not all ^{13}C signals visible in spectrum. ESI-HRMS: m/z calculated for $\text{C}_{16}\text{H}_{15}\text{N}_5\text{O}$ $[\text{M}+\text{H}]^+$ 294.1349, found 294.1357. RP-HPLC: t_R 8.02 min.

3-Isopropyl-5-(2-methoxybenzyl)-1H-pyrazolo[4,3-d]pyrimidin-7(6H)-one (**112**)



4-Amino-3-isopropyl-1H-pyrazole-5-carboxamide (**85**) (50 mg, 0.30 mmol), 2-(2-methoxyphenyl)acetic acid (50 mg, 0.30 mmol), bromo-tris-pyrrolidinophosphoniumhexafluorophosphate (152 mg, 0.33 mmol) and triethylamine (60 mg, 0.59 mmol) were combined in 1,2-dichloroethane (5 mL) and heated using microwave irradiation at 120 °C for 20 min. The reaction mixture was concentrated *in vacuo* to give a yellow oil. This material was passed through a short silica plug eluting with ethyl acetate. The filtrate was concentrated *in vacuo* to give a yellow solid. This solid was combined with 1 M potassium *t*-butoxide in tetrahydrofuran (67 mg, 0.60 mmol) in isopropanol (5 mL) and heated using microwave irradiation at 130 °C for 40 min. The reaction mixture was concentrated *in vacuo*. The residue was purified by column chromatography eluting with 10% methanol in ethyl acetate to afford **112** as a white solid (35 mg, 0.12 mmol, 40%). ^1H NMR (400 MHz, CD_3OD) δ 7.28 - 7.20 (m, 1H, ArH), 7.17 - 7.13 (m, 1H, ArH), 6.99 - 6.88 (m, 2H, ArH), 4.00 (s, 2H, CH_2), 3.85 (s, 3H, OCH_3), 3.65 - 3.62 (m, 1H, CH), 1.37 (d, $J = 7.0$ Hz, 6H, CH_3 , CH_3). ^{13}C NMR (101 MHz, DMSO) δ 156.9 (C=O), 130.9 (C), 130.5 (C), 129.4 (CH), 127.9 (CH), 120.2 (CH), 110.6 (CH), 45.4 (CH_2), 25.7 (CH), 21.7 (CH_3). Note: not all ^{13}C signals visible in spectrum. ESI-HRMS: m/z calculated for $\text{C}_{16}\text{H}_{18}\text{N}_4\text{O}_2$ $[\text{M}+\text{H}]^+$ 299.1503, found 299.1499. RP-HPLC: t_R 8.18 min.

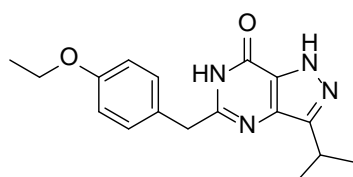
3-Isopropyl-5-(4-methoxybenzyl)-1H-pyrazolo[4,3-d]pyrimidin-7(6H)-one (113)

4-Amino-3-isopropyl-1H-pyrazole-5-carboxamide (85)

(50 mg, 0.30 mmol), 2-(4-methoxyphenyl)acetic acid

(50 mg, 0.30 mmol), bromo-tris-pyrrolidinophosphonium-

hexafluorophosphate (152 mg, 0.33 mmol) and triethylamine (60 mg, 0.59 mmol) were combined in 1,2-dichloroethane (5 mL) and heated using microwave irradiation at 120 °C for 20 min. The reaction mixture was concentrated *in vacuo* to give a yellow oil. This material was passed through a short silica plug eluting with ethyl acetate. The filtrate was concentrated *in vacuo* to give a yellow solid. This solid was combined with 1 M potassium *t*-butoxide in tetrahydrofuran (67 mg, 0.60 mmol) in isopropanol (5 mL) and heated using microwave irradiation at 130 °C for 40 min. The reaction mixture was concentrated *in vacuo*. The residue was purified by column chromatography eluting with 10% methanol in ethyl acetate to afford **113** as a white solid (42 mg, 0.14 mmol, 47%). ¹H NMR (400 MHz, CD₃OD) δ 7.26 - 7.20 (m, 2H, ArH), 6.85 - 6.82 (m, 2H, ArH), 3.91 (s, 2H, CH₂), 3.72 (s, 3H, OCH₃), 3.46 - 3.39 (m, 1H, CH), 1.40 (d, *J* = 7.5 Hz, 6H, CH₃, CH₃). ¹³C NMR (101 MHz, CD₃OD) δ 160.2 (C=O), 131.0 (C), 130.7 (C), 129.6 (CH), 115.1 (CH), 55.7 (CH₃), 41.0 (CH₂), 25.2 (CH), 22.3 (CH₃). Note: not all ¹³C signals visible in spectrum. ESI-HRMS: *m/z* calculated for C₁₆H₁₈N₄O₂ [M+H]⁺ 299.1503, found 299.1490. RP-HPLC: *t_R* 8.08 min.

3-Isopropyl-5-(4-methoxybenzyl)-1H-pyrazolo[4,3-d]pyrimidin-7(6H)-one (114)

4-Amino-3-isopropyl-1H-pyrazole-5-carboxamide (85)

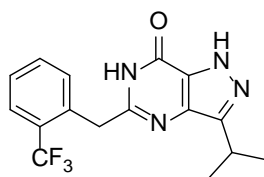
(50 mg, 0.30 mmol), 2-(2-(trifluoromethyl)phenyl)acetic

acid (54 mg, 0.30 mmol), bromo-trispyrrolidinophospho-

niumhexafluorophosphate (152 mg, 0.33 mmol) and triethylamine (60 mg, 0.59 mmol) were combined in 1,2-dichloroethane (5 mL) and heated using microwave irradiation at

120 °C for 20 min. The reaction mixture was concentrated *in vacuo* to give a yellow oil. This material was passed through a short silica plug eluting with ethyl acetate. The filtrate was concentrated *in vacuo* to give a yellow solid. This solid was combined with 1 M potassium *t*-butoxide in tetrahydrofuran (67 mg, 0.60 mmol) in isopropanol (5 mL) and heated using microwave irradiation at 130 °C for 40 min. The reaction mixture was concentrated *in vacuo*. The residue was purified by column chromatography eluting with 10% methanol in ethyl acetate to afford **114** as a white solid (58 mg, 0.19 mmol, 63%). ¹H NMR (400 MHz, CD₃OD) δ 7.23 (d, *J* = 8.8 Hz, 2H, ArH), 6.84 (d, *J* = 8.8 Hz, 2H, ArH), 3.98 (q, *J* = 7.0 Hz, 2H, OCH₂CH₃), 3.91 (s, 2H, CH₂), 3.45 - 3.38 (m, 1H, CH), 1.41 (d, *J* = 7.5 Hz, 6H, CH₃, CH₃), 1.35 (t, *J* = 7.0 Hz, 3H, CH₂CH₃). ¹³C NMR (101 MHz, CD₃OD) δ 159.5 (C=O), 155.0 (C), 130.7 (C), 129.6 (CH), 115.7 (CH), 64.5 (CH₂), 41.0 (CH₂), 27.3 (CH), 22.3 (CH₃), 15.1 (CH₃). Note: not all ¹³C signals visible in spectrum. ESI-HRMS: *m/z* calculated for C₁₇H₂₀N₄O₂ [M+H]⁺ 313.1659, found 313.1669. RP-HPLC: *t*_R 8.71 min.

3-Isopropyl-5-(2-(trifluoromethyl)benzyl)-1*H*-pyrazolo[4,3-*d*]pyrimidin-7(6*H*)-one (115)

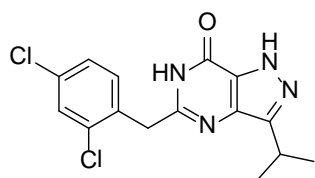


4-Amino-3-isopropyl-1*H*-pyrazole-5-carboxamide (**85**) (50 mg, 0.30 mmol), 2-(2-ethoxyphenyl)acetic acid (60 mg, 0.30 mmol), bromo-tris-pyrrolidinophosphonium-hexafluorophosphate

(152 mg, 0.33 mmol) and triethylamine (60 mg, 0.59 mmol) were combined in 1,2-dichloroethane (5 mL) and heated using microwave irradiation at 120 °C for 20 min. The reaction mixture was concentrated *in vacuo* to give a yellow oil. This material was passed through a short silica plug eluting with ethyl acetate. The filtrate was concentrated *in vacuo* to give a yellow solid. This solid was combined with 1 M potassium *t*-butoxide in tetrahydrofuran (67 mg, 0.60 mmol) in isopropanol (5 mL)

and heated using microwave irradiation at 130 °C for 40 min. The reaction mixture was concentrated *in vacuo*. The residue was purified by column chromatography eluting with 10% methanol in ethyl acetate to afford **115** as a white solid (62 mg, 0.18 mmol, 60%). ¹H NMR (400 MHz, DMSO) δ 7.73 (d, *J* = 7.7 Hz, 1H, ArH), 7.62 (t, *J* = 7.7 Hz, 1H, ArH), 7.48 (t, *J* = 7.7 Hz, 1H, ArH), 7.40 (d, *J* = 7.7 Hz, 1H, ArH), 4.12 (s, 2H, CH₂), 3.10 - 3.03 (m, 1H, CH), 1.20 (d, *J* = 7.0 Hz, 6H, CH₃, CH₃). ¹³C NMR (101 MHz, DMSO) δ 157.1 (C=O), 136.8 (C), 130.4 (CH), 129.6 (CH), 127.4 (C), 123.2 (CH), 122.1 (CH), 40.2 (CH₂), 27.2 (CH), 21.4 (CH₃). Note: not all ¹³C signals visible in spectrum. ESI-HRMS: *m/z* calculated for C₁₆H₁₅F₃N₄O [M+H]⁺ 337.1271, found 313.1273. RP-HPLC: *t*_R 9.33 min.

5-(2,4-Dichlorobenzyl)-3-isopropyl-1*H*-pyrazolo[4,3-*d*]pyrimidin-7(6*H*)-one (**116**)

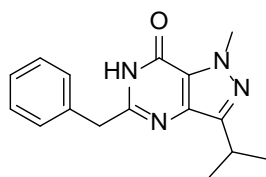


4-Amino-3-isopropyl-1*H*-pyrazole-5-carboxamide (**85**)
(50 mg, 0.30 mmol), 2-(2,4-dichlorophenyl)acetic acid
(61 mg, 0.30 mmol), bromo-trispyrrolidinophosphonium-
hexafluorophosphate (152 mg, 0.33 mmol) and triethylamine (60 mg, 0.59 mmol) were

combined in 1,2-dichloroethane (5 mL) and heated using microwave irradiation at 120 °C for 20 min. The reaction mixture was concentrated *in vacuo* to give a yellow oil. This material was passed through a short silica plug eluting with ethyl acetate. The filtrate was concentrated *in vacuo* to give a yellow solid. This solid was combined with 1 M potassium *t*-butoxide in tetrahydrofuran (67 mg, 0.60 mmol) in isopropanol (5 mL) and heated using microwave irradiation at 130 °C for 40 min. The reaction mixture was concentrated *in vacuo*. The residue was purified by column chromatography eluting with 10% methanol in ethyl acetate to afford **116** as a white solid (69 mg, 0.20 mmol, 67%). ¹H NMR (400 MHz, DMSO) δ 7.62 - 7.60 (m, 1H, ArH), 7.42 - 7.34 (m, 2H, ArH), 4.06 (s, 2H, CH₂), 3.17 - 3.10 (m, 1H, CH), 1.23 (d, *J* = 7.5 Hz, 6H, CH₃, CH₃).

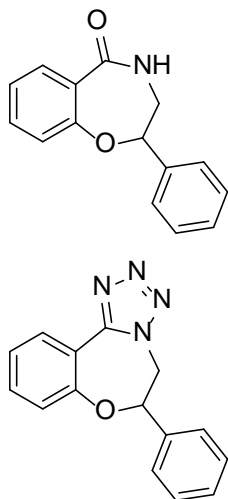
^{13}C NMR (101 MHz, DMSO) δ 134.0 (CH), 132.0 (CH), 128.0 (CH), 126.7 (C), 21.1 (CH₃). Note: not all ^{13}C signals visible in spectrum. ESI-HRMS: m/z calculated for C₁₅H₁₄Cl₂N₄O [M+H⁺]⁺ 337.0617, found 337.0609. RP-HPLC: t_R 9.68 min.

Synthesis of 5-benzyl-3-isopropyl-1-methyl-1*H*-pyrazolo[4,3-*d*]pyrimidin-7(6*H*)-one (117)



To a stirring solution of 5-Benzyl-3-isopropyl-1*H*-pyrazolo[4,3-*d*]pyrimidin-7(6*H*)-one (**99**) (30 mg, 0.11 mmol) in acetone (15 mL) was added dimethylsulfate (17 mg, 0.13 mmol) in acetone (10 mL) in a drop-wise manner. The reaction mixture was stirred at 60 °C for 16 h. The reaction mixture was concentrated *in vacuo* and the crude material was purified by column chromatography eluting with 50% ethyl acetate in hexane to afford **117** as a white solid (20 mg, 0.07 mmol, 63%). ^1H NMR (400 MHz, DMSO) δ 7.35 - 7.28 (m, 4H, ArH), 7.25 - 7.20 (m, 1H, ArH), 4.08 (s, 3H, NCH₃), 3.90 (s, 2H, CH₂), 3.26 - 3.17 (m, 1H, CH), 1.31 (d, J = 7.0 Hz, 6H, CH₃, CH₃). ^{13}C NMR (101 MHz, CD₃OD) δ 152.2 (C=O), 134.8 (C), 128.6 (CH), 126.9 (CH), 126.5 (CH), 40.4 (CH₂), 40.2 (CH₃), 26.3 (CH), 21.0 (CH₃). Note: not all ^{13}C signals visible in spectrum. ESI-HRMS: m/z calculated for C₁₆H₁₈N₄O [M+H⁺]⁺ 283.1553, found 283.1549. RP-HPLC: t_R 8.01 min.

7.2.2 Chapter 4 experimental

2-Phenyl-3,4-dihydrobenzo[f][1,4]oxazepin-5(2H)-one (121) and 6-phenyl-5,6-dihydrobenzo[f]tetrazolo[1,5-d][1,4]oxazepine (127)Method I:

Sodium azide (174 mg, 2.68 mmol) was added in portions to a stirring solution of 2-phenylchroman-4-one (300 mg, 1.34 mmol) in toluene (20 mL) at 0 °C. Concentrated sulfuric acid (2.0 mL) was added in a drop-wise manner over 30 min at 0 °C. The reaction mixture was allowed to warm to room temperature and stirring was continued for 16 h. The reaction mixture had water (20 mL) added and was extracted with toluene (3 × 15 mL). The combined organic extracts were dried (anhydrous sodium sulfate), filtered and concentrated *in vacuo* to afford a mixture of **121** and **127** (6:1) as a yellow oil. Purification by column chromatography eluting with 50% ethyl acetate in hexane afforded **121** as cream needles (after recrystallisation from ethanol) (206 mg, 0.86 mmol, 64%) and **127** as white needles (after recrystallisation from ethanol) (31 mg, 0.11 mmol, 8%).

Method II:

To a stirred solution of 2-phenylchroman-4-one (flavanone) (300 mg, 1.34 mmol) in 1,2-dichloroethane (20 mL) was added trimethylsilylazide (231 mg, 2.01 mmol) and iron (III) chloride (217 mg, 1.34 mmol). The mixture was stirred at room temperature for 16 h, and then concentrated *in vacuo*. The residue was diluted with water (40 mL) and extracted with ethyl acetate (3 × 20 mL). The combined organic extracts were dried (anhydrous sodium sulfate), filtered and concentrated *in vacuo* to yield a mixture of **121** and **127** (8:1) as a clear oil. Purification by column chromatography eluting with 30%

ethyl acetate in hexane afforded **121** as a cream solid (264 mg, 1.10 mmol, 82%) and **127** as a cream solid (43 mg, 0.02 mmol, 12%).

Method III:

(*E*)-2-Phenylchroman-4-one oxime (**135**) (100 mg, 0.42 mmol) was stirred in polyphosphoric acid (30 mL) at 120 °C for 2 h. The reaction mixture was poured into water (100 mL) and stirred at 75 °C for 2 h. The reaction mixture was cooled and extracted with ethyl acetate (3 × 20 mL). The combined organic extracts were washed with 5% aqueous sodium hydrogen carbonate (15 mL) and water (15 mL). The organic layer was dried (anhydrous sodium sulfate), filtered and concentrated *in vacuo* to afford **121** as a yellow oil (63 mg, 0.26 mmol, 79%).

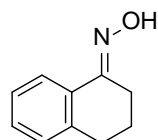
Method IV:

(*E*)-2-Phenylchroman-4-one oxime (**135**) (100 mg, 0.42 mmol), *p*-toluenesulfonic acid (22 mg, 0.13 mmol) and zinc (II) bromide (19 mg, 0.08 mmol) in acetonitrile (20 mL) were heated at 82 °C for 16 h. The reaction mixture was cooled and poured into saturated aqueous sodium hydrogen carbonate (40 mL) and extracted with ethyl acetate (3 × 20 mL). The combined organic extracts were dried (anhydrous sodium sulfate), filtered and concentrated *in vacuo* to afford **121** as a yellow oil (45 mg, 0.19 mmol, 45%).

121 - ^1H NMR (600 MHz, CDCl_3) δ 7.72 (dd, $J = 7.7, 1.3$ Hz, 1H, ArH), 7.38 - 7.30 (m, 2H, ArH), 7.29 - 7.18 (m, 4H, ArH), 7.07 (t, $J = 7.7$ Hz, 1H, ArH), 6.94 (d, $J = 8.1$ Hz, 1H, ArH), 5.33 (dd, $J = 6.2, 3.3$ Hz, 1H, CH), 3.57 - 3.47 (m, 1H, CHH), 3.42 (dt, $J = 15.4, 5.9$ Hz, 1H, CHH). ^{13}C NMR (101 MHz, CDCl_3) δ 171.2 (C=O), 154.7 (C), 139.2 (C), 133.5 (C), 131.1 (CH), 128.8 (CH), 126.4 (CH), 126.0 (CH), 124.1 (CH), 123.9 (CH), 122.6 (CH), 86.0 (CH_2), 46.5 (CH_3). ESI-HRMS: m/z calculated for $\text{C}_{15}\text{H}_{13}\text{NO}_2$ $[\text{M}+\text{H}]^+$ 240.1019, found 240.1027. RP-HPLC: t_R 9.35 min. M.p. 125 - 126 °C (lit.²⁸² M.p. 125 - 126 °C).

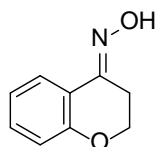
127 - ^1H NMR (600 MHz, CDCl_3) δ 8.59 (d, $J = 8.0$ Hz, 1H, ArH), 7.56 - 7.41 (m, 6H, ArH), 7.26 (dd, $J = 9.5, 5.8$ Hz, 1H, ArH), 7.18 (d, $J = 8.2$ Hz, 1H, ArH), 5.23 - 5.19 (m, 1H, CHH), 5.14 - 5.08 (m, 1H, CHH), 4.85 (dd, $J = 14.5, 9.5$ Hz, 1H, CH). ^{13}C NMR (101 MHz, CDCl_3) δ 157.0 (C), 152.1 (C), 136.5 (C), 133.4 (C), 130.6 (CH), 129.4 (CH), 129.3 (CH), 126.2 (CH), 124.2 (CH), 121.7 (CH), 113.2 (CH), 79.1 (CH), 56.4 (CH_2). ESI-HRMS: m/z calculated for $\text{C}_{15}\text{H}_{12}\text{N}_4\text{O}$ $[\text{M}+\text{H}]^+$ 265.1084, found 265.1079. RP-HPLC: t_R 10.85 min. M.p. 136 - 137 °C (lit.²⁸² M.p. 137 - 138 °C).

3,4-Dihydronaphthalen-1(2H)-one oxime (**131**)



Hydroxylamine hydrochloride (1.90 g, 27.4 mmol) was added in one portion to a stirring solution of 3,4-dihydronaphthalen-1(2H)-one (2.00 g, 13.7 mmol) and sodium acetate (2.24 g, 27.4 mmol) in ethanol (60 mL) at room temperature. The reaction mixture was then stirred at 78 °C for 2 h. The reaction mixture was cooled to 0 °C, water was added to give a precipitate, and the solid collected. Recrystallisation of the solid with ethanol afforded **131** as cream crystals (2.12 g, 13.2 mmol, 96%). ^1H NMR (400 MHz, CDCl_3) δ 7.89 (dd, $J = 7.8, 1.2$ Hz, 1H, ArH), 7.30 - 7.13 (m, 3H, ArH), 2.84 (t, $J = 6.5$ Hz, 2H, $\text{CH}_2\text{C}(\text{N})$), 2.77 (tt, $J = 6.5, 4.0$ Hz, 2H, Ar CH_2), 1.89 (t, $J = 4.0$ Hz, 2H, $\text{CH}_2\text{CH}_2\text{CH}_2$). ^{13}C NMR (101 MHz, CDCl_3) δ 155.6 (C=N), 139.9 (C), 130.7 (C), 129.3 (CH), 128.8 (CH), 126.6 (CH), 124.2 (CH), 30.0 (CH_2), 23.9 (CH_2), 21.5 (CH_2). ESI-MS: m/z 162.1 $[\text{M}+\text{H}]^+$. RP-HPLC: t_R 9.06 min. M.p. 101 - 102 °C (lit.³⁷⁶ M.p. 101 - 103 °C).

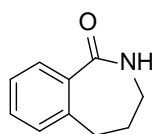
Chroman-4-one oxime (**132**)



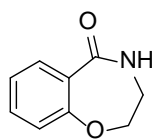
Hydroxylamine hydrochloride (469 mg, 6.75 mmol) was added in one portion to a stirring solution of chroman-4-one (500 mg, 3.37 mmol) and

sodium acetate (554 mg, 6.75 mmol) in ethanol (30 mL) at room temperature. The reaction mixture was then stirred at 78 °C for 2 h. The reaction mixture was cooled to 0 °C, water was added to give a precipitate, and the solid collected. Recrystallisation of the solid from ethanol afforded **132** as white crystals (502 mg, 3.08 mmol, 91%). ¹H NMR (400 MHz, CDCl₃) δ 7.82 (dd, *J* = 7.9, 1.5 Hz, 1H, ArH), 7.31 - 7.24 (m, 1H, ArH), 6.99 - 6.89 (m, 2H, ArH), 4.26 (t, *J* = 6.2 Hz, 2H, OCH₂), 3.02 (t, *J* = 6.2 Hz, 2H, CH₂C(N)). ¹³C NMR (101 MHz, CDCl₃) δ 159.0 (C=N), 149.2 (C), 131.2 (CH), 124.6 (CH), 121.7 (C), 120.4 (CH), 119.1 (CH), 65.6 (CH₂), 24.1 (CH₂). ESI-MS: *m/z* 164.2 [M+H]⁺. RP-HPLC: *t*_R 8.04 min. M.p. 139 - 140 °C (lit.³⁷⁷ M.p. 139 - 141 °C).

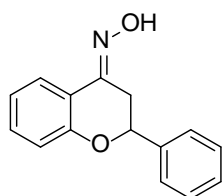
2,3,4,5-Tetrahydro-1*H*-benzo[*c*]azepin-1-one (133)



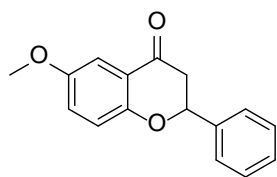
3,4-Dihydronaphthalen-1(2*H*)-one oxime (**131**) (50 mg, 0.31 mmol), *p*-toluenesulfonic acid (5 mg, 0.03 mmol) and zinc (II) bromide (8 mg, 0.04 mmol) in acetonitrile (15 mL) were heated at 82 °C for 16 h. The reaction mixture was cooled and poured into saturated aqueous sodium hydrogen carbonate (20 mL) and extracted with ethyl acetate (3 × 15 mL). The combined organic extracts were dried (anhydrous sodium sulfate), filtered and concentrated *in vacuo* to afford **133** as a yellow oil (45 mg, 0.26 mmol, 89%). ¹H NMR (400 MHz, CDCl₃) δ 7.92 - 7.87 (m, 1H, ArH), 7.31 - 7.18 (m, 2H, ArH), 7.16 (d, *J* = 7.5 Hz, 1H, ArH), 2.85 (t, *J* = 6.6 Hz, 2H, NHCH₂), 2.77 (t, *J* = 4.0 Hz, 2H, ArCH₂), 1.89 (tt, *J* = 6.6, 4.0 Hz, 2H, NHCH₂CH₂). ¹³C NMR (101 MHz, CDCl₃) δ 155.5 (C=O), 140.0 (C), 130.6 (C), 129.3 (CH), 128.8 (CH), 126.6 (CH), 124.2 (CH), 29.9 (CH₂), 24.0 (CH₂), 21.4 (CH₂). ESI-MS: *m/z* 162.2 [M+H]⁺. RP-HPLC: *t*_R 10.29 min. M.p. 97 - 98 °C (lit.³⁷⁸ M.p. 101 °C).

3,4-Dihydrobenzo[f][1,4]oxazepin-5(2H)-one (134)

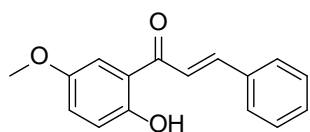
Chroman-4-one oxime (**132**) (50 mg, 0.31 mmol), *p*-toluenesulfonic acid (5 mg, 0.03 mmol) and zinc (II) bromide (8 mg, 0.04 mmol) in acetonitrile (15 mL) were heated at 82 °C for 16 h. The reaction mixture was cooled and poured into saturated aqueous sodium hydrogen carbonate (20 mL) and extracted with ethyl acetate (3 × 15 mL). The combined organic extracts were dried (anhydrous sodium sulfate), filtered and concentrated *in vacuo* to afford **134** as a yellow oil (40 mg, 0.24 mmol, 79%). ¹H NMR (400 MHz, CDCl₃) δ 7.76 (dd, *J* = 7.9, 1.8 Hz, 1H, ArH), 7.33 (ddd, *J* = 8.4, 7.2, 1.8 Hz, 1H, ArH), 6.90 - 6.82 (m, 2H, ArH), 4.40 (t, *J* = 8.0 Hz, 2H, OCH₂), 2.68 (t, *J* = 8.0 Hz, 2H, NHCH₂). ¹³C NMR (101 MHz, CDCl₃) δ 170.6 (C=O), 155.2 (C), 132.1 (CH), 130.9 (CH), 122.2 (C), 121.8 (CH), 120.9 (CH), 74.0 (CH₂), 40.2 (CH₂). ESI-MS: *m/z* 164.2 [M+H]⁺. RP-HPLC: *t_R* 10.42 min. M.p. 117 - 118 °C (lit.³⁷⁹ M.p. 114 - 116 °C).

2-Phenylchroman-4-one oxime (135)

Hydroxylamine hydrochloride (124 mg, 1.78 mmol) was added in one portion to a stirring solution of 2-phenylchroman-4-one (200 mg, 0.89 mmol) and sodium acetate (146 mg, 1.78 mmol) in ethanol (20 mL) at room temperature. The reaction mixture was then stirred at 78 °C for 2 h. The reaction mixture was cooled to 0 °C, water was added to give a precipitate, and the solid filtered to afford **135** as a white powder (196 mg, 0.82 mmol, 92%). ¹H NMR (400 MHz, CDCl₃) δ 7.88 (dd, *J* = 7.9, 1.7 Hz, 1H, ArH), 7.56 - 7.49 (m, 2H, ArH), 7.48 - 7.38 (m, 3H, ArH), 7.33 (ddd, *J* = 8.7, 7.2, 1.7 Hz, 1H, ArH), 7.08 - 6.97 (m, 2H, ArH), 5.14 (dd, *J* = 12.5, 3.0 Hz, 1H, CH), 3.62 (dd, *J* = 17.2, 3.1 Hz, 1H, CHH), 2.80 (dd, *J* = 17.2, 12.5 Hz, 1H, CHH). ESI-MS: *m/z* 240.3 [M+H]⁺. RP-HPLC: *t_R* 10.64 min.

6-Methoxy-2-phenylchroman-4-one (138)

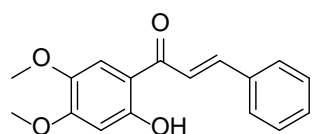
A solution of (*E*)-1-(2-hydroxy-5-methoxyphenyl)-3-phenylprop-2-en-1-one (**139**) (230 mg, 0.92 mmol) and sodium acetate (750 mg, 9.20 mmol) in ethanol (20 mL) was stirred at 78 °C for 16 h. The mixture was concentrated *in vacuo*. The residue was dissolved in water (30 mL) and extracted with dichloromethane (3 × 10 mL). The combined organic layers were dried (anhydrous sodium sulfate), filtered and concentrated *in vacuo*. Recrystallisation from ethanol afforded **138** as yellow needles (210 mg, 0.81 mmol, 90%). ¹H NMR (400 MHz, CDCl₃) δ 7.54 - 7.37 (m, 6H, ArH), 7.14 (dt, *J* = 7.4, 3.7 Hz, 1H, ArH), 7.05 - 6.99 (m, 1H, ArH), 5.47 (dd, *J* = 13.4, 2.9 Hz, 1H, CH), 3.82 (s, 3H, CH₃), 3.10 (dd, *J* = 17.0, 13.4 Hz, 1H, CHH), 2.91 (dd, *J* = 17.0, 2.9 Hz, 1H, CHH). ¹³C NMR (101 MHz, CDCl₃) δ 192.1 (C=O), 156.3 (C), 154.3 (C), 138.9 (C), 128.9 (CH), 126.2 (CH), 125.4 (CH), 120.8 (C), 119.5 (CH), 118.4 (CH), 107.4 (CH), 79.7 (CH), 55.8 (CH₃), 44.6 (CH₂). ESI-MS: *m/z* 255.2 [M+H]⁺. RP-HPLC: *t*_R 11.36 min. M.p. 97 - 98 °C (lit.³⁸⁰ M.p. 97 - 98 °C).

(*E*)-1-(2-Hydroxy-5-methoxyphenyl)-3-phenylprop-2-en-1-one (139)

A solution of benzaldehyde (100 mg, 0.94 mmol), 1-(2-hydroxy-5-methoxyphenyl)ethanone (160 mg, 0.94 mmol) and barium hydroxide (300 mg, 0.94 mmol) in ethanol (15 mL) was stirred at 40 °C for 16 h. The reaction mixture was cooled to room temperature, neutralised (pH ~ 7.0) with 1 M aqueous hydrochloric acid, and concentrated *in vacuo*. The residue was dissolved in water (30 mL), and extracted with ethyl acetate (3 × 10 mL). The combined organic layers were dried (anhydrous sodium sulfate), filtered and concentrated *in vacuo* to afford **139** as an orange solid (230 mg, 0.92 mmol, 97%). ¹H NMR (400 MHz, CDCl₃) δ 7.90 (d, *J* = 16.0 Hz, 1H, C(O)CH), 7.65 (s, 1H, ArH), 7.58 (d, *J* = 16.0 Hz, 1H,

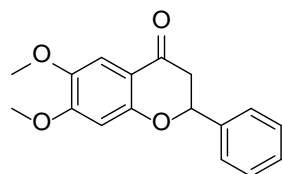
ArCH), 7.46 - 7.40 (m, 3H, ArH), 7.35 (s, 1H, ArH), 7.15 - 7.12 (m, 2H, ArH), 6.98 - 6.96 (m, 1H, ArH), 3.83 (s, 3H, CH₃). ¹³C NMR (101 MHz, CDCl₃) δ 190.8 (C=O), 161.4 (C), 144.4 (C), 143.1 (CH), 133.9 (C), 129.2 (CH), 129.1 (CH), 128.5 (CH), 122.2 (CH), 121.9 (CH), 112.8 (C), 110.4 (CH), 102.3 (CH), 61.8 (CH₃). ESI-MS: *m/z* 255.2 [M+H]⁺. RP-HPLC: *t*_R 11.92 min.

(*E*)-1-(2-Hydroxy-4,5-dimethoxyphenyl)-3-phenylprop-2-en-1-one (140a)



A solution of benzaldehyde (100 mg, 0.94 mmol), 1-(2-hydroxy-4,5-dimethoxyphenyl)ethanone (180 mg, 0.94 mmol) and barium hydroxide (300 mg, 0.94 mmol) in ethanol (15 mL) was stirred at 40 °C for 16 h. The reaction mixture was cooled to room temperature, neutralised (pH ~ 7.0) with 1 M aqueous hydrochloric acid, and concentrated *in vacuo*. The residue was dissolved in water (30 mL), and extracted with ethyl acetate (3 × 10 mL). The combined organic layers were dried (anhydrous sodium sulfate), filtered and concentrated *in vacuo* to afford **140a** as a yellow solid (250 mg, 0.89 mmol, 94%). ¹H NMR (400 MHz, CDCl₃) δ 7.90 - 7.84 (m, 1H, C(O)CH), 7.69 - 7.60 (m, 2H, ArCH), 7.52 - 7.47 (m, 3H, ArH, C(O)CHCH), 7.45 - 7.37 (m, 1H, ArH), 7.25 - 7.23 (m, 1H, ArH), 6.49 - 6.46 (m, 1H, ArH), 3.90 (s, 3H, CH₃), 3.89 (s, 3H, CH₃). ¹³C NMR (101 MHz, CDCl₃) δ 191.4 (C=O), 161.8 (C), 156.8 (C), 144.4 (C), 141.9 (CH), 134.8 (C), 130.6 (CH), 129.0 (CH), 128.5 (CH), 120.3 (CH), 112.0 (C), 111.0 (CH), 100.8 (CH), 60.32 (CH₃), 60.31 (CH₃). ESI-MS: *m/z* 285.2 [M+H]⁺. RP-HPLC: *t*_R 11.51 min.

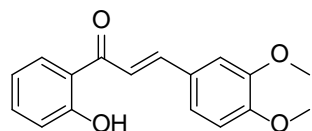
6,7-Dimethoxy-2-phenylchroman-4-one (140)



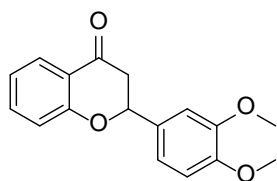
A solution of (*E*)-1-(2-hydroxy-4,5-dimethoxyphenyl)-3-phenylprop-2-en-1-one (**140a**) (200 mg, 0.70 mmol) and sodium

acetate (690 mg, 7.00 mmol) in ethanol (20 mL) was stirred at 78 °C for 16 h. The mixture was concentrated *in vacuo*. The residue was dissolved in water (30 mL) and extracted with dichloromethane (3 × 10 mL). The combined organic layers were dried (anhydrous sodium sulfate), filtered and concentrated *in vacuo*. Recrystallisation from ethanol afforded **140** as cream needles (190 mg, 0.68 mmol, 96%). ¹H NMR (400 MHz, CDCl₃) δ 7.39 - 7.22 (m, 5H, ArH), 7.17 (s, 1H, ArH), 6.42 (s, 1H, ArH), 5.35 - 5.32 (m, 1H, CH), 3.81 (s, 3H, CH₃), 3.78 (s, 3H, CH₃), 2.98 - 2.94 (m, 1H, CHH), 2.74 - 2.70 (m, 1H, CHH). ¹³C NMR (101 MHz, CDCl₃) δ 190.6 (C=O), 158.0 (C), 156.3 (C), 144.7 (C), 138.9 (C), 129.0 (CH), 128.8 (CH), 126.2 (CH), 113.2 (C), 106.7 (CH), 100.6 (CH), 80.3 (CH), 56.2 (CH₃), 56.0 (CH₃), 44.1 (CH₂). ESI-MS: *m/z* 285.2 [M+H]⁺. RP-HPLC: *t*_R 10.47 min. M.p. 170 - 171 °C (lit.³⁸¹ M.p. 170 - 171 °C).

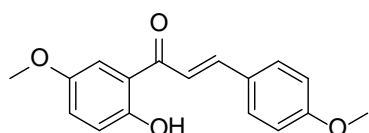
(E)-3-(3,4-Dimethoxyphenyl)-1-(2-hydroxyphenyl)prop-2-en-1-one (141a)



A solution of 3,4-dimethoxybenzaldehyde (300 mg, 1.81 mmol), 1-(2-hydroxyphenyl)ethanone (246 mg, 1.81 mmol) and barium hydroxide (569 mg, 1.81 mmol) in ethanol (15 mL) was stirred at 40 °C for 16 h. The reaction mixture was cooled to room temperature, neutralised (pH ~ 7.0) with 1 M aqueous hydrochloric acid, and concentrated *in vacuo*. The residue was dissolved in water (30 mL), and extracted with ethyl acetate (3 × 10 mL). The combined organic layers were dried (anhydrous sodium sulfate), filtered and concentrated *in vacuo* to afford **141a** as a yellow solid (500 mg, 1.76 mmol, 97%). ¹H NMR (400 MHz, CDCl₃) δ 7.95 - 7.84 (m, 2H, C(O)CH, ArCH), 7.54 - 7.39 (m, 3H, ArH), 7.25 (dd, *J* = 7.9, 2.2 Hz, 1H, ArH), 7.16 (d, *J* = 7.9 Hz, 1H, ArH), 7.04 - 6.86 (m, 2H, ArH), 3.95 (s, 3H, CH₃), 3.93 (s, 3H, CH₃). ESI-MS: *m/z* 285.2 [M+H]⁺. RP-HPLC: *t*_R 11.34 min.

2-(3,4-Dimethoxyphenyl)chroman-4-one (141)

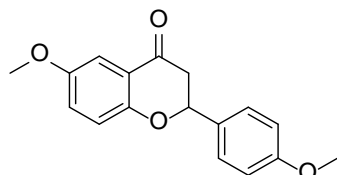
A solution of (*E*)-3-(3,4-dimethoxyphenyl)-1-(2-hydroxyphenyl)prop-2-en-1-one (**141a**) (300 mg, 1.06 mmol) and sodium acetate (866 mg, 10.6 mmol) in ethanol (20 mL) was stirred at 78 °C for 16 h. The reaction mixture was concentrated *in vacuo*. The residue was dissolved in water (30 mL) and extracted with dichloromethane (3 × 10 mL). The combined organic layers were dried (anhydrous sodium sulfate), filtered and concentrated *in vacuo*. Recrystallisation from ethanol afforded **141** as cream needles (274 mg, 0.96 mmol, 91%). ¹H NMR (400 MHz, CDCl₃) δ 7.41 - 7.35 (m, 2H, ArH), 7.26 - 7.18 (m, 1H, ArH), 7.11 - 7.01 (m, 4H, ArH), 5.36 (dd, *J* = 13.3, 2.6 Hz, 1H, CH), 3.96 (s, 3H, CH₃), 3.94 (s, 3H, CH₃), 3.11 (dd, *J* = 16.9, 13.3 Hz, 1H, CHH), 2.94 (dd, *J* = 16.9, 2.6 Hz, 1H, CHH). ESI-MS: *m/z* 285.3 [M+H]⁺. RP-HPLC: *t*_R 10.20 min. M.p. 121 - 122 °C (lit.³⁸² M.p. 124 - 125 °C).

(*E*)-1-(2-Hydroxy-5-methoxyphenyl)-3-(4-methoxyphenyl)prop-2-en-1-one (142a)

A solution of 4-methoxybenzaldehyde (100 mg, 0.73 mmol), 1-(2-hydroxy-5-methoxyphenyl)ethanone (120 mg, 0.73 mmol) and barium hydroxide (230 mg, 0.73 mmol) in ethanol (15 mL) was stirred at 40 °C for 16 h. The reaction mixture was cooled to room temperature, neutralised (pH ~ 7.0) with 1 M aqueous hydrochloric acid, and concentrated *in vacuo*. The residue was dissolved in water (30 mL), and extracted with ethyl acetate (3 × 10 mL). The combined organic layers were dried (anhydrous sodium sulfate), filtered and concentrated *in vacuo* to afford **142a** as an orange oil (190 mg, 0.68 mmol, 92%). ¹H NMR (400 MHz, CDCl₃) δ 7.90 (d, *J* = 15.5 Hz, 1H, C(O)CH), 7.59 (d, *J* = 15.5 Hz, 1H, ArCH), 7.40 - 7.34 (m, 3H, ArH), 7.19 - 7.12 (m, 2H, ArH), 7.07 - 7.00

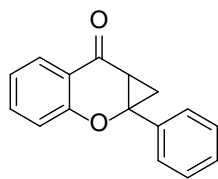
(m, 1H, ArH), 5.46 - 5.41 (m, 1H, ArH), 3.89 (s, 3H, CH₃), 3.86 (s, 3H, CH₃). ESI-MS: m/z 285.2 [M+H]⁺. RP-HPLC: t_R 12.21 min.

6-Methoxy-2-(4-methoxyphenyl)chroman-4-one (142)



A solution of (*E*)-1-(2-hydroxy-5-methoxyphenyl)-3-(4-methoxyphenyl)prop-2-en-1-one (**142a**) (200 mg, 0.70 mmol) and sodium acetate (580 mg, 7.00 mmol) in ethanol (20 mL) was stirred at 78 °C for 16 h. The mixture was concentrated *in vacuo*. The residue was dissolved in water (30 mL) and extracted with dichloromethane (3 × 10 mL). The combined organic layers were dried (anhydrous sodium sulfate), filtered and concentrated *in vacuo*. Recrystallisation from ethanol afforded **142** as orange needles (190 mg, 0.68 mmol, 96%). ¹H NMR (400 MHz, CDCl₃) δ 7.51 - 6.62 (m, 7H, ArH), 5.42 - 5.40 (m, 1H, CH), 3.83 (s, 3H, CH₃), 3.80 (s, 3H, CH₃), 3.05 (d, J = 16.0 Hz, 1H, CHH), 2.87 (d, J = 16.0 Hz, 1H, CHH). ESI-MS: m/z 285.2 [M+H]⁺. RP-HPLC: t_R 11.86 min. M.p. 156 - 157 °C (lit.³⁸⁰ M.p. 158 - 159 °C).

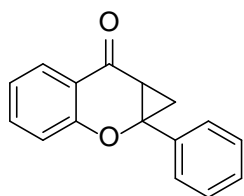
1a-Phenyl-1,7a-dihydrocyclopropa[b]chromen-7(1aH)-one (151)



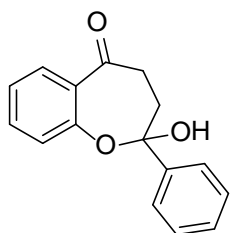
In a dry, three-neck round bottom flask equipped with a magnetic stirrer bar, thermometer and dropping funnel under a constant supply of N₂ gas was added anhydrous dimethylsulfoxide (10 mL). Sodium hydride (95%, 59 mg, 2.47 mmol) was added in portions, and following the exothermic reaction trimethylsulfoxonium iodide (545 mg, 2.47 mmol) was added in portions. The reaction mixture was stirred at room temperature under N₂ gas for 40 min. A solution of 2-phenyl-4*H*-chromen-4-one (500 mg, 2.25 mmol) in anhydrous dimethylsulfoxide (10 mL) was added in a drop-wise manner over 3 min. The solution was stirred vigorously for 30 min. at room temperature, before stirring at 50 °C for 16 h. The

reaction mixture was cooled to room temperature and poured onto ice. The aqueous layer was extracted with diethyl ether (2×20 mL) and ethyl acetate (2×20 mL). The combined organic extracts were dried (anhydrous sodium sulfate), filtered and concentrated *in vacuo* to afford **151** as a yellow oil (433 mg, 1.83 mmol, 81%). ^1H NMR (400 MHz, CDCl_3) δ 7.94 (dd, $J = 7.8, 1.7$ Hz, 1H, ArH), 7.56 - 7.34 (m, 6H, ArH), 7.08 (dd, $J = 14.7, 7.8$ Hz, 2H, ArH), 2.54 (dd, $J = 10.9, 6.2$ Hz, 1H, C(O)CH), 2.06 (dd, $J = 10.9, 7.1$ Hz, 1H, CHH), 1.74 (t, $J = 6.6$ Hz, 1H, CHH). ^{13}C NMR (101 MHz, CDCl_3) δ 189.8 (C=O), 157.1 (C), 138.0 (C), 135.7 (C), 128.8 (CH), 128.5 (CH), 127.1 (CH), 126.1 (CH), 122.0 (CH), 118.1 (CH), 118.0 (CH), 67.3 (C), 34.4 (CH), 15.0 (CH_2). ESI-MS: m/z 237.2 $[\text{M}+\text{H}]^+$. RP-HPLC: t_R 10.77 min.

1a-phenyl-1,7a-dihydrocyclopropa[b]chromen-7(1aH)-one (151) and 2-Hydroxy-2-phenyl-3,4-dihydrobenzo[b]oxepin-5(2H)-one (161) and



In a dry, three-neck round bottom flask equipped with a magnetic stirrer bar, thermometer and dropping funnel under a constant supply of N_2 gas was added anhydrous dimethylsulfoxide (20 mL).



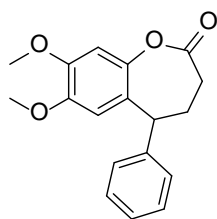
Sodium hydride (95%, 136 mg, 5.68 mmol) was added in portions, and following the exothermic reaction trimethylsulfoxonium iodide (1.25 g, 5.68 mmol) was added in portions. The reaction mixture

was stirred at room temperature under N_2 gas for 40 min. A solution of 2-phenyl-4H-chromen-4-one (1.15 g, 5.18 mmol) in anhydrous dimethylsulfoxide (20 mL) was added in a drop-wise manner over 3 min. The solution was stirred vigorously for 30 min. at room temperature, before stirring at 50°C for 16 h. The reaction mixture was poured onto ice and the aqueous layer was extracted with diethyl ether (2×30 mL) and ethyl acetate (2×30 mL). The combined organic extracts were dried (anhydrous sodium sulfate), filtered and concentrated *in vacuo* to afford a mixture of **151** and **161** (1:6) as a

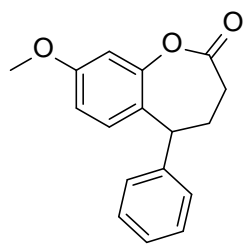
brown oil. Recrystallisation from ethanol afforded **161** as cream crystals (900 mg, 3.54 mmol, 68%) and **151** as a yellow oil (145 mg, 0.62 mmol, 12%).

161 - ^1H NMR (400 MHz, DMSO) δ 8.08 - 8.01 (m, 3H, ArH), 7.70 - 7.63 (m, 1H, ArH), 7.59 - 7.51 (m, 3H, ArH), 7.00 (dd, $J = 11.3, 4.5$ Hz, 2H, ArH), 3.52 - 3.39 (m, 4H, C(O)CH₂, C(O)CH₂CH₂). ^{13}C NMR (150 MHz, DMSO) δ 198.5 (C=O), 160.5 (C), 136.4 (C), 136.1 (CH), 136.0 (CH), 133.3 (CH), 130.6 (CH), 128.8 (CH), 127.9 (C), 120.3 (CH), 119.3 (CH), 117.7 (C), 33.2 (CH₂), 32.1 (CH₂). ESI-MS: m/z 255.4 [M+H]⁺. RP-HPLC: t_R 11.26 min.

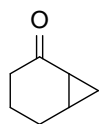
7,8-Dimethoxy-5-phenyl-4,5-dihydrobenzo[b]oxepin-2(3H)-one (**153**)



5-Phenyldihydrofuran-2-(3H)-one (3.00 g, 18.5 mmol) and 3,4-dimethoxyphenol (3.14 g, 20.4 mmol) were stirred in polyphosphoric acid (75%, 10 g) at room temperature for 7 h. The reaction mixture was poured onto ice and extracted with diethyl ether (4 × 30 mL). The combined organic layers were washed with 2 M aqueous sodium hydroxide (30 mL) and water (30 mL). The organic layer was dried (anhydrous sodium sulfate), filtered and concentrated *in vacuo* to yield a clear oil. Purification by column chromatography eluting with 2% methanol in dichloromethane afforded **153** as a white solid (4.53 g, 15.2 mmol, 82%). ^1H NMR (400 MHz, CDCl₃) δ 7.32 - 7.23 (m, 4H, ArH), 7.20 (dt, $J = 9.1, 4.3$ Hz, 1H, ArH), 6.58 (s, 1H, ArH), 6.40 (s, 1H, ArH), 4.23 (dd, $J = 10.0, 4.9$ Hz, 1H, CH), 3.72 (s, 3H, CH₃), 3.72 (s, 3H, CH₃), 2.37 - 2.28 (m, 4H, C(O)CH₂, CHCH₂). ^{13}C NMR (150 MHz, CDCl₃) δ 179.7 (C=O), 148.5 (C), 147.8 (C), 143.2 (C), 143.1 (C), 128.8 (CH), 128.2 (CH), 126.8 (C), 121.4 (CH), 112.3 (CH), 101.7 (CH), 56.9 (CH₃), 56.0 (CH₃), 42.8 (CH), 32.1 (CH₂), 29.5 (CH₂). ESI-HRMS: m/z calculated for C₁₈H₁₈O₄ [M+H]⁺ 299.1278, found 299.1275. RP-HPLC: t_R 8.53 min.

8-Methoxy-5-phenyl-4,5-dihydrobenzo[*b*]oxepin-2(3*H*)-one (154)

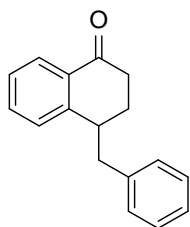
5-Phenyldihydrofuran-2-(3*H*)-one (200 mg, 1.23 mmol) and 4-methoxyphenol (153 mg, 1.23 mmol) were stirred in polyphosphoric acid (75%, 5 g) at room temperature for 7 h. The reaction mixture was poured onto ice and extracted with diethyl ether (4 × 20 mL). The combined organic layers were washed with 2 M aqueous sodium hydroxide (20 mL) and water (20 mL). The organic layer was dried (anhydrous sodium sulfate), filtered and concentrated *in vacuo* to yield a yellow oil. Purification by column chromatography eluting with 15% ethyl acetate in hexane afforded **154** as a cream solid (153 mg, 0.57 mmol, 46%). ¹H NMR (400 MHz, CDCl₃) δ 7.36 (ddd, *J* = 7.5, 4.5, 1.3 Hz, 2H, ArH), 7.31 - 7.23 (m, 3H, ArH), 7.02 (d, *J* = 8.7 Hz, 1H, ArH), 6.70 (dd, *J* = 8.7, 3.0 Hz, 1H, ArH), 6.26 - 6.22 (m, 1H, ArH), 4.37 (dd, *J* = 12.8, 6.4 Hz, 1H, CH), 3.61 (s, 3H, CH₃), 2.61 - 2.33 (m, 4H, C(O)CH₂, CH₂CH₂). ¹³C NMR (150 MHz, CDCl₃) δ 171.5 (C=O), 156.9 (C), 144.6 (C), 138.7 (C), 133.9 (C), 128.4 (CH), 127.1 (CH), 124.2 (CH), 119.5 (CH), 114.0 (CH), 111.4 (CH), 55.0 (CH₃), 42.7 (CH), 31.1 (CH₂), 30.6 (CH₂). ESI-HRMS: *m/z* calculated for C₁₇H₁₆O₃ [M+H]⁺ 269.1172, found 269.1169. RP-HPLC: *t*_R 10.76 min.

Bicyclo[4.1.0]heptan-2-one (160)

In a dry, three-neck round bottom flask equipped with a magnetic stirrer bar, thermometer and dropping funnel under a constant supply of N₂ gas was added anhydrous dimethylsulfoxide (10 mL). Sodium hydride (95%, 165 mg, 6.87 mmol) was added in portions, and following the exothermic reaction trimethylsulfoxonium iodide (1.51 g, 6.87 mmol) was added in portions. The reaction mixture was stirred at room temperature under N₂ gas for 40 min. A solution of 2-cyclohexenone (600 mg, 6.24 mmol) in anhydrous dimethylsulfoxide (10 mL) was

added in a drop-wise manner over 15 min. The solution was stirred vigorously for 30 min. at room temperature, before stirring at 50 °C for 2 h. The reaction mixture was poured onto ice and the aqueous layer was extracted with diethyl ether (2 × 20 mL) and ethyl acetate (2 × 20 mL). The combined organic extracts were dried (anhydrous sodium sulfate), filtered and concentrated *in vacuo* to yield a yellow oil which was purified by column chromatography eluting with 30% ethyl acetate in hexane to afford **160** as a yellow solid (606 mg, 5.50 mmol, 88%). ¹H NMR (400 MHz, CDCl₃) δ 1.93 - 1.90 (m, 1H, C(O)CH₂H), 1.81 - 1.74 (m, 1H, C(O)CH₂H), 1.58 - 1.42 (m, 3H, C(O)CH₂CH₂, C(O)CH₂CH₂CH₂), 1.24 - 1.15 (m, 3H, C(O)CH₂CH₂CH₂, C(O)CH₂CH₂CH₂), 0.77 - 0.73 (m, 1H, C(O)CH₂CH₂), 0.63 - 0.58 (m, 1H, C(O)CH₂CH₂). ¹³C NMR (101 MHz, CDCl₃) δ 171.1 (C=O), 38.1 (CH₂), 36.7 (CH₂), 25.8 (CH), 17.8 (CH), 17.4 (CH₂), 10.2 (CH₂). ESI-MS: *m/z* 111.2 [M+H]⁺. RP-HPLC: *t_R* 5.54 min.

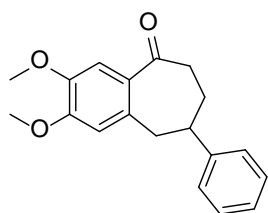
4-Benzyl-3,4-dihydronaphthalen-1(2H)-one (**169**)



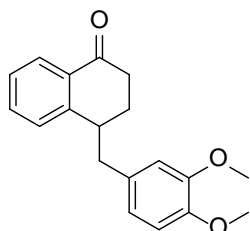
4,5-diphenylpentanoic acid (**176**) (100 mg, 0.39 mmol) was stirred in polyphosphoric acid (10 mL) at 80 °C for 4 h. The reaction mixture was poured into water (100 mL) and extracted with diethyl ether (4 × 20 mL). The combined organic extracts were washed with 5% aqueous sodium hydrogen carbonate (20 mL), dried (anhydrous sodium sulfate), filtered and concentrated *in vacuo* to afford **169** as a yellow oil (63 mg, 0.27 mmol, 67%). ¹H NMR (300 MHz, CDCl₃) δ 8.13 (d, *J* = 7.7 Hz, 1H ArH), 7.54 (t, *J* = 7.4 Hz, 1H, ArH), 7.45 - 7.35 (m, 3H, ArH), 7.26 (t, *J* = 6.2 Hz, 4H, ArH), 3.36 - 3.25 (m, 1H, CH), 3.25 - 3.12 (m, 1H, CHCH₂CH₂), 3.02 - 2.87 (m, 2H, ArCH₂CH), 2.72 - 2.58 (m, 1H, CHCH₂CH₂), 2.30 - 2.15 (m, 1H, CHCH₂CH₂), 2.07 - 1.94 (m, 1H, CHCH₂CH₂). ¹³C NMR (101 MHz, CDCl₃) δ 197.8 (C=O), 147.5 (C), 139.6 (CH), 133.4 (C), 132.0 (CH), 128.9 (CH), 128.5 (C), 128.4 (CH), 127.4 (CH), 126.8 (CH), 126.4 (CH), 41.1

(CH), 39.8 (CH₂), 34.6 (CH₂), 25.9 (CH₂). ESI-MS: m/z 237.2 [M+H]⁺. RP-HPLC: t_R 12.47 min.

2,3-Dimethoxy-8-phenyl-6,7,8,9-tetrahydro-5H-benzo[7]annulen-5-one (171) and 4-(3,4-dimethoxybenzyl)-3,4-dihydronaphthalen-1(2H)-one (172)



5-(3,4-dimethoxyphenyl)-5-oxo-4-phenylpentanoic acid (180)



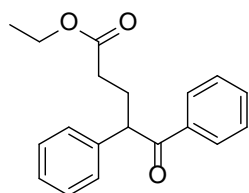
(300 mg, 0.95 mmol) was stirred in polyphosphoric acid (15 mL) at 80 °C for 4 h. The reaction mixture was poured into water (100 mL) and extracted with diethyl ether (4 × 20 mL). The combined organic extracts were washed with 5% aqueous sodium hydrogen carbonate (20 mL), dried (anhydrous sodium sulfate), filtered and concentrated *in vacuo* to afford a mixture of

171 and **172** (1:4) as a yellow oil (crude yield, 261.4 mg, 0.88 mmol, 92%). Purification of 80 mg of crude material through chiral chromatography (Amylose 2 stationary phase, isocratic mixture of 10% ethanol in petroleum spirits) afforded **171** as a clear oil (8 mg, 50%) and a mixture of **171** and **172** as a clear oil (22 mg, 34%).

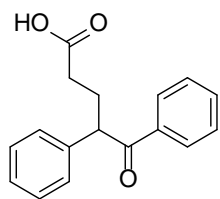
171 - ¹H NMR (400 MHz, CDCl₃) δ 7.44 (s, 1H, ArH), 7.33 - 7.27 (m, 2H, ArH), 7.24 - 7.21 (m, 1H, ArH), 7.16 - 7.14 (m, 2H, ArH), 6.54 (s, 1H, ArH), 3.94 (s, 3H, CH₃), 3.86 (s, 3H, CH₃), 3.26 - 3.09 (m, 3H, ArCH₂, CH), 3.00 - 2.95 (m, 1H, C(O)CHH), 2.78 - 2.74 (m, 1H, C(O)CHH), 2.19 (dd, *J* = 8.5, 5.9 Hz, 1H, C(O)CH₂CHH), 2.00 - 1.88 (m, 1H, C(O)CH₂CHH). ¹³C NMR (101 MHz, CDCl₃) δ 174.4 (C=O), 152.3 (C), 147.9 (C), 146.3 (C), 134.9 (C), 130.8 (C), 128.7 (CH), 127.3 (CH), 126.7 (CH), 113.5 (CH), 111.5 (CH), 56.22 (CH₃), 56.20 (CH₃), 43.2 (CH₂), 40.6 (CH), 40.0 (CH₂), 29.1 (CH₂). ESI-HRMS: m/z calculated for C₁₉H₂₀O₃ [M+H]⁺ 297.1485, found 297.1488. RP-HPLC: t_R 11.22 min.

172 - ^1H NMR (400 MHz, CDCl_3) δ 8.07 - 8.05 (m, 1H, ArH), 7.45 - 7.43 (m, 1H, ArH), 7.35 - 7.31 (m, 1H, ArH), 7.15 - 7.13 (m, 1H, ArH), 6.82 (s, 1H, ArH), 6.72 - 6.69 (m, 1H, ArH), 6.61 - 6.60 (m, 1H, ArH), 3.83 (s, 3H, OCH_3), 3.83 (s, 3H, OCH_3), 3.20 - 3.17 (m, 1H, ArCH), 3.07 - 3.02 (m, 1H, ArCHH), 2.86 - 2.77 (m, 2H, ArCHH, C(O)CHH), 2.62 - 2.55 (m, 1H, C(O)CHH), 2.23 - 2.16 (m, 1H, C(O)CH₂CHH), 2.02 - 1.96 (m, 1H, C(O)CH₂CHH). ESI-MS: m/z 297.2 $[\text{M}+\text{H}]^+$. RP-HPLC: t_R 11.22 min.

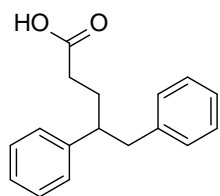
Ethyl 5-oxo-4,5-diphenylpentanoate (**174**)



To a solution of potassium *t*-butoxide (2.00 g, 17.8 mmol) in *t*-butanol (100 mL) was added deoxybenzoin (3.00 g, 15.3 mmol) with stirring. Ethyl acrylate (1.83 g, 18.3 mmol) was added in a drop-wise manner and stirring was continued at room temperature for 2 h and then concentrated *in vacuo*. The crude material was dissolved in water (100 mL) and extracted with diethyl ether (3×30 mL). The combined organic extracts were dried (anhydrous sodium sulfate), filtered and concentrated *in vacuo* to yield a pale yellow solid which was recrystallised from ethanol to afford **174** as white needles (4.46 g, 15.1 mmol, 98%). ^1H NMR (300 MHz, CDCl_3) δ 7.98 - 7.92 (m, 2H, ArH), 7.51 - 7.43 (m, 1H, ArH), 7.42 - 7.33 (m, 2H, ArH), 7.31 - 7.27 (m, 4H, ArH), 7.24 - 7.17 (m, 1H, ArH), 4.68 (t, $J = 7.2$ Hz, 1H, CH), 4.17 - 4.06 (m, 2H, OCH_2), 2.53 - 2.38 (m, 1H, CHCHH), 2.35 - 2.26 (m, 2H, CHCH₂CH₂), 2.24 - 2.10 (m, 1H, CHCHH), 1.26 - 1.19 (m, 3H, CH_3). ESI-MS: m/z 297.2 $[\text{M}+\text{H}]^+$. RP-HPLC: t_R 12.71 min. M.p. 55 - 56 °C. (lit.³³² M.p. 45 - 57 °C)

5-Oxo-4,5-diphenylpentanoic acid (175)

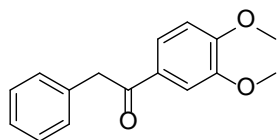
Ethyl-5-oxo-4,5-diphenylpentanoate (**174**) (1.42 g, 4.79 mmol) was dissolved in 1,4-dioxane/1 M aqueous sodium hydroxide (1:1, 50 mL) and stirred at 100 °C for 2 h. The reaction mixture was cooled, made acidic (pH ~ 2) with concentrated hydrochloric acid, and concentrated *in vacuo*. The residue was dissolved in ethyl acetate (50 mL) and washed with water (3 × 20 mL). The organic layer was dried (anhydrous sodium sulfate), filtered and concentrated *in vacuo* to yield a cream solid which was recrystallised from ethanol to afford **175** as white needles (1.22 g, 4.55 mmol, 95%). ¹H NMR (300 MHz, CDCl₃) δ 7.95 (d, *J* = 7.8 Hz, 2H, ArH), 7.48 (t, *J* = 7.2 Hz, 1H, ArH), 7.38 (t, *J* = 7.2 Hz, 2H, ArH), 7.32 - 7.27 (m, 4H, ArH), 7.25 - 7.17 (m, 1H, ArH), 4.67 (t, *J* = 7.2 Hz, 1H, CH), 2.51 - 2.40 (m, 1H, CHCHH), 2.40 - 2.32 (m, 2H, CHCH₂CH₂), 2.26 - 2.13 (m, 1H, CHCHH). ESI-MS: *m/z* 267.2 [M-H⁺]⁻. RP-HPLC: *t*_R 10.67 min. M.p. 135 - 136 °C.

4,5-Diphenylpentanoic acid (176)

To a stirred solution of 5-oxo-4,5-diphenylpentanoic acid (**175**) (250 mg, 0.93 mmol) in trifluoroacetic acid (10 mL) under an atmosphere of nitrogen was added triethylsilane (238 mg, 2.05 mmol) in a drop-wise manner. The reaction mixture was stirred at room temperature for 16 h, made basic (pH ~ 9) with aqueous sodium hydroxide, and washed with diethyl ether (15 mL). The aqueous extract was made acidic (pH ~ 4) with concentrated hydrochloric acid and extracted with diethyl ether (3 × 20 mL). The combined organic extracts were dried (anhydrous sodium sulfate), filtered and concentrated *in vacuo* to afford **176** as a pale yellow oil (201 mg, 0.79 mmol, 85%). ¹H NMR (300 MHz, CDCl₃) δ 7.41 - 7.31 (m, 3H, ArH), 7.31 - 7.23 (m, 3H, ArH), 7.20 (t, *J* = 6.6 Hz, 2H, ArH), 7.12 (d, *J* = 7.4 Hz, 2H, ArH), 3.05 - 2.95 (m, 2H, ArCH₂)

2.95 - 2.85 (m, 1H, CH), 2.34 - 2.22 (m, 2H, C(O)CH₂), 2.22 - 2.08 (m, 1H, CHCHH), 2.08 - 1.94 (m, 1H, CHCHH). ESI-MS: m/z 255.3 $[M+H]^+$. RP-HPLC: t_R 11.71 min.

1-(3,4-Dimethoxyphenyl)-2-phenylethanone (**177**)



Method I:

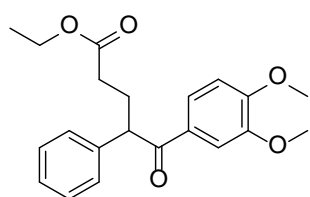
Phenylacetic acid (5.00 g, 34.7 mmol) was dissolved in thionyl chloride (30 mL) and stirred at 80 °C for 2.5 h. The reaction mixture was removed from heat and concentrated *in vacuo*. The crude material was dissolved in dichloromethane (50 mL) and cooled to 0 °C. 1,2-Dimethoxybenzene (4.80 g, 34.7 mmol) was added, followed by the gradual addition of aluminium trichloride (6.95 g, 52.1 mmol). The solution was warmed to room temperature then heated at 60 °C for 2 h. The mixture was cooled, poured onto ice, and made acidic (pH ~ 4) with concentrated hydrochloric acid. The organic phase was separated and the aqueous phase was extracted with dichloromethane (2 × 20 mL). The combined organic extracts were washed with water (30 mL), dried (anhydrous sodium sulfate), filtered and concentrated *in vacuo* to afford **177** as a yellow oil (5.55 g, 21.7 mmol, 62%).

Method II:

Phenylacetic acid (2.00 g, 14.7 mmol) and oxalyl chloride (1.24 g, 9.79 mmol) in dichloromethane (50 mL) were stirred at 60 °C for 1 h. The solution was cooled to room temperature and dimethoxybenzene (1.35 g, 9.79 mmol) was added followed by the gradual addition of aluminium trichloride (1.96 g, 14.7 mmol). The solution was stirred at 60 °C for 4 h. The mixture was cooled, poured into ice, and made acidic (pH ~ 4) with concentrated hydrochloric acid. The organic phase was separated and the aqueous phase was extracted with dichloromethane (2 × 20 mL). The combined organic extracts were washed with water (30 mL), dried (anhydrous sodium sulfate), filtered and concentrated *in vacuo* to give a yellow solid which was recrystallised from ethanol to

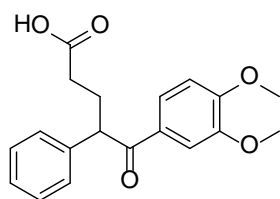
afford **177** as a white solid (2.14 g, 8.35 mmol, 85%). ^1H NMR (300 MHz, CDCl_3) δ 7.64 (d, $J = 8.4$ Hz, 1H, ArH), 7.53 (s, 1H, ArH), 7.34 - 7.18 (m, 5H, ArH), 6.85 (d, $J = 8.4$ Hz, 1H, ArH), 4.22 (s, 2H, CH_2), 3.91 (s, 3H, CH_3), 3.89 (s, 3H, CH_3). ESI-MS: m/z 257.2 $[\text{M}+\text{H}]^+$. RP-HPLC: t_R 10.28 min. M.p. 81 - 82 °C (lit.³³⁸ M.p. 82 °C).

Ethyl 5-(3,4-dimethoxyphenyl)-5-oxo-4-phenylpentanoate (**178**)



To a solution of potassium *t*-butoxide (2.00 g) in *t*-butanol (100 mL) was added 1-(3,4-dimethoxyphenyl)-2-phenylethanone (**177**) (3.00 g, 11.7 mmol) with stirring. Ethyl acrylate (1.41 g, 14.1 mmol) was added in a drop-wise manner and stirring was continued at room temperature for 2 h and then the reaction mixture was concentrated *in vacuo*. The crude material was dissolved in water (100 mL) and extracted with diethyl ether (3 \times 30 mL). The combined organic extracts were dried (anhydrous sodium sulfate), filtered and concentrated *in vacuo* to afford **178** as a pale yellow oil (3.89 g, 10.9 mmol, 93%). ^1H NMR (400 MHz, CDCl_3) δ 7.58 (dd, $J = 8.5, 2.0$ Hz, 1H, ArH), 7.50 (d, $J = 2.0$ Hz, 1H, ArH), 7.28 - 7.23 (m, 4H, ArH), 7.20 - 7.16 (m, 1H, ArH), 6.78 - 6.74 (m, 1H, ArH), 4.62 (t, $J = 7.3$ Hz, 1H, CH), 4.10 - 4.03 (q, $J = 7.3$ Hz, 2H, OCH_2), 3.83 (s, 6H, OCH_3 , OCH_3), 2.46 - 2.93 (m, 1H, CHCHH), 2.29 - 2.21 (m, 2H, $\text{C}(\text{O})\text{CH}_2$), 2.19 - 2.07 (m, 1H, CHCHH), 1.20 (t, $J = 7.1$ Hz, 3H, CH_3). ESI-MS: m/z 357.2 $[\text{M}+\text{H}]^+$. RP-HPLC: t_R 11.26 min.

5-(3,4-Dimethoxyphenyl)-5-oxo-4-phenylpentanoic acid (**179**)

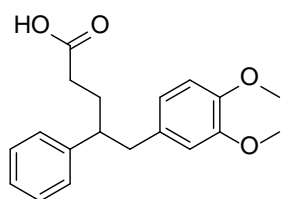


Ethyl 5-(3,4-dimethoxyphenyl)-5-oxo-4-phenylpentanoate (**178**) (3.48 g, 9.76 mmol) was dissolved in 1,4-dioxane/1 M aqueous sodium hydroxide (1:1, 50 mL) and stirred at 100 °C for 2 h.

The reaction mixture was cooled, made acidic (pH \sim 2) with concentrated hydrochloric

acid, and concentrated *in vacuo*. The residue was dissolved in ethyl acetate (50 mL) and washed with water (3×20 mL). The organic layer was dried (anhydrous sodium sulfate), filtered and concentrated *in vacuo* to afford **179** as a clear oil (3.09 g, 9.41 mmol, 96%). ^1H NMR (400 MHz, CDCl_3) δ 7.57 (dd, $J = 8.5, 2.0$ Hz, 1H, ArH), 7.50 (d, $J = 2.0$ Hz, 1H, ArH), 7.28 - 7.24 (m, 4H, ArH), 7.20 - 7.16 (m, 1H, ArH), 6.77 (dd, $J = 8.5, 4.1$ Hz, 1H, ArH), 4.61 (t, $J = 7.3$ Hz, 1H, CH), 3.86 (s, 3H, CH_3), 3.85 (s, 3H, CH_3), 2.49 - 2.37 (m, 1H, CHCHH), 2.32 (t, $J = 7.3$ Hz, 2H, $\text{C}(\text{O})\text{CH}_2$), 2.20 - 2.09 (m, 1H, CHCHH). ESI-MS: m/z 327.2 $[\text{M}-\text{H}]^+$. RP-HPLC: t_R 9.42 min.

5-(3,4-Dimethoxyphenyl)-4-phenylpentanoic acid (**180**)

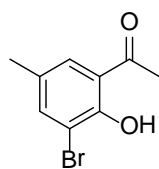


To a stirred solution of 5-(3,4-dimethoxyphenyl)-5-oxo-4-phenylpentanoic acid (**179**) (500 mg, 3.05 mmol) in trifluoroacetic acid (10 mL) under an atmosphere of nitrogen was added triethylsilane (779 mg, 6.70 mmol) in a drop-wise manner. The reaction mixture was stirred at room temperature for 1 h, and further equivalents of triethylsilane (779 mg, 6.70 mmol) were added. Stirring was continued at room temperature for 15 h. The reaction mixture was made basic (pH \sim 9) with aqueous 1 M sodium hydroxide, and washed with diethyl ether (15 mL). The aqueous extract was made acidic (pH \sim 4) with concentrated hydrochloric acid and extracted with diethyl ether (3×20 mL). The combined organic extracts were dried (anhydrous sodium sulfate), filtered and concentrated *in vacuo* to afford **180** as a pale yellow oil (881 mg, 2.81 mmol, 92%). ^1H NMR (400 MHz, CDCl_3) δ 7.29 - 7.23 (m, 2H, ArH), 7.20 - 7.15 (m, 1H, ArH), 7.09 (m, 2H, ArH), 6.70 (dd, $J = 8.1, 3.8$ Hz, 1H, ArH), 6.59 (dd, $J = 8.1, 1.9$ Hz, 1H, ArH), 6.40 (d, $J = 1.9$ Hz, 1H, ArH), 3.81 (s, 3H, CH_3), 3.70 (s, 3H, CH_3), 2.87 - 2.74 (m, 3H, CH, ArCH $_2$), 2.21 - 2.14 (m, 2H, $\text{C}(\text{O})\text{CH}_2$), 2.11 - 2.01 (m, 1H, CHCHH), 1.96 - 1.86 (m, 1H, CHCHH). ^{13}C NMR (101 MHz, CDCl_3) δ 179.6 (C=O), 148.5 (C), 147.3 (C),

143.6 (C), 132.8 (C), 128.6 (CH), 128.0 (CH), 126.6 (CH), 121.2 (CH), 112.6 (CH), 111.1 (CH), 55.9 (CH₃), 55.8 (CH₃), 47.6 (CH), 43.3 (CH₂), 32.2 (CH₂), 30.3 (CH₂).
ESI-MS: m/z 315.3 [M+H]⁺. RP-HPLC: t_R 8.20 min.

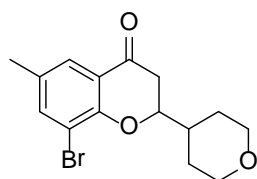
7.2.3 Chapter 5 experimental

1-(3-Bromo-2-hydroxy-5-methylphenyl)ethanone (**186**)



To a stirring solution of 1-(2-hydroxy-5-methylphenyl)ethanone (2.00 g, 13.3 mmol) and sodium acetate (1.20 g, 14.7 mmol) in glacial acetic acid (20 mL) at 0 °C was added in a drop-wise manner a solution of bromine (2.34 g, 14.7 mmol) in glacial acetic acid (5 mL). Stirring was continued at room temperature for 16 h and further portions of bromine (2.34 g, 14.7 mmol) and sodium acetate (1.20 g, 14.7 mmol) were added. Stirring was continued at room temperature for 2 h. The reaction mixture was poured onto ice and the resulting precipitate was filtered. Recrystallisation of the precipitate from ethanol afforded **186** as yellow needles (2.93 g, 12.8 mmol, 96%). ¹H NMR (400 MHz, CDCl₃) δ 7.60 - 7.58 (m, 1H, ArH), 7.51 - 7.50 (m, 1H, ArH), 2.66 (s, 3H, C(O)CH₃), 2.33 (s, 3H, CH₃). ESI-MS: m/z 229.4 [M-H]⁺. RP-HPLC: t_R 9.76 min. M.p. 87 - 88 °C (lit.³⁴⁸ M.p. 86 - 87 °C).

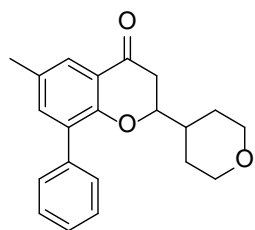
8-Bromo-6-methyl-2-(tetrahydro-2H-pyran-4-yl)chroman-4-one (**187**)



A solution of 1-(3-bromo-2-hydroxy-5-methylphenyl)ethanone (**186**) (1.00 g, 4.37 mmol), tetrahydro-2H-pyran-4-carbaldehyde (0.50 g, 4.37 mmol) and sodium tetraborate (3.33 g, 8.73 mmol) in ethanol/water (5:3, 32 mL) was stirred at 78 °C for 48 h. The reaction mixture was

concentrated *in vacuo*. The crude material was dissolved in ethyl acetate (80 mL), and washed with 1 M aqueous hydrochloric acid (30 mL) and saturated aqueous sodium chloride (30 mL). The organic extract was dried (anhydrous sodium sulfate), filtered and concentrated *in vacuo* to afford **187** as a cream solid (1.24 g, 3.81 mmol, 87%). ^1H NMR (400 MHz, CDCl_3) δ 7.62 (d, $J = 2.2$ Hz, 1H, ArH), 7.56 (d, $J = 2.2$ Hz, 1H, ArH), 4.29 - 4.18 (m, 1H, OCH), 4.11 - 4.02 (m, 2H, OCHH, OCHH), 3.44 - 3.40 (m, 2H, OCHH, OCHH), 2.74 - 2.70 (m, 2H, C(O)CH₂), 2.30 (s, 3H, CH₃), 2.06 - 1.99 (m, 2H, OCH₂CHH, OCH₂CHH), 1.64 - 1.56 (m, 3H, OCH₂CHH, OCH₂CHH, OCHCH). ^{13}C NMR (101 MHz, CDCl_3) δ 192.0 (C=O), 155.9 (C), 140.1 (CH), 132.0 (C), 126.2 (CH), 121.9 (C), 111.6 (C), 82.1 (CH), 67.8* (CH₂), 67.5* (CH₂), 40.1 (CH₂), 39.4 (CH), 28.8* (CH₂), 28.3* (CH₂), 20.3 (CH₃). ESI-HRMS: m/z calculated for $\text{C}_{15}\text{H}_{17}\text{BrO}_3$ $[\text{M}+\text{H}]^+$ 325.0434, found 325.0442. RP-HPLC: t_R 10.60 min.

6-Methyl-8-phenyl-2-(tetrahydro-2H-pyran-4-yl)chroman-4-one (188)



Method I:

1-(2-Hydroxy-5-methyl-[1,1'-biphenyl]-3-yl)ethanone (**189**) (51 mg, 0.23 mmol), tetrahydro-2H-pyran-4-carbaldehyde (26 mg, 0.23 mmol) and sodium tetraborate (172 mg, 0.45 mmol) in

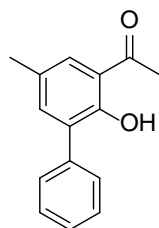
ethanol/water (5:3, 16 mL) were stirred at 78 °C for 48 h. The reaction mixture was concentrated *in vacuo*. The crude material was dissolved in ethyl acetate (40 mL), and washed with 1 M aqueous hydrochloric acid (15 mL) and saturated aqueous sodium chloride (15 mL). The organic layer was dried (anhydrous sodium sulfate), filtered and concentrated *in vacuo* to afford **188** as a yellow oil (30 mg, 0.09 mmol, 41%).

Method II:

To a degassed solution of 8-bromo-6-methyl-2-(tetrahydro-2*H*-pyran-4-yl)chroman-4-one (**187**) (70 mg, 0.22 mmol), cesium carbonate (140 mg, 0.43 mmol) and phenylboronic acid (34 mg, 0.28 mmol) in 1,4-dioxane (3 mL) was added palladium (II) acetate (spatula tip), tricyclohexylphosphine (spatula tip), tetra-*n*-butylammonium bromide (spatula tip) and water (0.5 mL). The reaction mixture was heated using microwave irradiation at 150 °C for 30 min. After cooling, the reaction mixture was filtered through celite. The filtrate was concentrated *in vacuo*, the residue was dissolved in ethyl acetate (20 mL) and washed with water (10 mL) and saturated aqueous sodium sulfate (10 mL). The organic layer was dried (anhydrous sodium sulfate), filtered and concentrated *in vacuo* to yield a yellow solid. Purification by column chromatography eluting with 30% ethyl acetate in hexane afforded **188** as a cream solid (65 mg, 0.20 mmol, 94%). ¹H NMR (400 MHz, CDCl₃) δ 7.61 - 7.58 (m, 1H, ArH), 7.41 - 7.37 (m, 2H, ArH), 7.34 - 7.28 (m, 2H, ArH), 7.26 - 7.25 (m, 1H, ArH), 7.15 (s, 1H, ArH), 4.07 (dd, *J* = 15.3, 8.0 Hz, 1H, OCH), 3.92 - 3.84 (m, 2H, OCHH, OCHH), 3.32 - 3.19 (m, 2H, OCHH, OCHH), 2.61 - 2.59 (m, 2H, C(O)CH₂), 2.24 (s, 3H, CH₃), 1.85 - 1.77 (m, 1H, OCH₂CHH), 1.68 - 1.64 (m, 1H, OCH₂CHH), 1.47 - 1.42 (m, 1H, OCHCH), 1.40 - 1.27 (m, 2H, OCH₂CHH, OCH₂CHH). ¹H NMR (400 MHz, DMSO) δ 7.57 (dd, *J* = 2.3, 0.8 Hz, 1H, ArH), 7.54 - 7.51 (m, 2H, ArH), 7.46 - 7.41 (m, 3H, ArH), 7.38 - 7.33 (m, 1H, ArH), 4.35 - 4.27 (m, 1H, OCH), 3.86 - 3.83 (m, 2H, OCHH, OCHH), 3.31 - 3.20 (m, 2H, OCHH, OCHH), 2.85 - 3.21 (m, 1H, C(O)CHH), 2.68 - 2.61 (m, 1H, C(O)CHH), 2.32 (s, 3H, CH₃), 1.95 - 1.80 (m, 1H, OCH₂CHH), 1.69 - 1.66 (m, 1H, OCH₂CHH), 1.53 - 1.50 (m, 1H, OCHCH), 1.41 - 1.28 (m, 2H, OCH₂CHH, OCH₂CHH). ¹³C NMR (101 MHz, CDCl₃) δ 192.9 (C=O), 156.6 (C), 138.1 (CH), 136.9 (C), 131.1 (C), 130.7 (C), 129.4 (CH), 128.0 (CH), 127.4 (CH), 126.1 (CH), 121.2 (C), 81.4 (CH), 67.7* (CH₂), 67.4* (CH₂), 40.4 (CH₂), 39.6 (CH), 28.7* (CH₂), 28.3* (CH₂),

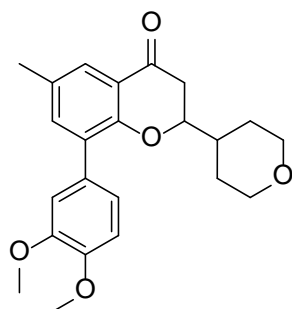
20.5 (CH₃). ¹³C NMR (101 MHz, DMSO) δ 192.3 (C=O), 156.1 (C), 137.4 (CH), 136.5 (C), 130.4 (C), 130.1 (C), 129.2 (CH), 128.0 (CH), 127.4 (CH), 125.4 (CH), 121.0 (C), 80.9 (CH), 66.62* (CH₂), 66.61* (CH₂), 38.7 (CH₂), 30.7 (CH), 27.9* (CH₂), 27.8* (CH₂), 20.0 (CH₃). ¹³C NMR (101 MHz, 323 K, DMSO) δ 192.7 (C=O), 156.7 (C), 137.8 (CH), 137.1 (C), 130.9 (C), 130.6 (C), 129.7 (CH), 128.4 (CH), 127.8 (CH), 125.9 (CH), 121.6 (C), 81.4 (CH), 67.1 (CH₂), 38.6 (CH₂), 31.1 (CH), 28.4 (CH₂), 20.4 (CH₃). ESI-HRMS: *m/z* calculated for C₂₁H₂₂O₃ [M+H]⁺ 323.1653, found 323.1642. RP-HPLC: *t_R* 11.33 min.

1-(2-Hydroxy-5-methyl-[1,1'-biphenyl]-3-yl)ethanone (**189**)

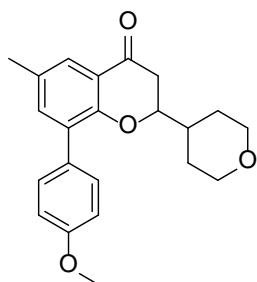


To a degassed solution of 1-(3-bromo-2-hydroxy-5-methylphenyl)ethanone (**186**) (100 mg, 0.44 mmol), potassium carbonate (151 mg, 1.09 mmol) and phenylboronic acid (69 mg, 0.57 mmol) in dimethylformamide/water (9:1, 5 mL) was added palladium (II) hydroxide (22 mg, 0.15 mmol). The reaction mixture was heated using microwave irradiation at 130 °C for 2.5 h. After cooling, the reaction mixture was filtered through celite, and the filtrate was lyophilised. The residue was dissolved in ethyl acetate (30 mL) and washed with water (10 mL) and saturated aqueous sodium chloride (10 mL). The organic layer was dried (anhydrous sodium sulfate), filtered and concentrated *in vacuo* to yield a cream solid. Purification by column chromatography eluting with 30% ethyl acetate in hexane afforded **189** as a white solid (91 mg, 0.40 mmol, 92%). ¹H NMR (400 MHz, CDCl₃) δ 7.48 - 7.43 (m, 2H, ArH), 7.42 - 7.39 (m, 1H, ArH), 7.34 - 7.28 (m, 2H, ArH), 7.27 - 7.20 (m, 2H, ArH), 2.53 (s, 3H, C(O)CH₃), 2.24 (s, 3H, CH₃). ESI-MS: *m/z* 227.2 [M+H]⁺. RP-HPLC: *t_R* 11.39 min.

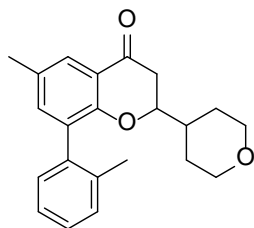
8-(3,4-Dimethoxyphenyl)-6-methyl-2-(tetrahydro-2H-pyran-4-yl)chroman-4-one
(190)



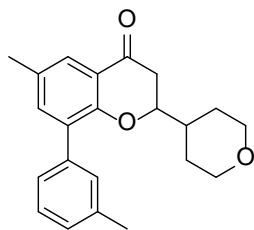
To a degassed solution of 8-bromo-6-methyl-2-(tetrahydro-2H-pyran-4-yl)chroman-4-one (**187**) (150 mg, 0.46 mmol), cesium carbonate (301 mg, 0.92 mmol) and (3,4-dimethoxyphenyl)boronic acid (109 mg, 0.60 mmol) in 1,4-dioxane (3 mL) was added palladium (II) acetate (spatula tip), tricyclohexylphosphine (spatula tip), tetra-*n*-butylammonium bromide (spatula tip) and water (0.5 mL). The reaction mixture heated using microwave irradiation at at 150 °C for 30 min. After cooling, the reaction mixture was filtered through celite. The filtrate was concentrated *in vacuo*, the residue dissolved in ethyl acetate (20 mL) and washed with water (10 mL) and saturated aqueous sodium sulfate (10 mL). The organic layer was dried (anhydrous sodium sulfate), filtered and concentrated *in vacuo* to yield a yellow solid. Purification by column chromatography eluting with 30% ethyl acetate in hexane afforded **190** as a cream solid (142 mg, 0.37 mmol, 81%). ¹H NMR (400 MHz, CDCl₃) δ 7.69 - 7.67 (m, 1H, ArH), 7.35 - 7.34 (m, 1H, ArH), 7.09 - 7.03 (m, 2H, ArH), 6.95 - 6.91 (m, 1H, ArH), 4.22 - 4.16 (m, 1H, OCH), 4.04 - 3.96 (m, 2H, OCHH, OCHH), 3.93 (s, 3H, OCH₃), 3.91 (s, 3H, OCH₃), 3.36 (m, 2H, OCHH, OCHH), 3.41 - 3.31 (m, 2H, C(O)CH₂), 2.34 (s, 3H, CH₃), 2.04 - 1.91 (m, 1H, OCH₂CHH), 1.84 - 1.75 (m, 1H, OCH₂CHH), 1.56 - 1.40 (m, 3H, OCH₂CHH, OCH₂CHH, OCHCH). ¹³C NMR (101 MHz, CDCl₃) δ 192.9 (C=O), 156.5 (C), 148.5 (C), 148.4 (C), 137.9 (CH), 130.8 (C), 130.7 (C), 129.7 (C), 125.8 (CH), 121.8 (CH), 121.2 (C), 112.8 (CH), 110.8 (CH), 81.4 (CH), 67.6* (CH₂), 67.4* (CH₂), 55.92 (CH₃), 55.91 (CH₃), 40.2 (CH₂), 39.6 (CH), 28.8* (CH₂), 28.4 (CH₂), 20.5 (CH₃). ESI-HRMS: *m/z* calculated for C₂₃H₂₆O₅ [M+H]⁺ 383.1814, found 383.1865. RP-HPLC: *t*_R 10.60 min.

8-(4-Methoxyphenyl)-6-methyl-2-(tetrahydro-2H-pyran-4-yl)chroman-4-one (191)

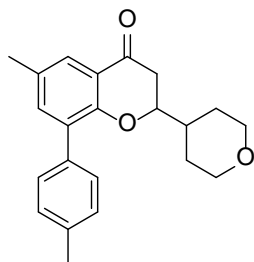
To a degassed solution of 8-bromo-6-methyl-2-(tetrahydro-2H-pyran-4-yl)chroman-4-one (**187**) (50 mg, 0.15 mmol), cesium carbonate (100 mg, 0.31 mmol) and (4-methoxyphenyl)boronic acid (30 mg, 0.20 mmol) in 1,4-dioxane (3 mL) was added palladium (II) acetate (spatula tip), tricyclohexylphosphine (spatula tip), tetra-*n*-butylammonium bromide (spatula tip) and water (0.5 mL). The reaction mixture was heated using microwave irradiation at 150 °C for 30 min. After cooling, the reaction mixture was filtered through celite. The filtrate was concentrated *in vacuo*, the residue dissolved in ethyl acetate (20 mL) and washed with water (10 mL) and saturated aqueous sodium sulfate (10 mL). The organic layer was dried (anhydrous sodium sulfate), filtered and concentrated *in vacuo* to yield a white solid. Purification by column chromatography eluting with 30% ethyl acetate in hexane afforded **191** as a white solid (45 mg, 0.13 mmol, 83%). ¹H NMR (400 MHz, CDCl₃) δ 7.67 - 7.67 (m, 1H, ArH), 7.47 - 7.42 (m, 2H, ArH), 7.34 - 7.34 (m, 1H, ArH), 6.98 - 6.93 (m, 2H, ArH), 4.24 - 4.14 (m, 1H, OCH), 4.04 - 3.96 (m, 2H, OCHH, OCHH), 3.86 (s, 3H, OCH₃), 3.44 - 3.31 (m, 2H, OCHH, OCHH), 2.73 - 2.68 (m, 2H, C(O)CH₂), 2.34 (s, 3H, CH₃), 2.00 - 1.87 (m, 1H, OCH₂CHH), 1.79 (ddd, *J* = 13.3, 3.6, 1.8 Hz, 1H, OCH₂CHH), 1.56 - 1.53 (m, 1H, OCHCH), 1.53 - 1.39 (m, 2H, OCH₂CHH, OCH₂CHH). ¹³C NMR (101 MHz, CDCl₃) δ 193.0 (C=O), 159.0 (C), 156.7 (C), 138.0 (CH), 130.9 (C), 130.8 (C), 130.6 (CH), 129.4 (CH), 125.7 (C), 121.3 (CH), 113.6 (C), 81.5 (CH), 67.8* (CH₂), 67.6* (CH₂), 55.5 (CH₃), 40.5 (CH₂), 39.7 (CH), 28.8* (CH₂), 28.4* (CH₂), 20.6 (CH₃). ESI-HRMS: *m/z* calculated for C₂₂H₂₄O₄ [M+H]⁺ 353.1747, found 353.1761. RP-HPLC: *t*_R 11.07 min.

6-Methyl-2-(tetrahydro-2H-pyran-4-yl)-8-(*o*-tolyl)chroman-4-one (192)

To a degassed solution of 8-bromo-6-methyl-2-(tetrahydro-2H-pyran-4-yl)chroman-4-one (**187**) (40 mg, 0.12 mmol), cesium carbonate (100 mg, 0.31 mmol) and *o*-tolylboronic acid (22 mg, 0.16 mmol) in 1,4-dioxane (3 mL) was added palladium (II) acetate (spatula tip), tricyclohexylphosphine (spatula tip), tetra-*n*-butylammonium bromide (spatula tip) and water (0.5 mL). The reaction mixture was heated using microwave irradiation at 150 °C for 30 min. After cooling, the reaction mixture was filtered through celite. The filtrate was concentrated *in vacuo*, the residue dissolved in ethyl acetate (20 mL) and washed with water (10 mL) and saturated aqueous sodium sulfate (10 mL). The organic layer was dried (anhydrous sodium sulfate), filtered and concentrated *in vacuo* to yield a white solid. Purification by column chromatography eluting with 30% ethyl acetate in hexane afforded **192** as a white solid (36 mg, 0.11 mmol, 87%). ¹H NMR (400 MHz, CDCl₃) δ 7.71 - 7.70 (m, 1H, ArH), 7.27 - 7.18 (m, 4H, ArH), 7.14 - 7.12 (m, 1H, ArH), 4.27 - 4.04 (m, 1H, OCH), 3.99 - 3.86 (m, 2H, OCHH, OCHH), 3.37 - 3.22 (m, 2H, OCHH, OCHH), 2.71 - 2.64 (m, 2H, C(O)CH₂), 2.33 (s, 3H, CH₃), 2.16 (s, 3H, CH₃), 1.83 - 1.77 (m, 1H, OCH₂CHH), 1.59 - 1.46 (m, 2H, OCH₂CHH, OCHCH), 1.42 - 1.28 (m, 2H, OCH₂CHH, OCH₂CHH). ¹³C NMR (101 MHz, CDCl₃) δ 193.0 (C=O), 156.8 (C), 138.4 (CH), 136.5 (C), 131.5 (C), 130.6 (C), 129.8 (C), 129.6 (CH), 127.2 (CH), 126.8 (CH), 126.0 (CH), 125.6 (CH), 120.9 (C), 81.4 (CH), 67.7* (CH₂), 67.4* (CH₂), 40.5 (CH₂), 39.6 (CH), 28.5* (CH₂), 28.2* (CH₂), 20.6 (CH₃), 20.1 (CH₃). ESI-HRMS: *m/z* calculated for C₂₂H₂₄O₃ [M+H]⁺ 337.1798, found 337.1803. RP-HPLC: *t*_R 11.46 min.

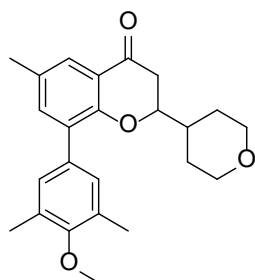
6-Methyl-2-(tetrahydro-2H-pyran-4-yl)-8-(*m*-tolyl)chroman-4-one (193)

To a degassed solution of 8-bromo-6-methyl-2-(tetrahydro-2H-pyran-4-yl)chroman-4-one (**187**) (50 mg, 0.15 mmol), cesium carbonate (100 mg, 0.31 mmol) and *m*-tolylboronic acid (27 mg, 0.20 mmol) in 1,4-dioxane (3 mL) was added palladium (II) acetate (spatula tip), tricyclohexylphosphine (spatula tip), tetra-*n*-butylammonium bromide (spatula tip) and water (0.5 mL). The reaction mixture was heated using microwave irradiation at 150 °C for 30 min. After cooling, the reaction mixture was filtered through celite. The filtrate was concentrated *in vacuo*, the residue dissolved in ethyl acetate (20 mL) and washed with water (10 mL) and saturated aqueous sodium sulfate (10 mL). The organic layer was dried (anhydrous sodium sulfate), filtered and concentrated *in vacuo* to yield a white solid. Purification by column chromatography eluting with 30% ethyl acetate in hexane afforded **193** as a cream solid (47 mg, 0.14 mmol, 91%). ¹H NMR (400 MHz, CDCl₃) δ 7.66 - 7.64 (m, 1H, ArH), 7.33 - 7.32 (m, 1H, ArH), 7.29 - 7.25 (m, 3H, ArH), 7.14 - 7.10 (m, 1H, ArH), 4.17 - 4.11 (m, 1H, OCH), 4.01 - 3.92 (m, 2H, OCHH, OCHH), 3.38 - 3.28 (m, 2H, OCHH, OCHH), 2.69 - 2.63 (m, 2H, C(O)CH₂), 2.36 (s, 3H, CH₃), 2.30 (s, 3H, CH₃), 1.94 - 1.82 (m, 1H, OCH₂CHH), 1.80 - 1.75 (m, 1H, OCH₂CHH), 1.57 - 1.36 (m, 3H, OCH₂CHH, OCH₂CHH, OCHCH). ¹³C NMR (101 MHz, CDCl₃) δ 193.0 (C=O), 156.7 (C), 138.1 (CH), 137.6 (C), 136.9 (C), 131.3 (C), 130.8 (C), 130.3 (CH), 128.3 (CH), 128.1 (CH), 126.6 (CH), 126.1 (CH), 121.3 (C), 81.5 (CH), 67.7* (CH₂), 67.5* (CH₂), 40.5 (CH₂), 39.8 (CH), 28.9* (CH₂), 28.4* (CH₂), 21.6 (CH₃), 20.6 (CH₃). ESI-HRMS: *m/z* calculated for C₂₂H₂₄O₃ [M+H]⁺ 337.1798, found 337.1814. RP-HPLC: *t*_R 11.68 min.

6-Methyl-2-(tetrahydro-2H-pyran-4-yl)-8-(*p*-tolyl)chroman-4-one (194)

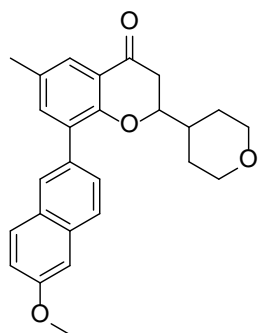
To a degassed solution of 8-bromo-6-methyl-2-(tetrahydro-2H-pyran-4-yl)chroman-4-one (**187**) (50 mg, 0.15 mmol), cesium carbonate (100 mg, 0.31 mmol) and *p*-tolylboronic acid (27 mg, 0.20 mmol) in 1,4-dioxane (3 mL) was added palladium (II) acetate (spatula tip), tricyclohexylphosphine (spatula tip), tetra-*n*-butylammonium bromide (spatula tip) and water (0.5 mL). The reaction mixture was heated using microwave irradiation at 150 °C for 30 min. After cooling, the reaction mixture was filtered through celite. The filtrate was concentrated *in vacuo*, the residue dissolved in ethyl acetate (20 mL) and washed with water (10 mL) and saturated aqueous sodium sulfate (10 mL). The organic layer was dried (anhydrous sodium sulfate), filtered and concentrated *in vacuo* to yield a white solid. Purification by column chromatography eluting with 30% ethyl acetate in hexane afforded **194** as a white solid (34 mg, 0.10 mmol, 66%). ¹H NMR (400 MHz, CDCl₃) δ 7.69 - 7.66 (m, 1H, ArH), 7.42 - 7.38 (m, 2H, ArH), 7.36 - 7.35 (m, 1H, ArH), 7.24 - 7.22 (m, 2H, ArH), 4.18 (dt, *J* = 8.7, 7.2 Hz, 1H, OCH), 4.03 - 3.98 (m, 2H, OCHH, OCHH), 3.43 - 3.32 (m, 2H, OCHH, OCHH), 2.73 - 2.69 (m, 2H, C(O)CH₂), 2.40 (s, 3H, CH₃), 2.34 (s, 3H, CH₃), 1.98 - 1.87 (m, 1H, OCH₂CHH), 1.83 - 1.76 (m, 1H, OCH₂CHH), 1.56 - 1.52 (m, 1H, OCHCH), 1.52 - 1.39 (m, 2H, OCH₂CHH, OCH₂CHH). ¹³C NMR (101 MHz, CDCl₃) δ 193.1 (C=O), 160.4 (C), 144.1 (CH), 138.1 (C), 137.3 (C), 134.1 (C), 131.2 (C), 129.4 (CH), 128.9 (CH), 126.0 (CH), 121.3 (C), 81.5 (CH), 67.8* (CH₂), 67.6* (CH₂), 40.5 (CH₂), 39.7 (CH), 28.8* (CH₂), 28.4* (CH₂), 21.4 (CH₃), 20.6 (CH₃). ESI-HRMS: *m/z* calculated for C₂₂H₂₄O₃ [M+H]⁺ 337.1798, found 337.1807. RP-HPLC: *t*_R 11.77 min.

8-(4-Methoxy-3,5-dimethylphenyl)-6-methyl-2-(tetrahydro-2H-pyran-4-yl)chroman-4-one (195)

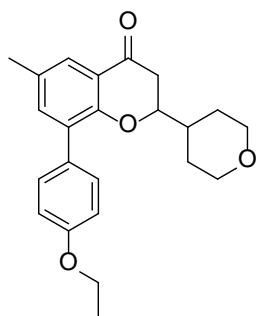


To a degassed solution of 8-bromo-6-methyl-2-(tetrahydro-2H-pyran-4-yl)chroman-4-one (**187**) (50 mg, 0.15 mmol), cesium carbonate (100 mg, 0.31 mmol) and (4-methoxy-3,5-dimethylphenyl)boronic acid (36 mg, 0.20 mmol) in 1,4-dioxane (3 mL) was added palladium (II) acetate (spatula tip), tricyclohexylphosphine (spatula tip), tetra-*n*-butylammonium bromide (spatula tip) and water (0.5 mL). The reaction mixture was heated using microwave irradiation at 150 °C for 30 min. After cooling, the reaction mixture was filtered through celite. The filtrate was concentrated *in vacuo*, the residue dissolved in ethyl acetate (20 mL) and washed with water (10 mL) and saturated aqueous sodium sulfate (10 mL). The organic layer was dried (anhydrous sodium sulfate), filtered and concentrated *in vacuo* to yield a white solid. Purification by column chromatography eluting with 30% ethyl acetate in hexane afforded **195** as a white solid (47 mg, 0.12 mmol, 80%). ¹H NMR (400 MHz, CDCl₃) δ 7.67 - 7.66 (m, 1H, ArH), 7.35 - 7.34 (m, 1H, ArH), 7.17 (s, 2H, ArH), 4.22 - 4.15 (m, 1H, OCH), 4.04 - 3.97 (m, 2H, OCHH, OCHH), 3.77 (s, 3H, OCH₃), 3.43 - 3.33 (m, 2H, OCHH, OCHH), 2.73 - 2.67 (m, 2H, C(O)CH₂), 2.34 (s, 3H, CH₃), 2.32 (s, 6H, CH₃, CH₃), 1.99 - 1.90 (m, 1H, OCH₂CHH), 1.90 - 1.83 (m, 1H, OCH₂CHH), 1.61 - 1.54 (m, 1H, OCHCH), 1.54 - 1.42 (m, 2H, OCH₂CHH, OCH₂CHH). ¹³C NMR (101 MHz, CDCl₃) δ 193.0 (C=O), 156.7 (C), 156.6 (C), 138.0 (CH), 132.4 (C), 130.9 (C), 130.8 (C), 130.5 (C), 130.1 (CH), 125.9 (CH), 121.4 (C), 81.5 (CH), 67.7* (CH₂), 67.5* (CH₂), 59.9 (CH₃), 40.6 (CH₂), 39.9 (CH), 29.1* (CH₂), 28.5* (CH₂), 20.6 (CH₃), 16.2 (CH₃). ESI-HRMS: *m/z* calculated for C₂₄H₂₈O₄ [M+H]⁺ 381.4915, found 381.4918. RP-HPLC: *t*_R 11.46 min.

8-(6-Methoxynaphthalen-2-yl)-6-methyl-2-(tetrahydro-2H-pyran-4-yl)chroman-4-one (196)

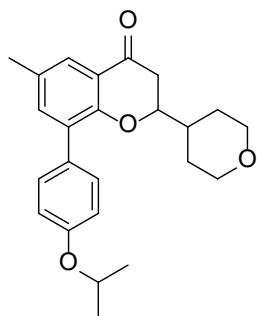


To a degassed solution of 8-bromo-6-methyl-2-(tetrahydro-2H-pyran-4-yl)chroman-4-one (**187**) (40 mg, 0.12 mmol), cesium carbonate (80 mg, 0.25 mmol) and (6-methoxynaphthalen-2-yl)boronic acid (32 mg, 0.16 mmol) in 1,4-dioxane (3 mL) was added palladium (II) acetate (spatula tip), tricyclohexylphosphine (spatula tip), tetra-*n*-butylammonium bromide (spatula tip) and water (0.5 mL). The reaction mixture was heated using microwave irradiation at 150 °C for 30 min. After cooling, the reaction mixture was filtered through celite. The filtrate was concentrated *in vacuo*, the residue dissolved in ethyl acetate (20 mL) and washed with water (10 mL) and saturated aqueous sodium sulfate (10 mL). The organic layer was dried (anhydrous sodium sulfate), filtered and concentrated *in vacuo* to yield a white solid. Purification by column chromatography eluting with 30% ethyl acetate in hexane afforded **196** as a yellow solid (43 mg, 0.11 mmol, 87%). ¹H NMR (400 MHz, CDCl₃) δ 7.88 - 7.88 (m, 1H, ArH), 7.78 - 7.74 (m, 4H, ArH), 7.72 - 7.72 (m, 2H, ArH), 7.62 (dd, *J* = 8.5, 1.7 Hz, 1H, ArH), 4.21 (dd, *J* = 15.4, 7.9 Hz, 1H, OCH), 4.00 - 3.97 (m, 2H, OCHH, OCHH), 3.95 (s, 3H, OCH₃), 3.40 - 3.28 (m, 2H, OCHH, OCHH), 2.74 - 2.72 (m, 2H, C(O)CH₂), 2.37 (s, 3H, CH₃), 1.93 - 1.90 (m, 1H, OCH₂CHH), 1.81 - 1.77 (m, 1H, OCH₂CHH), 1.57 - 1.43 (m, 3H, OCHCH, OCH₂CHH, OCH₂CHH). ¹³C NMR (101 MHz, CDCl₃) δ 193.0 (C=O), 158.1 (C), 156.9 (C), 138.3 (CH), 133.9 (C), 132.4 (C), 131.2 (C), 130.9 (C), 129.7 (CH), 128.9 (C), 128.3 (CH), 128.2 (CH), 126.3 (CH), 126.1 (CH), 121.4 (CH), 119.2 (C), 105.8 (CH), 81.6 (CH), 67.7* (CH₂), 67.5* (CH₂), 55.5 (CH₃), 40.5 (CH₂), 39.8 (CH), 28.9* (CH₂), 28.4* (CH₂), 20.6 (CH₃). ESI-HRMS: *m/z* calculated for C₂₆H₂₆O₄ [M+H]⁺ 403.1904, found 403.1922. RP-HPLC: *t_R* 11.87 min.

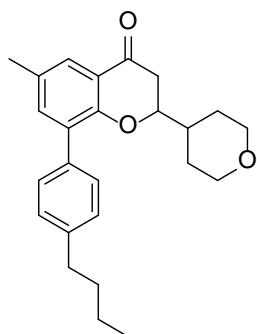
8-(4-Ethoxyphenyl)-6-methyl-2-(tetrahydro-2H-pyran-4-yl)chroman-4-one (197)

To a degassed solution of 8-bromo-6-methyl-2-(tetrahydro-2H-pyran-4-yl)chroman-4-one (**187**) (50 mg, 0.15 mmol), cesium carbonate (100 mg, 0.31 mmol) and (4-ethoxyphenyl)boronic acid (33 mg, 0.20 mmol) in 1,4-dioxane (3 mL) was added palladium (II) acetate (spatula tip), tricyclohexylphosphine (spatula tip), tetra-*n*-butylammonium bromide (spatula tip) and water (0.5 mL). The reaction mixture was heated using microwave irradiation at 150 °C for 30 min. After cooling, the reaction mixture was filtered through celite. The filtrate was concentrated *in vacuo*, the residue dissolved in ethyl acetate (20 mL) and washed with water (10 mL) and saturated aqueous sodium sulfate (10 mL). The organic layer was dried (anhydrous sodium sulfate), filtered and concentrated *in vacuo* to yield a white solid. Purification by column chromatography eluting with 30% ethyl acetate in hexane afforded **197** as a cream solid (41 mg, 0.11 mmol, 73%). ¹H NMR (400 MHz, CDCl₃) δ 7.66 - 7.65 (m, 1H, ArH), 7.45 - 7.41 (m, 2H, ArH), 7.34 - 7.33 (m, 1H, ArH), 6.95 - 6.93 (m, 2H, ArH), 4.19 - 4.13 (m, 1H, OCH), 4.08 (q, *J* = 7.0 Hz, 2H, OCH₂CH₃), 4.02 - 3.97 (m, 2H, OCHH, OCHH), 3.42 - 3.32 (m, 2H, OCHH, OCHH), 2.71 - 2.69 (m, 2H, C(O)CH₂), 2.33 (s, 3H, CH₃), 1.94 - 1.88 (m, 1H, OCH₂CHH), 1.81 - 1.78 (m, 1H, OCH₂CHH), 1.57 - 1.53 (m, 1H, OCHCH), 1.51 - 1.47 (m, 2H, OCH₂CHH, OCH₂CHH), 1.21 (t, *J* = 7.1 Hz, 3H, OCH₂CH₃). ¹³C NMR (101 MHz, CDCl₃) δ 193.1 (C=O), 158.5 (C), 156.7 (C), 137.9 (CH), 130.9 (C), 130.8 (C), 130.6 (C), 129.3 (CH), 125.7 (CH), 121.3 (C), 114.2 (CH), 81.5 (CH), 67.8* (CH₂), 67.6* (CH₂), 63.6 (CH₂), 40.5 (CH₂), 39.8 (CH), 28.9* (CH₂), 28.4* (CH₂), 20.6 (CH₃), 15.0 (CH₃). ESI-HRMS: *m/z* calculated for C₂₃H₂₆O₄ [M+H]⁺ 367.1904, found 367.1920. RP-HPLC: *t*_R 11.71 min.

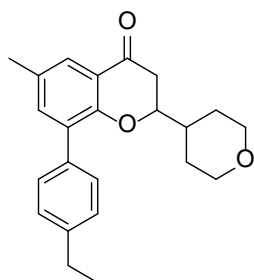
8-(4-Isopropoxyphenyl)-6-methyl-2-(tetrahydro-2H-pyran-4-yl)chroman-4-one
(198)



To a degassed solution of 8-bromo-6-methyl-2-(tetrahydro-2H-pyran-4-yl)chroman-4-one (**187**) (50 mg, 0.15 mmol), cesium carbonate (100 mg, 0.31 mmol) and (4-isopropoxyphenyl)boronic acid (36 mg, 0.20 mmol) in 1,4-dioxane (3 mL) was added palladium (II) acetate (spatula tip), tricyclohexylphosphine (spatula tip), tetra-*n*-butylammonium bromide (spatula tip) and water (0.5 mL). The reaction mixture was heated using microwave irradiation at 150 °C for 30 min. After cooling, the reaction mixture was filtered through celite. The filtrate was concentrated *in vacuo*, the residue dissolved in ethyl acetate (20 mL) and washed with water (10 mL) and saturated aqueous sodium sulfate (10 mL). The organic layer was dried (anhydrous sodium sulfate), filtered and concentrated *in vacuo* to yield a white solid. Purification by column chromatography eluting with 30% ethyl acetate in hexane afforded **198** as a yellow solid (55 mg, 0.14 mmol, 94%). ¹H NMR (400 MHz, CDCl₃) δ 7.66 - 7.65 (m, 1H, ArH), 7.44 - 7.39 (m, 2H, ArH), 7.34 - 7.33 (m, 1H, ArH), 6.95 - 6.90 (m, 2H, ArH), 4.63 - 4.57 (hept, *J* = 6.1 Hz, 1H, OCH(CH₃)₂), 4.22 - 4.11 (m, 1H, OCH), 4.05 - 3.93 (m, 2H, OCH₂H, OCH₂H), 3.44 - 3.30 (m, 2H, OCH₂H, OCH₂H), 2.70 - 2.68 (m, 2H, C(O)CH₂), 2.33 (s, 3H, CH₃), 1.95 - 1.91 (m, 1H, OCH₂CH₂H), 1.82 - 1.78 (m, 1H, OCH₂CH₂H), 1.59 - 1.41 (m, 3H, OCHCH₃, OCH₂CH₂H, OCH₂CH₂H), 1.37 (d, *J* = 4.5 Hz, 6H, CHCH₃, CHCH₃). ¹³C NMR (101 MHz, CDCl₃) δ 193.0 (C=O), 157.4 (C), 156.7 (C), 137.9 (CH), 130.9 (C), 130.7 (C), 130.6 (CH), 129.1 (C), 125.6 (CH), 121.3 (C), 115.4 (CH), 81.5 (CH), 70.0 (CH), 67.7* (CH₂), 67.5* (CH₂), 40.4 (CH₂), 39.7 (CH), 28.8* (CH₂), 28.4* (CH₂), 22.2 (CH₃), 20.6 (CH₃). ESI-HRMS: *m/z* calculated for C₂₄H₂₈O₄ [M+H]⁺ 381.2060, found 381.2078. RP-HPLC: *t*_R 11.81 min.

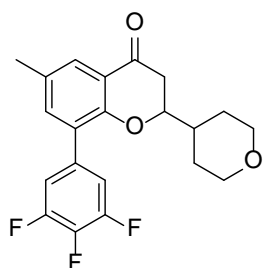
8-(4-Butylphenyl)-6-methyl-2-(tetrahydro-2H-pyran-4-yl)chroman-4-one (199)

To a degassed solution of 8-bromo-6-methyl-2-(tetrahydro-2H-pyran-4-yl)chroman-4-one (**187**) (50 mg, 0.15 mmol), cesium carbonate (100 mg, 0.31 mmol) and (4-butylphenyl)boronic acid (36 mg, 0.20 mmol) in 1,4-dioxane (3 mL) was added palladium (II) acetate (spatula tip), tricyclohexylphosphine (spatula tip), tetra-*n*-butylammonium bromide (spatula tip) and water (0.5 mL). The reaction mixture was heated using microwave irradiation at 150 °C for 30 min. After cooling, the reaction mixture was filtered through celite. The filtrate was concentrated *in vacuo*, the residue dissolved in ethyl acetate (20 mL) and washed with water (10 mL) and saturated aqueous sodium sulfate (10 mL). The organic layer was dried (anhydrous sodium sulfate), filtered and concentrated *in vacuo* to yield a white solid. Purification by column chromatography eluting with 30% ethyl acetate in hexane afforded **199** as a cream solid (42 mg, 0.11 mmol, 72%). ¹H NMR (400 MHz, CDCl₃) δ 7.68 - 7.68 (m, 1H, ArH), 7.43 - 7.41 (m, 2H, ArH), 7.37 - 7.36 (m, 1H, ArH), 7.26 - 7.22 (m, 2H, ArH), 4.20 - 4.15 (m, 1H, OCH), 4.02 - 3.97 (m, 2H, OCHH, OCHH), 3.42 - 3.32 (m, 2H, OCHH, OCHH), 2.71 - 2.69 (m, 2H, C(O)CH₂), 2.66 (t, *J* = 7.6 Hz, 2H, ArCH₂), 2.34 (s, 3H, CH₃), 1.95 - 1.91 (m, 1H, OCH₂CHH), 1.81 - 1.77 (m, 1H, OCH₂CHH), 1.69 - 1.61 (m, 3H, OCHCH, OCH₂CHH, OCH₂CHH), 1.49 - 1.35 (m, 4H, ArCH₂CH₂CH₂CH₃), 0.95 (t, *J* = 7.3 Hz, 3H, ArCH₂CH₂CH₃). ¹³C NMR (101 MHz, CDCl₃) δ 193.0 (C=O), 156.7 (C), 142.3 (C), 138.1 (CH), 134.2 (C), 131.2 (C), 130.7 (C), 129.3 (CH), 128.2 (CH), 125.9 (CH), 121.3 (C), 81.5 (CH), 67.7* (CH₂), 67.5* (CH₂), 40.4 (CH₂), 39.7 (CH), 35.5 (CH₂), 33.7 (CH₂), 28.8* (CH₂), 28.4* (CH₂), 22.5 (CH₂), 20.6 (CH₃), 14.1 (CH₃). ESI-HRMS: *m/z* calculated for C₂₅H₃₀O₃ [M+H]⁺ 379.2268, found 379.2286. RP-HPLC: *t*_R 13.47 min.

8-(4-Ethylphenyl)-6-methyl-2-(tetrahydro-2H-pyran-4-yl)chroman-4-one (200)

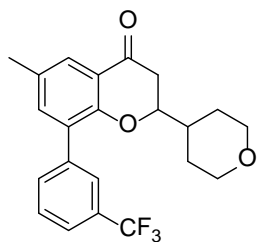
To a degassed solution of 8-bromo-6-methyl-2-(tetrahydro-2H-pyran-4-yl)chroman-4-one (**187**) (50 mg, 0.15 mmol), cesium carbonate (100 mg, 0.31 mmol) and (4-ethylphenyl)boronic acid (30 mg, 0.20 mmol) in 1,4-dioxane (3 mL) was added palladium (II) acetate (spatula tip), tricyclohexylphosphine (spatula tip), tetra-*n*-butylammonium bromide (spatula tip) and water (0.5 mL). The reaction mixture was heated using microwave irradiation at 150 °C for 30 min. After cooling, the reaction mixture was filtered through celite. The filtrate was concentrated *in vacuo*, the residue dissolved in ethyl acetate (20 mL) and washed with water (10 mL) and saturated aqueous sodium sulfate (10 mL). The organic layer was dried (anhydrous sodium sulfate), filtered and concentrated *in vacuo* to yield a white solid. Purification by column chromatography eluting with 30% ethyl acetate in hexane afforded **200** as a white solid (47 mg, 0.11 mmol, 87%). ¹H NMR (400 MHz, CDCl₃) δ 7.69 - 7.68 (m, 1H, ArH), 7.45 - 7.42 (m, 2H, ArH), 7.37 - 7.36 (m, 1H, ArH), 7.26 - 7.24 (m, 2H, ArH), 4.21 - 4.17 (m, 1H, OCH), 4.02 - 3.98 (m, 2H, OCHH, OCHH), 3.42 - 3.33 (m, 2H, OCHH, OCHH), 2.74 - 2.67 (m, 5H, C(O)CH₂, ArCH₂CH₃, OCHCH), 2.34 (s, 3H, CH₃), 1.95 - 1.90 (m, 1H, OCH₂CHH), 1.82 - 1.78 (m, 1H, OCH₂CHH), 1.56 - 1.54 (m, 2H, OCH₂CHH, OCH₂CHH), 1.29 (t, *J* = 10.8 Hz, 3H, ArCH₂CH₃). ¹³C NMR (101 MHz, CDCl₃) δ 193.1 (C=O), 156.8 (C), 143.7 (C), 138.2 (CH), 134.3 (C), 131.2 (C), 130.8 (C), 129.4 (CH), 127.7 (CH), 126.0 (CH), 121.4 (C), 81.5 (CH), 67.8* (CH₂), 67.6* (CH₂), 40.4 (CH₂), 39.7 (CH), 28.9* (CH₂), 28.7* (CH₂), 28.4 (CH₂), 20.6 (CH₃), 15.6 (CH₃). ESI-HRMS: *m/z* calculated for C₂₃H₂₆O₃ [M+H]⁺ 351.1955, found 351.1953. RP-HPLC: *t*_R 12.28 min.

6-Methyl-2-(tetrahydro-2H-pyran-4-yl)-8-(3,4,5-trifluorophenyl)chroman-4-one
(201)



To a degassed solution of 8-bromo-6-methyl-2-(tetrahydro-2H-pyran-4-yl)chroman-4-one (**187**) (50 mg, 0.15 mmol), cesium carbonate (100 mg, 0.31 mmol) and (3,4,5-trifluorophenyl)boronic acid (35 mg, 0.20 mmol) in 1,4-dioxane (3 mL) was added palladium (II) acetate (spatula tip), tricyclohexylphosphine (spatula tip), tetra-*n*-butylammonium bromide (spatula tip) and water (0.5 mL). The reaction mixture was heated using microwave irradiation at 150 °C for 30 min. After cooling, the reaction mixture was filtered through celite. The filtrate was concentrated *in vacuo*, the residue dissolved in ethyl acetate (20 mL) and washed with water (10 mL) and saturated aqueous sodium sulfate (10 mL). The organic layer was dried (anhydrous sodium sulfate), filtered and concentrated *in vacuo* to yield a white solid. Purification by column chromatography eluting with 30% ethyl acetate in hexane afforded **201** as a white solid (28 mg, 0.08 mmol, 48%). ¹H NMR (400 MHz, CDCl₃) δ 7.74 - 7.73 (m, 1H, ArH), 7.30 - 7.29 (m, 1H, ArH), 7.16 - 7.12 (m, 2H, ArH), 4.21 - 4.16 (m, 1H, OCH), 4.03 - 4.00 (m, 2H, OCHH, OCHH), 3.39 (qd, *J* = 11.7, 2.3 Hz, 2H, OCHH, OCHH), 2.75 - 2.68 (m, 2H, C(O)CH₂), 2.35 (s, 3H, CH₃), 1.97 - 1.91 (m, 1H, OCH₂CHH), 1.76 - 1.73 (m, 1H, OCH₂CHH), 1.59 - 1.55 (m, 1H, OCHCH), 1.55 - 1.42 (m, 2H, OCH₂CHH, OCH₂CHH). ¹³C NMR (101 MHz, CDCl₃) δ 192.3 (C=O), 156.3 (C), 151.0 (ddd, *J* = 249, 10, 4 Hz, CFCFC), 139.3 (dt, *J* = 252, 15 Hz, CFCFC), 137.5 (CH), 133.0 (dd, *J* = 8, 3 Hz, C), 131.2 (C), 128.1 (C), 127.4 (CH), 121.6 (C), 113.7 (dd, *J* = 16, 6 Hz, CFCH), 81.9 (CH), 67.6* (CH₂), 67.5* (CH₂), 40.4 (CH₂), 39.7 (CH), 28.9* (CH₂), 28.4* (CH₂), 20.5 (CH₃). ESI-HRMS: *m/z* calculated for C₂₁H₁₉F₃O₃ [M+H]⁺ 377.1360, found 377.1359. RP-HPLC: *t_R* 11.56 min.

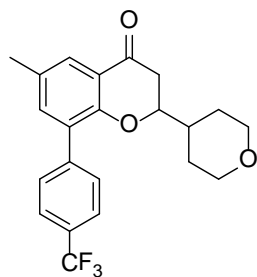
6-Methyl-2-(tetrahydro-2H-pyran-4-yl)-8-(3-(trifluoromethyl)phenyl)-chroman-4-one (202)



To a degassed solution of 8-bromo-6-methyl-2-(tetrahydro-2H-pyran-4-yl)chroman-4-one (**187**) (50 mg, 0.15 mmol), cesium carbonate (100 mg, 0.31 mmol) and (3-(trifluoromethyl)phenyl)boronic acid (38 mg, 0.20 mmol) in 1,4-dioxane (3 mL) was added palladium (II) acetate (spatula tip), tricyclohexylphosphine (spatula tip), tetra-*n*-butylammonium bromide (spatula tip) and water (0.5 mL). The reaction mixture was heated using microwave irradiation at 150 °C for 30 min. After cooling, the reaction mixture was filtered through celite. The filtrate was concentrated *in vacuo*, the residue dissolved in ethyl acetate (20 mL) and washed with water (10 mL) and saturated aqueous sodium sulfate (10 mL). The organic layer was dried (anhydrous sodium sulfate), filtered and concentrated *in vacuo* to yield a white solid. Purification by column chromatography eluting with 30% ethyl acetate in hexane afforded **202** as a cream solid (45 mg, 0.12 mmol, 75%). ¹H NMR (400 MHz, CDCl₃) δ 7.82 (s, 1H, ArH), 7.74 - 7.74 (m, 1H, ArH), 7.67 - 7.65 (m, 1H, ArH), 7.62 - 7.60 (m, 1H, ArH), 7.56 - 7.53 (m, 1H, ArH), 7.37 - 7.37 (m, 1H, ArH), 4.23 - 4.17 (m, 1H, OCH), 4.02 - 3.96 (m, 2H, OCHH, OCHH), 3.41 - 3.31 (m, 2H, OCHH, OCHH), 2.73 - 2.70 (m, 2H, C(O)CH₂), 2.36 (s, 3H, CH₃), 1.96 - 1.89 (m, 1H, OCH₂CHH), 1.77 - 1.72 (m, 1H, OCH₂CHH), 1.59 - 1.52 (m, 1H, OCHCH), 1.51 - 1.37 (m, 2H, OCH₂CHH, OCH₂CHH). ¹³C NMR (101 MHz, CDCl₃) δ 192.6 (C=O), 156.5 (C), 137.82 (CH), 137.81 (CH), 132.6 (C), 131.1 (C), 130.5 (q, *J* = 32 Hz, CCF₃), 129.6 (C), 128.8 (CH), 127.1 (CH), 126.6 (q, *J* = 4 Hz, CCCF₃), 124.31 (q, *J* = 273 Hz, CF₃), 124.30 (q, *J* = 4 Hz, CCCF₃), 121.5 (C), 81.7 (CH), 67.6* (CH₂), 67.5* (CH₂), 40.5 (CH₂), 39.9 (CH),

28.8* (CH₂), 28.3* (CH₂), 20.6 (CH₃). ESI-HRMS: m/z calculated for C₂₂H₂₁F₃O₃ [M+H]⁺ 391.1516, found 391.1518. RP-HPLC: t_R 11.72 min.

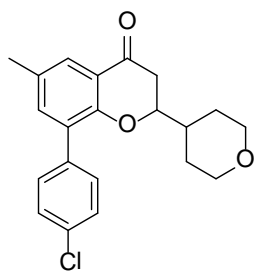
6-Methyl-2-(tetrahydro-2H-pyran-4-yl)-8-(4-(trifluoromethyl)phenyl)-chroman-4-one (203)



To a degassed solution of 8-bromo-6-methyl-2-(tetrahydro-2H-pyran-4-yl)chroman-4-one (**187**) (50 mg, 0.15 mmol), cesium carbonate (100 mg, 0.31 mmol) and 4-(trifluoromethyl)phenylboronic acid (38 mg, 0.20 mmol) in 1,4-dioxane (3 mL) was added palladium (II) acetate (spatula tip), tricyclohexylphosphine (spatula tip), tetra-*n*-butylammonium bromide (spatula tip) and water (0.5 mL). The reaction mixture was heated using microwave irradiation at 150 °C for 30 min. After cooling, the reaction mixture was filtered through celite. The filtrate was concentrated *in vacuo*, the residue dissolved in ethyl acetate (20 mL) and washed with water (10 mL) and saturated aqueous sodium sulfate (10 mL). The organic layer was dried (anhydrous sodium sulfate), filtered and concentrated *in vacuo* to yield a white solid. Purification by column chromatography eluting with 30% ethyl acetate in hexane afforded **203** as a cream solid (56 mg, 0.14 mmol, 93%). ¹H NMR (400 MHz, CDCl₃) δ 7.75 - 7.75 (m, 1H, ArH), 7.69 - 7.67 (m, 2H, ArH), 7.63 - 7.61 (m, 2H, ArH), 7.36 - 7.35 (m, 1H, ArH), 4.23 - 4.17 (m, 1H, OCH), 4.03 - 3.98 (m, 2H, OCHH, OCHH), 3.42 - 3.32 (m, 2H, OCHH, OCHH), 2.74 - 2.72 (m, 2H, C(O)CH₂), 2.36 (s, 3H, CH₃), 1.97 - 1.89 (m, 1H, OCH₂CHH), 1.74 - 1.70 (m, OCH₂CHH), 1.57 - 1.54 (m, 1H, OCHCH), 1.50 - 1.38 (m, 2H, OCH₂CHH, OCH₂CHH). ¹³C NMR (101 MHz, CDCl₃) δ 192.6 (C=O), 156.5 (C), 140.8 (C), 138.0 (CH), 131.1 (CH), 129.8 (C), 129.7 (q, *J* = 33 Hz, CCF₃), 129.5 (C), 127.2 (CH), 125.1 (q, *J* = 4 Hz, CCF₃), 124.4 (q, *J* = 272 Hz, CF₃), 121.1 (C),

81.8 (CH), 67.7* (CH₂), 67.5* (CH₂), 40.4 (CH₂), 39.7 (CH), 28.8* (CH₂), 28.4* (CH₂), 20.6 (CH₃). ESI-HRMS: m/z calculated for C₂₂H₂₁F₃O₃ [M+H]⁺ 391.1516, found 391.1511. RP-HPLC: t_R 12.04 min.

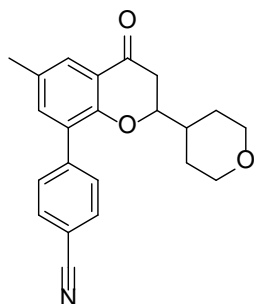
8-(4-Chlorophenyl)-6-methyl-2-(tetrahydro-2H-pyran-4-yl)chroman-4-one (**204**)



To a degassed solution of 8-bromo-6-methyl-2-(tetrahydro-2H-pyran-4-yl)chroman-4-one (**187**) (50 mg, 0.15 mmol), cesium carbonate (100 mg, 0.31 mmol) and (4-chlorophenyl)boronic acid (31 mg, 0.20 mmol) in 1,4-dioxane (3 mL) was added palladium (II) acetate (spatula tip), tricyclohexylphosphine (spatula tip), tetra-*n*-butylammonium bromide (spatula tip) and water (0.5 mL). The reaction mixture was heated using microwave irradiation at 150 °C for 30 min. After cooling, the reaction mixture was filtered through celite. The filtrate was concentrated *in vacuo*, the residue dissolved in ethyl acetate (20 mL) and washed with water (10 mL) and saturated aqueous sodium sulfate (10 mL). The organic layer was dried (anhydrous sodium sulfate), filtered and concentrated *in vacuo* to yield a white solid. Purification by column chromatography eluting with 30% ethyl acetate in hexane afforded **204** as a cream solid (49 mg, 0.14 mmol, 89%). ¹H NMR (400 MHz, CDCl₃) δ 7.72 - 7.71 (m, 1H, ArH), 7.46 - 7.38 (m, 4H, ArH), 7.33 - 7.32 (m, 1H, ArH), 4.18 (dd, *J* = 15.2, 7.9 Hz, 1H, OCH), 4.03 - 3.99 (m, 2H, OCHH, OCHH), 3.42 - 3.33 (m, 2H, OCHH, OCHH), 2.72 - 2.70 (m, 2H, C(O)CH₂), 2.35 (s, 3H, CH₃), 1.94 - 1.90 (m, 1H, OCH₂CHH), 1.77 - 1.72 (m, 1H, OCH₂CHH), 1.58 - 1.56 (m, 1H, OCHCH), 1.50 - 1.41 (m, 2H, OCH₂CHH, OCH₂CHH). ¹³C NMR (101 MHz, CDCl₃) δ 192.8 (C=O), 156.5 (C), 137.9 (CH), 135.5 (C), 133.6 (C), 131.0 (C), 130.8 (CH), 130.0 (C), 128.4 (CH), 126.6 (CH), 121.4 (C), 81.7 (CH), 67.7* (CH₂), 67.5* (CH₂), 40.4 (CH₂), 39.7 (CH), 28.8* (CH₂), 28.4* (CH₂),

20.6 (CH₃). ESI-HRMS: m/z calculated for C₂₁H₂₁ClO₃ [M+H]⁺ 357.1252, found 357.1264. RP-HPLC: t_R 11.93 min.

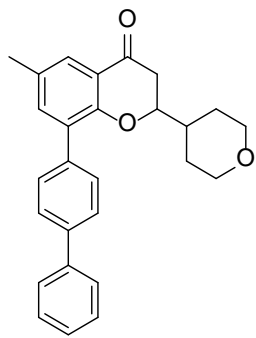
4-(6-Methyl-4-oxo-2-(tetrahydro-2H-pyran-4-yl)chroman-8-yl)benzonitrile (**205**)



To a degassed solution of 8-bromo-6-methyl-2-(tetrahydro-2H-pyran-4-yl)chroman-4-one (**187**) (50 mg, 0.15 mmol), cesium carbonate (100 mg, 0.31 mmol) and (4-cyanophenyl)boronic acid (24 mg, 0.20 mmol) in 1,4-dioxane (3 mL) was added palladium (II) acetate (spatula tip), tricyclohexylphosphine (spatula tip), tetra-*n*-butylammonium bromide (spatula tip) and water (0.5 mL). The reaction mixture was heated using microwave irradiation at 150 °C for 30 min. After cooling, the reaction mixture was filtered through celite. The filtrate was concentrated *in vacuo*, the residue dissolved in ethyl acetate (20 mL) and washed with water (10 mL) and saturated aqueous sodium sulfate (10 mL). The organic layer was dried (anhydrous sodium sulfate), filtered and concentrated *in vacuo* to yield a white solid. Purification by column chromatography eluting with 30% ethyl acetate in hexane afforded **205** as a yellow solid (49 mg, 0.14 mmol, 92%). ¹H NMR (400 MHz, CDCl₃) δ 7.75 - 7.74 (m, 1H, ArH), 7.74 - 7.69 (m, 3H, ArH), 7.62 - 7.60 (m, 2H, ArH), 4.19 (dd, *J* = 15.2, 7.8 Hz, 1H, OCH), 4.01 - 3.98 (m, 2H, OCHH, OCHH), 3.41 - 3.32 (m, 2H, OCHH, OCHH), 2.73 - 2.71 (m, 2H, C(O)CH₂), 2.35 (s, 3H, CH₃), 1.94 - 1.90 (m, 1H, OCH₂CHH), 1.71 - 1.67 (m, 1H, OCH₂CHH), 1.56 - 1.52 (m, 1H, OCHCH), 1.47 - 1.39 (m, 2H, OCH₂CHH, OCH₂CHH). ¹³C NMR (101 MHz, CDCl₃) δ 192.4 (C=O), 156.4 (CN), 141.9 (C), 137.7 (CH), 131.9 (CH), 131.2 (C), 130.2 (CH), 129.2 (C), 127.5 (CH), 121.5 (C), 118.9 (C), 111.3 (C), 81.8 (CH), 67.6* (CH₂), 67.4* (CH₂), 40.3

(CH₂), 39.6(CH), 28.7* (CH₂), 28.3* (CH₂), 20.5 (CH₃). ESI-HRMS: *m/z* calculated for C₂₂H₂₁NO₃ [M+H]⁺ 348.1594, found 348.1611. RP-HPLC: *t*_R 10.72 min.

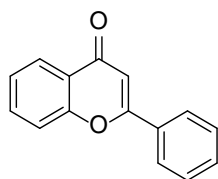
8-([1,1'-Biphenyl]-4-yl)-6-methyl-2-(tetrahydro-2*H*-pyran-4-yl)chroman-4-one
(206)



To a degassed solution of 8-bromo-6-methyl-2-(tetrahydro-2*H*-pyran-4-yl)chroman-4-one (**187**) (40 mg, 0.12 mmol), cesium carbonate (80 mg, 0.25 mmol) and [1,1'-biphenyl]-4-ylboronic acid (32 mg, 0.16 mmol) in 1,4-dioxane (3 mL) was added palladium (II) acetate (spatula tip), tricyclohexylphosphine (spatula tip), tetra-*n*-butylammonium bromide (spatula tip) and water (0.5 mL). The reaction mixture was heated using microwave irradiation at 150 °C for 30 min. After cooling, the reaction mixture was filtered through celite. The filtrate was concentrated *in vacuo*, the residue dissolved in ethyl acetate (20 mL) and washed with water (10 mL) and saturated aqueous sodium sulfate (10 mL). The organic layer was dried (anhydrous sodium sulfate), filtered and concentrated *in vacuo* to yield a white solid. Purification by column chromatography eluting with 30% ethyl acetate in hexane afforded **206** as a white solid (41 mg, 0.10 mmol, 84%). ¹H NMR (400 MHz, CDCl₃) δ 7.72 - 7.71 (m, 1H, ArH), 7.67 - 7.64 (m, 4H, ArH), 7.60 - 7.58 (m, 2H, ArH), 7.47 - 7.44 (m, 2H, ArH), 7.41 - 7.41 (m, 1H, ArH), 7.37 - 7.34 (m, 1H, ArH), 4.20 (dd, *J* = 15.4, 7.8 Hz, 1H, OCH), 4.02 - 3.97 (m, 2H, OCHH, OCHH), 3.41 - 3.31 (m, 2H, OCHH, OCHH), 2.72 - 2.70 (m, 2H, C(O)CH₂), 2.35 (s, 3H, CH₃), 1.98 - 1.89 (m, 1H, OCH₂CHH), 1.83 - 1.79 (m, 1H, OCH₂CHH), 1.57 - 1.54 (m, 1H, OCHCH), 1.48 - 1.45 (m, 2H, OCH₂CHH, OCH₂CHH). ¹³C NMR (101 MHz, CDCl₃) δ 192.8 (C=O), 156.7 (C), 140.7 (C), 140.3 (C), 138.0 (CH), 136.0 (C), 130.8 (C), 130.7 (C), 129.9 (CH), 128.9 (CH), 127.5 (CH), 127.1 (CH), 126.8 (CH), 126.3 (CH), 121.4 (C), 81.6 (CH), 67.7* (CH₂),

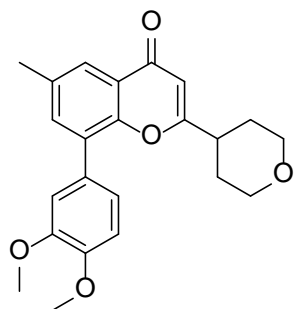
67.5* (CH₂), 40.4 (CH₂), 39.7 (CH), 28.8* (CH₂), 28.4* (CH₂), 20.5 (CH₃). ESI-HRMS: m/z calculated for C₂₇H₂₆O₃ [M+H]⁺ 399.1955, found 399.1973. RP-HPLC: t_R 12.24 min.

2-Phenyl-4*H*-chromen-4-one (207)

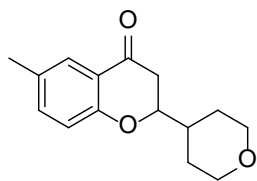


A solution of 2-phenylchroman-4-one (flavanone) (200 mg, 0.89 mmol) and iodine (226 mg, 0.89 mmol) in anhydrous pyridine (10 mL) was stirred at 90 °C for 3 h. The reaction mixture was poured into water (50 mL) and extracted with ethyl acetate (3 × 20 mL). The combined organic layers were washed with saturated aqueous sodium thiosulfate (20 mL) and water (20 mL). The organic layer was dried (anhydrous sodium sulfate), filtered and concentrated *in vacuo* to give a cream solid which was recrystallised from ethanol to afford **207** as white needles (112 mg, 0.50 mmol, 57%). ¹H NMR (400 MHz, CDCl₃) δ 8.20 - 8.19 (m, 1H, ArH), 7.92 - 7.88 (m, 2H, ArH), 7.66 - 7.65 (m, 1H, ArH), 7.53 - 7.49 (m, 4H, ArH), 7.39 - 7.37 (m, 1H, ArH), 6.78 (s, 1H, C(O)CH). ¹³C NMR (101 MHz, CDCl₃) δ 178.3 (C=O), 163.3 (C), 156.2 (C), 133.7 (CH), 131.61 (C), 131.60 (CH), 129.0 (CH), 126.2 (CH), 125.6 (CH), 125.2 (CH), 123.9 (C), 118.0 (CH), 107.5 (CH). ESI-MS: m/z 223.2 [M+H]⁺. RP-HPLC: t_R 10.61 min.

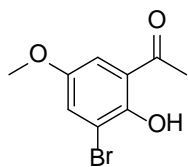
8-(3,4-Dimethoxyphenyl)-6-methyl-2-(tetrahydro-2H-pyran-4-yl)-4H-chromen-4-one (208)



A solution of 8-(3,4-dimethoxyphenyl)-6-methyl-2-(tetrahydro-2H-pyran-4-yl)chroman-4-one (**190**) (100 mg, 0.26 mmol) and iodine (66 mg, 0.26 mmol) in anhydrous pyridine (8 mL) was stirred at 90 °C for 16 h. The reaction mixture was poured into water (50 mL) and extracted with ethyl acetate (3 × 20 mL). The combined organic layers were washed with saturated aqueous sodium thiosulfate (20 mL) and water (20 mL). The organic layer was dried (anhydrous sodium sulfate), filtered and concentrated *in vacuo* to give a yellow solid. Purification by column chromatography eluting with 15% ethyl acetate in hexane afforded **208** as a yellow solid (22 mg, 0.06 mmol, 22%). ¹H NMR (400 MHz, CDCl₃) δ 7.95 - 7.94 (m, 1H, ArH), 7.49 - 7.45 (m, 1H, ArH), 7.10 - 7.03 (m, 2H, ArH), 7.00 - 6.96 (m, 1H, ArH), 6.20 (s, 1H, C(O)CH), 4.04 - 4.00 (m, 2H, OCHH, OCHH), 3.95 (s, 3H, OCH₃), 3.92 (s, 3H, OCH₃), 3.44 - 3.41 (m, 2H, OCHH, OCHH), 2.78 - 2.70 (m, 1H, OCH₂CH₂CH), 3.26 (s, 3H, CH₃), 1.85 - 1.71 (m, 4H, OCH₂CH₂, OCH₂CH₂). ¹³C NMR (101 MHz, CDCl₃) δ 178.8 (C=O), 170.9 (C), 151.7 (C), 149.10 (C), 148.8 (C), 135.9 (CH), 134.9 (CH), 131.3 (C), 128.9 (C), 124.1 (CH), 122.2 (CH), 112.9 (C), 111.2 (C), 108.1 (CH), 67.4 (CH₃), 56.1 (CH₃), 40.0 (CH₂), 30.0 (CH₂), 21.0 (CH₃). ESI-HRMS: *m/z* calculated for C₂₃H₂₄O₅ [M+H]⁺ 381.1697, found 381.1714. RP-HPLC: *t*_R 10.29 min.

6-Methyl-2-(tetrahydro-2H-pyran-4-yl)chroman-4-one (209)

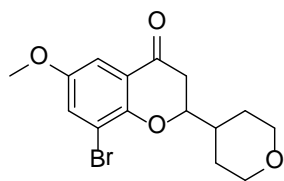
A solution of 1-(2-hydroxy-5-methylphenyl)ethanone (100 mg, 0.67 mmol) and tetrahydro-2H-pyran-4-carbaldehyde (84 mg, 0.73 mmol) and piperidine (113 mg, 1.33 mmol) in ethanol (20 mL) was stirred at 78 °C for 48 h. The reaction mixture was concentrated *in vacuo*. The residue was dissolved in ethyl acetate (40 mL) and washed with 1 M aqueous hydrochloric acid (15 mL) and saturated aqueous sodium chloride (15 mL). The organic layer was dried (anhydrous sodium sulfate), filtered and concentrated *in vacuo* to give a yellow solid. Purification by column chromatography eluting with 40% ethyl acetate in hexane afforded **209** as a yellow solid (63 mg, 0.25 mmol, 38%). ¹H NMR (400 MHz, CDCl₃) δ 7.65 (s, 1H, ArH), 7.29 - 7.26 (m, 1H, ArH), 6.86 (d, *J* = 8.4 Hz, 1H, ArH), 4.22 - 4.13 (m, 1H, OCH), 4.04 (d, *J* = 11.7 Hz, 2H, OCHH, OCHH), 3.46 - 3.36 (m, 2H, OCHH, OCHH), 2.70 - 2.64 (m, 2H, C(O)CH₂), 2.29 (s, 3H, CH₃), 1.95 (ddd, *J* = 11.1, 7.3, 3.4 Hz, 1H, OCH₂CHH), 1.89 (d, *J* = 13.3 Hz, 1H, OCH₂CHH), 1.60 - 1.50 (m, 3H, OCHCH, OCH₂CHH, OCH₂CHH). ¹³C NMR (101 MHz, CDCl₃) δ 192.7 (C=O), 159.7 (C), 137.2 (CH), 130.8 (C), 126.6 (C), 120.7 (CH), 117.7 (CH), 81.2 (CH), 67.7* (CH₂), 67.5* (CH₂), 40.2 (CH₂), 39.3 (CH), 28.5* (CH₂), 28.2* (CH₂), 20.5 (CH₃). ESI-HRMS: *m/z* calculated for C₁₅H₁₈O₃ [M+H]⁺ 247.1329, found 247.1321. RP-HPLC: *t*_R 8.77 min.

1-(2-Hydroxy-5-methoxyphenyl)ethanone (211)

To a stirring solution of 1-(2-hydroxy-5-methoxyphenyl)ethanone (2.00 g, 12.0 mmol) and sodium acetate (1.09 g, 13.2 mmol) in glacial acetic acid (20 mL) at 0 °C was added in a drop-wise manner a solution of bromine (2.12 g, 13.2 mmol) in glacial acetic acid (5 mL). Stirring was continued at

room temperature for 16 h and further portions of bromine (2.12 g, 13.2 mmol) and sodium acetate (1.09 g, 13.2 mmol) were added. Stirring was continued at room temperature for 2 h. The reaction mixture was poured onto ice and the resulting precipitate was filtered. Recrystallisation of the precipitate from ethanol afforded **211** as yellow needles (2.61 g, 10.7 mmol, 88%). ^1H NMR (400 MHz, CDCl_3) δ 7.73 - 7.59 (m, 1H, ArH), 7.19 - 7.17 (m, 1H, ArH), 3.79 (s, 3H, OCH₃), 2.63 (s, 3H, COCH₃). ESI-MS: m/z 246.1 $[\text{M}+\text{H}]^+$. RP-HPLC: t_R 9.41 min. M.p. 77 - 78 °C (lit.³⁴⁸ M.p. 76 - 78 °C).

8-Bromo-6-methoxy-2-(tetrahydro-2H-pyran-4-yl)chroman-4-one (**212**)



A solution of 1-(3-bromo-2-hydroxy-5-methoxyphenyl)ethanone (**211**) (1.00 g, 4.08 mmol), tetrahydro-2H-pyran-4-carbaldehyde (0.47 g, 4.08 mmol) and sodium tetraborate (3.11 g, 8.16 mmol) in ethanol/water (5:3, 32 mL) was stirred at 78 °C for 48 h. The reaction mixture was concentrated *in vacuo*. The crude material was dissolved in ethyl acetate (80 mL), and washed with 1 M aqueous hydrochloric acid (30 mL) and saturated aqueous sodium chloride (30 mL). The organic layer was dried (anhydrous sodium sulfate), filtered and concentrated *in vacuo* to afford **212** as a yellow oil (0.31 g, 0.91 mmol, 22%). ^1H NMR (400 MHz, CDCl_3) δ 7.37 (d, J = 3.1 Hz, 1H, ArH), 7.30 (d, J = 3.1 Hz, 1H, ArH), 4.25 - 4.19 (m, 1H, OCH), 4.11 - 4.02 (m, 2H, OCHH, OCHH), 3.79 (s, 3H, OCH₃), 3.49 - 3.38 (m, 2H, OCHH, OCHH), 2.75 - 2.70 (m, 2H, C(O)CH₂), 2.08 - 1.97 (m, 2H, OCH₂CHH, OCH₂CHH), 1.62 - 1.56 (m, 3H, OCH₂CHH, OCH₂CHH, OCHCH). ^{13}C NMR (101 MHz, CDCl_3) δ 191.9 (C=O), 154.1 (C), 152.8 (CH), 127.9 (C), 121.8 (CH), 112.6 (C), 107.9 (C), 82.1 (CH), 67.8* (CH₂), 67.5*

(CH₂), 56.2 (CH₃), 40.1 (CH₂), 39.4 (CH), 28.8* (CH₂), 28.4* (CH₂). ESI-HRMS: m/z calculated for C₁₅H₁₇BrO₄ [M+H]⁺ 341.0383, found 341.0393. RP-HPLC: t_R 10.28 min.

7.3 Biological assay general experimental

7.3.1 *Plasmodium falciparum* growth inhibition assay

Malstat reagent was prepared by combining 0.1 M Tris (pH 9.0) (50 mL), lactic acid (1.00 g) and Triton X-100 (100 μ L). The pH of the solution was adjusted (with aqueous sodium hydroxide) to 7.4. Acetylpyridine adenine dinucleotide (50 mg) was added to the solution, which was sealed and inverted several times to obtain a mixed solution. Malstat agent was stored at 4 °C and used with 14 days of preparation. Nitroblue reagent was prepared by dissolving nitroblue tetrazolium in water (2 mg/mL). The solution was stored at -14 °C and shielded from light. PES was prepared by dissolving phenazine ethosulfate in water (0.1 mg/mL). The solution was stored at -14 °C.

Into each well of 96-well, U-bottom assay plate was dispensed 100 μ L of red blood cell/parasite mixture (0.1% parasitaemia). Into each well was added test compound or vehicle (DMSO) (0.2 μ L). Well solutions were mixed thoroughly. Plates were incubated at 37 °C for 72 h in an atmosphere of 5% CO₂, 5% O₂, 95% N₂. Plates were then frozen at -70 °C overnight and then thawed at room temperature for 4-5 h.

To evaluate LDH activity, 75 μ L of LDH assay reagent (containing 10:1:1 of Malstat reagent/nitroblue reagent/PES) was dispensed into the wells of a 96-well plate (flat-bottom). To each well was added a 30 μ L aliquot of the corresponding parasite-drug solution described above. The 96-well plates were protected from light and incubated at

room temperature for 45 min. The absorbance of each well was then measured at 650 nm using a Thermo Scientific Multiskan Go plate reader operated by Thermo Scientific Skanit Software v3.2.

Data were analysed using GraphPad Prism v5.0 software.

7.3.2 Human phosphodiesterase inhibition assays

BPS Bioscience assays

The human phosphodiesterase inhibition assays of compounds **99** and **105** were conducted externally under contract by BPS Bioscience, SanDiego.

Compound dilutions ten-fold higher than test concentration were prepared with 10% DMSO in assay buffer and 5 µl of the dilution was added to a 50 µl reaction so that the final concentration of DMSO is 1% in all of reactions. The enzymatic reactions were conducted at rt for 60 min in a 50 µl mixture containing PDE assay buffer, 100 nM FAM-cAMP, or 100 nM FAM-cGMP, a PDE enzyme and the test compound. After the enzymatic reaction, 100 µl of a binding solution (1:100 dilution of the binding agent with the binding agent diluent) was added to each reaction and the reaction was performed at rt for 60 min. Fluorescence intensity was measured at an excitation of 485 nm and an emission of 528 nm using a Tecan Infinite M1000 microplate reader.

PDE activity assays were performed in duplicate at each concentration. Fluorescence intensity is converted to fluorescence polarisation using the Tecan Magellan6 software. The fluorescence polarisation data were analysed using the computer software, GraphPad Prism. The fluorescence polarisation (FP_t) in absence of the compound in

each data set was defined as 100% activity. In the absence of PDE and the compound, the value of fluorescent polarisation (FP_b) in each data set was defined as 0% activity. Some of the compounds emit fluorescence under the assay conditions; the FP value in absence of PDE only was subtracted from that in presence of PDE enzyme. The percent activity in the presence of the compound was calculated according to the following equation: % activity = (FP-FP_b)/(FP_t-FP_b)×100%, where FP= the fluorescence polarisation in the presence of the compound.

Scottish Biomedical assays

Performed a fluorescence polarisation assay (described above). All assays were performed in a 3% final concentration of DMSO. All compounds were tested at a concentration of 1 µM in duplicate and inhibitor potency was calculated as an average of the two data points. The data generated was analysed using GraphPad Prism software.

Chapter 8

References

1. Greenwood, B. M.; Bojang, K.; Whitty, C. J. M.; Targett, G. A. T., Malaria. *Lancet* **2005**, *365*, 1487-1498.
2. Sherman, I. W., Malaria. John Wiley & Sons, Ltd: **2001**.
3. Cox-Singh, J.; Davis, T. M. E.; Lee, K.-S.; Shamsul, S. S. G.; Matusop, A.; Ratnam, S.; Rahman, H. A.; Conway, D. J.; Singh, B., *Plasmodium knowlesi* malaria in humans is widely distributed and potentially life threatening. *Clin. Infect. Dis.* **2008**, *46*, 165-171.
4. Bray, R. S.; Garnham, P. C., The life-cycle of primate malaria parasites. *Br. Med. Bull.* **1982**, *38*, 117-122.
5. Peterson, I.; Eastman, R.; Lanzer, M., Drug-resistant malaria: Molecular mechanisms and implications for public health. *FEBS Lett.* **2011**, *585*, 1551-1562.
6. Hay, S.; Guerra, C.; Tatem, A.; Noor, A.; Snow, R., The global distribution and population at risk of malaria: Past, present and future. *Lancet Infect. Dis.* **2004**, *4*, 327-336.

7. Mendis, K.; Rietveld, A.; Warsame, M.; Bosman, A.; Greenwood, B.; Wernsdorfer, W. H., From malaria control to eradication: The WHO perspective. *Trop. Med. Int. Health.* **2009**, *14*, 1-7.
8. Greenwood, B.; Mutabingwa, T., Malaria in 2002. *Nature* **2002**, *415*, 670-672.
9. Beard, J., DDT and human health. *Sci. Total Environ.* **2006**, *355*, 78-89.
10. Seagren, E. A., DDT, human health, and the environment. *J. Environ. Eng.* **2005**, *131*, 1617-1619.
11. WHO *World Malaria Report 2011*; **2011**.
12. Trampuz, A.; Jereb, M.; Muzlovic, I.; Prabhu, R. M., Clinical review: Severe malaria. *Crit. Care* **2003**, *7*, 315-323.
13. White, N. J., *Plasmodium knowlesi*: The fifth human malaria parasite. *Clin. Infect. Dis.* **2008**, *46*, 172-173.
14. Mackintosh, C. L.; Beeson, J. G.; Marsh, K., Clinical features and pathogenesis of severe malaria. *Trends Parasitol.* **2004**, *20*, 597-603.
15. Chiang, P. K.; Bujnicki, J. M.; Su, X.; Lanar, D. E., Malaria: Therapy, genes and vaccines. *Curr. Mol. Med.* **2006**, *6*, 309-326.
16. Yuasa, K.; Mi-Ichi, F.; Kobayashi, T.; Yamanouchi, M.; Kotera, J.; Kita, K.; Omori, K., *PfPDE1*, a novel cGMP-specific phosphodiesterase from the human malaria parasite *Plasmodium falciparum*. *Biochem. J.* **2005**, *392*, 221-229.
17. Miller, L. H.; Baruch, D. I.; Marsh, K.; Doumbo, O. K., The pathogenic basis of malaria. *Nature* **2002**, *415*, 673-679.
18. Pasvol, G., Protective hemoglobinopathies and *Plasmodium falciparum* transmission. *Nat. Genet.* **2010**, *42*, 284-285.
19. Mayxay, M.; Pukrittayakamee, S.; Newton, P. N.; White, N. J., Mixed-species malaria infections in humans. *Trends Parasitol.* **2004**, *20*, 233-240.

20. Krotoski, W. A.; Krotoski, D. M.; Garnham, P. C.; Bray, R. S.; Killick-Kendrick, R.; Draper, C. C.; Targett, G. A.; Guy, M. W., Relapses in primate malaria: Discovery of two populations of exoerythrocytic stages. Preliminary note. *Br. Med. J.* **1980**, 280, 153-154.
21. Chin, W.; Contacos, P. G.; Coatney, G. R.; Kimball, H. R., A naturally acquired quotidian-type malaria in man transferable to monkeys. *Science* **1965**, 149, 865.
22. Sinden, R. E., Malaria: Parasite biology, pathogenesis and protection. In Sherman, I. W., Ed. ASM Press: Washington, D. C., **1998**, 25.
23. Leete, E., Biosynthesis of quinine and related alkaloids. *Acc. Chem. Res.* **1969**, 2, 59-64.
24. Schlitzer, M., Malaria chemotherapeutics part I: History of antimalarial drug development, currently used therapeutics, and drugs in clinical development. *ChemMedChem* **2007**, 2, 944-986.
25. Sa, J. M.; Chong, J. L.; Wellems, T. E., Malaria drug resistance: New observations and developments. *Essays Biochem.* **2011**, 51, 137-160.
26. Manson-Bahr, P., The action of plasmochin on malaria. *Proc. R. Soc. Med.* **1927**, 20, 919-926.
27. Peters, W., *Chemotherapy and drug resistance in malaria*, 2nd. edn. Harcourt Brace: London, **1987**.
28. Sweeney, A. W., The possibility of an 'X' factor. The first documented drug resistance of human malaria. *Int. J. Parasitol.* **1996**, 26, 1035-1061.
29. Burrows, J. N.; Chibale, K.; Wells, T. N. C., The state of the art in anti-malarial drug discovery and development. *Curr. Top. Med. Chem.* **2011**, 11, 1226-1254.
30. Burrows, J. N.; Waterson, D., Discovering new medicines to control and eradicate malaria. *Curr. Top. Med. Chem.* **2011**, 7, 125-180.

31. Stocks, P. A.; Raynes, K. J.; Ward, S. A., Novel Quinoline Antimalarials. In *Antimalarial chemotherapy: Mechanisms of action, resistance, and new directions in drug discovery* (ed. Rosenthal, P. J.) Humana, Totowa, **2001**, 235-253.
 32. Taylor, W. R.; White, N. J., Antimalarial drug toxicity: a review. *Drug Saf.* **2004**, 27, 25-61.
 33. Tilley, L.; Loria, P.; Foley, M., Chloroquine and other Quinoline Antimalarials. In *Antimalarial chemotherapy* (ed. Rosenthal, P. J.) Humana, Totowa, **2001**, 87-121.
 34. Egan, T. J., Haemozoin (malaria pigment): a unique crystalline drug target. *TARGETS* **2003**, 2, 115-124.
 35. O'Neill, P. M.; Ward, S. A.; Berry, N. G.; Jeyadevan, J. P.; Biagini, G. A.; Asadollaly, E.; Park, B. K.; Bray, P. G., A medicinal chemistry perspective on 4-aminoquinoline antimalarial drugs. *Curr. Top. Med. Chem.* **2006**, 6, 479-507.
 36. Warhurst, D. C.; Craig, J. C.; Adagu, I. S.; Meyer, D. J.; Lee, S. Y., The relationship of physico-chemical properties and structure to the differential antiplasmodial activity of the cinchona alkaloids. *Malaria J.* **2003**, 2, 1-14.
 37. Warhurst, D. C.; Craig, J. C.; Adagu, I. S.; Guy, R. K.; Madrid, P. B.; Fivelman, Q. L., Activity of piperazine and other 4-aminoquinoline antiplasmodial drugs against chloroquine-sensitive and resistant blood-stages of *Plasmodium falciparum*. Role of beta-haematin inhibition and drug concentration in vacuolar water- and lipid-phases. *Biochem. Pharmacol.* **2007**, 73, 1910-1926.
 38. Hawley, S. R.; Bray, P. G.; O'Neill, P. M.; Park, B. K.; Ward, S. A., The role of drug accumulation in 4-aminoquinoline antimalarial potency - the influence of structural substitution and physicochemical properties. *Biochem. Pharmacol.* **1996**, 52, 723-733.
-

-
39. Fitch, C. D., Ferriprotoporphyrin IX, phospholipids, and the antimalarial actions of quinoline drugs. *Life Sci.* **2004**, *74*, 1957-1972.
 40. Sullivan, D. J.; Gluzman, I. Y.; Russel, D. G.; Goldberg, D. E., On the molecular mechanisms of chloroquine's antimalarial action. *Proc. Natl. Acad. Sci. U.S.A.* **1996**, *93*, 11865-11870.
 41. Olliaro, P.; Yuthavong, Y., An overview of chemotherapeutic targets for antimalarial drug discovery. *Pharmacol. Ther.* **1999**, *81*, 91-110.
 42. Chen, C.; Tang, L.-H.; Chun, J., Studies on a new antimalarial compound: Pyronaridine. *Trans. R. Soc. Trop. Med. Hyg.* **1992**, *86*, 7-10.
 43. Wells, T. N. C., New medicines to combat malaria: An overview of the global pipeline of therapeutics. In *Treatment and prevention of malaria* (ed. Staines, H. M.; Krishna, S.), Springer Basel: **2012**, 227-247.
 44. Mzayek, F.; Deng, H.; Mather, F. J.; Wasilevich, E. C.; Liu, H.; Hadi, C. M.; Chansolme, D. H.; Murphy, H. A.; Melek, B. H.; Tenaglia, A. N.; Mushatt, D. M.; Dreisbach, A. W.; Lertora, J. J. L.; Krogstad, D. J., Randomized dose-ranging controlled trial of AQ-13, a candidate antimalarial, and chloroquine in healthy volunteers. *PLoS Clin. Trials* **2007**, 1-15.
 45. Luo, X.-D.; Shen, C.-C., The chemistry, pharmacology, and clinical applications of qinghaosu (Artemisinin) and its derivatives. *Med. Res. Rev.* **1987**, *7*, 29-52.
 46. O'Neill, P. A.; Posner, G. H., A medicinal chemistry perspective on artemisinin and related endoperoxides. *J. Med. Chem.* **2004**, *47*, 2945-2964.
 47. Hsu, E., The history of qing hao in the Chinese materia medica. *Trans. R. Soc. Trop. Med. Hyg.* **2006**, 505-508.
 48. Liang, X.-T.; Fang, W.-S., *Medicinal chemistry of bioactive natural products*. Hoboken, **2006**.
-

49. Meshnick, S. R.; Taylor, T. E.; Kamchonwongpaisan, S., Artemisinin and the antimalarial endoperoxides: From herbal remedy to targeted chemotherapy. *Microbiol. Rev.* **1996**, *60*, 301-315.
 50. White, N. J., Qinghaosu (artemisinin): The price of success. *Science* **2008**, *320*, 330-334.
 51. Hartwig, C. L.; Rosenthal, P. J.; D'Angelo, J.; Griffin, C. E.; Posner, G. H.; Cooper, R. A., Accumulation of artemisinin trioxane derivatives within a neutral lipids of *Plasmodium falciparum* malaria parasites is endoperoxide-dependent. *Biochem. Pharmacol.* **2009**, 322-336.
 52. Carvalho, L. H.; Rocha, E. M.; Raslan, D. S.; Oliveira, A. B.; Krettli, A. U., *In vitro* activity of natural and synthetic naphthoquinones against erythrocytic stages of *Plasmodium falciparum*. *Braz. J. Med. Biol. Res.* **1988**, *21*, 485-487.
 53. Fawaz, G.; Fieser, L. F., Naphthoquinone antimalarials. XXIV. A new synthesis of lapinone. *J. Am. Chem. Soc.* **1950**, *72*, 996-1000.
 54. Hudson, A. T., Atovaquone — a novel broad-spectrum anti-infective drug. *Parasitol. Today* **1993**, *9*, 66-68.
 55. Painter, H. J.; Morrissey, J. M.; Mather, M. W.; Vaidya, A. B., Specific role of mitochondrial electron transport in blood-stage *Plasmodium falciparum*. *Nature* **2007**, *446*, 88-91.
 56. Funck-Brentano, C.; Becquemont, L.; Leneveu, A.; Roux, A.; Jaillon, P.; Beaune, P., Inhibition by omeprazole of proguanil metabolism: Mechanism of the interaction *in vivo* experiments. *J. Pharmacol. Exp. Ther.* **1997**, *280*, 730-738.
 57. Dahl, E. L.; Rosenthal, P. J., Apicoplast translation, transcription and genome replication: targets for antimalarial antibiotics. *Trends Parasitol.* **2008**, *24*, 279-284.
-

-
58. <http://www.drugbank.ca/>. (accessed 13/12/2012)
59. Geary, T. G.; Divo, A. A.; Jensen, J. B., Activity of quinoline-containing antimalarials against chloroquine-sensitive and -resistant strains of *Plasmodium falciparum* in vitro. *Trans. R. Soc. Trop. Med. Hyg.* **1987**, *81*, 499-503.
60. Vennerstrom, J. L.; Nuzum, E. O.; Miller, R. E.; Dorn, A.; Gerena, L.; Dande, P. A.; Ellis, W. Y.; Ridley, R. G.; Milhous, W. K., 8-Aminoquinolines active against blood stage *Plasmodium falciparum* in vitro inhibit hemozoin polymerization. *Antimicrob. Agents Chemother.* **1999**, *43*, 598-602.
61. Dutta, G. P.; Puri, S. K.; Bhaduri, A. P.; Seth, M., Radical curative activity of a new 8-aminoquinoline derivative (CDRI 80/53) against *Plasmodium cynomolgi* B in monkeys. *Am. J. Trop. Med. Hyg.* **1989**, *41*, 635-637.
62. <http://www.cdsco.nic.in/html/DRUGSAPRVD.htm>. (accessed 13/12/2012)
63. Chou, A. C.; Fitch, C. D., Control of heme polymerase by chloroquine and other quinoline derivatives. *Biochem. Biophys. Res. Commun.* **1993**, *195*, 422-427.
64. Llinas, A.; Glen, R. C.; Goodman, J. M., Solubility challenge: Can you predict solubilities of thirty-two molecules using a database of one hundred reliable measurements? *J. Chem. Inf. Model.* **2008**, *48*, 1289-1303.
65. Wiesner, J.; Henschker, D.; Hutchinson, D. B.; Beck, E.; Jomaa, H., *In vitro* and *in vivo* synergy of fosmidomycin, a novel antimalarial drug, with clindamycin. *Antimicrob. Agents Chemother.* **2002**, *46*, 2889-2894.
66. White, N. J., Cardiotoxicity of antimalarial drugs. *Lancet Infect. Dis.* **2007**, *7*, 549-558.
67. Haynes, R. K.; Fugmann, B.; Stetter, J.; Rieckmann, K.; Heilmann, H.-D.; Chan, H.-W.; Cheung, M.-K.; Lam, W.-L.; Wong, H.-N.; Croft, S. L.; Vivas, L.; Rattray, L.; Stewart, L.; Peters, W.; Robinson, B. L.; Edstein, M. D.; Kotecka, B.; Kyle, D. E.; Beckermann, B.; Gerisch, M.; Radtke, M.; Schmuck, G.;
-

- Steinke, W.; Wollborn, U.; Schmeer, K.; Römer, A., Artemisone—a highly active antimalarial drug of the Artemisinin class. *Angew. Chem. Int. Ed.* **2006**, *45*, 2082-2088.
68. Brossi, A.; Venugopalan, B.; Dominguez, G. L.; Yeh, H. J. C.; Flippen-Anderson, J. L.; Buchs, P.; Luo, X. D.; Milhous, W.; Peters, W., Arteether, a new antimalarial drug: Synthesis and antimalarial properties. *J. Med. Chem.* **1988**, *31*, 645-650.
69. Fivelman, Q. L.; Adagu, I. S.; Warhurst, D. C., Modified fixed-ratio isobologram method for studying *in vitro* interactions between atovaquone and proguanil or dihydroartemisinin against drug-resistant strains of *Plasmodium falciparum*. *Antimicrob. Agents Chemother.* **2004**, *48*, 4097-4102.
70. Shmuklarsky, M. J.; Klayman, D. L.; Milhous, W. K.; Kyle, D. E.; Rossan, R. N.; Ager, A. L. J.; Tang, D. B.; Heiffer, M. H.; Canfield, C. J.; Schuster, B. G., Comparison of beta-artemether and beta-arteether against malaria parasites *in vitro* and *in vivo*. *Am. J. Trop. Med. Hyg.* **1993**, *48*, 377-384.
71. Eriksson, B.; Lebbad, M.; Bjorkman, A., *In vitro* activity of proguanil, chlorproguanil and their main metabolites against *Plasmodium falciparum*. *Trans. R. Soc. Trop. Med. Hyg.* **1989**, *83*, 488.
72. Vennerstrom, J. L.; Arbe-Barnes, S.; Brun, R.; Charman, S. A.; Chiu, F. C. K.; Chollet, J.; Dong, Y.; Dorn, A.; Hunziker, D.; Matile, H.; McIntosh, K.; Padmanilayam, M.; Santo, T. J.; Scheurer, C.; Scorneaux, B.; Tang, Y.; Urwyler, H.; Wittlin, S.; Charman, W. N., Identification of an antimalarial synthetic trioxolane drug development candidate. *Nature* **2004**, *430*, 900-904.
73. Kamchonwongpaisan, S.; Quarrell, R.; Charoensetakul, N.; Ponsinet, R.; Vilaivan, T.; Vanichtanankul, J.; Tarnchompoo, B.; Sirawaraporn, W.; Lowe, G.; Yuthavong, Y., Inhibitors of multiple mutants of *Plasmodium falciparum*
-

- dihydrofolate reductase and their antimalarial activities. *J. Med. Chem.* **2004**, *47*, 673-680.
74. Smilkstein, M. J.; Forquer, I.; Kanazawa, A.; Kelly, J.; Winter, R. W.; Hinrichs, D. J.; Kramer, D. M.; Riscoe, M. K., A drug-selected *Plasmodium falciparum* lacking the need for conventional electron transport. *Mol. Biochem. Parasitol.* **2008**, *159*, 64-68.
75. Dahl, E. L.; Shock, J. L.; Shenai, B. R.; Gut, J.; DeRisi, J. L.; Rosenthal, P. J., Tetracyclines specifically target the apicoplast of the malaria *P. falciparum*. *Antimicrob. Agents Chemother.* **2006**, *50*, 3124-3131.
76. Dahl, E. L.; Rosenthal, P. J., Multiple antibiotics exert delayed effects against the *Plasmodium falciparum* apicoplast. *Antimicrob. Agents Chemother.* **2007**, *51*, 3485-3490.
77. Wang, P.; Sims, P. F. G.; Hyde, J. E., A modified *in vitro* sulfadoxine susceptibility assay for *Plasmodium falciparum* suitable for investigating Fansidar resistance. *Parasitol.* **1997**, *115*, 223-230.
78. Zhang, Y.; Meshnick, S. R., Inhibition of *Plasmodium falciparum* dihydropteroate synthetase and growth *in vitro* by sulfa drugs. *Antimicrob. Agents Chemother.* **1991**, *35*, 267-271.
79. White, N. J., Antimalarial drug resistance. *J. Clin. Invest.* **2004**, *113*, 1084-1092.
80. Marsh, K., Malaria disaster in Africa. *Lancet* **1998**, *352*, 924-925.
81. Ginsburg, H., Should chloroquine be laid to rest? *Acta Tropica* **2005**, *96*, 16-23.
82. Nosten, F.; van Vugt, M.; Price, R.; Luxemburger, C.; Thway, K. L.; Brockman, A.; McGready, R.; ter Kuile, F.; Looareesuwan, S.; White, N. J., Effects of artesunate-mefloquine combination on incidence of *Plasmodium falciparum* malaria and mefloquine resistance in western Thailand: A prospective study. *Lancet* **2000**, *356*, 297-302.

-
83. Trape, J.-F.; Pison, G.; Preziosi, M.-P.; Enel, C.; du Loû, A. D.; Delaunay, V.; Samb, B.; Lagarde, E.; Molez, J.-F.; Simondon, F., Impact of chloroquine resistance on malaria mortality. *C. R. Acad. Sci. III* **1998**, *321*, 689-697.
 84. White, N., Antimalarial drug resistance and combination chemotherapy. *Philos. Trans. R. Soc. London [Biol]* **1999**, *354*, 739-749.
 85. Talisuna, A. O.; Bloland, P.; D'Alessandro, U., History, dynamics, and public health importance of malaria parasite resistance. *Clin. Microbiol. Rev.* **2004**, *17*, 235-254.
 86. Plowe, C. V., Monitoring antimalarial drug resistance: Making the most of the tools at hand. *J. Exp. Biol.* **2003**, *206*, 3745-3752.
 87. Verdier, F.; Le Bras, J.; Clavier, F.; Hatin, I.; Blayo, M. C., Chloroquine uptake by *Plasmodium falciparum*-infected human erythrocytes during *in vitro* culture and its relationship to chloroquine resistance. *Antimicrob. Agents Chemother.* **1985**, *27*, 561-564.
 88. Borst, P., New mechanisms of drug resistance in parasitic protozoa. *Annu. Microbiol.* **1995**, *49*, 427-460.
 89. Anderson, T. J. C.; Nair, S.; Qin, H.; Singlam, S.; Brockman, A.; Paiphun, L.; Nosten, F., Are transporter genes other than the Chloroquine Resistance Locus (*pfcr*) and Multidrug Resistance Gene (*pfmdr*) associated with antimalarial drug resistance? *Antimicrob. Agents Chemother.* **2005**, *49*, 2180-2188.
 90. Ariey, F.; Fandeur, T.; Durand, R.; Randrianarivelojosia, M.; Jambou, R.; Legrand, E.; Ekala, M.; Bouchier, C.; Cojean, S.; Duchemin, J.; Robert, V.; Le Bras, J.; Mercereau-Puijalon, O., Invasion of Africa by a single *pfcr* allele of South East Asian type. *Malaria J.* **2006**, *5*, 34-39.
-

-
91. Sidhu, A. B.; Valderramos, S. G.; Fidock, D. A., *Pfmdr1* mutations contribute to quinine resistance and enhance mefloquine and artemisinin sensitivity in *Plasmodium falciparum*. *Mol. Microbiol.* **2005**, *57*, 913-926.
 92. Nkrumah, L. J.; Riegelhaupt, P. M.; Moura, P.; Johnson, D. J.; Patel, J.; Hayton, K.; Ferdig, M. T.; Wellems, T. E.; Akabas, M. H.; Fidock, D. A., Probing the multifactorial basis of *Plasmodium falciparum* quinine resistance: Evidence for a strain-specific contribution of the sodium-proton exchanger *PfNHE*. *Mol. Biochem. Parasitol.* **2009**, *165*, 122-131.
 93. Cooper, R. A.; Ferdig, M. T.; Su, X.-Z.; Ursos, L. M. B.; Mu, J.; Nomura, T.; Fujioka, H.; Fidock, D. A.; Roepe, P. D.; Wellems, T. E., Alternative mutations at position 76 of the Vacuolar Transmembrane protein *PfCRT* are associated with chloroquine resistance and unique stereospecific quinine and quinidine responses in *Plasmodium falciparum*. *Mol. Pharmacol.* **2002**, *61*, 35-42.
 94. Cooper, R. A.; Lane, K. D.; Deng, B.; Mu, J.; Patel, J. J.; Wellems, T. E.; Su, X.; Ferdig, M. T., Mutations in transmembrane domains 1, 4 and 9 of the *Plasmodium falciparum* chloroquine resistance transporter alter susceptibility to chloroquine, quinine and quinidine. *Mol. Microbiol.* **2007**, *63*, 270-282.
 95. Stepniewska, K.; White, N. J., Pharmacokinetic determinants of the window of selection for antimalarial drug resistance. *Antimicrob. Agents Chemother.* **2008**, *52*, 1589-1596.
 96. Cowman, A.; Galatis, D.; Thompson, J. K., Selection for mefloquine resistance in *Plasmodium falciparum* is linked to amplification of the *pfmdr1* gene and cross-resistance to halofantrine and quinine. *Proc. Natl. Acad. Sci. U.S.A.* **1994**, *91*, 1143-1147.
 97. Sisowath, C.; Ferreira, P. E.; Bustamante, L. Y.; Dahlstrom, S.; Martensson, A.; Bjorkman, A.; Krishna, S.; Gil, J. P., The role of *pfmdr1* in *Plasmodium*
-

- falciparum* tolerance to artemether-lumefantrine in Africa. *Trop. Med. Int. Health* **2007**, *12*, 736-742.
98. Sisowath, C.; Strömberg, J.; Mårtensson, A.; Msellem, M.; Obondo, C.; Björkman, A.; Gil, J. P., *In vivo* selection of *Plasmodium falciparum* *pfmdr1* 86N coding alleles by artemether-lumefantrine (Coartem). *J. Infect. Dis.* **2005**, *191*, 1014-1017.
99. Price, R. N.; Uhlemann, A.-C.; van Vugt, M.; Brockman, A.; Hutagalung, R.; Nair, S.; Nash, D.; Singhasivanon, P.; Anderson, T. J. C.; Krishna, S.; White, N. J.; Nosten, F., Molecular and pharmacological determinants of the therapeutic response to artemether-lumefantrine in multidrug-resistant *Plasmodium falciparum* malaria. *Clin. Infect. Dis.* **2006**, *42*, 1570-1577.
100. Hughes, W. T.; Kennedy, W.; Shenep, J. L.; Flynn, P. M.; Hetherington, S. V.; Fullen, G.; Lancaster, D. J.; Stein, D. S.; Palte, S.; Rosenbaum, D.; Liao, S. H. T.; Blum, M. R.; Rogers, M. D., Safety and pharmacokinetics of 566C80, a hydroxynaphthoquinone with anti-pneumocystis carinii activity: A phase I study in Human Immunodeficiency Virus (HIV)-infected men. *J. Infect. Dis.* **1991**, *163*, 843-848.
101. Gil, J. P.; Nogueira, F.; Strömberg-Nörklit, J.; Lindberg, J.; Carrolo, M.; Casimiro, C.; Lopes, D.; Arez, A. P.; Cravo, P. V.; Rosário, V. E., Detection of atovaquone and Malarone™ resistance conferring mutations in *Plasmodium falciparum* cytochrome *b* gene (*cytb*). *Mol. Cell. Probes* **2003**, *17*, 85-89.
102. Boland, P. B. *Drug Resistance in Malaria*; World Health Organisation Report, Geneva, **2001**.
103. Jambou, R.; Legrand, E.; Niang, M.; Khim, N.; Lim, P.; Volney, B.; Ekala, M. T.; Bouchier, C.; Esterre, P.; Fandeur, T.; Mercereau-Puijalon, O., Resistance of

- Plasmodium falciparum* field isolates to *in-vitro* artemether and point mutations of the SERCA-type *PfATPase6*. *Lancet* **2005**, 366, 1960-1963.
104. Hunt, P.; Afonso, A.; Creasey, A.; Culleton, R.; Sidhu, A. B. S.; Logan, J.; Valderramos, S. G.; McNae, I.; Cheesman, S.; Rosario, V. d.; Carter, R.; Fidock, D. A.; Cravo, P., Gene encoding a deubiquitinating enzyme is mutated in artesunate- and chloroquine-resistant rodent malaria parasites. *Mol. Microbiol.* **2007**, 65, 27-40.
105. Roberts, L.; Enserink, M., Did they really say... eradication? *Science* **2007**, 318, 1544-1545.
106. www.rollbackmalaria.org/. (accessed 13/12/2012)
107. Wells, T. N. C.; Olliaro, P., The global portfolio of new antimalarial medicines under development. *Clin. Pharmacol. Ther.* **2009**, 85, 584-595.
108. <http://www.mmv.org/research-development/rd-portfolio>. (accessed 14/11/2012)
109. Zhang, Y.-K.; Plattner, J. J.; Freund, Y. R.; Easom, E. E.; Zhou, Y.; Ye, L.; Zhou, H.; Waterson, D.; Gamo, F.-J.; Sanz, L. M.; Ge, M.; Li, Z.; Li, L.; Wang, H.; Cui, H., Benzoxaborole antimalarial agents. Part 2: Discovery of fluoro-substituted 7-(2-carboxyethyl)-1,3-dihydro-1-hydroxy-2,1-benzoxaboroles. *Bioorg. Med. Chem. Lett.* **2012**, 22, 1299-1307.
110. Dong, Y.; Wittlin, S.; Sriraghavan, K.; Chollet, J.; Charman, S. A.; Charman, W. N.; Scheurer, C.; Urwyler, H.; Santo Tomas, J.; Snyder, C.; Creek, D. J.; Morizzi, J.; Koltun, M.; Matile, H.; Wang, X.; Padmanilayam, M.; Tang, Y.; Dorn, A.; Brun, R.; Vennerstrom, J. L., The structure–activity relationship of the antimalarial ozonide arterolane (OZ277). *J. Med. Chem.* **2009**, 53, 481-491.
111. Charman, S. A.; Arbe-Barnes, S.; Bathurst, I. C.; Brun, R.; Campbell, M.; Charman, W. N.; Chiu, F. C. K.; Chollet, J.; Craft, J. C.; Creek, D. J.; Dong, Y.; Matile, H.; Maurer, M.; Morizzi, J.; Nguyen, T.; Papastogiannidis, P.; Scheurer,

- C.; Shackleford, D. M.; Sriraghavan, K.; Stingelin, L.; Tang, Y.; Urwyler, H.; Wang, X.; White, K. L.; Wittlin, S.; Zhou, L.; Vennerstrom, J. L., Synthetic ozonide drug candidate OZ439 offers new hope for a single-dose cure of uncomplicated malaria. *Proc. Natl. Acad. Sci. U.S.A.* **2011**, *108*, 4400-4405.
112. Vennerstrom, J. L.; Arbe-Barnes, S.; Brun, R.; Charman, S. A.; Chiu, F. C. K.; Chollet, J.; Dong, Y.; Dorn, A.; Hunziker, D.; Matile, H.; McIntosh, K.; Padmanilayam, M.; Santo Tomas, J.; Scheurer, C.; Scorneaux, B.; Tang, Y.; Urwyler, H.; Wittlin, S.; Charman, W. N., Identification of an antimalarial synthetic trioxolane drug development candidate. *Nature* **2004**, *430*, 900-904.
113. Mäser, P.; Wittlin, S.; Rottmann, M.; Wenzler, T.; Kaiser, M.; Brun, R., Antiparasitic agents: New drugs on the horizon. *Curr. Opin. Pharmacol.* **2012**, *14*, 1-5.
114. Martyn, D. C.; Ramirez, A. P.; Beattie, M. J.; Cortese, J. F.; Patel, V.; Rush, M. A.; Woerpel, K. A.; Clardy, J., Synthesis of spiro-1,2-dioxolanes and their activity against *Plasmodium falciparum*. *Bioorg. Med. Chem. Lett.* **2008**, *18*, 6521-6524.
115. Fattorusso, C.; Campiani, G.; Catalanotti, B.; Persico, M.; Basilico, N.; Parapini, S.; Taramelli, D.; Campagnuolo, C.; Fattorusso, E.; Romano, A.; Tagliatalata-Scafati, O., Endoperoxide derivatives from marine organisms: 1,2-Dioxanes of the plakortin family as novel antimalarial agents. *J. Med. Chem.* **2006**, *49*, 7088-7094.
116. Sabbani, S.; Stocks, P. A.; Ellis, G. L.; Davies, J.; Hedenstrom, E.; Ward, S. A.; O'Neill, P. M., Piperidine dispiro-1,2,4-trioxane analogues. *Bioorg. Med. Chem. Lett.* **2008**, *18*, 5804-5808.
117. O'Neill, P. M.; Amewu, R. K.; Nixon, G. L.; Bousejra ElGarah, F.; Mungthin, M.; Chadwick, J.; Shone, A. E.; Vivas, L.; Lander, H.; Barton, V.;

- Muangnoicharoen, S.; Bray, P. G.; Davies, J.; Park, B. K.; Wittlin, S.; Brun, R.; Preschel, M.; Zhang, K.; Ward, S. A., Identification of a 1,2,4,5-tetraoxane antimalarial drug-development candidate (RKA 182) with superior properties to the semisynthetic artemisinins. *Angew. Chem. Int. Ed.* **2010**, *49*, 5693-5697.
118. Singh, C.; Pandey, S.; Sharma, M.; Puri, S. K., Orally active 1,2,4-trioxepanes: Synthesis and antimalarial activity of a series of 7-arylvinyl-1,2,4-trioxepanes against multidrug-resistant *Plasmodium yoelii* in Swiss mice. *Bioorg. Med. Chem.* **2008**, *16*, 1816-1821.
119. Dubar, F.; Khalife, J.; Brocard, J.; Dive, D.; Biot, C., Ferroquine, an ingenious antimalarial drug – thoughts on the mechanism of action. *Molecules* **2008**, *13*, 2900-2907.
120. Dubar, F.; Egan, T. J.; Pradines, B.; Kuter, D.; Ncokazi, K. K.; Forge, D.; Paul, J.-F. o.; Pierrot, C.; Kalamou, H.; Khalife, J.; Buisine, E.; Rogier, C.; Vezin, H.; Forfar, I.; Slomianny, C.; Trivelli, X.; Kapishnikov, S.; Leiserowitz, L.; Dive, D.; Biot, C., The antimalarial ferroquine: Role of the metal and intramolecular hydrogen bond in activity and resistance. *ACS Chem. Biol.* **2010**, *6*, 275-287.
121. Tschan, S.; Kremsner, P. G.; Mordmüller, B., Emerging drugs for malaria. *Expert Opin. Emerg. Drugs* **2012**, 1-15.
122. O'Neill, P. M.; Mukhtar, A.; Stocks, P. A.; Randle, L. E.; Hindley, S.; Ward, S. A.; Storr, R. C.; Bickley, J. F.; O'Neil, I. A.; Maggs, J. L.; Hughes, R. H.; Winstanley, P. A.; Bray, P. G.; Park, B. K., Isoquine and related amodiaquine analogues: A new generation of improved 4-aminoquinoline antimalarials. *J. Med. Chem.* **2003**, *46*, 4933-4945.
123. Coslédan, F.; Fraisse, L.; Pellet, A.; Guillou, F.; Mordmüller, B.; Kremsner, P. G.; Moreno, A.; Mazier, D.; Maffrand, J.-P.; Meunier, B., Selection of a

- trioxaquine as an antimalarial drug candidate. *Proc. Natl. Acad. Sci. U.S.A.* **2008**, *105*, 17579-17584.
124. Andrews, S.; Burgess, S. J.; Skaalrud, D.; Kelly, J. X.; Peyton, D. H., Reversal agent and linker variants of reversed chloroquines: Activities against *Plasmodium falciparum*. *J. Med. Chem.* **2009**, *53*, 916-919.
125. Gemma, S.; Campiani, G.; Butini, S.; Joshi, B. P.; Kukreja, G.; Coccone, S. S.; Bernetti, M.; Persico, M.; Nacci, V.; Fiorini, I.; Novellino, E.; Taramelli, D.; Basilico, N.; Parapini, S.; Yardley, V.; Croft, S.; Keller-Maerki, S.; Rottmann, M.; Brun, R.; Coletta, M.; Marini, S.; Guiso, G.; Caccia, S.; Fattorusso, C., Combining 4-aminoquinoline- and clotrimazole-based pharmacophores toward innovative and potent hybrid antimalarials. *J. Med. Chem.* **2008**, *52*, 502-513.
126. Ray, S.; Madrid, P. B.; Catz, P.; LeValley, S. E.; Furniss, M. J.; Rausch, L. L.; Guy, R. K.; DeRisi, J. L.; Iyer, L. V.; Green, C. E.; Mirsalis, J. C., Development of a new generation of 4-aminoquinoline antimalarial compounds using predictive pharmacokinetic and toxicology models. *J. Med. Chem.* **2010**, *53*, 3685-3695.
127. Natarajan, J. K.; Alumasa, J. N.; Yearick, K.; Ekoue-Kovi, K. A.; Casabianca, L. B.; de Dios, A. C.; Wolf, C.; Roepe, P. D., 4-N-, 4-S-, and 4-O-chloroquine analogues: Influence of side chain length and quinolyl nitrogen pKa on activity vs chloroquine resistant malaria. *J. Med. Chem.* **2008**, *51*, 3466-3479.
128. Iwaniuk, D. P.; Whetmore, E. D.; Rosa, N.; Ekoue-Kovi, K.; Alumasa, J.; de Dios, A. C.; Roepe, P. D.; Wolf, C., Synthesis and antimalarial activity of new chloroquine analogues carrying a multifunctional linear side chain. *Bioorg. Med. Chem.* **2009**, *17*, 6560-6566.
-

-
129. Dive, D.; Biot, C., Ferrocene conjugates of chloroquine and other antimalarials: The development of ferroquine, a new antimalarial. *ChemMedChem* **2008**, *3*, 383-391.
130. Khan, M. O. F.; Levi, M. S.; Tekwani, B. L.; Khan, S. I.; Kimura, E.; Borne, R. F., Synthesis and antimalarial activities of cyclen 4-aminoquinoline analogs. *Antimicrob. Agents Chemother.* **2009**, *53*, 1320-1324.
131. Gupta, L.; Srivastava, K.; Singh, S.; Puri, S. K.; Chauhan, P. M. S., Synthesis of 2-[3-(7-Chloro-quinolin-4-ylamino)-alkyl]-1-(substituted-phenyl)-2,3,4,9-tetrahydro-1H- β -carboline as a new class of antimalarial agents. *Bioorg. Med. Chem. Lett.* **2008**, *18*, 3306-3309.
132. Sunduru, N.; Srivastava, K.; Rajakumar, S.; Puri, S. K.; Saxena, J. K.; Chauhan, P. M. S., Synthesis of novel thiourea, thiazolidinedione and thioparabanic acid derivatives of 4-aminoquinoline as potent antimalarials. *Bioorg. Med. Chem. Lett.* **2009**, *19*, 2570-2573.
133. Mahajan, A.; Yeh, S.; Nell, M.; van Rensburg, C. E. J.; Chibale, K., Synthesis of new 7-chloroquinolinyl thioureas and their biological investigation as potential antimalarial and anticancer agents. *Bioorg. Med. Chem. Lett.* **2007**, *17*, 5683-5685.
134. Sunduru, N.; Sharma, M.; Srivastava, K.; Rajakumar, S.; Puri, S. K.; Saxena, J. K.; Chauhan, P. M. S., Synthesis of oxalamide and triazine derivatives as a novel class of hybrid 4-aminoquinoline with potent antiplasmodial activity. *Bioorg. Med. Chem.* **2009**, *17*, 6451-6462.
135. Shanks, G. D.; Oloo, A. J.; Aleman, G. M.; Ohrt, C.; Klotz, F. W.; Braitman, D.; Horton, J.; Brueckner, R., A new primaquine analogue, tafenoquine (WR 238605), for prophylaxis against *Plasmodium falciparum* malaria. *Clin. Infect. Dis.* **2001**, *33*, 1968-1974.
-

-
136. Nanayakkara, N. P. D.; Ager, A. L.; Bartlett, M. S.; Yardley, V.; Croft, S. L.; Khan, I. A.; McChesney, J. D.; Walker, L. A., Antiparasitic activities and toxicities of individual enantiomers of the 8-aminoquinoline 8-[(4-amino-1-methylbutyl)amino]-6-methoxy-4-methyl-5-[3,4-dichlorophenoxy]quinoline succinate. *Antimicrob. Agents Chemother.* **2008**, *52*, 2130-2137.
137. Pérez-Silanes, S.; Berrade, L.; García-Sánchez, R.; Mendoza, A.; Galiano, S.; Pérez-Solórzano, B.; Nogal-Ruiz, J.; Martínez-Fernández, A.; Aldana, I.; Monge, A., New 1-aryl-3-substituted propanol derivatives as antimalarial agents. *Molecules* **2009**, *14*, 4120-4135.
138. Milner, E.; McCalmont, W.; Bhonsle, J.; Caridha, D.; Carroll, D.; Gardner, S.; Gerena, L.; Gettayacamin, M.; Lanteri, C.; Luong, T.; Melendez, V.; Moon, J.; Roncal, N.; Sousa, J.; Tungtaeng, A.; Wipf, P.; Dow, G., Structure–activity relationships amongst 4-position quinoline methanol antimalarials that inhibit the growth of drug sensitive and resistant strains of *Plasmodium falciparum*. *Bioorg. Med. Chem. Lett.* **2010**, *20*, 1347-1351.
139. Dechy-Cabaret, O.; Benoit-Vical, F.; Robert, A.; Meunier, B., Preparation and antimalarial activities of “trioxaquines”, new modular molecules with a trioxane skeleton linked to a 4-aminoquinoline. *ChemBioChem* **2000**, *1*, 281-283.
140. Basco, L. K.; Dechy-Cabaret, O.; Ndounga, M.; Meche, F. S.; Robert, A.; Meunier, B., *In vitro* activities of DU-1102, a new trioxaquine derivative, against *Plasmodium falciparum* isolates. *Antimicrob. Agents Chemother.* **2001**, *45*, 1886-1888.
141. Grellepois, F.; Grellier, P.; Bonnet-Delpon, D.; Bégué, J.-P., Design, Synthesis and antimalarial activity of trifluoromethylartemisinin–mefloquine dual molecules. *ChemBioChem* **2005**, *6*, 648-652.
-

-
142. Coteron, J. M.; Marco, M. a.; Esquivias, J.; Deng, X.; White, K. L.; White, J.; Koltun, M.; El Mazouni, F.; Kokkonda, S.; Katneni, K.; Bhamidipati, R.; Shackleford, D. M.; Angulo-Barturen, I. i.; Ferrer, S. B.; Jiménez-Díaz, M. A. B. N.; Gamo, F.-J.; Goldsmith, E. J.; Charman, W. N.; Bathurst, I.; Floyd, D.; Matthews, D.; Burrows, J. N.; Rathod, P. K.; Charman, S. A.; Phillips, M. A., Structure-guided lead optimization of triazolopyrimidine-ring substituents identifies potent *Plasmodium falciparum* dihydroorotate dehydrogenase inhibitors with clinical candidate potential. *J. Med. Chem.* **2011**, *54*, 5540-5561.
143. Wu, T.; Nagle, A.; Kuhen, K.; Gagaring, K.; Borboa, R.; Francek, C.; Chen, Z.; Plouffe, D.; Goh, A.; Lakshminarayana, S. B.; Wu, J.; Ang, H. Q.; Zeng, P.; Kang, M. L.; Tan, W.; Tan, M.; Ye, N.; Lin, X.; Caldwell, C.; Ek, J.; Skolnik, S.; Liu, F.; Wang, J.; Chang, J.; Li, C.; Hollenbeck, T.; Tuntland, T.; Isbell, J.; Fischli, C.; Brun, R.; Rottmann, M.; Dartois, V.; Keller, T.; Diagana, T.; Winzeler, E.; Glynn, R.; Tully, D. C.; Chatterjee, A. K., Imidazolopiperazines: Hit to lead optimization of new antimalarial agents. *J. Med. Chem.* **2011**, *54*, 5116-5130.
144. Chatterjee, A. In *Discovery of novel antimalarials through cell-based medicinal chemistry optimization of HTS hits*, RSC/SCI Medicinal Chemistry Symposium, Churchill College, Cambridge UK, Churchill College, September 11-14, **2011**.
145. Rottmann, M.; McNamara, C.; Yeung, B. K. S.; Lee, M. C. S.; Zou, B.; Russell, B.; Seitz, P.; Plouffe, D. M.; Dharia, N. V.; Tan, J.; Cohen, S. B.; Spencer, K. R.; González-Páez, G. E.; Lakshminarayana, S. B.; Goh, A.; Suwanarusk, R.; Jegla, T.; Schmitt, E. K.; Beck, H.-P.; Brun, R.; Nosten, F.; Renia, L.; Dartois, V.; Keller, T. H.; Fidock, D. A.; Winzeler, E. A.; Diagana, T. T., Spiroindolones, a potent compound class for the treatment of malaria. *Science* **2010**, *329*, 1175-1180.
-

-
146. Gardner, M. J.; Hall, N.; Fung, E.; White, O.; Berriman, M.; Hyman, R. W.; Carlton, J. M.; Pain, A.; Nelson, K. E.; Bowman, S.; Paulsen, I. T.; James, K.; Eisen, J. A.; Rutherford, K.; Salzberg, S. L.; Craig, A.; Kyes, S.; Chan, M.-S.; Nene, V.; Shallom, S. J.; Suh, B.; Peterson, J.; Angiuoli, S.; Pertea, M.; Allen, J.; Selengut, J.; Haft, D.; Mather, M. W.; Vaidya, A. B.; Martin, D. M. A.; Fairlamb, A. H.; Fraunholz, M. J.; Roos, D. S.; Ralph, S. A.; McFadden, G. I.; Cummings, L. M.; Subramanian, G. M.; Mungall, C.; Venter, J. C.; Carucci, D. J.; Hoffman, S. L.; Newbold, C.; Davis, R. W.; Fraser, C. M.; Barrell, B., Genome sequence of the human malaria parasite *Plasmodium falciparum*. *Nature* **2002**, *419*, 498-511.
147. Carlton, J. M.; Adams, J. H.; Silva, J. C.; Bidwell, S. L.; Lorenzi, H.; Caler, E.; Crabtree, J.; Angiuoli, S. V.; Merino, E. F.; Amedeo, P.; Cheng, Q.; Coulson, R. M. R.; Crabb, B. S.; del Portillo, H. A.; Essien, K.; Feldblyum, T. V.; Fernandez-Becerra, C.; Gilson, P. R.; Gueye, A. H.; Guo, X.; Kanga, S.; Kooij, T. W. A.; Korsinczky, M.; Meyer, E. V. S.; Nene, V.; Paulsen, I.; White, O.; Ralph, S. A.; Ren, Q.; Sargeant, T. J.; Salzberg, S. L.; Stoeckert, C. J.; Sullivan, S. A.; Yamamoto, M. M.; Hoffman, S. L.; Wortman, J. R.; Gardner, M. J.; Galinski, M. R.; Barnwell, J. W.; Fraser-Liggett, C. M., Comparative genomics of the neglected human malaria parasite *Plasmodium vivax*. *Nature* **2008**, *455*, 757-763.
148. Zhou, Y.; Ramachandran, V.; Kumar, K. A.; Westenberger, S.; Refour, P.; Zhou, B.; Li, F.; Young, J. A.; Chen, K.; Plouffe, D.; Henson, K.; Nussenzweig, V.; Carlton, J.; Vinetz, J. M.; Duraisingh, M. T.; Winzeler, E. A., Evidence-based annotation of the malaria parasite's genome using comparative expression profiling. *PLoS ONE* **2008**, *3*, 1570.
-

149. Bumol, T. F.; Watanabe, A. M., Genetic information, genomic technologies, and the future of drug discovery. *JAMA* **2001**, *285*, 551-555.
150. Payne, D. J.; Gwynn, M. N.; Holmes, D. J.; Pompliano, D. L., Drugs for bad bugs: Confronting the challenges of antibacterial discovery. *Nat. Rev. Drug Discovery* **2007**, *6*, 29-40.
151. Kirk, K., Membrane transport in the malaria-infected erythrocyte. *Physiol. Rev.* **2001**, *81*, 495-537.
152. Hart, C. P., Finding the target after screening the phenotype. *Drug Discov. Today* **2005**, *10*, 513-519.
153. Plouffe, D.; Brinker, A.; McNamara, C.; Henson, K.; Kato, N.; Kuhen, K.; Nagle, A.; Adrián, F.; Matzen, J. T.; Anderson, P.; Nam, T.-g.; Gray, N. S.; Chatterjee, A.; Janes, J.; Yan, S. F.; Trager, R.; Caldwell, J. S.; Schultz, P. G.; Zhou, Y.; Winzeler, E. A., *In silico* activity profiling reveals the mechanism of action of antimalarials discovered in a high-throughput screen. *Proc. Natl. Acad. Sci. U.S.A.* **2008**, *105*, 9059-9064.
154. Gamo, F.-J.; Sanz, L. M.; Vidal, J.; de Cozar, C.; Alvarez, E.; Lavandera, J.-L.; Vanderwall, D. E.; Green, D. V. S.; Kumar, V.; Hasan, S.; Brown, J. R.; Peishoff, C. E.; Cardon, L. R.; Garcia-Bustos, J. F., Thousands of chemical starting points for antimalarial lead identification. *Nature* **2010**, *465*, 305-310.
155. Guiguemde, W. A.; Shelat, A. A.; Bouck, D.; Duffy, S.; Crowther, G. J.; Davis, P. H.; Smithson, D. C.; Connelly, M.; Clark, J.; Zhu, F.; Jiménez-Díaz, M. B.; Martinez, M. S.; Wilson, E. B.; Tripathi, A. K.; Gut, J.; Sharlow, E. R.; Bathurst, I.; Mazouni, F. E.; Fowble, J. W.; Forquer, I.; McGinley, P. L.; Castro, S.; Angulo-Barturen, I.; Ferrer, S.; Rosenthal, P. J.; DeRisi, J. L.; Sullivan, D. J.; Lazo, J. S.; Roos, D. S.; Riscoe, M. K.; Phillips, M. A.; Rathod, P. K.; van

- Voorhis, W. C.; Avery, V. M.; Guy, R. K., Chemical genetics of *Plasmodium falciparum*. *Nature* **2010**, *465*, 311-315.
156. <http://www.ebi.ac.uk/chemblntd>. (accessed 12/12/2012)
157. <http://www.collaborativedrug.com/>. (accessed 08/11/2012)
158. <http://pubchem.ncbi.nlm.nih.gov/>. (accessed 04/09/2012)
159. Rathore, D.; McCutchan, T. F.; Sullivan, M.; Kumar, S., Antimalarial drugs: Current status and new developments. *Expert Opin. Invest. Drugs* **2005**, *14*, 871-883.
160. Biagini, G. A.; O'Neill, P. M.; Bray, P. G.; Ward, S. A., Current drug development portfolio for antimalarial therapies. *Curr. Opin. Pharmacol.* **2005**, *5*, 473-478.
161. WHO Guidelines for the treatment of malaria, World Health Organisation report, **2006**.
162. Agüero, F.; Al-lazikani, B.; Aslett, M.; Berriman, M.; Buckner, F. S.; Campbell, R. K.; Carmona, S.; Carruthers, I. M.; Chan, A. W. E.; Chen, F.; Crowther, G. J.; Doyle, M. A.; Hertz-fowler, C.; Hopkins, A. L.; McAllister, G.; Nwaka, S.; Overington, J. P.; Pain, A.; Paolini, G. V.; Pieper, U.; Ralph, S. A.; Riechers, A.; Roos, D. S.; Sali, A.; Shanmugam, D.; Suzuki, T.; Van Voorhis, W. C.; Verlinde, C. L. M. J., Genomic-scale prioritization of drug targets: the TDR targets database. *Nat. Rev. Drug Discovery* **2008**, *7*, 900-907.
163. Wentzinger, L.; Bopp, S.; Tenor, H.; Klar, J.; Brun, R.; Beck, H. P.; Seebeck, T., Cyclic nucleotide-specific phosphodiesterases of *Plasmodium falciparum*: PfPDE α , a non-essential cGMP-specific PDE that is an integral membrane protein. *Int. J. Parasitol.* **2008**, *38*, 1625-1637.

-
164. Beghyn, T.; Charton, J.; Leroux, F.; Laconde, G.; Bourin, A.; Cos, P.; Maes, L.; Deprez, B., Drug to genome to drug: Discovery of new antiplasmodial compounds. *J. Med. Chem.* **2011**, *54*, 3222-3240.
165. Beghyn, T. B.; Charton, J.; Leroux, F.; Henninot, A.; Reboule, I.; Cos, P.; Maes, L.; Deprez, B., Drug-to-genome-to-drug, step 2: Reversing selectivity in a series of antiplasmodial compounds. *J. Med. Chem.* **2011**, *55*, 1274-1286.
166. Taylor, C. J.; McRobert, L.; Baker, D. A., Disruption of a *Plasmodium falciparum* cyclic nucleotide phosphodiesterase gene causes aberrant gametogenesis. *Mol. Microbiol.* **2008**, *69*, 110-118.
167. Bland, N. D.; Wang, C.; Tallman, C.; Gustafson, A. E.; Wang, Z.; Ashton, T. D.; Ochiana, S. O.; McAllister, G.; Cotter, K.; Fang, A. P.; Gechijian, L.; Garceau, N.; Gangurde, R.; Ortenberg, R.; Ondrechen, M. J.; Campbell, R. K.; Pollastri, M. P., Pharmacological validation of *Trypanosoma brucei* phosphodiesterases B1 and B2 as druggable targets for African sleeping sickness. *J. Med. Chem.* **2011**, *54*, 8188-8194.
168. Wang, C.; Ashton, T. D.; Gustafson, A.; Bland, N. D.; Ochiana, S. O.; Campbell, R. K.; Pollastri, M. P., Synthesis and evaluation of human phosphodiesterases (PDE) 5 inhibitor analogs as trypanosomal PDE inhibitors. Part 1. Sildenafil analogs. *Bioorg. Med. Chem. Lett.* **2012**, *22*, 2579-2581.
169. Ochiana, S. O.; Gustafson, A.; Bland, N. D.; Wang, C.; Russo, M. J.; Campbell, R. K.; Pollastri, M. P., Synthesis and evaluation of human phosphodiesterases (PDE) 5 inhibitor analogs as trypanosomal PDE inhibitors. Part 2. Tadalafil analogs. *Bioorg. Med. Chem. Lett.* **2012**, *22*, 2582-2584.
170. Liu, S.; Mansour, M. N.; Dillman, K. S.; Perez, J. R.; Danley, D. E.; Aeed, P. A.; Simons, S. P.; LeMotte, P. K.; Menniti, F. S., Structural basis for the
-

- catalytic mechanism of human phosphodiesterase 9. *Proc. Natl. Acad. Sci. U.S.A.* **2008**, *105*, 13309-13314.
171. Ke, H.; Wang, H., Crystal structures of phosphodiesterases and implications on substrate specificity and inhibitor selectivity. *Curr. Top. Med. Chem.* **2007**, *7*, 391-403.
172. Chen, Y.; David, N.; Kye-Im, J., Regulation and function of cyclic nucleotide phosphodiesterases in vascular smooth muscle and vascular diseases. In *Cyclic Nucleotide Phosphodiesterases in Health and Disease*, CRC Press: **2006**.
173. Zhang, K. Y. J.; Card, G. L.; Suzuki, Y.; Artis, D. R.; Fong, D.; Gillette, S.; Hsieh, D.; Neiman, J.; West, B. L.; Zhang, C.; Milburn, M. V.; Kim, S.-H.; Schlessinger, J.; Bollag, G., A glutamine switch mechanism for nucleotide selectivity by phosphodiesterases. *Mol. Cell.* **2004**, *15*, 279-286.
174. Jeon, Y. H.; Heo, Y. S.; Kim, C. M.; Hyun, Y. L.; Lee, T. G.; Ro, S.; Cho, J. M., Phosphodiesterase: overview of protein structures, potential therapeutic applications and recent progress in drug development. *Cell. Mol. Life Sci.* **2005**, *62*, 1198-1220.
175. Beavo, J. A.; Hardman, J. G.; Sutherland, E. W., Stimulation of adenosine 3',5'-monophosphate hydrolysis by guanosine 3',5'-monophosphate. *J. Biol. Chem.* **1971**, *246*, 3841-3846.
176. Beavo, J. A., Cyclic nucleotide phosphodiesterases: Functional implications of multiple isoforms. *Physiol. Rev.* **1995**, *10*, 3841-3846.
177. Bender, A. T.; Beavo, J. A., Cyclic nucleotide phosphodiesterases: Molecular regulation to clinical use. *Pharmacol. Rev.* **2006**, *58*, 488-520.
178. Amer, M. S.; Kreighbaum, W. E., Cyclic nucleotide phosphodiesterases: Properties, activators, inhibitors, structure–activity relationships, and possible role in drug development. *J. Pharm. Sci.* **1975**, *64*, 1-37.
-

179. Conti, M.; Beavo, J. A., Biochemistry and physiology of cyclic nucleotide phosphodiesterases: Essential components in cyclic nucleotide signaling. *Annu. Rev. Biochem.* **2006**, *76*, 481-511.
180. Omori, K.; Kotera, J., Overview of PDEs and their regulation. *Circ. Res.* **2007**, *100*, 309-327.
181. Lugnier, C., Cyclic nucleotide phosphodiesterase (PDE) superfamily: A new target for the development of specific therapeutic agents. *Pharmacol. Ther.* **2006**, *109*, 366-398.
182. Boswell-Smith, V.; Spina, D.; Page, C. P., Phosphodiesterase inhibitors. *Br. J. Pharmacol.* **2006**, *147*, 252-257.
183. Xu, R. X.; Hassell, A. M.; Vanderwall, D.; Lambert, M. H.; Holmes, W. D.; Luther, M. A.; Rocque, W. J.; Milburn, M. V.; Zhao, Y.; Ke, H.; Nolte, R. T., Atomic structure of PDE4: Insights into phosphodiesterase mechanism and specificity. *Science* **2000**, *288*, 1822-1825.
184. Manallack, D. T.; Hughes, R. A.; Thompson, P. E., The next generation of phosphodiesterase inhibitors: Structural clues to ligand and substrate selectivity of phosphodiesterases. *J. Med. Chem.* **2005**, *48*, 3449-3462.
185. Card, G. L.; England, B. P.; Suzuki, Y.; Fong, D.; Powell, B.; Lee, B.; Luu, C.; Tabrizizad, M.; Gillette, S.; Ibrahim, P. N.; Artis, D. R.; Bollag, G.; Milburn, M. V.; Kim, S.-H.; Schlessinger, J.; Zhang, K. Y. J., Structural basis for the activity of drugs that inhibit phosphodiesterases. *Structure* **2004**, *12*, 2233-2247.
186. Ghosh, R.; Sawant, O.; Ganpathy, P.; Pitre, S.; Kadam, V. J., Phosphodiesterase inhibitors: Their role and implications. *Int. J. Pharm. Tech. Research* **2009**, *1*, 1148-1160.
187. Beavo, J. A., *Cyclic nucleotide phosphodiesterases in health and disease*. **2006**.

188. Weiss, B.; Hait, W. N., Selective cyclic nucleotide phosphodiesterase inhibitors as potential therapeutic agents. *Annu. Rev. Pharmacol. Toxicol.* **1977**, *17*, 441-477.
189. Murray, K. J., Phosphodiesterase V inhibitors. *Drug News Perspect.* **1993**, *6*, 150-156.
190. Merkel, L., Zaprinast: A cGMP-selective phosphodiesterase inhibitor. *Cardiovasc. Drug Rev.* **1993**, *11*, 501-515.
191. Lugnier, C.; Stierle, A.; Beretz, A.; Schoeffter, P.; Lebec, A.; Wermuth, C. G.; Cazenave, J. P.; Stoclet, J. C., Tissue and substrate specificity of inhibition by alkoxy-aryl-lactams of platelet and arterial smooth muscle cyclic nucleotide phosphodiesterases relationship to pharmacological activity. *Biochem. Biophys. Res. Commun.* **1983**, *113*, 954-959.
192. Saeki, T.; Adachi, H.; Takase, Y.; Yoshitake, S.; Souda, S.; Saito, I., A selective type V phosphodiesterase inhibitor, E4021, dilates porcine large coronary artery. *J. Pharmacol. Exp. Ther.* **1995**, *272*, 825-831.
193. Zeller, E.; Stief, H. J.; Pflug, B.; Sastre-y-Hernández, M., Results of a phase II study of the antidepressant effect of rolipram. *Pharmacopsychiatry* **1984**, *17*, 188-190.
194. Wachtel, H., Potential antidepressant activity of rolipram and other selective cyclic adenosine 3',5'-monophosphate phosphodiesterase inhibitors. *Neuropharmacology* **1983**, *22*, 267-272.
195. Bobon, D.; Breulet, M.; Gerard-Vandenhove, M. A.; Guiot-Goffioul, F.; Plomteux, G.; Sastre-y-Hernández, M.; Schratzer, M.; Troisfontaines, B.; Frenckell, R.; Wachtel, H., Is phosphodiesterase inhibition a new mechanism of antidepressant action? *Eur. Arch. Psychiatr. Neurol. Sci.* **1988**, *238*, 2-6.

196. Kawamoto, F.; Alejo-Blanco, R.; Fleck, S. L.; Kawamoto, Y.; Sinden, R. E., Possible roles of Ca^{2+} and cGMP as mediators of the exflagellation of *Plasmodium berghei* and *Plasmodium falciparum*. *Mol. Biochem. Parasitol.* **1990**, *42*, 101-108.
197. Kawamoto, F.; Fujioka, H.; Murakami, R.; Syafruddin Hagiwara, M.; Ishikawa, T.; Hidaka, H., The roles of Ca^{2+} /calmodulin- and cGMP-dependent pathways in gametogenesis of a rodent malaria parasite, *Plasmodium berghei*. *Eur. J. Cell. Biol.* **1993**, *60*, 101-107.
198. Moon, R. W.; Taylor, C. J.; Bex, C.; Schepers, R.; Goulding, D.; Janse, C. J.; Waters, A. P.; Baker, D. A.; Billker, O., A cyclic GMP signalling module that regulates gliding motility in a malaria parasite. *PLoS Pathogens* **2009**, *5*, 1-14.
199. DeNinno, M. P.; Andrews, M.; Bell, A. S.; Chen, Y.; Eller-Zarbo, C.; Eshelby, N.; Etienne, J. B.; Moore, D. E.; Palmer, M. J.; Visser, M. S.; Yu, L. J.; Zavadoski, W. J.; Michael Gibbs, E., The discovery of potent, selective, and orally bioavailable PDE9 inhibitors as potential hypoglycemic agents. *Bioorg. Med. Chem. Lett.* **2009**, *19*, 2537-2541.
200. Cavasotto, C. N.; Phatak, S. S., Homology modeling in drug discovery: Current trends and applications. *Drug Discov. Today* **2009**, *14*, 676-683.
201. Hillisch, A.; Pineda, L. F.; Hilgenfeld, R., Utility of homology models in the drug discovery process. *Drug Discov. Today* **2004**, *9*, 659-669.
202. van Dongen, M.; Weigelt, J.; Uppenberg, J.; Schultz, J.; Wikström, M., Structure-based screening and design in drug discovery. *Drug Discov. Today* **2002**, *7*, 471-478.
203. Chenna, R.; Sugawara, H.; Koike, T.; Lopez, R.; Gibson, T. J.; Higgins, D. G.; Thompson, J. D., Multiple sequence alignment with the Clustal series of programs. *Nucleic Acids Res.* **2003**, *31*, 3497-3500.

204. Chen, V. B.; Arendall, W. B. I.; Headd, J. J.; Keedy, D. A.; Immormino, R. M.; Kapral, G. J.; Murray, L. W.; Richardson, J. S.; Richardson, D. C., MolProbity: All-atom structure validation for macromolecular crystallography. *Acta Crystallogr.* **2010**, *66*, 12-21.
205. Sung, B. J.; Hwang, K. Y.; Jeon, Y. H.; Lee, J. I.; Heo, Y. S.; Kim, J. H.; Moon, J.; Yoon, J. M.; Hyun, Y. L.; Kim, E.; Eum, S. J.; Park, S. Y.; Lee, O. J.; Lee, T. G.; Ro, S.; Cho, J. M., Structure of the catalytic domain of human phosphodiesterase 5 with bound drug molecules. *Nature* **2003**, *425*, 98-102.
206. Read, L. K.; Mikkelsen, R. B., Comparison of adenylate cyclase and cAMP-dependent protein kinase in gametocytogenic and nongametocytogenic clones of *Plasmodium falciparum*. *J. Parasitol.* **1991**, *77*, 346-352.
207. Wang, H.; Yan, Z.; Geng, J.; Kunz, S.; Seebeck, T.; Ke, H., Crystal structure of the *Leishmania major* phosphodiesterase *LmjPDEB1* and insight into the design of the parasite-selective inhibitors. *Mol. Microbiol.* **2007**, *66*, 1029-1038.
208. Higgins, D. G.; Sharp, P., M., CLUSTAL: A package for performing multiple sequence alignment on a microcomputer. *Gene* **1988**, *73*, 237-244.
209. Laurent, W.; Thomas, S., Protozoal Phosphodiesterases. In *Cyclic Nucleotide Phosphodiesterases in Health and Disease*, CRC Press: **2006**.
210. Rose, F. L., New syntheses based on 5-aminopyrimidines. *J. Chem. Soc.* **1952**, 3448-3464.
211. Hamilton, H. W.; Ortwine, D. F.; Worth, D. F.; Bristol, J. A., Synthesis and structure-activity relationships of pyrazolo[4,3-d]pyrimidin-7-ones as adenosine receptor antagonists. *J. Med. Chem.* **1987**, *30*, 91-96.
212. Carson, D. A.; Chang, K.-P., Phosphorylation and anti-leishmanial activity of formycin B. *Biochem. Biophys. Res. Commun.* **1981**, *100*, 1377-1383.
-

213. de Koning, H. P.; Jarvis, S. M., Adenosine transporters in bloodstream forms of *Trypanosoma brucei*: Substrate recognition motifs and affinity for trypanocidal drugs. *Mol. Pharmacol.* **1999**, *56*, 1162-1170.
214. Koyama, G.; Maeda, K.; Umezawa, H., The structural studies of formycin and formycin b. *Tetrahedron Lett.* **1966**, *6*, 597-602.
215. Perry, C. M.; Faulds, D., Valaciclovir. A review of its antiviral activity, pharmacokinetic properties and therapeutic efficacy in herpesvirus infections. *Drugs* **1996**, *52*, 754-772.
216. Lok, A. S. F.; McMahon, B. J., Chronic hepatitis B: Update 2009. *Hepatology* **2009**, *50*, 661-662.
217. Haning, H.; Niewöhner, U.; Schenke, T.; Lampe, T.; Hillisch, A.; Bischoff, E., Comparison of different heterocyclic scaffolds as substrate analog PDE5 inhibitors. *Bioorg. Med. Chem. Lett.* **2005**, *15*, 3900-3907.
218. Terrett, N. K.; Bell, A. S.; Brown, D.; Ellis, P., Sildenafil (VIAGRATM), a potent and selective inhibitor of type 5 cGMP phosphodiesterase with utility for the treatment of male erectile dysfunction. *Bioorg. Med. Chem. Lett.* **1996**, *6*, 1819-1824.
219. Veitch, G. E.; Bridgwood, K. L.; Ley, S. V., Magnesium nitride as a convenient source of ammonia: Preparation of primary amides. *Org. Lett.* **2008**, *10*, 3623-3625.
220. Robins, R. K.; Holum, L. B.; Furcht, F. W., Potential purine antagonists. V. Synthesis of some 3-methyl-5,7-substituted pyrazolo[4,3-*d*]pyrimidines. *J. Org. Chem.* **1956**, *21*, 833-836.
221. Bridgwood, K. L.; Veitch, G. E.; Ley, S. V., Magnesium nitride as a convenient source of ammonia: Preparation of dihydropyridines. *Org. Lett.* **2008**, *10*, 3627-3629.
-

-
222. Krystof, V.; Moravcova, D.; Paprskarova, M.; Barbier, P.; Peyrot, V.; Hlobilkova, A.; Havlicek, L.; Strnad, M., Synthesis and biological activity of 8-azapurine and pyrazolo[4,3-*d*]pyrimidine analogues of myoseverin. *Eur. J. Med. Chem.* **2006**, *41*, 1405-1411.
223. Daw, P.; Sinha, A.; Rahaman, S. M. W.; Dinda, S.; Bera, J. K., Bifunctional water activation for catalytic hydration of organonitriles. *Organometallics* **2012**, *31*, 3790-3797.
224. Kankan, R. N. R.; Rao, D. R. A novel process for the synthesis of sildenafil citrate. International Publication Number, WO 01/19827, **2001**.
225. Trager, W.; Jensen, J., Human malaria parasites in continuous culture. *Science* **1976**, *193*, 673-675.
226. Mishra, M. N.; Misra, R. N., Immunochromatographic methods in malaria diagnosis. *Med. J. Armed Forces India* **2007**, *63*, 127-129.
227. Mayer, K. M.; Arnold, F. H., A colorimetric assay to quantify dehydrogenase activity in crude cell lysates. *J. Biomol. Screen.* **2002**, *7*, 135-140.
228. Lehane, A. M.; Saliba, K. J., Common dietary flavonoids inhibit the growth of the intraerythrocytic and malaria parasite. *Biomed. Res.* **2008**, *1*, 26-30.
229. Chen, Y. T.; Zheng, R. L.; Jia, Z. J.; Ju, Y., Flavonoids as super oxide scavengers and antioxidant. *Free Radical Biol. Med.* **1990**, *9*, 19-21.
230. Clack, W.; Mackay, E., Effect of flavonoid substances on histamine toxicity, anaphylactic shock and histamine enhanced capacity to die. *J. Allergy* **1950**, *21*, 133-147.
231. Hertog, M. G.; Hollman, P. C.; Katan, M. B.; Kromhout, D., Intake of potentially anticarcinogenic flavonoids and their determinants in adults in The Netherlands. *Nutr. Cancer* **1993**, *20*, 21-29.
-

232. Ferrandiz, M. L.; Alcaraz, M. J., Anti-inflammatory activity and inhibition of arachidonic acid metabolism by flavonoid. *Agents Actions* **1991**, 32, 283-288.
233. Maschi, O.; Cero, E. D.; Galli, G. V.; Caruso, D.; Bosisio, E.; Dell'Agli, M., Inhibition of human cAMP-phosphodiesterase as a mechanism of the spasmolytic effect of *Matricaria recutita*. *J. Agricult. Food Chem.* **2008**, 56, 5015-5020.
234. Edenhardder, R.; Von Petersdorff, I.; Rauscher, R., Antimutagenic effects of flavonoids, chalcones and structurally related compounds on the activity of 2-amino-3-methylimidazole[4,5-*f*]quinoline (IQ) and other heterocyclic amine mutagens from cooked food. *Mutat. Res.* **1993**, 287, 261-274.
235. Narayana, K. R.; Reddy, M. S.; Chaluvadi, M. R.; Krishna, D. R., Bioflavonoids classification, pharmacological, biochemical effects and therapeutic potential. *Indian J. Pharmacol.* **2001**, 33, 2-16.
236. Brahmachari, G.; Gorai, D., Progress in the research on naturally occurring flavones and flavonols: An overview. *Curr. Org. Chem.* **2006**, 10, 873-898.
237. Beretz, A.; Anton, R.; Stoclet, J. C., Flavonoid compounds are potent inhibitors of cyclic AMP phosphodiesterase. *Experientia* **1978**, 34, 1054-1055.
238. Ruckstuhl, M.; Beretz, A.; Anton, R.; Landry, Y., Flavonoids are selective cyclic GMP phosphodiesterase inhibitors. *Biochem. Pharmacol.* **1979**, 28, 535-538.
239. Ferrell, J. E.; Chang Sing, P. D. G.; Leow, G.; King, R.; Mansour, J. M.; Mansour, T. E., Structure/activity studies of flavonoids as inhibitors of cyclic AMP phosphodiesterase and relationship to quantum chemical indices. *Mol. Pharmacol.* **1979**, 16, 556-568.
-

-
240. Kuppusamy, U. R.; Das, N. P., Effects of flavonoids on cyclic AMP phosphodiesterase and lipid mobilization in rat adipocytes. *Biochem. Pharmacol.* **1992**, *44*, 1307-1315.
241. Orallo, F.; Camina, M.; Alvarez, E.; Basaran, H.; Lugnier, C., Implication of cyclic nucleotide phosphodiesterase inhibition in the vasorelaxant activity of the citrus-fruits flavonoid (+)-naringenin. *Planta Med.* **2005**, *71*, 99-107.
242. Ning, H.; Xin, Z. C.; Lin, G.; Banie, L.; Lue, T. F.; Lin, C. S., Effects of icariin on phosphodiesterase-5 activity *in vitro* and cyclic guanosine monophosphate level in cavernous smooth muscle cells. *Urology* **2006**, *68*, 1350-1354.
243. Nagai, H.; He, J. X.; Tani, T.; Akao, T., Antispasmodic activity of Licochalcone A, a species-specific ingredient of *Glycyrrhiza inflanta* roots. *J. Pharm. Pharmacol.* **2007**, *59*, 1421-1426.
244. Liu, B.; Yang, J.; Wen, Q.; Li, Y., Isoliquiritigenin, a flavonoid from licorice, relaxes guinea-pig tracheal smooth muscle *in vitro* and *in vivo*: Role of cGMP/PKG pathway. *Eur. J. Pharmacol.* **2008**, *587*, 252-266.
245. Ko, W. C.; Chen, M. C.; Wang, S. H.; Lai, Y. H.; Chen, J. H.; Lin, C. N., 3-O-methylquercetin more selectively inhibits phosphodiesterase subtype 3. *Planta Med.* **2003**, *69*, 310-315.
246. Shin, H. J.; Kim, H. J.; Kwak, J. H.; Chun, H. O.; Kim, J. H.; Park, H., A prenylated flavonol, sophoflavescenol: A potent and selective inhibitor of cGMP phosphodiesterase 5. *Bioorg. Med. Chem.* **2002**, *12*, 2313-2316.
247. Lines, T. C.; Ono, M., FRS 1000, an extract of red onion peel, strongly inhibits phosphodiesterase 5A (PDE 5A). *Phytomedicine* **2006**, *13*, 236-239.
248. Dell'Agli, M.; Galli, G. V.; Vrhovsek, U.; Mattivi, F.; Bosisio, E., *In vitro* inhibition of human cGMP-specific phosphodiesterase-5 by polyphenols from red grapes. *J. Agricult. Food Chem.* **2005**, *53*.
-

-
249. Ko, W.-C.; Shih, C.-M.; Lai, Y.-H.; Chen, J.-H.; Huang, H.-L., Inhibitory effects of flavonoids on phosphodiesterase isozymes from guinea pig and their structure–activity relationships. *Biochem. Pharmacol.* **2004**, *68*, 2087-2094.
250. Kanokmedhakul, S.; Kanokmedhakul, K.; Nambuddee, K.; Kongsaree, P., New bioactive prenylflavonoids and dibenzocycloheptene derivative from roots of *dendrobium lanceolatum*. *J. Nat. Prod.* **2004**, *67*, 968-972.
251. Beldjoudi, N.; Mambu, L.; Labaïed, M.; Grellier, P.; Ramanitrahasimbola, D.; Rasoanaivo, P.; Martin, M. T.; Frappier, F., Flavonoids from *Dalbergia louvelii* and their antiplasmodial activity. *J. Nat. Prod.* **2003**, *66*, 1447-1450.
252. Auffret, G.; Labaied, M.; Frappier, F.; Rasoanaivo, P.; Grellier, P.; Lewin, G., Synthesis and antimalarial evaluation of a series of piperazinyl flavones. *Bioorg. Med. Chem. Lett.* **2007**, *17*, 959-963.
253. Tasdemir, D.; Lack, G.; Brun, R.; Rüedi, P.; Scapozza, L.; Perozzo, R., Inhibition of *Plasmodium falciparum* fatty acid biosynthesis: Evaluation of FabG, FabZ, and FabI as drug targets for flavonoids. *J. Med. Chem.* **2006**, *49*, 3345-3353.
254. Ferreira, J. F. S.; Luthria, D. L.; Sasaki, T.; Heyerick, A., Flavonoids from *Artemisia annua* L. as antioxidants and their potential synergism with artemisinin against malaria and cancer. *Molecules* **2010**, *15*, 3135-3170.
255. Liu, K. C. S.; Yang, S. L.; Roberts, M. F.; Elford, B. C.; Phillipson, J. D., The contribution of flavonoids to the antimalarial activity of *Artemisia annua*. *Planta Med.* **1989**, *55*, 654-655.
256. Lim, S. S.; Kim, H.-S.; Lee, D.-U., *In vitro* antimalarial activity of flavonoids and chalcones. *Bull. Korean Chem. Soc.* **2007**, *28*, 24595-2497.
-

-
257. Petty, F.; Trivedi, M. H.; Fulton, M.; Rush, A. J., Benzodiazepines as antidepressants: Does GABA play a role in depression? *Biol. Psychiatry* **1995**, *38*, 578-591.
258. Kennett, G. A.; Dourish, C. T.; Curzon, G., Antidepressant-like action of 5-HT_{1A} agonists and conventional antidepressants in an animal model of depression. *Eur. J. Pharmacol.* **1987**, *134*, 265-274.
259. McLeod, M. C.; Scarr, E.; Dean, B., Effects of benzodiazepine treatment on cortical GABA(A) and muscarinic receptors: Studies in schizophrenia and rats. *Psychiatry Res.* **2010**, *179*, 139-146.
260. Galantay, E. E.; Simpson, R.; Corriveau, G.; Denzer, M.; Knorr, D. C.; Strohschein, R. J.; Paoletta, N. A.; Uike, Y.; Gogerty, J. H.; Ryan, E. A.; Louis, C. I., Novel tricyclic systems. Oxazole, thiazole, and imidazole analogs of the amitriptyline type. *J. Med. Chem.* **1974**, *17*, 1316-1327.
261. Klemm, L. H.; Bower, G. M., Reformatskii reaction in syntheses of ω , ω -diarylalkonic acids and related compounds. *J. Org. Chem.* **1958**, *23*, 344-348.
262. Kofron, W. Process for preparation of diphenyl alkonic acids. U.S. Patent Number 3,412,146, **1968**.
263. Galantay, E. E. 5,9-Epoxy-6,7,8,9-tetrahydro-5H-benzocyclohepten-5-ols and process for preparing same. U.S. Patent Number 3,432,526, **1969**.
264. Kukla, M. J., Synthesis of 1-amino-5-phenyl-4,5-dihydro-3H-2-benzazepines and the isomeric 2-amino-1-benzazepines. *J. Heterocycl. Chem.* **1977**, *14*, 933-935.
265. Ackerman, K.; Horning, D. E.; Muchowski, J. M., New synthesis of 5-phenyl-2,3-dihydro- and 2,3,4,5-tetrahydro-1H-2-benzazepin-1-ones. *Can. J. Chem.* **1972**, *50*, 3886-3891.
-

266. Werner, L. H.; Ricca, S.; Rossi, A.; De Stevens, G., Imidazoline derivatives with antiarrhythmic activity. *J. Med. Chem.* **1967**, *10*, 575-582.
267. Jackson, P. F.; Li, J.-H.; Maclin, K. M.; Zhang, J. Aryl and heteroaryl poly(ADP-ribose) polymerase (PARP) inhibitors, preparation, and pharmaceutical compositions, and methods of therapeutic use. U.S. Patent Number 6,635,642, **2003**.
268. Li, J.-H.; Tays, K. L.; Zhang, J. Oxo-substituted heterocyclic compounds, therapeutic methods, and compositions for inhibiting poly(ADP-ribose) polymerase (PARP) activity. U.S. Patent Number 2002/0022636, **2002**.
269. Li, J.-H.; Tays, K. L.; Zhang, J. Oxo-substituted heterocyclic compounds, therapeutic methods, and compositions for inhibiting poly(ADP-ribose) polymerase (PARP) activity. International Publication Number WO 9911624, **1999**.
270. Jackson, P. F.; Li, J.-H.; Maclin, K. M.; Zhang, J. Preparation of PARP inhibitors. International Publication Number WO 9911649, **1999**.
271. Yadav, J. S.; Reddy, B. V. S.; Reddy, U. V. S.; Praneeth, K., Azido-Schmidt reaction for the formation of amides, imides and lactams from ketones in the presence of FeCl₃. *Tetrahedron Lett.* **2008**, *49*, 4742-4745.
272. Mphahlele, M. J.; Mampa, R. M., Synthesis and spectroscopic studies of oximes derived from 2-aryl-1,2,3,4-tetrahydro-1,4-benzoheterazepin-5(4*H*)-ones. *Phosphorus, Sulfur Silicon Relat. Elem.* **2001**, *176*, 227-235.
273. Kaye, P. T.; Mphahlele, M. J., Regioselective A-ring chlorination of benzodiazepine analogues using *tert*-butyl hypochlorite. *Synth. Commun.* **1994**, *24*, 1971-1978.
274. Schmidt, K. F., Über den imin-rest. *Ber. Dtsch. Chem. Ges.* **1924**, *57*, 704-706.
-

-
275. Greco, C. V.; Gray, R. P., Selective ring expansion of 5,10-octalin-1,6-diones via the Schmidt reaction. *Tetrahedron* **1970**, *26*, 4329-4337.
276. Bach, R. D.; Wolber, G. J., Theoretical study of the barrier to nitrogen inversion in N-cyano- and N-diazoformimine. Mechanism of the Schmidt reaction. *J. Org. Chem.* **1982**, *47*, 239-245.
277. Hassner, A.; Fibiger, R.; Amarasekara, A. S., Synthetic methods. 25. Titanium tetrachloride-catalyzed addition of hydrazoic acid to aldehydes and ketones. Thermolysis and photolysis of α -azido ethers. *J. Org. Chem.* **1988**, *53*, 22-27.
278. Song, D.; Rostami, A.; West, F. G., Domino electrocyclization/azide-capture/schmidt rearrangement of dienones: One-step synthesis of dihydropyridones from simple building blocks. *J. Am. Chem. Soc.* **2007**, *129*, 12012-12011.
279. Amer, F. A.; Hammouda, M.; El-Ahl, A. A. S.; Abdel-Wahab, B. F., 3-Pyrrolidinones. Michael addition and Schmidt rearrangement reactions. *Synth. Commun.* **2009**, *39*, 416-425.
280. Kurhade, S. E.; Enhawade, T.; Bhuniya, D.; Palle, V. P.; Reddy, D. S., Synthesis of novel sugar-lactam conjugates using the Aube reaction. *Org. Biomol. Chem.* **2011**, *9*, 744-747.
281. Krapcho, J.; Turk, C. F., Substituted 2,3-dihydro-1,5-benzothiazepin-4(5H)-one and related compounds. II. A new class of antidepressants. *J. Med. Chem.* **1966**, *9*, 191-195.
282. Misiti, D.; Rimatori, V., 2,3-Dihydro-2-phenyl-1,4-benzoxazepin-5(4H)-one from the reaction of the flavanone with hydrazoic acid. A reappraisal. *Tetrahedron Lett.* **1970**, *11*, 947-950.
283. Beckmann, E., Zur kenntniss der isonitrosoverbindungen. *Chem. Ber.* **1886**, *19*, 988.
-

-
284. Eaton, P. E.; Carlson, G. R.; Lee, J. T., Phosphorus pentoxide-methanesulfonic acid. Convenient alternative to polyphosphoric acid. *J. Org. Chem.* **1973**, *38*, 4071-4073.
285. Bakale, R. P.; Scialdone, M. A.; Johnson, C. R., Tin-directed Baeyer-Villiger and Beckmann fragmentations. *J. Am. Chem. Soc.* **1990**, *112*, 6729-6731.
286. Blaszczyk, K.; Koenig, H.; Mel, K.; Paryzek, Z., Abnormal Beckmann rearrangement of steroidal α -chlorocyclobutanone oximes: the fragmentation-substitution reaction. *Tetrahedron* **2006**, *62*, 1069-1078.
287. Pathak, U.; Pandey, L. K.; Mathur, S.; Suryanarayana, M. V. S., Ketoximes to N-substituted thioamides *via* PSCl_3 mediated Beckmann rearrangement. *Chem. Commun.* **2009**, *36*, 5409-5411.
288. Vilas, M.; Tojo, E., A mild and efficient way to prepare ϵ -caprolactam by using a novel salt related with ionic liquids. *Tetrahedron Lett.* **2010**, *53*, 4125-4128.
289. Crosby, I. T.; Shin, J. K.; Capuano, B., The application of the Schmidt reaction and Beckmann rearrangement to the synthesis of bicyclic lactams: Some mechanistic considerations. *Aus. J. Chem.* **2010**, *63*, 211-226.
290. Kim, D.; Ham, K.; Hong, S., Synthetic approach to flavanones and flavones *via* ligand-free palladium(II)-catalyzed conjugate addition of arylboronic acids to chromones. *Org. Biomol. Chem.* **2012**, *10*, 7305-7312.
291. Saengchantara, S. T.; Wallace, T. W., Conjugate addition of cuprate reagents to chromones: A route to 2-substituted chroman-4-ones. *Tetrahedron* **1990**, *46*, 3029-3036.
292. Meyer, A. M.; Katz, C. E.; Li, S.-W.; Vander Velde, D.; Aubé, J., A tandem Prins/Schmidt reaction approach to marine alkaloids: Formal and total syntheses of Lepadiformines A and C. *Org. Lett.* **2010**, *12*, 1244-1247.
-

-
293. Pi, H.-J.; Dong, J.-D.; An, N.; Du, W.; Deng, W.-P., Unexpected results from the re-investigation of the Beckmann rearrangement of ketoximes into amides by using TsCl. *Tetrahedron* **2009**, *65*, 7790-7793.
294. Xiao, L.-F.; Xia, C.-G.; Chen, J., *p*-Toluenesulfonic acid mediated zinc chloride: Highly effective catalyst for the Beckmann rearrangement. *Tetrahedron Lett.* **2007**, *48*, 7218-7221.
295. Fridén-Saxin, M.; Pemberton, N.; da Silva Andersson, K.; Dyrager, C.; Friberg, A.; Grøtli, M.; Luthman, K., Synthesis of 2-alkyl-substituted chromone derivatives using microwave irradiation. *J. Org. Chem.* **2009**, *74*, 2755-2759.
296. Chandrasekhar, S.; Vijeender, K.; Reddy, K. V., New synthesis of flavanones catalyzed by L-proline. *Tetrahedron Lett.* **2005**, *46*, 6991-6993.
297. Sathyanarayana, S.; Krishnamurty, H. G., Corroborative studies on the highly efficient preparation of 2'-hydroxychalcones using partially dehydrated barium hydroxide catalyst. *Curr. Sci.* **1988**, *57*, 1114-1116.
298. Chimenti, F.; Fioravanti, R.; Bolasco, A.; Chimenti, P.; Secci, D.; Rossi, F.; Yáñez, M.; Orallo, F.; Ortuso, F.; Alcaro, S.; Cirilli, R.; Ferretti, R.; Sanna, M. L., A new series of flavones, thioflavones, and flavanones as selective monoamine oxidase-B inhibitors. *Bioorg. Med. Chem.* **2010**, *18*, 1273-1279.
299. Ying, H.; Hu, Y.; He, Q.; Li, R.; Yang, B., Synthesis and anticancer activity of a novel class of flavonoids: 2,4-Diarylchromane[4,3-*d*]-1,9*b*-1,2,3-thiadiazolines. *Eur. J. Med. Chem.* **2007**, *42*, 226-234.
300. Tatsuoka, T.; Imao, K.; Suzuki, K.; Shibata, M.; Satoh, F., Synthesis of 2-phenyl-2,3,4,5-tetrahydro-1-benzoxepin-5-ones. *Heterocycles* **1990**, *30*, 749-752.
301. Martz, K. E.; Dorn, A.; Baur, B.; Schattel, V.; Goettert, M. I.; Mayer-Wrangowski, S. C.; Rauh, D.; Laufer, S. A., Targeting the hinge glycine flip and
-

- the activation loop: Novel approach to potent p38 α inhibitors. *J. Med. Chem.* **2012**, *55*, 7862-7874.
302. Barrett, I.; Meegan, M. J.; Hughes, R. B.; Carr, M.; Knox, A. J. S.; Artemenko, N.; Golfis, G.; Zisterer, D. M.; Lloyd, D. G., Synthesis, biological evaluation, structural–activity relationship, and docking study for a series of benzoxepin-derived estrogen receptor modulators. *Bioorg. Med. Chem.* **2008**, *16*, 9554-9573.
303. Tandon, V. K.; Khanna, J. M.; Chandra, A.; Anand, N., Phenethylamine in a rigid framework : Synthesis, stereochemistry and reactions of *cis* and *trans*-4-amino-2,3,4,5-tetrahydro-1-benzoxepin-5-ols and their derivatives. *Tetrahedron* **1990**, *46*, 2871-2882.
304. Ratier, M.; Pereyre, M., Organotin route for specific reductive ring opening of vinylcyclopropanes. *Tetrahedron Lett.* **1976**, *17*, 2273-2276.
305. Tatsuoka, T.; Suzuki, K.; Imao, K.; Sumoto, K. A diaryl butyric acid derivative and the production process thereof. Patent Number (Japan) 0187524, **1985**.
306. Corey, E. J.; Chaykovsky, M., A new synthesis of ketones. *J. Am. Chem. Soc.* **1964**, *86*, 1639-1640.
307. Corey, E. J.; Chaykovsky, M., Dimethylsulfoxonium methylide. *J. Am. Chem. Soc.* **1962**, *84*, 867-868.
308. Mae, M.; Matsuura, M.; Amii, H.; Uneyama, K., A facile synthesis of difluoromethylaziridines. *Tetrahedron Lett.* **2002**, *43*, 2069-2072.
309. Saito, T.; Sakairi, M.; Akiba, D., Enantioselective synthesis of aziridines from imines and alkyl halides using a camphor-derived chiral sulfide mediator *via* the imino Corey–Chaykovsky reaction. *Tetrahedron Lett.* **2001**, *42*, 5451-5454.
310. Vacher, B.; Bonnaud, B.; Funes, P.; Jubault, N.; Koek, W.; Assié, M.-B.; Così, C.; Kleven, M., Novel derivatives of 2-pyridinemethylamine as selective, potent,

- and orally active agonists at 5-HT_{1A} receptors. *J. Med. Chem.* **1999**, 42, 1648-1660.
311. Li, A.-H.; Dai, L.-X.; Aggarwal, V. K., Asymmetric ylide reactions: Epoxidation, cyclopropanation, aziridination, olefination, and rearrangement. *Chem. Rev.* **1997**, 97, 2341-2372.
312. Corey, E. J.; Cheng, H.; Baker, C. H.; Matsuda, S. P. T.; Li, D.; Song, X., Methodology for the preparation of pure recombinant *S. cerevisiae* lanosterol synthase using a baculovirus expression system. Evidence that oxirane cleavage and A-ring formation are concerted in the biosynthesis of lanosterol from 2,3-oxidosqualene. *J. Am. Chem. Soc.* **1997**, 119, 1277-1288.
313. Corey, E. J.; Chaykovsky, M., Methylsulfinyl carbanion ($\text{CH}_3\text{-SO-CH}_2^-$). Formation and applications to organic synthesis. *J. Am. Chem. Soc.* **1965**, 87, 1345-1353.
314. Corey, E. J.; Chaykovsky, M., Dimethyloxosulfonium methylide ($((\text{CH}_3)_2\text{SOCH}_2)$) and dimethylsulfonium methylide ($((\text{CH}_3)_2\text{SCH}_2)$). Formation and application to organic synthesis. *J. Am. Chem. Soc.* **1965**, 87, 1353-1364.
315. Grygorenko, O. O.; Artamonov, O. S.; Palamarchuk, G. V.; Zubatyuk, R. I.; Shishkin, O. V.; kamarov, I. V., Stereoselective synthesis of 2,4-methanoproline homologues. *Tetrahedron: Asymmetry* **2006**, 17, 252-258.
316. Dean, F. M.; Johnson, R. S., Reactions between 3-nitrochromone and diazoalkanes; Michael additions catalysed by diazoalkanes and nitrogen bases. *J. Chem. Soc., Perkin Trans. 1* **1980**, 2049-2053.
317. McCague, R.; Kuroda, R.; Leclercq, G.; Stoessel, S., Synthesis and estrogen receptor binding of 6,7-dihydro-8-phenyl-9-[4-[2-(dimethylamino)ethoxy]phenyl]-5*H*-benzocycloheptene, a nonisomerizable

- analogue of tamoxifen. X-ray crystallographic studies. *J. Med. Chem.* **1986**, *29*, 2053-2059.
318. Fillion, E.; Fishlock, D.; Wilsily, A.; Goll, J. M., Meldrum's acids as acylating agents in the catalytic intramolecular Friedel–Crafts reaction. *J. Org. Chem.* **2005**, *70*, 1316-1327.
319. Beletskiy, E. V.; Sudheer, C.; Douglas, C. J., Cooperative catalysis approach to intramolecular hydroacylation. *J. Org. Chem.* **2012**, *77*, 5884-5893.
320. Murineddu, G.; Ruiu, S.; Loriga, G.; Manca, I.; Lazzari, P.; Reali, R.; Pani, L.; Toma, L.; Pinna, G. A., Tricyclic pyrazoles. 3. Synthesis, biological evaluation, and molecular modeling of analogues of the cannabinoid antagonist 8-chloro-1-(2',4'-dichlorophenyl)-*N*-piperidin-1-yl-1,4,5,6-tetrahydrobenzo[6,7]cyclohepta-[1,2-*c*]pyrazole-3-carboxamide. *J. Med. Chem.* **2005**, *48*, 7351-7362.
321. Gilmore, R. C.; Horton, W. J., Seven-membered ring compounds. I. 7,8,9,10-tetrahydrocyclohepta[*d,e*]naphthalene. *J. Am. Chem. Soc.* **1951**, *73*, 1411-1414.
322. Huisgen, R.; Rietz, U., Medium rings. XIII. Intramolecular acylation of ω -(1-naphthyl) fatty acids. *Tetrahedron* **1958**, *2*, 271-288.
323. Isabelle, M. E.; Wightman, R. H.; Avdovich, H., W.; Laycock, D. E., Tricyclic aromatic ketones by cycliacylation of carboxylic acid derivatives of indian, tetralin, and benzosuberane. *Can. J. Chem.* **1980**, *58*, 1344-1349.
324. Negoro, N.; Sasaki, S.; Mikami, S.; Ito, M.; Suzuki, M.; Tsujihata, Y.; Ito, R.; Harada, A.; Takeuchi, K.; Suzuki, N.; Miyazaki, J.; Santou, T.; Odani, T.; Kanzaki, N.; Funami, M.; Tanaka, T.; Kogame, A.; Matsunaga, S.; Yasuma, T.; Momose, Y., Discovery of TAK-875: A potent, selective, and orally bioavailable GPR40 agonist. *ACS Med. Chem. Lett.* **2010**, *1*, 290-294.
325. Ho, T.-L.; Po-Fei, Y., Synthesis of phenolic sesquiterpenes *via* oxidative cleavage of benzocycloalkenols. *Tetrahedron* **1995**, *51*, 181-192.

-
326. Gardner, P. D.; Horton, W. J., Seven-membered ring compounds. II. 7,8-Dihydrocyclohepta[*d,e*]naphthalene-1,2,8,9,10,10a-hexahydrocyclohepta[*k,l,m*]-benz[*e*]indene and the attempted synthesis of cyclohepta[*d,e*]naphthalene. *J. Am. Chem. Soc.* **1952**, *74*, 657-660.
327. Hendrickson, J. B.; Hussoin, M. S., Reactions of carboxylic acids with phosphonium anhydrides. *J. Org. Chem.* **1989**, *54*, 1144-1449.
328. Gao, P.; Sun, X.; Qiu, T., Synthesis of 2,3-benzosuberone. *Jingxi Huagong* **2010**, *27*, 929-932.
329. Christol, H.; Delhoste, Y.; Mousseron, M., Acid-catalyzed rearrangements. VIII. The synthesis of β,γ -benzotropolones. *Bull. Soc. Chim. Fr.* **1959**, 1238-1243.
330. Dodd, J. H. In *Polyphosphoric Acid*. John Wiley & Sons, Ltd., **2001**.
331. Thompson, P. E. Design and synthesis of CNS-active adrenergic and analgesic compounds. University of Melbourne, **1991**.
332. Murray, R. J.; Schmiesing, R. J. Diphenyl-2-piperidinone and 2-pyrrolidinone derivatives having anti-convulsant and neuroprotective activity. International Publication Number WO 9,532,135, **1995**.
333. Reddy, M. P.; Rao, G. S. K., Synthesis of 5-*p*-hydroxybenzyl-5,6-dihydro-2-naphthol, (+)-sequirin D. *J. Chem. Soc., Perkin Trans. I* **1981**, *10*, 2662-2665.
334. Kursanov, D. N.; Parnes, Z. N.; Bassova, G. I.; Loim, N. M.; Zdanovich, V. I., Ionic hydrogenation of the ethylene bond and the double bond of the carbonyl group. *Tetrahedron* **1967**, *23*, 2235-2242.
335. Tyllick, C.; El-Zohry, M. F.; Li, M.; Roberts, R. M., Cyclialkylation studies. I. A practical synthetic approach to the 2,3:6,7-dibenzocyclo[3.2.2]nona-2,6-diene system. *J. Org. Chem.* **1991**, *56*, 2938-2940.
-

-
336. Quiclet-Sire, B. a.; Tölle, N.; Zafar, S. N.; Zard, S. Z., Oxime derivatives as α -electrophiles. From α -tetralone oximes to tetracyclic frameworks. *Org. Lett.* **2011**, *13*, 3266-3269.
337. Oh, S.-H.; Sato, T., Metal-catalyzed organic photoreactions. Photoreaction of 2-chloroacetophenone with functionalized olefins in the presence of silver trifluoromethanesulfonate. *J. Org. Chem.* **1994**, *59*, 3744-3746.
338. Dyke, S. F.; Tiley, E. P.; White, A. W. C.; Gale, D. P., α -Aminonitriles—I: A simple synthesis of deoxybenzoins. *Tetrahedron* **1975**, *31*, 1219-1222.
339. Antus, S.; Baitz-Gacs, E.; Boross, F.; Nogradi, M.; Solyom, A., Oxidation von 1,3-diphenyl-1,3-propandionen mit thallium-(III)-nitrat in methanol. *Liebigs. Ann. Chem.* **1980**, *8*, 1271-1282.
340. Abbott, B. M.; Thompson, P. E., PDE2 inhibition by the PI3 kinase inhibitor LY294002 and analogues. *Bioorg. Med. Chem. Lett.* **2004**, *14*, 2847-2851.
341. Abbott, B. M.; Thompson, P. E., Analysis of anti-PDE3 activity of 2-morpholinochromone derivatives reveals multiple mechanisms of anti-platelet activity. *Bioorg. Med. Chem. Lett.* **2006**, *16*, 969-973.
342. Nakamura, J.; Okamura, N.; Kawakami, Y., Augmentation of lipolysis in adipocytes from fed rats, but not from starved rats, by inhibition of rolipram-sensitive phosphodiesterase 4. *Arch. Biochem. Biophys.* **2004**, *425*, 106-114.
343. Berkowitz, D. E.; Gregg, C. J.; Steppan, J.; Gonzalez, D. R.; Champion, H. C.; Phan, A. C.; Nhyan, D.; Shoukas, A. A.; Hare, J. M.; Barouch, L. A., A beta(2)-adrenergic receptor-coupled phosphoinositide 3-kinase constrains cAMP-dependent increases in cardiac intropy through phosphodiesterase 4 activation. *Anesth. Analg.* **2010**, *111*.
-

-
344. Gharbi, S. I.; Zvelebil, M. J.; Shuttleworth, S. J.; Hancox, T.; Saghir, N.; Timms, J. F.; Waterfield, M. D., Exploring the specificity of the PI3K family inhibitor LY294002. *Biochem. J.* **2007**, *404*, 15-21.
345. Nankervis, J. L. Small molecule inhibitors of PDE4. Monash University, Monash Institute of Pharmaceutical Sciences, **2012**.
346. Dillard, L. W.; Yuan, J.; Jia, L.; Zheng, Y. Inhibitors of beta-secretase. International Publication Number WO 2010/021680, **2010**.
347. Csajernyik, G.; Karlstrom, S.; Kers, A.; Kolmodin, K.; Nylof, M.; Ohberg, L.; Rakos, L.; Sandberg, L.; Sehgelmeble, F.; Soderman, P.; Swahn, B.-M.; von Berg, S. Compounds and their use as BACE inhibitors. International Publication Number WO 2012/087236, **2012**.
348. Abbott, B.; Thompson, P., Synthetic studies of the phosphatidylinositol 3-kinase inhibitor LY294002 and related analogues. *Aus. J. Chem.* **2003**, *56*, 1099-1106.
349. Friden-Saxin, M.; Pemberton, N.; Andersson, K. d. S.; Dyrager, C.; Friberg, A.; Grotli, M.; Luthman, K., Synthesis of 2-alkyl-substituted chromone derivatives using microwave irradiation. *J. Org. Chem.* **2009**, *74*, 2755-2759.
350. Bedford, R. B.; Blake, M. E.; Butts, C. P.; Holder, D., The Suzuki coupling of aryl chlorides in TBAB-water mixtures. *Chem. Commun.* **2003**, 466-467.
351. Bedford, R. B.; Butts, C. P.; Hurst, T. E.; Lidstrom, P., The Suzuki coupling of aryl chlorides under microwave heating. *Adv. Synth. Catal.* **2004**, *346*, 1627-1630.
352. Dong, X.; Liu, T.; Yan, J.; Wu, P.; Chen, J.; Hu, Y., Synthesis, biological evaluation and quantitative structure-activities relationship of flavonoids as vasorelaxant agents. *Bioorg. Med. Chem.* **2009**, *17*, 716-726.
353. Klier, L.; Bresser, T.; Nigst, T. A.; Karaghiosoff, K.; Knochel, P., Lewis acid-triggered selective zincation of chromones, quinolones, and thiochromones:
-

- Application to the preparation of natural flavones and isoflavones. *J. Am. Chem. Soc.* **2012**, *134*, 13584-13587.
354. Lipinski, C. A., Drug-like properties and the causes of poor solubility and poor permeability. *J. Pharmacol. Toxicol. Methods* **2000**, *44*, 235-249.
355. Lipinski, C. A., Lead- and drug-like compounds: The Rule-of-Five revolution. *Drug Discov. Today: Tech.* **2004**, *1*, 337-341.
356. Bathurst, I.; Hentschel, C., Medicines for Malaria Venture: Sustaining antimalarial drug development. *Trends Parasitol.* **2006**, *22*, 301-307.
357. Tanner, M.; Savigny, D. D., Malaria eradication back on the table. *Bull. WHO* **2008**, *86*, 82-82.
358. *Bill and Melinda Gates Foundation Malarial Forum, Day 2 [Transcript]*; 17 October, **2007**.
359. Burrows, J. N.; Leroy, D.; Lotharius, J.; Waterson, D., Challenges in antimalarial drug discovery. *Future Med. Chem.* **2011**, *3*, 1401-1412.
360. Craft, J. C., Challenges facing drug development for malaria. *Curr. Opin. Microbiol.* **2008**, *11*, 428-433.
361. Pink, R.; Hudson, A.; Mouries, M.-A.; Bendig, M., Opportunities and challenges in antiparasitic drug discovery. *Nat. Rev. Drug Discov.* **2005**, *4*, 727-740.
362. Gelb, M. H., Drug discovery for malaria: A very challenging and timely endeavor. *Curr. Opin. Chem. Biol.* **2007**, *11*, 440-445.
363. Fidock, D. A., Drug discovery: Priming the antimalarial pipeline. *Nature* **2010**, *465*, 297-298.
364. Sahu, N. K.; Sahu, S.; Kohli, D. V., Novel molecular targets for antimalarial drug development. *Chem. Biol. Drug Des.* **2008**, *71*, 287-297.
365. Wiesner, J.; Ortmann, R.; Jomaa, H.; Schlitzer, M., New antimalarial drugs. *Angew. Chem. Int. Ed.* **2003**, *42*, 5274-5293.

-
366. Weisman, J. L.; Liou, A. P.; Shelat, A. A.; Cohen, F. E.; Kiplin Guy, R.; DeRisi, J. L., Searching for new antimalarial therapeutics amongst known drugs. *Chem. Biol. Drug Des.* **2006**, *67*, 409-416.
367. Dandapani, S.; Marcaurelle, L. A., Accessing new chemical space for 'undruggable' targets. *Nat. Chem. Biol.* **2010**, *6*, 861-863.
368. Lipinski, C. A.; Hopkins, A., Navigating chemical space for biology and medicine. *Nature* **2004**, *432*, 855-861.
369. Keller, T. H.; Pichota, A.; Yin, Z., A practical view of 'druggability'. *Curr. Opin. Chem. Biol.* **2006**, *10*, 357-361.
370. Dobson, C. M., Chemical space and biology. *Nature* **2004**, *432*, 824-828.
371. Eichelbaum, M.; Gross, A. S., Stereochemical aspects of drug action and disposition. In *Advances in Drug Research*, (Eds. Bernard, T.; Urs, A. M.) Academic Press: **1996**, *28*, 1-64.
372. Clayden, J.; Moran, W. J.; Edwards, P. J.; LaPlante, S. R., The challenge of atropisomerism in drug discovery. *Angew. Chem. Int. Ed.* **2009**, *48*, 6398-6401.
373. Soderling, S. H.; Bayuga, S. J.; Beavo, J. A., Identification and characterization of a novel family of cyclic nucleotide phosphodiesterases. *J. Biol. Chem.* **1998**, *273*, 15553-15558.
374. Still, W. C.; Kahn, M.; Mitra, A., Rapid chromatographic technique for preparative separations with moderate resolution. *J. Org. Chem.* **1978**, *43*, 2923-2925.
375. Gottlieb, H. E.; Kotlyar, V.; Nudelman, A., NMR chemical shifts of common laboratory solvents as trace impurities. *J. Org. Chem.* **1997**, *62*, 7512-7515.
376. Delgado, A.; Garcia, J. M.; Mauleon, D.; Minguillon, C.; Subirats, J. R.; Feliz, M.; Lopez, F.; Velasco, D., Synthesis and conformational analysis of 2-amino-1,2,3,4-tetrahydro-1-naphthalenols. *Can. J. Chem.* **1988**, *66*, 517-527.
-

377. Clive, D. L. J.; Pham, M. P.; Subedi, R., Carbocyclization by radical closure onto *O*-trityl oximes: Dramatic effect of diphenyl diselenide. *J. Am. Chem. Soc.* **2007**, *129*, 2713-2717.
378. Meyers, A. I.; Hutchings, R. H., The asymmetric synthesis of 1-alkyl-2,3,4,5-tetrahydro-benzazepines and benzo[β]-1-azabicyclo[5,3,1]decanes. *Tetrahedron* **1993**, *49*, 1807-1820.
379. Huckle, D.; Lockhart, I. M.; Wright, M., The preparation of some 2,3-dihydro-1,4-benzoxazepin-5(4*H*)-ones and related compounds. *J. Chem. Soc.* **1965**, 1137-1141.
380. Aitmambetov, A.; Dalimov, D.; Kubzheterova, A., Synthetic analogs of natural flavolignans. XV. Isomerization of 2'-hydroxychalcones into flavanones using triethylamine. *Chemistry of Natural Compounds* **2001**, *37*, 421-423.
381. Bargallini, G., Flavone, flavanone and flavonol derivatives of hydroxyquinone. *Gazz. Chim. Ital.* **1947**, *70*, 170-178.
382. Dauzonne, D.; Monneret, C., A new synthesis of flavanones. *Synthesis* **1997**, 1305-1308.

Appendices

Appendix 1

Chapter 2 publication

Howard, B. L.; Thompson, P. E.; Manallack, D. T. Active site similarity between human and *Plasmodium falciparum* phosphodiesterases: Considerations for antimalarial drug design. *Journal of Computer-Aided Molecular Design* **2011**, 25, 753-762.

Active site similarity between human and *Plasmodium falciparum* phosphodiesterases: considerations for antimalarial drug design

Brittany L. Howard · Philip E. Thompson ·
David T. Manallack

Received: 31 March 2011 / Accepted: 8 July 2011 / Published online: 16 July 2011
© Springer Science+Business Media B.V. 2011

Abstract The similarity between *Plasmodium falciparum* phosphodiesterase enzymes (PfPDEs) and their human counterparts have been examined and human PDE9A was found to be a suitable template for the construction of homology models for each of the four PfPDE isoforms. In contrast, the architecture of the active sites of each model was most similar to human PDE1. Molecular docking was able to model cyclic guanosine monophosphate (cGMP) substrate binding in each case but a docking mode supporting cyclic adenosine monophosphate (cAMP) binding could not be found. Anticipating the potential of PfPDE inhibitors as anti-malarial drugs, a range of reported PDE inhibitors including zaprinast and sildenafil were docked into the model of PfPDE α . The results were consistent with their reported biological activities, and the potential of PDE1/9 inhibitor analogues was also supported by docking.

Keywords Malaria · *Plasmodium falciparum* · Phosphodiesterase · Homology modelling · Molecular modelling · Molecular docking

Introduction

Malaria is an infectious disease caused by protozoan parasites and is transmitted through the bite of infected female Anopheles mosquitoes [1, 2]. The malaria parasite belongs to the genus *Plasmodium*, with the majority of human infections caused by four species (*P. falciparum*, *P. vivax*, *P. malariae*, and *P. ovale*). *P. falciparum* is the most pathogenic form and the only species where life-threatening complications such as cerebral malaria, severe anaemia and renal failure are frequently seen [3]. The life-cycle of *P. falciparum* consists of complex sexual stages in the mosquito and asexual replicating stages in the human host [4].

Despite the range of drug therapies available (including quinolones, artemisinins, antifolates, atovaquone/proguanil combinations, and antibiotics), there is a paucity of simple and effective drug regimes for treating malaria. More importantly, drug resistance in *P. falciparum* has limited the number of viable treatment options [5, 6]. The challenge therefore faced by the drug discovery community is to find new targets in an effort to help treat malaria. Great advances have been made in genomics and the provision of laboratory methods to enable research into parasite life cycles. Recent work has looked at further interventions in the blood and liver stages as well as the potential for developing a range of vaccines [7].

While targeting essential metabolic pathways that are present in the parasite but absent or non-essential in the human host has had some success, the alternative approach is to seek targets common to both organisms for which a range of human therapeutic substances have been developed. An example of the latter strategy is to target phosphodiesterase (PDE) enzymes [8]. The PDEs are a superfamily of metal ion-dependent enzymes whose primary role is to terminate the cyclic nucleotide second

Dedicated to the memory of Kate Burt.

Electronic supplementary material The online version of this article (doi:10.1007/s10822-011-9458-5) contains supplementary material, which is available to authorized users.

B. L. Howard · P. E. Thompson · D. T. Manallack (✉)
Medicinal Chemistry and Drug Action, Monash Institute
of Pharmaceutical Sciences, Monash University,
381 Royal Parade, Parkville, VIC 3052, Australia
e-mail: [REDACTED]

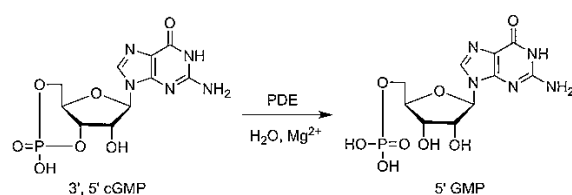


Fig. 1 Reaction catalysed by phosphodiesterase illustrated with cGMP as the substrate

messenger signal within a cell through hydrolysis of the 3'-phosphoester bond of cyclic adenosine monophosphate (cAMP) and cyclic guanosine monophosphate (cGMP; Fig. 1) [9–11].

Four PDEs (*Pf*PDE α – δ) are present in the genome of *P. falciparum* which have been cloned and characterised [12–14]. Furthermore, various studies have indicated that cyclic nucleotides are likely to play a major role in the cell biology of *P. falciparum* (including sexual development, hepatocyte infection, gametocytogenesis, cell cycle control, and exocytosis) [15, 16]. As a consequence, it has been suggested that targeting *P. falciparum* PDEs should disrupt a range of physiological processes and weaken or kill the organism [15–19]. Interest in this area has been focussed on understanding the role of PDEs in the parasite life cycle [15, 16, 20]. In addition, Yuasa and co-workers have screened compounds against *Pf*PDE α which has identified potential starting points for medicinal chemistry [21]. Interestingly, zaprinast was able to inhibit *Pf*PDE α with an IC₅₀ of 3.8 μ M and to inhibit parasite proliferation with an EC₅₀ of 35 μ M [21]. More recently, Beghyn and co-workers [22] developed a series of tadalafil analogues as potential inhibitors of *Pf*PDEs with the best compound (Fig. 2) showing potent antiplasmodial activity (IC₅₀ 0.5 μ M). Additional work on these compounds is required to determine whether blockade of *Pf*PDEs was responsible

for the inhibition of proliferation. Certainly, the provision of more potent and selective compounds will aid this research.

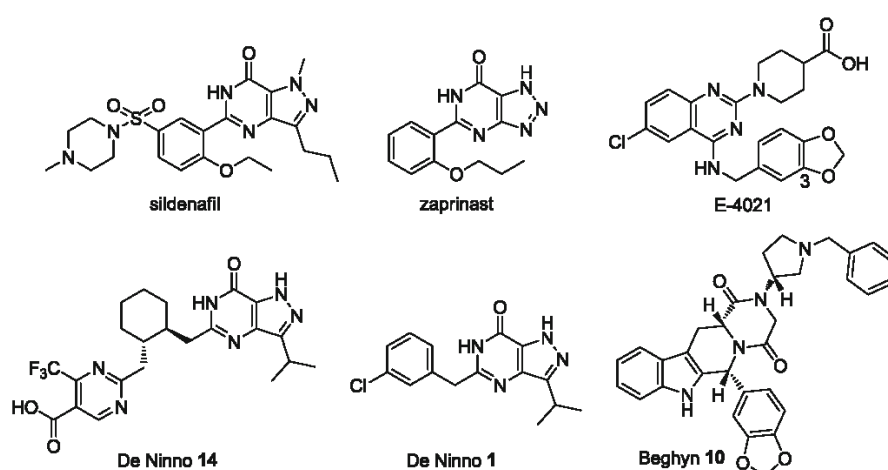
As crystal structures of *P. falciparum* PDEs have yet to be described, homology models of these enzymes based on a human PDE template could facilitate our drug discovery efforts. The human genome encodes for 21 PDEs that are classified into 11 families, with up to 46% sequence homology at the amino acid level [14, 23–25]. This current study has focussed on the generation of *Pf*PDE homology models for each of the four isoforms. Molecular docking experiments have also been undertaken to gain insights into cyclic nucleotide selectivity and the binding modes of known inhibitors.

Computational methods

Sequence alignment, template selection

Protein sequences of both human and malarial PDEs were retrieved from the UniProtKB database [26]. The Lalign [27] global alignment method was employed to compare sequences to determine percentage homologies and to suggest likely alignments. Further adjustments to the sequence alignments were undertaken to coincide with previous work in our laboratories [28] (suppl. data). Usually this involved moving gaps out of helical regions to loop sections. This optimised alignment utilised the 16 amino acids known to be conserved among the human enzymes as a guide to give the appropriate overlay of these invariant residues. These adjustments align residues that play a key structural role in the protein. From these analyses potential template proteins were identified and additional criteria were examined to select the most appropriate crystal structure for homology modelling purposes.

Fig. 2 Structures of the ligands used in the docking studies. Compounds De Ninno 1 and De Ninno 14 were taken from the study by De Ninno and co-workers [31] while compound Beghyn 10 was taken from the research recently described by Beghyn et al. [22], and in each case utilises their numbering schemes



Model building and minimisation

Each homology model was generated using Prime version 2.2 (Maestro version 9.1, Schrödinger, LLC, New York, USA) employing the optimised sequence alignment. The model building process used the PDE9A structure 3DYN [29] and retained the endogenous cGMP ligand, metal ions together with their coordinated water molecules. Minimisation of the model was undertaken using MacroModel version 9.8 (Maestro version 9.1, Schrödinger, LLC, New York, USA), employing the PRCG method and the OPLS_2005 force field. Initially, amino acid side chains were minimised with the ligand, metals, water molecules and protein backbone held rigid. Steric clashes were addressed by the rotation of strained residues. Typically this was a result of the substitution of a smaller amino acid for a larger one and manual inspection was required to look for alternative conformations to reduce steric strain. This involved examining other PDE crystal structures with similar amino acids in these positions to provide clues to likely low energy conformations. Following this, the model was further minimised while maintaining the previous constraints. A final minimisation was conducted without constraints and the models were assessed using MolProbity [30] which included a Ramachandran analysis.

Docking

Docking was performed using Glide version 5.6 (Maestro version 9.1, Schrödinger, LLC, New York, USA) employing the XP (extra precision) mode. Both cyclic nucleotides (cAMP and cGMP) were docked into each *Pf*PDE model. In each case, two conformations of the terminal carboxamide of the invariant purine-scanning glutamine (Gln453; the numbering used in this study refers to the 3DYN crystal structure [29]) were explored. Additionally, each cyclic nucleotide was minimized in the protein using both conformations of the carboxamide of the purine-scanning glutamine. This was undertaken to gain insight into the conformation of this residue and was applied to the docking of a series of PDE inhibitors (Fig. 2).

Results and discussion

The similarity between *h*PDE and *Pf*PDE has been previously recognized and Wentzinger and Seebeck suggested that the sequences of the *Pf*PDEs conformed to the general Class I grouping of the mammalian PDEs [32]. This is indirectly supported by the crystal structure of *Leishmania major* (*Lmj*PDEB1) which similarly adopts the general fold of the Class I PDEs, drawing the link between mammalian and protozoan PDEs [33].

The full-length PDE proteins have been depicted as having three regions: an N-terminal splicing region, a regulatory domain, and a C-terminal catalytic domain. Within the catalytic domain of each PDE enzyme are 16 α -helices which can be further divided into three subdomains (helices 1–7, 8–11, and 12–16). The active site exists at the interface of the three subdomains, where 11 of the 16 invariant amino acids of the catalytic domain are situated [34]. The catalytic site consists of four subsites that influence substrate binding: a metal-binding site (M-site), core pocket (Q pocket), hydrophobic pocket (H pocket) and lid region (L region) [24].

Protein sequence comparison

An examination of the full length *Pf*PDE sequences has predicted that they contain three to six transmembrane helices, suggesting that they are integral membrane proteins [28]. Sequence analysis of these full length *Pf*PDEs has also shown that they represent a new PDE family [21]. Interestingly, they show a low degree of relatedness to *h*PDE9A as well as *Dictyostelium* PDE, RegA [21] from an evolutionary perspective. An analysis of the catalytic domains of the four *Pf*PDEs showed that their sequence identities varied from 25 to 37% (Table 1). Again the *Pf*PDEs did not fall into any known human PDE families when these catalytic domains were compared in isolation. On average, the four *Pf*PDEs showed a sequence identity of 23% to the human PDEs, with approximately 50% of residues being indicated as highly similar. *Lmj*PDEB1 showed 26% average sequence identity with the human PDEs which was in contrast to its similarity to the *Pf*PDEs (22%). Given that the sequence identities were quite low and did not vary considerably across the human PDEs, the choice of template for the *Pf*PDEs was influenced by the earlier finding of the evolutionary relatedness between the *Pf*PDEs and *h*PDE9A. The comparison of *h*PDE9A to *Pf*PDE α showed a 27% sequence identity with just over 50% of residues being considered highly similar.

There are 16 amino acids that are absolutely conserved among the 21 human PDE enzymes, and of these 13 are also fully conserved across the series of four *Pf*PDE enzymes. The changes that would result from the lack of conservation of the three outstanding residues are not expected to alter the gross structure of the proteins. An invariant asparagine in human enzymes (N253) at the beginning of helix 6 is conserved in *Pf*PDE β , γ and δ but was found to be a threonine residue in *Pf*PDE α . In the *h*PDEs this asparagine residue may provide structural stability to the enzyme by forming a hydrogen bond with adjacent backbone amides of isoleucine, valine and alanine residues. Within helix 9, serine replaces a conserved alanine (A312) in *Pf*PDE α , β and γ . This alanine residue is

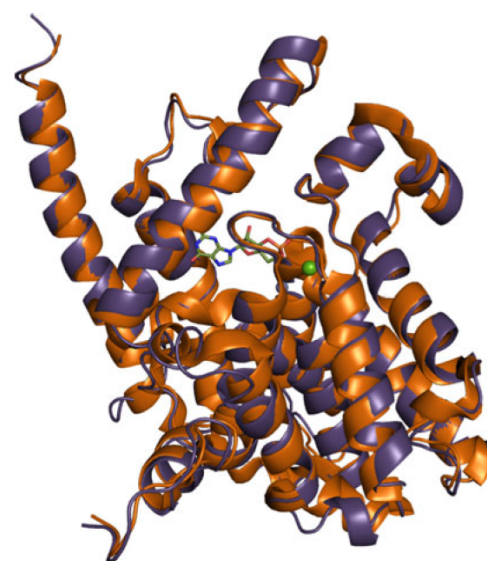
Table 1 Percent homologies of human and protozoan PDE enzymes

		<i>Pf</i> PDE α	<i>Pf</i> PDE β	<i>Pf</i> PDE γ	<i>Pf</i> PDE δ	<i>Lmj</i> PDEB1
<i>Pf</i> PDE	α					21.9
	β	30.9				23.1
	γ	29.8	36.8			21.9
	δ	25.3	27.8	27		21.1
<i>hPDE</i>	1A	21.2	26.7	24.6	21.1	24
	1B	23.6	25.8	26.3	21.9	24.6
	1C	20.9	25.2	25.8	22.7	24.1
	2A	23.9	24.9	24.3	18.4	28.3
	3A	22.6	22.8	23.9	20.2	21.4
	3B	21.2	23.1	24.9	20	23.2
	4A	24.1	24.9	25.6	19.9	27.7
	4B	25.4	24.4	26.5	18.9	28
	4C	23.9	24.7	26.8	20.6	27.9
	4D	24.3	25.6	27.4	18.2	27.6
	5A	19.9	23.3	22.5	20.2	27.8
	6A	20.4	21.8	22.4	17.4	25.7
	6B	21.5	23.2	23	16.5	24.9
	6C	20.3	23.8	23	18.5	26
	7A	26.5	27.3	24.6	22.5	26.9
	7B	21.6	24.8	22.1	23.2	26
	8A	22.5	24	26.4	21.3	26.2
	8B	23.2	24	26.1	19.2	26.4
	9A	26.8	27.5	23.1	21.1	25.7
	10A	20.9	22.9	22.1	17.6	26.4
	11A	21.3	25.8	23.4	18.2	30.7

positioned in a cavity on the outside of the protein where there is sufficient room to accommodate the additional hydroxyl group of the serine. Thirdly, histidine (H324) in helix 10 is replaced by a tyrosine residue in all four *Pf*PDEs and appears to be coupled to a complementary change at an acidic residue (usually aspartic acid; PDE1 is the only exception, where it is a glutamic acid) between helices 7 and 8 (D295). This acidic residue in human enzymes is replaced with a glycine residue in the *Pf*PDE enzymes that presumably allows room for the larger tyrosine residue.

Homology models

Homology models of the four *Pf*PDEs were constructed based on the co-ordinates of the *hPDE9A* crystal structure (pdb code: 3DYN) [29]. In this structure, *hPDE9A* is in complex with the endogenous ligand cGMP at 2.10 Å resolution [29]. When superimposed onto the *hPDE9A* crystal structure template (Fig. 3), the only noticeable deviations from that structure arose from small insertions in the loop regions. These insertions were not in close

**Fig. 3** Overlay of the fully minimised *Pf*PDE α homology model (light) with the 3DYN crystal structure (dark) [29]

proximity to the binding site in any of the models generated and would not be expected to significantly affect substrate or inhibitor binding. Each of the models was assessed using MolProbity [30] and a Ramachandran plot analysis (suppl. data) that showed backbone phi and psi angles in the expected regions and required no further refinement.

hPDE binding sites are characterised primarily by a critical conserved purine-scanning glutamine (Gln453) residue and ‘hydrophobic clamp’ comprised of an aromatic purine-stacking residue at the roof of the binding site (Phe456) and a hydrophobic residue, isoleucine, valine or leucine at the bottom of the site (Leu420, R5 in Table 2) [11, 23, 25, 28]. This forms the basis of adenine or guanine binding of the cyclic nucleotides.

The models in this study were built retaining cGMP, the metal ions and coordinated water molecules in the binding site to ensure that the binding cavity would not collapse during the building or minimisation of the models. This helped maintain the integrity of the hydrogen bond network within the site, and ensured the hydrophobic clamp remained in position. Thus the resultant models are constructed around these features, yielding a cGMP substrate bound conformer of the *Pf*PDEs. Removal of the endogenous ligand and subsequent full minimisation did not result in any significant change to the positions of the metal ions nor to the shape or volume of the binding cavity (Fig. 4; suppl. data). These ‘cGMP-specific’ models were considered to be suitable for further modelling work, as experimental work by Yuasa and co-workers had previously shown *Pf*PDE α to be cGMP specific [21].

Table 2 A list of the 25 residues associated with the active site of human, *P. falciparum* and *L. major* PDEs

3DYN residue number	Region	Phosphodiesterase																
		<i>Human</i>											<i>P. falciparum</i>				<i>L. major</i>	
		1 (A, B, C)	2	3	4	5	6	7 (A, B)	8	9	10	11	α	β	γ	δ	B1	
292	(i)	M	H	H	H	H	H	H	H	H	H	H	H	H	H	H	H	H
293	(i)	M	D	D	D	D	D	D	D	D	D	D	D	D	D	D	D	D
296	(i)	M	H	H	H	H	H	H	H	H	H	H	H	H	H	H	H	H
322	(i)	M	E	E	E	E	E	E	E	E	E	E	E	E	E	E	E	E
325	(i)	M	H	H	H	H	H	H	H	H	H	H	H	H	H	H	H	H
402	(i)	M	D	D	D	D	D	D	D	D	D	D	D	D	D	D	D	D
251	(R3)	Q	Y	Y	Y	Y	Y	Y	Y	Y	F	Y	Y	Y	Y	Y	Y	Y
405	(R1)	Q	H	D	G	N	A	A	N	N	N	S	A	H	H	H	H	N
413	(R2)	Q	H	T	H	Y	Q	Q	S	C	A	T	S	H	H	H	H	S
420	(R5)	Q + H	L	I	I	I	V	V	V	I	L	I	V	I	V	L	V	V
423	(i)	Q	E	E	E	E	E	E	E	E	E	E	E	E	E	E	E	E
453	(R6) (i)	Q	Q	Q	Q	Q	Q	Q	Q	Q	Q	Q	Q	Q	Q	Q	Q	Q
456		Q	F	F	F	F	F	F	F	F	F	F	W	F	F	F	F	F
490	(R7)	Q	W	W	W	Y	W	W	W	W	Y	W	W	W	W	W	W	I
421		H	M, L, M	Y	V	M	A	A	T, C	S	L	Y	T	N ^a	L	V	S	T
424		H	F	F	F	F	F	F	F	Y	Y	F	F	F	F	F	F	F
441		H	L (ii)	M	F	M	L	M	L	V	F	M	I	C ^a	L	L	I	M
301		L	N	N	N	N	N	N	Q	N	N	N	N	N	N	N	N	N
302		L	N, N, S	S	A	Q	S	L	P	S	T	S	A	Y ^a	L	I	S	S
303		L	F	F	F	F	Y	Y	F	F	Y	Y	Y	F	F	F	Y	F
452		L	S	L	L	S	M	L	I	S	A	G	L	S	S	I ^c	T ^d	G
455		L	G	S	S	G	G	G	G	S	G	G	E	D ^a	T	T	Y ^d	G
459		L	F	H	H	Y	A	F	Y	Y	F	A	S	H	F	E ^c	I ^d	F
406	(R8)	(iii)	P	Q	P	P	I	I	P	P	E	V	V	S ^a	G ^b	N ^c	T ^d	V
417	(R4)	(iii)	T	A	T	T	A	A	S	A	V	A	A	T	C ^b	V	T	A

Numbering is based on the 3DYN pdb crystal structure [29]. (i) indicates an invariant residue, (ii) while a list of amino acids has been compiled for this hydrophobic region position, this amino acid falls in a loop region. Each of the PDEs have differing lengths for this loop and thus in a 3-dimensional sense it may be difficult to make comparisons. Having said that, PDEs 3, 4, 5 and 9 overlay quite well while PDE1 is distorted at this point, (iii) no region assigned to this residue. R numbers in brackets refers to numbering from ref [28]

^a Residue as unique to *PfPDE α* at this position

^b Residue as unique to *PfPDE β* at this position

^c Residue as unique to *PfPDE γ* at this position

^d Residue as unique to *PfPDE δ* at this position

Active site analysis

With models established that preserved the basic fold of the PDE catalytic domain, we then examined the residues associated with the active site of the *PfPDEs*. This may be a means to predict or understand the cyclic nucleotide or inhibitor selectivity of the isozymes. Firstly, the sequence similarity of the cyclic nucleotide binding site was assessed by sequence alignment on the key residues in the M (metal-binding), H (hydrophobic pocket), L (lid region) and Q (core pocket) regions (Table 2) as defined by Sung et al. [24]. Within the active site itself, the purine-stacking phenylalanine is conserved while at the opposite side of

this site the amino acid (R5) varies between the following hydrophobic residues: isoleucine (α), valine (β , δ) and leucine (γ).

With regard to the purine-scanning glutamine residue (R6, Table 2), it has been shown that in human PDEs the terminal carboxamide group of this residue exists in either one of two conformations (through a 180° rotation) and forms complementary hydrogen bonds to either of the cyclic nucleotide substrates [25]. This ‘glutamine switch’ mechanism has been proposed to explain PDE substrate preference for cAMP and cGMP. Both cAMP- and cGMP-specific enzymes hold the glutamine in the appropriate conformation through a network of hydrogen bonds.

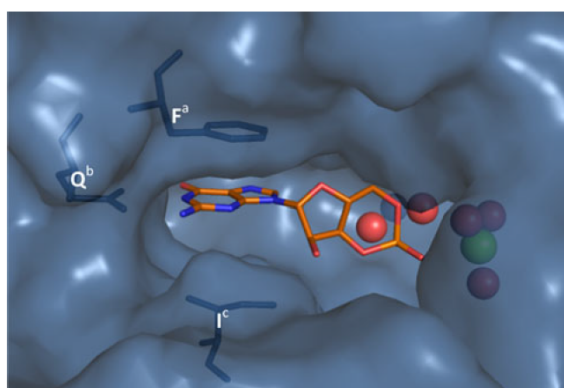


Fig. 4 Surface representation of the *PfPDEα* binding site shown complexed with cGMP. Mg^{2+} , Zn^{2+} and water molecules are represented by spheres. The purine-scanning glutamine is also shown together with the hydrophobic clamp residues. ^aEquates to F456, ^bequates to Q453 and ^cequates to L420 using 3DYN numbering

PDE9A is a cGMP specific isozyme and the crystal structure shows that the purine-scanning glutamine residue (Gln453) is anchored via hydrogen-bonding to an adjacent glutamine (Gln406) which locks it into a cGMP-specific conformation. In dual-specific PDEs, the glutamine residue is free to rotate and adopt either conformation, allowing both cAMP and cGMP to bind as substrates [25].

The ability of the *PfPDEα* models to accommodate cAMP was investigated through a manual rotation of the carboxamide group of the purine-scanning glutamine residue (R6, Table 2) and energy minimisation of the structure. Notably, a clash with the adjacent histidine residue (R2, Table 2) prevented the glutamine from presenting a conformer suitable for cAMP binding for any of the four *PfPDEs* (Fig. 5). This clash could not be relieved by energy minimisation nor by any manual rotation of the histidine residues to accommodate cAMP. This may support the observation that *PfPDEα* is cGMP specific [32]. As each *PfPDE* shares histidine residues in positions R1 and R2, this suggests that they too may be cGMP selective. That none of the four identified isozymes can hydrolyse cAMP would be surprising given the apparent role of *PfPKA* in parasite signalling [35].

Another region of interest is located next to the purine-scanning glutamine in the active site. In *Leishmania major* and *Trypanosoma* protozoa the residue preceding this glutamine is a glycine residue. This effectively opens up a pocket near the glutamine residue that is apparent only in *hPDE10* and has been suggested as a selectivity pocket for drug design against these parasites [33]. As the *PfPDE* enzymes do not share the glycine residue adjacent to the purine-scanning glutamine, it is presumed that the additional pocket found in *hPDE10* and other protozoan enzymes will not exist in *PfPDEs*.

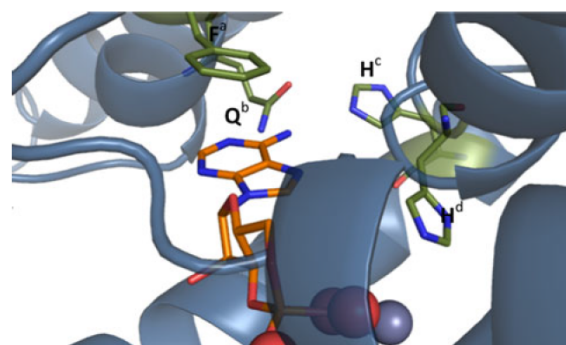


Fig. 5 Diagram illustrating the close arrangement of the purine-scanning glutamine (Q^b) and histidine (H^c) in the *PfPDEα* active site. ^aEquates to F456, ^bequates to Q453, ^cequates to N405, and ^dequates to H413 using 3DYN numbering

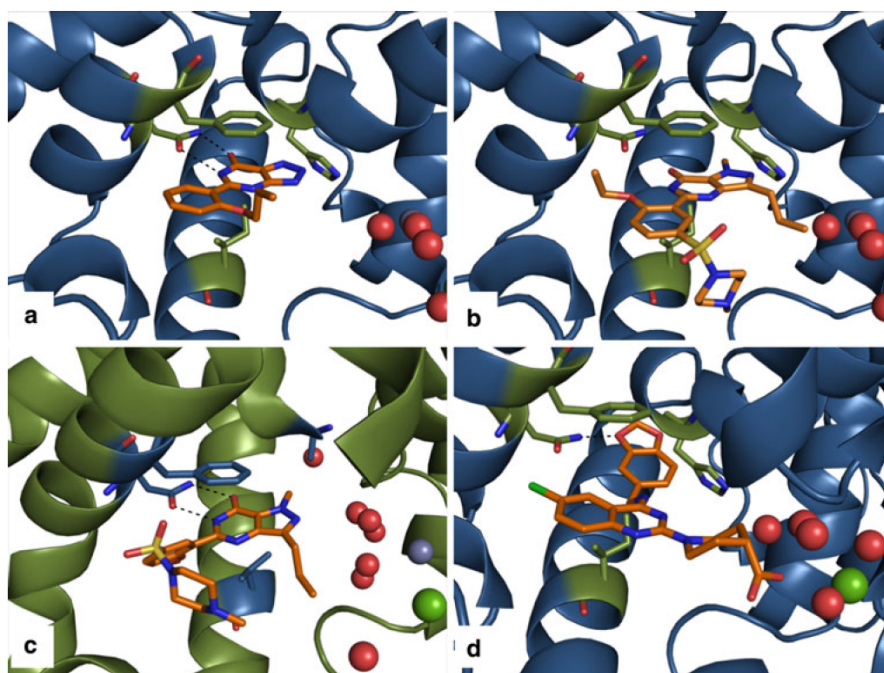
This analysis has highlighted potentially important differences between *PfPDEs* and *hPDE9A* from which the models were built. Most strikingly, the relationship to *hPDE9A* in the binding site is lost at positions R1 and R2 (Table 2) and all the *PfPDEs* have two histidine residues that are only found in *hPDE1*. The relationship to *hPDE1* is strongest for *PfPDEβ* and *PfPDEγ* (Table 2), and these latter two enzymes are highly similar (37%) to each other. *PfPDEα* was found to be most similar to *hPDE3* in this region, showing the same residues in positions R4 and R5 in the active site. *PfPDEα*, β and γ also show binding site similarities to *hPDE1* and *hPDE3*. *PfPDEδ* in contrast, shows similarity to *hPDEs* 5, 6 and 11 and this may be attributed to residues within the lid region as well as position R5 (Val) in the active site. On balance however, the residues closely associated with the active site (i.e. R1–R8) suggest that the *PfPDEs* appear to be mostly *hPDE1*-like (particularly residues R1 and R2).

Docking

The value of homology models is primarily to expedite the design of new inhibitors of *PfPDEs* which will be the crucial tools for delineating isozyme function and validating the clinical potential of *PfPDE* inhibition. To date the only pharmacological data relating to *PfPDE* activity concerns a selection of PDE inhibitors screened against *PfPDEα* [32]. Our plan is to perform large scale virtual screens of chemical libraries to enrich the selection of inhibitors prior to the availability of in vitro assays.

Seebeck and co-workers [32] reported the inhibitory activity of several PDE inhibitors against *PfPDEα*. Of the compounds tested, the *hPDE1/5* inhibitor, zaprinast (*hPDE1* IC_{50} = 6 μ M, *hPDE5A* IC_{50} = 0.81 μ M, *hPDE9A* IC_{50} = 29–46 μ M [36]) was the most potent inhibitor with an IC_{50} value of 3.8 μ M [32]. The PDE inhibitors E4021 (*hPDE5A*

Fig. 6 **a** Zaprinasat docked into the *Pf*PDE α model, **b** Sildenafil docked into the *Pf*PDE α model, **c** Sildenafil bound to the *h*PDE5A 1TBF crystal structure, and **d** E4021 docked into the *Pf*PDE α model. Purine-scanning glutamine, hydrophobic clamp and histidine residues are highlighted. Mg^{2+} , Zn^{2+} and water molecules are represented by spheres. Hydrogen bonds are shown with dashed lines



$IC_{50} = 6.2$ nM [36]) and sildenafil (*h*PDE5A $IC_{50} = 1.6$ nM, *h*PDE9A $IC_{50} = 2.6$ – 11 μ M [36]) were also reported to exhibit moderate activity against *Pf*PDE α (IC_{50} values of 46 and 56 μ M, respectively) [32].

When zaprinast was docked into the *Pf*PDE α models, it adopted a pose analogous to the binding of the pyrazolo-pyrimidinone core of sildenafil in the *h*PDE5A crystal structures, 1TBF [25] and 1UDT [24] (Fig. 6a). The expected contacts to the purine-scanning glutamine residue were evident, as well as aromatic stacking with the hydrophobic clamp. Furthermore, the pendant aryl groups superimpose, although the alkoxy groups project in different directions. The docked binding mode of sildenafil in the *Pf*PDE α model (Fig. 6b), while also similar to the *h*PDE5A crystal structure binding modes (1TBF [25] and 1UDT [24]; Fig. 6c), does not hydrogen bond as closely to the purine-scanning glutamine. This appears to be due to a clash between the histidine residue (R1, Table 2) and the pyrazole *N*-methyl substituent of sildenafil. In *h*PDE5A, the presence of a smaller alanine residue in this position avoids this clash. Interestingly, the bicyclic ring system of zaprinast lacks the *N*-methyl substituent and is thus able to fully enter the binding site to make the key interactions with the purine-scanning glutamine residue. Sildenafil also has additional interactions with the *h*PDE5A binding site through the bulky sulfonamide group that are not reproduced in *Pf*PDE α . Thus the docking mode of zaprinast appears convincing in light of crystal structures of

sildenafil in *h*PDE5A and may explain the relative potency of the two molecules against *Pf*PDE α .

Very recently, Beghyn et al. [22] implemented a ‘drug to genome to drug’ approach to design and test a series of *Pf*PDE inhibitors based on tadalafil. Docking of compound 10 from the Beghyn study [22] (Fig. 2) was undertaken using our *Pf*PDE α model. Given that the binding mode of tadalafil in *h*PDE5A (pdb code 1XOZ) places the benzodioxole in a pocket adjacent to the purine-scanning glutamine residue [37], then a similar sized pocket would be required to successfully dock this compound into the *Pf*PDE α model. However, as the *Pf*PDE homology models do not possess a cavity of the right dimensions, the tadalafil analogues could not be successfully docked. Interestingly, the bottom of the *h*PDE5A benzodioxole binding pocket is lined with an alanine residue [A783, 1XOZ], while the *Pf*PDEs have larger amino acids in this position (N, L, V, S for α , β , γ and δ , respectively). In addition, the *h*PDE5A pocket in structure 1XOZ is made larger by the movement of helix 15 in a direction away from the metal atoms. The size of the amino acids, plus large scale protein movement results in a pocket that is capable of binding the benzodioxole group but this is precluded in our models. Clearly this requires further work to examine the amino acids lining this pocket as well as undertaking molecular dynamics experiments. This is the current subject of our research.

While crystal structures are not available to show the binding mode of E4021 in any available PDE enzyme, we

docked this ligand into the binding site of *Pf*PDE α . Docking suggests a binding mode for E4021 where the catechol ring system interacts with the purine-scanning glutamine through a single hydrogen bond and the piperidine carboxylic acid terminus resides near the metal ions of the binding site (Fig. 6d). In contrast, when E4021 was docked into the *h*PDE5A crystal structures 1UDT [24] and 1TBF [25], the binding mode showed that the ether oxygen in the 3-position formed a hydrogen bond with the purine-scanning glutamine.

Finally, as the sequence analyses comparing the human and *Pf*PDE enzymes showed similarity to both *h*PDE9A and *h*PDE1 (active site), we investigated a series of *h*PDE1/9 inhibitors recently reported by De Ninno and co-workers [31]. For example, compounds De Ninno **1** and **14** (Fig. 2) from that study were shown to have good activity at *h*PDE1 and 9, with compound **14** exhibiting useful selectivity for *h*PDE9A over *h*PDE1. When docked into each of the *Pf*PDE models, these compounds made two contacts to the purine-scanning glutamine residue and aromatic stacking with the purine-stacking phenylalanine in a manner similar to most PDE inhibitors. Like zaprinast, the pyrazolopyrimidinone core of De Ninno **1** and **14** was able to dock into the active site to form key interactions with the purine-scanning glutamine (Fig. 7). The same molecules could also be successfully docked into *h*PDE1 and *h*PDE9A structures, again making contacts to the purine-scanning glutamine and aromatic interactions with the purine-stacking phenylalanine.

Gaining selectivity for malarial PDEs

Prior studies on the *Pf*PDE biochemistry of zaprinast [32] and tadalafil analogues [22], as well as the docking of the *h*PDE9A and *h*PDE1 selective inhibitors described above show the potential for developing *Pf*PDE inhibitors from *h*PDE ligands. An important further element is the need to remove *h*PDE potency while retaining *Pf*PDE potency to achieve selectivity for the malarial PDEs. From the docking results it would appear that there may be several

chemical fragments that could be explored to develop *Pf*PDE inhibitors such as the benzodioxole group of E4021 or the guanine mimics within zaprinast and sildenafil. It is clear however, that to obtain *Pf*PDE selectivity, binding site residues that are unique to the enzyme of interest need to be targeted. This approach has been successful in the development of highly selective and potent human PDE inhibitors [38]. It is therefore logical to target differences within the 25 binding residues associated with the active site (Table 2). Of the 25 amino acids, five residues within *Pf*PDE α are unique to this enzyme (Table 2, Fig. 8). We propose that targeting these particular residues will introduce selectivity for *Pf*PDE α over both human and other malarial PDEs. In a similar manner, targeting residues identified as being unique to *Pf*PDE β , γ and δ (Table 2) may offer a means by which selectivity toward each isozyme may be achieved. Beghyn and co-workers [22] designed a set of tadalafil analogues where the N-methyl group was replaced with benzyl substituted pyrrolidine or

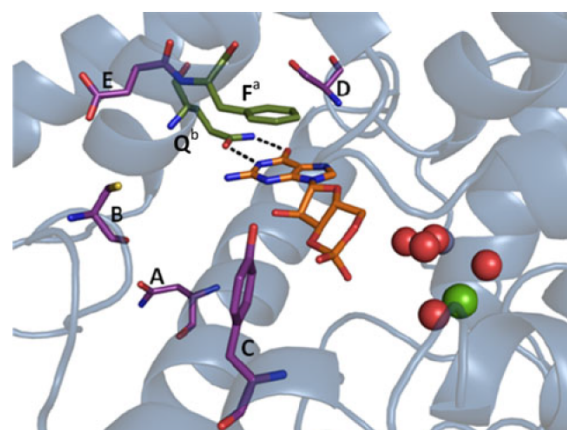
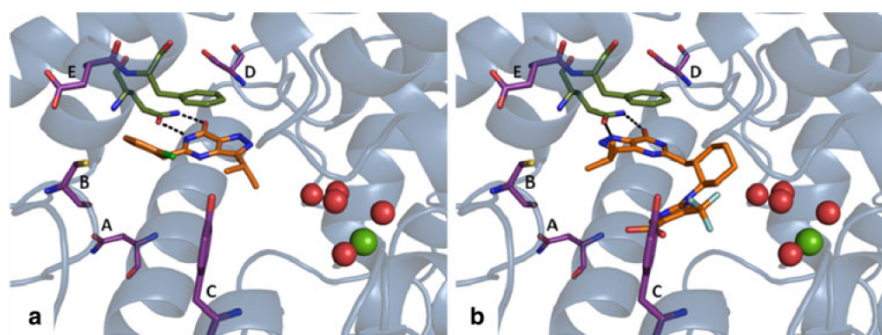


Fig. 8 Residues A–E (highlighted) that are unique to *Pf*PDE α that may offer a route to selectivity over other PDE enzymes if targeted through inhibitor design. ^aEquates to F456 and ^bequates to Q453 using 3DYN numbering. cGMP is shown within the active site. Mg²⁺, Zn²⁺ and water molecules are represented by spheres. Hydrogen bonds are shown with dashed lines

Fig. 7 **a** Docking of De Ninno **1** into the *Pf*PDE α model and **b** docking of De Ninno **14** into the *Pf*PDE α model. Mg²⁺, Zn²⁺ and water molecules are represented by spheres. Hydrogen bonds are shown with dashed lines. Purine-scanning glutamine and purine-stacking phenylalanine residues are highlighted, as well as residues unique to *Pf*PDE α (A–E)



piperidine rings. These substituents are thought to be oriented towards the periphery of the active site where they can encounter residues unique to *Pf*PDEs. While further assays are needed to confirm their ability to inhibit *Pf*PDEs, these promising results are very positive and have encouraged us to continue our design and synthesis work.

Other means of introducing groups to gain selectivity may be gained by substitution from the 5-position of the guanine ring of cGMP and its related analogues to specifically target the R8 residue in the *Pf*PDEs (Residue E in Fig. 8). As the R8 residue is unique to each *Pf*PDE (Table 2), this simplistic approach could provide the basis for which selectivity may be obtained. Notwithstanding that their inhibitory potency is unknown, the De Ninno compounds **1** and **14**, which have been extended from this 2-position, show promising results when docked into each of the *Pf*PDE models (Fig. 7). The chlorobenzyl group at the 2-position of De Ninno **1** appears to extend toward the unique serine residue in *Pf*PDE α (residue D in Fig. 7). In the case of De Ninno **14**, docking favours an interaction between the pyrimidinetrifluoro carboxylic acid moiety and the metal binding site within the enzyme. Extending the molecule toward the unique tyrosine residue in each of the *Pf*PDEs (residue C in Fig. 7) should not be overlooked in the design strategy.

Conclusions

In anticipation of the potential of the four *Pf*PDE isozymes as targets for antimalarial drug design, we have constructed homology models based on gene sequence data and homology to their human counterparts. Interestingly, our models show that the binding site topology of the *Pf*PDEs have a high resemblance to *h*PDE1 and our modelling explains the cGMP selectivity of *Pf*PDE α . Docking of the reported *Pf*PDE α inhibitors zaprinast, E4021 and sildenafil, suggested plausible binding modes consistent with their relative potencies. Our docking studies also support the pursuit of *h*PDE1/9 inhibitors as starting points for the design of *Pf*PDE α inhibitors.

We hope that this information may provide a useful tool for screening compound libraries, either diversity-based or developed from the large PDE inhibitor pool. The generalized homology to *h*PDEs, coupled to observable differences in the binding sites might support structure-based design of pan-*Pf*PDE inhibitors that select against human isoforms, or also potentially *Pf*PDE-isoform selective inhibitors. The renewed fight against malaria requires the identification and validation of targets for therapy. With a pathway for conducting virtual screening for *Pf*PDEs, we hope that the road to finding molecules active against the parasite might be smoothed.

Acknowledgments The authors would like to thank Dr Paul Gilson for his helpful discussions.

References

1. Miller LH, Baruch DI, Marsh K, Doumbo OK (2002) Nature 415:673–679
2. Greenwood BM, Bojang K, Whitty CJ, Targett GA (2005) Lancet 365:1487–1498
3. Heddini A (2002) Int J Parasitol 32:1587–1598
4. Chiang PK, Bujnicki JM, Su X, Lanar DE (2006) Curr Mol Med 6:309–326
5. Woster PM (2003) New therapies for malaria. In: Doherty AM (ed) Annual reports in medicinal chemistry, vol 38. Elsevier, Amsterdam, pp 203–212
6. Ridley RG (2002) Nature 415:686–693
7. Kappe SH, Vaughan AM, Boddey JA, Cowman AF (2010) Science 328:862–866
8. Wentzinger L, Bopp S, Tenor H, Klar J, Brun R, Beck HP, Seebeck T (2008) Int J Parasitol 38:1625–1637
9. Lugnier C (2006) Pharmacol Ther 109:366–398
10. Conti M, Beavo J (2007) Ann Rev Biochem 76:481–511
11. Jeon YH, Heo YS, Kim CM, Hyun YL, Lee TG, Ro S, Cho JM (2005) Cell Mol Life Sci 62:1198–1220
12. Baker DA, Kelly JM (2004) Trends Parasitol 20:227–232
13. Gardner MJ, Hall N, Fung E, White O, Berriman M, Hyman RW, Carlton JM, Pain A, Nelson KE, Bowman S, Paulsen IT, James K, Eisen JA, Rutherford K, Salzberg SL, Craig A, Kyes S, Chan MS, Nene V, Shallom SJ, Suh B, Peterson J, Angiuoli S, Pertea M, Allen J, Selengut J, Haft D, Mather MW, Vaidya AB, Martin DM, Fairlamb AH, Fraunholz MJ, Roos DS, Ralph SA, McFadden GI, Cummings LM, Subramanian GM, Mungall C, Venter JC, Carucci DJ, Hoffman SL, Newbold C, Davis RW, Fraser CM, Barrell B (2002) Nature 415:498–511
14. Beavo JA (1995) Physiol Rev 75:725–748
15. Taylor CJ, McRobert L, Baker DA (2008) Mol Microbiol 69:110–118
16. Moon RW, Taylor CJ, Bex C, Schepers R, Goulding D, Janse CJ, Waters AP, Baker DA, Billker O (2009) PLoS Pathog 5(9):e1000599
17. McRobert L, Taylor CJ, Deng W, Fivelman QL, Cummings RM, Polley SD, Billker O, Baker DA (2008) PLoS Biol 6(6):e139
18. Taylor HM, McRobert L, Grainger M, Sicard A, Dluzewski AR, Hopp CS, Holder AA, Baker DA (2010) Eukaryot Cell 9:37–45
19. Beraldo FH, Almeida FM, da Silva AM, Garcia CR (2005) J Cell Biol 170:551–557
20. Young JA, Fivelman QL, Blair PL, de la Vega P, Le Roch KG, Zhou Y, Carucci DJ, Baker DA, Winzeler EA (2005) Mol Biochem Parasitol 143:67–79
21. Yuasa K, Mi-Ichi F, Kobayashi T, Yamanouchi M, Kotera J, Kita K, Omori K (2005) Biochem J 392:221–229
22. Beghyn TB, Charton J, Leroux F, Laconde G, Bourin A, Cos P, Maes L, Deprez B (2011) J Med Chem 54:3222–3240
23. Ke H, Wang H (2007) Curr Top Med Chem 7:391–403
24. Sung BJ, Hwang KY, Jeon YH, Lee JJ, Heo YS, Kim JH, Moon J, Yoon JM, Hyun YL, Kim E, Eum SJ, Park SY, Lee JO, Lee TG, Ro S, Cho JM (2003) Nature 425:98–102
25. Zhang KY, Card GL, Suzuki Y, Artis DR, Fong D, Gillette S, Hsieh D, Neiman J, West BL, Zhang C, Milburn MV, Kim SH, Schlessinger J, Bollag G (2004) Mol Cell 15:279–286
26. Fry M, Beesley J (1991) Parasitol Today 102:17–26
27. Chenna R, Sugawara H, Koike T, Lopez R, Gibson TJ, Higgins DG, Thompson JD (2003) Nucleic Acids Res 31:3497–3500

28. Manallack DT, Hughes RA, Thompson PE (2005) *J Med Chem* 48:3449–3462
29. Liu S, Mansour MN, Dillman KS, Perez JR, Danley DE, Aeed PA, Simons SP, Lemotte PK, Menniti FS (2008) *Proc Natl Acad Sci USA* 105:13309–13314
30. Chen VB, Arendall WB 3rd, Headd JJ, Keedy DA, Immormino RM, Kapral GJ, Murray LW, Richardson JS, Richardson DC (2010) *Acta Crystallogr D Biol Crystallogr* 66(Pt 1):12–21
31. De Nino MP, Andrews M, Bell AS, Chen Y, Eller-Zarbo C, Eshelby N, Etienne JB, Moore DE, Palmer MJ, Visser MS, Yu LJ, Zavadoski WJ, Gibbs ME (2009) *Bioorg Med Chem Lett* 19:2537–2541
32. Wentzinger L, Seebeck T (2006) Protozoal phosphodiesterases. In: Beavo J (ed) *Cyclic nucleotide phosphodiesterases in health and disease*. CRC Press, Boca Raton, Florida, pp 275–301
33. Wang H, Yan Z, Geng J, Kunz S, Seebeck T, Ke H (2007) *Mol Microbiol* 66:1029–1038
34. Xu RX, Hassell AM, Vanderwall D, Lambert MH, Holmes WD, Luther MA, Rocque WJ, Milburn MV, Zhao Y, Ke H, Nolte RT (2000) *Science* 288:1822–1825
35. Read LK, Mikkelsen RB (1991) *J Parasitol* 77:346–352
36. Saeki T, Adachi H, Takase Y, Yoshitake S, Souda S, Saito I (1995) *J Pharmacol Exp Ther* 272:825–831
37. Card GL, England BP, Suzuki Y, Fong D, Powell B, Lee B, Luu C, Tabrizi M, Gillette S, Ibrahim PN, Artis DR, Bollag G, Milburn MV, Kim SH, Schlessinger J, Zhang KY (2004) *Structure* 12:2237–2247
38. Verhoest PR, Chapin DS, Corman M, Fonseca K, Harms JF, Hou X, Marr ES, Menniti FS, Nelson F, O'Connor R, Pandit J, Proulx-Lafrance C, Schmidt AW, Schmidt CJ, Suiciak JA, Liras S (2009) *J Med Chem* 52:5188–5196

Appendix 2

Sequence alignment of the catalytic domains of human and protozoan phosphodiesterases

Below is the sequence alignment of the catalytic domains of the human (*hPDE1-11*) and protozoan (*PfPDEα-δ* and *LmjPDEB1*) phosphodiesterase enzymes. This sequence alignment has been generated through an initial alignment in ClustalW, followed by manual alignment of the key residues, as discussed in section 2.2.1 and 7.1.1.

	*h1*****	*h2****	
hPDE1A	RKTYHMGVGLAYPAAVIVTLKDVKWSFDVFALNEASG---	EH	173
hPDE1C	RRTSNMVGLSYPPAVIEALKDVKWSFDVFSLNEASG---	DH	183
hPDE1B	RRTYTSVGPITYSTAVLNCLKNLDLWCFDVFSLNQAAD---	DH	178
hPDE3A	DKPILAPEPLVMDNLDSEIMEQLNTWNFPFIDLVENIGRKCGR		709
hPDE3B	IEQEVSLDLILVEEYDSLIEKMSNWNFPFIFELVEKMGKSGR		694
hPDE4A	NIPRFGVKTDQEELLAQLEENLNKWGLNIFCVSDYAG---	GR	389
hPDE4B	SISRFGVNTENEDHLAKELEDLNKWGLNIFNVAGYSH---	NR	362
hPDE4C	TVPRFGVQTDQEEQLAKELEDTNKWGLDVFKVAELSG---	NR	344
hPDE4D	SIPRFGVKTEQEDVLAKELEDVNKWGLHVFRIAELSG---	NR	418
hPDE8A	NIITPISLDDVPPRIARAMENEEYWDFDIFELEAATH---	NR	512
hPDE8B	HLAMPITINDVPPCISQLLDNEESWDFNIFELEAITH---	KR	571
hPDE7A	SNSLNILDDDYNGQAKCMLKEKVGNNWDFDIFLFDRLTN---	GN	168
hPDE7B	QAPLHLLDDEDYLGQARHMLSKVGMWDFDIFLFDRLTN---	GN	129
hPDE5A	EETRELQSLAAAVVPSAQTLKITDFSFSDFELS-----	DL	569
hPDE11	SKAEVDKFK-AANIPLVSELAIDDIHFDDFSLD-----	VD	675
hPDE6A	KEPWECEEEELAEILQALPDADKYEINKFHFSDLPLT--	EL	515
hPDE6B	KEPADCEDELGEILKEELPGPTTFDIYEFHFSDELECT--	EL	514
hPDE6C	DVIDDCEEKQLVAILKEDLPDRPSAELEYFRFSDFPLT--	EH	519
hPDE10	SYHSICTSEEWQGLMQFTLPVRLCKEIELFHFDIGPF---	EN	474
hPDE2A	HMKVSDDEYTKLLHDGIQPVAAIDSNFASFTYTPRSLP--	ED	613
hPDE9A	TPRRDVPTYPKYLLSPETIEALRKPTFDVWLWE-----	PN	269
		:	
PfPDEα	ISFNSFSNMHSLLSKFQEHYNDIYDWNGNIENIY----	KA	
PfPDEβ	KQIKKFLKQINISQLTKMIQFIDNKLSDWDFNCLTY---	FD	

*Pf*PDEγ DEFNVKKEMDMNLKCDNVNLDIWNTSFLNNETL-----E
*Pf*PDEδ IAYEVVLKNIKKINCDEIGKNWDYSFIDSEYG-----KS
*Lmj*PDE IAVTPEEREAVMSIDFGGAYDFTSPGFNLFVREKYS-EPMD

*h3***** *h4** *h5***** *h6*****
*hp*PDE1A SLKFMiYELfTRYDLINRFKIPVSLITFAEALEVGYSKYKNPYHNLiHAADVTQTvHYIM 234
*hp*PDE1C ALKFIFyELLTRYDLISRFKIPISALVSFVEALEVGYSKHKNPYHNLiMHAADVTQTvHYLL 244
*hp*PDE1B ALRTiVfELLTRHNLISRFKIPTVFLMSFLDALETGYGKYKNPYHNQiHAADVTQTvHCFL 239
*hp*PDE3A ILSQvSYRLfEDMGLFEAFKIPIREFMNYFHALEIGYR--DIPYHNRIHATDVLHAVvYLT 768
*hp*PDE3B ILSQvMYTLfQDTGLLEIFKIPTQQFMNYFRALENGYR--DIPYHNRIHATDVLHAVvYLT 753
*hp*PDE4A SLTCiMYMIFQERDLLKKFRIPVDTMVtYMLTLEDHYH-ADVAYHNSLHAADVLQSTHvLL 449
*hp*PDE4B PLTCiMYAiFQERDLLKtFRISSDTfITYMMTLEDHYH-SDVAYHNSLHAADVAQSTHvLL 422
*hp*PDE4C PLTAiIfSIFQERDLLKtFQIPADTLATyLLMLEGHYH-ANVAYHNSLHAADVAQSTHvLL 404
*hp*PDE4D PLTvIMHTiFQERDLLKtFKIPVDTLiTYLMTLEDHYH-ADVAYHNNiHAADVvQSTHvLL 478
*hp*PDE8A PLiYlGLKMFARFGiCEFLHCSEStLSwLQIIEANYH-SSNPYHNStHSAADVlHATAYfL 572
*hp*PDE8B PLvYlGLKVFfSRFGVCEfLNCSEtTLRAWfQVIEANYH-SSNAYHNStHAADVlHATAfFL 631
*hp*PDE7A SLvSLtFHLfSLHGLiEYfHLDMMKLRRfLVMiQEDYH-SQNPYHNNAVHAADVTQAMHCyL 228
*hp*PDE7B SLvTLlChLFNTHGLiHHfKLDMVtLHRfLVMVQEDYH-SQNPYHNNAVHAADVTQAMHCyL 189
*hp*PDE5A ETAlCTiRMfTDNLvQNfQMKEVlCRWILSVKKNYRK-NVAYHNWRHAFNTAQCMFAAL 629
*hp*PDE11 AMITAAALRMfMELGMvQKfKIDYETlCRWLLTVRKNYR--MVLYHNWRHAFNVQCMLFAML 734
*hp*PDE6A ELvKCGiQMYyELKVVdKFHiPQEAALvRFMYSLSKGYR--KiTYHNWRHGfNVGQTMfSLl 574
*hp*PDE6B DLvKCGiQMYyELGVVRKfQIPQEVlVRfLFSISKGYR--RiTYHNWRHGfNVAQTMfTLl 573
*hp*PDE6C GLiKCGiRLfFEiNVvEKfKVPVEVlTRWMyTVRKGYR--AVTYHNWQHGFNVGQTMfTLl 578
*hp*PDE10 MWPGiFvYMVHRSCGTSCfEL--EKLCRFiMSVKKNYR--RVPyHNWKHAvTVAHCMyAIL 531
*hp*PDE2A DTSMAlLSMLQDMNFINNYKiDCPTLARfCLMVKKGYR--DPPYHNWMHAFSVSHfCYLLY 672
*hp*PDE9A EMLSCLEHMYHDLGLVRdFSiNPVTLRRWLFcvHDNYR--NNPfHNfRHCFcVAQMMYSMV 328
 : : : : * : ** * :
 AA A
*Pf*PDEα NTFiSiGYKLLYPLGVLEANFDKEKLKKfLFRiCSyYn--DiPYHTSLHAAQVAHfSKSML
*Pf*PDEβ ESEYpFFDiNLSLiCTiDHNiPiNiIiNfLCfVEKQYn--NVPyHNTiHATMvTQKfFLA
*Pf*PDEγ DiFiHiGNKLLKMYyTTNHNiPSEtLYSLLYEMKNGYn--NVPyHNSiHAAMvTHHCNVlV
*Pf*PDEδ TLvILEVGYHLiSPYiENNENKKKKLQLfLLLiNSMYf--PNPyHNANHGATvCHLSKCLA
*Lmj*PDE AAAGVVYnLLWNSGLpEKfGCREQTLNfILQCRRYR--RVPyHNfYHVVDVCQTLHTYl

*hp*PDE1A LHTG-----IMHWLTeLEiLA 250
*hp*PDE1C YKTG-----VANWLTeLEiFA 260
*hp*PDE1B LRTG-----MVHCLSEiELLA 255
*hp*PDE3A TQPiPGLSTViNDHGStSDSDSGfTHGHMGYVfSKTYNVtDDKYGCLSGNiPALELMA 828
*hp*PDE3B TRPVPGLQqIHNGCGTGNETDSDGRiNHGfiAYiSSKSCSNPDESYGCLSSNiPALELMA 813
*hp*PDE4A ATPA-----LDAVfTDLEiLA 465
*hp*PDE4B STPA-----LDAVfTDLEiLA 438
*hp*PDE4C ATPA-----LEAVfTDLEiLA 420
*hp*PDE4D STPA-----LEAVfTDLEiLA 494
*hp*PDE8A SKER-----IKETLDPiDEVA 588
*hp*PDE8B GKER-----VKGSLDQLDEVA 647
*hp*PDE7A KEPK-----LANSvTPWDiLL 244
*hp*PDE7B KEPK-----LASfLTPLDiML 205
*hp*PDE5A KAGK-----IQNKLTDEiLA 645
*hp*PDE11 TTAG-----FQDiLTeVEiLA 750
*hp*PDE6A VTGK-----LKRYfTDLEALA 590
*hp*PDE6B MTGK-----LKSYyTDLEAFA 589
*hp*PDE6C MTGR-----LKKYyTDLEAFA 594
*hp*PDE10 QNNH-----TLfTDLERK 545
*hp*PDE2A KNLE-----LTNYLEDiEiFA 688
*hp*PDE9A WLCS-----LQEKfSQTDiLi 344
 :
*Pf*PDEα FMLD-----MNHKiSAiDEfC
*Pf*PDEβ KKLg-----iYDDLEyKiKLv
*Pf*PDEγ SNLN-----TANiLRDNElGA
*Pf*PDEδ HiTD-----YDSYLNNTYMiC
*Lmj*PDE YTGKASE-----LLTeLECYVLLV

```

hpDE1A      -----PEGIDRAKTMSLILHAADISHPAKSWKLHYRWTMALMEEFFLQGDKEAELG 403
hpDE1C      -----PEAIEKPKALSMLLHTADISHPAKAWDLHHRWTMSLLEEFFRQGDREAELG 414
hpDE1B      -----LERIDKPKALSLLHAADISHPTKQWLVSHRWTKALMEEFFRQGDKEAELG 408
hpDE3A      -----DWTNENDRLLVCQMCIKLADINGPAKCKELHLQWTDGIVNEFYEQGDEEASLG 988
hpDE3B      -----EWSNENDRLLVCQVCIKLADINGPAKVRDLHLKWTEGIVNEFYEQGDEEANLG 975
hpDE4A      ---VLLLDNYSDRIQVLRNMVHCADLSNPTKPLELYRQWTDRIMAEFFQGGDRERERG 629
hpDE4B      ---VLLLDNYTDRIQVLRNMVHCADLSNPTKSLELYRQWTDRIMEEFFQGGDKERERG 602
hpDE4C      ---VLLLDNYSDRIQVLQNLVHCADLSNPTKPLPLYRQWTDRIMAEFFQGGDRERESG 584
hpDE4D      ---VLLLDNYSDRIQVLQNMVHCADLSNPTKPLQLYRQWTDRIMEEFFRQGGDRERERG 658
hpDE8A      EVINTMLRTPENRTLIKRMLIKCADVSNPCRPLQYCIEWAARISEEYFSQTDEEKQQG 765
hpDE8B      NPAG--KNFPENQILIKRMMIKCADVANPCRPDLCIEWAGRISEEYFAQTDEEKRQG 820
hpDE7A      ---DLCLEDTRHRHLVLQMALKCADICNPCRTWELSKQWSEKVTEEFFHQGDIEKKYH 400
hpDE7B      ---DLRLEDAQDRHFMLQIALKCADICNPCRIWEMSKQWSERVCEEFYRQGELEQKFE 361
hpDE5A      ---QFNLEDPHQKELFLAMLMTACDLSAITKPWPIQQRIAELVATEFFDQGGDRERKEL 803
hpDE11      ---EYDWNIKNHRDIFRSMLMTACDLGAVTKPWEISRQVAELVTSEFFEQGGDRERLEL 909
hpDE6A      EWTQYMMLEQTRKEIVMAMMMTACDLSAITKPWEVQSQVALLVAAEFWEQGDLERTVL 758
hpDE6B      SWVEYLSLETTRKEIVMAMMMTACDLSAITKPWEVQSKVALLVAAEFWEQGDLERTVL 757
hpDE6C      EAIKYVTVDPTKKEIIMAMMMTACDLSAITKPWEVQSQVALMVANEFWEQGDLERTVL 762
hpDE10      --GSLNLNNQSHRDRVIGLMMTACDLSVTKLWPVTKLTANDIAEYFAEWAEGDEMKKLG 702
hpDE2A      ---GYDNNNKQHHRLLLCLLMTSCDLSDQTKGWKTTRKIAELIYKEFFSQGDLEKAMG 846
hpDE9A      ---FDYSNEEHMTLLKMILIKCCDISNEVRPMEVAEPWVDCLLEEYFMQSDREKSEG 500
      : . * : : : * : : :
      A A

```

```

PfPDEα      -----NDQIWQIFCLILKASDIGHSTLEWNKHLEWTLKINEEFFYLQGLLEKSLN
PfPDEβ      ---FDYIKNSDDLLILTKMIIKSADISHGSVSWSEHYCWCQRVLSEFYTQGDDEELKNK
PfPDEγ      ---IKSYIEKNIIILCLKMIIKAADLSHNCVDWSEHYQWVKRLVNEFYEGDELFQMG
PfPDEδ      ---QNFDISDTDAINLGTINIKLADIGHTCLKWKDHAKWTMLVSEEFFSQKRVEELHK
LmjPDE      ---GFEKDNDTHRRLVMETLIKAGDVSNVTKPFETSRMWAMAVTEEFYRQGDMEKEKG

```

```

hpDE1A      -----LP 405
hpDE1C      -----LP 416
hpDE1B      -----LP 410
hpDE3A      -----LP 990
hpDE3B      -----LP 977
hpDE4A      -----ME 631
hpDE4B      -----ME 604
hpDE4C      -----LD 586
hpDE4D      -----ME 660
hpDE8A      -----LP 767
hpDE8B      -----LP 822
hpDE7A      -----LG 402
hpDE7B      -----LE 363
hpDE5A      -----NI 805
hpDE11      -----KL 911
hpDE6A      -----QQ 760
hpDE6B      -----DQ 759
hpDE6C      -----QQ 764
hpDE10      -----I 704
hpDE2A      -----N 848
hpDE9A      -----LP 502

```

```

PfPDEα      -----IQ
PfPDEβ      -----MP
PfPDEγ      -----YK
PfPDEδ      NKNIDPLNFSNFGKEDNIDEGMIFNYENIYINYINNINNTYDYSYIK
LmjPDE      -----VE

```

```

      *h15a***** *h15b*****
hpDE1A      FS-PLCDRKST-MVAQSQIGFIDFIVEPTFSLLTDSTEKIVI 440
hpDE1C      FS-PLCDRKST-MVAQSQVGFIDFIVEPTFTVLTDMTEKIVS 451
hpDE1B      FS-PLCDRTST-LVAQSQIGFIDFIVEPTFSVLTDVAEKSVQ 446
hpDE3A      IS-PFMDRSAP-QLANLQESFISHIVGPLCNSYDSAGLMPGK 1026
hpDE3B      IS-PFMDRSSP-QLAKLQESFITHIVGPLCNSYDAAGLLPGQ 1012

```

hpDE4A	IS-PMCDKHTA-SVEKSQVGFIDYIVHPLWETWADLVHPD--	664
hpDE4B	IS-PMCDKHTA-SVEKSQVGFIDYIVHPLWETWADLVQPD--	637
hpDE4C	IS-PMCDKHTA-SVEKSQVGFIDYIAHPLWETWADLVHPD--	619
hpDE4D	IS-PMCDKHNA-SVEKSQVGFIDYIVHPLWETWADLVHPD--	693
hpDE8A	VVMPVFDNTC-SIPKSIQSFIDYFITDMFDAWDAFVD----	798
hpDE8B	VVMPVFDNTC-SIPKSIQSFIDYFITDMFDAWDAFAH----	853
hpDE7A	VS-PLCDRHTE-SIANIQIGFMTYLVLEPLFTEWARFS-NTRL	436
hpDE7B	IS-PLCNQQKD-SIPSIQIGFMSYIVEPLFREWAHFTGNSTL	398
hpDE5A	EPTDLMNREKKNKIPSMQVGFIDAICQLYEALTHVSED---	838
hpDE11	TPSAIFDRNRKDELPRQLQLEWIDSICMPLYQALVKVNVK---	944
hpDE6A	NPIPMMDRNKADELPKLQVGFIDFVCTFVYKEFSRFHEE---	793
hpDE6B	QPIPMMDRNKADELPKLQVGFIDFVCTFVYKEFSRFHEE---	792
hpDE6C	QPIPMMDRNKRDELPKLQVGFIDFVCTFVYKEFSRFHKE---	797
hpDE10	QPIPMMDRDKKDEVPQQLGFYNAVAIPCYTTLTQILPP---	737
hpDE2A	RPMEEMDREKA-YIPELQISFMEHIAMPIYKLLQDLFPK---	880
hpDE9A	VA-PFMDRDKV-TKATAQIGFIKFVLIPMFETVTKLFPMV--	535
	: * :	
	A	
PfPDE α	NSFLCDINTMN-KLALSQIDFLKHLCIPLFNELNYICKNNDV	
PfPDE β	LS-PLCDRTKHNEVCKSQITFLKFVVMPLFEELSHIDNNKFI	
PfPDE γ	IN-PLFDRNCHNNFIQIQRTFLKELVYPLIISLKTLDNTSI-	
PfPDE δ	LN-FIHHDHFVKSIPSTQVYFFEIIVMPLIKELQSMESKKE	
LmjPDE	VL-PMFDRSKNNELARGQIGFIDFVAGKFFRDIVGNLFGMQ	
hpDE1A	PLIEEASKAETSSYVASSSTTIVGLHIADALRRSNTKGSMDSGYSYSPDYSLAAVDLKSF	499
hpDE1C	PLIDETSQTGGTGQRRSSLNSISSDAKRSGVKTSGSEGSAPINNSVISVDYKSF----	506
hpDE1B	PLADEDSKSKNQPSFQWRQPSLDVEVGDPNPDVVSF-----	482
hpDE3A	WVEDSDESGDTDDPEEEEEEAAPNEEETCENNESPKKKTFK-RRKI-----	1072
hpDE3B	WLEAEEDN-DTESGDDEDEGE-LDTEDEEMENNLNPKPPRRKSRRRI-----	1057
hpDE4A	-----	
hpDE4B	-----	
hpDE4C	-----	
hpDE4D	-----	
hpDE8A	-----	
hpDE8B	-----	
hpDE7A	-----	
hpDE7B	-----	
hpDE5A	-----	
hpDE11	-----	
hpDE6A	-----	
hpDE6B	-----	
hpDE6C	-----	
hpDE10	-----	
hpDE2A	-----	
hpDE9A	-----	
PfPDE α	-----	
PfPDE β	-----	
PfPDE γ	-----	
PfPDE δ	I-----	
LmjPDE	W-----	
	*h16*****	
hpDE1A	KNNLVDI IQQNKERWKE LA AQEARTSSQKCE	530
hpDE1C	KATWTEVVHINRERWRAKVPKEEKAKKEAEE	537
hpDE1B	RSTWVKRIQENQKWKERAASGITNQMSIDE	513
hpDE3A	YCQITQHLLQNHKMWKVIEEQRLAGIENQ	1103
hpDE3B	FCQLMHHLTENHKIWKEIVEEECKKADGNK	1088
hpDE4A	AQEILD TLEDNRDWYSAIRQSPSPPPPEES	695
hpDE4B	AQDILD TLEDNRNWYQSMIPQSPSPPLDEQN	668
hpDE4C	AQDLLD TLEDNREWYQSKIPRSPDLTNPER	650
hpDE4D	AQDILD TLEDNREWYQSTIPQSPSPAPDDPE	724
hpDE8A	LPDLMQHLDNNFKYWKGLDEMKLRLNLRPPPE	829

hpDE8B	LPALMQHLADNYKHWKTLDDLKCKSLRLPSD	884
hpDE7A	SQTM LGHVGLNKASWGLQREQSSSEDTDA	467
hpDE7B	SENMLGHLAHNKAQWKSLLPRQHRSRGSSGS	429
hpDE5A	CFPLLDGCRKNRQKQALAEQQEKMLINGES	869
hpDE11	LKPMLDSVATNRSKWEELHQKRLLASTASSS	975
hpDE6A	ITPMLDGITNNRKEWKALADEYDAKMKVQEE	824
hpDE6B	ILPMFDRLQNNRKEWKALADEYEAKVKALEE	823
hpDE6C	ITPMLSGLQNNRVEWKSLADEYDAKMKVIEE	828
hpDE10	TEPLLKACRDNLSQWEKVIERGEETATWISSP	768
hpDE2A	AAELYERVASNGEHWTKVSHKFTIRGIPSN	911
hpDE9A	EEIMLQPLWESRDRYEELKRIDDAMKELQKK	566
	:	
PfPDE α	YTHCIQPIENNIERWESHKNDNQNLGLHEKY	
PfPDE β	KSFCLKRLNSNCIMWDTLMKEEKTIEVYDPA	
PfPDE γ	TQDMINNVKRNYSKWTKIEKCQIKKKYLINE	
PfPDE δ	TQKVLHNLNINLQTWRLIEKNINLIFYNTEKM	
LmjPDE	CVDTVNSNRAKWQEILDGRDSIRSSIV---	

The numbering scheme has been taken from the SwissProt database.

Helix numbering is intended as a guide and refers to the PDE4 structure 1PTW.

Differences occur in overall structure between PDE isoforms such as helices 1, 8 and 9.

"*" indicates that the residues in that column are identical in all sequences in the alignment

":" indicates that conserved substitutions have been observed

":" indicates that semi-conserved substitutions are observed

"A" indicates that this residue is in the active site

The multiple sequence alignment was conducted using Clustal W (1.82) on the <http://www.ebi.ac.uk/clustalw/> web site. Modifications to the Clustal W alignment were required at the start of the sequences shown here, between helices 2 and 3, and between helices 15 and 16. In some cases further manual changes to the alignment were needed to coincide with alignments observed in the crystal structures themselves.

Appendix 3

Calculated physicochemical properties of synthesised compounds

The following table lists the predicted physicochemical properties of the compounds synthesised within this thesis. An assessment of the predicted physicochemical properties, including pass or failure of Lipinski's Rule, is relevant in a medicinal chemistry campaign to focus synthetic efforts toward drug-like compounds. The physicochemical properties of the synthesised compounds are referred to in sections 3.3 and 5.3 of this thesis, as the physicochemical properties of the compounds were monitored during the syntheses of both the pyrazolopyrimidinone compound library and the 2-tetrahydropyranchromanone compound library.

Table A3. Calculated physicochemical properties of synthesised compounds.

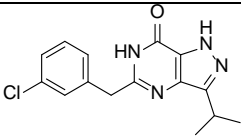
<i>Compound</i>	<i>Molecular weight</i>	<i>Heavy atoms</i>	<i>PSA</i>	<i>cLogP</i>	<i>cLogD_{7.4}</i>	<i># H-bond donors</i>	<i># H-bond acceptors</i>	<i>Lipinski (4 of 4)</i>
 77	302.76	21	70.14	2.81	2.80	2	3	Pass

Table A3 continued. Calculated physicochemical properties of synthesised compounds.

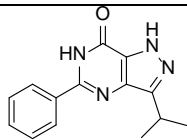
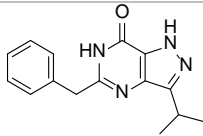
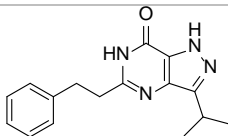
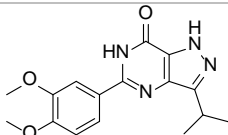
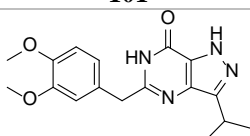
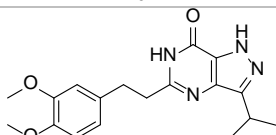
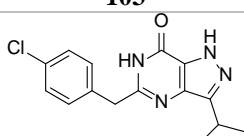
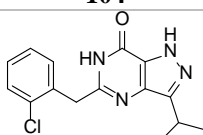
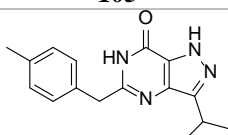
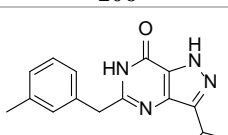
<i>Compound</i>	<i>Molecular weight</i>	<i>Heavy atoms</i>	<i>PSA</i>	<i>cLogP</i>	<i>cLogD_{7.4}</i>	<i># H-bond donors</i>	<i># H-bond acceptors</i>	<i>Lipinski (4 of 4)</i>
 98	254.29	19	70.14	2.23	2.22	2	3	Pass
 99	268.31	20	70.14	2.21	2.19	2	3	Pass
 100	282.34	21	70.14	2.65	2.64	2	3	Pass
 101	314.34	23	88.6	1.91	1.90	2	5	Pass
 102	328.37	24	88.6	1.89	1.88	2	5	Pass
 103	343.39	25	88.6	2.34	2.32	2	5	Pass
 104	302.76	21	70.14	2.81	2.80	2	3	Pass
 105	302.76	21	70.14	2.81	2.80	2	3	Pass
 106	282.34	21	70.14	2.72	2.71	2	3	Pass
 107	282.34	21	70.14	2.72	2.71	2	3	Pass

Table A3 continued. Calculated physicochemical properties of synthesised compounds.

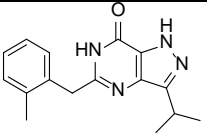
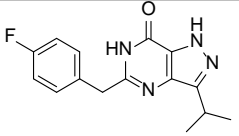
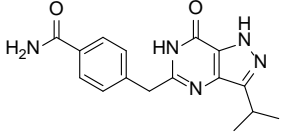
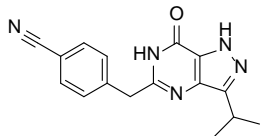
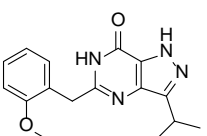
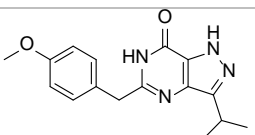
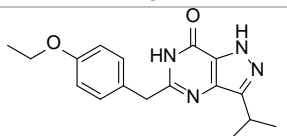
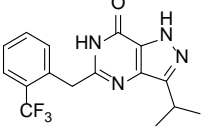
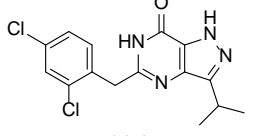
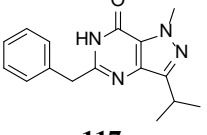
<i>Compound</i>	<i>Molecular weight</i>	<i>Heavy atoms</i>	<i>PSA</i>	<i>cLogP</i>	<i>cLogD_{7.4}</i>	<i># H-bond donors</i>	<i># H-bond acceptors</i>	<i>Lipinski (4 of 4)</i>
 108	282.34	21	70.14	2.72	2.71	2	3	Pass
 109	286.30	21	70.14	2.35	2.34	2	3	Pass
 110	311.34	23	113.23	1.06	1.05	3	4	Pass
 111	293.32	22	93.93	2.06	2.05	2	4	Pass
 112	298.34	22	79.37	2.05	2.04	2	4	Pass
 113	298.34	22	79.37	2.05	2.04	2	4	Pass
 114	312.37	23	79.37	2.41	2.39	2	4	Pass
 115	336.31	24	70.14	3.08	3.07	2	3	Pass
 116	337.20	22	70.14	3.41	3.40	2	3	Pass
 117	282.34	21	59.28	2.33	2.33	1	3	Pass

Table A3 continued. Calculated physicochemical properties of synthesised compounds.

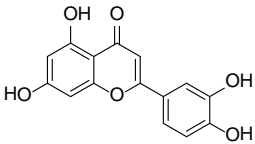
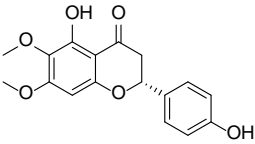
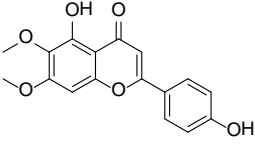
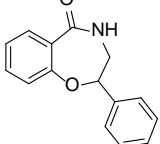
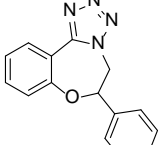
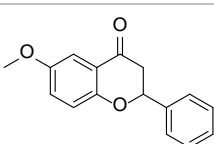
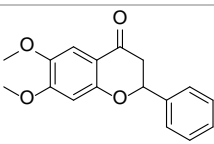
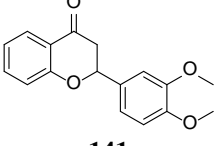
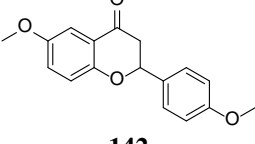
<i>Compound</i>	<i>Molecular weight</i>	<i>Heavy atoms</i>	<i>PSA</i>	<i>cLogP</i>	<i>cLogD_{7.4}</i>	<i># H-bond donors</i>	<i># H-bond acceptors</i>	<i>Lipinski (4 of 4)</i>
 Luteolin	286.24	21	110.05	2.40	0.39	4	6	Pass
 118	316.31	23	85.22	2.82	2.82	2	6	Pass
 119	314.29	23	85.22	2.69	2.37	2	6	Pass
 121	239.27	18	38.33	2.50	2.50	1	2	Pass
 127	264.28	20	52.83	2.83	2.83	0	4	Pass
 138	254.28	19	35.53	2.94	2.94	0	3	Pass
 140	284.31	21	44.76	2.78	2.78	0	4	Pass
 141	284.31	21	44.76	2.78	2.78	0	4	Pass
 142	284.31	21	44.76	2.78	2.78	0	4	Pass

Table A3 continued. Calculated physicochemical properties of synthesised compounds.

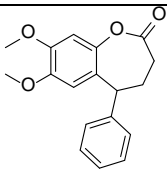
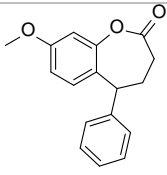
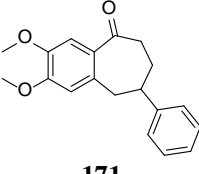
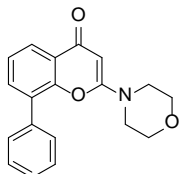
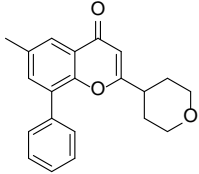
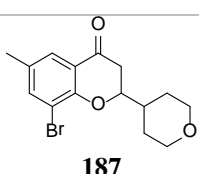
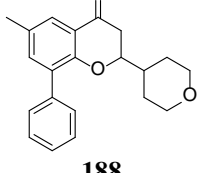
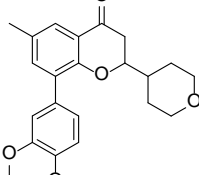
<i>Compound</i>	<i>Molecular weight</i>	<i>Heavy atoms</i>	<i>PSA</i>	<i>cLogP</i>	<i>cLogD_{7.4}</i>	<i># H-bond donors</i>	<i># H-bond acceptors</i>	<i>Lipinski (4 of 4)</i>
 153	298.33	22	44.76	3.44	3.44	0	3	Pass
 154	268.31	20	35.53	3.59	3.59	0	2	Pass
 171	296.36	22	35.53	3.83	3.83	0	3	Pass
 182	307.34	23	38.77	3.41	3.41	0	4	Pass
 183	320.38	24	35.53	4.10	4.10	0	3	Pass
 187	325.20	19	35.53	3.08	3.08	0	3	Pass
 188	322.40	24	35.53	3.95	3.95	0	3	Pass
 190	382.45	28	53.99	3.64	3.64	0	5	Pass

Table A3 continued. Calculated physicochemical properties of synthesised compounds.

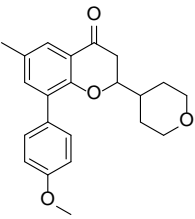
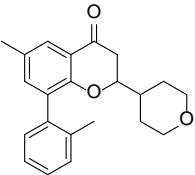
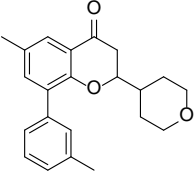
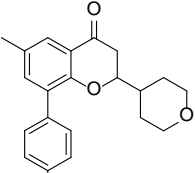
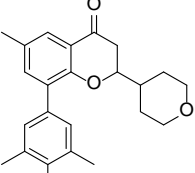
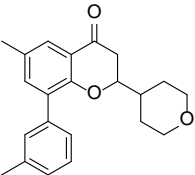
<i>Compound</i>	<i>Molecular weight</i>	<i>Heavy atoms</i>	<i>PSA</i>	<i>cLogP</i>	<i>cLogD_{7.4}</i>	<i># H-bond donors</i>	<i># H-bond acceptors</i>	<i>Lipinski (4 of 4)</i>
 191	352.42	26	44.76	3.80	3.80	0	4	Pass
 192	336.42	25	35.53	4.47	4.47	0	3	Pass
 193	336.42	25	35.53	4.47	4.47	0	3	Pass
 194	336.42	25	35.53	4.47	4.47	0	3	Pass
 195	380.48	28	44.76	4.82	4.82	0	4	Pass
 196	402.48	30	44.76	4.79	4.79	0	4	Pass

Table A3 continued. Calculated physicochemical properties of synthesised compounds.

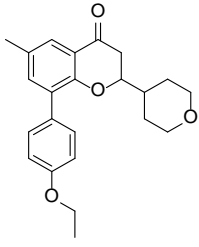
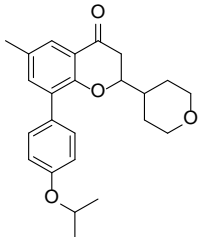
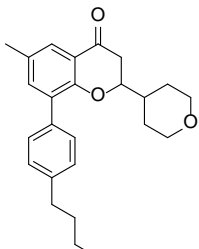
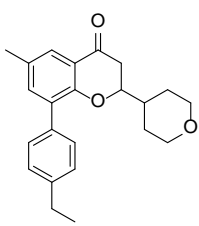
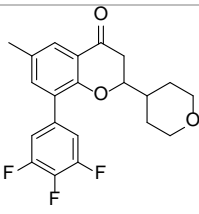
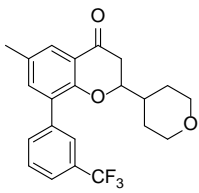
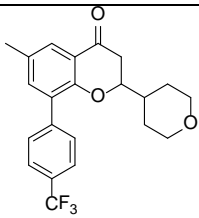
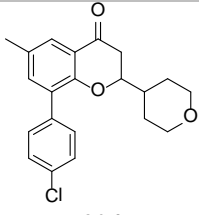
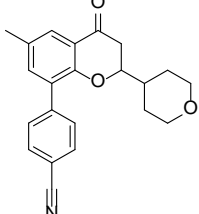
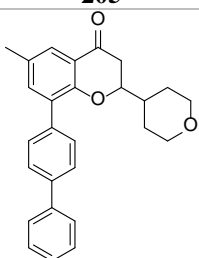
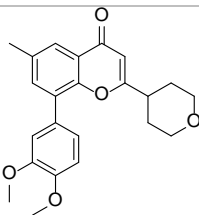
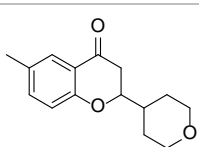
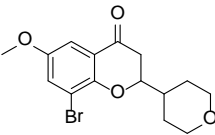
<i>Compound</i>	<i>Molecular weight</i>	<i>Heavy atoms</i>	<i>PSA</i>	<i>cLogP</i>	<i>cLogD_{7.4}</i>	<i># H-bond donors</i>	<i># H-bond acceptors</i>	<i>Lipinski (4 of 4)</i>
 197	366.45	27	44.76	4.15	4.15	0	4	Pass
 198	380.48	28	44.76	4.57	4.57	0	4	Pass
 199	378.50	28	35.53	5.80	5.80	0	3	Fail
 200	350.45	26	35.53	4.91	4.91	0	3	Pass
 201	376.37	27	35.53	4.38	4.38	0	3	Pass
 202	390.40	28	35.53	4.83	4.83	0	3	Pass

Table A3 continued. Calculated physicochemical properties of synthesised compounds.

<i>Compound</i>	<i>Molecular weight</i>	<i>Heavy atoms</i>	<i>PSA</i>	<i>cLogP</i>	<i>cLogD_{7.4}</i>	<i># H-bond donors</i>	<i># H-bond acceptors</i>	<i>Lipinski (4 of 4)</i>
 203	390.40	28	35.53	4.83	4.83	0	3	Pass
 204	356.84	25	35.53	4.56	4.56	0	3	Pass
 205	347.41	26	59.32	3.81	3.81	0	4	Pass
 206	398.49	30	35.53	5.60	5.60	0	3	Fail
 208	380.43	28	53.99	3.78	3.78	0	5	Pass
 209	246.30	18	35.53	2.31	2.31	0	3	Pass
 212	341.20	20	44.76	2.40	2.40	0	4	Pass

Appendix 4

Summary of biological activities of synthesised compounds

The following table summarises the biological activities of the compounds synthesised within this thesis. Both *Plasmodium falciparum* growth inhibition and human PDE inhibitory activities are listed where they have been obtained. Furthermore, determined IC₅₀ values are shown against selected hPDE isoforms where they have been obtained. The inhibitory activities of the synthesised compounds are discussed in detail in sections 3.5, 4.2.4, and 5.4 of this thesis.

Table A4. Summary of the biological activities of synthesised compounds.

Compound	<i>Pf</i> parasite growth IC ₅₀ (μM)	<i>Human PDE % inhibition at 1 μM (IC₅₀ in μM)</i>										
		1A	2A	3CAT	4CAT	5CAT	6AB	7A	8A	9A	10A	11A
77	16- >100	-	-	-	-	-	-	-	-	(0.01) ^a	-	-
98	3.7- 10.4	-	-	-	-	-	-	-	-	-	-	-
99	0.08- 0.72	44	13	8	8	67	64	0	16	(0.03) ^a	0	19
100	1.6-2.7	-	-	-	-	-	-	-	-	-	-	-

Table A4 continued. Summary of the biological activities of synthesised compounds.

<i>Compound</i>	<i>Pf parasite growth IC₅₀ (μM)</i>	<i>Human PDE % inhibition at 1 μM (IC₅₀ in μM)</i>										
		<i>1A</i>	<i>2A</i>	<i>3CAT</i>	<i>4CAT</i>	<i>5CAT</i>	<i>6AB</i>	<i>7A</i>	<i>8A</i>	<i>9A</i>	<i>10A</i>	<i>11A</i>
101	>100	-	-	-	-	-	-	-	-	-	-	-
102	33-92	-	-	-	-	-	-	-	-	-	-	-
103	27-54	-	-	-	-	-	-	-	-	-	-	-
104	0.26-1.7	-	-	-	-	-	-	-	-	-	-	-
105	0.06-0.97	21	0	1	0	22	30	1	0	(1.80) ^a	0	15
106	3.3-6.6	-	-	-	-	-	-	-	-	-	-	-
107	2.0-4.6	-	-	-	-	-	-	-	-	-	-	-
108	0.64-1.2	-	-	-	-	-	-	-	-	-	-	-
109	0.22-1.5	-	-	-	-	-	-	-	-	-	-	-
110	2.0-3.3	-	-	-	-	-	-	-	-	-	-	-
111	8.0-9.7	-	-	-	-	-	-	-	-	-	-	-
112	>100	-	-	-	-	-	-	-	-	-	-	-
113	3.2-4.7	-	-	-	-	-	-	-	-	-	-	-
114	2.4-5.3	-	-	-	-	-	-	-	-	-	-	-
115	0.61-0.84	-	-	-	-	-	-	-	-	-	-	-
116	5.0-7.2	-	-	-	-	-	-	-	-	-	-	-
117	>100	-	-	-	-	-	-	-	-	-	-	-

Table A4 continued. Summary of the biological activities of synthesised compounds.

<i>Compound</i>	<i>Pf parasite growth IC₅₀ (μM)</i>	<i>Human PDE % inhibition at 1 μM (IC₅₀ in μM)</i>										
		<i>1A</i>	<i>2A</i>	<i>3CAT</i>	<i>4CAT</i>	<i>5CAT</i>	<i>6AB</i>	<i>7A</i>	<i>8A</i>	<i>9A</i>	<i>10A</i>	<i>11A</i>
121	4.2-9.4	62	-	-	5	-	-	-	-	3	-	-
127	>100	7	-	-	17	-	-	-	-	0	-	-
138	>100	3	-	-	14	-	-	-	-	0	-	-
140	>100	0	-	-	8	-	-	-	-	0	-	-
141	42- >100	-	-	-	-	-	-	-	-	-	-	-
142	>100	9	-	-	14	-	-	-	-	0	-	-
153	>100	20	-	-	6	-	-	-	-	3	-	-
154	>100	-	-	-	-	-	-	-	-	-	-	-
182	-	11	(40) 23	(100) 0	41 ^b	50	25 ^c	0	0	0	(1.3) 85	(4.1) 65
187	>100	4	-	-	11	-	-	-	-	3	-	-
188	>100	39	-	-	31	-	-	-	-	0	-	-
190	2.6-4.1	94	13	14	(1.6) 90	45	0	33	54	2	53	51
191	5.7-9.0	73	-	-	48	-	-	-	-	0	-	-
192	>100	3	-	-	32	-	-	-	-	10	-	-
193	9.9-48	6	-	-	37	-	-	-	-	76	-	-
194	5.6-7.0	84	7	8	48	30	0	0	27	0	6	24

Table A4 continued. Summary of the biological activities of synthesised compounds.

Compound	<i>Pf</i> parasite growth IC_{50} (μM)	<i>Human PDE % inhibition at 1 μM (IC_{50} in μM)</i>										
		1A	2A	3CAT	4CAT	5CAT	6AB	7A	8A	9A	10A	11A
195	>100	-	-	-	-	-	-	-	-	-	-	-
196	>100	0	-	-	4	-	-	-	-	1	-	-
197	4.2-11	82	-	-	31	-	-	-	-	3	-	-
198	3.0-5.4	68	-	-	22	-	-	-	-	3	-	-
199	1.1-1.3	77	-	-	22	-	-	-	-	0	-	-
200	6.6-12	25	-	-	44	-	-	-	-	3	-	-
201	7.9-52	-	-	-	-	-	-	-	-	-	-	-
202	>100	-	-	-	-	-	-	-	-	-	-	-
203	1.7-3.1	74	-	-	10	-	-	-	-	6	-	-
204	85- >100	6	-	-	35	-	-	-	-	1	-	-
205	3.8-4.2	72	0	3	33	34	0	4	34	1	9	32
206	2.3-3.7	0	-	-	1	-	-	-	-	0	-	-
208	4.7-9.7	99	29	29	(0.2) 94	60	0	44	83	4	82	75
209	>100	68	-	-	6	-	-	-	-	0	-	-
212	>100	-	-	-	-	-	-	-	-	-	-	-

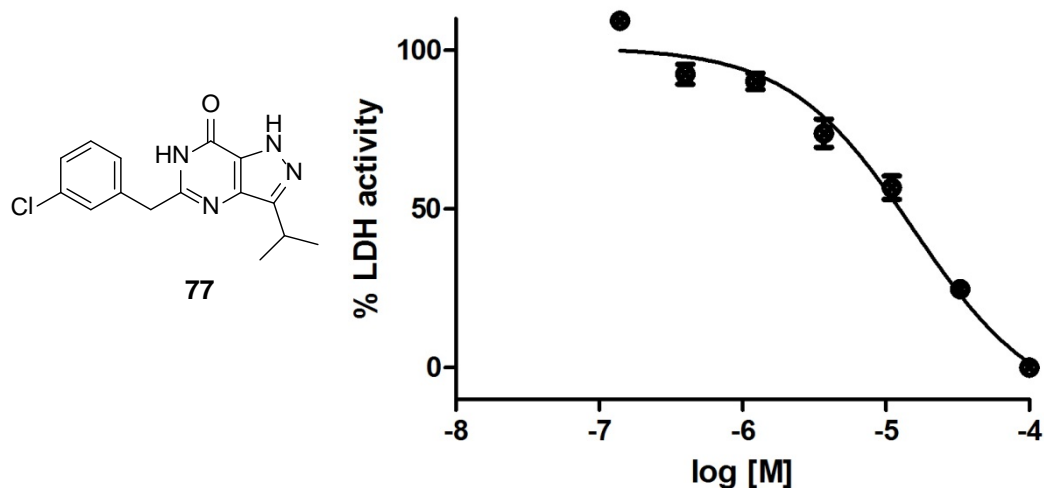
Each value represents the mean of duplicate determinations where each replicate was within 6% of the mean value. Values shown in brackets are determined IC_{50} values, in μM . Compounds **99** and **105** were assayed externally by BPS Bioscience, San Diego (see section 7.3.2 for experimental methods). The remainder of the compounds were assayed externally by Scottish Biomedical, Glasgow (see section 7.3.2 for experimental methods).

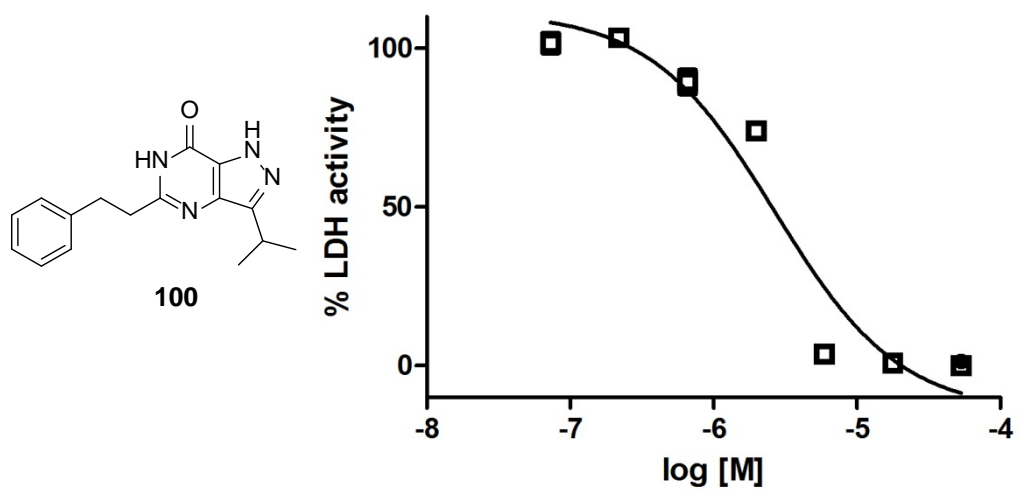
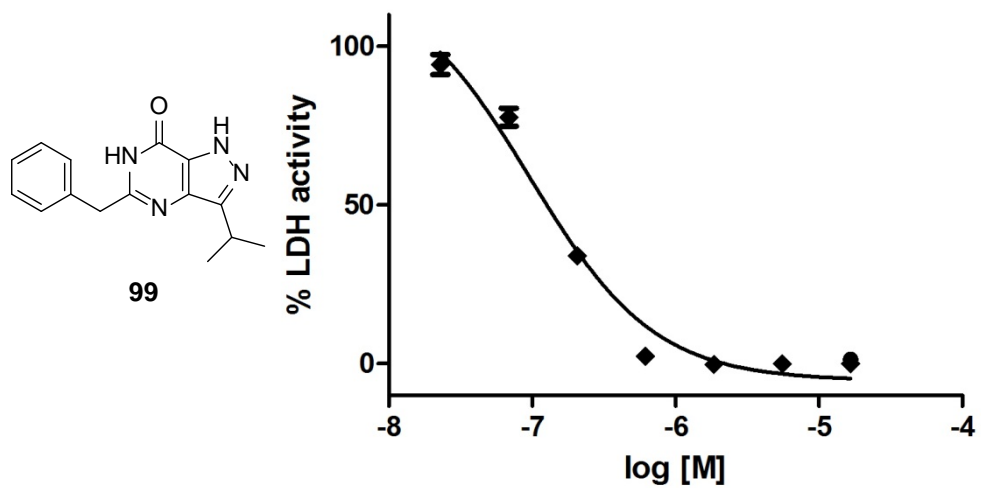
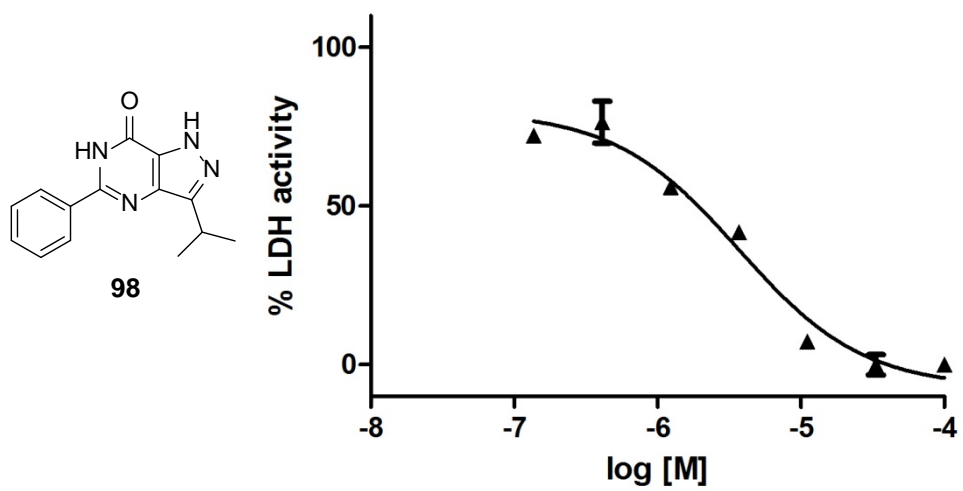
^a IC_{50} values determined by DeNinno *et al.*¹⁹⁹; ^b assessed against PDE4A; ^c assessed against PDE6C

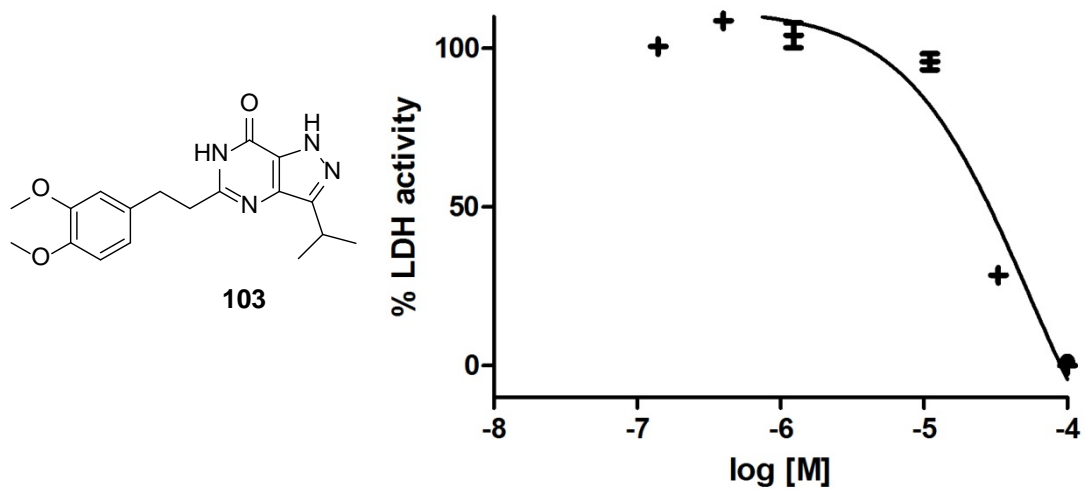
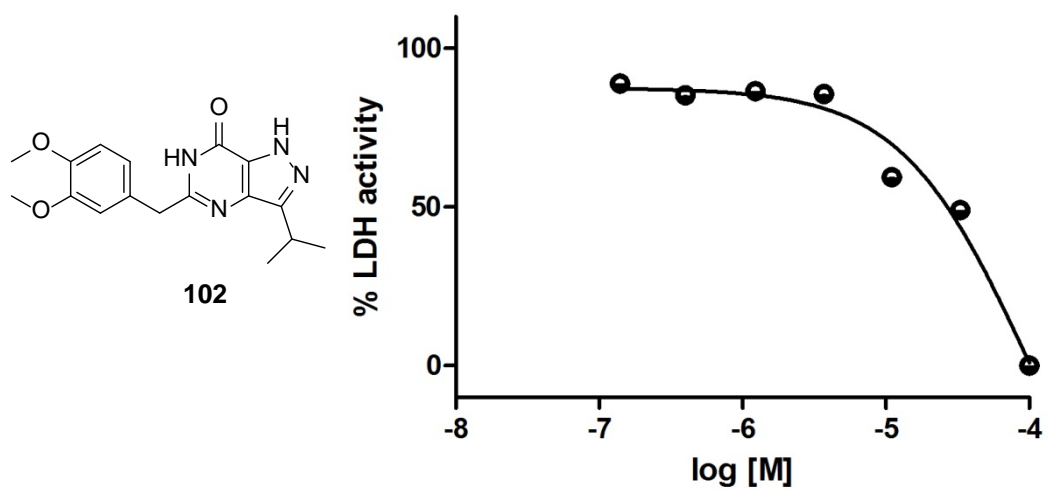
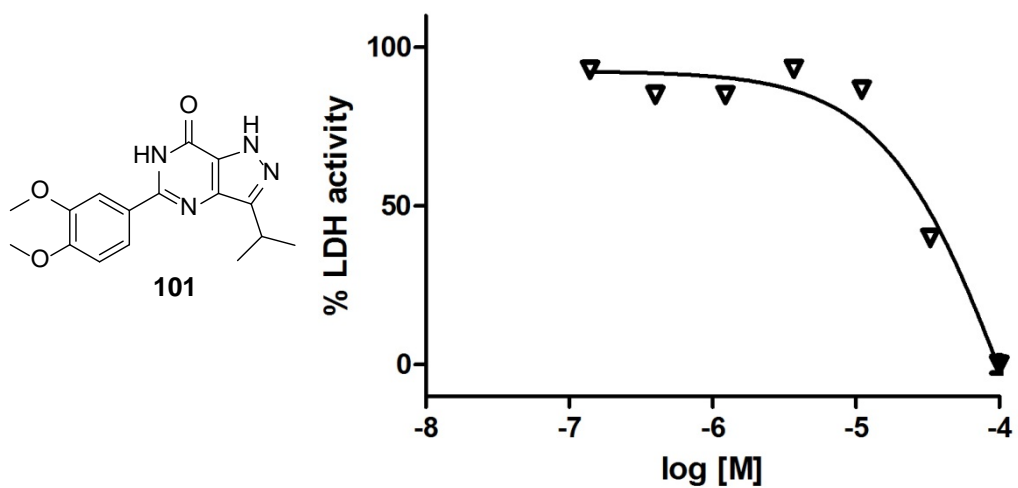
Appendix 5

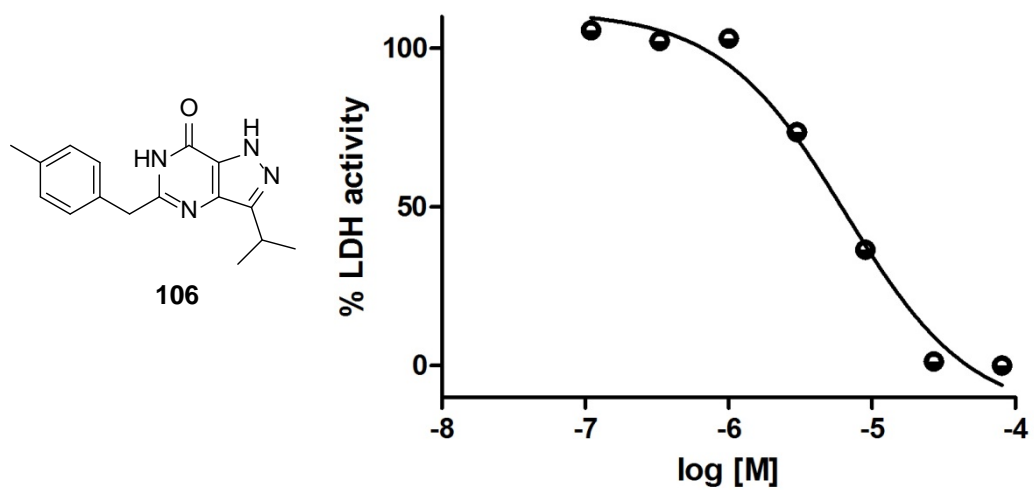
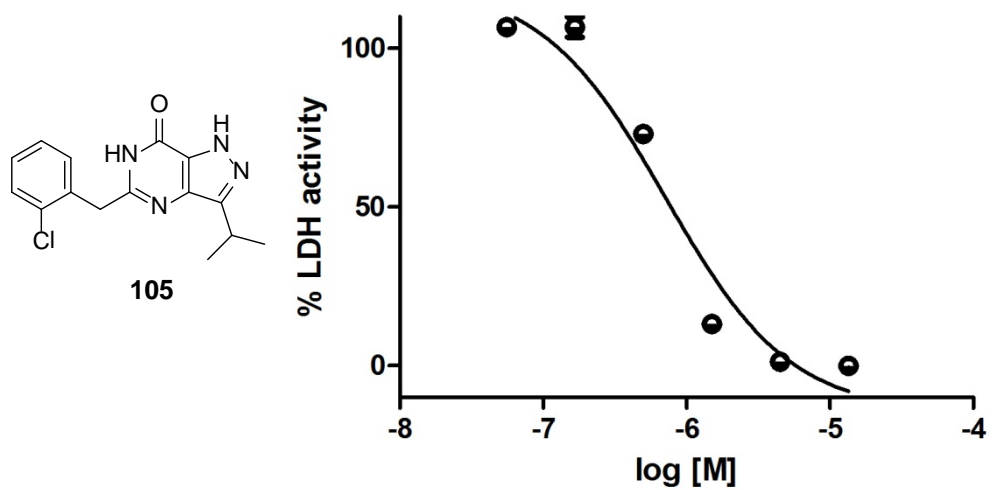
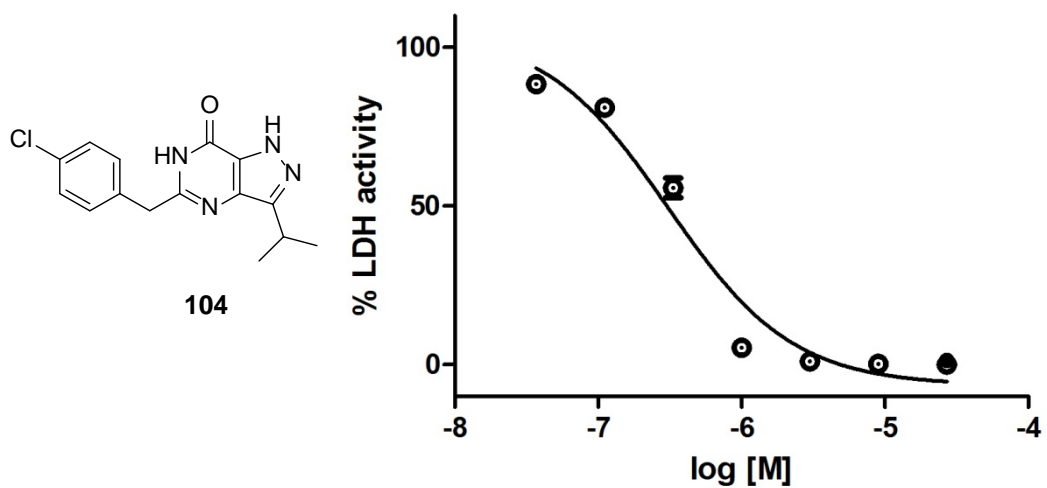
IC₅₀ curves of synthesised compounds

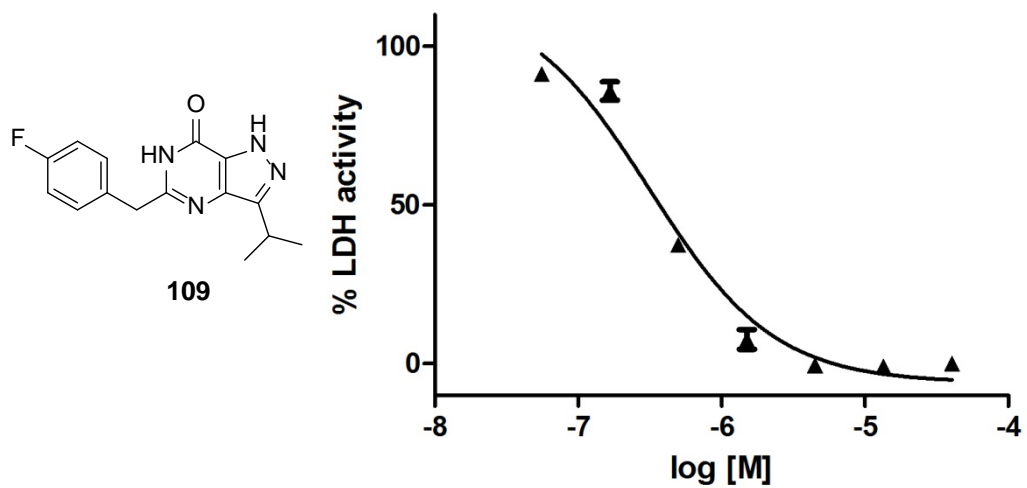
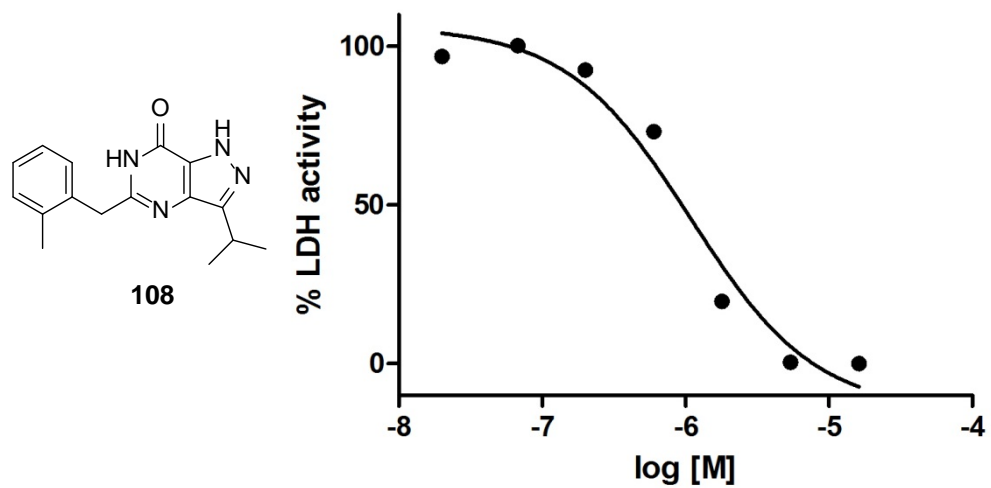
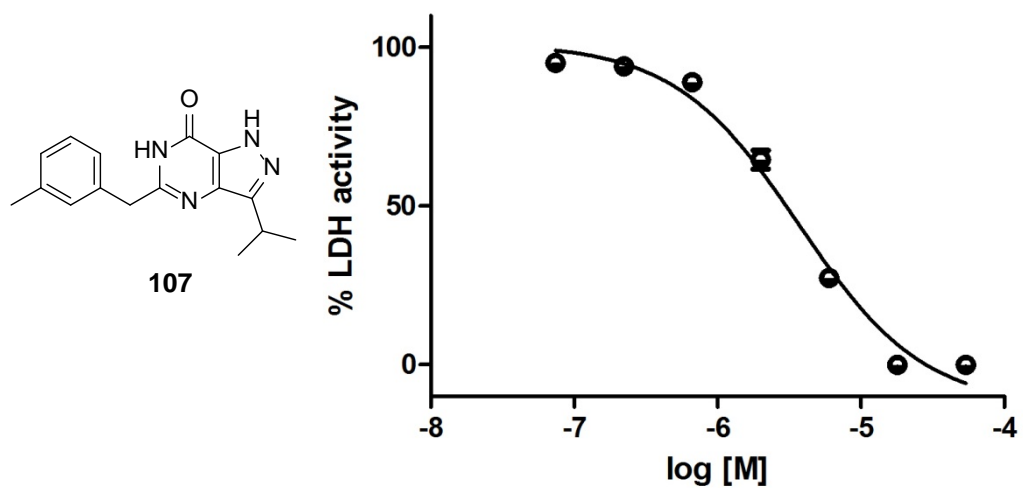
Depicted below are the IC₅₀ curves of *Plasmodium falciparum* growth inhibition. Each of the synthesised pyrazolopyrimidinone compounds and 2-tetrahydropyranchromanone compounds were assessed for antiplasmodial growth inhibition and are discussed in sections 3.5 and 5.4 of this thesis. The curves shown are one trace which is representative of a minimum of three replicates.

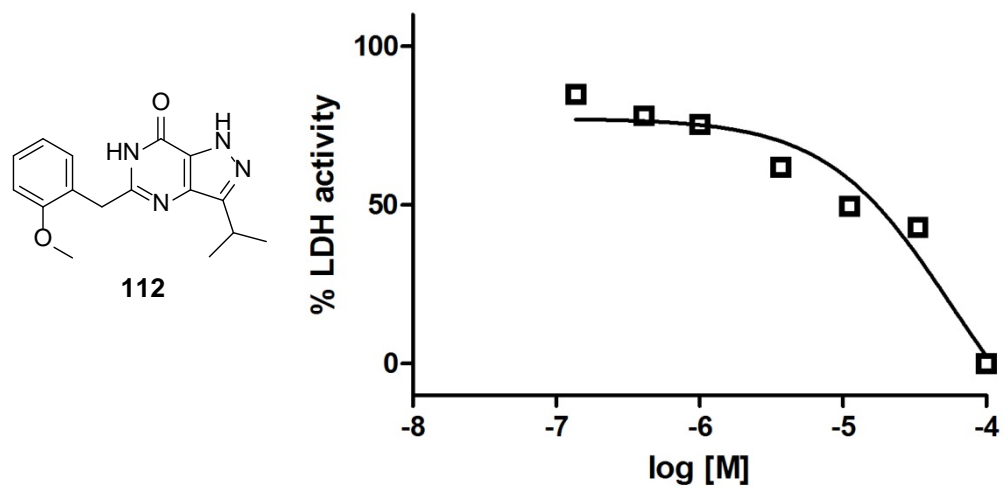
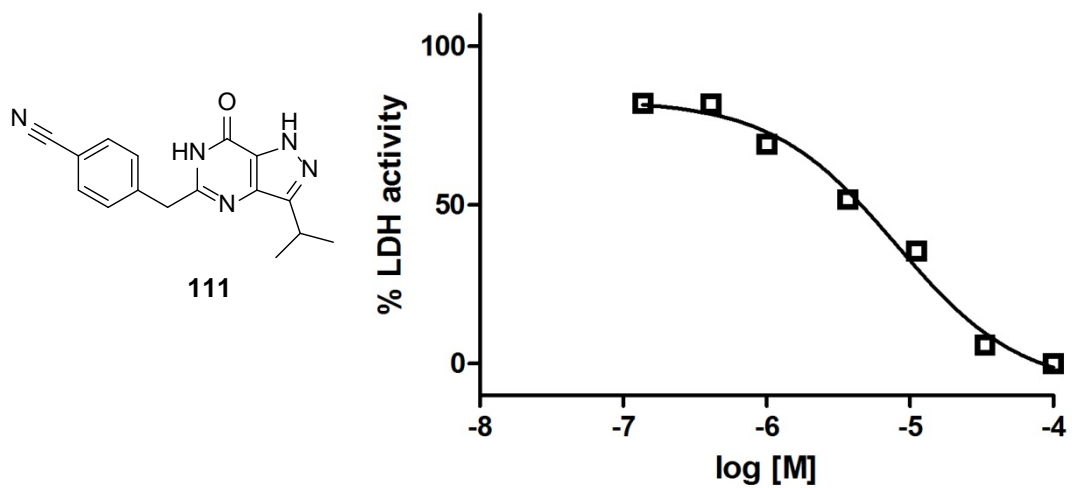
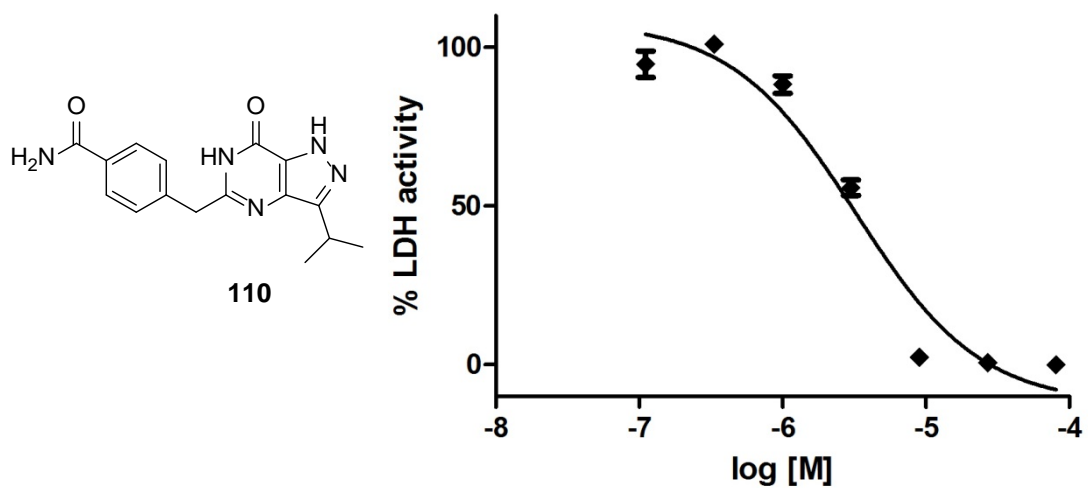


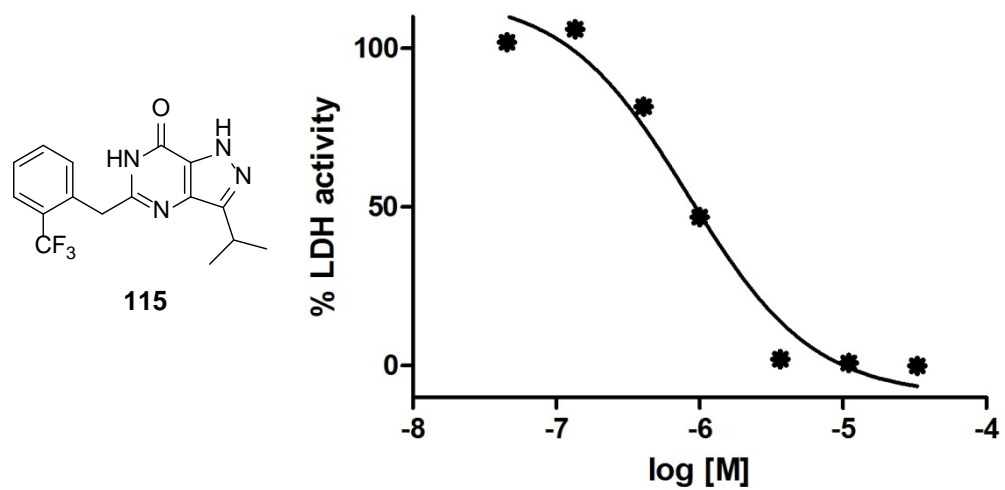
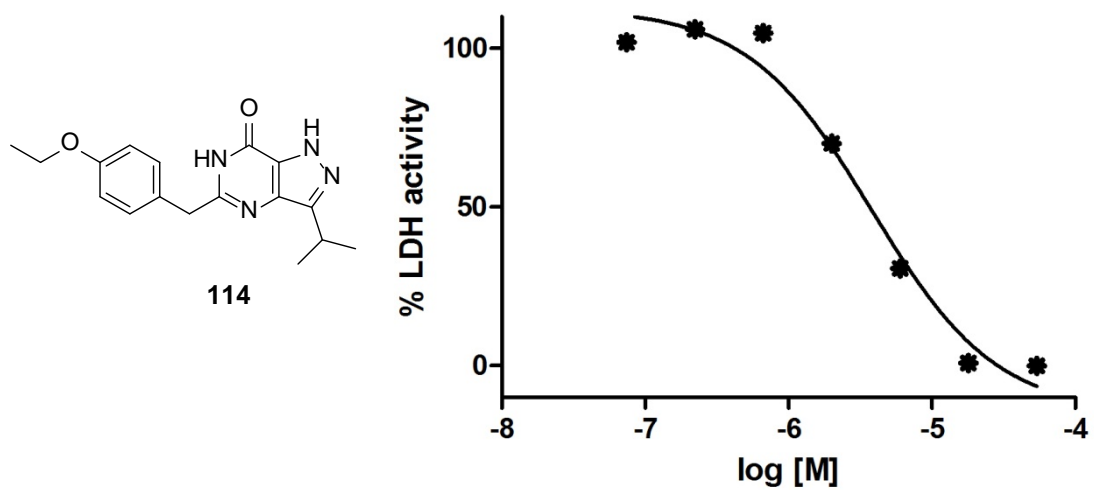
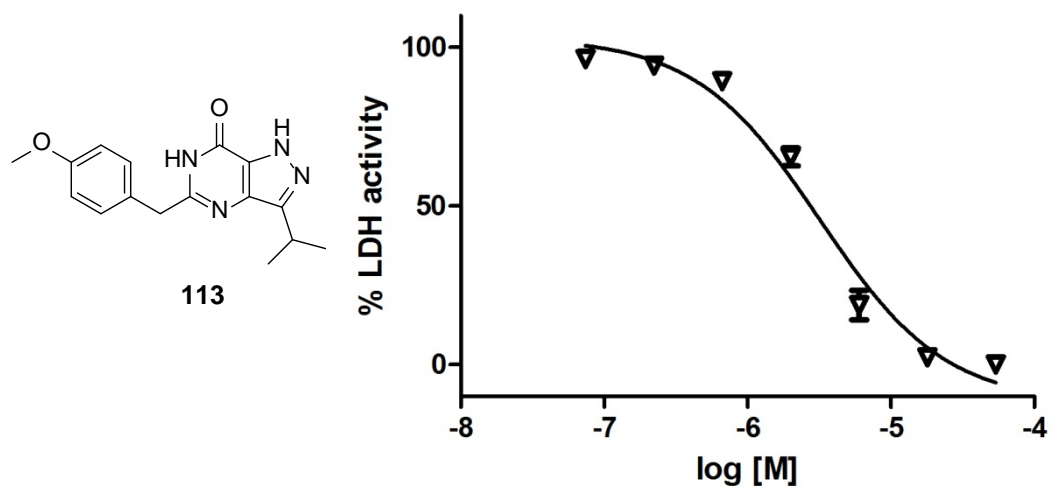


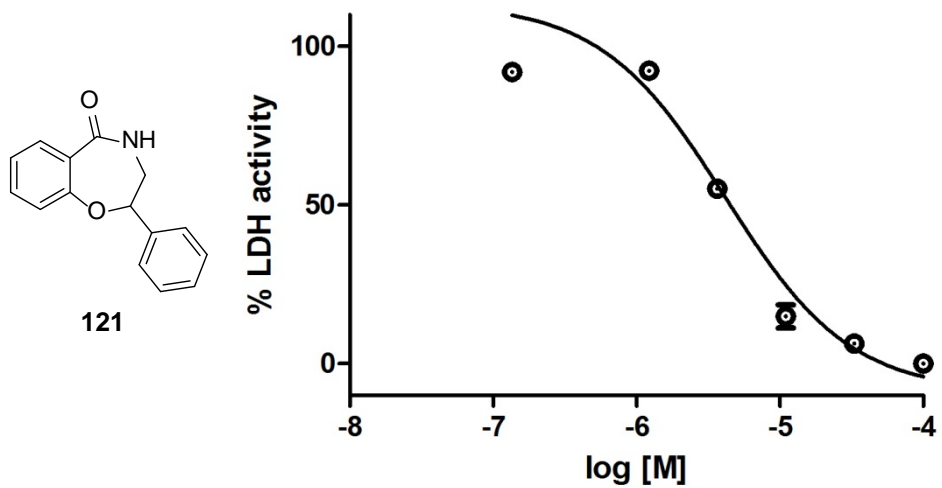
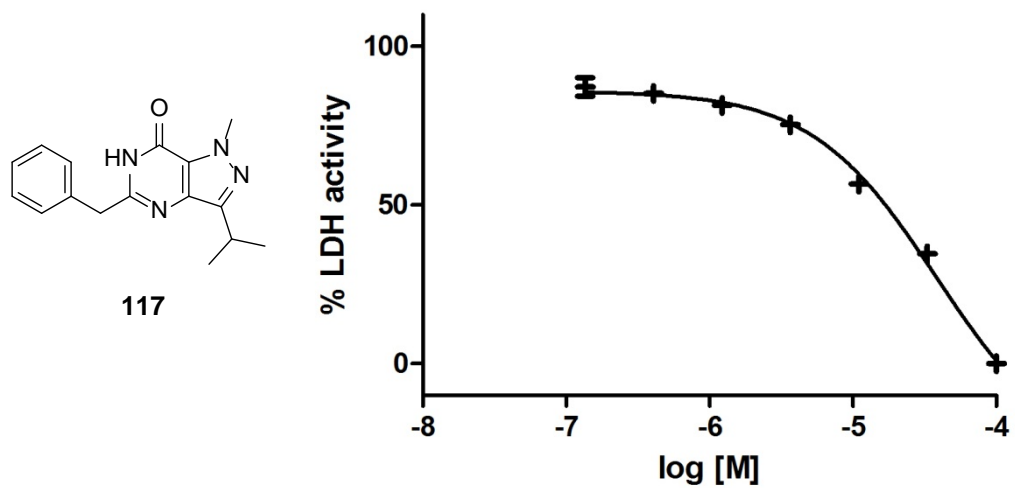
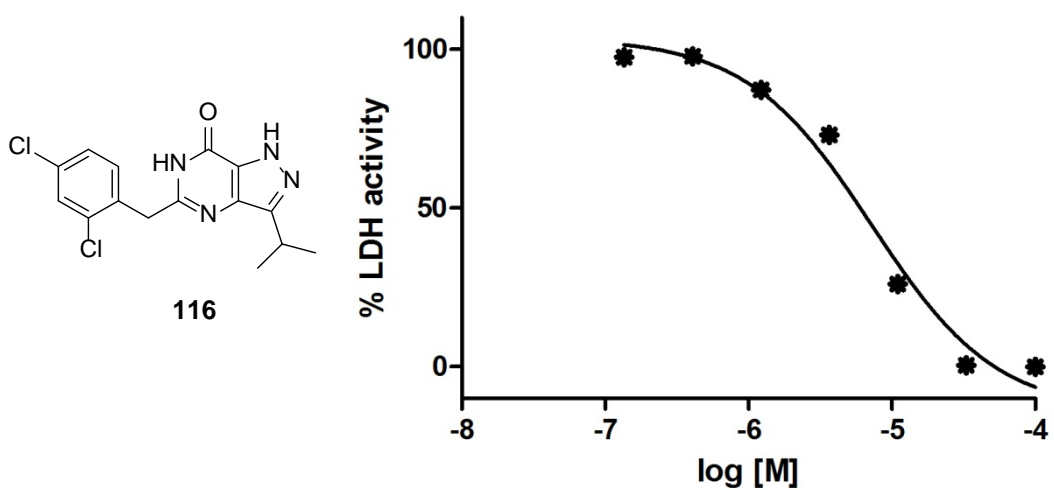


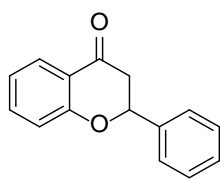




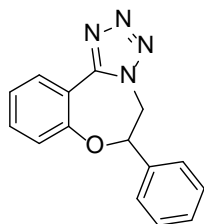
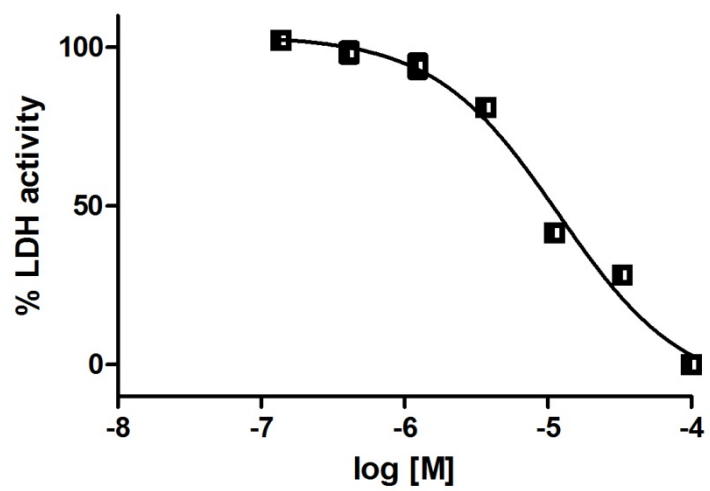




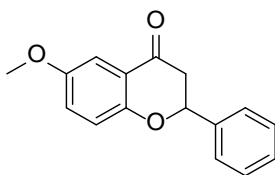
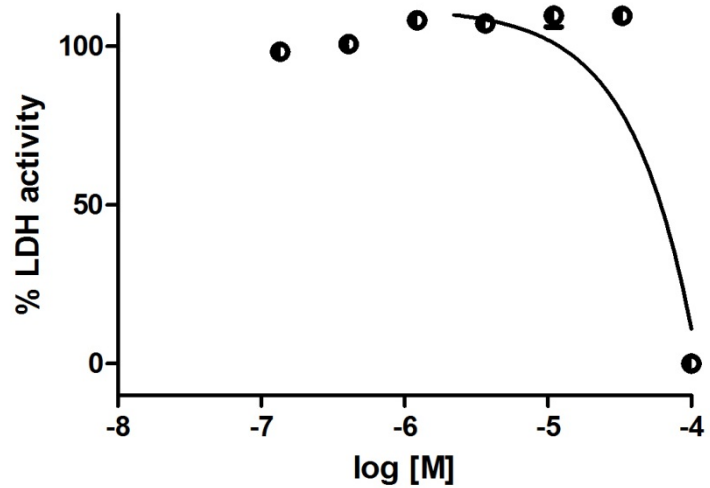




125



127



138

